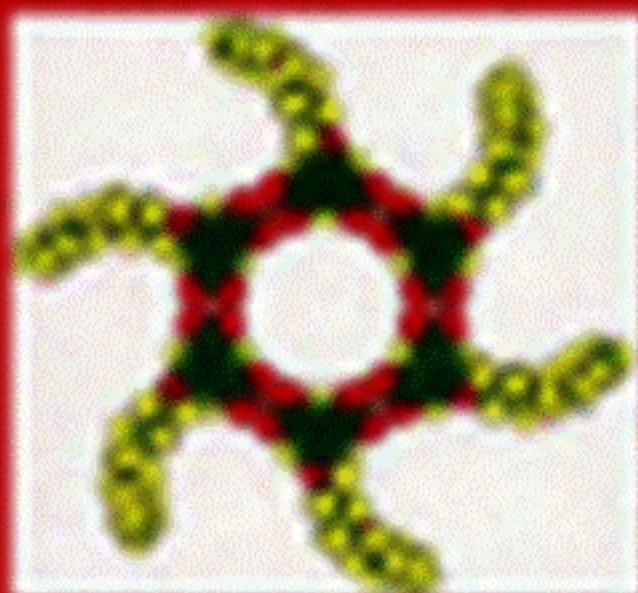


*Advances in
Supramolecular
Chemistry*

FOUNDED BY J. H. DINEEN



Supramolecular Control of Structure and Reactivity

Edited by

Andrew D. Hamilton

Supramolecular Control of Structure and Reactivity

Editorial Board

Founding Editor

J.-M. Lehn, Collège de France, Chimie des Interactions Moléculaires, 11 Place Marcelin Berthelot, 75005 Paris, France

Editors

J.-P. Behr, Université Louis Pasteur, Institut le Bel, 4 Rue Blaise Pascal, F-67070 Strasbourg, France

G. R. Desiraju, University of Hyderabad, School of Chemistry, Hyderabad 500134, India

A. D. Hamilton, University of Pittsburgh, Department of Chemistry, Pittsburgh, PA 15260, USA

T. Kunitake, Kyushu University, Faculty of Engineering, Hakozaki, Fukuoka 812, Japan

D. N. Reinhoudt, University of Twente, Faculty of Chemical Technology, PO Box 217, NL-7500 AE Enschede, The Netherlands

J.-P. Sauvage, Université Louis Pasteur, Institut le Bel, 4 Rue Blaise Pascal, F-67070 Strasbourg, France

Supramolecular Control of Structure and Reactivity

*Perspectives in
Supramolecular Chemistry
Volume 3*

EDITED BY ANDREW D. HAMILTON

University of Pittsburgh, USA

JOHN WILEY & SONS

Chichester · New York · Brisbane · Toronto · Singapore

Copyright © 1996 by John Wiley & Sons Ltd,
Baffins Lane, Chichester,
West Sussex PO19 1UD, England

National 01243 779777
International (+44) 1243 779777
e-mail (for orders and customer service enquiries): cs-books@wiley.co.uk
Visit our Home Page on <http://www.wiley.co.uk>
or <http://www.wiley.com>

All Rights Reserved. No part of this publication may be reproduced, stored in a retrieval system, or transmitted, in any form or by any means, electronic, mechanical, photocopying, recording, scanning or otherwise, except under the terms of the Copyright, Designs and Patents Act 1988 or under the terms of a licence issued by the Copyright Licensing Agency, 90 Tottenham Court Road, London, UK W1P 9HE, without the permission in writing of the publisher.

Other Wiley Editorial Offices

John Wiley & Sons, Inc., 605 Third Avenue,
New York, NY 10158-0012, USA

Jacaranda Wiley Ltd, 33 Park Road, Milton,
Queensland 4064, Australia

John Wiley & Sons (Canada) Ltd, 22 Worcester Road,
Rexdale, Ontario M9W 1L1, Canada

John Wiley & Sons (Asia) Pte Ltd, 2 Clementi Loop #02-01,
Jin Xing Distripark, Singapore 129809

Library of Congress Cataloging-in-Publication Data

Supramolecular control of structure and reactivity / edited by Andrew
D. Hamilton.

p. cm.—(Perspectives in supramolecular chemistry : v. 3)
Includes bibliographical references and index.

ISBN 0-471-95920-0 (cloth)

1. Macromolecules. 2. Self-organizing systems. I. Hamilton,

Andrew D. II. Series.

QP801.P64S86 1996

96-944

574.8'8—dc20

CIP

British Library Cataloguing in Publication Data

A catalogue record for this book is available from the British Library

ISBN 0-471-95920-0

Typeset in 10/12pt Times by Dobbie Typesetting Limited, Tavistock, Devon
Printed and bound in Great Britain by Biddles Ltd, Guildford and King's Lynn

This book is printed on acid-free paper responsibly manufactured from sustainable forestation,
for which at least two trees are planted for each one used for paper production.

Contents

Contributors	vii
Preface	ix
1 Metal Template Control of Self-Assembly in Supramolecular Chemistry John R. Fredericks and Andrew D. Hamilton	1
2 A Survey of Supramolecular Chemistry (1993–1994) Uday Maitra	41
3 Control of Reactivity in Aggregates of Amphiphilic Molecules Paolo Scrimin	101
4 Models of Hemoprotein Active Sites Michel Momenteau	155
5 Recent Developments in the Design of Self-Replicating Systems Edward A. Wintner and Julius Rebek Jr	225
6 Synthetic Control of DNA Triplex Structure Through Chemical Modifications Krishna N. Ganesh, Vijayanti A. Kumar and Dinesh A. Barawkar	263
Cumulative Author Index	329
Cumulative Title Index	331
Index	333

Contributors

Dinesh A. Barawkar, Division of Organic Chemistry, National Chemical Laboratory, Pune 411008, India

John R. Fredericks, Department of Chemistry, University of Pittsburgh, Pittsburgh, PA 15260, USA

Krishna N. Ganesh, Division of Organic Chemistry, National Chemical Laboratory, Pune 411008, India

Andrew D. Hamilton, Department of Chemistry, University of Pittsburgh, Pittsburgh, PA 15260, USA

Vaijayanti A. Kumar, Division of Organic Chemistry, National Chemical Laboratory, Pune 411008, India

Uday Maitra, Department of Organic Chemistry, Indian Institute of Science, Bangalore 560012, India

Michel Momenteau, Institut Curie, Section de Biologie, U.219 INSERM, Bâtiment 112, Centre Universitaire, 91405 Orsay Cedex, France

Julius Rebek Jr, Massachusetts Institute of Technology, Department of Chemistry, 77 Massachusetts Avenue, Room 18-390, Cambridge, MA 02139, USA

Paolo Scrimin, University of Trieste, Department of Chemical Sciences, 34127 Trieste, Italy

Edward A. Wintner, Massachusetts Institute of Technology, Department of Chemistry, 77 Massachusetts Avenue, Room 18-390, Cambridge, MA 02139, USA

Preface

In recent years there has been an explosion of interest in the burgeoning new field of supramolecular chemistry. Building on the pivotal work of Pedersen, Cram and Lehn, scientists from many nations have been investigating the chemistry of noncovalent interactions. Particular focus has been placed on the design of synthetic molecules that can mimic biological systems and achieve significant recognition or catalytic activities. Crucial for success in this endeavor is an understanding of the interplay between different binding interactions and how they contribute to the recognition of ground state or transition state structures. What can be learned from or achieved with artificial receptor molecules and why is this study important in the context of biochemical processes? This is a critical question at the heart of all modern supramolecular chemistry research and the answer is manifold. While the study of the natural system may answer “how” an enzyme functions, the study of small synthetic analogs can help us understand “why” it works. Small molecule mimics of biological function provide an opportunity to study the intrinsic chemistry of molecular recognition and catalysis away from the complex environment of a biopolymer. Small molecules provide considerably greater detail and precision in the study of their structure and of the thermodynamics and kinetics of their recognition interactions. Modifications can be easily made to the position, orientation and nature of binding groups as well as the solvent environment, leading to new insights into the underlying chemistry of the biological process. Understanding the “why” of an enzyme function gives us not only increased mechanistic understanding but also the ability to reproduce biological levels of reactivity in synthetic systems.

This book provides a broad view of the different approaches that have been taken to control structure and reactivity in supramolecular systems. Six researchers from around the world describe different approaches to novel supramolecular systems ranging from amphiphiles with catalytic activity to synthetic entities that recognize and bind to the major groove of DNA. Other

contributions describe the use of metal templates to construct synthetic receptors and also the design of molecules with the capacity for self-replication. A comprehensive discussion of the use of small molecule models of heme protein function is also included as well as a review of recent contributions in the general area of supramolecular chemistry.

Andrew D. Hamilton
Pittsburgh
May 1996

Chapter 1

Metal Template Control of Self-Assembly in Supramolecular Chemistry

JOHN R. FREDERICKS AND ANDREW D. HAMILTON

University of Pittsburgh, PA, USA

1. INTRODUCTION

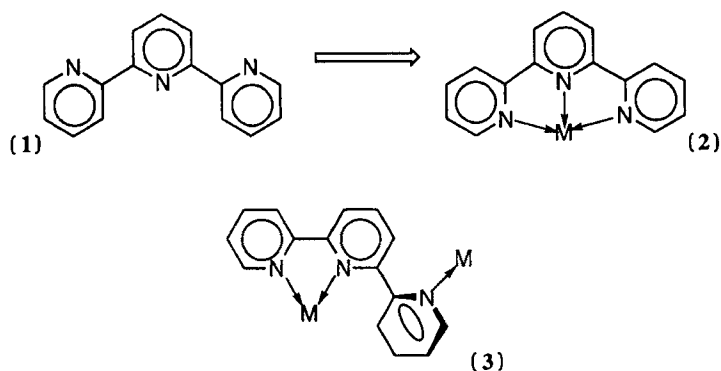
There is enormous current interest in the development of molecules that self-assemble into aggregates of well-defined shape and function [1]. A key to success is the identification of both strong and directional binding forces to hold together the different components of the structure. To this end, extensive use has been made of intermolecular hydrogen bonds [2], π - π stacking interactions [3] and metal-ligand coordination (the subject of this review) to build large, multicomponent aggregates. Such structures form the foundation of the burgeoning field of nanoarchitecture. Self-assembled systems have been designed which can act as host molecules for organic guests [4] and enclathrating agents [5]. A molecule has been developed that can act as a molecular abacus [6], and various modular strategies to the formation of molecular building sets have been proposed [7,8]. Although the long-term goal of much of this work is the design of functioning devices, important progress is also being made in understanding the factors that influence the formation of self-assembled aggregates. For example, recent studies have emphasized the role of preorganization [9–11], analyzed the detailed thermodynamics and kinetics of self-assembly [12], incorporated error-checking mechanisms into aggregate formation [13] and demonstrated cooperativity [14].

Metal–ligand coordination has been widely utilized in designing self-assembling aggregates. In this chapter, we will first give an overview of the use of metals to control the formation of novel structures, and then describe their role in the design of some functioning aggregates. There are several factors which influence the self-assembly process for these structures: the nature of and substitution pattern on the ligand, the ability of an aromatic ligand to π -stack with itself or other ligands, and the stereochemical preference of the metal ion. This last factor has been shown to be the most important in determining the final shape and structure of a templated aggregate, though the other two factors certainly have an effect.

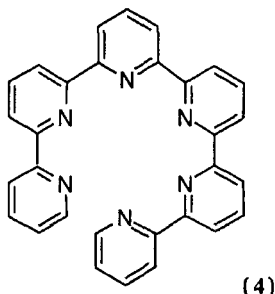
2. METAL TEMPLATE CONTROL OF SUPRAMOLECULAR STRUCTURE

2.1 Self-Assembly of Double- and Triple-Helical Structures

The ability of certain metal ions to coordinate with pyridine has been used in designing various double-helical structures. Linking three pyridine rings produces the molecule 2,2':6',2''-terpyridine (terpy). In the solid state, terpy takes a planar *trans,trans*-conformation (1). Coordinating terpy with most metal ions causes the ligand to adopt a planar *cis,cis*-conformation (2). To use oligopyridines to form helices, the rings must be induced to take up a nonplanar or “twist” geometry. This type of conformation can be induced by coordinating two metals to the terpy. The steric and electrostatic repulsion of the metal centers leads to a twist geometry as shown in (3) [15].



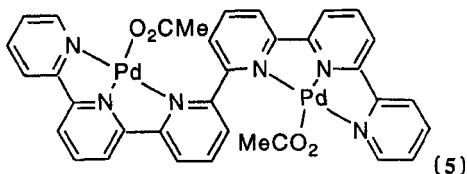
Using the longer oligopyridine ligand 2,2':6',2'':6'',2''':6''',2''':6''''-sexipyridine (spy) (4), Constable *et al.* have shown that some metal ions can induce the formation of double-helical aggregates. In particular, (4) was allowed to complex with six different metal ions and the resultant structure of each aggregate was determined [16].



When the ligand was allowed to react with manganese(II) acetate, a complex of formula $[\text{Mn}_2(\mathbf{4})_2][\text{PF}_6]_4$ resulted. This was determined to be a double helix, with each manganese atom displaying six-coordinate geometry. Evidence for the formation of a double helix was found in the cyclic voltammetry and electron spin resonance (ESR) data. The voltammogram revealed four well-separated reductions, but no oxidation wave. The aggregate may be stabilized with respect to reduction because of the close proximity of the two manganese(II) centers. ESR data suggest that both manganese atoms are in identical environments and that there is a magnetic interaction between them. The complex formed between iron(II) and (4) behaved similarly, though it was not as resistant to oxidation as the manganese complex.

The crystal structure of the complex between (4) and cadmium(II) also shows the formation of a double-helical structure between two equivalents of ligand and two equivalents of metal ion (Figure 1). Both left-handed and right-handed helices form. The two cadmium(II) ions are in identical six-coordinate sites. The metal-metal distance of 4.173 Å (1 Å = 0.1 nm) does not permit direct cadmium-cadmium interactions. It is notable that ligand (4) arranges itself so that stacking interactions are present. Data from the ^1H nuclear magnetic resonance (NMR) spectra suggest that this complex persists in solution.

The importance of octahedral, six-coordinate geometry in helix formation was established in the reaction of (4) with the normally four-coordinate square planar palladium(II). This forms a 1:2 ligand:metal complex as in (5), with each palladium(II) in a distorted square planar environment.



A complex of the formula $[\text{Cu}_3(\mathbf{4})_2][\text{PF}_6]_3$ results from the reaction of (4) with Copper(I). Molecular models and ^1H NMR data suggest the structure shown in Figure 2, with each copper (I) ion in a distorted tetrahedral environment.

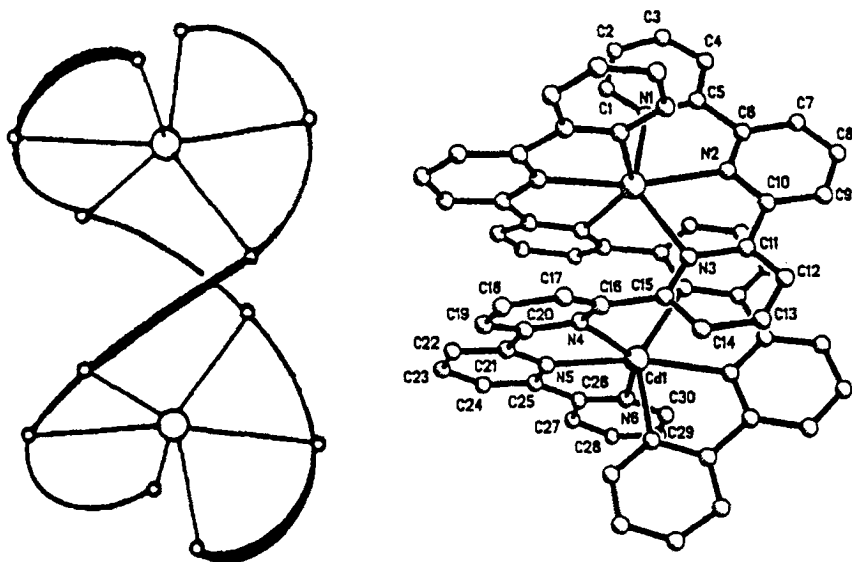
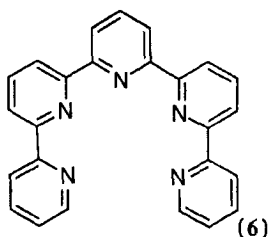


Figure 1 Structure of the double-helical complex formed between (4) and cadmium(II). Reproduced by permission from *J. Am. Chem. Soc.* **112**, 1256–1258 (1990)

The stoichiometry of the complex formed between silver(I) and (4) is the same as for the copper(I) complex, although the structures are unlikely to be identical. The silver(I) ion has a radius over 30% larger than copper(I), so one ligand must “slip” relative to the others to accommodate three silver(I) ions [17].

Most self-assembled helices have been constructed using only a single type of metal ion. Constable and Walker have designed a helix which contains two different metals using the quinquepyridine (qpy) (6) as the ligand. Two qpy ligands can provide only 10 metal-coordinating sites. Thus, in a double-helical structure one site will be appropriate for a six-coordinate metal with pseudooctahedral geometry and the other for a four-coordinate metal with pseudotetrahedral geometry. When methanolic or ethanolic solutions of $[\text{Co}(\text{6})(\text{MeCN})_2]^{2+}$ were treated with Cu^+ or Ag^+ , complexes $[\text{CoAg}(\text{6})_2]^{3+}$ and $[\text{CoCu}(\text{6})_2]^{3+}$ were formed. Cyclic voltammetry, fast-atom bombardment mass spectrometry (FABMS) and ^1H NMR all gave data consistent with the formation of a heterobinuclear double-helical complex [18].



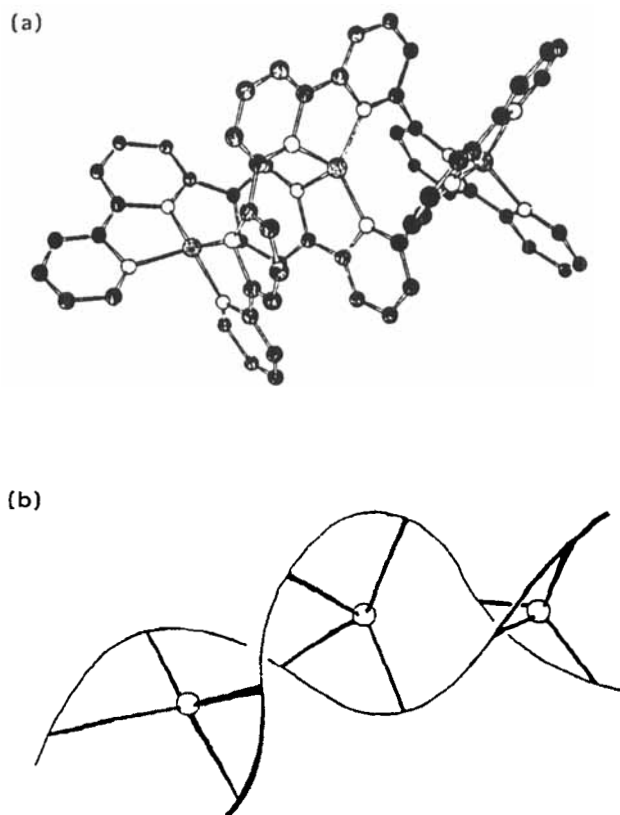
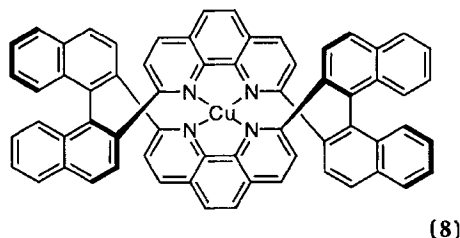
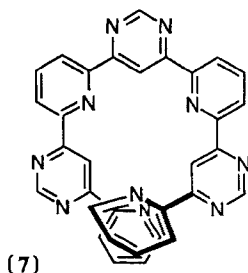
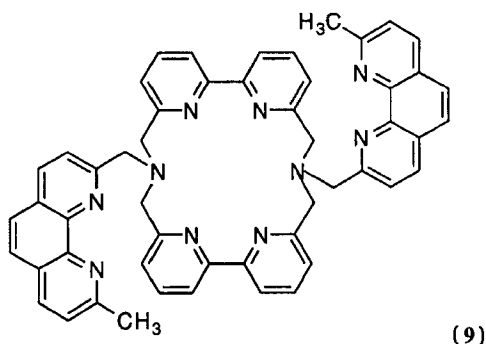


Figure 2 Proposed structure (a) for the cation $[\text{Cu}_3(\mathbf{4})_2]^{3+}$ together with a schematic representation (b). Reproduced by permission of the Royal Society of Chemistry

The propensity for double-helix formation in these complexes is so strong that the metals can be used to template the synthesis of the oligopyridine ligands [19]. The combination of one sexipyridine ligand (**4**) and nickel(II) templates the coupling of two terpyridines. Demetalating the complex using aqueous KCN gives (**4**) in an overall yield of 50%, much improved over the nontemplated method. Lehn and coworkers have recently shown that incorporation of alternating pyridine–pyrimidine groups into a ligand, such as (**7**), leads to electrostatic repulsion of the nitrogen atoms and significant stabilization of a helical structure, even in the absence of metal ions [20]. The helical environment for metal coordination can also be imposed by covalent connections, as Cram and coworkers have shown in the combination of phenanthroline and binaphthyl subunits in (**8**) [21].



All of the helices we have seen to this point have been constructed using ligands which have two or more identical metal-binding sites connected by spacers. A self-assembling double helix has been designed around a ligand (9) which contains two distinct transition metal-binding sites. This ligand can coordinate one metal ion in the central pyridine-based macrocycle, and two more metal ions with its phenanthroline sidearms. The metal ions complexed by the sidearms are then free to complex with another ligand and form a double helix. Reaction of (9) with excess copper(I) gave a helicate structure in the solid state, as shown in Figure 3. Each copper(I) ion is in a distorted tetrahedral environment, and the overall symmetry is C_2 . The structure persisted in solution according to ^1H and ^{13}C NMR, FABMS and ultraviolet (UV)-visible spectroscopy. The ^1H NMR titration data show that the helix is the only species present, indicating positive cooperativity for the helicate formation. A similar helicate was confirmed in solution for the product of ligand (9) and excess silver(I) ion [22].



Lehn and coworkers have designed many double-helical compounds. Copper(I), cobalt(II) and iron(II) were allowed to complex with the ethylene-bridged bis(bipyridine) (10) and bis(phenanthroline) (11) to examine the stereochemical preferences of the metal ions. When ligand (10) was treated with copper(I), a complex of 2:2 stoichiometry (molecular weight confirmed by

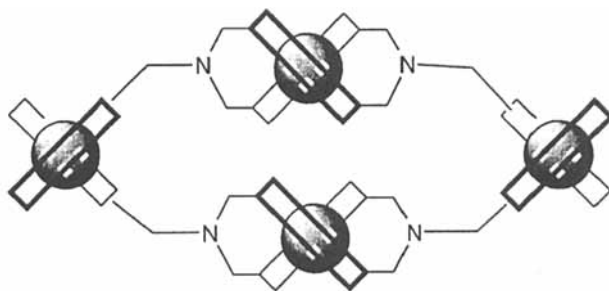
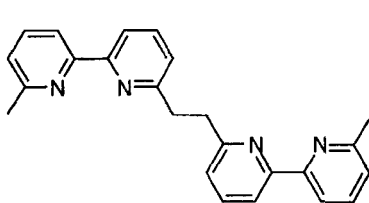
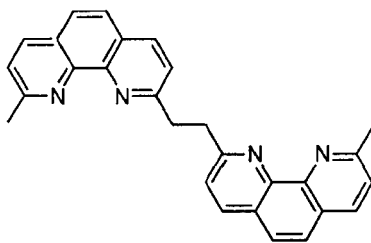


Figure 3 Schematic structure of the helical aggregate between (9) and Copper(I)

FABMS) with a double-helical conformation was formed (Figure 4). Each copper atom possesses a distorted tetrahedral geometry, and the complex was shown to persist in solution by ^1H NMR and cyclic voltammetry. In contrast, when ligand (11) was treated with cobalt(II), a 1:1 complex was formed. The crystal structure reveals that the aggregate is not a double helix, and the cobalt possesses a distorted octahedral geometry [23].



(10)



(11)

This metal–bipyridine motif was used to design a self-assembling chiral helix. The strategy was to incorporate stereogenic centers directly on the backbone of the ligand. Ligands (12a) and (12b) were synthesized and allowed to react with copper(I) and silver(I). FABMS and UV–visible spectra showed that both copper(I) and silver(I) formed 2:3 ligand:metal complexes with both ligands. Achiral (12b) gave, as expected, a racemic mixture of right-handed and left-

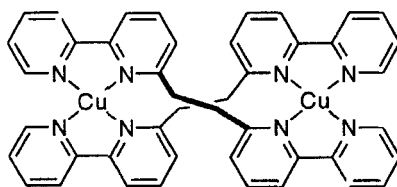
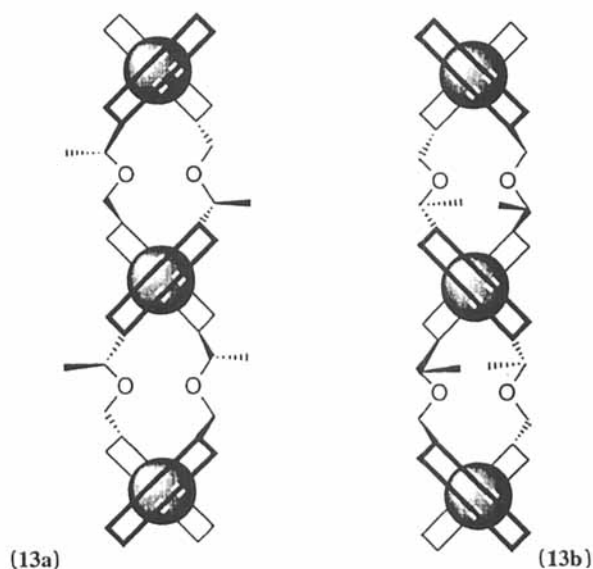
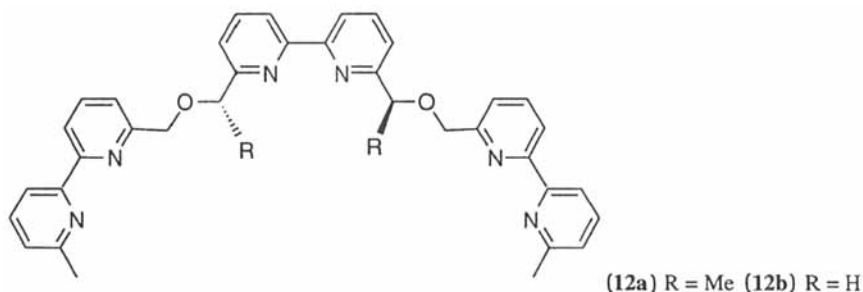


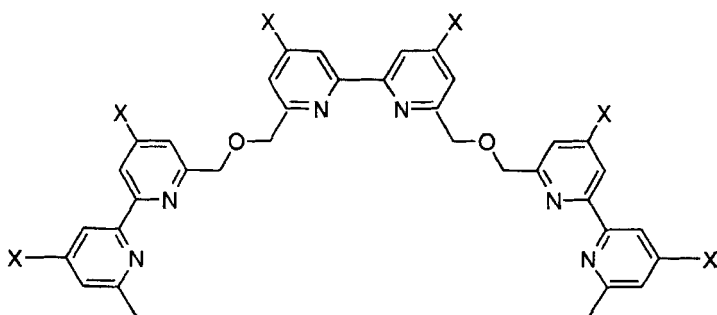
Figure 4 Representation of the structure of $[\text{Cu}_2(\text{10})_2]^{2+}$

handed helices. However, chiral (**12a**) would be expected to lead to preferential formation of one diastereomeric helix. The circular dichroism (CD) spectrum of $[\text{Cu}_3(\textbf{12a})_2]^{3+}$ displays a strong, positive Cotton effect. This, along with the ^1H NMR data, points to a very high helical induction (95%). Consideration of space-filling and preliminary molecular mechanics calculations suggested that the complexes take the conformation of a right-handed helix as in (**13a**) rather than the left-handed diastereomer (**13b**) [24].

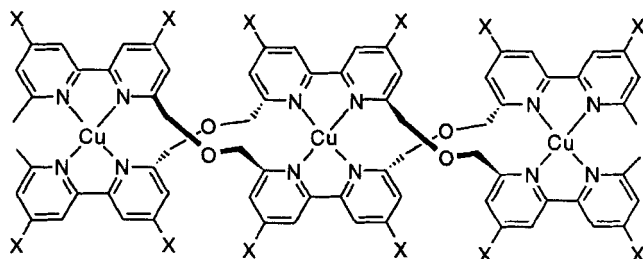


Related double-helical metal complexes have been used to investigate the role of cooperativity in self-assembly. Ligands (**14a**) and (**14b**) were allowed to react with CuBF_4 to form the corresponding helicates (**15a**) and (**15b**). The formation of helicates (**15a**) and (**15b**) was confirmed in solution by spectrophotometric titration. Two sharp isosbestic points are seen in the spectrum, and the excess absorbance diagram is linear even at a very low

ligand-to-metal ratio, indicating the clean generation of a single species. A Scatchard analysis of this complexation showed the concave downward shape characteristic of a system which displays positive cooperativity. Also, a Hill plot gave a maximum slope of 1.75, which, being greater than unity, provides evidence for positive cooperativity [25]. The approximate values $\Delta H^\circ = -168 \pm 10 \text{ kJ mol}^{-1}$ and $\Delta S^\circ = -218 \pm 30 \text{ J K}^{-1} \text{ mol}^{-1}$ indicate that the helicate formation reaction $3\text{M} + 2\text{L} \rightarrow \text{M}_3\text{L}_2$ displays a large negative entropy. This is presumably owing to the formation of one aggregate from five separate components.



(14a) X = CO₂Et (14b) X = H

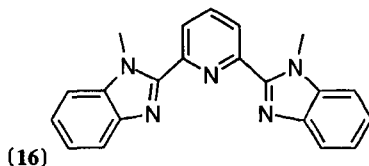


(15a) X = CO₂Et (15b) X = H

It would be expected that if several different ligands and two different metal ions were all present in solution, the resulting aggregates would contain many different coordination products. Lehn and coworkers have designed self-assembling systems which do not give a mixture of products, but rather only a few well-defined aggregates. These systems show self-discrimination or nonself-discrimination, and exhibit the phenomenon of error checking. Reaction of copper(I) with a solution of several ligands containing different numbers of bipyridine units gave only matched helicates with ligands of the same length. No mixed ligand species were present. Self-recognition can occur even if several different metal ions are present. A mixture of copper(I) (which shows a preference for pseudotetrahedral geometry) and nickel(II) (which shows a

preference for pseudooctahedral geometry) results exclusively in the formation of a copper(I)-based double helix and a nickel(II)-based triple helix with oligobipyridine ligands [13].

The conformations of helices formed between metals and ligands are dictated by the stereochemical preferences of the metal ions. However, structural features of the ligand, such as the ability to position aromatic rings in a π -stacking arrangement, can promote the formation of helices. The relative importance of these factors was examined by Williams and coworkers by investigating complex formation with a range of different ligands [11]. Copper(I) forms a binuclear double helix with ligand (16) as shown in Figure 5. The bridging pyridine places the copper(I) ions in a distorted tetrahedral environment. Removal of the bridging nitrogen should therefore destroy the helicity of the complexes. Stacking interactions can be seen between the benzimidazole moieties. Replacement of the bridging pyridine with a nonaromatic bridge should reveal the importance of these stacking interactions.



The ligands exist in two different conformations: *cis,cis*, as in (16), and *trans,trans*, as in the phenyl analogue (17). The *cis,cis*-ligand should promote the formation of a helix, while the *trans,trans*-ligand will not. In its complex with copper(I), (16) has taken the *cis,cis*-conformation. In contrast, the copper(I) complex with (17) does not form a helical structure. The structure of the complex $[\text{Cu}_2(17)_2]^{2+}$ is shown in Figure 6. Stacking interactions are present in this structure between the two bridging benzene rings. It is notable that the Cu–N bond distance is almost identical to that in $[\text{Cu}_2(16)_2]^{2+}$. Examination of molecular models of these two compounds reveals that they may be interconverted merely by rotating the Cu–N and benzimidazole–

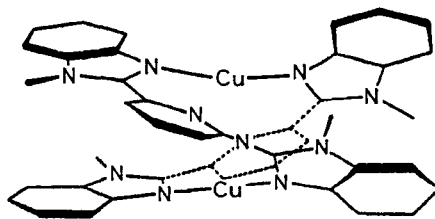
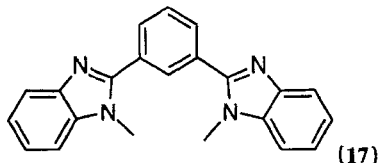


Figure 5 Representation of the structure of $[\text{Cu}_2(16)_2]^{2+}$. Reproduced by permission from *J. Am. Chem. Soc.* **114**, 4230–4237 (1992)

pyridine or benzimidazole–benzene bonds. These two structures may be regarded as pseudostereoconformers of one another. The complex $[\text{Cu}_2(\mathbf{17})_2]^{2+}$ persists in solution in polar aprotic solvents, as evidenced by data from cyclic voltammetry, UV–visible spectroscopy and ^1H NMR spectroscopy.



The complex between (18) and copper(I) is revealing in determining which factors encourage double-helix formation. The complex has 1:1 stoichiometry with T-shaped coordination of the copper, even though a double-helical conformation is also possible. The benzimidazole–benzimidazole stacking interactions and bridging groups do not seem in themselves to be sufficient to cause formation of a helical structure. Williams and coworkers suggest that $[\text{Cu}_2(\mathbf{16})_2]^{2+}$ undergoes double-helix formation because the mononuclear complex is unstable. The geometry of copper(I) would not favor a mononuclear complex because the bite angle α , estimated to be in the range $200\text{--}206^\circ$, would be too large a distortion of the ideal geometry of 120° (Figure 7). In contrast, ligand (19) forms the three-coordinate complex $[\text{Cu}(\mathbf{19})(\text{MeCN})]^+$ with approximately trigonal coordination of the copper. The extended Hückel molecular orbital (EHMO) method can also be applied to this system, and shows poor orbital overlap as the angle α increases from 120° to 180° to 200° . These studies support the idea that although the presence of bridging groups and stacking interactions may enhance the stability of metal–ligand helices, the coordination preference of the metal is a greater factor in the determination of the structure [11].

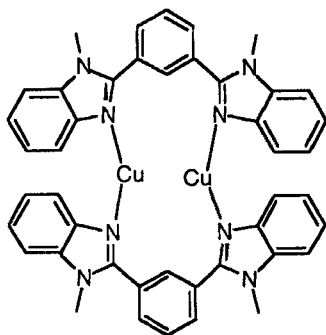


Figure 6 Representation of the structure of $[\text{Cu}_2(\mathbf{17})_2]^{2+}$

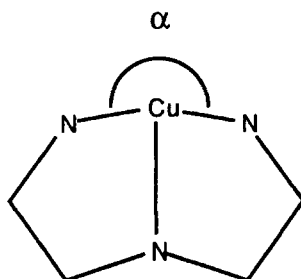
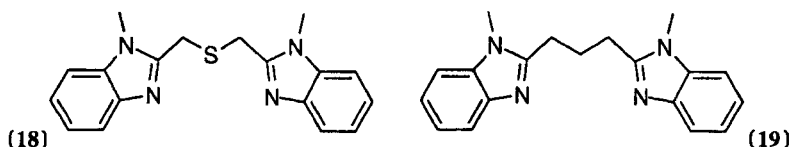
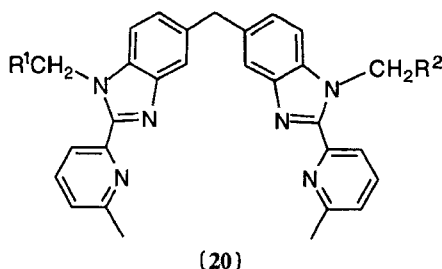


Figure 7 Bite angle involved in the formation of tridentate copper(I) complexes



The effect of metal ion stereochemical preference in mediating the final structure of a self-assembling helix was examined by Williams and coworkers using the ligand **(20)** [26]. The formation of a double-helical structure is seen from the reaction of two equivalents of copper(I) and two equivalents of **(20)** (Figure 8). This structure, with pseudotetrahedral geometry around the metal centers, was found to exist in solution by UV-visible spectroscopy, ^1H NMR and cyclic voltammetry. The double helix does not appear to be the only species existing in solution: mononuclear $[\text{Cu}(\text{20})_2]^+$ was observed by ^1H NMR spectroscopy. The ^1H NMR spectrum of the complex between copper(I) and **(20)** suggests that at room temperature, there may be a rapid equilibrium between the mononuclear complex and the binuclear complex.



In contrast, cobalt(II) and **(20)** (Figure 9) led to the formation of a triple-helical complex with pseudooctahedral geometry around the metal centers. The

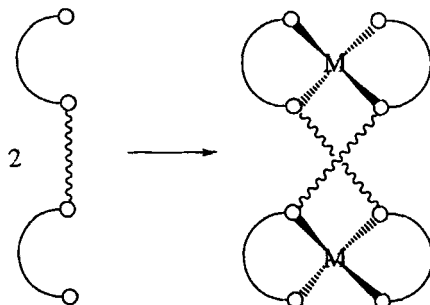


Figure 8 Schematic structure of the double-helical complex formed from (20) and copper(I)

triple helix was observed in the crystal structure, and also confirmed in solution with UV-visible spectroscopy, ^1H NMR, ^{13}C NMR and cyclic voltammetry. This triple-helical structure was the sole species found, suggesting that cooperativity is present with the first cobalt(II) creating a favorable coordination environment for the second. The double-helical species $[\text{Co}_2(\mathbf{20})_2]^{4+}$ might be expected to form because the cobalt octahedral-tetrahedral transition shows the smallest loss of ligand field stabilization energy. No stacking interactions were observed in the triple-helical complex, and molecular models suggest that stacking interactions are also absent from the double helix. This implies that the self-assembly is directed by the stereochemical preferences of the metal ions and not by interligand interactions. A related triple helix was also seen in the complex of (20) and cobalt(III) [27].

The behavior of zinc(II) is more complicated since it is known to be able to accommodate either a pseudotetrahedral or a pseudooctahedral geometry.

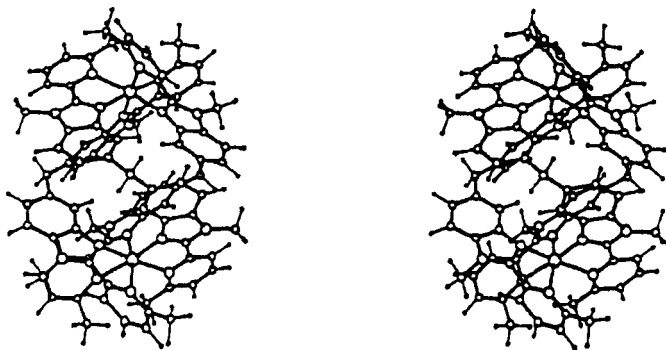


Figure 9 Stereoview of the triple-helical complex $[\text{Co}_2(\mathbf{20})_3]^{4+}$. Reproduced by permission of the Royal Society of Chemistry

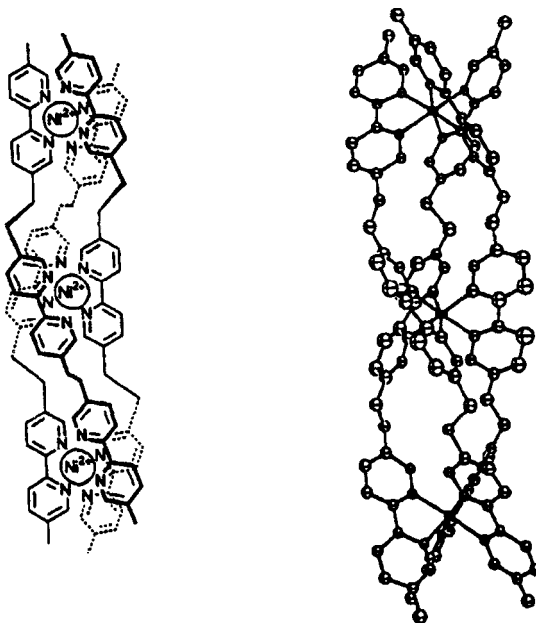


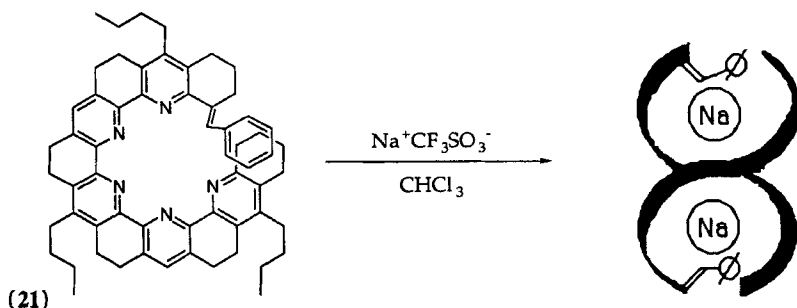
Figure 10 Representations of the crystal structure of a self-assembled trinuclear triple helix. Reproduced by permission of Angewandte Chemie

UV-visible spectroscopic analysis of the reaction between zinc(II) and (20) shows one complex whose stoichiometry suggests a double-helical structure and one complex whose stoichiometry suggests a triple-helical structure. The complex $[\text{Zn}_3(\text{20})_2]^{2+}$ is also observed in the analysis, and may have a structure which has a tetrahedral Zn^{2+} bridging two $[\text{Zn}(\text{20})]^{2+}$ units [26].

A related triple-helical structure has been characterized by Lehn and coworkers based on the templating effects of three Ni^{2+} ions. A tris(bipyridine) ligand related to (14b) was prepared, with in this case an ethylene spacer linked through the 5-positions of the pyridine rings. The crystal structure of this triple helix is shown in Figure 10, and confirms that no π -stacking interactions are present. The molecule does not display the regular triple-helical symmetry of D_3 , but rather has a C_2 axis perpendicular to the Ni–Ni–Ni axis, crossing through the middle of the central C–C bond of the central bipyridine unit of one strand. This symmetry suggests that the helix is chiral, with two enantiomers possible. Crystals of the complex were studied by CD, though the optical purity of the helix has not been determined [28]. Potts *et al.* have prepared a tricopper(I) triple helix based on a terpyridine ligand with ethynyl group spacers between each pyridine [29].

A helix has been designed which does not involve a transition metal, but rather the alkali metal sodium ion. Because the interaction of Na^+ with

organic ligands is weak and nondirectional, the formation of the helix is controlled by preorganizing the ligand. Ligand (**21**) is an example of a heterohelicene that is less flexible than oligopyridines, and is preorganized into a helical shape by the ethylene bridges. In solution, (**21**) exists as a racemic mixture of left- and right-handed isomers. The interconversion between the two enantiomers occurs at a rate of $>100\text{ s}^{-1}$.

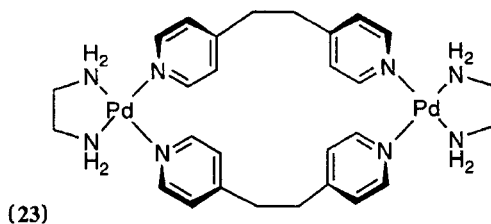
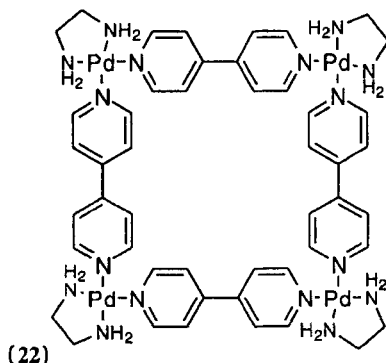


When sodium triflate (NaOTf) is introduced into a solution of ligand (**21**), the double helix $[\text{Na}_2(\text{21})_2][\text{OTf}]_2$ is formed. The species $[\text{Na}(\text{21})][\text{OTf}]$ is also detected, but equilibrates to form $[\text{Na}_2(\text{21})][\text{OTf}]_2$ if allowed to stand in the dark. The stoichiometry of the complex was confirmed by mass spectrometry (MS). Diastereotopic CH_2 protons are seen in the ^1H NMR spectrum of the complex as interconversion between left- and right-handed enantiomers is no longer rapid. Shielding effects are observed between benzylidene groups and the pyridine rings of the other ligand strand, showing that they lie above one another in the helical structures. This is an example of a metal–ligand aggregate whose assembly is dictated solely by the conformation of the ligand [30].

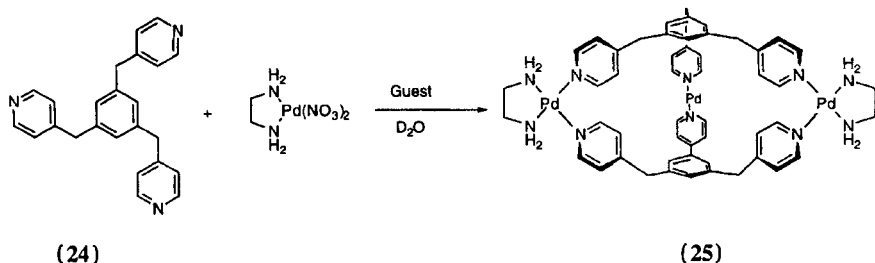
2.2 Self-Assembly of Box Structures

Metal ions that form four-coordinate, square planar complexes are inactive in the formation of helices, but show particular value as corner pieces in the construction of cubic or boxlike structures. Fujita *et al.* have elegantly shown that palladium(II) nitrate complexes react with 4,4'-bipyridines to form 4+4 complexes like (**22**) [31]. The bipyridines function as the sides and the palladium(II) ions as the corners of a square macrocycle. ^1H NMR analysis shows this complex to be the thermodynamically stable product of the reaction with slow exchange between (**22**) and smaller fragments. Moreover, the central cavity in (**22**) is of sufficient size to encapsulate aromatic guests. Addition of 1,3,5-trimethoxybenzene to an aqueous solution of (**22**) leads to upfield shifts of the guest resonances and the measurement of a K_a of 750 M^{-1} . By changing the size of the pyridine component (to diazapyrene and diazaperylene), Stang *et al.* have shown that palladium-based boxes of much

larger size can be prepared [32]. Use of 1,2-bis(4-pyridyl)ethane in place of 4,4'-bipyridine leads to the 2:2 complex (23) with a differently shaped cavity [33]. The size and recognition characteristics of the macrocycle could be changed by varying the spacer between the pyridine rings.

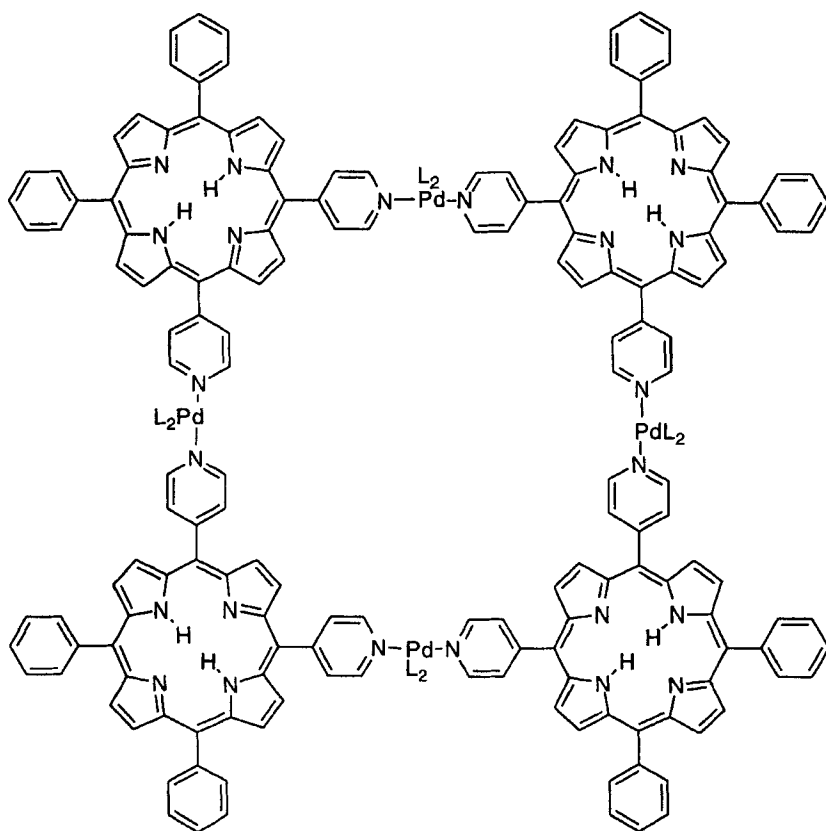


A further refinement of this strategy has recently been shown by the self-assembly of the cage complex (25) formed from the reaction of three palladium(II) ions with 1,3,5-tris(4-pyridylmethyl)benzene (24) [34]. A key feature of this process is the critical role played by aromatic guests (such as 4-methoxyphenylacetic acid) in templating the formation of (25). In the absence of guest, only ill-defined, oligomeric metal complexes are formed.



In an extension of this basic approach, Stang and Zhdankin have prepared molecular boxes with four iodonium ions as corners and four biphenyl groups as sides in a structure directly analogous to (22) [35].

Drain and Lehn have further extended the metal-templated box strategy with the synthesis of 5,10-bis(4-pyridyl)-15,20-diphenylporphine. In the presence of palladium(II) or platinum(II) this self-assembles into the 4:4 complex (26) with four porphyrins occupying the four walls of the box [36].

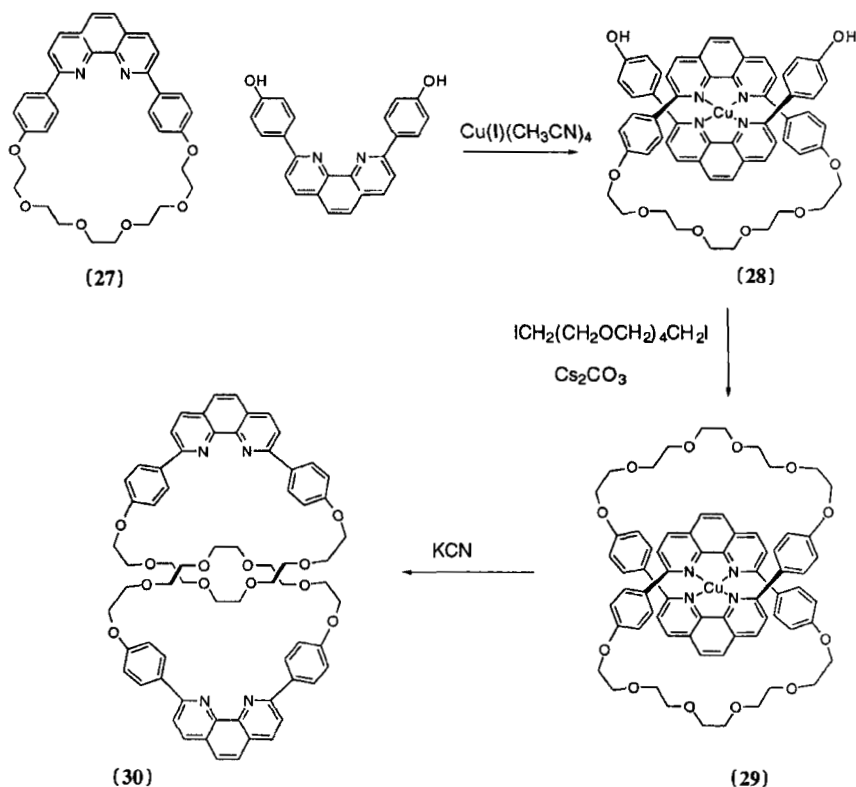


(26)

2.3 Self-Assembly of Catenanes

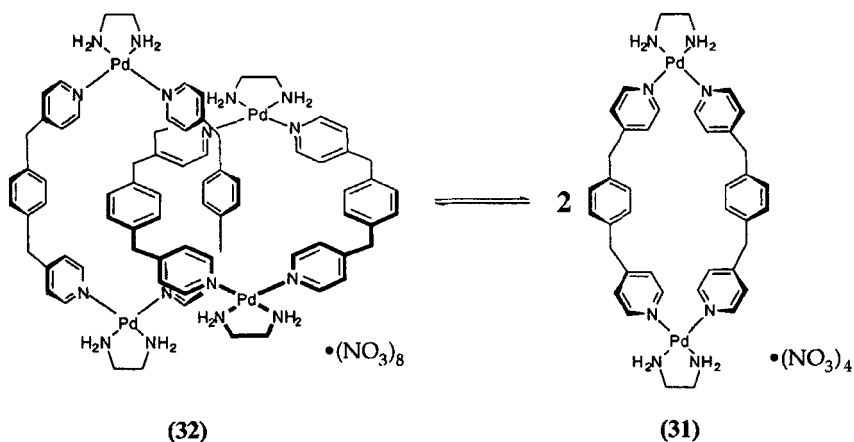
In a seminal series of papers, Sauvage and coworkers have demonstrated the use of transition metals in templating the formation of catenated structures [37]. This area has been extensively reviewed [38–40] and will only be covered briefly here. The central strategy has been to use the perpendicular positioning

of two phenanthroline ligands around a copper(I) center effectively to thread one strand of a macrocycle through a second. Reaction of macrocycle (27) and 2,9-bis(4-hydroxyphenyl)phenanthroline with copper(I) salt leads to the threaded tetrahedral complex (28), which has the two phenolic hydroxy groups positioned above and below the plane of the other phenanthroline ring. These can be linked via a Williamson ether synthesis using the appropriate diiodide. The result is the catenated structure (29) templated around the copper(I) center. Treatment of templated (29) with KCN leads to the metal-free catenand structure (30) containing interlocked macrocyclic rings. This unusual, linked bis(phenanthroline) ligand can be used to bind other transition metals and stabilize normally reactive oxidation states, such as nickel(I) [41]. This strategy has recently been extended to the formation of more complex catenated structures, including a [3]catenane containing two smaller rings threaded onto a larger macrocycle [42].



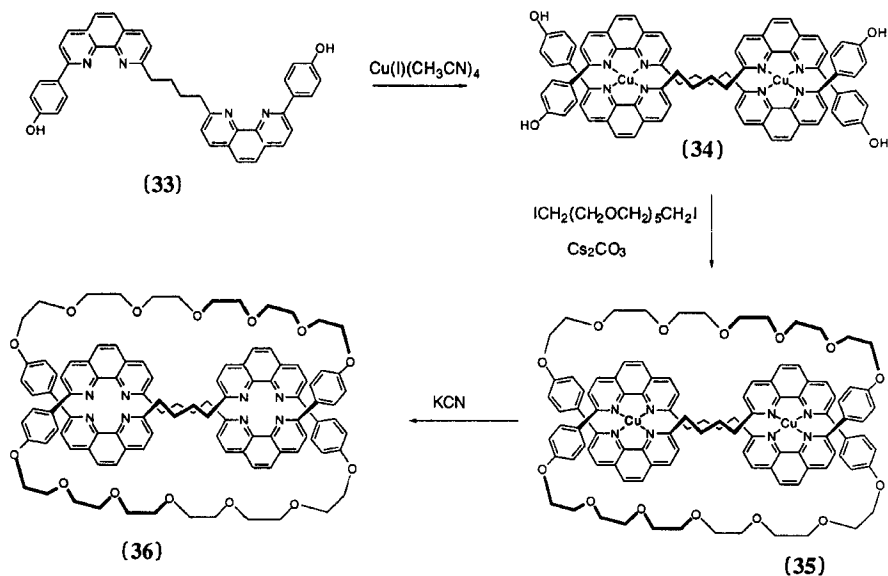
The metal coordination strategy of Fujita has been used to design a [2]catenane whose behavior is remarkably like that of “magic rings” – able to

link and unlink depending on solution conditions. The single ring (31) was self-assembled via coordination with two palladium(II) ions, as seen above with (23). At low concentrations (< 50 mM in D_2O), the major species in solution is the single ring. When the concentration is increased above 50 mM, more than 90% of the species in solution exist as the [2]catenane (32), as confirmed by 1H NMR, FABMS and electrospray mass spectrometry (EMS). The equilibrium could also be controlled by varying the solvent. More polar solvents promoted the formation of the [2]catenane and the ratio of [2]catenane to single ring could be varied between 99:1 and 1:99. The linking and unlinking of the rings are caused by the breaking and reforming of the palladium–nitrogen coordination, an interaction which is known to be reversible. When platinum is substituted for palladium, this behavior is not observed because platinum coordinates with pyridine irreversibly [43].



2.4 Template Formation of Knotted Structures

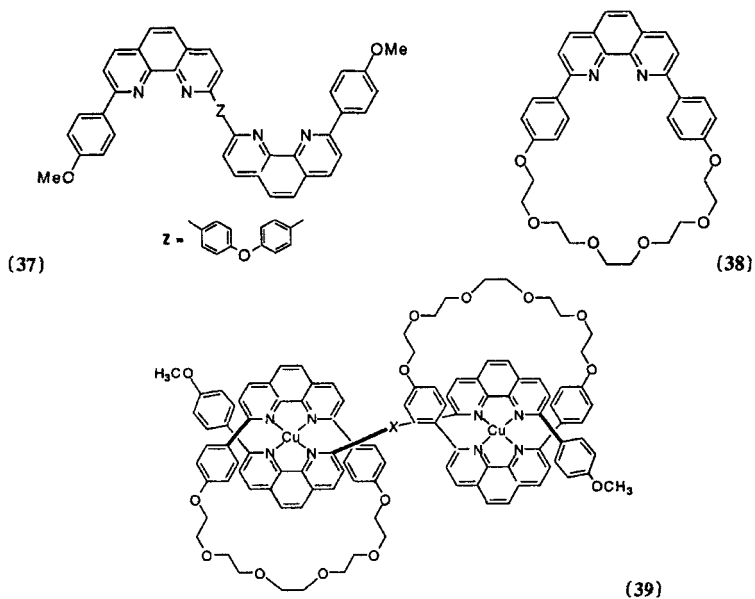
Several molecular knots have been designed which use metal–ligand coordination to hold the two ends of the knot in place so that they can be “tied” together [44]. Linkage of two phenanthroline units through oligomethylene, as in (33), or *p*-xylyl spacers leads to the formation of double-helical bis(metal) complexes of type (34). Connection of the four hydroxy groups in the correct combination through oligoethyleneoxy linkers gives the templated knot complex (35) which can be demetalated using KCN to the molecular knot (36). The structures of the knotted molecules were confirmed by 1H NMR and X-ray crystallography [45].



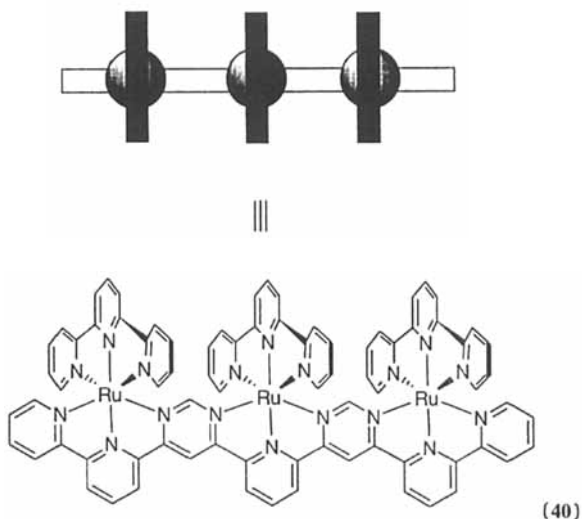
This strategy has been further extended to the synthesis of a triply twisted tris[bis(phenanthroline)copper(I)] complex analogous to (35) which, after correct linking of the termini and demetalation, leads to a doubly interlocked catenane structure [46].

2.5 Metal-Templated Formation of Rotaxanes and Other Rack or Grid Structures

Metal coordination has been used to design rotaxane structures in which macrocycles are threaded onto linear molecular strands [47]. The “thread” and “bead” are organic ligands held together by coordination to the copper(I) ion. The ligand (37) was used as a simple thread with two potential coordination sites. The “bead” was the macrocycle (38), large enough to slip over the thread. Addition of a copper(I) salt leads to the formation of the double-threaded complex (39). The tris(phenanthroline) thread homologous to (37) does not form a tris(rotaxane)analogous to (39). Instead, one copper coordinates with two sites on the thread, and the other copper coordinates with the remaining coordination site on the thread and one macrocyclic bead.



In a related strategy, Lehn and coworkers have prepared more rigid two-metal-binding and three-metal-binding ligands based on fused terpyridine derivatives, and have shown that these organize two or three terpyridine metal complexes in a rack-type arrangement, as in (40). The structures were supported by ^1H and ^{13}C NMR spectroscopy, and a crystal structure for the diruthenium system was obtained [48].



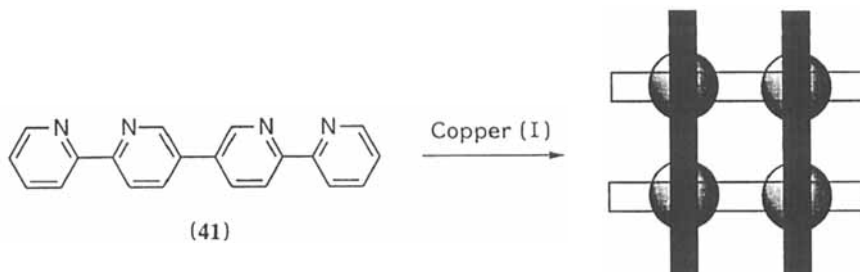


Figure 11 Formation of gridlike complexes from the self-assembly of (41) and copper(I)

The ability of copper(I) to form pseudotetrahedral coordination complexes with bipyridine units has recently been used to design several unusual complexes. When $[\text{Cu}(\text{OTf})_2 \cdot \text{C}_6\text{H}_6]$ is allowed to complex with the ligand 3,6-bis(2'-pyridyl)pyridazine (41) in a methanolic solution, an aggregate composed of four ligands and four metal ions results. The crystal structure of the aggregate shows a gridlike arrangement (Figure 11) with the copper atoms exhibiting a distorted tetrahedral geometry and π -stacking interactions between the parallel pairs of (41). These stacking interactions may be responsible for the nonideal geometry of the copper atoms. The persistence of the tetracopper complex in solution was confirmed using ^1H and ^{13}C NMR, infrared (IR) spectroscopy and cyclic voltammetry, and its self-assembly was shown to be cooperative. In acetone, a dark-green precipitate of $[\text{Cu}(\text{41})_2(\text{OTf})]$ was formed which dissolved in CD_3CN immediately to give the tetrakis(metal) complex. This suggests that the formation of the aggregate is under thermodynamic control, and the assembly of complexes such as $[\text{Cu}(\text{41})_2(\text{OTf})]$ is possible if they can form rapidly and reversibly [49].

The approach could be further extended to grid-type structures containing six triply chelating ligands (42), organizing nine metal ions into a self-assembled structure composed of 15 subunits [50]. Treatment of (42) with silver triflate led to the formation of a 3×3 grid of the chelating units stabilized by the tetrahedral geometry preference of nine silver(I) ions, as shown schematically in Figure 12.

A three-dimensional example of this type of supramolecular control has been reported by Lehn and coworkers based on the hexaphenylhexaazatriphenylene unit (43). When two equivalents of (43) were combined with three equivalents of dimethyl-(41) and six equivalents of copper(I), the result was a barrel-shaped aggregate, shown in Figure 13, composed of 11 subunits [51]. Data from ^1H NMR, ^{13}C NMR and FABMS were used to confirm the existence of the complexes in solution. The hexakis(metal) complex is actually more stable than the corresponding tris(metal) system, formed from bipyridine, (43) and

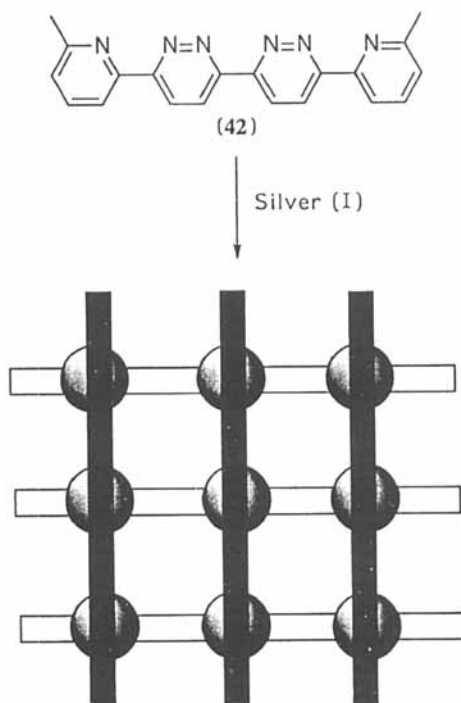


Figure 12 Formation of gridlike complexes from the self-assembly of (42) and silver(I)

copper(I). After repeated recrystallizations, the smaller complex began to decompose, whereas the larger was quite stable. Lehn and coworkers have further carried out an analysis of the usefulness of EMS in analyzing these types of complexes [52].

3. METAL TEMPLATE FORMATION OF FUNCTIONAL AGGREGATES

This section describes several examples of aggregated structures that have been designed with a particular purpose in mind. In each case the “cement” which holds these aggregates together is the metal–ligand interaction.

3.1 Photoactive Multimetal Systems

A large number of synthetic multimetal complexes have been prepared as potential photoinduced electron-transfer systems [53]. In these designs the metal complexes can act both as structural templates and as photoactive units in their own right.

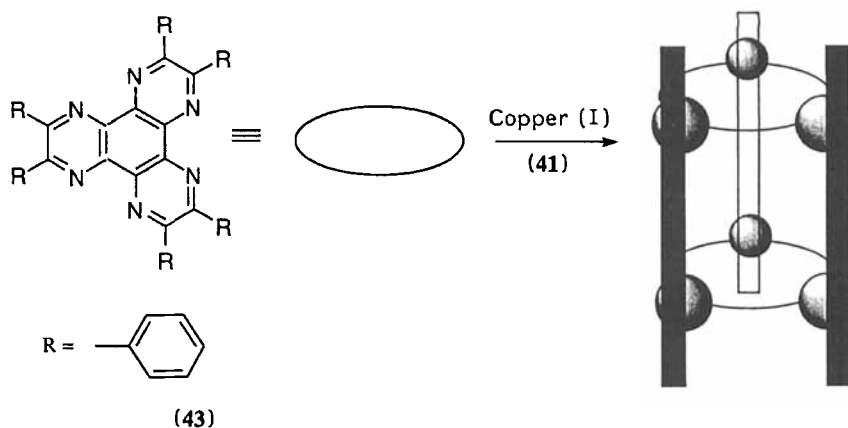
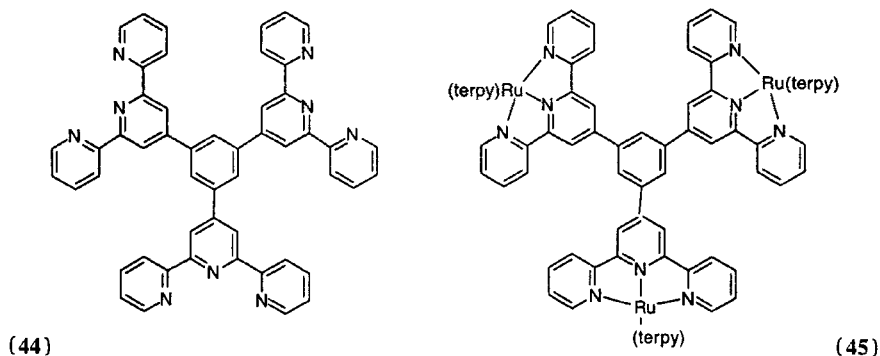


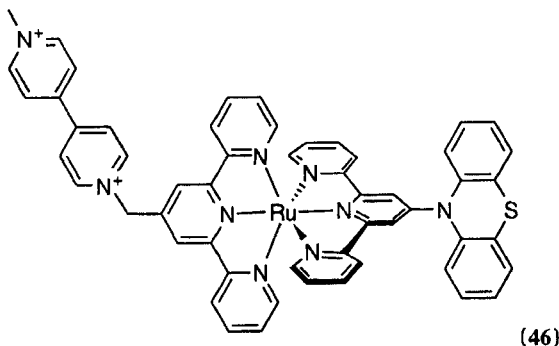
Figure 13 Formation of a barrel-shaped aggregate from the self-assembly of (41), (43) and copper(I)

Several self-assembling systems based on substituted terpyridine derivatives have been designed. For example, Constable and Cargill Thompson have prepared the triply-chelating ligand 1,3,5-tris[4'-(2,2':6',2''-terpyridyl)]benzene (ttpy) (**44**) [54]. Reaction with $[\text{Ru}(\text{terpy})\text{Cl}_3]$ in methanol gave the triruthenium complex (**45**) with three photoactive metal centers held at a fixed distance around the central benzene ring. This strategy has been further exploited in the design of both linear and three-dimensional multimetal complexes [55]. Replacement of terpy in (**45**) by (**44**) or another ligand could lead to a branch point for the assembly of starburstlike coordination oligomers.



In a related strategy, Sauvage *et al.* have used a bis(terpyridine) complex both as a photoactive center and as a means for separating, on a rigid template, electron-donor and electron acceptor sites [56]. For example, reaction of a

phenothiazine-linked terpyridine with RuCl_3 followed by a viologen-linked terpyridine leads to the three-component redox system (46) containing a photoactive metal center flanked by electron-donor and electron-acceptor groups. Detailed photophysical studies on these and other related systems showed strong electronic coupling between the redox centers.



Using a combination of 2,2'-bipyridine and 2,3-bis(2-pyridyl)pyrazine as the chelating units, Balzani and coworkers [57] and Campagna *et al.* [58] have reported the preparation of a number of multimetal complexes with interesting photophysical properties.

3.2 Metal-Templated Recognition Sites

Metal templates can be used in a simple way to bring together different substrate recognition sites. This is an attractive strategy as it allows the rapid construction of a large number of different artificial receptors. A family of subunits can be prepared containing a metal-binding (constant) domain and a substrate-binding (variable) domain (Figure 14). Addition of a templating metal ion to the subunits should have no effect on the substrate recognition site but instead should cause the recruitment of two (or more) metal-chelating (constant) regions. This will lead to the formation of a well-defined substrate-binding region.

We have established the concept of metal-templated receptors by using phenanthroline derivatives in the constant metal-binding region. The synthesis of phenanthrolines (47) substituted by an acylaminopyridine recognition site is shown in Figure 15. Addition of $[\text{Cu}(\text{MeCN})_4][\text{BF}_4]$ to a CH_2Cl_2 solution of (47) leads to chelation of two phenanthrolines and formation of a bis(acylaminopyridine) recognition site as in (48) [59]. A key feature of (48) is that the copper(I) ion does not interfere with the aminopyridine region but interacts preferentially with the stronger-chelating phenanthroline group, thus separating the template and binding functions. Dicarboxylic acids bind strongly to (48) in CDCl_3 (e.g. $K_a = 4.9 \times 10^4 \text{ M}^{-1}$ for glutaric acid). The ^1H

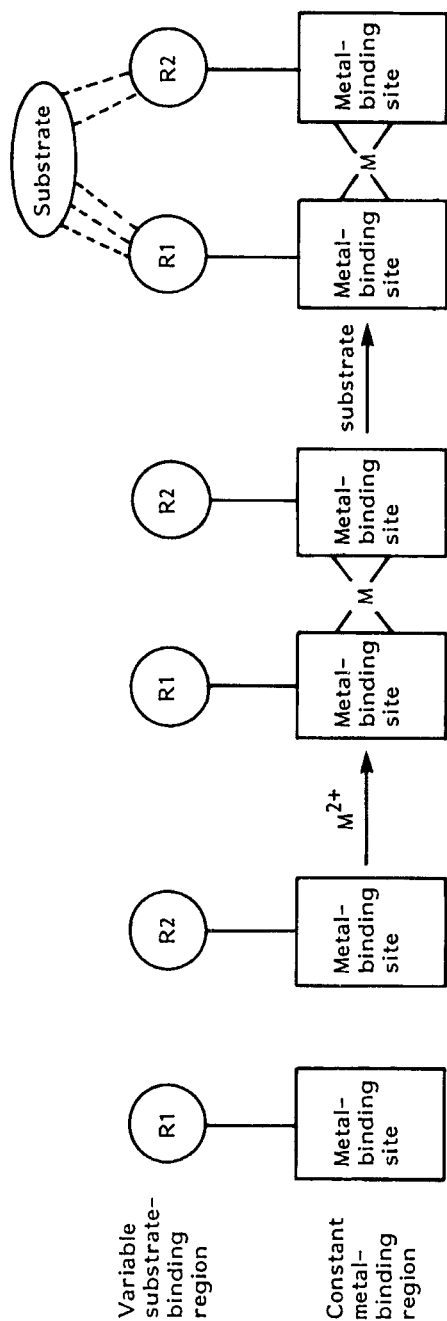


Figure 14 Schematic approach to metal-templated receptors

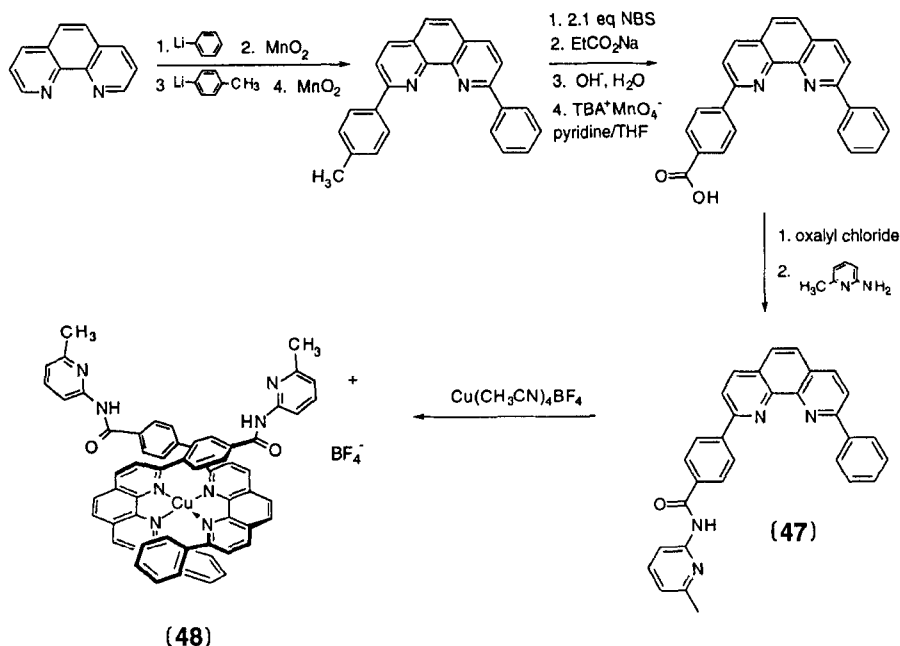
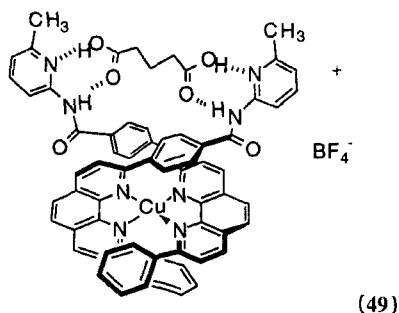


Figure 15 Synthesis of self-assembling receptors based on copper(I) complexes of phenanthroline

NMR changes (large downfield shift of NH resonances and shifts of the glutarate protons) are all consistent with a complex containing four hydrogen bonds as shown in (49). Related complexes with similar affinity are formed by bis(acylaminopyridine) derivatives linked through covalent spacers [60].



In the case of (48), the metal-templated self-assembly is crucial for substrate recognition, as the simple subunit (47) binds dicarboxylic acids only weakly in the absence of metal ions. Significantly, there is a slight color change (red-

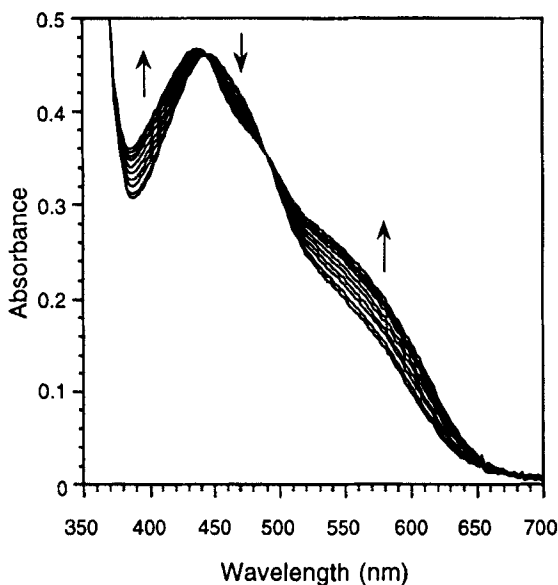
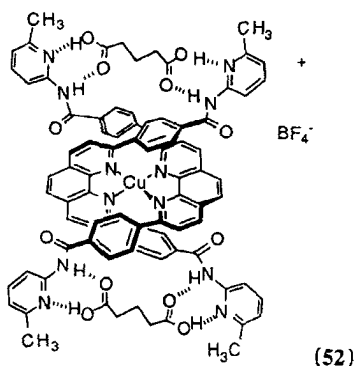
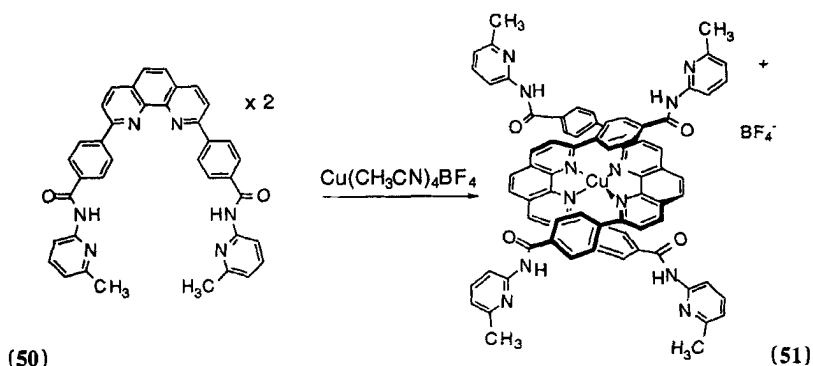


Figure 16 UV-visible spectra of (48)-glutaric acid

orange to orange-red) on diacid binding. The UV-visible changes for (48) on addition of glutaric acid (Figure 16) show a substantial increase of $\sim 30\%$ in the relative absorptivity at 550 nm and a blue shift in λ_{\max} of 9 nm. These changes are smaller for diacids that are less well bound (e.g. for pimelic acid, $K_a = 1.5 \times 10^4 \text{ M}^{-1}$, 15% change at 550 nm and $\Delta\lambda_{\max} = 5 \text{ nm}$), confirming that substrate selectivity follows spectroscopic changes. The key conclusion in this first self-assembled receptor is that the metal ion plays the role not only of template but also of a spectroscopic reporter group detecting substrate binding. Copper(I) complex (48) is a chiral receptor, reminiscent of other C_2 -symmetric receptors studied by ourselves [61] and others [62]. Addition of an optically pure dicarboxylic acid, such as *N*-Cbz-L-glutamic acid, to a racemic mixture of (48) leads to two diastereomeric complexes and a splitting of the receptor peaks into two distinct sets of signals.

In an attempt to amplify the spectroscopic changes that result on substrate binding with the single receptor (48), we have prepared the corresponding double receptor (51). Once again, this can be formed by the metal-templated self-assembly of two subunits (50). In this case, two potential recognition sites are present in the molecule and able to bind to two equivalents of a dicarboxylic acid as in (52). ^1H NMR analysis shows a very similar binding affinity for glutaric acid and other dicarboxylic acids as compared to (48). The most important difference, however, is that on addition of glutaric acid to a

CH_2Cl_2 solution of (51), a dramatic color change from orange to dark red takes place. In particular, a large increase ($> 100\%$) in the intensity of the shoulder at 550 nm takes place (Figure 17a). This is a much larger chromogenic effect than that seen with (48), but shows a similar dependence on the length of the diacid, with glutaric acid giving a greater change than longer diacids (Figure 17b). The origin of the chromogenic effect presumably derives from either a distortion of the coordination geometry around the copper(I) or a change in the conformation of the benzoylaminopyridyl sidearms [63].



There are two possible modes of glutaric acid binding to (51): interphenanthroline, as in (52), and intraphenanthroline (to give a catenated structure). Molecular modeling was used to address this question. The uncoordinated receptor (51) was minimized using the Amber force field within the MacroModel program and manually coordinated to a copper(I) ion, utilizing bond angles and lengths from the X-ray crystal structure of the similar bis(2,9-diphenyl-1,10-phenanthroline)copper(I) complex [64]. The model of the

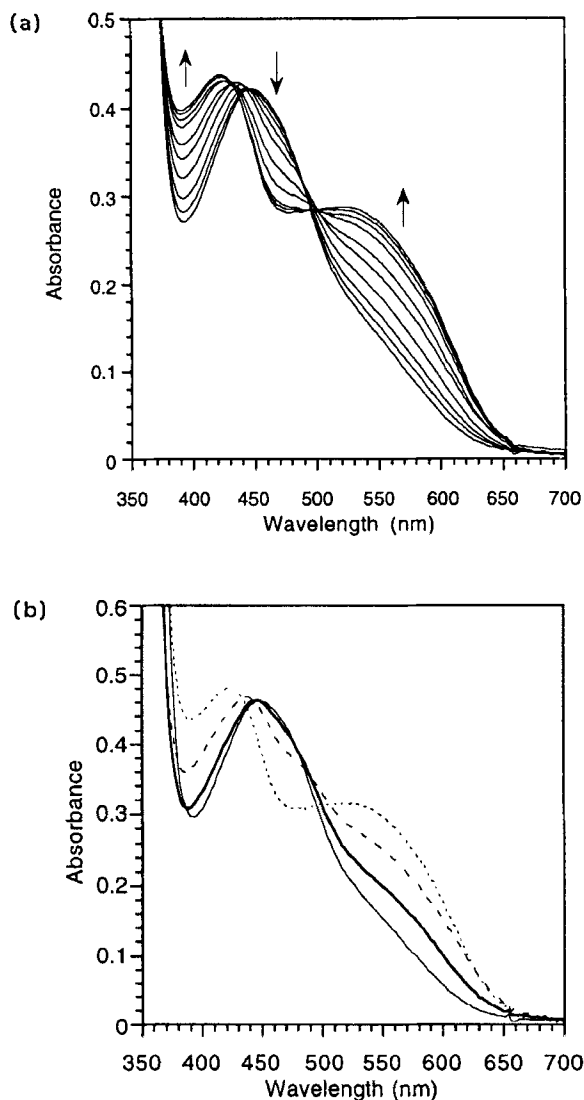


Figure 17 (a) UV-visible spectra for (51)-glutaric acid. (b) Comparison of the UV-visible spectral changes for (48) and (51), (—) [Cu(47)₂][BF₄]; (---) [Cu(47)₂][BF₄]-glutaric acid; (—) [Cu(50)₂][BF₄]; and (---) [Cu(50)₂][BF₄]-glutaric acid

receptor-substrate complex between [Cu(50)₂][BF₄] and two glutaric acids is shown in Figure 18(a). The acylaminopyridine binding sites in this structure are well oriented for forming strong hydrogen bonds to dicarboxylic acids. An alternative binding mode can be envisioned in which a single dicarboxylic acid

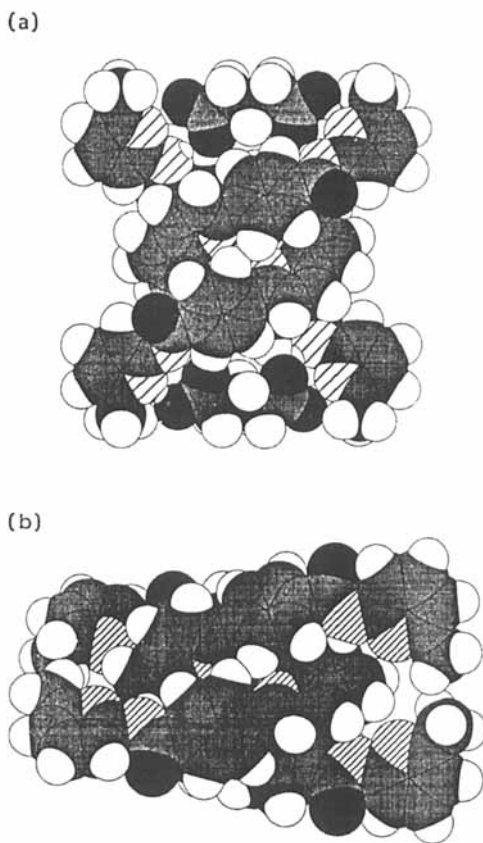


Figure 18 Glutaric acid complex in the productive conformation (a) and the unproductive conformation (b)

binds to two acylaminopyridines on the same ligand, resulting in an interlocking loop structure. Modeling suggests that this type of structure is unlikely (Figure 18b) since, when the acylaminopyridines are turned to face each other, the resulting binding site is both too small for glutaric acid and is blocked by the phenanthroline ring of the second ligand.

Copper(I) has drawbacks as a general metal template in this study. Most notably, it is limited to tetrahedral (T_d) or distorted tetrahedral (D_{2d}) geometry and shows relatively fast ligand exchange, which would complicate the study of templated receptors with two different substrate-binding regions. To overcome this problem we have prepared the first of a large family of tridentate chelating

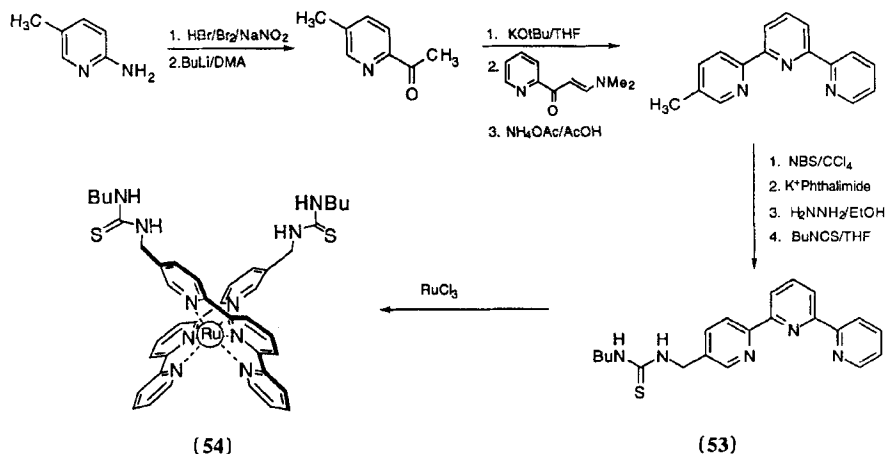
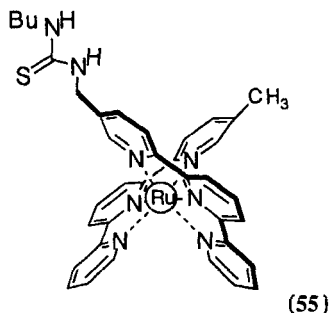


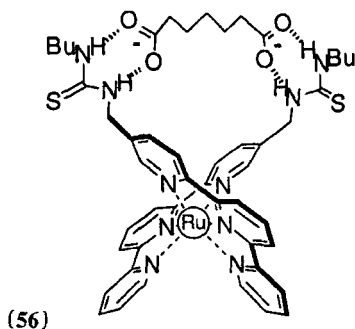
Figure 19 Synthesis of self-assembling receptors based on ruthenium(II) complexes of terpyridine

subunits that can bind to a wide range of first-row, second-row and third-row transition metals in an octahedral geometry. These consist of a terpyridine constant (metal-binding) domain linked to a variable thiourea (substrate-binding) domain.

The key terpyridine–thiourea subunit (53) was prepared easily by the route outlined in Figure 19. Reaction of (53) with half an equivalent of RuCl_3 led in quantitative yield to the bis(terpyridine)ruthenium(II) receptor (54) which contains two thiourea groups positioned across an octahedral metal complex. As in (48) and (51), the metal template reacts exclusively with the constant chelating region (phenanthroline or terpyridine) with no disruption of the variable (substrate-binding) region. By modifying the original metal salt to $[\text{RuCl}_2(\text{DMSO})_4](\text{DMSO} = \text{dimethyl sulfoxide})$ [65], we can carry out a stepwise synthesis, reacting first with 5-methylterpyridine to form the intermediate complex of RuCl_2 with one terpyridine, and then with (53) to give the mixed terpyridine–terpyridine–thiourea complex (55) [66a]. While not interesting as a receptor, (55) shows the ease with which a large library of metal-templated receptors with different substrate-binding regions can be prepared by this route [66b]. In addition, the substitution-inert character of ruthenium(II) chelates renders unsymmetrical complexes such as (55) stable, even in the presence of other potential ligands (such as carboxylate) that may be present in the target substrate. In contrast, the corresponding iron(II) complex of (53) undergoes displacement of the terpyridine ligands upon addition of dicarboxylates.



Large changes in the chemical shifts were observed for the NH protons for receptor (54) upon addition of small aliquots of dicarboxylate ($\Delta\delta \approx 3.0$ – 3.5 ppm) in pure DMSO- d_6 . These are similar to those seen in fully covalent receptors [67] and consistent with the formation of a complex containing four hydrogen bonds as shown in (56). In addition, the diastereotopic methylene protons between the terpyridine and thiourea groups, which have identical chemical shifts in the absence of any guest, give an AB pattern in the presence of excess pimelate (Figure 20), reflecting the formation of a bridged 1:1 complex similar to (56). Binding constants were too high ($K_a > 10^4 \text{ M}^{-1}$) to be measured accurately in pure DMSO- d_6 by ^1H NMR spectroscopy. This strong binding presumably derives in part from an additional electrostatic interaction between the doubly cationic ruthenium ion and the dianionic dicarboxylate. The 1:1 stoichiometry was confirmed by a Job NMR titration. The binding affinity could be reduced by adding hydroxylic solvents to the solution and more accurate K_a values were measured in 5% D_2O –DMSO- d_6 for a variety of dicarboxylates (Table 1). Since it was not possible to follow the NH signals in this solvent system, binding was measured by following the signal of the 4'-proton of the terpyridine group. Strong binding was observed for all substrates studied, reflecting a somewhat flexible binding cavity. Similar changes in the NMR spectra were noted in this solvent mixture as in pure DMSO- d_6 , and 1:1 stoichiometry was confirmed by a Job plot.



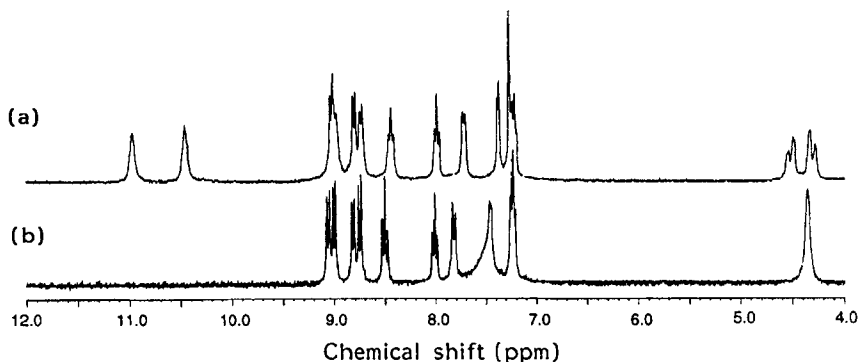
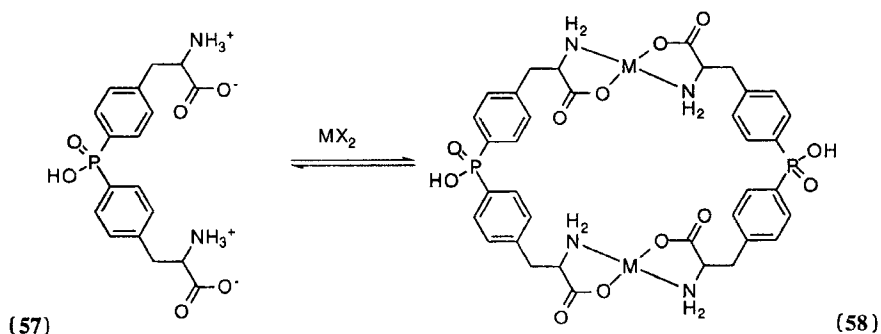


Figure 20 ^1H NMR spectra of (54) in the presence (a) and in the absence (b) of pimelate in DMSO-d_6

Table 1 Binding constants for $[(54)]\text{PF}_6]_2$ with tetrabutylammonium dicarboxylates in 5% D_2O – DMSO-d_6

Dicarboxylate	Binding constant, $10^{-3}K_a \text{ (M}^{-1}\text{)}$
Glutarate	8.3
Adipate	2.9
Pimelate	6.0
Isophthalate	3.5
1,3-Phenylenediacetate	6.2

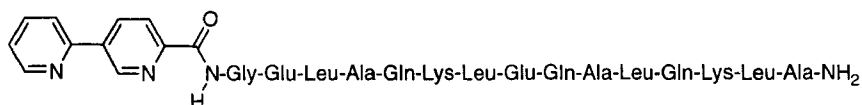
In a completely different approach to metal-templated receptors, Schwabacher *et al.* have prepared a series of bis(amino acid) derivatives like (57) which, on addition of transition metals such as nickel(II) or cobalt(II), dimerize to form cyclophane-like macrocycles (58) that are capable of substrate recognition in water [68]. These designs have the advantage that the metal can provide electrostatic binding to polar substituents on the substrate in addition to the primarily hydrophobic interactions [69].



Other approaches to self-assembling receptors have been reported in recent years. A self-assembling, trimeric palladium complex based on the bis(benzimidazole) ligand (**17**) was designed by Williams and coworkers [4]. The complex contains a hydrophobic cavity that in the X-ray structure has included a molecule of acetonitrile. In a different context, Schepartz and McDevitt [70] have used the chelation of nickel(II) by *N,N'*-bis(salicylaldehyde)ethylenediamine (salen) derivatives to control the position of K^+ -binding glyme chains, and it has been shown that these self-assembled ionophores influence alkali metal transport across liquid membranes [71]. Also, Shinkai and coworkers [72] and Schneider and Ruf [73] have used metal chelation to induce an allosteric effect on binding at a second site.

3.3 Metal-Templated Protein Bundles

The major obstacle in the design of proteins has been how to progress from the one-dimensional information present in the peptide sequence to the three-dimensional tertiary structure of the protein. Insights gained from other self-assembling metal-ligand systems have led to the design of self-assembling triple-helical bundle proteins by Ghadiri *et al.* [74] and Lieberman and Sasaki [75]. An oligopeptide sequence was constructed and functionalized at the nitrogen terminus with a bipyridine subunit, as in (**59**). The 15-residue sequence was chosen to avoid any predisposition toward triple-helix formation. Three of these molecules will be able to bind to a metal ion through their bipyridine groups. Nickel(II), cobalt(II) and ruthenium(II) all formed 1:3 metal:ligand complexes with the polypeptide. The stoichiometry was confirmed with absorption spectroscopy, size exclusion chromatography (SEC) and FABMS. Circular dichroism measurements provided valuable insights into the nature of the complex. In the absence of a transition metal ion, the polypeptide sequence displays only 30% α -helicity. When the metal ions are added, the α -helicity increases to >70%. This indicates that the peptide has undergone a metal-ion-assisted self-assembly process.

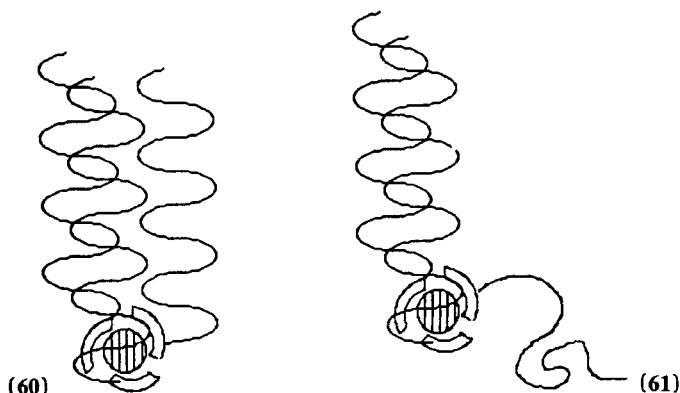


Gly = glycine, Glu = glutamic acid, Leu = leucine, Ala = alanine, Gln = glutamine, Lys = lysine

(**59**)

There are two possible topologies which explain this increase in α -helicity. Either the desired triple-helical bundle has formed as in (**60**), or only two of the peptide subunits interact to form a two-stranded helical coil with the other

subunit adopting a random orientation in solution as in (61). The absence of a concentration dependence on α -helix formation indicated that the desired triple-stranded topology was formed.



This strategy has been extended to form a four-helix bundle metalloprotein. The oligopeptide was functionalized with a pyridine moiety to allow four of the peptides to bind to a metal ion. Ruthenium(II) was chosen as the metal ion because it is known to have a strong affinity for nitrogen-containing aromatic heterocycles. When the peptide was allowed to complex with ruthenium(II), a four-helix bundle metalloprotein was formed. Circular dichroism revealed that the complex exhibited >90% α -helicity with no dependence on concentration [76].

In a related strategy, Cuenand and Schepartz [77] have exploited bis(terpyridine) ion complexes to link two peptides that recognize and bind to deoxyribonucleic acid (DNA). Furthermore, in an important development of the use of metal-templating structures to mimic biomolecules, Sakai and Sasaki have linked a single carbohydrate to a bipyridine ligand. Transition metals were then used to assemble three chelate-linked sugars to mimic the recognition behavior of oligosaccharides [78].

4. REFERENCES

1. J. S. Lindsay, *New J. Chem.*, **15**, 153 (1991).
2. G. M. Whitesides, J. P. Mathias and C. M. Seto, *Science*, **254**, 1312 (1991).
3. P. R. Ashton, C. L. Brown, E. J. T. Chrystal, T. T. Goodnow, A. E. Kaifer, K. P. Parry, A. M. Z. Slawin, N. Spencer, J. F. Stoddart and D. J. Williams, *Angew. Chem., Int. Ed. Engl.*, **30**, 1039 (1991).
4. S. Rüttimann, G. Bernardinelli and A. F. Williams, *Angew. Chem., Int. Ed. Engl.*, **32**, 392 (1993).
5. M. Simard, D. Su and J. D. Wuest, *J. Am. Chem. Soc.*, **113**, 4696 (1991).

6. P. R. Ashton, R. A. Bissell, N. Spencer, J. F. Stoddart and M. S. Tolley, *Synlett*, 914 (1992); P. R. Ashton, R. A. Bissell, R. Gorski, D. Philp, N. Spencer, J. F. Stoddart and M. S. Tolley, *Synlett*, 919 (1992).
7. P. Kaszynski, A. C. Friedli and J. Michl, *J. Am. Chem. Soc.*, **114**, 601 (1992).
8. P. L. Anelli, P. R. Ashton, R. Ballardini, V. Balzani, M. Delgado, M. T. Gandolfi, T. T. Goodnow, A. E. Kaifer, D. Philp, M. Pietraszkiewicz, L. Prodi, M. V. Reddington, A. M. Z. Slawin, N. Spencer, J. F. Stoddart, C. Vicent and D. S. Williams, *J. Am. Chem. Soc.*, **114**, 193 (1992).
9. C. T. Seto and G. M. Whitesides, *J. Am. Chem. Soc.*, **115**, 905 (1993).
10. M. V. Gallant, M. T. P. Viet and J. D. Wuest, *J. Org. Chem.*, **56**, 2284 (1991).
11. S. Ruttiman, C. Piguet, G. Bernardinelli, B. Bocquet and A. F. Williams, *J. Am. Chem. Soc.*, **114**, 4230 (1992).
12. C. T. Seto and G. M. Whitesides, *J. Am. Chem. Soc.*, **115**, 1330 (1993).
13. R. Kramer, J. M. Lehn and A. Marquis-Rigault, *Proc. Natl. Acad. Sci. USA*, **90**, 5394 (1993).
14. J. Rebek Jr, *Acc. Chem. Res.*, **23**, 399 (1990).
15. E. C. Constable, *Tetrahedron*, **48**, 10013 (1992).
16. E. C. Constable, M. D. Ward and D. A. Tocher, *J. Am. Chem. Soc.*, **112**, 1256 (1990).
17. E. C. Constable, M. D. Ward and D. A. Tocher, *J. Chem., Soc. Dalton Trans.*, 1675 (1991).
18. E. C. Constable and J. V. Walker, *J. Chem. Soc., Chem. Commun.*, 884 (1992).
19. E. C. Constable and R. Chotalia, *J. Chem. Soc., Chem. Commun.*, 64 (1992).
20. G. S. Hanan, J. M. Lehn N. Kyritsakas and J. Fischer, *J. Chem. Soc., Chem. Commun.*, 765 (1995).
21. J. K. Judice, S. J. Keipert and D. J. Cram, *J. Chem. Soc., Chem. Commun.*, 1323 (1993).
22. R. Ziessel and M. T. Youinou, *Angew. Chem., Int. Ed. Engl.*, **32**, 877 (1993).
23. M. T. Youinou, R. Ziessel and J. M. Lehn, *Inorg. Chem.*, **30**, 2144 (1991).
24. W. Zarges, J. Hall, J. M. Lehn and C. Bolm, *Helv. Chim. Acta*, **74**, 1843 (1991).
25. A. Pfeil and J. M. Lehn, *J. Chem. Soc., Chem. Commun.*, 838 (1992).
26. C. Piguet, G. Bernardinelli, B. Bocquet, A. Quattropiani and A. F. Williams, *J. Am. Chem. Soc.*, **114**, 7440 (1992).
27. L. J. Charbonniere, G. Bernardinelli, C. Piguet, A. Sargeson and A. F. Williams, *J. Chem. Soc., Chem. Commun.*, 1419 (1994).
28. R. Kramer, J. M. Lehn, A. De Cian and J. Fischer, *Angew. Chem., Int. Ed. Engl.*, **32**, 703 (1993).
29. K. T. Potts, C. P. Horwitz, A. Fessak, M. Keshavarz, K. E. Nash and P. J. Toscano, *J. Am. Chem. Soc.*, **115**, 10444 (1993).
30. T. W. Bell and H. Jousselin, *Nature*, **367**, 441 (1994).
31. M. Fujita, J. Yazaki and K. Ogura, *J. Am. Chem. Soc.*, **112**, 5645 (1990).
32. P. J. Stang, D. H. Cao, S. Saito and A. M. Arif, *J. Am. Chem. Soc.*, **117**, 6273 (1995).
33. M. Fujita, S. Nagao, M. Lida, K. Ogata and K. Ogura, *J. Am. Chem. Soc.*, **115**, 1574 (1993).
34. M. Fujita, S. Nagao and K. Ogura, *J. Am. Chem. Soc.*, **117**, 1649 (1990).
35. P. J. Stang and V. V. Zhdankin, *J. Am. Chem. Soc.*, **115**, 9808 (1993).
36. C. M. Drain and J. M. Lehn, *J. Chem. Soc., Chem. Commun.*, 2313 (1994).
37. C. O. Dietrich-Buchecker, J. P. Sauvage and J. P. Kinzanger, *Tetrahedron Lett.*, **24**, 5095 (1983).
38. C. O. Dietrich-Buchecker and J. P. Sauvage, *Chem. Rev.*, **87**, 795 (1987).
39. J. P. Sauvage, *Acc. Chem. Res.*, **23**, 319 (1990).

40. C. O. Dietrich-Buchecker and J. P. Sauvage, *Tetrahedron*, **46**, 503 (1990).
41. C. O. Dietrich-Buchecker, J. M. Kern and J. P. Sauvage, *J. Chem. Soc., Chem. Commun.*, 760 (1985).
42. N. Armaroli, V. Balzani, F. Barigelli, L. De Cola, L. Flamigni, J. P. Sauvage and C. Hemmert, *J. Am. Chem. Soc.*, **116**, 5211 (1994).
43. M. Fujita, F. Ibukuro, H. Hagihara and K. Ogura, *Nature*, **367**, 720 (1994).
44. C. O. Dietrich-Buchecker, J. F. Nierengarten and J. P. Sauvage, *Tetrahedron Lett.*, **33**, 3625 (1992).
45. C. O. Dietrich-Buchecker and J. P. Sauvage, in *Supramolecular Chemistry* (eds V. Balzani and L. De Cola), Kluwer, Dordrecht, 1992, p. 259.
46. J. F. Nierengarten, C. O. Dietrich-Buchecker and J. P. Sauvage, *J. Am. Chem. Soc.*, **116**, 375 (1994).
47. J. C. Chambron, C. O. Dietrich-Buchecker, J. F. Nierengarten and J. P. Sauvage, *J. Chem. Soc., Chem. Commun.*, 801 (1993).
48. G. S. Hanan, C. R. Arana, J. M. Lehn and D. Fenske, *Angew. Chem. Int. Ed. Engl.*, **34**, 112 (1995).
49. M. T. Youinou, N. Rahmouni, J. Fischer and J. A. Osborn, *Angew. Chem. Int. Ed. Engl.*, **31**, 733 (1992).
50. P. N. W. Baxter, J. M. Lehn, J. Fischer and M. T. Youinou, *Angew. Chem. Int. Ed. Engl.*, **33**, 2284 (1994).
51. P. Baxter, J. M. Lehn, A. DeCian and J. Fischer, *Angew. Chem. Int. Ed. Engl.*, **32**, 69 (1993).
52. E. Leize, A. Van Dorsselaer, R. Kramer and J. M. Lehn, *J. Chem. Soc., Chem. Commun.*, 990 (1993).
53. P. Besler, *Chimia*, **48**, 347 (1994).
54. E. C. Contable and A. M. W. Cargill Thompson, *J. Chem. Soc., Chem. Commun.*, 617 (1992).
55. E. C. Constable, A. M. W. Cargill Thompson and D. A. Tocher, in *Supramolecular Chemistry* (eds V. Balzani and L. De Cola), Kluwer, Dordrecht, p. 219.
56. J. P. Sauvage, J. P. Colin, J. C. Chambron, S. Guillerez, C. Coudret, V. Balzani, F. Barigelli, L. De Cola and L. Flamigni, *Chem. Rev.*, **94**, 993 (1994).
57. G. Denti, S. Campagna, S. Serroni, M. Ciano and V. Balzani, *J. Am. Chem. Soc.*, **114**, 2944 (1992) and references therein.
58. S. Campagna, A. Giannetti, S. Serroni, G. Denti, S. Trusso, F. Mallamace and N. Micali, *J. Am. Chem. Soc.*, **117**, 1754 (1995).
59. M. S. Goodman, J. Wess and A. D. Hamilton, *Tetrahedron Lett.*, **35**, 8943 (1994).
60. F. Garcia-Tellado, S. Goswami, S. K. Chang, S. J. Geib and A. D. Hamilton, *J. Am. Chem. Soc.*, **112**, 7393 (1990).
61. F. Garcia-Tellado, J. Albert and A. D. Hamilton, *J. Chem. Soc., Chem. Commun.*, 1761 (1991).
62. L. Owens, C. Thilgen, F. Diederich and C. B. Knobler, *Helv. Chim. Acta*, **76**, 2757 (1993).
63. A. K. I. Crushurst, D. R. McMillin, C. O. Dietrich-Buchecker and J. P. Sauvage, *Inorg. Chem.*, **28**, 4070 (1989); J. P. Sauvage and J. Weiss, *J. Am. Chem. Soc.*, **107**, 6108 (1985).
64. P. J. Burke, K. Herrick and D. R. McMillin, *Inorg. Chem.*, **21**, 1881 (1982); D. Q. McDonald and W. C. Still, *Tetrahedron*, **33**, 7743 (1992); W. C. Still, *MacroModel*, Columbia University, New York.
65. I. P. Evans, A. Spencer and G. Wilkinson, *J. Chem. Soc., Dalton Trans.*, 204 (1973).
- 66a. M. S. Goodman, V. Jubian and A. D. Hamilton, *Tetrahedron Lett.*, **36**, 2551 (1995).

- 66b. M. S. Goodman, V. Jubian, B. Linton and A. D. Hamilton, *J. Am. Chem. Soc.*, **117**, 11610 (1995).
- 67. E. Fan, S. A. Van Arman, S. Kincaid and A. D. Hamilton, *J. Am. Chem. Soc.*, **115**, 369 (1993).
- 68. A. Schwabacher, J. Lee and H. Lei, *J. Am. Chem. Soc.*, **114**, 7597 (1992).
- 69. J. Lee and A. Schwabacher, *J. Am. Chem. Soc.*, **116**, 8382 (1994).
- 70. A. Schepartz and J. P. McDevitt, *J. Am. Chem. Soc.*, **111**, 5976 (1989).
- 71. J. P. Costes, F. Dahan and J. P. Laurent, *Inorg. Chem.*, **33**, 2738 (1994).
- 72. G. Deng, T. D. James and S. Shinkai, *J. Am. Chem. Soc.*, **115**, 8091 (1993).
- 73. H.-J. Schneider and D. Ruf, *Angew. Chem., Int. Ed. Engl.*, **29**, 1159 (1990).
- 74. M. R. Ghadiri, C. Soares and C. Choi, *J. Am. Chem. Soc.*, **114**, 825 (1992).
- 75. M. Lieberman and T. Sasaki, *J. Am. Chem. Soc.*, **113**, 1470 (1991).
- 76. M. R. Ghadiri, C. Soares and C. Choi, *J. Am. Chem. Soc.*, **114**, 4000 (1992).
- 77. B. Cuenoud and A. Schepartz, *Science*, **259**, 510 (1993).
- 78. S. Sakai and T. Sasaki, *J. Am. Chem. Soc.*, **116**, 1587 (1994).

Chapter 2

A Survey of Supramolecular Chemistry (1993–1994)

UDAY MAITRA

Indian Institute of Science, Bangalore, India

1. INTRODUCTION

Fischer's "lock-and-key" concept for explaining the specificity of enzymatic action has been known since 1894. However, deliberate attempts to mimic (and thereby better understand) such biological processes in the laboratory started much later. The early work with cyclodextrins first gave an impression that new chemistry can be developed using host–guest complexation. The discovery of crown ethers ushered in a new era of research in the design, synthesis, evaluation and applications of synthetic molecular receptors. The number of papers published in this area is increasing every year. If one examines the developments in synthetic receptor chemistry during the past quarter of a century, it becomes quite apparent that during the last five years there has been a different trend in the design of such molecules. From 1970 to 1990, a variety of fairly complex receptors were synthesized. The complexity in the synthesis was to some extent a result of the dogma that the synthetic receptors would have to be highly preorganized. It is needless to say that many of these approaches were quite successful. More recently, however, it has been recognized that in order to achieve the efficient synthesis of a variety of receptors, the construction of these molecules must be as simple as possible. The use of specific hydrogen-bonding interactions to hold a host and a guest together is also being examined ever more. The construction of new types of supramolecular assemblies through polytopic receptors and guests has also been the focus of attention of various research groups. Additionally, several

groups have been interested in the study of the details of host–guest interactions. Another point to be noted is that such molecular receptors are increasingly being used for the development of molecular devices such as sensors.

A number of review articles and monographs have appeared in the current literature summarizing the developments in certain specific areas of molecular recognition [1]. In this survey, an attempt is made to highlight the research achievements in the general area of supramolecular chemistry during the period 1993–1994. Because of space limitations, this review is illustrative rather than comprehensive. The important area of self-assembly in supramolecular chemistry has been largely ignored in this survey since this is the subject of Chapter 1 in this monograph. The arrangement of the sub-areas is somewhat arbitrary (and clearly there is considerable overlap), but the author hopes that the changing pattern of molecular recognition research in the early 1990s will be transparent from this article.

2. CYCLODEXTRIN DERIVATIVES AS HOSTS

This subject has recently been reviewed by Wenz [2]. Various attempts have been made in recent years to improve the synthesis of cyclodextrin derivatives such as the aldehyde [3]. A synthesis of benzylated cycloisomaltohexoside has been published [4]. An electrochemical approach to study the inclusion complexation of substrates with cyclodextrins has been reported [5]. Significant changes in the electrochemical properties of a number of substrates were observed in the presence of cyclodextrins.

Ueno and coworkers have been studying functionalized cyclodextrins in order to understand energy-transfer processes [6–8]. A recent communication from this group reported the synthesis of a rhenium complex connected to a cyclodextrin unit (Figure 1). They have demonstrated energy transfer from a bound *N,N*-diethylaniline to the metal center. β -Cyclodextrin bearing a covalently bound *p*-(dimethylamino)benzamide (DMAB) unit has been examined as a fluorescent sensor of molecular recognition. In the absence of any guest, the DMAB unit intramolecularly binds to the cyclodextrin cavity.

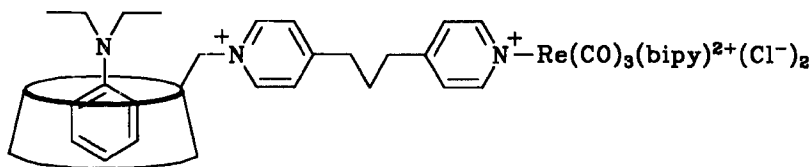


Figure 1 *N,N*-Diethylaniline bound in β -cyclodextrin functionalized with a rhenium complex (bipy = 2,2'-bipyridyl) [6]

However, in the presence of a guest molecule (cyclic alcohols, monoterpenes, steroids) binding to the cyclodextrin cavity, the twisted intramolecular charge-transfer (TICT) emission of the host decreases significantly, indicating the process schematically shown in Figure 2.

Nagata *et al.* have studied the pH-responsive guest binding to β -cyclodextrin functionalized with poly(γ -methyl L-glutarate-*co*-L-glutamic acid) [9]. The pH dependence of the conformation of the peptide was investigated by circular dichroism, and the pH dependence of the binding of 8-anilidonaphthalene-1-sulfonate (ANS) was monitored by fluorescence. The data indicated that at high pH ANS did not bind since the β -cyclodextrin unit was concealed in the random coil of the polypeptide. At lower pH, however, a random coil \rightarrow α -helix transition of the polypeptide exposed the cyclodextrin to the aqueous phase, thereby enabling ANS binding (Figure 3).

The binding of fluorophores 6-(4-toluidino)naphthalene-2-sulfonate (TNS) and 6-(4-*tert*-butylanilino)naphthalene-2-sulfonate (BNS) by bis(cyclodextrin)s has been studied by Sikorski and Petter [10]. The spacer length between the

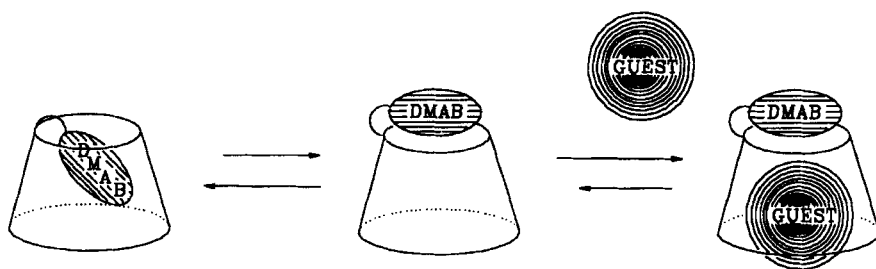


Figure 2 DMAB- β -cyclodextrin for the detection of guest binding by twisted intramolecular charge-transfer (TICT) fluorescence [7,8]

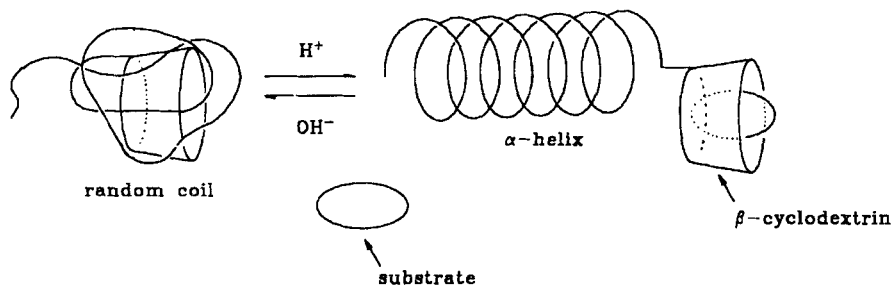


Figure 3 The pH-responsive guest binding by a polypeptide cyclodextrin [9]

two β -cyclodextrin units was varied. They observed that the best BNS binder (K_a of $8.2 \times 10^6 \text{ M}^{-1}$) was a bis(cyclodextrin) with an $\text{S}(\text{CH}_2)_2\text{S}$ spacer (Figure 4). Interestingly, they also found that increasing the spacer length by one methylene unit resulted in the decrease of the free energy of association by 0.25 kcal mol^{-1} (1 cal = 4.186 J).

The binding of nucleosides, nucleotides and sugars by amino- β -cyclodextrins has been studied by Eliseev and Schneider [11]. A β -cyclodextrin derivative with seven aminomethyl groups attached to the 6-position exhibited very tight binding to adenosine 5'-triphosphate (ATP) (K_a of $\sim 10^6 \text{ M}^{-1}$). An A,D-functionalized bis(aminomethyl) derivative showed discrimination of the guests based on nucleobase structure, sugar type and position of the phosphate group.

Cyclodextrins have also been used for the solubilization of a synthetic charge-transfer receptor [12]. The solubilized electron acceptor (Figure 5) in water was demonstrated to form π -complexes with various water-soluble π -bases.

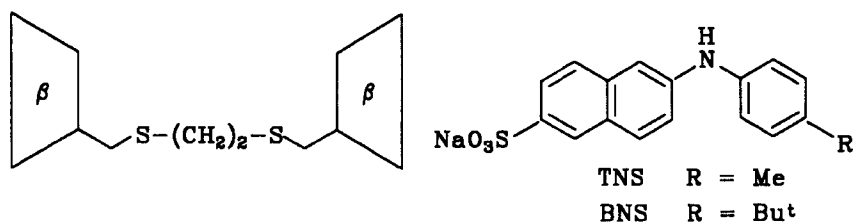


Figure 4 A bis(β -cyclodextrin) for binding BNS and TNS [10]

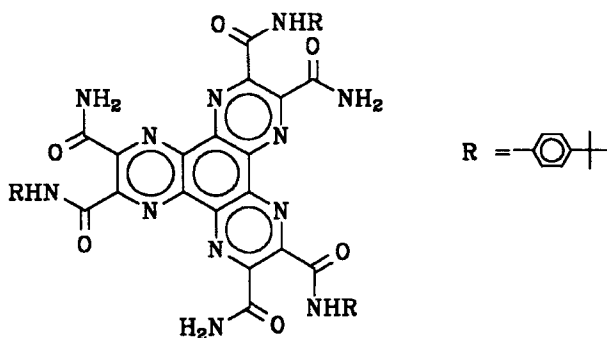


Figure 5 A charge-transfer receptor solubilized in water by β -cyclodextrin [12]

3. CROWN ETHERS

Since the discovery of crown ethers in 1967 by Pedersen, thousands of crown ethers have been synthesized and their properties studied. In recent years, there has been a great deal of interest in using crown ethers for designing metal ion sensors (*vide supra*). In this section the construction of novel crown ether molecules with interesting properties is highlighted.

Crown ethers have been used for improving the detection of fullerenes by electrospray mass spectrometry [13]. Sawada *et al.* have developed a FABMS methodology for the determination of chiral recognition of amino acid esters by crown ethers [14]. This method requires that the racemic mixture of the guests contains one enantiomer in its isotopically labeled form. Mass spectral analysis of the molecular ion peaks for $H + G_{(R)}$ and $H + G_{(S)}$ allows a direct comparison of their relative abundances, where H and G are host and guest, respectively.

The effect of anions on the selectivity of alkali metal ion extraction by crown ethers has been investigated by Olsher *et al.* [15]. They have shown that the overall extraction efficiency decreases in the order $ClO_4^- > I^-$, $SCN^- > NO_3^- > Br^-$. It was also shown that this efficiency is dependent upon the solvation energy of the anion in both phases, but not upon the anion softness parameter. On the other hand, the extraction selectivity (for K^+/Rb^+ by *cis*, *syn*, *cis*-dicyclohexano-18-crown-6) decreased in the order $NO_3^- > SCN^- > ClO_4^- \geq I^- > Br^-$. They concluded that higher selectivity was observed with nonspherical counterions.

A novel bis(crown ether) based on Kemp's triacid has recently been reported [16]. It has been shown that this molecule forms a sandwich-type complex with alkali metal ions. This crown ether (shown in Figure 6) was reported to exhibit a higher preference for potassium ions over sodium ions (85% K^+ versus 46% Na^+ extracted).

The photoresponsive thioindigocrown ether shown in Figure 7 has been constructed by Fatah-ur Rahman and Fukunishi [17]. They have demonstrated a reversible photochemical *cis-trans* isomerization of the crown ether. It has also been shown that the *cis*-form extracts metal ions with higher efficiency

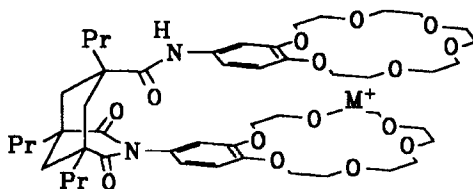


Figure 6 A Kemp's-triacid-derived bis(crown ether) [16]

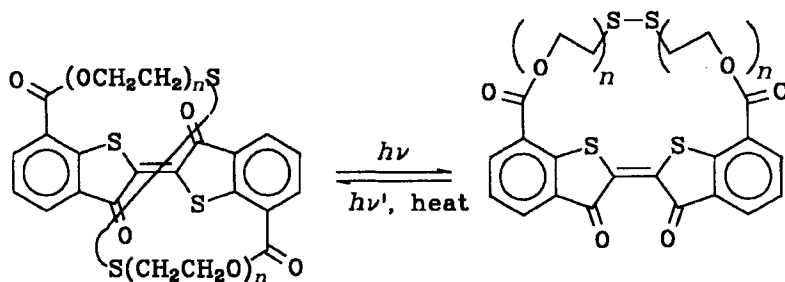


Figure 7 A photoresponsive thioindigocrown ether for metal ion binding [17]

than the *trans*-form. Interestingly, heavy-metal ions were found to have no interaction with this macrocycle.

A novel multisite crown ether receptor based on a P_3N_3 heterocycle has been synthesized by Mitjaville *et al.* (Figure 8) [18]. This class of receptors will be of interest for multiple metal ion binding.

A “cholacrown” has been reported by us (Figure 9), which was synthesized in one step from cholic acid [19]. As expected, this crown binds alkali metal ions and primary ammonium cations. The rigid juxtaposition of a functionalizable hydroxy group to the crown ether moiety in this molecule makes it attractive for the design of potential catalysts.

Joly *et al.* have reported the synthesis of a variety of crown ethers from D-hexopyranosides and D-mannitol [20]. Partial enantioselective complexation of phenylglycine methyl ester salts by some of the chiral crown ethers were reported (an example is shown in Figure 10). Joly and coworkers have synthesized a crown ether with a pendent amino group [21]. This compound was shown to extract dopamine from an aqueous solution. The pendent amino group was suggested to interact with a phenolic hydroxy group on dopamine (Figure 11). Other D-glucose-derived crown ethers have been reported by Mani and Kanakamma [22].

Schall and Gokel have reported the construction of “molecular boxes” derived from nucleic acid bases and azacrown ethers [23]. Detailed NMR studies provided evidence for the association of A-crown-A with T-crown-T in chloroform. Formation of a ternary receptor complex with α , ω -diammonium compounds (Figure 12) was also suggested.

Cation binding by permethylated cycloinulohexose (Figure 13) and cycloinuloheptose has been studied by Sawada *et al.* [24]. This 18-crown-6 analogue complexed alkali metal ions with association constants roughly two orders of magnitude lower than those observed with 18-crown-6 itself. Analysis of the crystal structure of the complex with Ba^{2+} showed that the metal ion was complexed in the pocket with the upper-rim 3-methoxy and the crown ether oxygens.

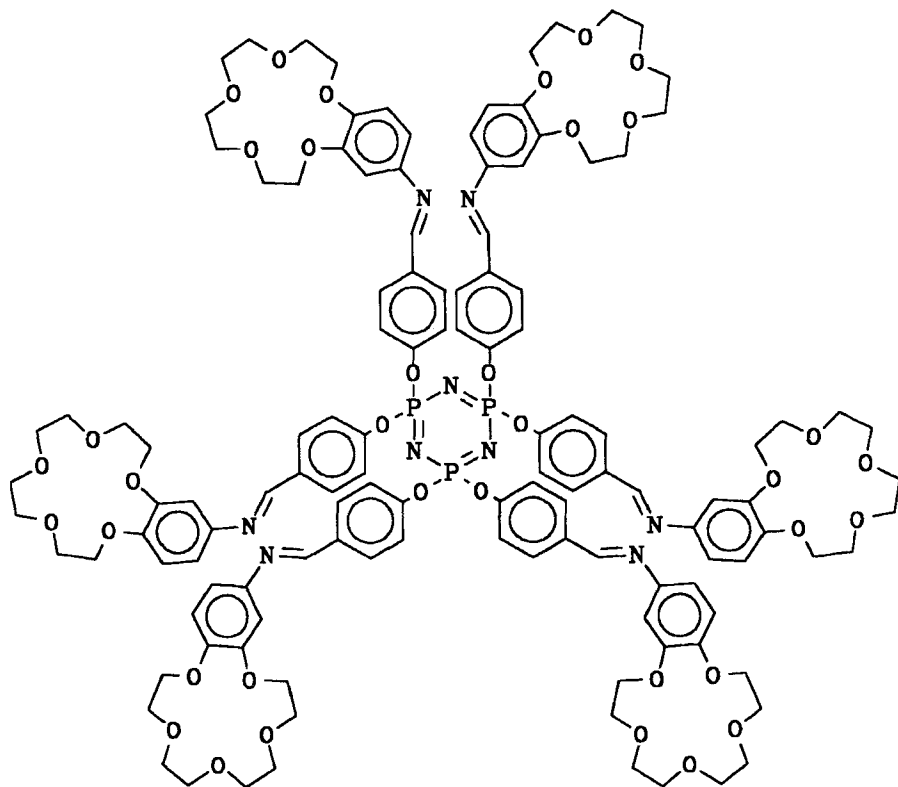


Figure 8 A hexacrown based on a P₃N₃ unit [18]

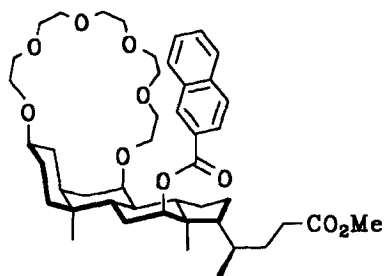


Figure 9 A bile-acid-derived crown ether ("cholacrown") [19]

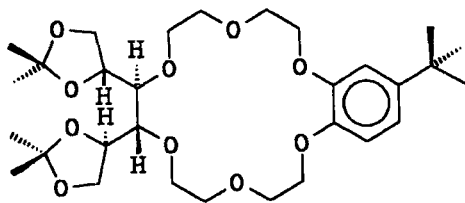


Figure 10 A D-mannitol-derived crown ether for the complexation of amino acid esters [20]

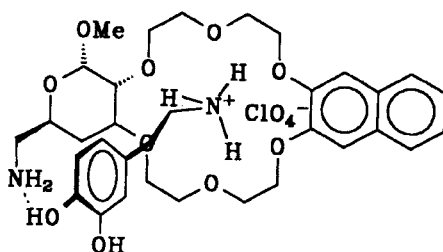


Figure 11 Complexation of dopamine by a carbohydrate-derived crown ether [21]

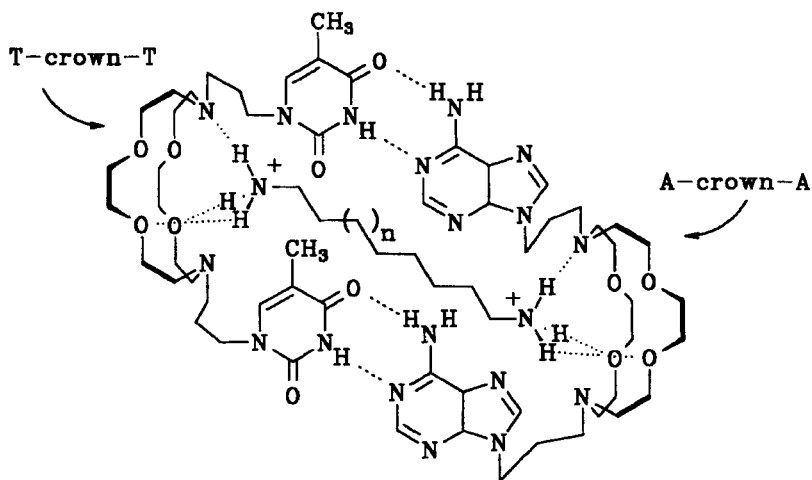


Figure 12 The complex from a "molecular box" and a diammonium guest [23]

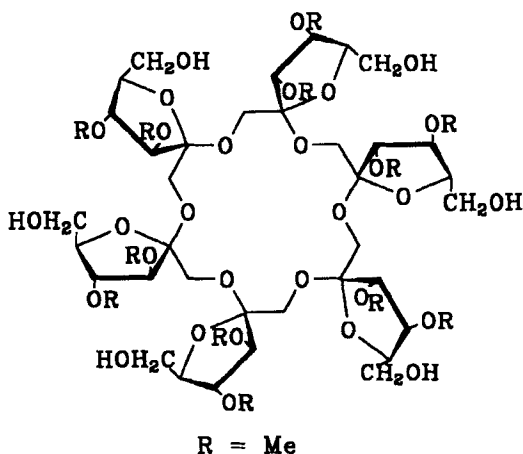


Figure 13 Permethylated cyclonulohexose as a crown ether mimic [24]

4. CALIXARENES AND RELATED HOSTS

Calixarenes have attracted the attention of a number of groups for constructing a wide variety of receptors. Functionalized higher calix[*n*]arenes (*n* = 6 and 8) are also being increasingly synthesized.

A furan-derived macrocycle (“calixfuran”), obtained by the condensation of furan with 2-hydroxymethylfuran, has been reported by Musau and Whiting (Figure 14) [25]. Higher oligomers (cyclic pentamer, hexamer and the octamer) were also isolated in small quantities. Functionalized calixfurans are likely to be of interest for further investigations.

Alam *et al.* have described the synthesis of a variety of mono- and tetrasubstituted calix[4]arenes *via* the quinonemethide route shown in Figure 15 [26].

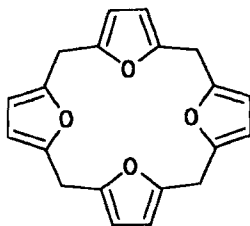


Figure 14 A furan-derived, calixarene-type macrocycle [25]

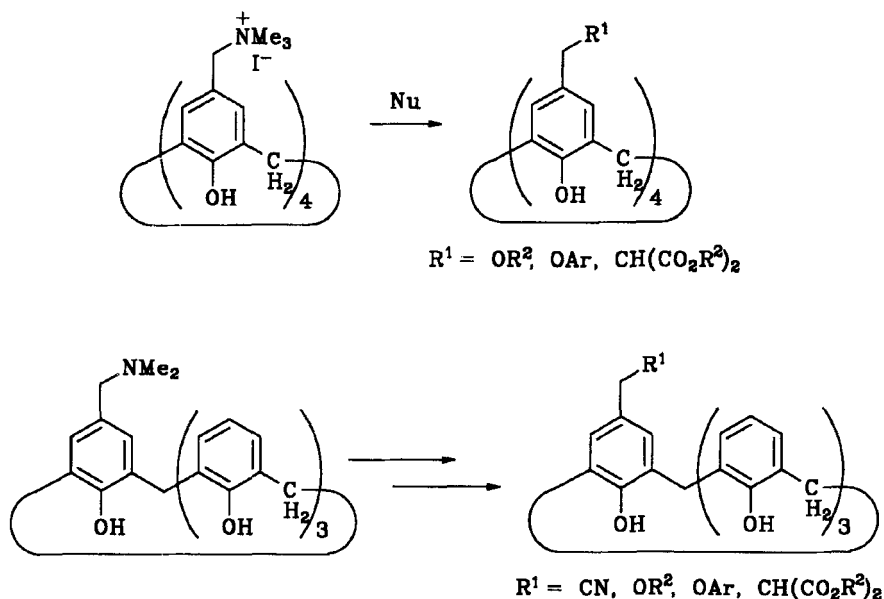


Figure 15 Mono- and tetrasubstituted calix[4]arenes [26]

The synthesis of p-t-butyltetraathio-calix[4]arene has been reported Gibbs and Gutsche [27]. Interestingly, this compound (Figure 16) was found to exist in the 1,3-alternate conformation.

The binding of simple alcohols by a resorcinol cyclic tetramer derivative (Figure 17) in chloroform has been studied by NMR and induced CD spectroscopy [28]. Acceptable binding constants for borneol (54 M^{-1}) and 3-oxo-2-butanol (35 M^{-1}) were measured. Cooperative CH- π and hydrogen-bonding interactions were suggested to be responsible for the binding. It was also observed that acetyl groups significantly promoted complexation, possibly owing to enhanced CH- π interaction involving the polarized C—H bonds of the acetyl group. A value of up to $1.4 \text{ kcal mol}^{-1}$ has been suggested for the CH- π interaction.

Reinhoudt and coworkers have synthesized novel bis(calix[4]arene)zinc tetraarylporphyrins [29]. The resulting molecules have large cavities, and will

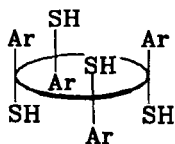


Figure 16 A tetraathio-calix[4]arene derivative [27]

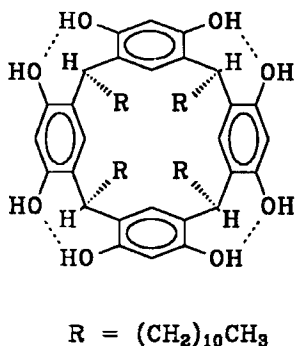


Figure 17 A resorcinol cyclic tetramer used for CH- π interaction studies [28]

be of interest in binding appropriate guest molecules. Reinhoudt and coworkers have also reported a detailed NMR study on the conformational aspects of calix[6]arenes with 1,3,5-*O*-alkyl substituents (Figure 18) [30]. A new and efficient synthesis of calixspherands, in which a calix[4]arene is bridged with a *m*-terphenyl (Figure 19), has also been reported by Reinhoudt and coworkers [31]. Their studies show that these molecules form kinetically stable complexes with Na^+ , K^+ and Rb^+ . It has been suggested that the high kinetic stability in polar solvents can be utilized for *in vivo* applications:

A “holand” has recently been described by Reinhoudt and coworkers which was constructed by the assembly of two calix[4]arenes and two resorcinol-based cavitands (schematically shown in Figure 20) [32]. This extremely rigid host has a shielded hole of nanosize dimensions, with an estimated hole volume of 1 nm^3 . Reinhoudt and coworkers have also reported the synthesis of a cryptocalix[6]arene (Figure 21), and studied its dynamic behavior [33]. A novel type of stereoisomerism has been reported in carcaplexes of dimethylacetamide and *N*-methylpyrrolidone with a calix[4]arene-based carcerand. This isomerism

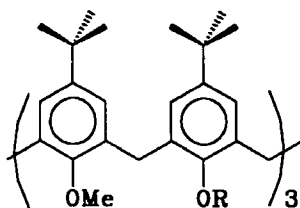


Figure 18 Calix[6]arenes with 1,3,5-*O*-alkyl substituents [30]

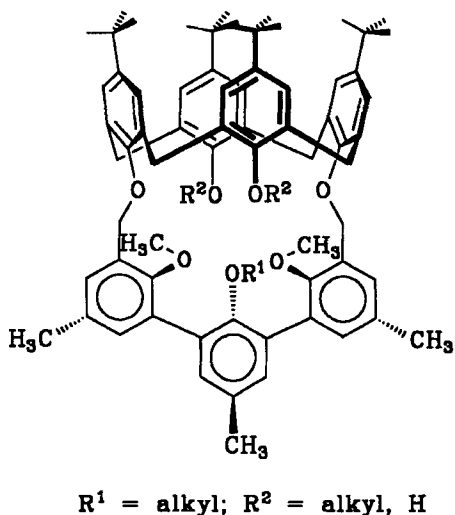
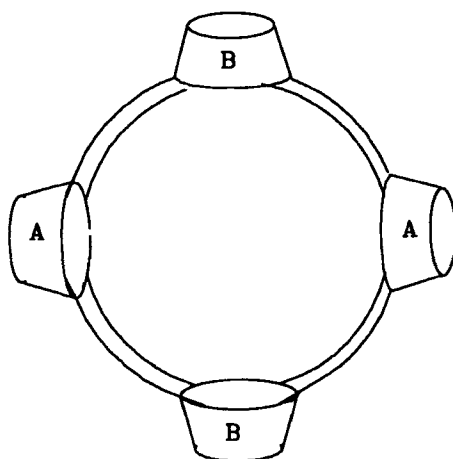


Figure 19 A calixspherand [31]



A = resorcinol based cavitand
B = calix[4]arene

Figure 20 Schematic representation of a host with a large, rigid cavity [32]

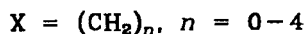
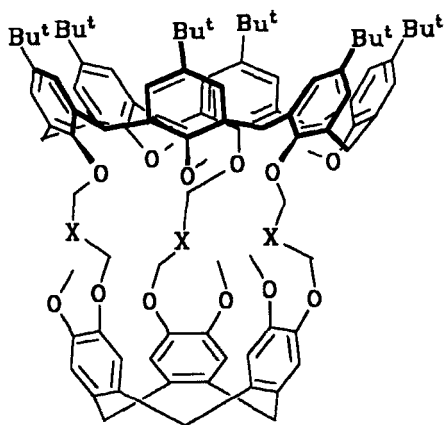


Figure 21 A cryptocalix[6]arene [33]

results from the hindered rotation of a noncovalently bound molecule inside the cavity [34].

Kubo *et al.* have reported the synthesis of an indoaniline-derived calix[6]arene (Figure 22) which showed a pronounced color change ($\Delta\lambda$ of 60 nm) in the presence of UO_2^{2+} [35]. Other cations studied (alkali metal ions, Sr^{2+} , Ba^{2+}) showed a much less pronounced color change ($\Delta\lambda$ less than 10 nm).

The crystal structure of a host–guest complex between triethylammonium sulfate and a calix[4]arene derived from resorcinol (Figure 23) has been reported by Mann and coworkers [36]. The host was found to exist in an approximately conical form. Alternating hydrophilic and hydrophobic layers were found in the crystal.

5. HYDROGEN-BONDING RECEPTORS

Savage and Gellman have constructed a novel macrocycle incorporating a phosphine oxide and two sulfoxide functionalities (Figure 24) [37]. The binding of hexosammonium ions was investigated in a mixture of CD_3OD and CDCl_3 (1 : 9). A β -glucosammonium derivative showed a K_a of 3000 M^{-1} . Evidence for binding contributions from $\text{OH}\cdots\text{OH}$ hydrogen bonds in this medium (2.5 M in methanol) was provided.

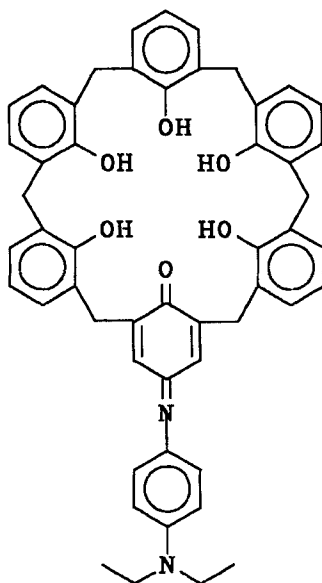


Figure 22 A calix[6]arene-based uranyl ion sensor [35]

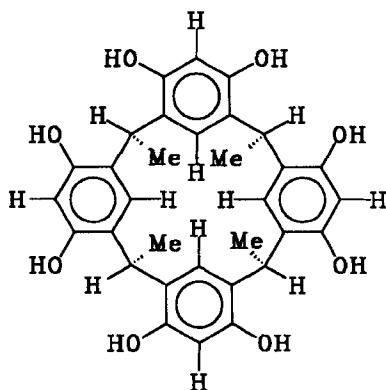


Figure 23 A resorcinol-derived host for binding alkylammonium guests [36]

A number of bis(guanidinium) receptors (Figure 25) have been synthesized (*meso* and *d, l*) by Anslyn and coworkers [38]. These molecules mimic part of the active site of staphylococcal nuclease. The binding of dibenzyl phosphate was investigated in detail by ^1H and ^{31}P NMR spectroscopy. It was found that binding occurred through the formation of four hydrogen bonds between the

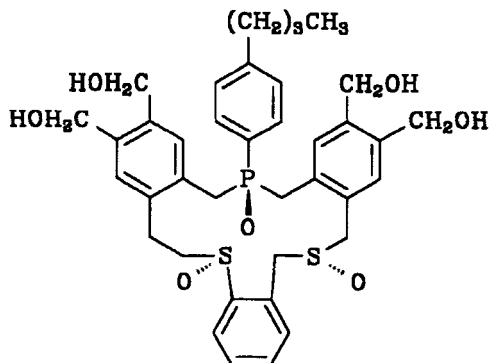


Figure 24 A hexosammonium ion receptor [37]

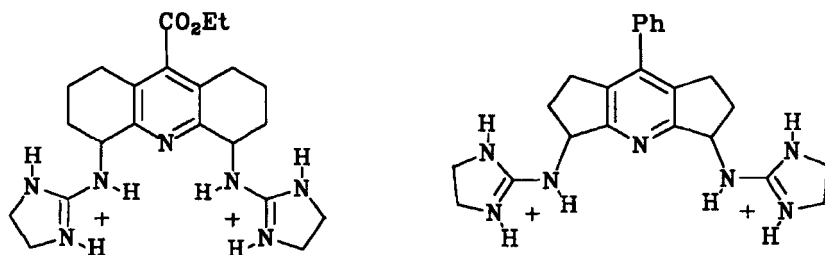
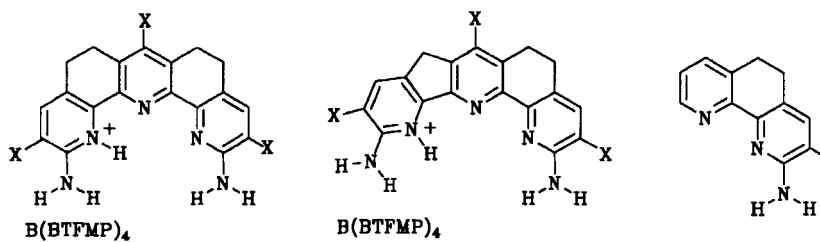


Figure 25 Phosphodiester receptors [38]



X = CO₂Et; B(BTFMP)₄ = tetrakis(3,5-bis(trifluoromethyl)phenyl)borate

Figure 26 Polyaza clefts for binding phosphoric acid diesters [39]

host and the guest. Complexation was observed even in highly competitive solvents. The effects of counterions, solvent mixtures and cavity flexibility on complexation were studied. One of the *meso*-compounds was found to act as a catalyst for ribonucleic acid (RNA) hydrolysis. Subsequently, Anslyn and coworkers reported the synthesis of the related molecules shown in Figure 26. Very tight binding of dinaphthyl hydrogen phosphate with a receptor was observed in chloroform [39].

Thummel and coworkers have systematically studied the binding of urea derivatives using the pyrido[3,2-*g*]indole subunit [40]. They have demonstrated, using hosts which offer two, three and four hydrogen-bonding sites, that tighter binding is observed with more than two hydrogen bonds ($A > B > C = D$, Figure 27 and Table 1).

Shippo and Rebek have designed a new cleft (*cf.* Figure 79) based on two xanthene skeletons separated by a porphyrin spacer unit (Figure 28) [41]. They demonstrated a high ($> 10^5 \text{ M}^{-1}$) binding constant with 1,4-diazabicyclo[2.2.2]octane (DABCO) in chloroform.

Hamilton and coworkers have reported the formation of helical structures, both in solution and in the solid state, from a simple combination of pyridine-2,6-dicarboxamide and anthranilamides (Figure 29) [42]. The helical secondary

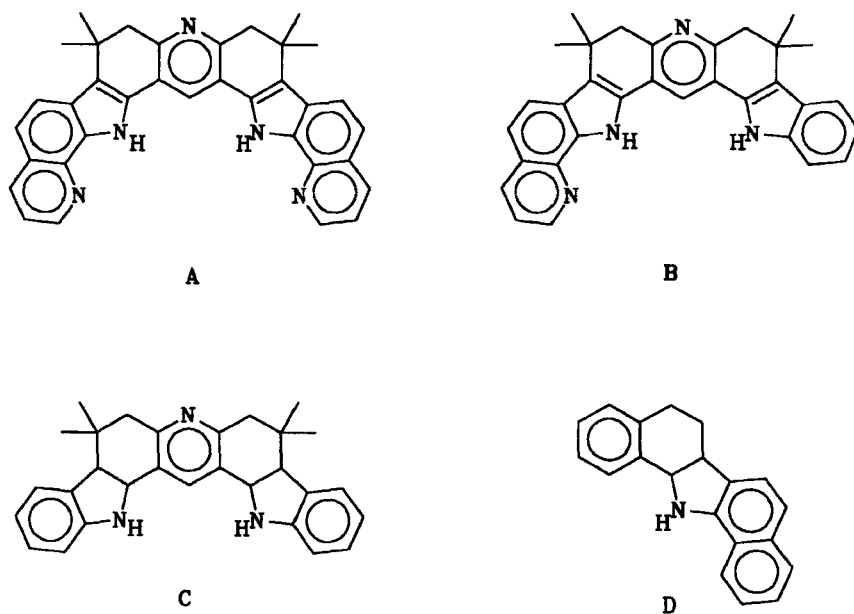
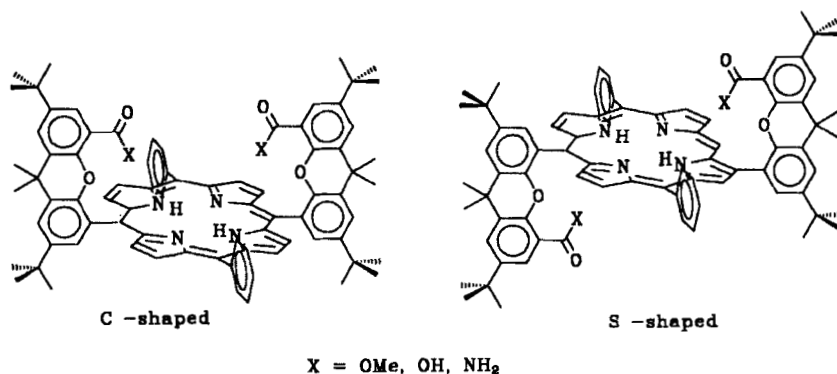
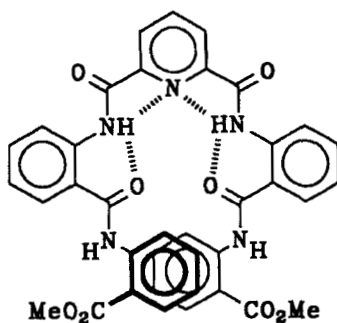


Figure 27 Receptors for urea and amide derivatives [40]

Table 1 Association constants at 18 °C for host–guest complexation in CDCl₃

Guest	Association constants, K_a (M ⁻¹)			
	Host A	Host B	Host C	Host D
Imidazolidone	8300	130	41	17
<i>n</i> -Butylurea	1200	260	38	15
<i>N,N'</i> -Dimethylurea	117	124	20	9
Butyrolactam	165	144	43	9
Barbital	3.92×10^4	406		95

**Figure 28** A porphyrin–xanthene-based molecular cleft [41]**Figure 29** A helical anthranilamide [42]

structure was found to be stabilized in part by *intramolecular* hydrogen-bonding.

Binding of 1,2-diols with phosphonates in acetonitrile has recently been reported by Das and Hamilton [43]. Association constants for the binding of

1,2-diols and alkyl glycosides with methyl benzylphosphonate were found to be of the order of 100^{-1} M^{-1} and 1000^{-1} M^{-1} , respectively. The binding constants of the same glycosides with a bis(phosphonate) (Figure 30) were higher, with K_a of the order of 10^4 M^{-1} . Hamilton and coworkers have designed an elegant self-assembling receptor for dicarboxylic acids [44]. Two phenanthroline-containing subunits chelate a copper(I) and orient the two pyridine-2-carboxamide moieties for hydrogen bonding to the ends of an α,ω -dicarboxylic acid (Figure 31). Binding constants of the order of 10^4 M^{-1} were reported for glutaric, pimelic and (N-Cbz)-L-glutamic acids.

Hunter and coworkers have reported a “molecular zipper” in which two different but complementary amide oligomers formed a 1 : 1 *heterocomplex* in a mixture of chloroform and methanol (19 : 1) [45]. The association constant for the formation of the *heterodimer* (240 M^{-1}) was an order of magnitude higher than the association constants for the two possible *homodimers*. NMR

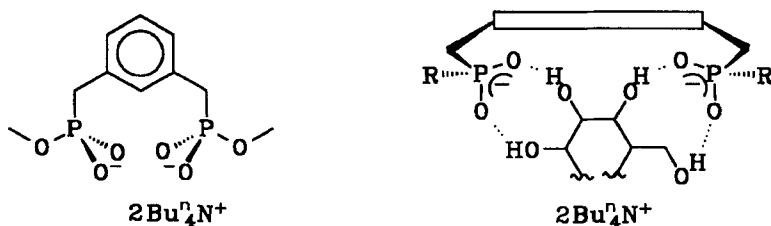


Figure 30 A bis(phosphonate) receptor for alkyl glycosides [43]

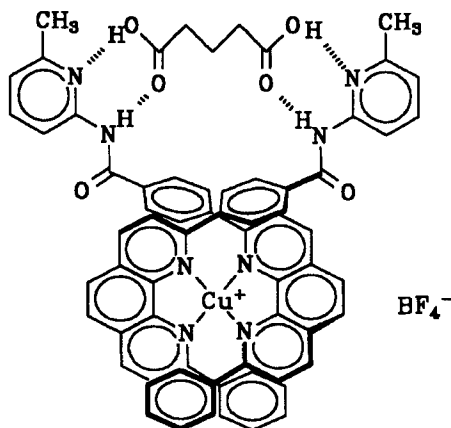


Figure 31 A self-assembling dicarboxylic acid receptor shown as its complex with glutaric acid [44]

experiments [including rotational Overhauser effect spectroscopy (ROESY)] suggested the structure shown in Figure 32. Hunter and Sarson published an example of a self-assembled porphyrin receptor (Figure 33) which binds terephthalic acid amides in CDCl_3 by hydrogen bonding, with association constants of the order of 1000 M^{-1} [46].

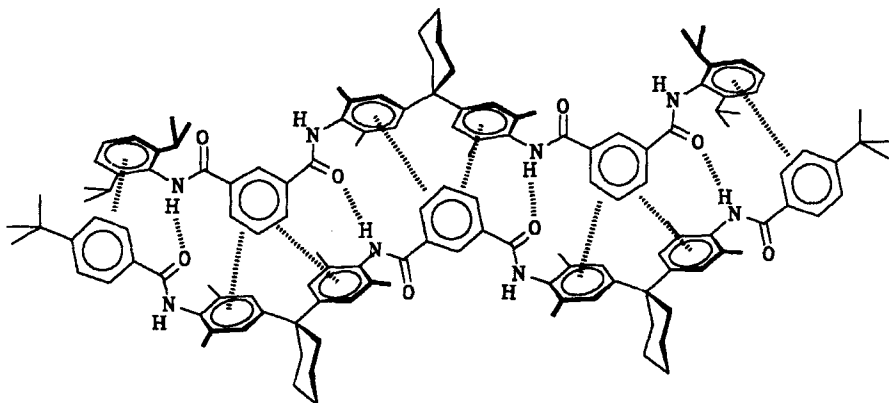


Figure 32 A "molecular zipper" [45]

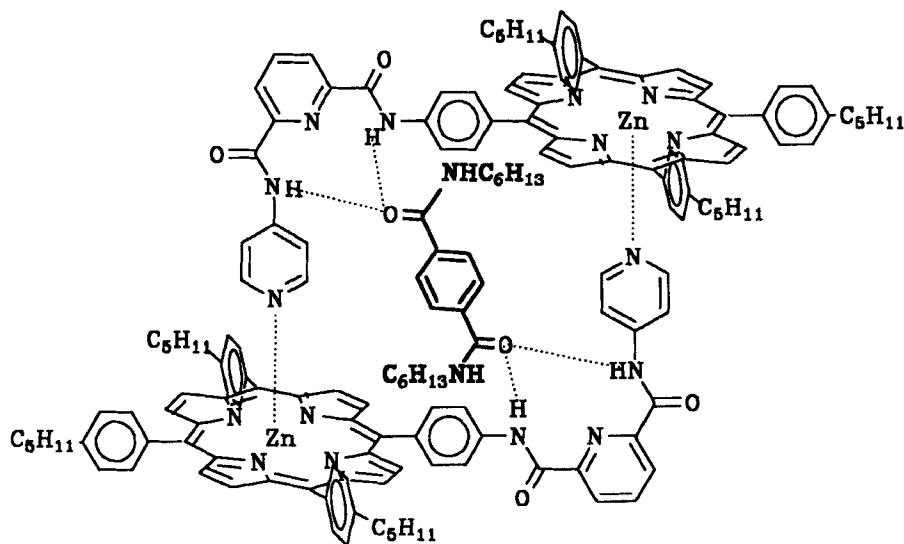


Figure 33 A self-assembled porphyrin receptor shown as its complex with a terephthalic acid derivative [46]

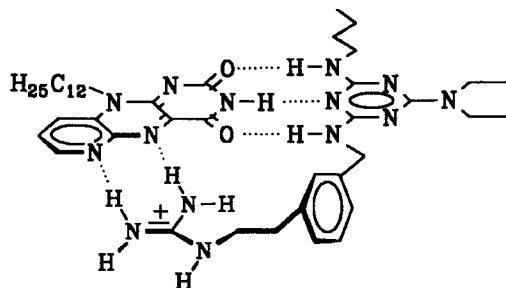


Figure 34 The complex between 6-azaflavin and its melamine-based receptor [47]

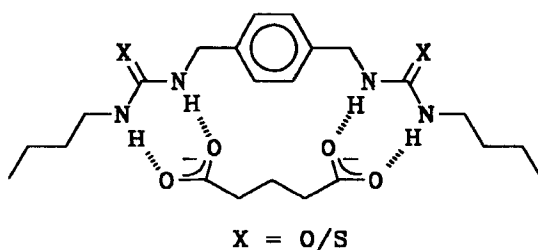


Figure 35 Binding of glutaric acid in D_2O - $DMSO-d_6$ [48]

A melamine derivative containing a guanidinium functionality has been constructed by Yano and coworkers which has exhibited very tight binding (K_a of $1.4 \times 10^5 M^{-1}$ in chloroform) to 6-azaflavin [47]. The proposed structure of the complex has five hydrogen bonds between the host and the guest (Figure 34).

Although hydrogen-bonding interactions have been utilized for host–guest complexation, most studies have been carried out in noncompetitive solvents such as chloroform. Hamilton and coworkers have demonstrated that by modifying both the location and charge of hydrogen-bonding sites, strong binding can be achieved even in highly competitive environments [48]. For example, the receptor–glutarate complex shown in Figure 35 showed K_a values of greater than $5 \times 10^4 M^{-1}$, $8500 M^{-1}$ and $480 M^{-1}$ in $DMSO-d_6$, 12% D_2O - $DMSO-d_6$ and 25% D_2O - $DMSO-d_6$, respectively.

6. BILE-ACID-BASED RECEPTORS

The unique structure and the presence of three hydroxy groups of different reactivity in cholic acid have attracted the attention of a number of research groups for the construction of a variety of receptors.

The inclusion of aromatic guests in the crystal of cholic acid has been investigated by Nassimbeni and coworkers [49]. Crystallographic, thermodynamic and molecular mechanics studies showed that cholic acid prefers nitrobenzene to aniline.

Davis and coworkers have carried out the synthesis of “cholaphanes” which exhibit selectivity in the binding of various octyl glycosides [50].

A strategy involving a polymer-bound, bile-acid-derived host library (Figure 36) for binding opioid peptides has recently been reported by Still and coworkers [51].

The synthesis of bile acid-drug conjugates has recently been reported [52,53]. These molecules are of considerable interest for selective targeting of a drug to the liver. Detailed biological studies on a bile-acid-derived 3-hydroxy-3-methylglutaryl coenzyme A (HMG-CoA) reductase inhibitor have also been reported. The most potent compound (Figure 37) showed an IC_{50} value (concentration for 50% inhibition) of $0.7 \mu M$ [54].

A novel steroidal cyclopeptide (Figure 38) has been synthesized by Albert and Feigl from a steroidal amino acid [55]. Since a variety of amino acids can be incorporated into the macrocycle, this strategy offers attractive possibilities for the construction of functionalized macrocycles for catalyst design.

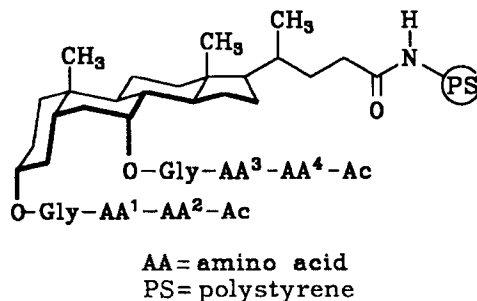


Figure 36 A bile-acid-derived receptor library for opioid peptides [51]

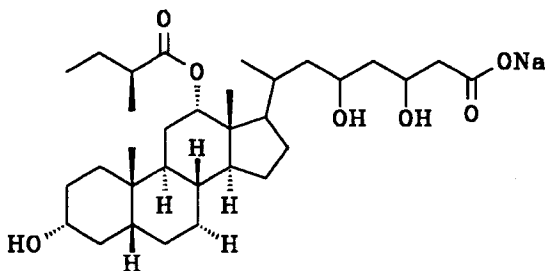


Figure 37 A bile-acid-derived HMG-CoA reductase inhibitor [54]

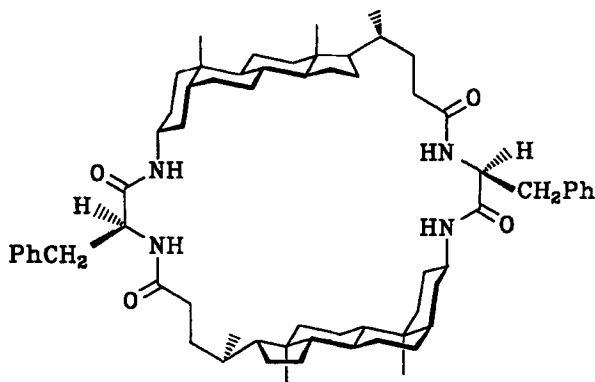


Figure 38 A bile-acid-derived macrocycle with amino acid linkers [55]

The synthesis of the two bile-acid-derived macrocycles shown in Figure 39 were recently reported by us [56]. Even though Corey–Pauling–Koltun (CPK) models showed that the cavities in these two compounds would be able to encapsulate monocyclic aromatic compounds, detailed binding studies carried out in organic solvents with a variety of aromatic compounds did not show any evidence for appreciable binding. There is clearly scope for design improvement to overcome this problem since the construction of this type of macrocycle is synthetically rather flexible.

Some new examples of semi-rigid molecular tweezers have also been constructed by us (Figure 40) which showed moderate association with electron-deficient aromatic compounds in CDCl_3 [57]. The variation in K_a (with the variation of the C7 substituent) was found to correlate with the O3–O12 distance. Novel chromatographic supports may possibly be generated by immobilizing these molecular tweezers [58].

7. BORONIC-ACID-BASED RECEPTORS

The boronic acid functionality is being increasingly used in many ways to complex guests containing diols and carboxylic acid units. A few examples are described below.

Mohler and Czarnik have shown that an *N*-cholanylpyridiniumboronic acid (Figure 41) acts as an efficient carrier of uridine over other nucleosides for transport through liquid membranes [59]. This carrier increased the rates of transport (compared to the background) for adenosine, inosine, cytidine and uridine by 13-fold, 36-fold, 10-fold and 140-fold, respectively.

Shinkai and coworkers have been using the phenylboronic acid moiety for the complexation of saccharides. They have recently shown that the coupling

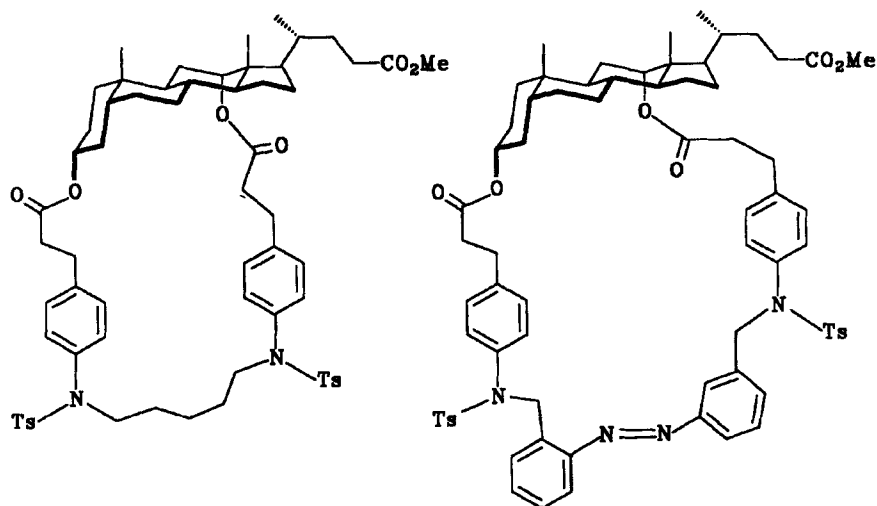


Figure 39 Bile-acid-derived macrocycles [56]

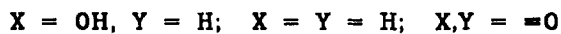
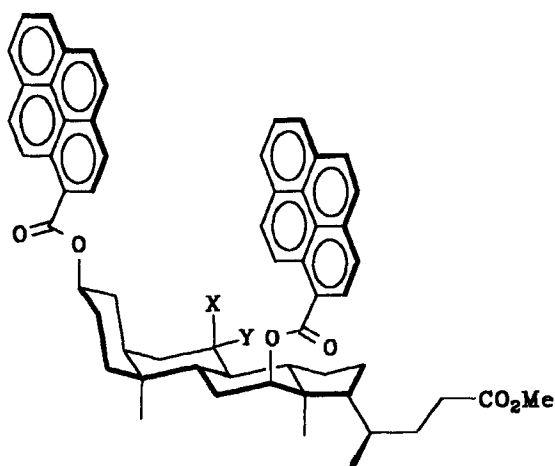


Figure 40 Bile-acid-derived, semirigid molecular tweezers [57]

of this moiety to cholesterol produces a receptor (Figure 42) which can be used for the chiral recognition of monosaccharides in a cholesteric liquid crystal system [60]. Shinkai and coworkers have also shown that stilbene-3,3'-diboronic acid (Figure 43) can act as a fluorescence sensor specifically for

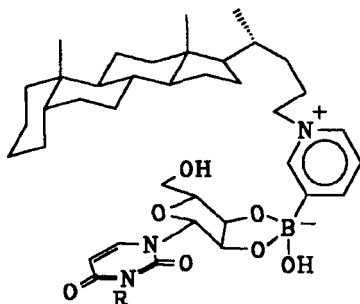


Figure 41 A synthetic carrier for ribonucleoside transport [59]

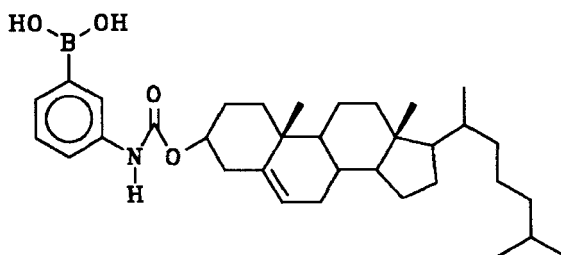


Figure 42 A cholesterol-based monosaccharide sensor [60]

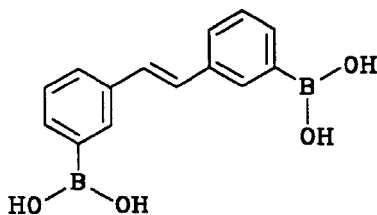


Figure 43 A boronic-acid-based disaccharide sensor [61]

disaccharides [61]. This molecule showed strongly enhanced fluorescence in the presence of melibiose. Simultaneous complexation of both boronic acid groups by the two sugar units was suggested to enhance the fluorescence by preventing the rotation of the excited stilbene chromophore about the ethylenic double bond. A saccharide sensor (Figure 44) has also been developed by Sandanayake and Shinkai [62]. They showed that some saccharides (e.g. D-fructose) gave rise to an observable color change at neutral pH. A glucose-

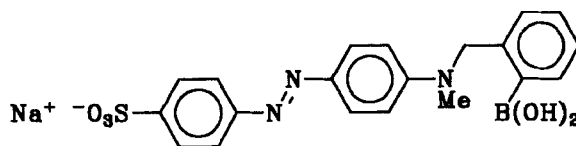


Figure 44 A boronic-acid-based saccharide sensor [62]

selective molecular fluorescence sensor (Figure 45) has also been reported by Shinkai and coworkers. This compound was used in an assay of glucose in the presence of low concentrations of D-fructose and D-galactose [63].

A phenylboronic-acid-functionalized 18-crown-6 system (Figure 46) has been constructed as a ditopic carrier for dopamine [64]. Under defined experimental conditions, this carrier increased dopamine transport through a liquid membrane 160-fold. Selectivity for the transport of dopamine over epinephrine, norepinephrine, tyramine and a few glycosides was reported. It has been suggested that dopamine transport occurs through a zwitterionic species formed by the complexation of the ammonium group with the crown, and the catechol unit with the boronic acid. Interestingly, Reetz *et al.* have shown that simply by mixing a phenylboronic acid with a crown ether, an amino acid such as L-phenylamine can be transported through a chloroform

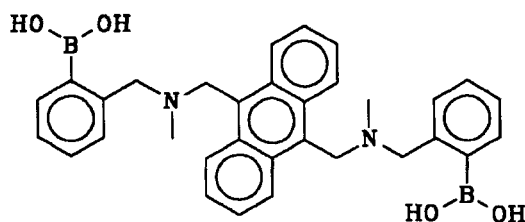


Figure 45 A glucose-selective fluorescence sensor [63]

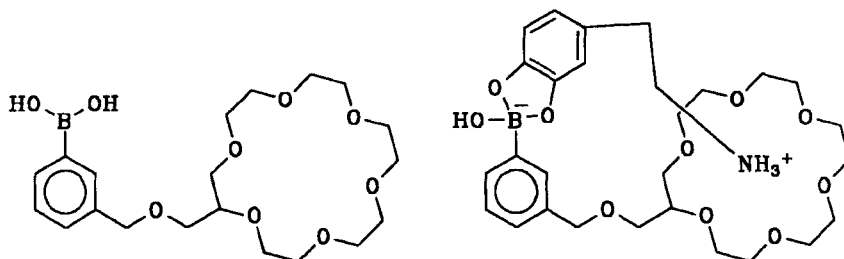


Figure 46 A crown boronic acid for selective dopamine transport [64]

liquid membrane. Using 18-crown-6 and 3,5-bis(trifluoromethyl)phenylboronic acid they showed that the transport rate was enhanced by a factor of 1270. The structure shown in Figure 47 has been postulated for the species which carries the zwitterionic amino acid through a liquid membrane. The crystal structure of phenylalanine with the carrier system has provided evidence for this structure for the complex [65].

8. ANION RECOGNITION [66]

Sessler and coworkers have recently developed a high-performance liquid chromatography (HPLC) support with sapphyrin-functionalized silica gel [67]. Oxyanions were found to interact with the sapphyrin unit, and thus they were retained longer compared to an appropriate control support. The separations of adenosine, adenosine 5'-phosphate (AMP), adenosine 5'-diphosphate (ADP) and ATP, and dimers to nonamers of polydeoxyadenylic acids at *neutral* pH were also achieved.

Reinhoudt and coworkers have shown a calix[4]arene UO_2 -salen complex (Figure 48) to be a selective receptor for H_2PO_4^- in DMSO, in which other anions such as chloride, bisulfate and perchlorate showed insignificant binding [68].

A bifunctional receptor constructed by coupling two crown ether fragments to a UO_2 -salen complex has been reported for the simultaneous complexation of anions and cations [69]. This compound, shown in Figure 49, showed high selectivity in binding potassium dihydrogen phosphate. Selectivity of the membrane transport of H_2PO_4^- (over Cl^-) has also been shown [70].

A number of simple amides and sulfonamides (Figure 50) have been shown by Reinhoudt and coworkers to bind anions exclusively through hydrogen bonding. For example, the naphthalenesulfonamide binds H_2PO_4^- , HSO_4^- and Cl^- with association constants of $1.42 \times 10^4 \text{ M}^{-1}$, 38 M^{-1} and 1600 M^{-1} , respectively [71].

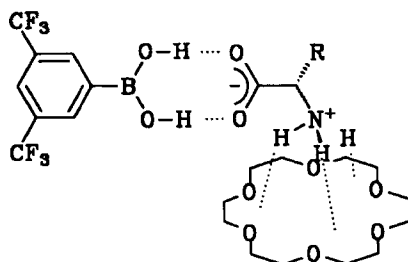


Figure 47 A complex of an amino acid with a crown ether and an arylboronic acid [65]

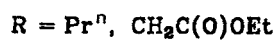
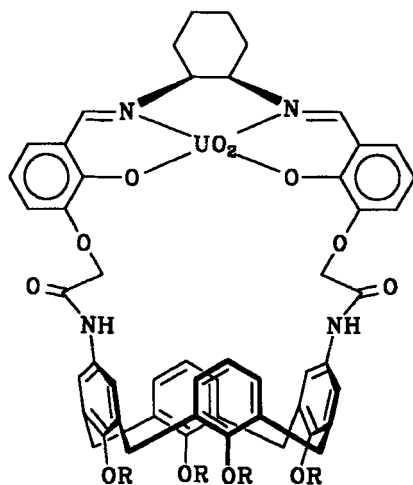


Figure 48 A bifunctional receptor for NaH_2PO_4 [68]

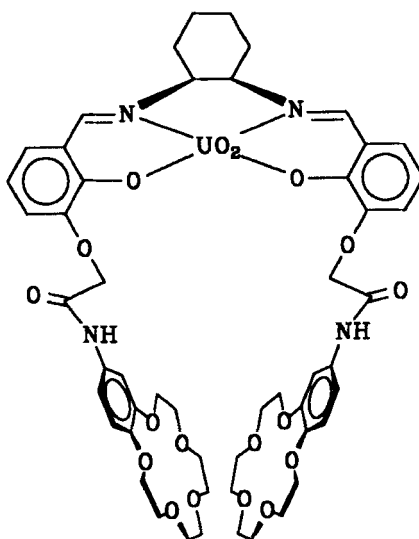


Figure 49 A bifunctional cleft for KH_2PO_4 [69]

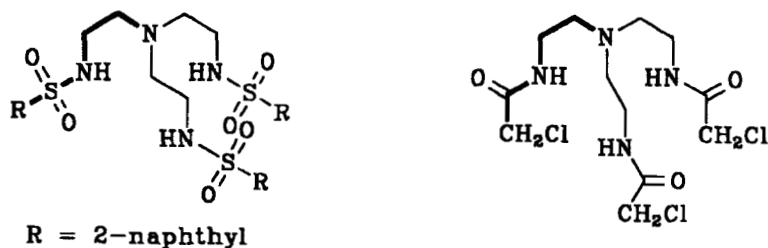


Figure 50 Neutral anion receptors with high selectivity for H_2PO_4^- [71]

Beer *et al.* have constructed a bipyridylruthenium(II) calix[4]arene receptor (Figure 51) for anion recognition [72]. Electrochemical studies showed this receptor to recognize H_2PO_4^- in the presence of a 10-fold excess of bisulfate or chloride.

Beer *et al.* have also reported the design and synthesis of a variety of chloride and bromide “chelators” by the combination of a charged or neutral organometallic and coordinated transition metal Lewis acidic center with amide NH groups (Figure 52) [73]. Electrostatic interactions and favorable $\text{NH}\cdots\text{X}^-$ hydrogen bonding were found to be responsible for the binding

Mussons *et al.* have shown that the phosphoramidate shown in Figure 53 binds 1,1-diacids very tightly, in some cases with a K_a of the order of 10^5 M^{-1} [74].

Gellman and coworkers have reported the binding of ammonium ions, as well as halide ions, in methanol–chloroform by a macrocycle containing a phosphine oxide and two sulfoxide functionalities (Figure 54) [75]. Monoalkylammonium halides (except fluoride) were found to bind *via* both anion and cation complexation.

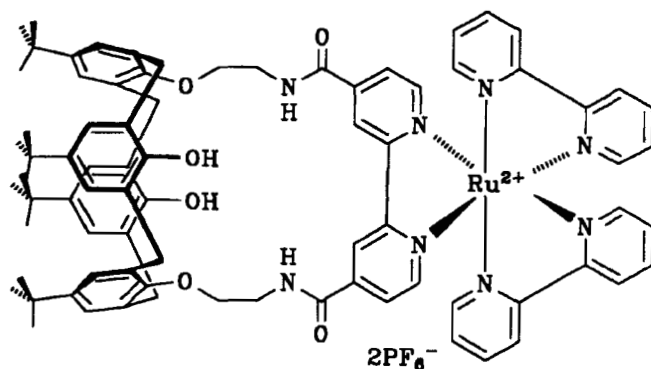


Figure 51 A bipyridylruthenium(II) calix[4]arene receptor for anions [72]

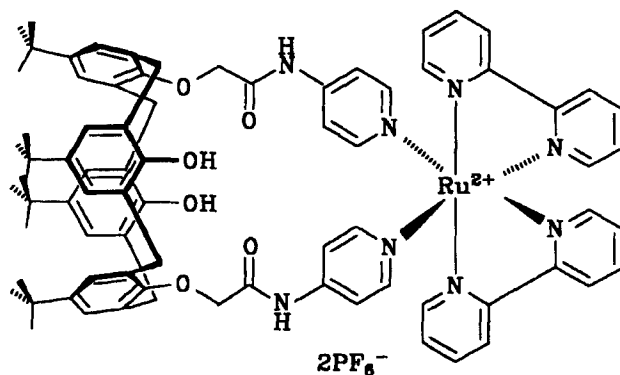


Figure 52 A calix[4]arene-based anion receptor [73]

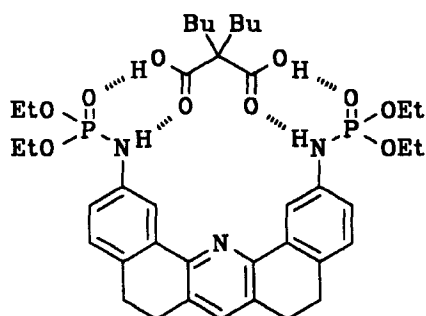


Figure 53 Dibutylmalonic acid binding by a phosphoramidate [74]

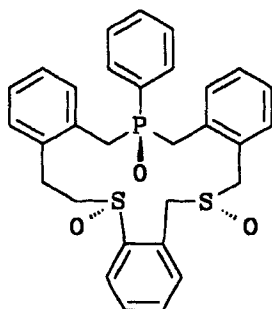


Figure 54 A phosphine oxide sulfoxide macrocycle for anion and ion pair complexation [75]

9. WATER-SOLUBLE RECEPTORS

Wennemers and Still have recently reported that common, commercially available dyes (such as rhodamine methyl ester, crystal violet, Safranin O, phenol red, xlenol orange, etc.) bind certain acylated tripeptides attached to hydrophilic poly(ethylene glycol)–polystyrene beads with high selectivity in water [76]. They suggested that hydrophobic interactions and electrostatic interactions are the driving forces for the binding.

Peterson and Diederich have recently synthesized a water-soluble macrocycle containing a large hydrophobic cavity (Figure 55) [77]. This molecule has been shown to increase the water solubility of steroids severalfold. A 1 mM solution of the host was found to increase the water solubility of cholesterol to $850\ \mu\text{M}$ (from $4.7\ \mu\text{M}$ in pure water). It has been suggested by these authors that further studies along these lines might lead to the development of alternative drugs for the dissolution of cholesterol deposits *in vivo*.

Collet and coworkers have investigated the binding of acetylcholine and related ammonium ions to water-soluble cryptophanes [78]. The receptor shown in Figure 56 was found to bind choline and acetylcholine with moderate affinity (the highest affinity being shown by the tetramethylammonium cation). Interestingly, the ΔG° values of binding for choline and acetylcholine (*ca.* $-5\ \text{kcal mol}^{-1}$) are comparable to those reported for acetylcholine esterases. These authors have suggested that a loose association, rather than a tight lock-and-key fit, is required for tight binding in this system.

A water-soluble cyclic AMP (cAMP) receptor (Figure 57) has been reported by Rebek and coworkers [79]. Both 2',3'-cAMP and 3',5'-cAMP were shown to bind to this receptor with association constants of 660 and $600\ \text{M}^{-1}$,

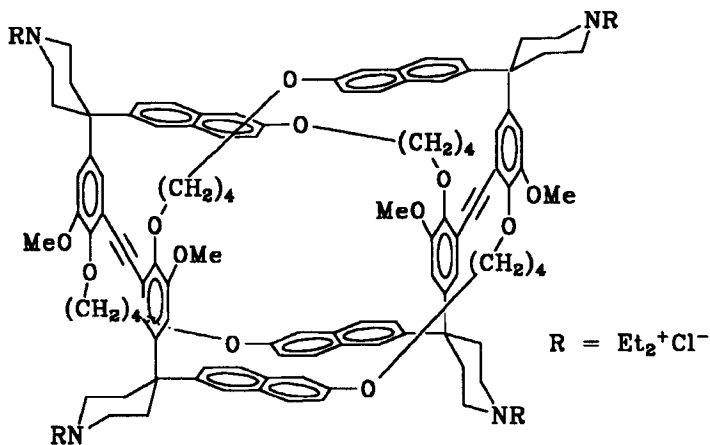


Figure 55 A water-soluble receptor for the dissolution of cholesterol [77]

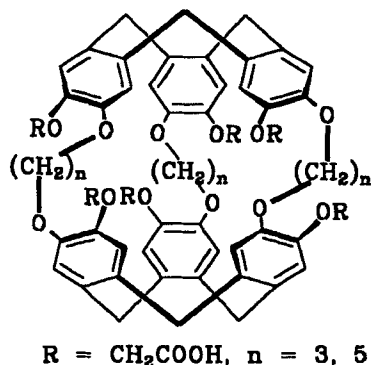


Figure 56 A water-soluble cryptophane for binding alkylammonium guests [78]

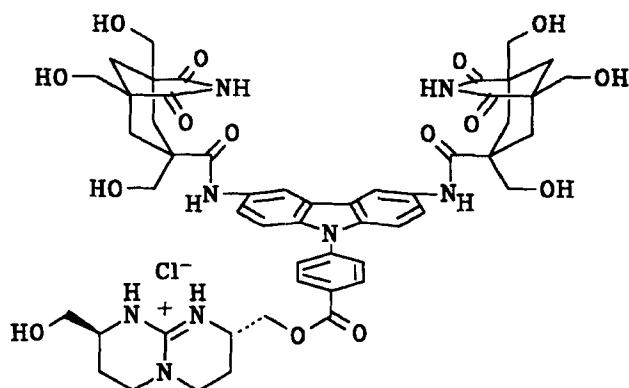


Figure 57 A water-soluble cAMP receptor [79]

respectively. These authors have estimated the phosphate–guanidinium electrostatic interaction in this system, and have reported a contribution of $\sim 0.6 \text{ kcal mol}^{-1}$ at 51 mM ionic strength.

A systematic study to design neutral, water-soluble calix[4]arenes has been carried out by Gansey *et al.*, and this has led to the synthesis of calixarene derivatives with water solubility up to 0.3 M [80].

A water-soluble cyclophane receptor (Figure 58) has been reported to form intracavity complexes with adenine derivatives with association constants of the order of 100 M^{-1} [81].

A polysulfonated calix[6]arene host (Figure 59) in water has been investigated for its binding to ferrocene derivatives by cyclic voltammetry and NMR [82]. Association constants of the order of 10^3 – 10^4 M^{-1} were observed. Polysulfonated calix[*n*]arenes for $n=4, 6$ and 8 were also found to include chiral quaternary ammonium guests in water (Figure 60) [83]. This

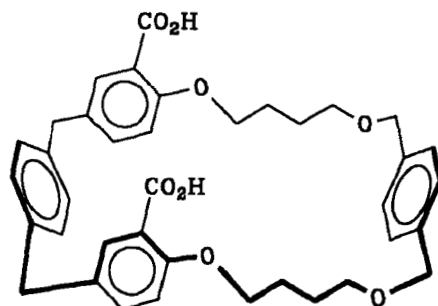


Figure 58 A water-soluble cyclophane receptor for adenine derivatives [81]

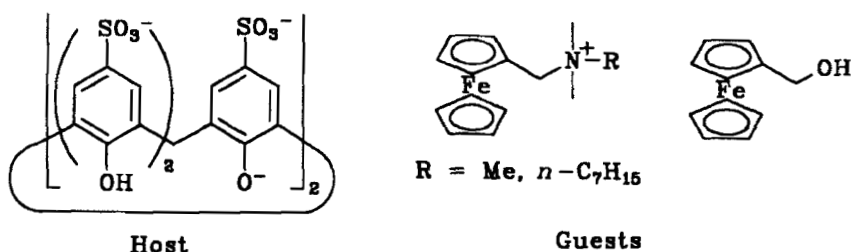


Figure 59 A water-soluble calix[6]arene host and ferrocene-derived guests [82]

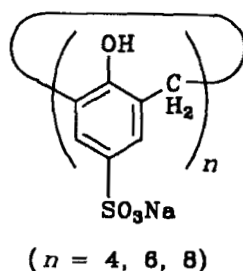


Figure 60 Calixarene-based receptors for ammonium cations [83]

binding was monitored by NMR and also by the induced circular dichroism exhibited by the host as a result of the guest-induced asymmetric deformation.

Molecular recognition in micelles has been studied by Nowick *et al.* [84]. Sodium dodecyl sulfate (SDS) micelles were used to provide a microenvironment to achieve hydrogen-bonding interactions between appropriate partners solubilized in the micelle. Nowick *et al.* observed that the adenine and thymine

derivatives, shown in Figure 61, base *pair* in SDS, whereas in the absence of the detergent they base *stack*. A model has been proposed in which the adenine derivative partitions between the exterior and interior of the micelles and the thymine binds the *intramicellar* adenine.

10. MISCELLANEOUS RECEPTORS

Shea *et al.* have prepared an imprinted polymer (a matrix of polymethacrylate) using 9-ethyladenine (9-EA) as a template (Figure 62) [85]. They have shown that the average association constant for this substrate is of the order of $7.6 \times 10^4 \text{ M}^{-1}$. This polymer showed high selectivity for adenine derivatives over other nucleic acid bases. These imprinted polymers are easy to synthesize, and are likely to provide great analytical opportunities.

Kemp's triacid has been utilized extensively by Rebek and coworkers in constructing a variety of molecular clefts. Recently, Curran *et al.* have synthesized an amino diacid variant of this versatile molecule (Figure 63) [86].

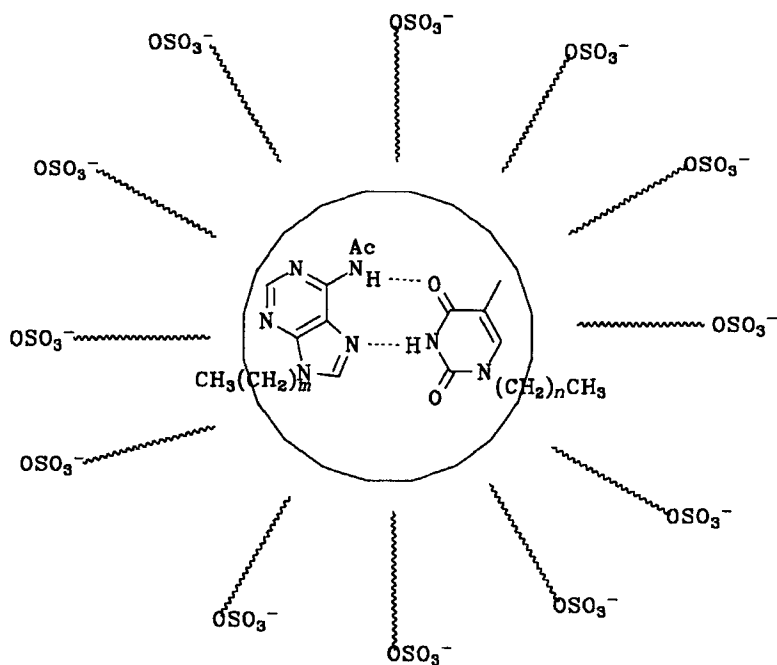


Figure 61 Molecular recognition in aqueous micelles [84]

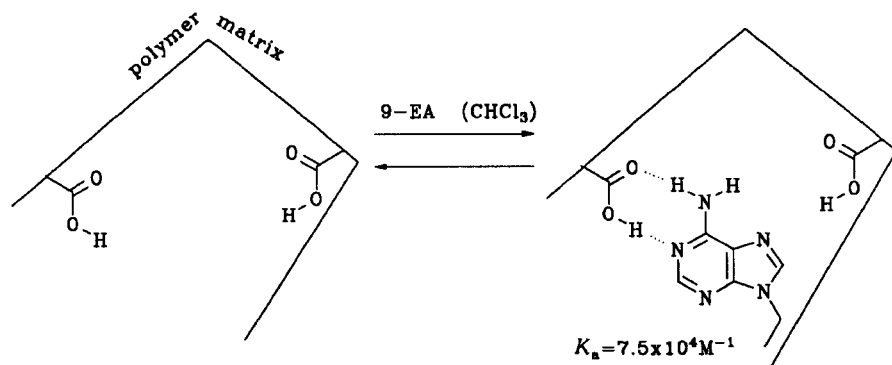


Figure 62 An imprinted polymer host for binding adenine derivatives [85]

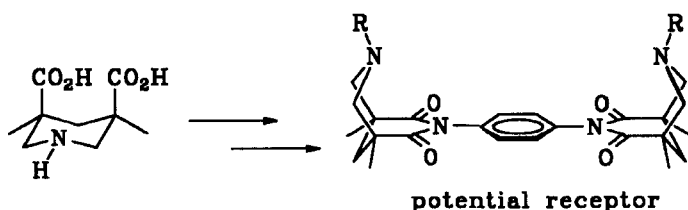


Figure 63 An amino diacid variant of Kemp's triacid and the structure of a potential receptor [86]

This amino diacid is likely to be of interest to design new types of molecular receptors.

Lindsay *et al.* have described the synthesis of porphyrin building blocks for the modular construction of bioorganic model systems, particularly for the construction of systems for studying energy transfer [87].

Cram and coworkers have crafted a variety of carcerands and hemicarcerands and studied their properties. The complexed guest has also been made to undergo chemical transformations [88].

Martinez-Diaz *et al.* have reported the synthesis of chiral podands and macrocycles based on 1,2,4-triazole (Figure 64) [89]. They have observed enantioselective transportation of chiral ammonium cations through supported liquid membranes.

Diederich and coworkers have reported the chiral recognition of cinchona alkaloids at the minor and major grooves of 1,1'-binaphthyl receptors (Figure 65) [90]. Diederich and Carcanague have reported the construction of large, water-soluble cyclophane receptors (Figure 66) with convergent *intracavity* functionalities [91]. The binding constants of some naphthalene derivatives were found to be of the order of $10\text{--}100 \text{ M}^{-1}$.

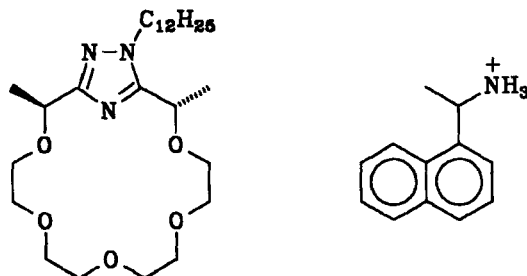


Figure 64 A chiral crown ether based on 1,2,4-triazole, and its guest [89]

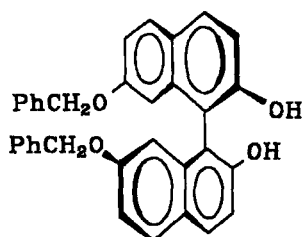


Figure 65 A chiral receptor for cinchona alkaloids [90]

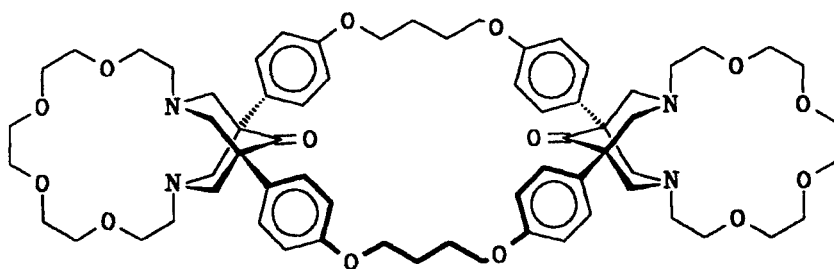


Figure 66 A cyclophane with intracavity functionalities [91]

A neutral ditopic receptor for AMP has been reported by Lacy *et al.* which was synthesized by coupling a UO_2 -salen to a thymine unit. This receptor binds $H_2PO_4^-$ and 9-butyladenine. The association constant in DMSO for adenosine 3'-phosphate was estimated to be 1200 M^{-1} . The proposed structure for the complex is shown in Figure 67 [92].

Collet and coworkers have reported studies with a cryptophane (Figure 68) which binds methane and chlorofluorocarbons in 1,1,2,2-tetrachloroethane [93]. The association constants were of the order of 100 M^{-1} , and the authors

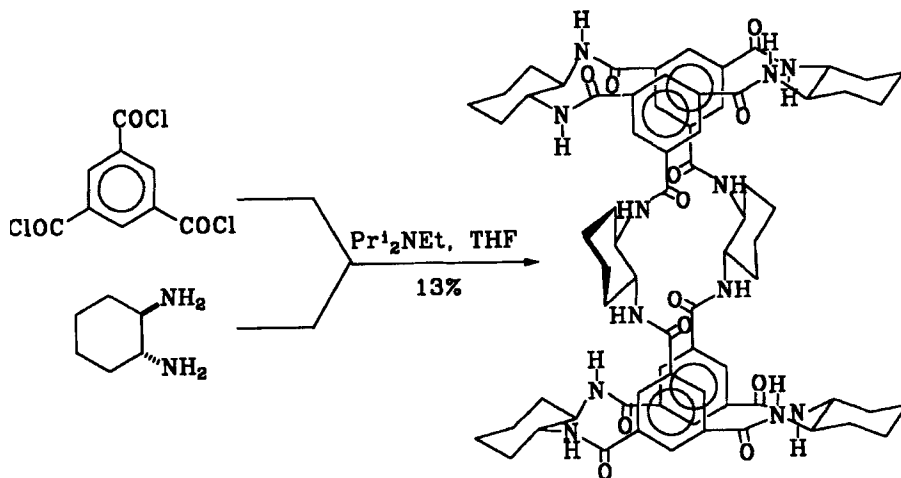


Figure 69 A synthetic, high-enantiodifferentiation receptor for peptides [94]

binding. Assignment of the amino acid sequence *via* an assay involving electron-capture gas chromatography (GC) helped in the identification of the tight-binding substrates. This method, however, is limited to substrates which are easy to prepare by combinatorial methods.

A related bowl-shaped host modified with a dye (Figure 71) has also been used by the same researchers in an analogous manner in order to test the binding of a library of peptides [96]. Highly selective binding of (L)X–(L)Pro–(L)X (Pro = proline) was observed, with a binding constant of $2.5 \times 10^5 \text{ M}^{-1}$ for $\text{Pr}^i\text{CO}-(\text{L})\text{Ala}-(\text{L})\text{Pro}-(\text{L})\text{Ala}-\text{NHC}_{12}\text{H}_{25}$.

Rebek and coworkers have also recently published a procedure for the synthesis of libraries of small organic molecules, and have designed a screening method for the isolation of active compounds from such libraries. A trypsin inhibitor with a K_i of $9 \mu\text{M}$ was found from the screening of a library [97].

A basket-shaped, macrotricyclic cyclophane receptor with a deep cavity (Figure 72) has been utilized by Meric *et al.* for binding quaternary ammonium cations [98]. Association constants of the order of 10^3 – 10^4 M^{-1} were reported.

A receptor for *cis*-1,3,5-cyclohexanetricarboxylic acid has been reported by Ballester *et al.* (Figure 73) [99]. Evidence for three pairs of hydrogen bonds between the host and the guest was reported. An association constant greater than 10^5 M^{-1} was estimated.

Kuroda *et al.* have reported a porphyrin-based “molecular trench” (Figure 74) with highly complementary binding sites for tartaric acid dialkyl esters showing association constants as high as 10^6 M^{-1} [100].

A synthetic molecular tweezer in which two dibenzofuran units are oriented parallel with a separation of $\sim 10 \text{ \AA}$ has recently been reported by Harmata *et*

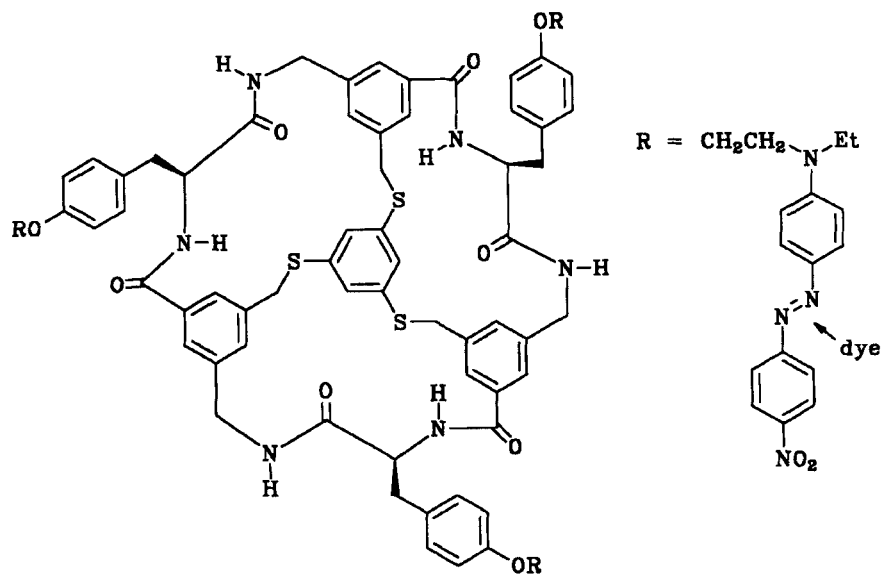


Figure 70 A dye-linked receptor for binding an encoded library of small peptides [95]

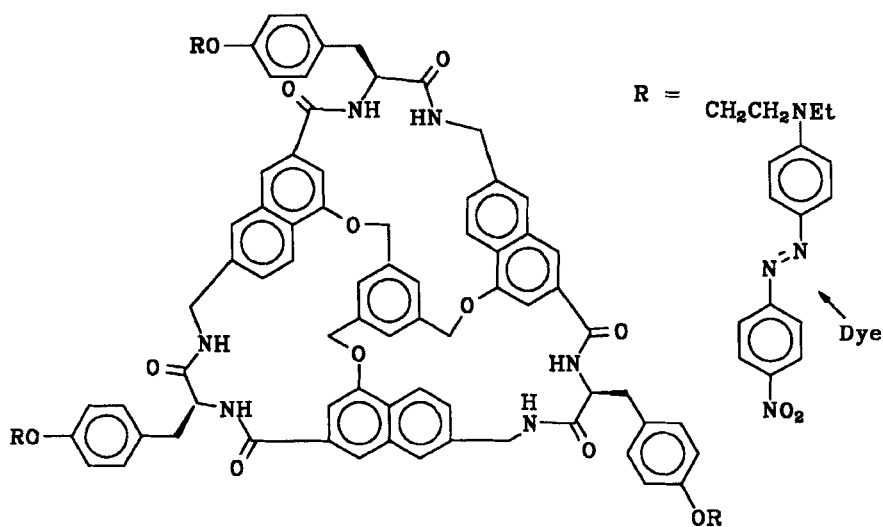


Figure 71 A dye-linked receptor for the internal residues of a peptide chain [96]

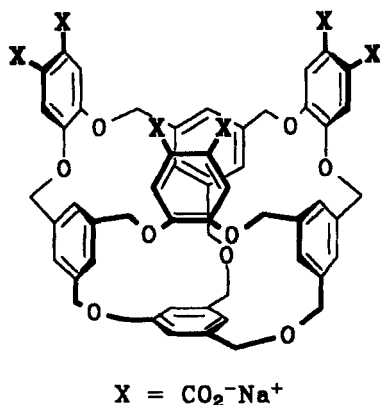


Figure 72 A basket-shaped macrotricyclic receptor for the complexation of quaternary ammonium cations [98]

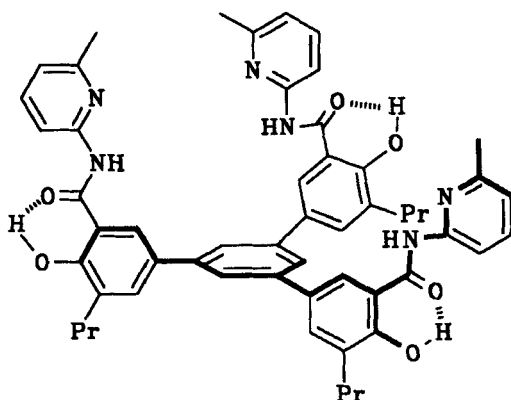


Figure 73 A receptor for *cis*-1,3,5-cyclohexanetricarboxylic acid [99]

al. [101]. The host and the crystal structure of its complex with 1,3,5-trinitrobenzene are schematically shown in Figure 75. This structure clearly shows the inclusion of two π -systems in the cleft.

A zinc(II) complex of 1,4,7,10-tetraazacyclododecane with a pendent acridine unit (Figure 76) has shown tight binding with N3-deprotonated 2'-deoxythymidine (dT) ($\log K_a$ of 7.2) [102]. The acridine unit was found to increase the binding by a factor of ~ 60 . Also 2'-deoxyguanosine (dG) in its N1-deprotonated form showed a $\log K_a$ of 5 whereas 2-deoxycytidine (dC) and 2-deoxyadenosine (dA) did not bind at all.

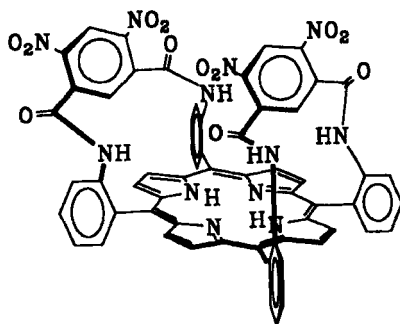


Figure 74 A “molecular trench” for the complexation of tartaric acid dialkyl esters [100]

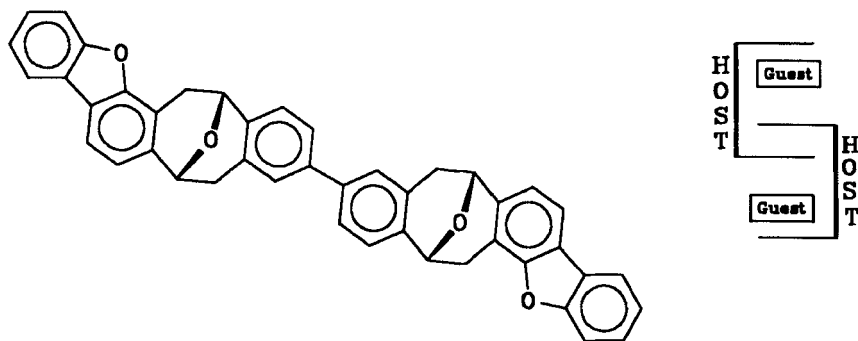


Figure 75 A molecular tweezer and schematic representation of its crystal structure with 1,3,5-trinitrobenzene as the guest [101]

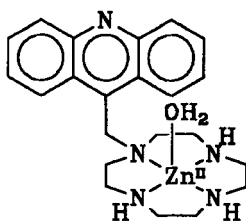


Figure 76 A polytopic receptor for nucleobases [102]

Ballardini *et al.* have reported detailed photophysical studies with a cylindrical macrotricyclic receptor (Figure 77) and its complexes with protons, ammonium ions and $[\text{Pt}(\text{NH}_3)_2(\text{bipy})]^{2+}$ [103].

Murakami *et al.* have reported binding studies on (4Z, 15Z)-bilirubin IX α and pamoic acid with a water-soluble, chiral, cage-type cyclophane (Figure 78)

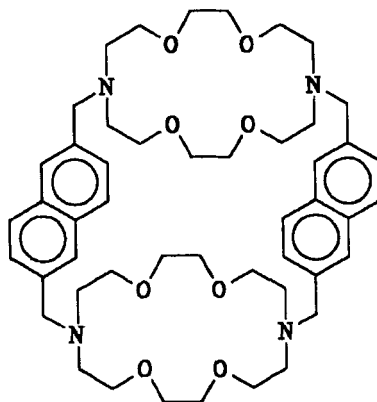


Figure 77 A cylindrical macrotricyclic receptor [103]

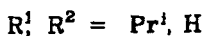
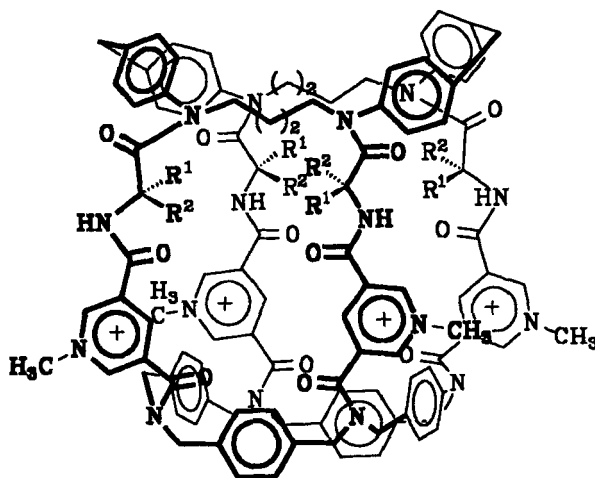


Figure 78 A chiral, water-soluble cyclophane for enantioselective binding [104]

using CD spectroscopy [104]. Their results showed that the host was able to discriminate the conformational enantiomers of these two guest molecules. It was concluded from the analysis of CD spectra that the (+)-host selectively bound bilirubin with (*S*)-helicity.

A number of new preorganized molecular clefts (an example is shown in Figure 79) have been synthesized by Rebek and coworkers [105]. The molecule

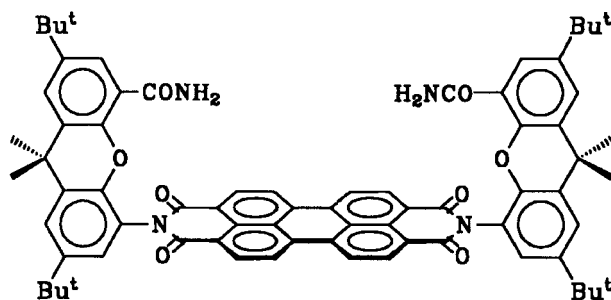


Figure 79 A perylene-based molecular cleft [105]

in Figure 79 was demonstrated to bind phenazine (1 : 1 complex) in chloroform with an association constant of 149 M^{-1} . Rebek and coworkers have also reported the synthesis of a water-soluble receptor which binds an association constant of 70 M^{-1} .

Evidence for ditopic binding by a self-assembled receptor (Figure 80) has been presented by Lee and Schwabacher [106]. They studied the binding of several indole and naphthalene derivatives bearing carboxylate sidearms. 1-Naphthyloxy acetate and the corresponding 1,5-diacetate showed the tightest binding (K_D of $\sim 10^{-4}$ and $\sim 10^{-5} \text{ M}$, respectively).

The binding of various nucleobases by a molecular tweezer has been studied by Vögtle and coworkers [107]. They found that this receptor (Figure 81) bound 2,6-diaminopurine and adenine with K_a of the order of 10^4 M^{-1} . 2-Aminopurine, cytosine, guanine and 2,4-dihydroxypteridine did not show any observable binding.

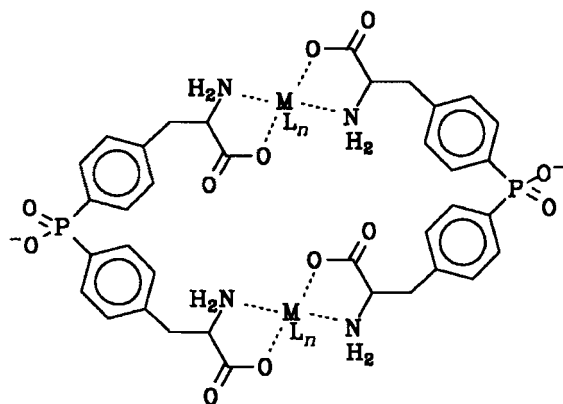


Figure 80 A self-assembled receptor for ditopic binding [106]

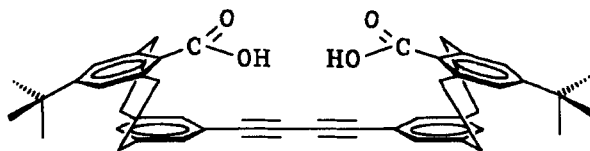


Figure 81 A molecular tweezer for binding nucleobases [109]

A boxlike cyclophane receptor has been reported to complex *p*-nitrophenol with an association constant greater than $4 \times 10^5 \text{ M}^{-1}$ in CDCl_3 (Figure 82) [108]. Large K_a values were observed in solvents such as chloroform and tetrachloroethane, whereas smaller solvent molecules such as CD_2Cl_2 and 1,2-dichloroethane lowered the binding. A similar effect was earlier reported by Chapman and Still [109].

11. CATALYSIS

Breslow and Zhang have reported the cleavage of phosphate di- and triesters by a cyclodextrin dimer (Figure 83) in the presence of La^{3+} and H_2O_2 [110]. High rate acceleration, up to $\sim 10^8$, was reported for this enzyme mimic.

Selective oxidation of benzylic alcohols (bearing phenolic functionalities) by a metallohost (Figure 84) containing a substrate-binding site and two

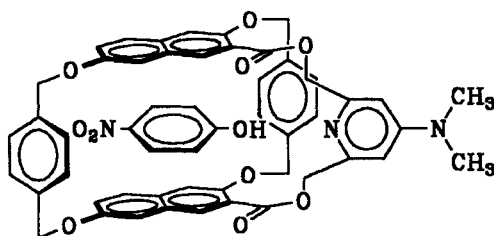


Figure 82 An efficient *p*-nitrophenol receptor [108]

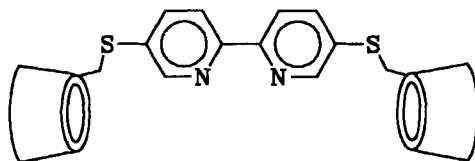


Figure 83 A bis(β -cyclodextrin) catalyst for the hydrolysis of phosphate esters [110]

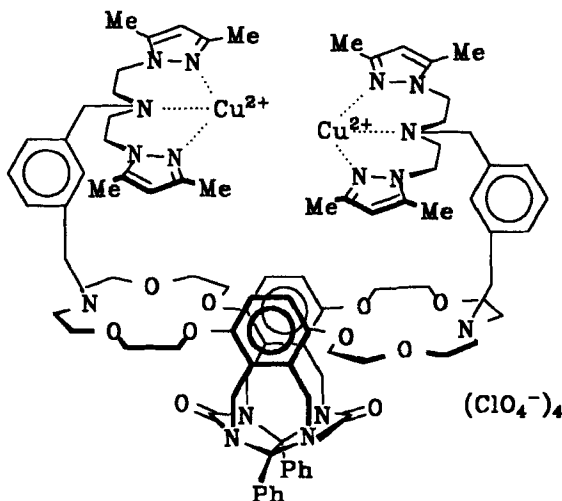


Figure 84 A catalyst for the oxidation of benzylic alcohols [111]

copper(II) ions has been reported by Nolte and coworkers [111]. Rate enhancements of at least four orders of magnitude were reported for 3-hydroxy- and 3,5-dihydroxybenzyl alcohols.

A recent publication from Moran and coworkers reports a molecule which catalyzes the Michael addition of pyrrolidine to 2(5H)furanone [112]. The ground-state molecule does not bind very tightly; however, the 1,4-addition of pyrrolidine creates a carboxylate like species (Figure 85) which is expected to bind more tightly. As the data in Table 2 show, the addition of 10 mol% of the catalyst considerably speeded up the reaction.

Gobel *et al.* have prepared a synthetic phosphodiesterase by combining an amidinium binding unit and a hydroxy nucleophile [113a]. More recently, a chiral version of a similar structure has been reported by Gobel and coworkers

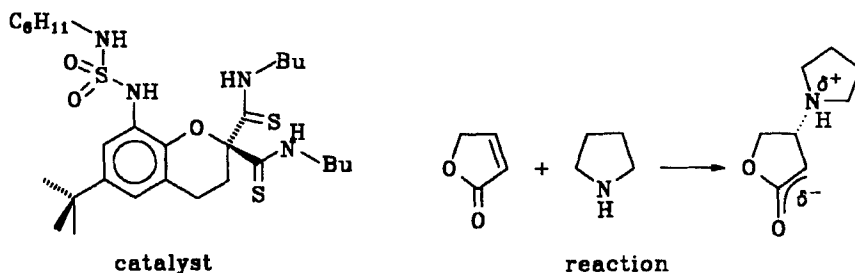


Figure 85 Catalysis of a Michael reaction [112]

Table 2 Rate data for the reaction shown in Figure 85

Conditions	Half-life, $t_{1/2}$ (min)
No catalyst	125
With 10 mol% catalyst	16

(Figure 86) [113b]. Functionalized forms of these chiral molecules will be of interest in designing new catalytic systems.

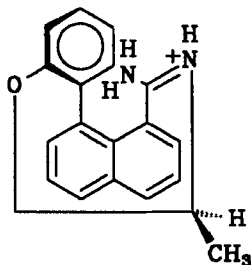
Sanders and coworkers have reviewed their strategy toward the construction of synthetic enzymes based on porphyrins and steroids [114]. One notable example is the acceleration of a Diels–Alder reaction between a pyridine-appended diene and dienophile in the presence of the catalyst, shown in Figure 87. The reaction partners bind to the inside of the host, resulting in a close proximity of their reactive ends.

12. MOLECULAR AND IONIC SENSORS

Murakami and Shinkai have reported a calix[4]arene-based molecular receptor which changes from a closed form (*intramolecular* hydrogen bonds) to an open form (*intermolecular* hydrogen bonds with a pteridine guest) upon Na^+ binding (Figure 88) [115]. Reduction of the fluorescence of the pteridine unit was observed in the presence of Na^+ and the receptor, thereby providing evidence for the structure of the complex as shown.

Shinkai and coworkers have developed a highly selective Ca^{2+} extractant based on *t*-butylcalix[4]arene (Figure 89) [116]. They showed that at pH 5.3, ~60% of Ca^{2+} was extracted from a mixture also containing Mg^{2+} , Sr^{2+} and Ba^{2+} . The other alkaline-earth metal ions were not extracted at all.

An anthracene-derived chemosensor has been synthesized by Hong and Czarnik. They have shown that this molecule (Figure 90) acts as a *metal-ion-insensitive* polyanion sensor [117]. This molecule was used for a real-time assay

**Figure 86** An axially chiral amidinium species [113b]

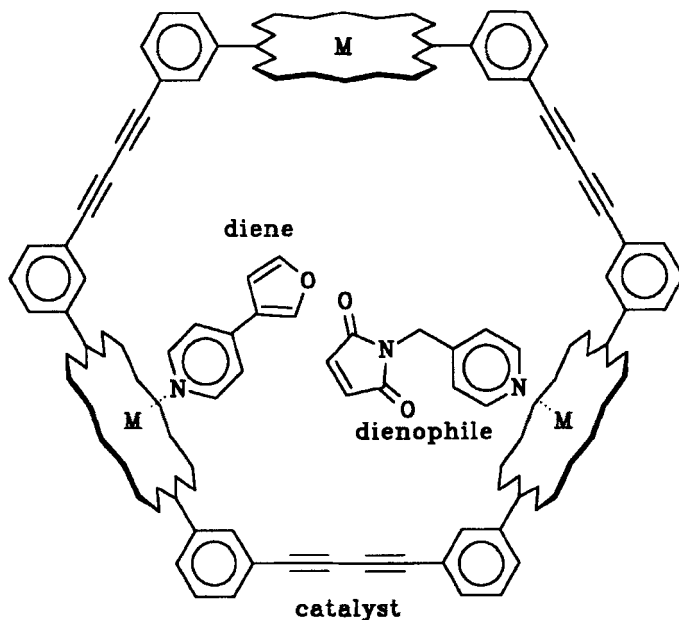


Figure 87 A porphyrin-based catalyst for the Diels-Alder reaction [114]

to monitor the hydrolysis of single-stranded and double-stranded DNA, permitting the rapid survey of metal activations.

Vance and Czarnik have also developed a new chemosensor for pyrophosphate based on an anthracene chromophore (Figure 91) [118]. This compound exhibits low fluorescence. However, upon binding pyrophosphate, the fluorescence increases considerably. It has been shown by Vance and Czarnik that inorganic pyrophosphatase can be assayed in real time using this chemosensor since the inorganic phosphate produced does not affect the fluorescence of this molecule.

Inouye *et al.* have designed a sensitive and selective cryptand-type crown spirobenzopyran sensor for alkaline-earth metal cations (Figure 92) [119]. Upon metal ion complexation, the spirocycle opens up, resulting in a large increase in the absorption in the visible range. For $n=1$ and 2 the selectivity orders were found to be $\text{Ca}^{2+} > \text{Mg}^{2+} > \text{Sr}^{2+}$ and $\text{Sr}^{2+} > \text{Ba}^{2+} > \text{Ca}^{2+}$, respectively.

An anthracene-based fluorescent sensor for transition metal ions (Figure 93) has been developed by Fabbrizzi *et al.* [120]. They have shown that at an appropriate pH (6–8), the addition of Mn^{2+} , Co^{2+} or Zn^{2+} does not affect the fluorescence. However, the addition of Cu^{2+} or Ni^{2+} ions results in a sharp

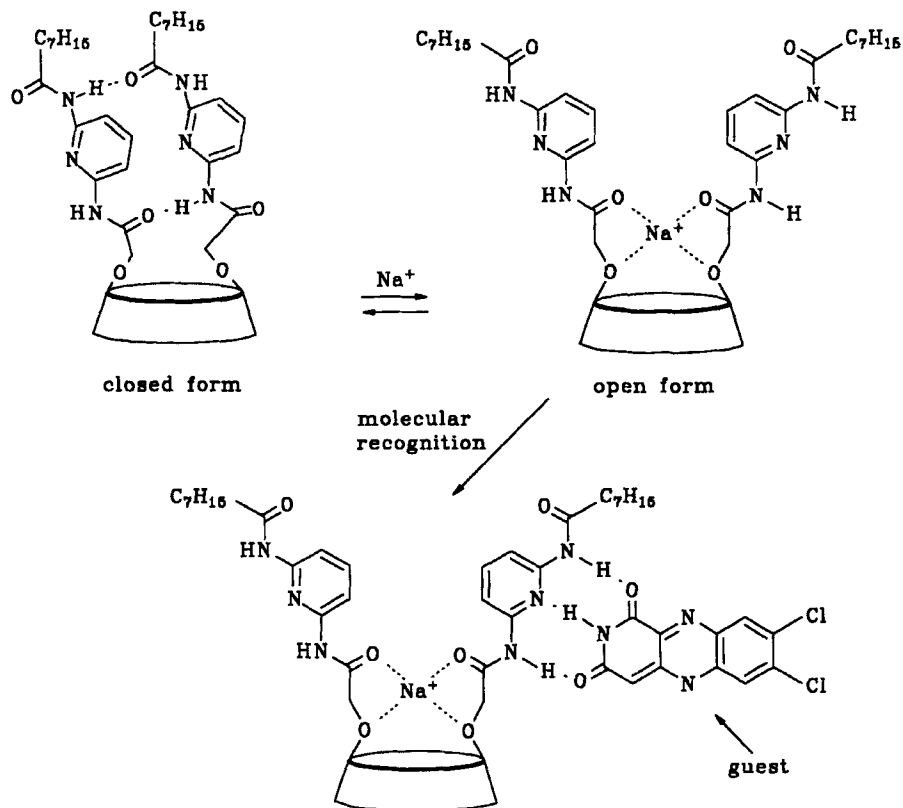


Figure 88 A fluorescence sensor for a molecular recognition process [115]

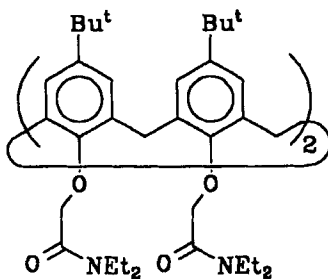


Figure 89 A Ca^{2+} -selective calixarene extractant [116]

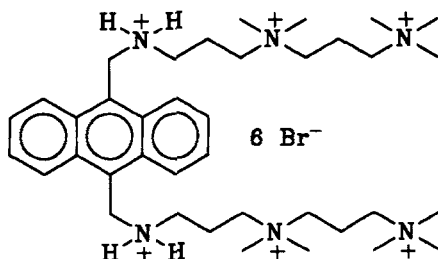


Figure 90 A metal-ion-insensitive polyanion chemosensor [117]

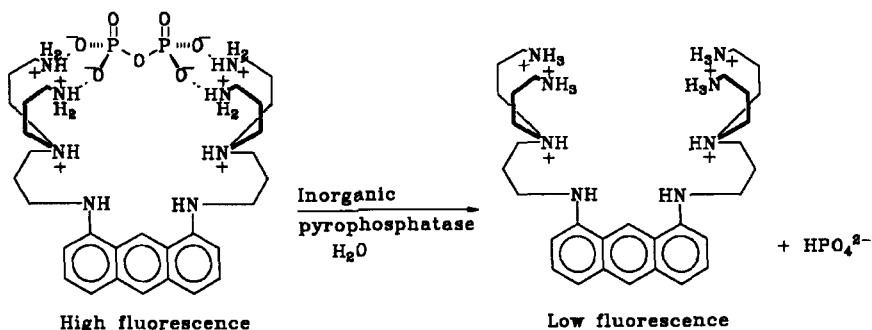


Figure 91 Inorganic phosphatase assay using a synthetic chemosensor [118]

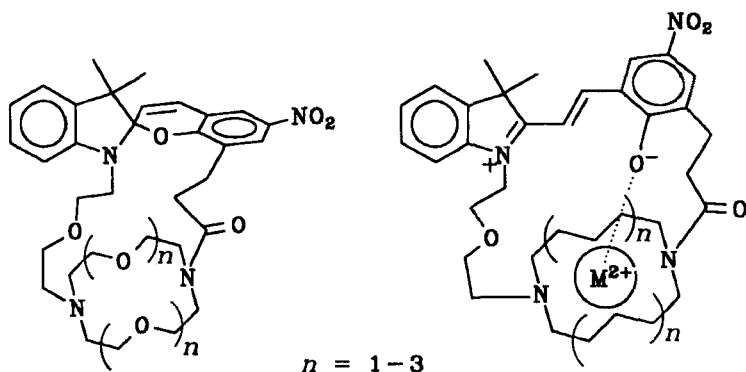


Figure 92 A crown-spirobenzopyran-based alkaline-earth metal ion sensor [119]

decrease in the fluorescence. They have also shown that this sensor can discriminate Cu^{2+} and Ni^{2+} at pH 7.1, at which only Cu^{2+} can be sensed.

Nabeshima *et al.* have designed a macrocycle containing an S-S bridge within the cavity (Figure 94) [121]. In the closed form it does not complex metal

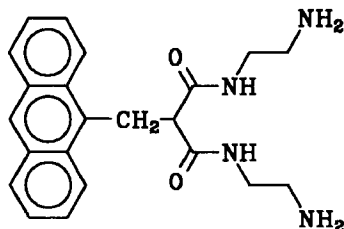


Figure 93 An anthracene-based fluorescent sensor for Cu^{2+} and Ni^{2+} [120]

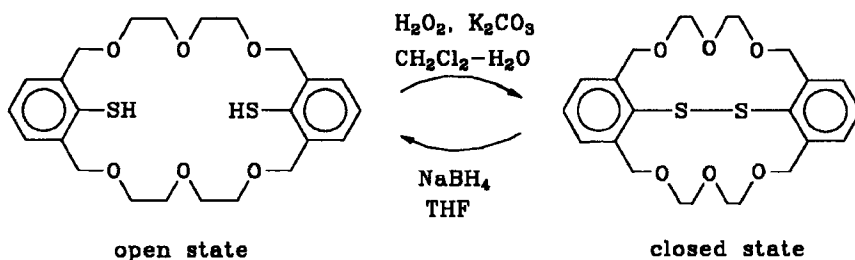


Figure 94 An Ag^+ receptor with a redox gate (the open state binds Ag^+ [121])

ions. However, the reduction of the disulfide to the dithiol results in the binding of thiophilic metal ions, in particular Ag^+ , Pb^{2+} and Cu^{2+} . The silver ion was found to have the highest specificity. The reducing agent thus acts as an on–off switch.

A pyridinium betaine derivative of a phenolic cryptand has been reported by Dolman and Sutherland (Figure 95) [122]. It has been demonstrated to be a fairly specific chromogenic reagent for Na^+ . Azophenolic cryptands acting as selective chromogenic reagents for Pb^{2+} have also been synthesized by Sutherland and coworkers (Figure 96). [123]. The same cryptand was shown earlier to have higher selectivity for Ca^{2+} over Na^+ or K^+ [124].

Chawla and Srinivas have synthesized new chromogenic calix[8]arenes (Figure 97) which exhibit observable color changes (with $\Delta\lambda$ up to 100 nm) with mono- and diamines, the shift being larger for diamines [125]. Diamines were also detected in the presence of an excess of monoamines.

Marsella and Swager have studied conducting-polymer-based sensors for selective ionochromic response [126]. For example, the polymer (molecular weight ~ 2800) depicted in Figure 98 showed a $\Delta\lambda$ of 15 nm, 63 nm and 10 nm in the presence of Li^+ , Na^+ and K^+ , respectively.

Beer *et al.* have been active in developing electrochemical sensors for nonredox-active metal ions. A potassium-selective, sulfide-linked, redox-active ferrocene ionophore has been reported by this group (Figure 99) [127]. This

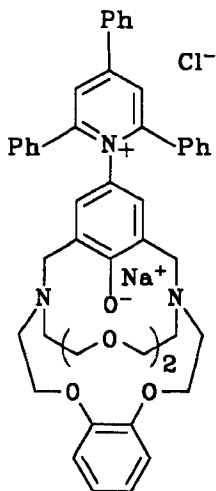


Figure 95 A pyridinium betaine derivative of a phenolic cryptand [122]

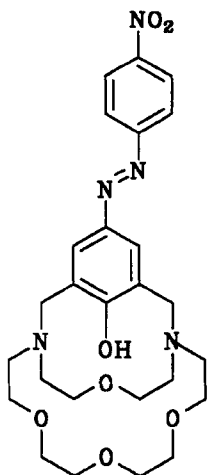


Figure 96 A chromogenic reagent for Pb^{2+} [123]

ferrocene-crown ether conjugate showed an expected anodic perturbation of its half-wave potential in the presence of Na^+ ions. However, an unexpected *cathodic* shift of the order of 60 mV was observed in the presence of K^+ ions. It was suggested that in the sandwich (1 : 1) complex the sulfur lone pairs adopt a conformation which directs electron density toward the ferrocene unit.

A novel calix[4]arene-diquinone crown ether has also been recently reported by Beer *et al.* which forms thermodynamically stable complexes with group 1,

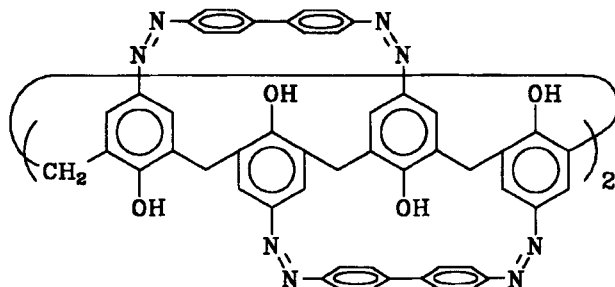


Figure 97 A chromogenic calix[8]arene for the detection of amines [125]

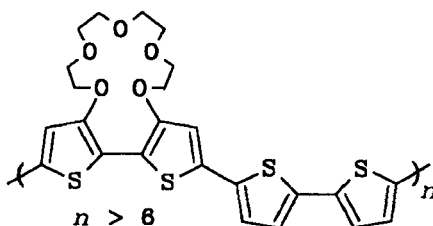


Figure 98 A conducting-polymer-based alkali metal ion sensor [126]

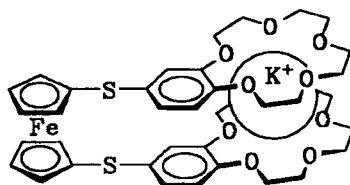


Figure 99 A K^+ -selective, redox-active ferrocene ionophore [127]

group 2 and ammonium cations (Figure 100) [128]. Electrochemical measurements indicated that these cations can be sensed via a substantial anodic perturbation effect of the redox potential (see Table 3).

A diaza-18-crown-6 derivative containing two phenanthridynyl units has been shown to detect alkaline-earth metal ions through an enhancement of the fluorescence (Figure 101) [129].

13. BINDING INTERACTION STUDIES

Schneider has studied pairwise interactions in supramolecular chemistry in order to correlate the binding energies observed in a large number of host–

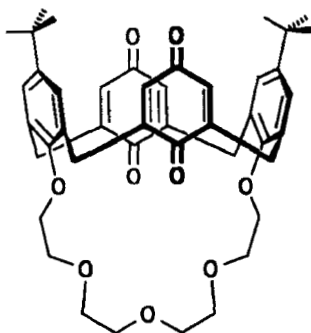


Figure 100 A calix[4]arene-diquinone crown ether for cation binding [128]

Table 3 Electrochemical data for cation complexes of the crown ether shown in Figure 100

Cation	ΔE (mV)
K^+	210
Na^+	255
Ba^{2+}	555
NH_4^+	405
$BuNH_3^+$	355

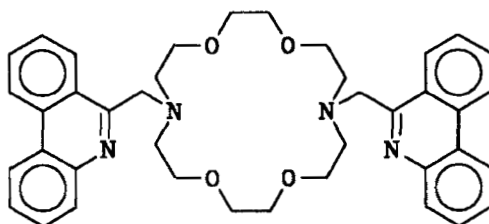
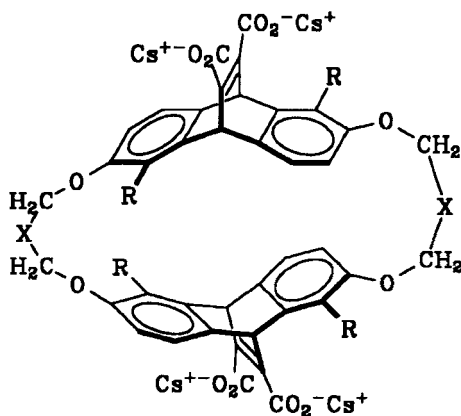


Figure 101 A fluorescence sensor for alkaline-earth metal ions [129]

guest complexes [130]. Interestingly, a linear free energy relationship was observed in a number of cases. It remains to be seen if this approach could be used for the prediction of the binding energies of new synthetic receptors.

Molecular recognition in aqueous media has been extensively studied by Dougherty and coworkers using host of the type shown in Figure 102 [131]. The binding of a variety of cationic and neutral molecules has been examined in order to gain new insights into the cation- π interaction. A free energy of



X: aromatic spacer; R: H, Br

Figure 102 A water-soluble receptor for studying cation- π interactions [131]

complexation as high as $9.4 \text{ kcal mol}^{-1}$ has been observed with an azulene derivative. Kim *et al.* have theoretically studied cation- π interactions using *ab initio* methods, and concluded that charge-quadrupole and charge-polarizability interactions play important roles in the complexation of Me_4N^+ with benzene [132].

Schwabacher *et al.* have studied the directionality of the cation- π effect by measuring the association constants of guests of various sizes with cationic and anionic water-soluble macrocycles (Figure 103) [133]. These studies have provided support for ion-quadrupole interactions contributing to the binding in the anionic host.

Sherman and coworkers have carried out a detailed study of carcaplex formation in the presence of a variety of guest molecules [134]. Competition experiments were done to find out the relative carcaplex formation abilities.

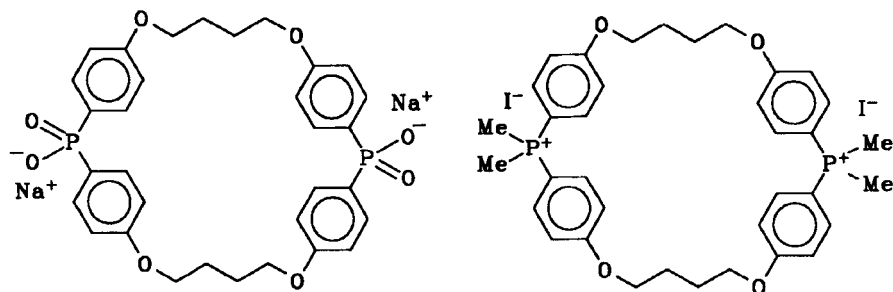


Figure 103 Water-soluble cationic and anionic macrocycles [133]

Pyrazine, 1,4-dioxane, dimethyl sulfide, DMSO and so on were found to be good “templating” molecules, whereas *N*-methyl-2-pyrrolidene (NMP), dimethylformamide (DMF), DMA and so on were poor “templating” molecules. The general observations which were made are as follows: (1) for the reported carcerand a maximum of seven nonhydrogen atoms is allowed; (2) the guest should be neither too polar nor too nonpolar; (3) higher symmetry results in easier carcarplex formation; (4) secondary amines are not encapsulated; and (5) cyclic molecules act as better templates than acyclic molecules.

Newcomb and Gellman have examined aromatic stacking interactions in aqueous solution by studying intramolecular stacking interactions in the compounds shown in Figure 104 [135]. Their studies showed that neither hydrophobic nor dispersion interactions are responsible for the stacking observed under the conditions studied.

The role of aromatic–aromatic interactions in molecular recognition has recently been reviewed by Hunter [136, 137].

Kelly and Kim have carried out a detailed study of the relative binding affinities of carboxylate, nitro, phosphate, phosphonate, sulfonate and δ -lactones with a urea-derived host (Figure 105) [138]. The effects of solvents on the binding affinity were also studied. This bis(urea) receptor was found to bind isophthalate in DMSO- d_6 with a K_a greater than 10^4 M^{-1} .

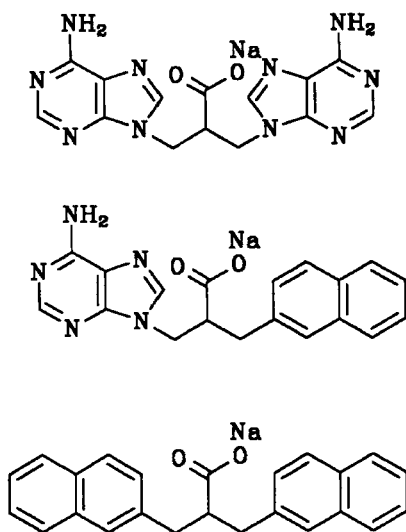


Figure 104 Substrates used for studying aromatic stacking interactions in water [135]

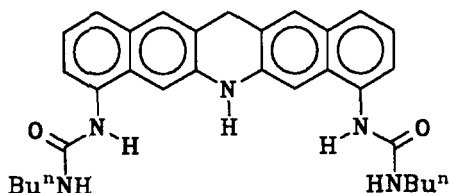


Figure 105 A ditopic receptor for studying the relative binding affinities of carboxylate and its isosteres [138]

A strategy for an experimental study of weak molecular recognition forces has been reported by Wilcox and coworkers [139]. From the equilibrium shown in Figure 106, the edge-to-face interaction was estimated to be of the order of $0.5 \text{ kcal mol}^{-1}$. Interestingly, aliphatic groups such as cyclohexyl and *t*-butyl also showed preference for the “folded” conformation.

14. CONCLUSIONS AND FUTURE OUTLOOK

The advances made in supramolecular chemistry in the period 1993–1994 have certainly been spectacular considering the wide range of studies carried out by various groups around the world. The most remarkable trend seen during this period is undoubtedly the approach taken by many research groups to construct simple structures packed with a variety of functions. It is inevitable that some of the newly synthesized receptors will find practical applications as molecular sensors with a degree of specificity never observed before. Such specificity has already been observed for the detection of metal ions. Developing a sensor for a small organic molecule in the presence of many others is still a problem, but is likely to be overcome with further advances in receptor design. The construction of synthetic receptors for binding to proteins with (sequence) specificity has not yet been addressed in a general sense, but

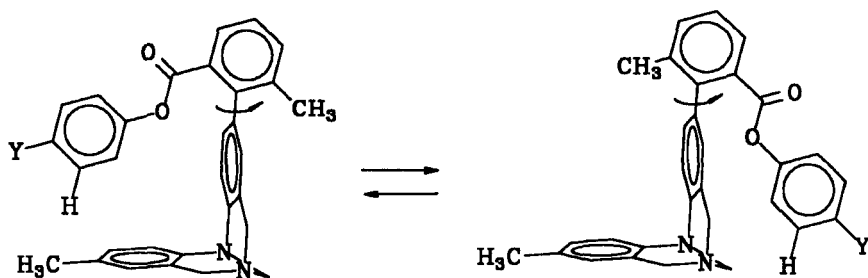


Figure 106 A “molecular torsion balance” for determining weak aromatic–aromatic interactions [139]

such studies are certainly going to be involved in the major future directions of supramolecular chemistry research. It is also clear that systematic studies of host-guest binding interactions will throw additional light on the contributions of various interaction forces in different media. The future of supramolecular chemistry appears to be bright, with many areas yet to be explored [140].

15. ACKNOWLEDGMENTS

I thank my coworkers, who are mentioned in the references, for the work on bile-acid-derived molecular receptors carried out at Bangalore. Financial support by the Department of Science and Technology and by the Department of Biotechnology is gratefully acknowledged. I also thank Mr Koushik Das Sarma for drawing all the structures for this article.

16. REFERENCES

1. (a) C. Seel and F. Vögtle, *Angew. Chem., Int. Ed. Engl.*, **31**, 528 (1992); (b) H. An, J. S. Bradshaw and R. M. Izatt, *Chem. Rev.*, **92**, 543 (1992); (c) A. J. Kirby, *Angew. Chem., Int. Ed. Engl.*, **33**, 551 (1994); (d) F. C. J. M. van Veggel, W. Verboom and D. N. Reinhoudt, *Chem. Rev.*, **94**, 279 (1994); (e) A. P. Davis, *Chem. Soc. Rev.*, 243 (1993); (f) T. H. Webb and C. S. Wilcox, *Chem. Soc. Rev.*, 383 (1993); (g) H. C. Visser, D. N. Reinhoudt and F. de Jong, *Chem. Soc. Rev.*, 900 (1994); (h) S. Anderson, H. L. Anderson and J. K. M. Sanders, *Acc. Chem. Res.*, **26**, 469 (1993); (i) H. An, J. S. Bradshaw, R. M. Izatt and Z. Yan, *Chem. Rev.*, **94**, 939 (1994); (j) J. L. Sessler, G. Memmi, T. D. Mody, T. Murai, A. Burrell and S. W. Young, *Acc. Chem. Res.*, **27**, 43 (1994). Additional references may be found in many of the papers cited here.
2. G. Wenz, *Angew. Chem., Int. Ed. Engl.*, **33**, 803 (1994).
3. K. A. Martin and A. W. Czarnik, *Tetrahedron Lett.*, **35**, 6781 (1994).
4. S. Houdier and P. J. A. Vottero, *Angew. Chem., Int. Ed. Engl.*, **32**, 354 (1993).
5. A. Essalim, E. Saint-Aman and D. Serve, *Bull. Soc. Chim. Fr.*, **131**, 407 (1994).
6. A. Nakamura, S. Okutsu, Y. Oda, A. Ueno and F. Toda, *Tetrahedron Lett.*, **35**, 7241 (1994).
7. K. Hamasaki, A. Ueno, F. Toda, I. Suzuki and T. Osa, *Bull. Chem. Soc. Jpn.*, **67**, 516 (1994).
8. K. Hamasaki, H. Ikeda, A. Nakamura, A. Ueno, F. Toda, I. Suzuki and T. Osa, *J. Am. Chem. Soc.*, **115**, 5035 (1994).
9. Y. Nagata, T. Aso, T. Kinoshita, Y. Tsujita, H. Yoshimizu and N. Minoura, *Bull. Chem. Soc. Jpn.*, **67**, 495 (1994).
10. C. T. Sikorski and R. C. Petter, *Tetrahedron Lett.*, **35**, 4275 (1994).
11. A. V. Eliseev and H.-J. Schneider, *J. Am. Chem. Soc.*, **116**, 6081 (1994).
12. J. T. Rademacher and A. W. Czarnik, *J. Am. Chem. Soc.*, **115**, 3018 (1993).
13. S. R. Wilson and Y. Wu, *J. Chem. Soc., Chem. Commun.*, 784 (1993).
14. M. Sawada, Y. Takai, H. Yamada, T. Kaneda, K. Kamada, T. Mizooku, K. Hirose, Y. Tobe and K. Naemura, *J. Chem. Soc., Chem. Commun.*, 2497 (1994).
15. U. Olsher, M. G. Hankins, Y. D. Kim and R. A. Bartsch, *J. Am. Chem. Soc.*, **115**, 3370 (1993).

16. K.-S. Jeong and S. Y. Pyun, *Tetrahedron Lett.*, **35**, 7041 (1994).
17. S. M. Fatah-ur Rahman and K. Fukunishi, *J. Chem. Soc., Chem. Commun.*, 917 (1994).
18. J. Mitjaville, A.-M. Caminade and J.-P. Majoral, *Tetrahedron Lett.*, **35**, 6865 (1994).
19. U. Maitra and B. G. Bag, *J. Org. Chem.*, **59**, 6114 (1994).
20. J.-P. Joly, M. Nazhaoui and B. Dumont, *Bull. Soc. Chim. Fr.*, **131**, 369 (1994).
21. D. B. Dumont, M.-F. Schmitt and J.-P. Joly, *Tetrahedron Lett.*, **35**, 4773 (1994).
22. N. S. Mani and P. P. Kanakamma, *Tetrahedron Lett.*, **35**, 3629 (1994).
23. O. F. Schall and G. W. Gokel, *J. Am. Chem. Soc.*, **116**, 6089 (1994).
24. M. Sawada, S. Takahashi, M. Shiro, M. Kawamura and T. Uchiyama, *J. Org. Chem.*, **59**, 2967 (1994).
25. R. M. Musau and A. Whiting, *J. Chem. Soc., Chem. Commun.*, 1029 (1993).
26. I. Alam, S. K. Sharma and C. D. Gutsche, *J. Org. Chem.*, **59**, 3716 (1994).
27. C. G. Gibbs and C. D. Gutsche, *J. Am. Chem. Soc.*, **115**, 5338 (1993).
28. K. Kobayashi, Y. Asakawa, Y. Kikuchi, H. Toi and Y. Aoyama, *J. Am. Chem. Soc.*, **115**, 2648 (1993).
29. D. M. Rudkevich, W. Verboom and D. N. Reinhoudt, *Tetrahedron Lett.*, **35**, 7131 (1994).
30. J. P. M. van Duynhoven, R. G. Janssen, W. Verboom, S. M. Franken, A. Casnati, A. Pochini, R. Ungaro, J. de Mendoza, P. M. Nieto, P. Prados and D. N. Reinhoudt, *J. Am. Chem. Soc.*, **116**, 5814 (1994).
31. W. I. Iwema Bakker, M. Haas, C. Khoo-Beattie, R. Ostaszewski, S. M. Franken, H. J. den Hertog Jr, W. Verboom, D. de Zeeuw, S. Harkema and D. N. Reinhoudt, *J. Am. Chem. Soc.*, **116**, 123 (1994).
32. P. Timmerman, W. Verboom, F. C. J. M. van Veggel, W. P. van Hoorn and D. N. Reinhoudt, *Angew. Chem., Int. Ed. Engl.*, **33**, 1292 (1994).
33. R. G. Janssen, W. Verboom, J. P. M. van Duynhoven, E. J. J. van Velzen and D. N. Reinhoudt, *Tetrahedron Lett.*, **35**, 6555 (1993).
34. P. Timmerman, W. Verboom, F. C. J. M. van Veggel, J. P. M. van Duynhoven and D. N. Reinhoudt, *Angew. Chem., Int. Ed. Engl.*, **33**, 2345 (1994).
35. Y. Kubo, S. Maeda, M. Nakamura and S. Tokita, *J. Chem. Soc., Chem. Commun.*, 1725 (1994).
36. T. Lippmann, H. Wilde, M. Pink, A. Schafer, M. Hesse and G. Mann, *Angew. Chem., Int. Ed. Engl.*, **32**, 1195 (1993).
37. P. B. Savage and S. H. Gellman, *J. Am. Chem. Soc.*, **115**, 10448 (1993).
38. D. M. Kneeland, K. Ariga, V. M. Lynch, C.-Y. Huang and E. V. Anslyn, *J. Am. Chem. Soc.*, **115**, 10042 (1993).
39. F. Chu, L. S. Flatt and E. V. Anslyn, *J. Am. Chem. Soc.*, **116**, 4194 (1994).
40. C.-Y. Hung, T. Hopfner and R. P. Thummel, *J. Am. Chem. Soc.*, **115**, 12601 (1993).
41. G. Shipp Jr and J. Rebek Jr, *Tetrahedron Lett.*, **35**, 6823 (1994).
42. Y. Hamuro, S. J. Geib and A. D. Hamilton, *Angew. Chem., Int. Ed. Engl.*, **33**, 446 (1994).
43. G. Das and A. D. Hamilton, *J. Am. Chem. Soc.*, **116**, 11139 (1994).
44. M. S. Goodman, J. Weiss and A. D. Hamilton, *Tetrahedron Lett.*, **35**, 8943 (1994).
45. A. P. Bisson, F. J. Carver, C. A. Hunter and J. P. Waltho, *J. Am. Chem. Soc.*, **116**, 10292 (1994).
46. C. A. Hunter and L. D. Sarson, *Angew. Chem., Int. Ed. Engl.*, **33**, 2313 (1994).
47. N. Tamura, T. Kajiki, T. Nabeshima and Y. Yano, *J. Chem. Soc., Chem. Commun.*, 2583 (1994).

48. E. Fan, S. A. Van Arman, S. Kincaid and A. D. Hamilton, *J. Am. Chem. Soc.*, **115**, 369 (1993).
49. M. R. Caira, L. R. Nassimbeni and J. L. Scott, *J. Chem. Soc., Chem. Commun.*, 612 (1993).
50. A. P. Davis, *Chem. Soc. Rev.*, 243 (1993).
51. R. Boyce, G. Li, H. P. Nestler, T. Suenaga and W. C. Still, *J. Am. Chem. Soc.*, **116**, 7955 (1994).
52. G. Wess, W. Kramer, A. Enhsen, H. Glombik, K.-H. Baringhaus, K. Bock, H. Kleine and W. Schmitt, *Tetrahedron Lett.*, **34**, 817 (1993).
53. G. Wess, W. Kramer, G. Schubert, A. Enhsen, K.-H. Baringhaus, H. Glombik, S. Müllner, K. Bock, H. Kleine, M. John, G. Neckermann and A. Hoffmann, *Tetrahedron Lett.*, **34**, 819 (1993).
54. W. Kramer, G. Wess, A. Enhsen, K. Bock, E. Falk, A. Hoffmann, G. Neckermann, D. Gantz, S. Schultz, L. Nickau, E. Petzinger, S. Turley and J. M. Dietschy, *Biochim. Biophys. Acta*, **1227**, 137 (1994).
55. D. Albert and M. Feigel, *Tetrahedron Lett.*, **35**, 565 (1994).
56. U. Maitra and S. Balasubramanian, *J. Chem. Soc., Perkin Trans. 1*, 83 (1995).
57. U. Maitra and L. J. D'Souza *J. Chem. Soc., Chem. Commun.*, 2793 (1994).
58. S. C. Zimmerman and K. W. Saionz, *J. Am. Chem. Soc.*, **117**, 1175 (1995).
59. L. K. Mohler and A. W. Czarnik, *J. Am. Chem. Soc.*, **115**, 2998 (1993).
60. T. D. James, T. Harada and S. Shinkai, *J. Chem. Soc., Chem. Commun.*, 857 (1993).
61. K. R. A. S. Sandanayake, K. Nakashima and S. Shinkai, *J. Chem. Soc., Chem. Commun.*, 1621 (1994).
62. K. R. A. S. Sandanayake and S. Shinkai, *J. Chem. Soc., Chem. Commun.*, 1083 (1994).
63. T. D. James, K. R. A. S. Sandanayake and S. Shinkai, *Angew. Chem., Int. Ed. Engl.*, **33**, 2207 (1994).
64. M.-F. Paugam, L. S. Valencia, B. Bogges and B. D. Smith, *J. Am. Chem. Soc.*, **116**, 11203 (1994).
65. M. T. Reetz, J. Huff, J. Rudolph, K. Töllner, A. Deege and R. Goddard, *J. Am. Chem. Soc.*, **116**, 11588 (1994).
66. D. E. Kaufmann and A. Otten, *Angew. Chem., Int. Ed. Engl.*, **33**, 1832 (1994).
67. B. L. Iverson, R. E. Thomas, V. Kral and J. L. Sessler, *J. Am. Chem. Soc.*, **116**, 2663 (1994).
68. D. M. Rudkevich, W. Verboom and D. N. Reinhoudt, *J. Org. Chem.*, **116**, 3683 (1994).
69. D. M. Rudkevich, Z. Brzozka, M. Palys, H. C. Visser, W. Verboom and D. N. Reinhoudt, *Angew. Chem., Int. Ed. Engl.*, **33**, 467 (1994).
70. H. C. Visser, D. M. Rudkevich, W. Verboom, F. de Jong and D. N. Reinhoudt, *J. Am. Chem. Soc.*, **116**, 11554 (1994).
71. S. Valiyaveetil, J. F. J. Engbersen, W. Verboom and D. N. Reinhoudt, *Angew. Chem., Int. Ed. Engl.*, **32**, 900 (1993).
72. P. D. Beer, Z. Chen, A. K. Goulden, A. Grieve, D. Heseck, F. Szemes and T. Wear, *J. Chem. Soc., Chem. Commun.*, 1269 (1994).
73. P. D. Beer, C. A. P. Dickson, N. Fletcher, A. J. Goulden, A. Grieve, J. Hodacova and T. Wear, *J. Chem. Soc., Chem. Commun.*, 828 (1993).
74. M. L. Mussons, C. Raposo, M. Crego, J. Anaya, M. C. Cabarello and J. R. Moran, *Tetrahedron Lett.*, **35**, 7061 (1994).
75. P. B. Savage, S. K. Holmgren and S. H. Gellman, *J. Am. Chem. Soc.*, **116**, 4069 (1994).
76. H. Wennemers and W. C. Still, *Tetrahedron Lett.*, **35**, 6413 (1994).

77. B. R. Peterson and F. Diederich, *Angew. Chem., Int. Ed. Engl.*, **33**, 1625 (1994).
78. L. Garel, B. Lozach, J.-P. Dutasta and A. Collet, *J. Am. Chem. Soc.*, **115**, 11 652 (1993).
79. Y. Kato, M. M. Conn and J. Rebek Jr, *J. Am. Chem. Soc.*, **116**, 3279 (1994).
80. M. H. B. G. Gansey, W. Verboom and D. N. Reinhoudt, *Tetrahedron Lett.*, **35**, 7127 (1994).
81. M. C. Rotger, J. F. Gonzalez, P. Ballester, P. M. Deya and A. Costa, *J. Org. Chem.*, **59**, 4501 (1994).
82. L. Zhang, A. Macias, T. Lu, J. I. Gordon, G. W. Gokel and A. E. Kaifer, *J. Chem. Soc., Chem. Commun.*, 1017 (1993).
83. T. Morozumi and S. Shinkai, *J. Chem. Soc., Chem. Commun.*, 1219 (1994).
84. J. S. Nowick, T. Cao and G. Noronha, *J. Am. Chem. Soc.*, **116**, 3285 (1994).
85. K. J. Shea, D. A. Spivak and B. Sellergren, *J. Am. Chem. Soc.*, **115**, 3368 (1994).
86. T. P. Curran, M. P. Smith and M. P. Pollastri, *Tetrahedron Lett.*, **35**, 4515 (1994).
87. J. S. Lindsay, S. Prathapan, T. E. Johnson and R. W. Wagner, *Tetrahedron*, **50**, 8941 (1994).
88. R. A. Robbins, C. B. Knobler, D. R. Bellew and D. J. Cram, *J. Am. Chem. Soc.*, **116**, 111 (1994); C. N. Eid Jr, C. B. Knobler, D. A. Gronbeck and D. J. Cram, *J. Am. Chem. Soc.*, **116**, 8506 (1994).
89. M. V. Martinez-Diaz, J. de Mendoza and T. Torres, *Tetrahedron Lett.*, **35**, 7669 (1994).
90. J. Reeder, R. P. Castro, C. B. Knobler, E. Martinborough, L. Owens and F. Diederich, *J. Org. Chem.*, **59**, 3151 (1994).
91. F. Diederich and D. R. Carcanague, *Helv. Chim. Acta.*, **77**, 800 (1994).
92. S. M. Lacy, D. M. Rudkevich, W. Verboom and D. N. Reinhoudt, *Tetrahedron Lett.*, **35**, 5953 (1994).
93. L. Garel, J.-P. Dutasta and A. Collet, *Angew. Chem., Int. Ed. Engl.*, **32**, 1169 (1993).
94. S. S. Yoon and W. C. Still, *J. Am. Chem. Soc.*, **115**, 823 (1993).
95. A. Borchardt and W. C. Still, *J. Am. Chem. Soc.*, **116**, 373 (1994).
96. A. Borchardt and W. C. Still, *J. Am. Chem. Soc.*, **116**, 7467 (1994).
97. T. Carell, E. A. Wintner, A. Bashir-Hashemi and J. Rebek Jr, *Angew. Chem., Int. Ed. Engl.*, **33**, 3059 (1994); T. Carell, E. A. Wintner and J. Rebek Jr, *Angew. Chem., Int. Ed. Engl.*, **33**, 2061 (1994).
98. R. Meric, J.-M. Lehn and J.-P. Vigneron, *Bull. Soc. Chim. Fr.*, **131**, 579 (1994).
99. P. Ballester, A. Costa, P. M. Deya, J. F. Gonzalez, M. C. Rotger and G. Deslongchamps, *Tetrahedron Lett.*, **35**, 3813 (1994).
100. Y. Kuroda, Y. Kato, M. Ito, J.-Y. Hasegawa and H. Ogoshi, *J. Am. Chem. Soc.*, **116**, 8392 (1994).
101. M. Harmata, C. L. Barnes, S. R. Karaa and S. Elahmad, *J. Am. Chem. Soc.*, **116**, 8392 (1994).
102. M. Shionoya, T. Ikeda, E. Kimura and M. Shiro, *J. Am. Chem. Soc.*, **116**, 3848 (1994).
103. R. Ballardini, V. Balzani, A. Credi, M. T. Gandolfi, F. Kotzbya-Hilbert, J.-M. Lehn and L. Prodi, *J. Am. Chem. Soc.*, **116**, 5741 (1994).
104. Y. Murakami, O. Hayashida and Y. Nagai, *J. Am. Chem. Soc.*, **116**, 2611 (1994).
105. K. D. Shimizu, T. M. Dewey and J. Rebek Jr, *J. Am. Chem. Soc.*, **116**, 5145 (1994).
106. J. Lee and A. W. Schwabacher, *J. Am. Chem. Soc.*, **116**, 8382 (1994).
107. R. Guthrie, M. Nieger and F. Vögtle, *Angew. Chem., Int. Ed. Engl.*, **32**, 601 (1993).
108. B. J. Whitlock and H. W. Whitlock, *J. Am. Chem. Soc.*, **116**, 2301 (1994).
109. K. T. Chapman and W. C. Still, *J. Am. Chem. Soc.*, **111**, 3075 (1989).
110. R. Breslow and B. Zhang, *J. Am. Chem. Soc.*, **116**, 7893 (1994).
111. C. M. Martens, R. J. M. Klein Gebbink, M. C. Feiters and R. J. M. Nolte, *J. Am. Chem. Soc.*, **116**, 5667 (1994).

112. C. Raposo, M. Almaraz, M. Crego, M. L. Mussons, N. Perez, M. C. Caballero and J. R. Moran, *Tetrahedron Lett.*, **35**, 7065 (1994).
113. (a) M.W. Gobel, J. W. Bats and G. Dürner, *Angew. Chem., Int. Ed. Engl.*, **31**, 207 (1992); (b) S. Lehr, K. Schutz, M. Bauch and M. W. Gobel, *Angew. Chem., Int. Ed. Engl.*, **33**, 984 (1994).
114. R. P. Bonar-Law, L. G. Mackay, C. J. Walter, V. Marvaud and J. K. M. Sanders, *Pure Appl. Chem.*, **66**, 803 (1994).
115. H. Murakami and S. Shinkai, *J. Chem. Soc., Chem. Commun.*, 1533 (1993).
116. M. Ogata, K. Fujimoto and S. Shinkai, *J. Am. Chem. Soc.*, **116**, 4505 (1994).
117. S.-Y. Hong and A. W. Czarnik, *J. Am. Chem. Soc.*, **115**, 3330 (1994).
118. D. H. Vance and A. W. Czarnik, *J. Am. Chem. Soc.*, **116**, 9397 (1994).
119. M. Inouye, Y. Noguchi and K. Isagawa, *Angew. Chem., Int. Ed. Engl.*, **33**, 1163 (1994).
120. L. Fabbrizzi, M. Licchelli, P. Pallavicini, A. Perotti and D. Sacchi, *Angew. Chem., Int. Ed. Engl.*, **33**, 1975 (1994).
121. T. Nabeshima, H. Furusawa and Y. Yano, *Angew. Chem., Int. Ed. Engl.*, **33**, 1750 (1994).
122. M. Dolman and I. O. Sutherland, *J. Chem. Soc., Chem. Commun.*, 1793 (1993).
123. A. Mason, A. Sheridan, I. O. Sutherland and A. Vincent, *J. Chem. Soc., Chem. Commun.*, 2627 (1994).
124. A. Mason and I. O. Sutherland, *J. Chem. Soc., Chem. Commun.*, 1131 (1994).
125. H. M. Chawla and J. Srinivas, *J. Chem. Soc., Chem. Commun.*, 2593 (1994).
126. M. J. Marsella and T. M. Swager, *J. Am. Chem. Soc.*, **115**, 12214 (1993).
127. P. D. Beer, J. P. Danks, D. Hesek and J. F. McAleer, *J. Chem. Soc., Chem. Commun.*, 1735 (1993).
128. P. D. Beer, Z. Chen, M. G. B. Drew and P. A. Gale, *J. Chem. Soc., Chem. Commun.*, 2207 (1994).
129. S. Alihodzic, M. Zinic, B. Klaić, R. Kiraly, B. Kojic-Prodic, M. Herceg and Z. Cimerman, *Tetrahedron Lett.*, **34**, 8345 (1993).
130. H.-J. Schneider, *Chem. Soc. Rev.*, 227 (1994).
131. P. C. Kearney, L. S. Mizoue, R. A. Kumpf, J. E. Forman, A. McCurdy and D. A. Dougherty, *J. Am. Chem. Soc.*, **115**, 9907 (1993).
132. K. S. Kim, J. Y. Lee, S. J. Lee, T.-K. Ha and D. H. Kim, *J. Am. Chem. Soc.*, **116**, 7399 (1994).
133. A. W. Schwabacher, S. Zhang and W. Davy, *J. Am. Chem. Soc.*, **115**, 6995 (1993).
134. R. G. Chapman, N. Chopra, E. D. Cochien and J. C. Sherman, *J. Am. Chem. Soc.*, **116**, 369 (1994).
135. L. F. Newcomb and S. H. Gellman, *J. Am. Chem. Soc.*, **116**, 4993 (1994).
136. C. A. Hunter, *Angew. Chem., Int. Ed. Engl.*, **32**, 1584 (1993).
137. C. A. Hunter, *Chem. Soc. Rev.*, 101 (1994).
138. T. R. Kelly and M. H. Kim, *J. Am. Chem. Soc.*, **116**, 7072 (1994).
139. S. Paliwal, S. Geib and C. S. Wilcox, *J. Am. Chem. Soc.*, **116**, 4497 (1994).
140. The author will be happy to share his collection of molecular-recognition-related references (titles, authors, journal details). This can be e-mailed in ASCII or WordPerfect 6.1 format. Please e-mail/fax your requests (e-mail, maitra@orgchem.iisc.ernet.in; fax, international code +91-80-334-1683). For a comprehensive treatment of this subject see: *Comprehensive Supramolecular Chemistry*, J.-M. Lehn (Chairman, Editorial Board), 11 volume set, Elsevier Science, Oxford, 1996.

Chapter 3

Control of Reactivity in Aggregates of Amphiphilic Molecules

PAOLO SCRIMIN

University of Trieste, Italy

1. INTRODUCTION

Aggregates of amphiphilic molecules (those of natural occurrence are known as lipids) constitute some of the most widespread self-organized structures in biological systems [1]. They make up 30–70% (by weight) of the components of biological membranes, and are among the most intriguing supramolecular structures known. The peculiar characteristics of amphiphilic molecules have, since the early development of chemistry, attracted the attention of many scientists, including those whose interests are oriented towards the understanding of biological systems. Indeed, spontaneous aggregates of amphiphilic molecules (or surfactants) are fascinating not only because they pose challenging questions concerning their structure and the forces that hold them together [2, 3], but also because they may be considered as a reaction medium [4, 5] with completely different properties with respect to aqueous solution, where the surfactants are dispersed.

This chapter deals with some features of reactivity in organized assemblies and is not intended as a review of the topic, but rather an attempt to highlight aspects of reactivity in these systems in order to define their peculiarity with respect to homogeneous solutions. As recently pointed out by Menger [6], “groups of molecules, properly assembled, can obviously accomplish much more than an equal number of molecules functioning separately”. Reference to

review articles rather than to original papers is given whenever possible to limit the otherwise quite long list of references. The literature on the topic is vast and still growing. For example, the *Current Contents* database contains ~5000 entries under the title key word "surfactant" for only the last five years.

2. STRUCTURE OF THE AGGREGATES [1, 5, 7]

Before entering into the details of reactivity in aggregates, it is useful to survey the structure of these systems. Usually, a surfactant is a molecule with a hydrophilic head-group and a lipophilic backbone. The head-group may be a charged moiety (like ammonium or sulfate) or neutral (like a polyether). The backbone may be made of one or more long hydrocarbon chains. Examples of amphiphilic molecules are shown in Table 1. However, any molecule presenting separate hydrophilic and lipophilic regions may form aggregates in water. For instance, Diederich and Dick [9] and Scrimin and coworkers [10] have clearly shown that water-soluble cyclophanes (or similar molecules) encompassing charged ammonium groups and rigid

Table 1 Some amphiphilic molecules, the aggregates they form in water and their critical aggregate concentrations

Amphiphilic	Aggregate	Critical aggregate concentration (cac) ^a (M)
$n - C_{16}H_{33}NMe_3^+Br^-$ (CTAB)	Micelle	9×10^{-4}
$n - C_{12}H_{25}N^+(\text{cyclohexyl})Br^-$	Micelle	1×10^{-2}
$(n - C_{12}H_{25})_2NMe_2^+Br^-$	Vesicle ^b	3×10^{-5}
$(n - C_{16}H_{33})_2NMe_2^+Br^-$	Vesicle ^b	8×10^{-6}
$n - C_{12}H_{25}OSO_3^-Na^+$ (SDS)	Micelle	8×10^{-3}
$n - C_{12}H_{25}(OCH_2CH_2)_6OH$	Micelle	1×10^{-4}
$(n - C_{12}H_{25}OCH_2)_2CH(OCH_2CH_2)_{10}OH$	Vesicle ^b	2×10^{-6}
$n - C_{12}H_{25}NMe_2(CH_2)_3SO_3^-$ (DDAPS)	Micelle	4×10^{-3}
$(n - C_{16}H_{33}O)_2PO_2^-Na^+$ (DHP)	Vesicle ^b	5×10^{-6}
$n - C_{15}H_{31}CO_2CH_2$	Vesicle	4×10^{-10}
$n - C_{15}H_{31}CO_2CHCH_2OPO_2^-$ $O(CH_2)_2NMe_3^+$ (DPPC)		

^aThe cac may vary depending on the ionic strength of the solution and the addition of hydrophobic additives.

^bThe aggregates may be open bilayers depending on the method of preparation [8].

hydrophobic cavities made of aromatic residues may, in water, spontaneously form aggregates. More recently, it has been shown that glycopeptide antibiotics like teicoplanin do aggregate [11] in aqueous solutions, and this leads to changes in some of their properties.

Aggregation of amphiphilic molecules occurs specifically in the presence of water (see Figure 1) (recently, though, aggregation has been observed in other solvents [12]) above the critical aggregate concentration (cac), dubbed the critical micelle concentration (cmc) in the case of the most simple of these aggregates: the micelle.

In the case of simple amphiphilic molecules, like CTAB (see Table 1), the aggregates formed are called micelles and have roughly a globular structure with the polar head-group at the micelle-water interface (see Figure 2). The surface of micelle is quite rough [13] and water molecules easily permeate the aggregate [14]. The aggregate is rather fluid and the hydrocarbon tails can

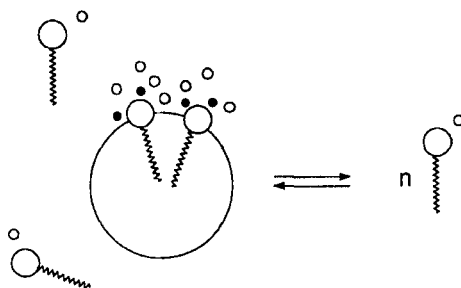
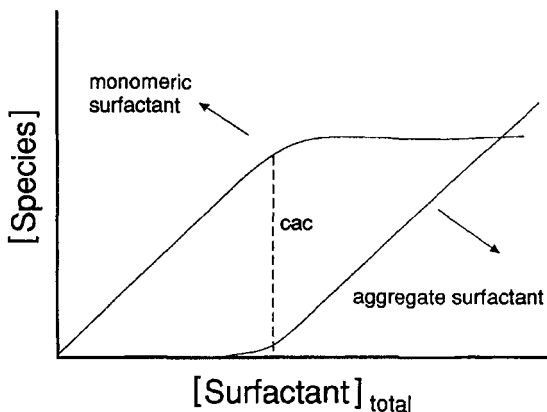


Figure 1 Surfactant molecules are soluble in aqueous solutions as monomers up to [surfactant] = cac. Above the cac, monomers are in equilibrium with aggregates

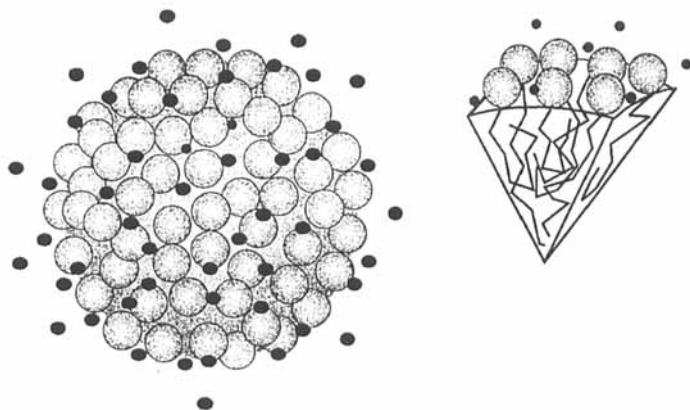


Figure 2 Schematic representation of a spherical micelle and a section showing the disordered arrangement of the hydrocarbon chains

easily float on the surface exposed to the bulk water solution. Furthermore, the monomeric surfactant molecules are in equilibrium with those in the aggregate. The rate of the exchange process depends on the values of the cmc [15] and is usually very fast (microsecond timescale) for $\text{cmc} \geq 10^{-3} \text{ M}$, but can be very slow (half-lives of minutes or hours) for $\text{cmc} < 10^{-6} \text{ M}$. As a consequence, these systems can be present in solution under conditions far from the thermodynamic equilibrium. In spite of the above kinetic processes, micelles constitute a pseudophase distinct from bulk water where they are dispersed, and this pseudophase has its own physicochemical characteristics. In this regard, a single example may give an idea of the new environment defined by the micellar aggregates; for instance, polypeptides bound to micelles experience the same tendency to organization (like the formation of helices) that they experience in classical “organizing” solvents [16].

Amphiphilic molecules with two or more hydrocarbon chains and a single polar head-group usually form [17] different aggregates [5, 7, 8] than micelles: these are called vesicles or liposomes. However, other aggregates, morphologically different from vesicles, can be obtained with these lipids (see Jain [1] and Fendler [5] for details); all share the presence of a bilayer structure (lamellae). In the simplest vesicles, the surfactants aggregate to form, again, a roughly spherical structure. However, they are organized in such a way as to form a bilayer (membrane) made of two leaflets of surfactants packed with the hydrocarbon tails facing each other and the polar head-groups on both surfaces exposed to water. In this way, a water pool is trapped inside the vesicle (Figure 3). Because of the very low solubility of amphiphiles that form vesicles, the aggregation must usually be induced by supplying extra energy (like by swirling or by sonication). The aggregates typically assume a flat lamellar

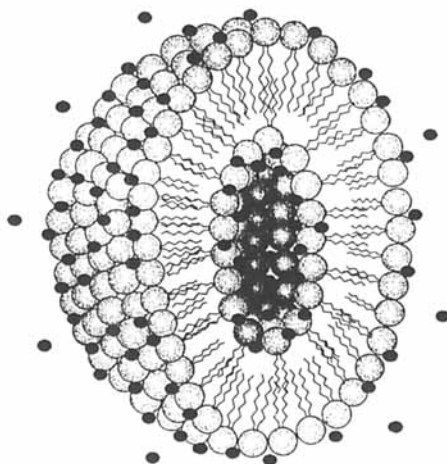


Figure 3 Schematic representation of the cross-section of a unilamellar vesicle. The high curvature of each leaflet in this rendition emphasizes the difference in population between the outer and inner layers

structure that eventually bends to form the spherical vesicles [18]. The packing requirements of a surfactant in the vesicle bilayer are much more stringent than in a micelle. This has two important implications. First, the “order” of the aggregate is higher than the “order” of the micelle. Second, permeation of water or polar solutes across the membrane is quite difficult [19, 20]. Because of the “order” of the hydrocarbon chains in the bilayer of vesicles, rotation around the C–C bonds requires much more energy than in micelles and usually occurs only in a cooperative manner, like in the melting of crystals. Accordingly, bilayer membranes of vesicles (and similar aggregates) are characterized by a phase transition temperature (T_c). Above this temperature, kinks occur in the hydrocarbon chains which are present only in an *s-trans*-conformation below this temperature [21]. Above T_c the bilayer becomes more fluid and permeation phenomena across the membrane may become significant. Many other kinetic processes occurring in the membrane [movement of the lipids within a layer; exchange of lipids from one leaflet to the other (flip-flop)] are also influenced by the fluidity of the bilayer. The control of permeation of solutes across biological membranes is of critical importance for the existence of living organisms.

The size of vesicles ranges from 20 nm to 500 nm, while that of conventional micelles is smaller (6–10 nm). The simple vesicle described above is not the only one that can be obtained. For instance, depending on the preparation conditions, it is possible to obtain multilayer (onionlike) vesicles. Furthermore,

it is possible to obtain vesicles from single-tail surfactants [8, 22] or macrocyclic surfactants with two polar head-groups (dubbed "bola") [23].

Micelles and vesicles constitute only two of the self-organized systems that can be obtained by dispersion of amphiphilic molecules in water. However, they give a clear idea of the kind of systems we are dealing with in this chapter. It must be pointed out that aggregates can also be obtained in wet organic solvents where the surfactant solubilizes water droplets of different size (microemulsions). A schematic representation of the extraordinary variety of aggregates that can be obtained by dispersion of amphiphilic molecules in aqueous (and wet organic) solutions is given in Figure 4.

I cannot complete this section without mentioning what is the energetic "glue" that keeps together surfactant assemblies. Hydrophobic interactions [2]

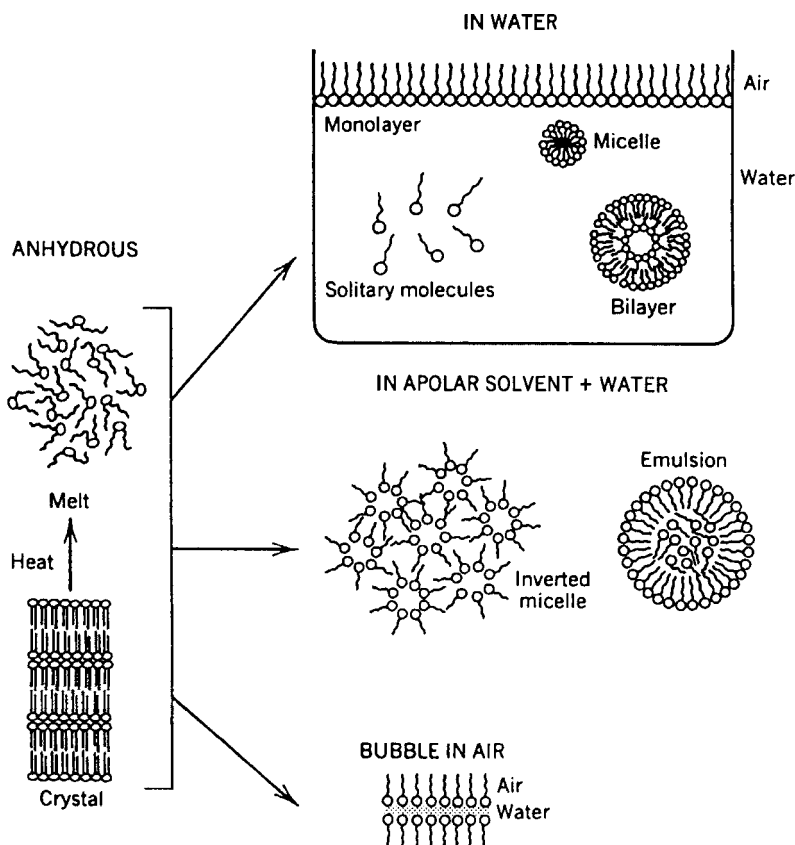


Figure 4 Representation of some of the aggregates obtained by dispersion of amphiphilic molecules in aqueous (and organic) solutions. Reproduced by permission from *Introduction to Biological Membranes*, 2nd edn, John Wiley & Sons, Inc, New York, 1988

commonly denote the tendency of relatively apolar molecules to aggregate in aqueous solution, and one will surely find the term “hydrophobic effect” used in other chapters of this book as these interactions are involved in many systems operating in water (including biological systems, of course). The basis of the hydrophobic effect has been the subject of many investigations [2, 3, 5]. However, the matter is still debated and several traditional views appear quite unsatisfactory according to more recent investigations. In a recent review, Engberts and Blokzijl [24] suggest that hydrophobic interactions “reflect the limited capacity of water to accommodate an apolar solute and maintain its original network of hydrogen bonds”. They question the previously accepted wisdom [2] of the hydrophobic effect as the result of water with enhanced structure at the surface of an apolar molecule. Clearly, central to the aggregation of amphiphilic molecules in water are the unique characteristics of water itself [25]: its strong tendency to form an extended network of hydrogen bonds and its exceptionally low molecular volume.

3. REACTIVITY IN AGGREGATES

As said above, micellar aggregates and, even more, the bilayer membranes of vesicles constitute a pseudophase with solvating properties different from those of the bulk water solution. Lipophilic substrates partition quite favorably into the aggregate by the same agents that bring the surfactant molecules together (see Figure 5): hydrophobic interactions. So, in the small volume of the aggregate a relatively high concentration of substrate is realized. Taking advantage of this fact, one can obtain large rate accelerations for reactions of substrates in aggregates [4, 5, 26, 27] involving lipophilic reactants but also employing synthetically modified surfactants with reactive functional groups [28] (functional surfactants), and even for reactions involving a lipophilic substrate and a hydrophilic reactant. In fact, surfactants with ionic head-groups interact strongly with counterions, offsetting the repulsions between the charged amphiphilic moieties. This also affects the energetics of aggregation. The concentration of ions at the micellar surface (often called the Stern layer) depends, among other parameters, on charge density, and those having low charge density are usually more strongly bound [29, 30].

On the basis of the above arguments, it appears clear that reactions in micelles can be accelerated by realizing high local concentrations of reactants. Obviously, for opposite reasons reactions can be retarded. This happens, for instance, when only one of the reacting species is transferred into the aggregate. The basic requisite for the occurrence of a reaction, the encounter of the reactants is prevented in this case. Aspects of reactivity in organized assemblies have been reviewed [4–6, 26–29], and this topic continues to attract the interest of several research groups. The analysis of reactivity has also led to quantitative treatments

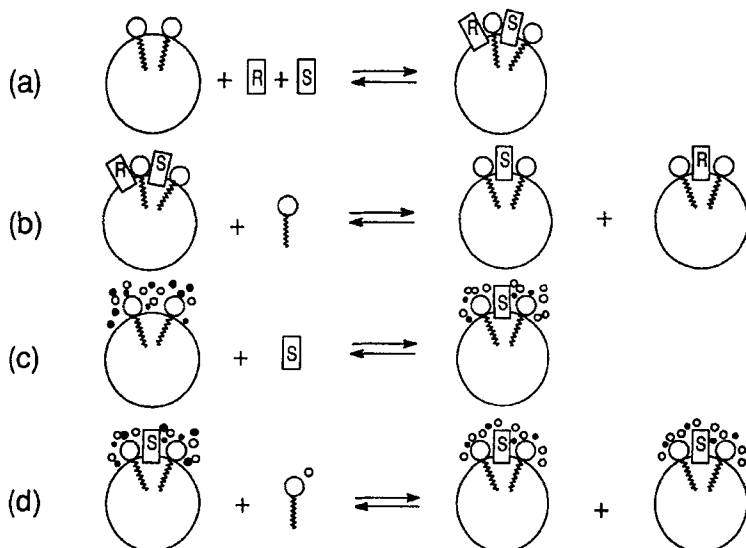


Figure 5 Aggregates may interact with lipophilic substrates (R = reactant, S = substrate) which favorably partition in the aggregate pseudophase (a). This situation gives an increase in concentration of the two reacting species with increase of the observed rate of the reaction. On further addition of surfactant the two reacting species begin to be “diluted” in different aggregates (b); the observed rate decreases with respect to the situation in (a). The substrate may also interact with ions (●) other than the counterions (○) of the ionic surfactant (c). Further addition of ionic surfactant brings into the Stern layer more nonreacting counterions which compete with the reacting ions, thus inhibiting the reaction (d)

of rates [27, 29, 31]. Though a detailed analysis of this aspect is beyond the scope of this chapter, the kinds of reactivity profiles that are usually observed and how they can be analyzed will be briefly discussed. Rate modifications of reactions of lipophilic substrates in aggregates are typically found in (1) reactions of a charged, polar molecule in assemblies made of nonfunctional, ionic surfactants; (2) reactions of a lipophilic reagent in aggregates of nonfunctional surfactants; and (3) reactions where the reactant is a functional surfactant.

In all cases, the rate versus [surfactant] profiles are characterized by a sharp change of the rate at $[\text{surfactant}] \geq \text{cac}$. This is the typical behavior of systems that operate on a cooperative basis [32]. Here the cooperativity occurs at the level of the association of the monomeric surfactant to form the aggregate with the onset of its new properties. The outburst of reactivity associated with the spontaneous formation of aggregates once the cac is reached has stimulated Luisi and coworkers [33, 34] to introduce the provocative idea of “autopoiesis”. According to their definition, an autopoietic system is an organizational unit capable of self-maintenance and, hence, self-reproduction. To illustrate this point they have [33],

for instance, added ethyl caprylate (a highly lipophilic ester) to an NaOH solution ($\text{pH} > 9$), obtaining a biphasic system as the ester is practically insoluble in the aqueous solution. This heterogeneous mixture is stable for several hours since hydrolysis of the ester is very slow because of its insolubility. Nevertheless, the hydrolysis proceeds and small amounts of soluble sodium caprylate are produced. When the cmc of caprylate is reached, micelles begin to form and increasing amounts of lipophilic ester are solubilized in the micellar pseudophase with a consequent enormous increase in the rate of hydrolysis. With the onset of micelles the timescale of the hydrolysis changes completely, and since the ester itself produces the micelle-forming surfactant the system is autocatalytic. The autopoietic process is then started with parent micelles generating new breeds of identical micelles until all ethyl caprylate is consumed (Figure 6).

This quite provocative representation of micellar catalysis may allow us to speculate on a possible relation to the origin of life and evolution, as the authors have done. However, in our context it gives clear evidence of the

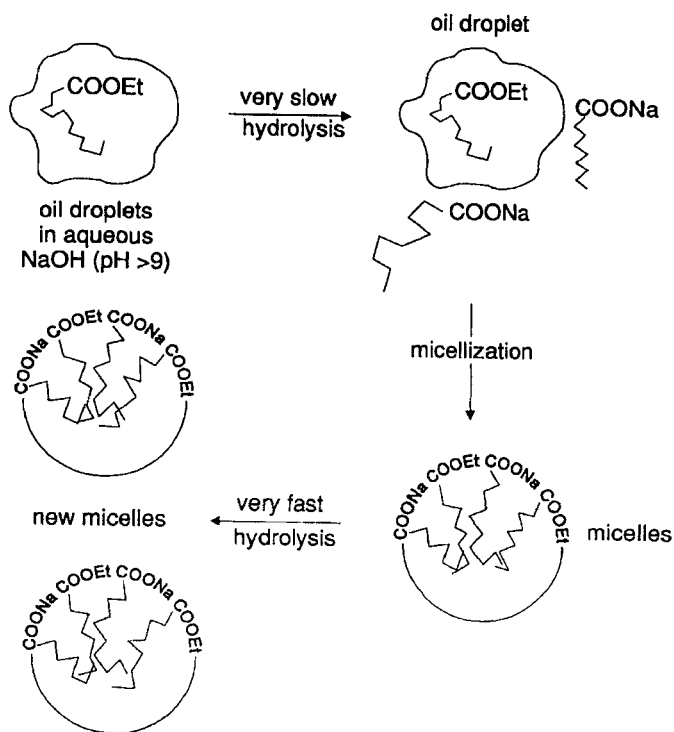


Figure 6 The experiment of Luisi and coworkers with ethyl caprylate leading to micelles of sodium caprylate by hydrolysis. Because of the continuous supply of ethyl caprylate, the micellar system self-replicates

impressive change of reactivity associated with the spontaneous phenomenon of self-aggregation of surfactants.

Since an increase in the surfactant concentration results in a higher fraction of substrate bound to the aggregate, an increase of the rate effects is expected, as seen in the above example, as [surfactant] increases and when [surfactant] \geq cac. Consequently, an enzymelike rate versus concentration profile is anticipated with a tendency of the curve to plateau when all the substrate is transferred into the aggregate. However, this is correct only in case (3) and in case (1) when the counterion of the added ionic surfactant is the reactive species (Figure 7, right). In case (1) when the reactive ion is not added as the counterion of the ionic surfactant (and is, consequently, kept constant in concentration) and in case (2), reaction profiles go through a maximum as the concentration of surfactant is increased (Figure 7, left).

A simple example of the first situation is given by the nucleophilic attack of OH^- at 2,4-dinitrochloronaphthalene [35] in CTAB (a cationic surfactant). At low CTAB concentration, owing to the transfer of the substrate into the aggregate, rate acceleration prevails, but at higher [CTAB] the anion Br^- favorably competes with OH^- in the Stern layer of the aggregate, leading to a decrease in local $[\text{OH}^-]$. Since this is the region where the reaction occurs, a decrease in the reaction rate is observed.

An attempt to quantify this phenomenon has led Bunton and Romsted to develop the "pseudophase exchange model" [27, 29] and alternative treatments [36].

When case (2) is dealt with, in order to explain the inhibition effect observed at high surfactant concentration one has to consider the "dilution" of substrate

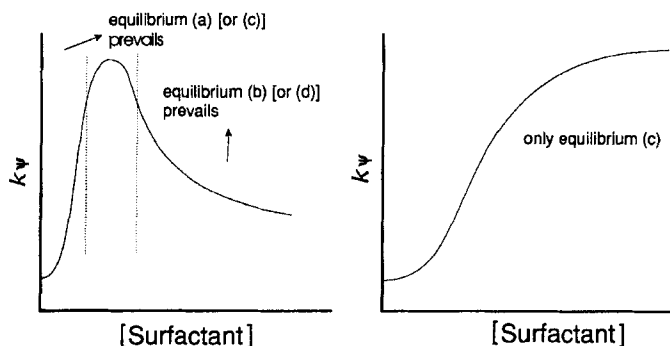




Figure 7 Rate constant (k_p) profiles expected for the different situations illustrated in Figure 5. A maximum is typically observed when neither the surfactant nor its counterion is the reacting species. The enzymelike profile of the curve on the right is found with functional surfactants or with reacting counterions. The inflection at very low [surfactant] denotes the kinetic cac

and lipophilic reactant in an increasing number of aggregates. As a result it becomes highly probable that they, in fact, are not bound to the same aggregate, and hence the concentration effect vanishes. In Section 9 are reported the equations commonly used to fit the experimental kinetic data with these different systems.

To complete this concise picture, I should mention that spontaneous monomolecular and water-catalyzed reactions are also affected by the presence of aggregates. The aggregates behave as a submicroscopic solvent, and to a large extent their effects can be explained on the basis of the known kinetic solvent effects in these reactions.

With the exception of a few examples, bimolecular reactions in micelles are largely controlled by the local concentration (and pH) realized at the micellar pseudophase. The data reported in Table 2 [28, 31] give a comparison of the second-order rate constants measured for a series of functional derivatives in aqueous and micellar pseudophases. The ratios of the two rate constants (taking into account concentration and deprotonation effects in micelles) are all close to unity, confirming the above assertion. Finally, although the quantification of rate accelerations has been done mainly with micellar aggregates, the reactivity in vesicles appears to follow basically the same rules with minor differences due to the different lipophilicity and/or order of the membrane [37].

Table 2 Second-order rate constants for reactions catalyzed by different functional groups in water (k_2^w) and in micelles (k_2^m). The data are corrected for the difference in pK_a of the functional groups in the two phases

Catalyst ^{a,b}	Substrate					
	PNPA ^c			PNPH ^d		
	k_2^m (s ⁻¹ M ⁻¹)	k_2^w (s ⁻¹ M ⁻¹)	k_2^m/k_2^w	k_2^m (s ⁻¹ M ⁻¹)	k_2^w (s ⁻¹ M ⁻¹)	k_2^m/k_2^w
RCONHCHCH ₂ -  CO ₂ ⁻	0.076	0.19	0.4	0.031	0.16	0.2
 -CH ₂ NRMe ₂ ⁺	31	16	1.9	19	24	0.8
RMe ₂ N ⁺ (CH ₂) ₂ S ⁻	5.1	2.8	1.8	5	1.3	0.4

^aR = Me or Et for monomeric catalysts, R = *n*-C₁₆H₃₃ for micellar catalysts.

^bWith added CTAB to ensure solubilization.

^cPNPA = *p*-nitrophenyl acetate.

^dPNPH = *p*-nitrophenyl hexanoate.

In making the above statements I am not diminishing the relevance of the rate accelerations that can be observed in aggregate-catalyzed reactions, I am only trying to put them in the correct perspective. So, for example, the increase of local pH or the shifting of protonation equilibria toward the more nucleophilic conjugate base in cationic aggregates without changing the pH of the bulk solution easily explains the source of large rate accelerations in aggregates. (It is important to note that the buffers control the pH of the bulk water solution and not that of the micellar pseudophase.) However, one has to acknowledge that this feature allows the reaction to be run under milder conditions than those otherwise required in homogeneous aqueous solutions.

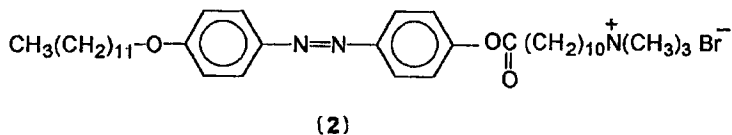
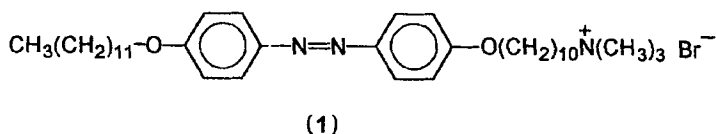
If we accept the idea recently put forward by Menger [38] that enzyme-like rate acceleration can be achieved only when the two reacting groups are forced to stay at van der Waals contact distances for finite times, we should not expect enzyme-like rates in aggregates. Two aspects of substrate–aggregate interaction operate against the achievement of such a goal: the nonspecific binding and the usually fast movements of the molecules within the aggregate. Under particular conditions these aspects may change and the control of kinetic processes and of the mode of binding may allow less predictable changes of reactivity.

Having presented the general aspects of micellar catalysis with its interesting features but also with its limitations, I will focus on a personal selection of examples of reactivity in aggregates and to show how these self-assembling systems may reveal, in some instances, unique properties that cannot be totally explained with the simple concept introduced above.

4. CONTROL OF REACTIVITY

4.1 Surfactant–Surfactant Interactions

When a solute is solubilized in a solvent [39], in the absence of specific intermolecular interactions it is surrounded by solvent molecules. This may not be true when a lipophilic (or amphiphilic) molecule is “solubilized” in the pseudophase constituted by the bilayer of a liposome [1, 40]. In fact, sorting of species embedded in biological membranes seems to be more frequent than expected [41]. An elegant example proving the formation of clusters of molecules in vesicular aggregates with consequences on reactivity has been reported by Kunitake and coworkers [42]. They have dispersed the azo dyes (1) and (2) in bilayer membranes made of the lipid $2C_{16}Br$. Below the phase transition temperature of the bilayer matrix (i.e. in its gel state), (1) is not homogeneously dispersed, instead, it forms clusters (domains) easily monitored by their characteristic absorption spectrum. Domains disappear as the membrane melts ($T > T_c$), as shown in Figure 8.



If we allow for the difference in temperature, the alkaline hydrolysis of (2) is faster when it is homogeneously dispersed in the matrix than when it is present as a cluster. Clustering, or phase separation, consequently influences its reactivity. Analogous behavior was observed with the imidazole-functionalized azo derivative (3). In this case clustering could be observed even when the matrix was in its fluid state (i.e. above T_c) upon control of the pH or addition of copper(II) ions. Phase separation occurs when the histidine subunit is zwitterionic or when it is coordinated to the metal ion. Accordingly, since charge-charge interactions, metal coordination or a change in temperature induces the formation of domains by controlling these parameters the reactivity in the aggregate may also be controlled.

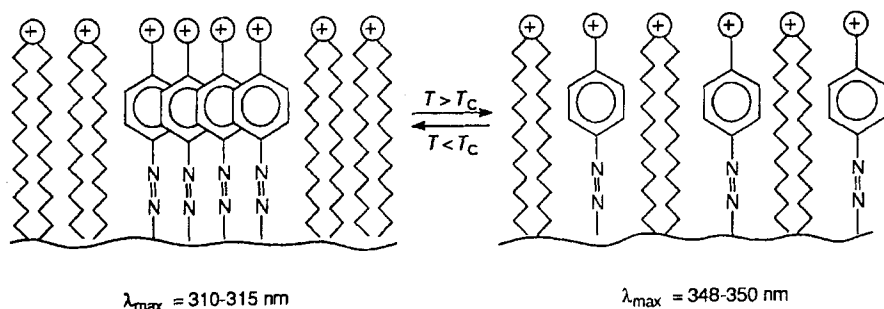
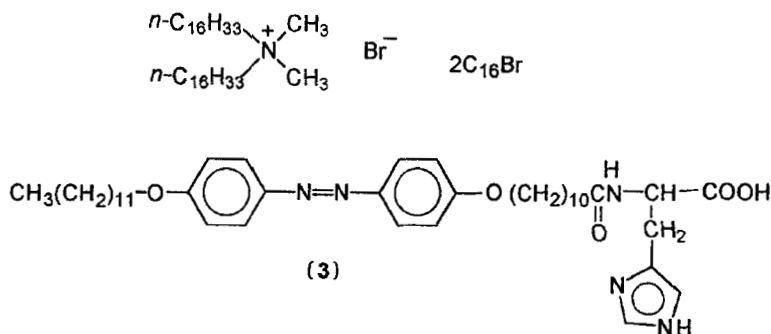
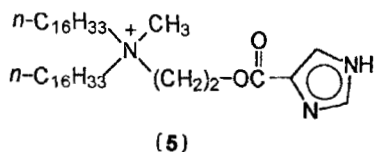
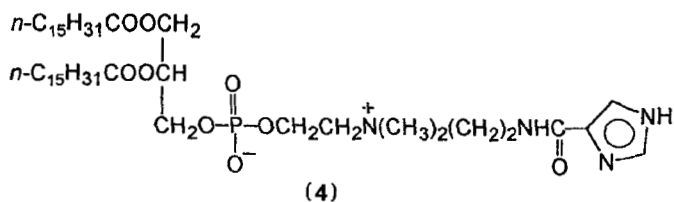


Figure 8 Schematic representation of the equilibrium governing the formation of domains of an azo derivative in aggregates of $2\text{C}_{16}\text{Br}$ as a function of the temperature



The above example shows a case of the control of reactivity through interactions that occur in both the lipophilic and hydrophilic regions of the bilayer membrane. The imidazole-functionalized phospholipid (4) provides an example of the control of reactivity by tuning the charge-charge interactions [43]. Vesicular aggregates of (4) constitute a classical example of a functional surfactant as the acylimidazole can act as a catalyst in the hydrolysis of carboxylate esters. Similarly functionalized cationic micelles [44] and vesicles [45] are also good catalysts of this reaction. Surprisingly, the reactivity of vesicular (4) toward the lipophilic ester *p*-nitrophenyl hexanoate (PNPH) was very sluggish. For example, at pH 8 PNPH is cleaved 2.7×10^4 times faster by cationic vesicles made of (5) than by pure vesicular (4). Interestingly, the efficiency of the imidazole group of (4) can be enhanced by the addition of the cationic amphiphile $2\text{C}_{16}\text{Br}$.



It has been suggested that this change of reactivity is controlled by the accessibility of the imidazole moieties to the substrate. It is known that phosphatidylcholine vesicles feature extensive electrostatic interaction between the N^+ and $\text{P}-\text{O}^-$ groups in their polar region, forcing them to lie parallel to the bilayer surface [46]. This may bury the imidazole in a region of the aggregate less accessible to PNPH. The cationic additive $2\text{C}_{16}\text{Br}$ may replace

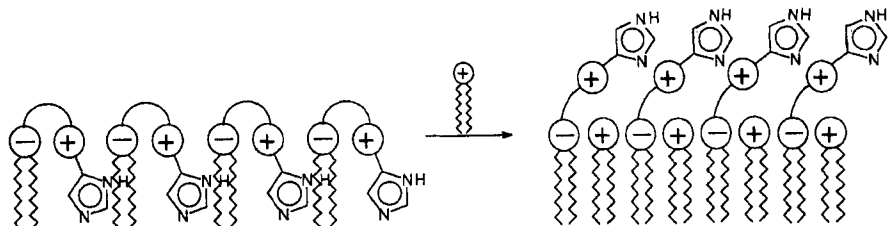


Figure 9 Schematic rendition of the effect of adding cationic surfactant $2C_{16}Br$ to vesicles of pure (4)

the ammonium group of (4) in the interaction with $P-O^-$ groups, thus releasing the imidazole moiety into a region more accessible to the substrate (Figure 9). The permeability of vesicular (4) to PNPH appears to be controlled by the fluidity of the bilayer and, consequently, by the temperature. Above the T_c of pure (4) ($36^\circ C$) the reactivity becomes sharply higher. This phenomenon occurs at much lower temperature in the blend of (4) and $2C_{16}Br$ ($T_c = 27^\circ C$).

4.2 Metallomicelles

The switching on of reactivity is not a peculiarity of vesicular aggregates, it may also be observed in micelles. The following is an example. It is known that the hydrolysis of α -amino esters can be greatly accelerated by the addition of transition metal ions, copper(II) in particular [47]. The coordination of the metal ion to proper ligands also influences the rate of cleavage, and, if new nucleophilic species are introduced, new products (or intermediates) may originate. Aggregates made of amphiphilic copper(II) complex (6) dubbed "metallomicelles" [48], accelerate the hydrolytic cleavage of esters. This occurs via the acylation of the alcohol group of the ligand followed by hydrolysis of the intermediate. In contrast, addition of the corresponding hydrophilic ligand to the copper(II) solution with formation of complex (7) (unable to form aggregates) inhibits the hydrolytic process. With the *p*-nitrophenyl ester of picolinic acid (PNPP) under the conditions $[(6)]$ or $[(7)] = [copper(II)] = 1.3 \times 10^{-4} M$, the reaction is almost 1000 times faster in the micellar system than in the monomeric one, amounting to a roughly 100-fold acceleration of the reaction in metallomicelles with respect to the effects of copper(II) alone and to a roughly 10-fold inhibition by the water-soluble complex. We demonstrated that this different behavior was attributable to the shifting of the equilibrium of coordination of the alcoholic arm of the ligand. In fact, with the water-soluble monomeric complex (7) the ROH group is not involved in coordination to the metal ion. The coordination occurs only in micelles, and consequently this system can capitalize on the nucleophilicity of the copper(II)-bound alcohol group which acts as a pseudointramolecular nucleophile (Figure 10).

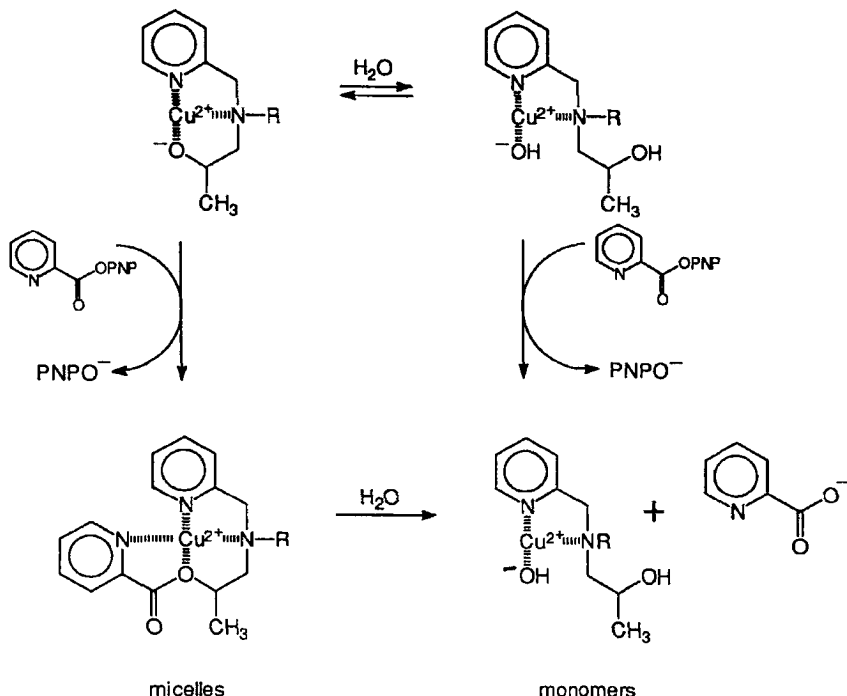
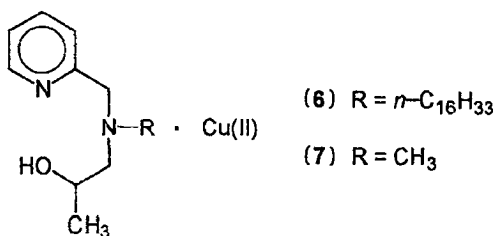


Figure 10 Micellar (6)·Cu(II) ($R = n\text{-C}_{16}\text{H}_{33}$) reacts with PNPP with acylation of the hydroxy group followed by hydrolysis. Monomeric (7)·Cu(II) ($R = \text{Me}$) hydrolyzes the substrate directly because the alcohol group is not bound to the metal ion



This tendency of metalloaggregates to modulate the coordination to transition metal ions appears quite general. For instance, very recently we have observed [49] that copper(II) metallomicelles made of the ligand shown in Figure 11 shift the coordination equilibrium toward the five-coordinate complex even at very low pH, while the water-soluble ligand is only tetracoordinated with the second imidazole in its protonated form. Clearly, the cationic metalloaggregate drives the deprotonation of the second

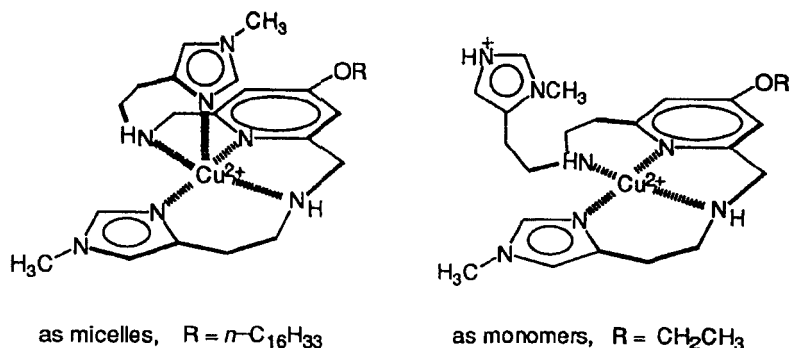
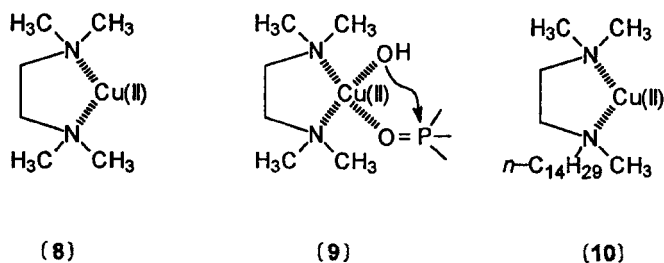
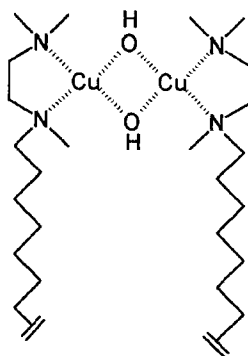


Figure 11 Micellization controls the composition of the coordination sphere of the complex shown. The imidazole resides in the apical position at a (bulk water) pH as low as 4 in micelles, while a pH higher than 6.5 is necessary with the monomeric system

imidazole. This difference in the coordination sphere of copper(II) leads to different properties in the monomeric and aggregated complexes.

The modulation of the coordination to the transition metal has not necessarily positive implications on the reactivity. For instance, we observed [50] that the copper(II) complex (8) of tetramethyl-1,2-diaminoethane catalyzes the hydrolysis of the phosphoric acid triester PNPDPP via an electrophilic mechanism which involves the pseudointramolecular attack of deprotonated water, as illustrated in (9). The electrophilic mechanism contribution to the hydrolytic process totally disappears in micellar aggregates made of the amphiphilic complex (10). Clearly, micellization does not allow the P-O group of the substrate to interact with the metal ion. This could be a result of steric constraint of the substrate when bound to the micelle and/or the formation of binuclear dihydroxy complexes, like (11), in the aggregate. So, in spite of the quite large rate accelerations observed [51] in the cleavage of PNPDPP in metallomicelles made of the amphiphilic complex (10), the second-order rate constant [allowing for the difference in $\text{p}K_a$ of the H_2O molecules bound to copper(II) in micelles and monomers] is higher for (8) than for (10) ($k_2^w/k_2^m > 250$).





(11)

4.3 Enantioselectivity

The conventional wisdom [52] is that the loose, nonspecific interactions usually realized in aggregates are not good premises for the achievement of highly enantioselective processes. Though this is largely correct, particularly when the aggregate, though chiral, is not directly involved in the process being studied, there are notable exceptions. More than 20 years ago, Moss *et al.* [53] provided an early example of the way in which aggregation may control the stereochemical course of a reaction. In studying the deamination of the chiral primary amine (12) in water below and above its cmc and in the presence of different counterions, they found a dramatic influence of both parameters on the stereochemistry of the reaction. While deamination of (12) below the cmc proceeds with 22% net inversion and extensive racemization (depending on the lifetime of the carbocationlike intermediate), above the cmc it proceeds with 10% net retention of configuration. This trend from inversion toward retention of configuration was also observed upon changing the length of the hydrocarbon chain in the amine (from 2-aminobutane to 2-aminodecane), and was associated with the onset of micellization as the amine became more hydrophobic. The modification of stereochemistry was explained by the authors by suggesting a tight interaction of the carbocationlike intermediate with hydrophobic counterions (BF_4^- , ClO_4^-) in the aggregate such that it can be approached by the nucleophile (water) only by the side of the leaving N_2 (Figure 12). More hydrophilic counterions (Cl^- , Br^-) did not allow control of the stereochemical outcome of the reaction.

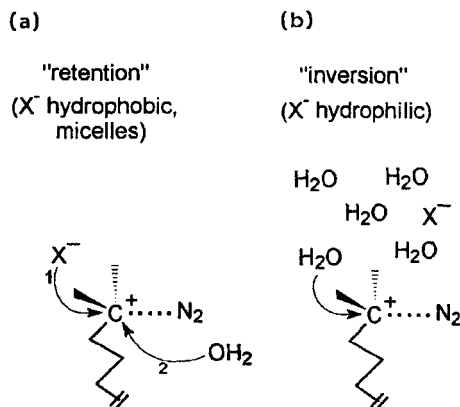
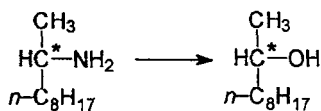
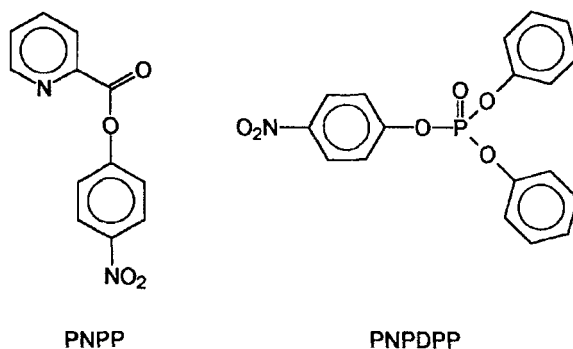
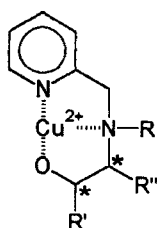


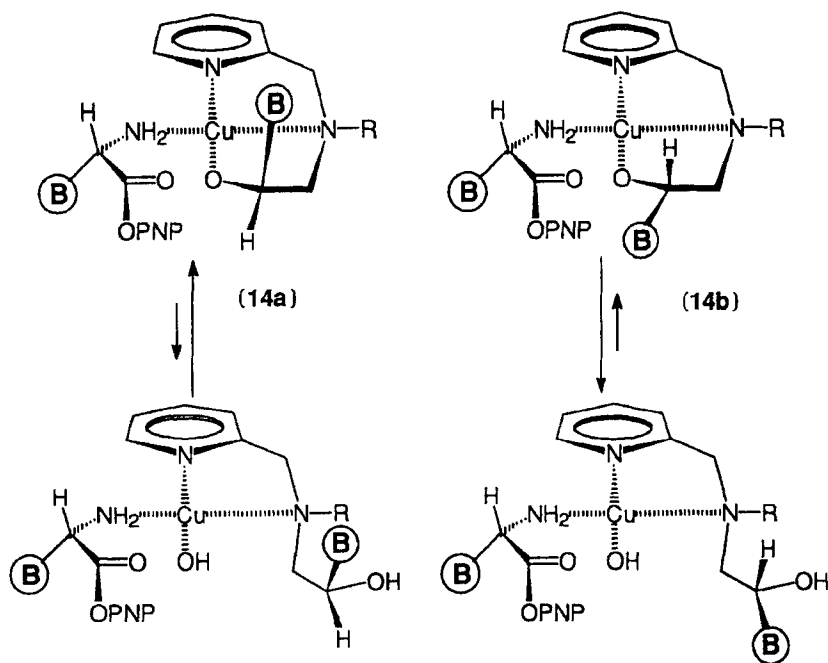
Figure 12 The stereochemical outcome of the deamination of chiral primary amines in micelles (a) is explained by a tight counterion-carbocationlike intermediate interaction (1) so that the nucleophile (H_2O) can reach the reaction center from the same side as the leaving N_2 (2). In monomers (b), the counterions are solvated by water molecules and the attack of the nucleophile is on the opposite side from the leaving group



When enantioselectivity is studied using chiral, functional surfactants it appears that one of the most important aspects leading to high stereoselectivity is the compartmentalization (within the same aggregate) of the two reacting enantiomers. This means that the reaction for the two of them occurs in different loci of the aggregate where small differences in polarity and/or solvation of the species lead to different reactivities. Examples confirming this statement have been recently reported by Nolte and coworkers [54] and others [55]. We have observed [56] that enantioselectivity in chiral metalloaggregates appears to be governed by differences in the solubilization site of the two enantiomers taking part in the reacting diastereomeric complex. For instance, using the chiral, amphiphilic copper(II) complex (13), we explained the relatively high enantioselectivities observed in the cleavage of the *p*-nitrophenyl esters of α -amino acids ($k_{(R)}/k_{(S)} \approx 12$) in terms of the different solvation requirements of the two diastereomeric complexes (14a) and (14b) (B denotes the bulky substituent at chiral carbon). The occurrence of the reaction in regions of the aggregate of different hydration influences the nature of the actual nucleophile. In a more hydrated environment the slower nucleophilic attack of copper(II)-bound OH^- prevails, while in the more hydrophobic regions the faster nucleophilic attack of the alkoxide ligand governs the reaction path. The net result is the difference in reactivity of the two enantiomers achieved through the reaction with two different nucleophiles (OH^- or RO^-). We suggest that at the basis of the observed phenomena is the mode of binding of ligand and substrate to copper(II) which, as a function of the stereochemistry at the stereogenic carbons, modulates the hydration of the metal center.



- (13) $\text{R} = n\text{-C}_{12}\text{H}_{25}$ or $n\text{-C}_{16}\text{H}_{33}$
 $\text{R}' = \text{CH}_3$ or H
 $\text{R}'' = \text{H}$ or CH_3 , or $(\text{CH}_3)_2\text{CH}$,
 Ph or CH_2Ph



In view of the higher order that can be achieved in vesicles, one could expect better results in the bilayer membranes of these aggregates. This is in fact the case [57]. In a matrix made of the cationic amphiphiles 2C₁₆Br or 2C₁₈Br, the enantioselectivity becomes almost three times higher ($k_{(R)}/k_{(S)} \approx 30$) than in micelles. What is particularly intriguing is the Arrhenius profile observed for the reaction of the two enantiomers (Figure 13). What we learn from these plots is that (1) the enantioselectivity is higher below the phase transition of the matrix (2) dramatic changes occur close to the phase transition temperature and (3) the reactivity above the phase transition tends to become similar for the two enantiomers. The above observations are consistent with the explanation of the enantioselectivity driven by compartmentalization and by solubilization of the two reacting complexes (14a) and (14b) in two different loci of the aggregate. The increase in temperature above the phase transition of the bilayer is associated with an increase of its fluidity; consequently, the segregation of the different species becomes less efficient. The faster enantiomer moves into a more hydrated region, the mechanism of the reaction changes and the overall reaction rate becomes slower in spite of the increase in temperature.

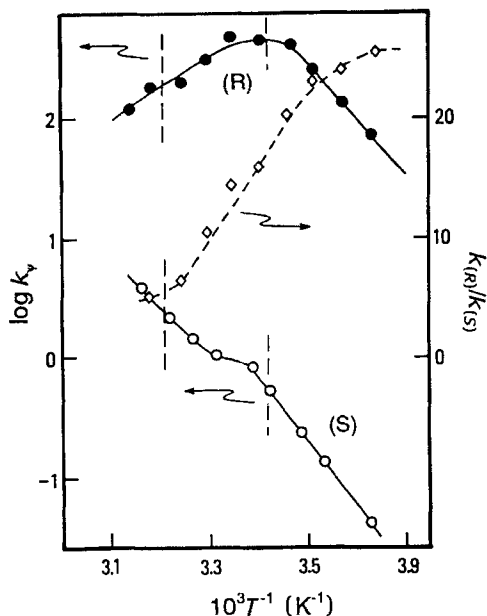
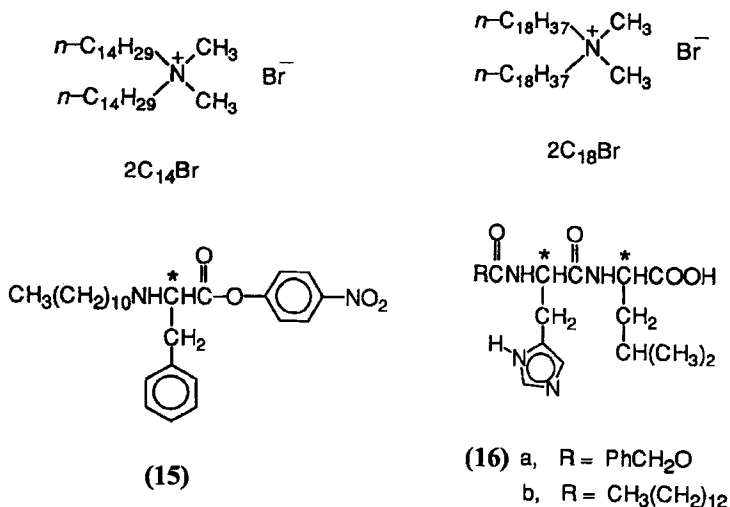


Figure 13 Arrhenius-type plots for the cleavage of the *p*-nitrophenyl esters of phenylglycine by the (*S*)-enantiomer of complex (13) ($R^1 = n\text{-C}_{12}\text{H}_{25}$, $R^2 = \text{H}$, $R^3 = \text{Pr}^i$) in a $2\text{C}_{18}\text{Br}$ vesicular matrix

The decrease in the fluidity of the membrane or the alteration of the order of the system seems to play a relevant role in controlling the stereoselectivity of reactions in other aggregates. Work done by many researchers, Ueoka and Moss [58] in particular, gives further insight on this aspect. Ueoka *et al.* have studied [58] the hydrolysis of the *p*-nitrophenyl ester of phenylalanine made lipophilic by protection of the amino group as the amide of a fatty acid (15). This substrate is totally bound to the aggregates where the reaction has been studied. The host matrix was made of an inert surfactant and the nucleophiles studied were lipophilic di- or tripeptides containing the histidine residue (16). Two parameters seem to influence the enantioselectivity of the reaction. The first one is, again, the fluidity of the membrane, as seen from kinetic studies run in a vesicular aggregate made of pure $2\text{C}_{14}\text{Br}$ as the host matrix. Below the phase transition, the $k_{(L)}/k_{(D)}$ ratios increase with increasing temperature, reaching a maximum at T_c and decreasing sharply thereafter. The phase transition temperature appears to be the optimum one for maximum enantioselectivity.



Second, the addition of the inert, single-chain surfactant CTAB dramatically enhances the stereoselectivity. The authors show how the change in ratio of double-chain to single-chain surfactant is also associated with a change in size of the aggregates from practically spherical vesicles (100% $2\text{C}_{14}\text{Br}$ with 300 Å average diameter to large rodlike aggregates (33% $2\text{C}_{14}\text{Br}$, 67% CTAB), as shown in Figure 14. It is conceivable that these morphological changes of the

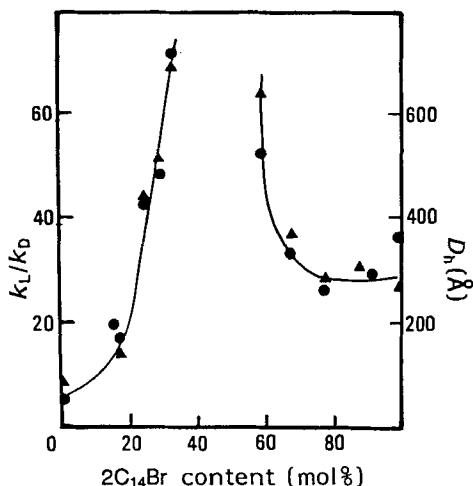


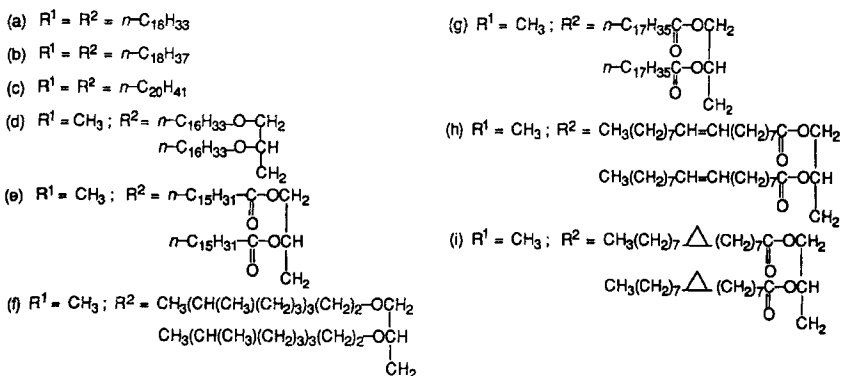
Figure 14 Enantioselectivity ratios (k_L/k_D), ●, and hydrodynamic diameters, ▲, of the aggregates as a function of surfactant composition in the cleavage of the enantiomers of (15) by (16a). Reproduced by permission from *J. Am. Chem. Soc.*, **107**, 2185 (1985)

aggregates bring about the formation of domains which differ remarkably in order and polarity [59]. It is likely that the two diastereomeric complexes are preferentially bound to different regions of the aggregate. This would lead to large differences in rate constants.

4.4 Cleavable Probes

Reactivity in aggregates may be used to get useful information on mobility in these systems. Vesicles are particularly amenable to these studies because, as mentioned earlier, mobility in these aggregates is lower than in micelles. For instance, it is estimated that above T_c , lateral diffusion of the lipids within the plane of the vesicle bilayer is very fast (diffusion coefficient of $\sim 10^{-8} \text{ cm}^2 \text{ s}^{-1}$, in the fluid phase), though three orders of magnitude slower than in an aqueous medium. Accordingly, randomization of a lipid in a leaflet of the bilayer of a 500 Å vesicle will occur in milliseconds, whereas the slow transverse (flip-flop) movement from one leaflet to another may take up to several days [1, 7, 60].

In 1986, Moss and Swarup [61] introduced the idea that a lipid functionalized with a cleavable group (like a carboxylate or phosphate ester) could be used to monitor kinetic phenomena related to the two most peculiar structural features of vesicles: the compartmentalization of water pools and the exchange of surfactants between the leaflets of the bilayer (flip-flop; see above). These processes are of paramount importance in biological membranes because they allow controlled permeation of ions across the membrane itself and the exchange of different chemical species [62]. Later, Moss and coworkers [63] synthesized a series of ester surfactants sharing a cleavable *p*-nitrophenyl benzoate group and differing in the structure and total charge of the amphiphilic residue (**17**). Notably, once cleaved, the ester surfactants (**17**) are converted into the *p*-nitrophenol-functionalized surfactants (**18**). The formation of these can be easily monitored at 400 nm by visible spectroscopy. By creating vesicles containing the functional lipids (**18**) in the selected matrix at low pH (~ 4) and subsequently increasing the pH of the bulk aqueous solution (to a pH of ~ 8) and exposing the external surface of the aggregate to glutathione (RS^-), they were able to monitor the kinetics of the permeation of H^+ and OH^- (in fact, concurrent counterions) and the dynamics of the lipids. The fast reaction with RS^- ($t_{1/2} \approx 6 \text{ s}$) generates surface-differentiated liposomes having on the exterior leaflet the cleaved surfactants (**18**) and on the interior layer the intact ester lipid (**17**). Cleavage of the internal surfactant substrate can be achieved by slow equilibration of the pH via permeation of ions or via exchange of the lipids residing on the two layers. Spectroscopically, they observed a fast increase of absorbance [accounting for ~ 50 – 60% of (**17**) present] followed by a much slower process accounting for the remaining substrate. A schematic representation is given in Figure 15.



If step (2) results in an enhanced rate of transbilayer movement of the functional lipid because of the raised temperature, one would expect, upon bringing the pH back to ~ 8 [step 3], to detect a new fast process accounting for the ester lipid that has moved from the interior to the exterior of the vesicles. This is in fact what the authors were able to monitor. By repetition of cycles (1)–(3), all the ester surfactant is eventually cleaved. By variation of the incubation time, a lifetime ($t_{1/2}$) of the flip–flop process could be determined. The $t_{1/2}$ data are reported in Table 3. Scrutiny of this table reveals that apart from the above-mentioned temperature of phase transition, the flip–flop process is also affected by the structure of the lipid backbone. For instance, dialkylammonium amphiphiles are much more mobile than those featuring a glycerollike backbone; increasing the length of the chain decreased the rate of

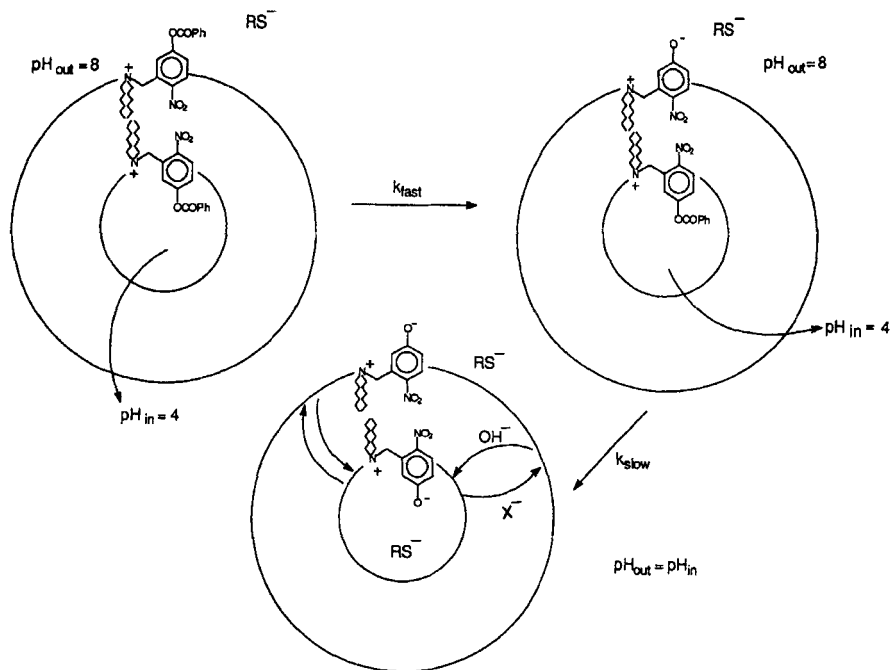


Figure 15 Surface differentiation with functional liposomes. The aggregates are formed at pH 4. Thereafter the external pH is raised to 8 and glutathione (RS^-) is added. This leads to fast cleavage of the external ester only. Later, pH equilibration and complete cleavage occur eventually in a much slower process

the process, while branching exerts the opposite effect; similarly, unsaturation and the presence of cyclopropane groups accelerate the kinetics.

Within the same context, it is worth mentioning that Menger *et al.* [65], Ladika *et al.* [66] and Moss *et al.* [67] have recently demonstrated that macrocyclic lipids decrease the mobility of the membrane by raising the phase transition temperature and decreasing the permeation of ionic species and the flip-flop rate.

Using the same concept outlined above, we were able to study the permeation of copper(II) ions across artificial liposomes made of cationic surfactants [68]. For this purpose, we synthesized the ester surfactant (**19**). The ester functional group in this case is a derivative of picolinic acid, a molecule known for its hydrolytic lability in the presence of transition metal ions [69] [copper(II) in particular] even at a pH close to neutrality. Vesicles made of cationic surfactants $2\text{C}_{16}\text{Br}$, $2\text{C}_{18}\text{Br}$ and $2\text{C}_{16}\text{GlyBr}$ containing 10% (molar ratio) of the ester surfactant (**19**) were obtained by sonication at pH 5. Upon

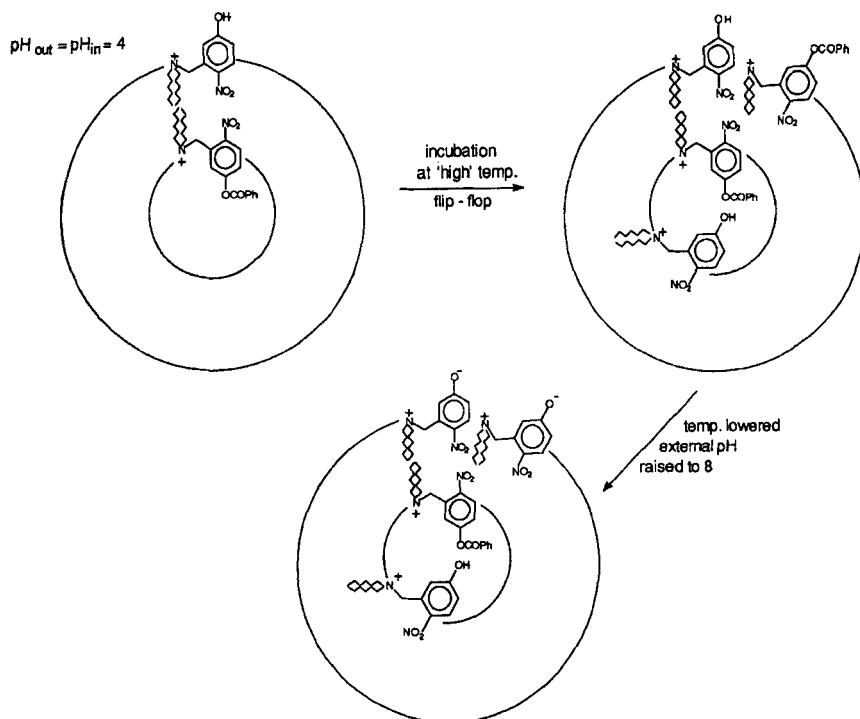


Figure 16 Protocol used for the flip-flop experiments by Moss and coworkers. After surface differentiation (see Figure 15), the external pH is decreased to 4 and the system incubated for different times at higher temperatures. The amount of unreacted substrate which moved to the outer layer is then determined by cleavage, raising the external pH back to 8

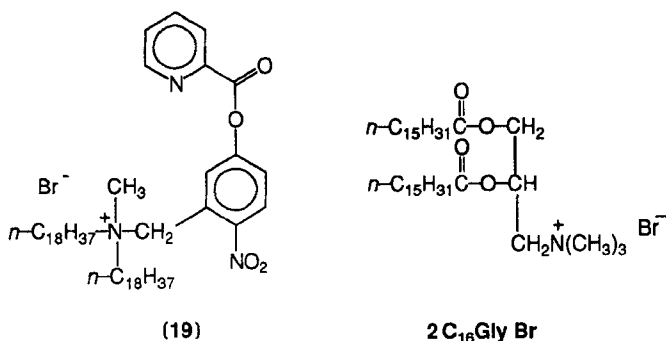
addition of copper(II) ions to the vesicular solution, two distinct situations were observed depending on the matrix used and the temperature at which experiments were run: (1) a monophasic (first-order) and fast hydrolysis of all ester present in solution, or (2) a fast hydrolysis of only 50–60% of the ester present in the vesicles followed by a slower process. While the fast process was dependent on the copper(II) concentration, the slower one was independent of this concentration and was associated with the metal-uncatalyzed hydrolysis of the surfactant substrate in the cationic aggregate matrix at the operational pH. Biphasic kinetic behavior was only observed at a temperature below the phase transition temperature and was a clear indication of no permeation of copper(II) ions since only the ester groups residing on the outer leaflet of the bilayer were rapidly cleaved in a copper(II)-catalyzed process. The presence of a monoexponential kinetic profile above T_c could be associated with a fast flip–

Table 3 Influence of the lipid backbone on the transbilayer and permeation kinetics of functional lipids (17a)–(17i), as measured by Moss and coworkers

Lipid	T_c (°C)	$t_{1/2}$ (flip–flop) (min)	$k_{\text{permeation}}$ (s ^{−1})
(17a)	26	1 (25) ^a	1.8×10^{-2} (15) ^a
(17b)	39	> 12 (25), ~2 (38)	1.8×10^{-3} (25)
(17c)	48	~10 (40), ~1 (50)	1.7×10^{-4} (25)
(17d)	37	~5 (40), ~1 (45)	1.0×10^{-3} (25)
(17e)	44	~5 (55), ~1 (65)	6.2×10^{-5} (25)
(17f)	< 10	< 1 (12)	Not detected
(17g)	59	> 30 (40)	4.0×10^{-5} (25)
<i>trans</i> -(17h)	14	~8 (15)	1.0×10^{-3} (25)
<i>cis</i> -(17h)	< 10	~3 (15), < 1 (25)	2.3×10^{-3} (25)
(17i)	< 10	~16 (25)	4.6×10^{-4} (25)

^aThe numbers in parentheses in these two columns are the temperatures (degrees Celsius) at which the measurements were made.

flop of the functional surfactant rather than copper(II) permeation (Figure 17). Consequently, we were able to demonstrate that in the cationic vesicles we have studied, copper(II) ions do not permeate the bilayer membrane even when this is in its fluid state (see Figure 18).



The phenomenon of metal permeation has consequences on the reactivity of metallovessicles when these are studied as catalysts of the cleavage of PNPP. To get insights on the reactivity of these systems in vesicular aggregates, we synthesized [70] ligands (20) and (21) which share the same coordinating subunit and ammonium group but differ in the lipophilic backbone. Vesicles were obtained by sonication of 1:10 mixtures of the above ligand surfactants and nonfunctional surfactants 2C₁₆Br and 2C₁₆GlyBr. Upon addition of both the metal ion [copper(II)] and the substrate after the creation of the vesicles made of the (21)–2C₁₆GlyBr blend, the reactivity observed was only roughly half that expected for the stoichiometric amount of catalyst present [the

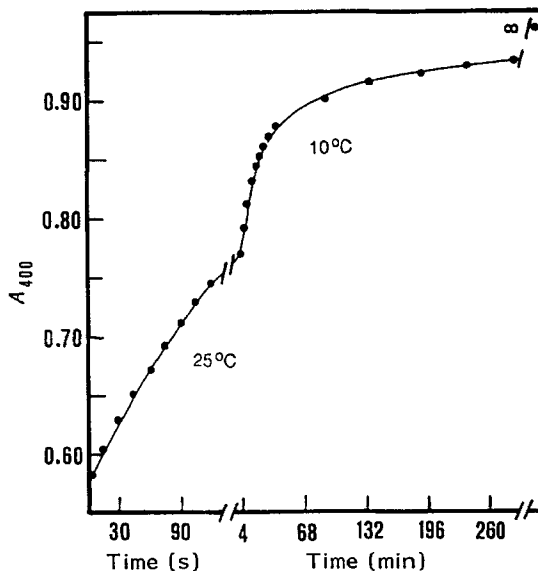


Figure 17 Time course of the kinetic experiment performed with surfactant substrate (19) in vesicular $2C_{16}Br$ upon addition of $Cu(NO_3)_2$ ($[copper(II)] = 5 \times 10^{-3} M$, pH 5). The first part was run at $25^\circ C$, i.e. above the T_c of the membrane. At this temperature the kinetics are monophasic. The second part was run at $10^\circ C$. If during the time at $25^\circ C$ copper(II) permeation occurred, monophasic kinetics would be expected since all the substrate (in the internal and external layers) is exposed to the metal ion. Since a biphasic process is observed, no permeation has occurred and the stay of the vesicles above T_c involves only flip-flop of (19)

complex Cu^{II} (21)] and, in fact, observed with vesicular (20)– $2C_{16}Br$. This was in agreement with the fact that with the first system, namely (21)– $2C_{16}GlyBr$, only ligands on the outer leaflet of the bilayer could interact with the metal ion. However, the ligands may also act as carriers of copper(II) [71], at least when the membrane is in its fluid state. We have seen previously that hydrated metal ions are unable to permeate the membrane under any fluidity condition; replacement of water molecules with a lipophilic ligand changes the partition coefficient of the ions between bulk water and the membrane. If carrier-mediated permeation is faster than the cleavage process studied, all ligands become exposed to the metal ions and the full reactivity of the system can be observed even when the metal ions are added after the creation of the vesicles, as in our case. Control experiments supported the hypothesis that the dialkylammonium derivative (20) was acting as a carrier of copper (II) in the vesicle, while (21) was totally inefficient in this respect. Clearly, the transbilayer mobility of this ligand (in agreement with the results of Moss and coworkers

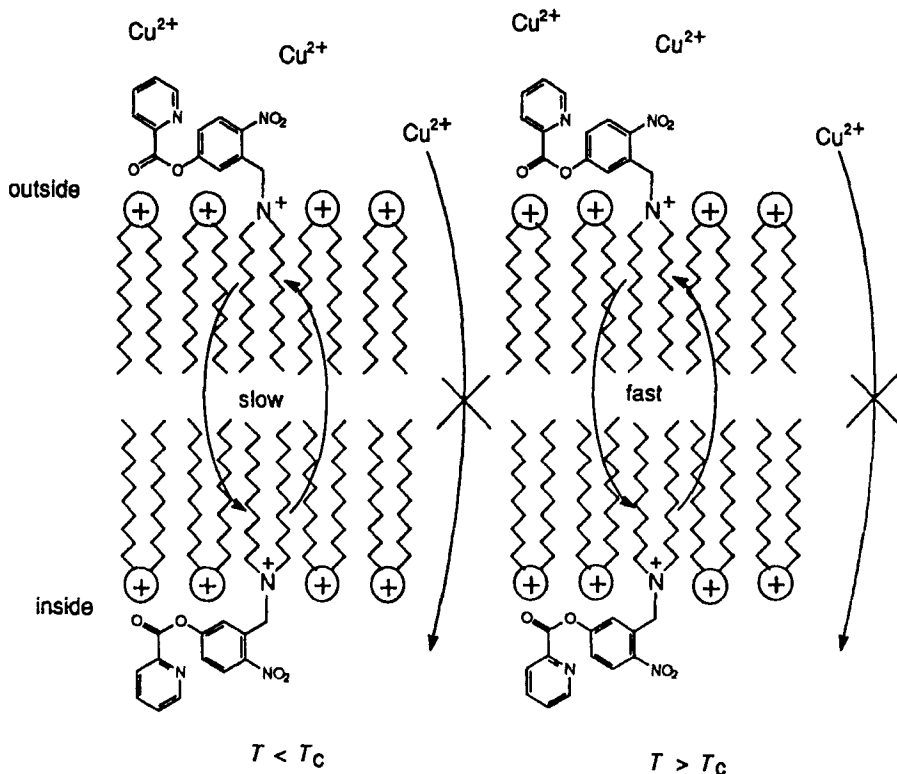
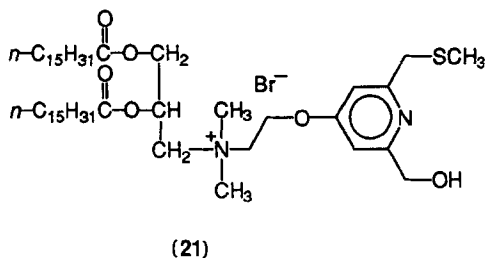
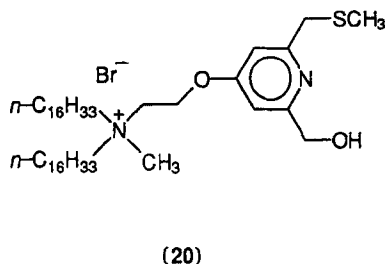


Figure 18 Schematic representation of the kinetic phenomena occurring below and above T_c in vesicles containing the surfactant probe (19). Note that copper(II) ions are added after the creation of the vesicles

described above) is far lower than that of (20). So, the reactivity of the system made of the vesicular blend (21)– $2\text{C}_{16}\text{GlyBr}$ can only take advantage of the formation of around half of the complex because the remainder of the potentially available ligand is not accessible to copper(II) ions (Figure 19).



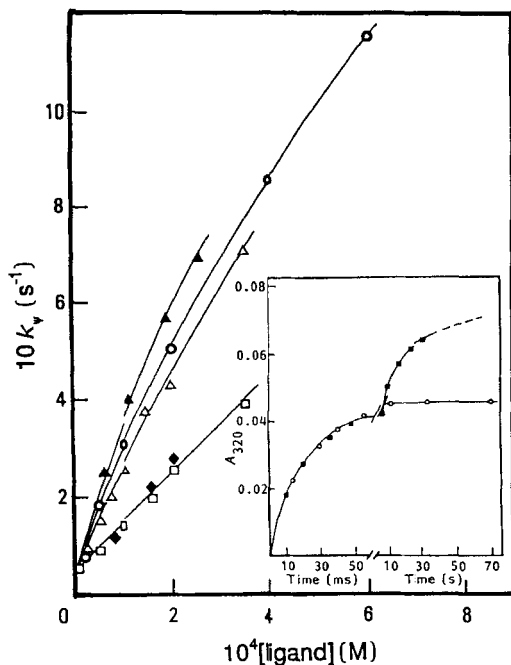


Figure 19 Dependence of the observed rate constant ($k\psi$) for the cleavage of PNPP on the ligand concentration in different vesicular blends (25 °C, [copper(II)] = 1.8×10^{-4} M), (20) and $2\text{C}_{16}\text{Br}$, ▲; CTABr, ○; $2\text{C}_{16}\text{GlyBr}$, △; (21) and $2\text{C}_{16}\text{Br}$, ■; $2\text{C}_{16}\text{GlyBr}$, □. The inset shows the time course of the absorbance increase observed upon addition of $\text{Cu}(\text{NO}_3)_2$ to the two different vesicular blends (20), ■; (21), ○. Only vesicles made of (20) and $2\text{C}_{16}\text{Br}$ show clearly biphasic behavior. The fast uptake of copper(II) by the ligand on the outer layer of the bilayer is followed by a much slower process, probably copper(II) permeation

4.5 Preaggregates

All the examples discussed so far concern the reactivity of (or in) aggregates above their cac. However, it must be pointed out that aggregation is not a sudden process; for instance, at concentrations below the cac, amphiphilic molecules form clusters that grow in size and monomer composition (aggregation number). The cac denotes the concentration at which this growth has reached the maximum size compatible with the structure of the amphiphile, the composition of the aqueous solution and the presence of lipophilic species. Evidence supporting the existence of these small clusters has been reported [72]. These small preaggregates may also influence reactivity. A striking example has been reported recently by Menger and Fei [73a]. Using equimolar amounts of premicellar concentrations (2×10^{-5} M) of the surfactant amide (22) and hexadecanoate at pH 8, they observed a very fast cleavage of (22) with formation

of the anhydride (**23**). The $t_{1/2}$ of the process was 3.1 min, in contrast to the immeasurably low rate of cleavage of the amide alone (half-life estimated at over one year). Furthermore, when large amounts of acetate are used as reactant instead of the hexadecanoate, the reaction still has $t_{1/2} > 450$ h (estimated). Accordingly, hexadecanoate is at least 10^8 times more effective than acetate in inducing the process. The authors suggest the formation of small clusters that they call “clumps”, defining them as “a multicomponent mixture of weakly associated species... that can function in concert”. Clearly, hydrophobic interactions and charge-charge interactions are at play here (Figure 20), so it is conceivable that the reaction occurs *via* a pseudointramolecular process as highlighted by the observed first-order kinetics, in spite of the equimolar concentrations of the two reactants.

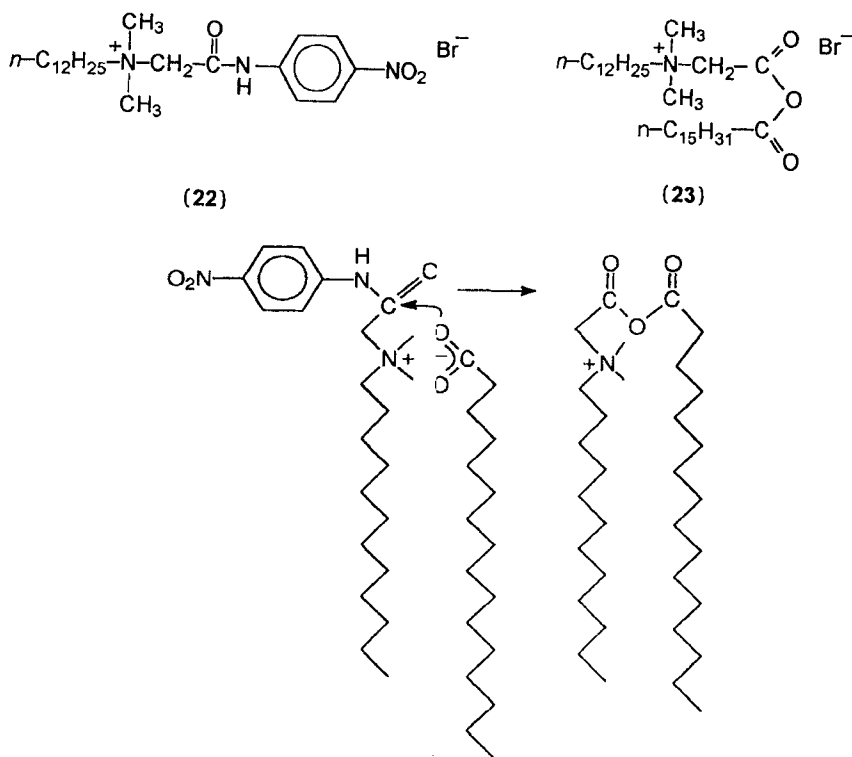


Figure 20 The cationic and amphiphilic substrate (**22**) interacts with anionic hexadecanoate to give (**23**) at a premicellar concentration. Both the hydrophobic and charge-charge interactions are needed to achieve the formation of the “clump”, as the system has been dubbed by Menger and Fei [73a] (these results have been questioned and the change of absorbance appears to be due to precipitation rather than to hydrolysis [73b])

5 AGGREGATES AS MICROREACTORS

Until now, we have seen clearly examples where the aggregates constitute the medium for the occurrence of the chemical reaction. The surfactant may take part in the reaction and compartmentalization within the same aggregate may give interesting modifications of reactivity. However, aggregates may also play the role of microreactors, allowing the solubilization of reagents in otherwise hostile environments or, even more challenging, the physical separation of reagents so that they may interact only when the proper conditions are realized. The parallel with macroscopic reactors is evident, though it must be clear that in the case of aggregates we are dealing with clear, optically transparent solutions without real phase separations. Membranes in living organisms also play this crucial role.

5.1 Enzymes in Hydrocarbon Solution

The use of enzymes in organic synthesis often poses the problem of the efficient interaction of the (usually) water-soluble protein with many substrates that are sparingly soluble in the aqueous medium. A possible solution comes from the solubilization of enzymes in reverse micelles in hydrocarbon solution. Reverse micelles (see Figure 4) are water pools surrounded by surfactants in hydrophobic solvents. The polar head-groups of the surfactant interact with water, while the hydrocarbon chains are solubilized in the organic solvent. These water pools can host several proteins, including enzymes as shown by the work done by Luisi [74], Martinek *et al.* [75a], Rahaman and Hatton [75b], Robinson and coworkers [76] and others [77]. Many of these enzymes remain active in this environment and do not experience denaturation of the protein structures. Since the activity of water in the aqueous pool inside the reverse micelle may be quite different from that of bulk water of the same pH and ionic composition because of the strong interaction with the charged head-groups of the surfactants, the reactivity of the enzymes may also be different. In some cases, even large rate accelerations have been observed [75a]. The hydrophobic substrate dissolved in the organic solvent may reach the enzyme through "holes" in the surfactant shell of the water pool where less hydrated regions of the protein may be exposed to the hydrocarbon solution. Other mechanisms to allow the binding of the substrate to the enzyme are possible and the matter is still being debated. A pictorial representation is given in Figure 21.

In some instances, water may not be necessary at all for the solubilization of the enzyme in a hydrocarbon solvent. A striking example has been provided by Okahata and coworkers [78] who solubilized lipase in benzene or *n*-hexane by coating the enzyme with the nonionic surfactant (**24**) or $2C_{16}Br$. The lipid-coated lipase showed activity for the synthesis of di- and triglycerides from monoglycerides and aliphatic acids.

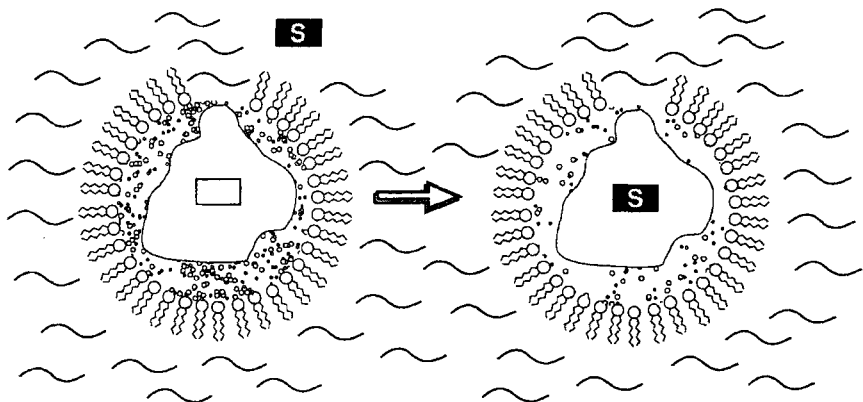
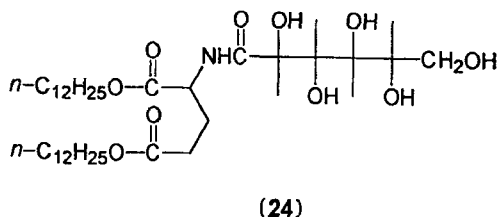


Figure 21 An enzyme entrapped in the water pool of a reverse micelle may interact with a water-insoluble substrate. The surfactant layer separating the aqueous from the hydrocarbon phase is in fast movement (very much like in regular micelles) and regions of the enzyme may be exposed to the organic solvent



5.2 Precipitation and Crystallization

Many living organisms are able to use vesicles as containers to be filled with salts for subsequent mineral formation [79]. Indeed, biological mineralization [79, 80] (biomineralization) plays an important role in life on earth as organisms ranging from plants to animals are able to produce minerals used to perform a wide variety of functions. Though current understanding of the processes that control biomineralization *in vivo* is very superficial, there is enormous interest in reproducing them in the chemical laboratory. It is obvious that the possibility of constructing organized microscopic (nanoscale) inorganic materials is of importance in electronics, catalysis, magnetism and sensory devices [80, 81].

An early example of the precipitation of Ag_2O crystallites within unilamellar vesicles was reported by Mann and coworkers [82] in 1983. They were able to obtain small particles of controlled size (~ 10 nm) by applying the following protocol (Figure 22). Phosphatidylcholine vesicles containing silver(I) ions were obtained by sonication at a temperature above T_c of pH 5 solutions of lipid very concentrated in AgNO_3 . The resulting aggregates were then passed

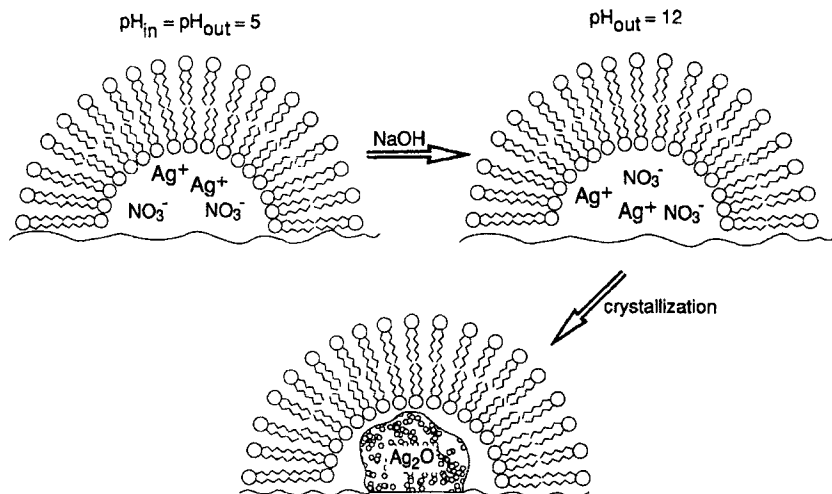


Figure 22 Schematic representation of the protocol followed by Mann and coworkers [82] for the precipitation of crystallites of Ag_2O 10 nm in size inside unilamellar phosphatidylcholine vesicles

down a cation-exchange column in order to remove external silver(I) ions. The pH was subsequently raised to ~ 12 by addition of NaOH solution to the vesicle dispersion. This caused the darkening of the solution owing to the formation of intravesicular Ag_2O crystallites. Crystallization of the oxide was shown to be dependent on the permeation of OH^- across the membrane. The kinetic process appears to be controlled by the in-out rate of diffusion of the trapped counterion of silver(I). Since the precipitates consisted of single-domain crystallites, the authors suggested that crystallization initiates at a single site on the internal leaflet of the vesicle.

More recently, Fendler and coworkers have used surfactant vesicles as hosts for colloidal semiconductor particles [83]. For instance, dihexadecyl phosphate (DHP) and $2\text{C}_{18}\text{Br}$ vesicles incorporating CdS, ZnS and mixed CdS–ZnS particles have been obtained and used for the realization of nanoscale photoelectric devices (see later). It is important to point out, however, that the presence of the closed vesicle does not appear, at least with these systems, to be of critical importance for the control of the size of the particles, as similar phenomena also occurs in Langmuir–Blodgett films [84], suggesting that a crucial role in nucleation is played mainly by the surface.

ZnSe-coated DHP vesicles led to charge separation upon irradiation and to electron transfer to methylviologen in the presence of sacrificial electron donors like glucose or cysteine [85]. The process is pH dependent as no current was observed below pH 9, while above this pH the photocurrent was linearly dependent on pH. The anodic photocurrent results from electrohole

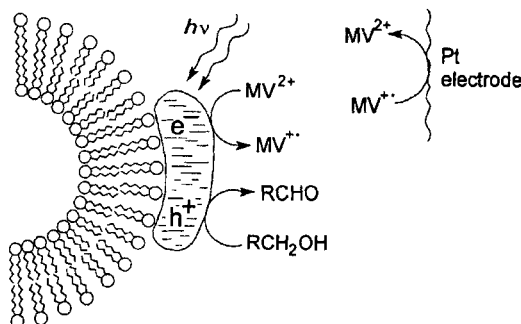


Figure 23 ZnSe particles on the surface of DHP vesicles lead to charge separation [$ZnSe(e^- + h^+)$] upon irradiation [85]. $ZnSe(e^-)$ reacts with methylviologen (MV^{2+}) to give $MV^{\bullet+}$. Glucose (RCH_2OH) depletes the holes (h^+) by electron transfer and is oxidized, while the electrode reconverts $MV^{\bullet+}$ to MV^{2+} .

photoproduction followed by electron transfer to methylviologen and subsequent reoxidation of the formed radical cation at the external electrode surface (Figure 23).

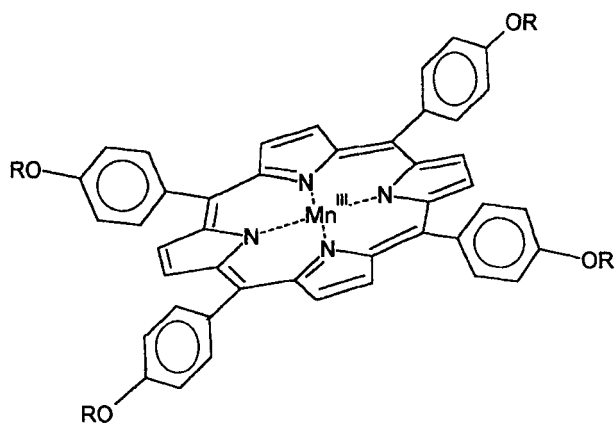
5.3 Redox Processes

The ability of membranes to compartmentalize reagents and control the permeation of chemical species may also allow the control of electron transfer in a more sophisticated way within the aggregate bilayer [86]. Photosynthetic processes occur specifically in membranes [87] (thylakoid membranes) so there is continuous interest in mimicking these phenomena with synthetic vesicles [86]. Though a large amount of information is available on the components of biological systems that operate electron transport, the actual mechanism of the process is far from being understood in detail.

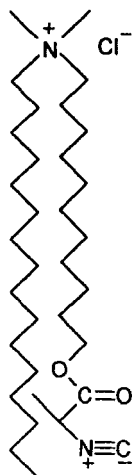
Other membrane-bound enzymes are known to catalyze oxygen transfer. Among them, cytochrome-P450-dependent monooxygenases catalyze a large number of reaction including the epoxidation of alkenes by molecular oxygen [88]. A few systems mimicking the oxygen activation and transfer step of cytochrome P450 in model vesicular membranes have recently been described.

In 1986, Nolte and coworkers reported a membrane-bound manganese porphyrin that was effective in the epoxidation of styrene and 2,5-dihydrofuran [89]. The system comprises a polymerized vesicular aggregate made of cationic surfactant (**26**), the lipophilic manganese(III) porphyrin (**25**) and membrane-bound methylene blue (**27**) (Figure 24). Recent investigation [90] showed that this porphyrin lies at the interface between the two leaflets of the membrane. The vesicles contain colloidal platinum entrapped in the internal water pool. In an O_2 - H_2 atmosphere, H_2 converts (**27**) to its reduced form; this is then reoxidized by manganese(III), in this way producing the manganese(II)

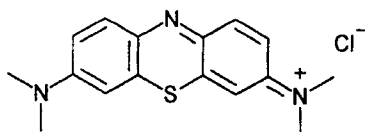
porphyrin that reduces molecular oxygen to give the species that eventually oxidizes the alkene. The overall process consists in the conversion of H_2 and O_2 into H_2O (nonproductive reaction) and the oxidation of the substrate, in strict analogy with the enzymatic transformation. The polymerized vesicular membrane not only provides the proper environment for the occurrence of the chemical transformation but also allows the compartmentalization of the reactants involved in the redox cascade described above.



(25) $R = n-C_{16}H_{33}$



(26)



(27)

The realization of the above system is quite interesting; however, it would be even more challenging to take advantage of the relative order of the vesicular membrane to achieve site-selective oxidation of a substrate. Successful results in this direction have been obtained by Groves and Neumann. They synthesized the iron(III) porphyrin (28) which includes four appended steroid moieties. They were able to demonstrate that in dimyristoylphosphatidylcholine (DMPC) vesicles, the porphyrin ring was buried in the middle of the bilayer and parallel to the plane defined by the membrane-water interface [91], as schematically shown in Figure 25. The four lipophilic steroid moieties do not protrude from the same side of the porphyrin plane; instead, two stick out from one side and two from the other in an alternating fashion. Obviously, amphiphilic substrates interact with the vesicular membrane with their lipophilic portion inserted into the apolar interior of the bilayer close to the porphyrin. As a consequence, if more than one double bond is present in the substrate, only that closest to the lipophilic end of the molecule is oxidized regardless of its intrinsic reactivity (as determined from experiments in homogeneous solution). For instance, oxidation of desmosterol (29) leads to the formation of the 24,25-epoxide and not of the 5,6-epoxide, even though the 5,6-double bond is the more reactive in homogeneous solution (by a factor of around four).

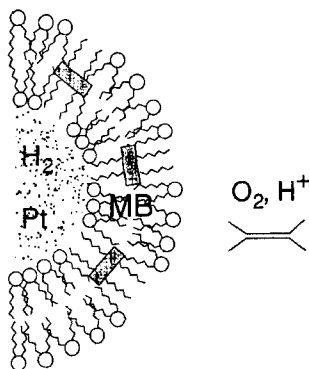


Figure 24 Polymerized vesicles made of the surfactant (26) and containing the membrane-bound manganese(III) porphyrin (25) were used by Nolte and coworkers to mimic cytochrome P450 oxidation of alkenes. The vesicles contain colloidal platinum in the internal water pool. Within the microreactor H_2 and O_2 are converted to H_2O and the alkene is epoxidized [89]. MB denotes membrane-bound methylene blue (27)

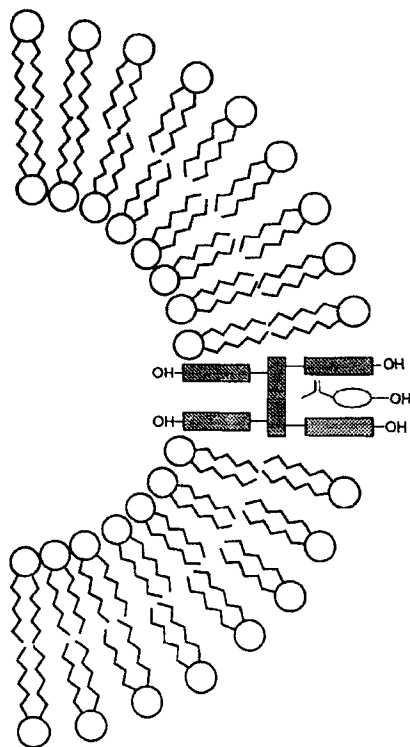
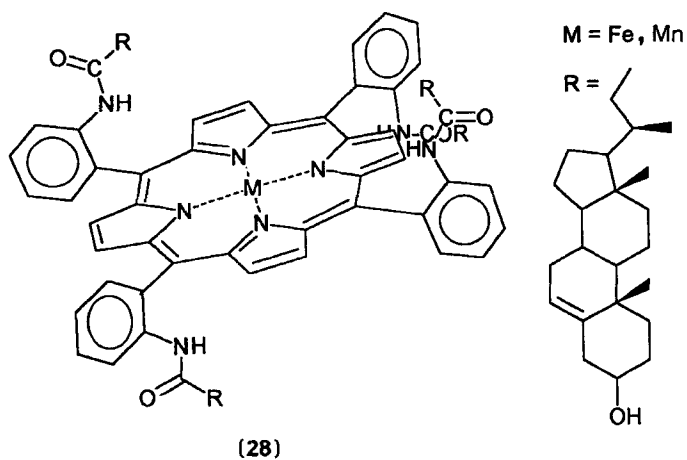
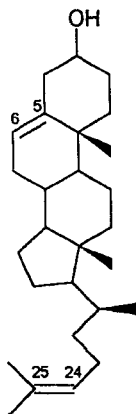


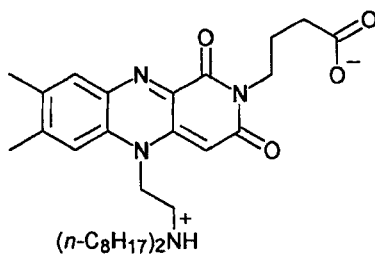
Figure 25 Schematic rendition of the mode of binding of the steroid-functionalized porphyrin (**28**) and the possible interaction with a steroid substrate at the site of oxidation, as suggested by Groves and Neumann [91]





(29)

The manganese(III) complex of the same porphyrin has been used, again by Groves, as part of a multicomponent catalytic vesicular assembly in which electrons derived from the decarboxylation of pyruvic acid (by pyruvate oxidase) reduce manganese(III). The manganese(III) porphyrin complex then mediates molecular oxygen activation and transfer [92]. A schematic representation of such a process is given in Figure 26. The substrate is ethylbenzene, which is converted into acetophenone in a catalytic manner with 20 turnovers of the manganese(III) porphyrin catalyst. The transfer of electrons from the enzyme to the porphyrin is mediated by the amphiphilic flavin derivative (30).



(30)

The above examples from the laboratories of Groves and Nolte provide quite impressive evidence of the way in which a vesicular membrane can host a variety of systems which eventually cooperate for the achievement of a chemical transformation. The last example I am going to discuss shows

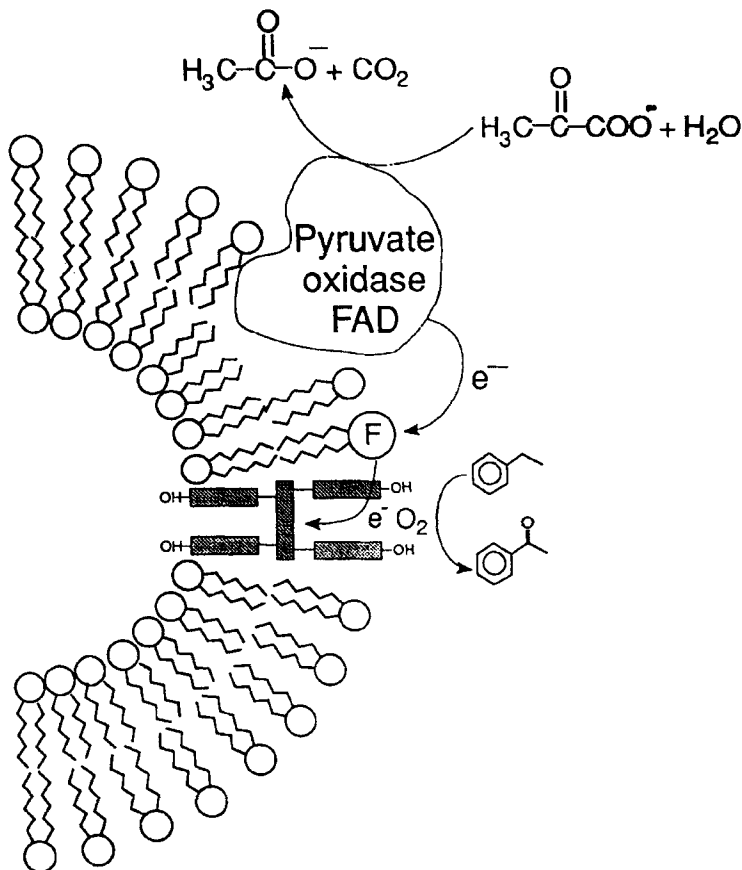
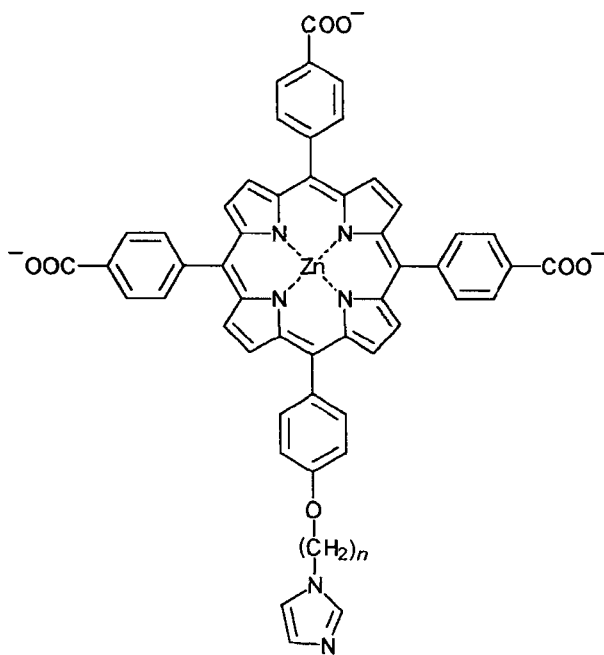


Figure 26 The manganese(III) steroid porphyrin (28) embedded in a DPPC membrane acts as an oxidation catalyst and converts ethylbenzene into acetophenone. An e^- cascade mediated by the amphiphilic flavin derivative (30) (F in the picture) reduces manganese(III) porphyrin to manganese(II) porphyrin which activates and transfers molecular oxygen [92] (FAD denotes tightly bound flavin adenine dinucleotide cofactor)

beautifully how the membrane may allow the correct positioning (relative distance, geometry) of reacting species, an aspect mastered by natural systems.

It has been shown that the rate of electron transfer (actually $\ln k_{\text{ET}}$) varies linearly with distance [93] between electron donors and acceptors. This relationship has been established by studying covalently bound systems where the distances are known and determined by the way the different molecules have been designed. A lipid membrane, however, may provide the proper environment for hosting the donor and acceptor molecules and, providing they

are properly compartmentalized and segregated one from the other, a precise spacing between the two of them may be achieved with consequent control of the rate of electron transfer. This idea was experimentally realized by Groves *et al.* quite recently. They [94] studied the transfer of electrons to ferricytochrome c from the membrane-bound manganese(II) porphyrin (**28**). For the experiment, they prepared small, unilamellar vesicle made of an 8:2 blend of DPPC and DMPC containing manganese(III) porphyrin (**28**). As we have seen above, this steroid porphyrin binds to the membrane in the middle of the bilayer between the two leaflets of lipids. The metal center of this porphyrin binds to the tethered imidazole of the anionic porphyrin (**31**), which, consequently, is anchored on the surface of the membrane. Externally added cytochrome c specifically binds to the vesicles on the surface where (**31**) is located through electrostatic interactions with the anionic carboxylate groups and the positively charged lysine patch which is known to surround the heme edge of the protein. This three-component ensemble is depicted in Figure 27. Irradiation of the solution with a xenon arc lamp led to photoreduction of manganese(III) to manganese(II) followed by electron transfer to ferricytochrome c. The rate of this process was shown to be in good accord with the distance (~ 22 Å) between donor and acceptor as imposed by the thickness of a single leaflet of the bilayer.



(31)

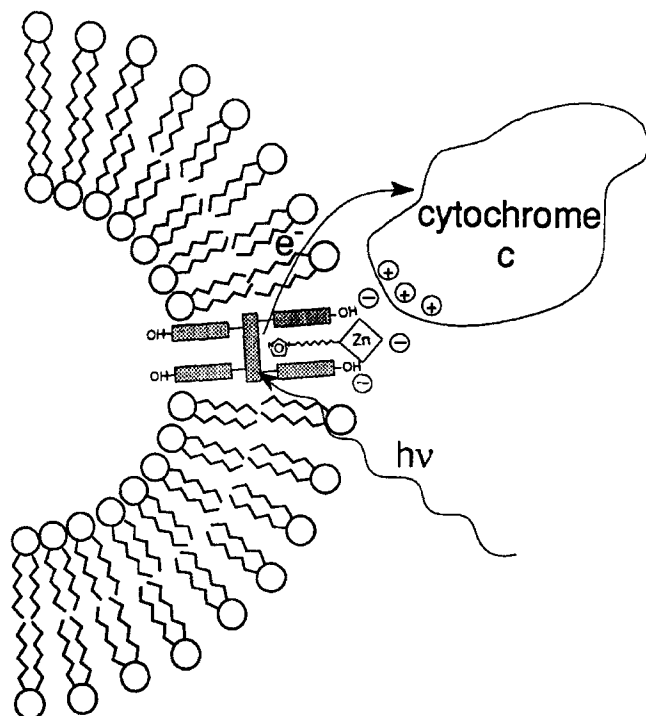
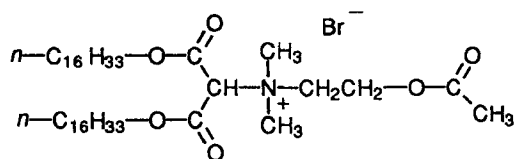


Figure 27 The ternary system made of manganese(II) porphyrin (28), tethered porphyrin (31) and ferricytochrome c, held together by the liposome bilayer, allows, upon irradiation, the electron transfer from porphyrin (28) to cytochrome c [94]

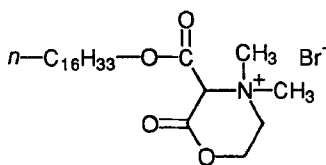
5.4 Drug Delivery

The idea of using vesicles as Trojan horses to deliver drugs *in vivo* is not new. However, in the past the feasibility of such an approach has been hampered by several practical problems. These have largely to do with the instability of many of these aggregates in biological fluids. Obviously, if the liposomal structure is rapidly lost with consequent release of the encapsulated or membrane-bound drug, the possibility to target the delivery of the drug is lost. This problem has recently been solved with the introduction of poly(ethylene glycol)-functionalized lipids (32), which, when used in 5–10% mixtures with natural lipids, greatly enhance the stability of the resulting liposome. It is believed [96] that the enhanced liposome stability is due to the prevention of the interaction of the liposomal membrane with the macromolecules as a result of the barrier constituted by the polymeric polar head of (32). These sterically stabilized liposomes have reached the market and are known as Stealth (a registered trade name of Liposome Technology Inc.) liposomes. A pictorial

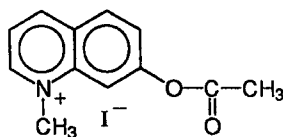
An example of enzyme-induced leakage of a trapped molecule has recently been reported by Menger and Johnston [98]. Their approach has been that of devising an amphiphilic molecule that can be cleaved by an enzyme. It is obviously quite interesting to realize a vesicular system that can be "opened" by an enzyme residing on the target site, in this way leading to the selective release of the drug. They have synthesized the cationic amphiphile (33) which, because it possesses two long hydrocarbon tails, forms vesicles in aqueous solution. Since (33) features an acetylcholinelike moiety, it reacts with the enzyme acetylcholinesterase. The enzyme hydrolyzes the acetyl group of the molecule and the alcoholic residue formed reacts intramolecularly to give (34) and *n*-hexadecanol. Compound (34) is still an amphiphilic molecule but with a single hydrocarbon tail, so it cannot sustain a bilayer structure. As a consequence, the vesicle is destroyed and the reaction, started by the acetylcholinesterase, leads to the final release of all molecules trapped inside. The occurrence of such a process was proved by encapsulating compound (35) inside vesicles made of surfactant (33). The quinolinium derivative (35), once deacetylated, becomes fluorescent. Upon addition of acetylcholinesterase to the above vesicular dispersion, the authors observed a very rapid outburst of fluorescence: the enzyme destroys the vesicles and, in hydrolyzing released (35), allows the detection of the decapsulation process. Notably, heat-denatured acetylcholinesterase, or a different enzyme, like acid phosphatase, is totally incapable of inducing vesicle "lesion" and destruction. This highlights the high selectivity of the process. The overall decapsulation protocol is illustrated in Figure 29.



(33)



(34)



(35)

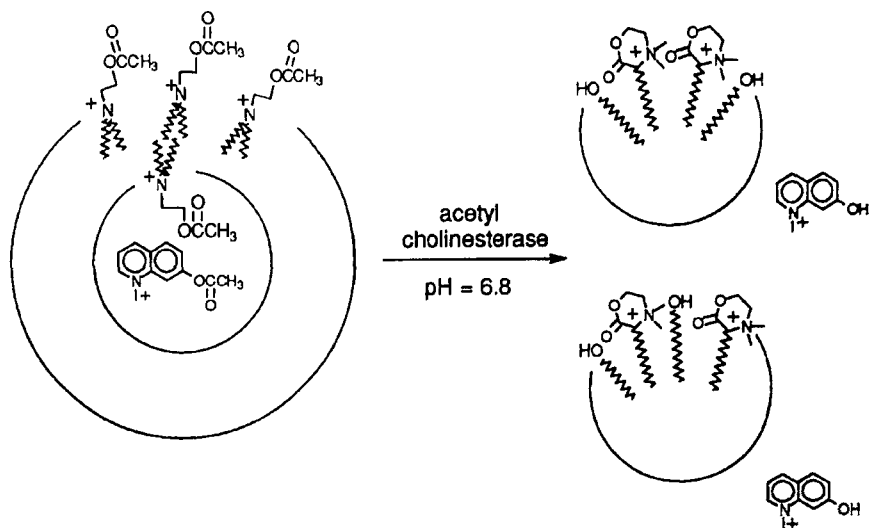


Figure 29 Vesicles made of the double-tailed surfactant (33) and containing in the internal water pool the quinolinium derivative (35) are destroyed by acetylcholinesterase, very probably leading to the formation of micelles made of (34) and *n*-hexadecanol. In the process, (35) is also released and cleaved by the enzyme [98]

Finally, it should be mentioned that the release of hydrophilic compounds entrapped in liposomes by means of the interaction of the liposomes with hydrophobic polyelectrolytes has recently been reported and shown to be pH sensitive [99].

6. CONCLUSION

The late 1970s and early 1980s were devoted to understanding the principles governing reactivity in aggregates (particularly micelles). Attention is now focused on more complex structures like vesicles, for which many interesting features relevant to reactivity in these aggregates are not fully understood. However, the challenge for the turn of the century is to realize systems able to work as molecular-scale devices where the scientist controls, by properly designing the monomeric lipids and their assemblies, the specific functions that he wants to trigger.

In the very near future, we will see the realization of new biomolecular materials [100] or totally synthetic materials able to take advantage of the unique properties of aggregates of molecules. The fact that biological systems use lipid aggregates for performing so many processes indicates that the potential of such systems is enormous and should be fully exploited.

I hope that this chapter will stimulate new research in this area and help to bring about new, exciting developments in the next few years.

7. ACKNOWLEDGMENTS

I am deeply indebted to my friends and colleagues (listed in alphabetical order) C. A. Bunton, R. A. Moss and U. Tonellato. Association with them has stimulated my interest in this field. Special thanks are due to Dr P. Tecilla with whom I have shared the excitement (and occasional disappointments) of much of our research reported here. Our technician, Mr E. Castiglione, was involved in producing the artwork for this chapter.

8. REFERENCES

1. M. Jain, *Introduction to Biological Membranes*, 2nd edn, Wiley, New York.
2. C. Tanford, *The Hydrophobic Effect*, 2nd edn, Wiley, New York, 1980.
3. J. N. Israelachvili, *Intermolecular and Surface Forces*, 2nd edn, Academic Press, London, 1992.
4. J. H. Fendler and E. J. Fendler, *Catalysis in Micellar and Macromolecular Systems*, Academic Press, New York, 1975.
5. J. H. Fendler, *Membrane Mimetic Chemistry*, Wiley, New York, 1982.
6. F. M. Menger, *Angew. Chem., Int. Ed. Engl.*, **30**, 1086 (1991).
7. D. D. Lasic, *Liposomes*, Elsevier, Amsterdam, 1993.
8. T. Kunitake, *Angew. Chem., Int. Ed. Engl.*, **31**, 709 (1992).
9. F. Diederich and K. Dick, *J. Am. Chem. Soc.*, **106**, 8024, (1984).
10. R. Fornasier, F. Reniero, P. Scrimin and U. Tonellato, *J. Inclusion Phenom.*, **6**, 175 (1988).
11. S. Pistorello, P. Scrimin, P. Tecilla, U. Tonellato, B. P. Andreini and L. F. Zerilli, *J. Org. Chem.*, **59**, 5080 (1994).
12. (a) M. Ramadan, D. F. Evans, R. Lumry and S. Philison, *J. Phys. Chem.*, **89**, 3405 (1985); (b) I. Rico and A. Lattes, *J. Phys. Chem.*, **90**, 5870 (1986); (c) H. Garibi, R. Palepu, G. J. T. Tiddy, D. G. Hall and E. Wyn-Jones, *J. Chem. Soc., Chem. Commun.*, 115 (1990); (d) A. Lattes, M. J. Marti, I. Rico, C. Petipas and X. Anvray, in *Surfactants in Solution* (eds K. L. Mittal and D. O. Shah), Vol 11, Plenum Press, New York, 1991, p. 127.
13. (a) P. Smit, P. A. J. Hilbers, K. Esselink, L. A. M. Rupert, N. M. van Os and A. G. Schlijper, *Nature*, **348**, 624 (1990); (b) J. J. Wendoloski, S. J. Kimatian, C. E. Schutt and F. R. Salemme, *Science*, **243**, 636 (1989); (c) F. M. Menger and D. W. Doll, *J. Am. Chem. Soc.*, **106**, 1109 (1984).
14. (a) F. M. Menger, J. M. Jerkunica and J. C. Johnston, *J. Am. Chem. Soc.*, **100**, 4676, (1978); (b) F. M. Menger and C. F. Mounier, *J. Am. Chem. Soc.*, **115**, 12 222 (1993).
15. (a) M. Corti and L. Cantù, *Surfactants in Solution* (eds K. L. Mittal and D. O. Shah) Vol 11, Plenum Press, New York, 1991, p. 171; (b) L. Cantu, M Corti and P. Salina, *J. Phys. Chem.*, **95**, 5981, (1991).

16. (a) E. Bairaktari, D. F. Mierke, S. Mammi and E. Peggion, *Biochemistry*, **29**, 10 090 (1990); (b) R. Battistutta, A. Bisello, S. Mammi and E. Peggion, *Biopolymers*, **34**, 1535, (1994).
17. Exceptions are known; for example, see L. Cantù, M. Corti, S. Sonnino and G. Tettamanti, *Chem. Phys. Lipids*, **41**, 315, (1986).
18. The ionic strength of the solution also appears to be critical for the formation of closed vesicles; for example, see (a) R. B. Pansu, B. Arrio, J. Roncin and J. Faure, *J. Phys. Chem.*, **94**, 796, (1990); (b) R. B. Pansu, L. Lan, J. Faure and J. Roncin, *New J. Chem.*, **14**, 105, (1990).
19. F. M. Menger, P. Aikens and M. Wood Jr, *J. Chem. Soc., Chem Commun.*, 180 (1988).
20. (a) D. W. Deamer and J. Bramhall, *Chem. Phys. Lipids*, **40**, 167 (1986); (b) E. A. Disalvo, *Adv. Colloid Interface Sci.*, **29**, 141 (1988).
21. A. G. Lee, *Prog. Biophys Biol.*, **29**, 3 (1975).
22. E. W. Kaler, A. Kalamakara Murthy, B. E. Rodriguez and J. A. N. Zasadzinski, *Science*, **245**, 1371, (1989).
23. (a) J.-H. Fuhrhop, H.-H. David, J. Mathieu, U. Liman, H.-J. Winter and E. Boekema, *J. Am. Chem. Soc.*, **108**, 1785, (1986); (b) G. H. Escamilla and G. R. Newkome, *Angew. Chem., Int. Ed. Engl.*, **33**, 1937 (1994).
24. J. B. F. N. Engberts and W. Blokzijl, *Angew. Chem., Int. Ed. Engl.*, **32**, 1545 (1993).
25. H. Bertagnolli, *Angew. Chem., Int. Ed. Engl.*, **31**, 1577 (1992) and references therein.
26. T. Kunitake and S. Shinkai, *Adv. Phys. Org. Chem.*, **17**, 435 (1980).
27. C. A. Bunton and G. Savelli, *Adv. Phys. Org. Chem.*, **22**, 213 (1986).
28. U. Tonellato, *Coll. Surf.*, **35**, 121 (1989).
29. C. A. Bunton, F. Nome, F. H. Quina and L. S. Romsted, *Acc. Chem. Res.*, **24**, 357 (1991).
30. An approach for the determination of the interfacial composition of ions (and water) in aggregates has recently been described: (a) A. Chadhuri, J. A. Longhlin, L. S. Romsted and J. Yao, *J. Am. Chem. Soc.*, **115**, 8351 (1993); (b) A. Chadhuri, L. S. Romsted and J. Yao, *J. Am. Chem. Soc.*, **115**, 8362 (1993); (c) J. Yao and L. S. Romsted, *J. Am. Chem. Soc.*, **116**, 11 779 (1994).
31. R. Fornasier and U. Tonellato, *J. Chem. Soc., Faraday Trans. 1*, **76**, 1301 (1980).
32. K. J. Laidler and P. S. Bunting, *The Chemical Kinetics of Enzyme Action*, 2nd edn, Clarendon Press, Oxford, 1973, Chap. 11.
33. P. A. Bachman, P. Walde, P. L. Luisi and J. Lang, *J. Am. Chem. Soc.*, **113**, 8204, (1991).
34. For other systems outlining the same concept see (a) P. A. Bachman, P. Walde, P. L. Luisi and J. Lang, *Nature*, **357**, 57 (1992); (b) P. K. Schmidli, P. Schurtenberger and P. L. Luisi, *J. Am. Chem. Soc.*, **113**, 8127 (1991); (c) P. A. Bachman, P. L. Luisi and J. Lang, *Nature*, **357**, 57 (1992); (d) P. Walde, R. Wick, M. Fresta, A. Mangone and P. L. Luisi, *J. Am. Chem. Soc.*, **116**, 11 649 (1994).
35. C. A. Bunton and J. R. Moffatt, *J. Phys. Chem.*, **90**, 538, (1986).
36. C. A. Bunton, in *Surfactants in Solution* (eds K. L. Mittal and D. O. Shah), Vol 11, Plenum Press, New York, 1991, p. 17.
37. T. Kunitake, Y. Okahata, R. Ando, S. Shinkai and S. Hirakawa, *J. Am. Chem. Soc.*, **102**, 7877 (1980).
38. (a) F. M. Menger, *Acc. Chem. Res.*, **18**, 128 (1985); (b) F. M. Menger, *Acc. Chem. Res.*, **26**, 206 (1993).
39. C. Reichardt, *Solvent and Solvent Effects in Organic Chemistry*, 2nd edn, VCH, Weinheim, 1988, p. 27.

40. (a) M. K. Jain, J. Rogers, L. Simpson and L. Gierasch, *Biochim. Biophys. Acta*, **816**, 153 (1985); (b) M. K. Jain and H. B. White, *Adv. Lipid Res.*, **15**, 1 (1977).
41. M. Jain *Introduction to Biological Membranes*, 2nd edn, Wiley, New York, 1988, Chap. 5.
42. (a) T. Kunitake, H. Ihara and Y. Okahata, *J. Am. Chem. Soc.*, **105**, 6070 (1983); (b) M. Shimomura and T. Kunitake, *J. Am. Chem. Soc.*, **104**, 1757 (1982).
43. R. A. Moss, P. Scrimin, S. Bhattacharya and S. Swarup, *J. Am. Chem. Soc.*, **109**, 6209 (1987).
44. (a) A. Ochoa-Solano, G. Romero and C. Gitler, *Science*, **156**, 1243 (1967); (b) C. Gitler and A. Ochoa-Solano, *J. Am. Chem. Soc.*, **90**, 5004 (1968); (c) W. Tagaki, M. Chigira, T. Ameda and Y. Yano, *J. Chem. Soc., Chem. Commun.*, 219 (1972); (d) J. M. Brown and C. A. Bunton, *J. Chem. Soc., Chem. Commun.*, 969 (1974); (e) U. Tonellato, *J. Chem. Soc., Perkin Trans. 2*, 771 (1976); (f) U. Tonellato, *J. Chem. Soc., Perkin Trans. 2* 821 (1977); (g) R. A. Moss, R. C. Nahas and S. Ramaswami, *J. Am. Chem. Soc.*, **99**, 627 (1977).
45. R. A. Moss and K. Y. Kim, *Isr. J. Chem.*, **25**, 11 (1985).
46. (a) P. L. Yeagle, *Acc. Chem. Res.*, **11**, 321 (1978); (b) K. Beyer, *Biochim. Biophys. Acta*, **855**, 365 (1986); (c) L. A. Meijer, F. A. M. Leermakers and J. Lyklema, *Recl. Trav. Chim. Pays-Bas*, **113**, 167 (1994).
47. P. Scrimin, P. Tecilla and U. Tonellato, *J. Phys. Org. Chem.*, **5**, 619 (1992) and references therein.
48. For details on metallomicelles see (a) R. Fornasier, P. Scrimin, P. Tecilla and U. Tonellato, *J. Am. Chem. Soc.*, **111**, 224 (1989); (b) W. Tagaki and K. Ogino, *Top. Curr. Chem.*, **128**, 144 (1985); (c) S. H. Gellman, R. Petter and R. Breslow, *J. Am. Chem. Soc.*, **108**, 2388 (1986); (d) J. G. J. Weijnen, A. Kondijs and J. F. J. Engbersen, *J. Chem. Soc., Perkin Trans. 2*, 1121 (1991); (e) P. Scrimin, P. Tecilla and U. Tonellato, *J. Org. Chem.*, **56**, 161 (1991).
49. G. Ghirlanda, P. Scrimin and U. Tonellato, unpublished results.
50. C. A. Bunton, P. Scrimin and P. Tecilla, *J. Chem. Soc., Perkin Trans. 2*, 419 (1996).
51. F. M. Menger, L. H. Gan, E. Johnson and D. H. Durst, *J. Am. Chem. Soc.*, **109**, 2600 (1987).
52. J. H. Fendler, *Membrane Mimetic Chemistry*, Wiley, New York, 1982, p. 322.
53. R. A. Moss, C. J. Talkowski, D. W. Reger, and C. E. Pewell, *J. Am. Chem. Soc.*, **95**, 5215 (1973).
54. M. C. Cleij, W. Drenth, and R. J. M. Nolte, *J. Org. Chem.*, **56**, 3883 (1991).
55. J. G. J. Wijnen, A. Koudijs and J. F. J. Engbersen, *J. Org. Chem.*, **57**, 7258 (1992).
56. P. Scrimin, P. Tecilla and U. Tonellato, *J. Org. Chem.*, **59**, 4194 (1994).
57. P. Scrimin, P. Tecilla and U. Tonellato, *Langmuir*, in press.
58. (a) R. Ueoka, R. A. Moss, S. Swarup, Y. Matsumoto, G. Strauss and Y. Murakami, *J. Am. Chem. Soc.*, **107**, 2185 (1985); (b) R. Ueoka, Y. Matsumoto, R. A. Moss, S. Swarup, A. Sugii, K. Harada, J. Kikuchi and Y. Murakami, *J. Am. Chem. Soc.*, **110**, 1588 (1988); (c) R. Ueoka, Y. Matsumoto, T. Yoshima, N. Watanabe, K. Omura and Y. Marakami, *Chem. Lett.*, 1743 (1986); (d) Y. Ihara, K. Igata, Y. Okubo and M. Nango, *J. Chem. Soc., Chem. Commun.*, 1900 (1989).
59. For an example of sorting within the same aggregate of surfactants of different shape see M. Corti, L. Cantù and P. Salina, *Adv. Colloid Interface Sci.*, **36**, 153 (1991).
60. D. D. Lasiz, *Liposomes*, Elsevier, Amsterdam, 1993, p. 52.
61. R. A. Moss and S. Swarup, *J. Am. Chem. Soc.*, **108**, 5341 (1986).
62. D. W. Deamer and J. Bramhall, *Chem. Phys. Lipids*, **40**, 167 (1986); (b) E. A. Disalvo, *Adv. Colloid Interface Sci.*, **29**, 141 (1988).

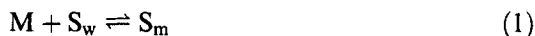
63. (a) R. A. Moss, S. Bhattacharya and S. Chatterjee, *J. Am. Chem. Soc.*, **111**, 3680 (1989); (b) R. A. Moss, T. Fujita and S. Ganguli, *Langmuir*, **6**, 1197 (1990); (c) R. A. Moss, S. Ganguli, Y. Okumura and T. Fujita, *J. Am. Chem. Soc.*, **112**, 6391 (1990); (d) R. A. Moss and T. Fujita, *Tetrahedron Lett.*, **31**, 2377 (1990); (e) R. A. Moss and T. Fujita, *Tetrahedron Lett.*, **31**, 7559 (1990); (f) R. A. Moss, T. Fujita and Y. Okumura, *Langmuir*, **7**, 2415 (1991); (g) R. A. Moss, T. Fujita and Y. Okumura, *Langmuir*, **7**, 400 (1991); (h) R. A. Moss and J.-M. Li, *J. Am. Chem. Soc.*, **114**, 9227 (1992); (i) R. A. Moss, T. Fujita, Y. Okumura, Z. Hua, R. Mendelson and L. Senak, *Langmuir*, **8**, 1731 (1992); (j) R. A. Moss, *Pure Appl. Chem.*, **66**, 851 (1994).
64. For other surface-differentiated vesicles see P. Tundo, K. Kurihara, D. J. Kippenberger, M. Politi and J. H. Fendler, *Angew. Chem., Int. Ed. Engl.*, **21**, 81 (1982).
65. F. M. Menger, X. Y. Chen, S. Brocchini, H. P. Hopkins and D. Hamilton, *J. Am. Chem. Soc.*, **115**, 6600 (1993).
66. M. Ladika, T. E. Fisk, W. W. Wu and S. D. Jons, *J. Am. Chem. Soc.*, **116**, 12093 (1994).
67. R. A. Moss, G. Li and J.-M. Li, *J. Am. Chem. Soc.*, **116**, 805 (1994).
68. G. Ghirlanda, P. Scrimin, P. Tecilla and U. Tonellato, *J. Org. Chem.*, **58**, 3025 (1993).
69. T. H. Fife and T. J. Przystas, *J. Am. Chem. Soc.*, **107**, 1041 (1985).
70. P. Scrimin, P. Tecilla and U. Tonellato, *J. Am. Chem. Soc.*, **114**, 5086 (1992).
71. P. Scrimin, P. Tecilla and U. Tonellato, *Tetrahedron*, **51**, 217 (1995).
72. (a) Y. Okahata, R. Ando and T. Kunitake, *J. Am. Chem. Soc.*, **99**, 3067 (1977); (b) C. A. Bunton and C. Quan, *J. Org. Chem.*, **49**, 5012 (1984); (c) G. Biresow and C. A. Bunton, *J. Org. Chem.*, **51**, 2525 (1986).
73. (a) F. M. Menger and Z. X. Fei, *Angew. Chem., Int. Ed. Engl.*, **33**, 346 (1994); (b) W. K. Fife and S. Liu, *Angew. Chem., Int. Ed. Engl.*, **34**, 2718 (1995).
74. P. L. Luisi, *Angew. Chem., Int. Ed. Engl.*, **24**, 439 (1985).
75. (a) K. Martinek, A. V. Levashov, Y. L. Khmelnitsky, N. L. Klyachko and I. V. Berezin, *Science*, **218**, 889 (1982); (b) R. S. Rahaman and T. A. Hatton, *J. Phys. Chem.*, **95**, 1799 (1991).
76. (a) P. D. I. Fletcher, A. M. Howe, B. Robinson and D. C. Steytler, in *Reverse Micelles—Technological and Biological Relevance*, (eds. P. L. Luisi and B. Straub) Plenum Press, New York, 1984, p. 73; (b) B. H. Robinson, D. Steytler and R. Tack, *J. Chem. Soc., Faraday Trans. 1*, **75**, 481 (1979).
77. (a) R. Hilhorst, C. Laane and C. Veeger, *FEBS Lett.*, **159**, 31 (1988); (b) C. Kumar and D. Balasubramanian, *J. Colloid Interface Sci.*, **74**, 64 (1980).
78. (a) Y. Okahata and K. Ijio, *J. Chem. Soc., Chem. Commun.*, 1392 (1988); (b) Y. Okahata, Y. Fujimoto and K. Ijio, *Tetrahedron Lett.*, **29**, 5133 (1988).
79. L. Addadi and S. Weiner, *Angew. Chem., Int. Ed. Engl.*, **31**, 153 (1992).
80. (a) S. Mann, *Nature*, **365**, 499 (1993); (b) S. Mann, *J. Chem. Soc., Dalton Trans.*, 1 (1993).
81. J. H. Fendler, *Chem. Rev.*, **87**, 877 (1987).
82. S. Mann and R. J. P. Williams, *J. Chem. Soc., Dalton Trans.*, 311 (1983); (b) S. Mann, M. J. Kim, R. G. Ratcliffe and R. J. P. Williams, *J. Chem. Soc., Dalton Trans.*, 771 (1983).
83. (a) Y.-M. Tricot and J. H. Fendler, *J. Am. Chem. Soc.*, **106**, 2475, 7359 (1984); H. J. Watzke and J. H. Fendler, *J. Phys. Chem.*, **91**, 581 (1987).
84. (a) S. Xu, X. K. Zhao and J. H. Fendler, *Adv. Mater.*, **2**, 183 (1990); (b) Y. Yuan, I. Cabasso and J. H. Fendler, *Chem. Mater.*, **2**, 226 (1990).
85. A.-C. Chang, W. F. Pfeiffer, B. Guillaume, S. Baral and J. H. Fendler, *J. Phys. Chem.*, **94**, 4284 (1990).

86. J. N. Robinson and D. J. Cole-Hamilton, *Chem. Soc. Rev.*, **20**, 49 (1991).
87. M. Calvin, *Photochem Photobiol*, **37**, 349 (1983).
88. R. E. White and H. J. Coon, *Annu. Rev. Biochem.*, **49**, 315 (1980).
89. J. H. van Esch, M. F. M. Roks and R. J. M. Nolte, *J. Am. Chem. Soc.*, **108**, 6093 (1986).
90. J. T. Groves and S. B. Ungashe, *J. Am. Chem. Soc.*, **112**, 7796 (1990).
91. (a) J. T. Groves and R. Neumann, *J. Am. Chem. Soc.*, **111**, 2900 (1989); (b) J. T. Groves and R. Neumann, *J. Org. Chem.*, **53**, 3891 (1988); (c) J. T. Groves and R. Neumann, *J. Am. Chem. Soc.*, **109**, 5045 (1987).
92. J. T. Groves and S. B. Ungashe, *J. Am. Chem. Soc.*, **112**, 7796 (1990).
93. C. C Moser, J. M. Keske, K. Warcke, R. S. Farid and P. L. Dutton, *Nature*, **355**, 796 (1992).
94. J. T. Groves, G. D. Fate and J. Lahiri, *J. Am. Chem. Soc.*, **116**, 5477 (1994).
95. D. D. Lasic, *Liposomes*, Elsevier, Amsterdam, 1993, p. 265.
96. D. D. Lasic, *Angew. Chem., Int. Ed. Engl.*, **33**, 1685 (1994).
97. V. C. Anderson and D. H. Thompson, in *Macromolecular Assemblies* (eds P. Stroeve and E. Balasz), American Chemical Society, Washington, DC, 1992, p. 154.
98. F. M. Menger and D. E. Johnston Jr, *J. Am. Chem. Soc.*, **113**, 5467 (1991).
99. (a) J. L. Thomas and D. A. Tirrell, *Acc. Chem. Res.*, **25**, 336 (1992); (b) J. L. Thomas, H. You and D. A. Tirrell, *J. Am. Chem. Soc.*, **117**, 2949 (1995).
100. J. G. Tirrell, M. J. Fournier, T. L. Mason and D. A. Tirrell, *Chem. Eng. News*, December 19, 40 (1994).
101. A. Fehrst, *Enzyme Structure and Mechanism*, Freeman, Reading, UK, 1977, Ch. 3.
102. L. S. Romsted, in *Surfactants in Solution* (eds K. L. Mittal and B. Lindman) Vol.2, Plenum Press, New York, p. 1015.

9. APPENDIX: QUANTITATIVE TREATMENT OF KINETIC DATA IN AGGREGATES

The quantitative treatment of kinetic data is based on the pseudophase separation approach, i.e. the assumption that the aggregate constitutes a (pseudo)phase separated from the bulk solution where it is dispersed. Some of the equations below are reminiscent of the well-known Michaelis-Menten equation of enzyme kinetics [101]. This formal similarity has led many authors to draw a parallel between micelle and enzyme catalysis. However, the analogy is limited because most enzymatic reactions are studied with the substrate in a large excess over the enzyme. Even for systems showing a real catalytic behavior of micelles and/or vesicles, the above assumption of the aggregate as a pseudophase does not allow operation with excess substrate. The condition $[S] \ll [M]$ must be valid for the applicability of the equations given below (where S is the substrate and M is the micellized surfactant).

Let us consider first the system described as case (3) [27, 31] in Section 3 representing a functional aggregate. This is the simplest case. The following equations must be considered.



and

$$k_\psi = \frac{k^w + k^m K_s [M]}{1 + K_s [M]} \quad (4)$$

where k^w is the pseudo-first-order rate constant of the substrate S in the aqueous medium; k^m is the pseudo-first-order rate constant of the substrate in the micellar pseudophase; K_s is the thermodynamic binding constant of the substrate based on the concentration of micellized surfactant (see equation (1)); and $[M]$ is the concentration of micellized surfactant i.e. $[M] = [\text{surfactant}]_{\text{total}} - \text{cac}$).

The second-order rate constant in the aggregate can be obtained by multiplying k^m by the molar volume V_m of the reactive region in the aggregate

$$k_2^m = k^m V_m \quad (5)$$

Let us consider now cases (1) and (2) [29, 102] from Section 3. The reactant in these systems is not the surfactant itself but a third molecule Y (ion or lipophilic compound). We now have to consider the equilibrium



It is more convenient to separate the second-order rate constants. Accordingly

$$k_w = k_2^w [Y]_w \text{ and } k_m = k_2^m \frac{[Y]_m}{[M] V_m} \quad (7)$$

where $[Y]_w$ is the concentration of Y in water and $[Y]_m/[M]V_m$ represents the molar ratio of the reacting species in the aggregates divided by the molar volume (in liters per mole) of the reactive region. This allows us to take into account the higher local concentration of the reacting species (Y) caused by the smaller volume of the aggregate pseudophase. Now, k_2^w and k_2^m are the second-order rate constants in the aqueous and micellar pseudophases, respectively. Substituting equations (7) into equation (4), we obtain

$$k\psi = \frac{k_2^w[Y]_w + k_2^m K_S[Y]_m / V_m}{1 + K_S[M]} \quad (8)$$

It must be pointed out that the condition $[S] \ll [Y]_m \ll [M]$ must be valid in the entire concentration interval explored.

If the concentration of the reactant is held constant while the concentration of surfactant is increased, the reactivity profile goes through a maximum, as experimentally observed. At low $[M]$ the observed rate constant increases with $[Y]_m$ owing to the binding of the reactant (and the substrate) to the aggregate; at high $[M]$, $[Y]_m$ does not increase any more since $[Y]_m$ approaches $[Y]_{\text{total}}$ (all reactant bound to the aggregate), and consequently the dilution of reactants in the aggregate prevails. The situation is relatively simple for a lipophilic reactant [case 2] and more complex for an ionic species where $[Y]_m$ is controlled by the ion exchange between the reacting ion (Y) and the nonreacting counterion (X) at the (ionic) micelle interface [29, 30]

$$K_Y^X = \frac{[Y]_w[X]_m}{[Y]_m[X]_w} \quad (9)$$

Note that the observed behavior supports the assumption that the substrate in one aggregate unit (micelle, vesicle) does not react with the reactant in another: this is further evidence of effective compartmentalization in aggregates.

Chapter 4

Models of Hemoprotein Active Sites

MICHEL MOMENTEAU

Institut Curie, Orsay, France

1. INTRODUCTION

The mechanisms by which structure modulates reactivity at protein active sites pose one of the fundamental problems of molecular bioorganic and bioinorganic chemistry. The lack of detailed understanding of the connection between structure and function has impeded in many ways the development of new methodologies based on the concept of model building during the two past decades and on the current advances in genetic engineering.

In the biomimetic chemical approach to biological systems, it is possible to estimate the relative importance of chemical and stereochemical parameters which contribute to the overall activity of the proteins. Thus, in the case of metalloproteins, it becomes possible to design superstructured models of the active site which lack a macromolecular peptide backbone but contain chemical groups involved in biological processes.

Hemoproteins, ubiquitous among plants and animals, perform at least five important functions related to dioxygen and the production of energy: (1) dioxygen transport and storage by hemoglobin and myoglobin; (2) catalytic oxidation of organic compounds by cytochrome-P450-dependent monooxygenases; (3) decomposition and utilization of hydrogen peroxide by catalases and peroxidases; (4) reduction of dioxygen by cytochrome c oxidase; and (5) electron transfer by cytochromes. Although all these natural compounds contain iron porphyrin (heme) as a prosthetic group, the great variety of their remarkable properties is most probably related both to the

axial ligations of the metal and to the protein chains surrounding the heme. The former govern the electronic distribution on the metal and consequently the ligand binding on the other face of the macrocyclic ring. The latter offer a microenvironment able to modulate the reactivity of the prosthetic group without participating directly in the reaction. Thus, the study of metalloporphyrins is of interest for the detailed understanding of the function of the hemoproteins. However, studies of simple iron porphyrins show that the characteristics of the metal (spin state, oxidation state and coordination number) can vary depending on the nature of the solvent and the axial ligands. Until recently, particular attention has been paid to the reactivity of superstructured metalloporphyrins in which superstructures linked to the porphyrin macrocycle allow us to create cavities mimicking the protein pockets surrounding the active sites and controlling ligand affinity or substrate oxidation. This chapter focuses exclusively on the superstructured metalloporphyrins as model systems of dioxygen carriers, catalases and cytochrome P450 monooxygenases. These major themes have attracted a great deal of interest in the last two decades, as evidenced by the large number of original publications cited and by the availability of numerous review articles [1–10] addressing some of the topics covered here.

2. SYNTHETIC MODELS FOR REVERSIBLE OXYGENATION

2.1 General Considerations

In dioxygen-carrying hemoproteins (hemoglobin and myoglobin), the active site consists essentially of an iron(II) complex of protoporphyrin IX (**1**) (Figure 1) embedded in a water-resistant pocket and tightly bound to the protein through a single coordinate bond between the imidazole group of the proximal histidine residue (F8) and the iron atom [11]. Hemoglobin (Hb), which transports dioxygen in the blood, is a tetrameric molecule with an $\alpha_2\beta_2$ -subunit structure, from which the dioxygen is transferred to another dioxygen-binding hemoprotein, namely myoglobin (Mb). This is a monomeric polypeptide chain. In the native deoxy form, the iron(II) ion of the heme is in a five-coordinate state. It reversibly binds molecular dioxygen in the sixth, vacant coordination site. A variety of other small ligands (CO, NO and alkyl isocyanides) also bind to the sixth coordination site of the iron.

In hemoglobin, the interactions between the subunits are known under the general term of allosteric properties and are of great physiological importance. They determine the cooperative binding of O₂. In the deoxy form, the iron atom of each heme is in a high-spin ($S=2$) five-coordinate iron(II) state and lies about 0.5 Å out of the heme plane in the direction of the proximal histidine [12]. The Fe–N(imidazole) bond vector has $\sim 10^\circ$ tilt off the heme normal.

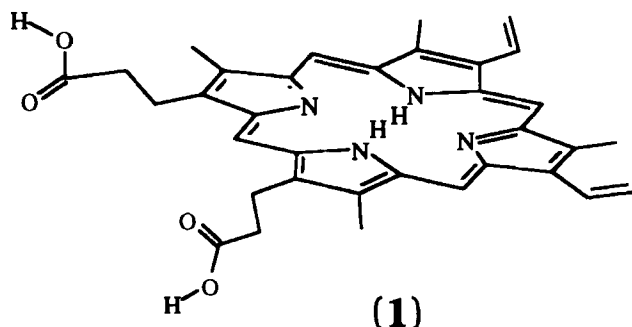
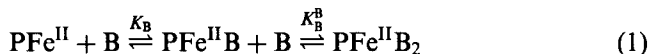


Figure 1 Structure of protoporphyrin IX, the prosthetic group in hemoproteins

The binding of O_2 modifies both the structure and electronic configuration of the heme. The oxygenated heme adopts a low-spin ($S=0$) six-coordinate state with the iron atom more nearly centered in the porphyrin plane. Furthermore, the Fe-N(imidazole) off-axis vector is reduced along with a lateral shift of the protein F helix. The O_2 molecule is bound in a bent geometry [13, 14]. Recent X-ray studies of HbO_2 [15] and neutron diffraction studies of MbO_2 [16] have provided strong evidence for hydrogen bonding between the imidazole NH of the distal histidine (His E7) and bound O_2 . Furthermore, the distal histidine cannot form a direct coordinate bond with iron in the deoxy forms of hemoproteins because it is too far away. Several structural studies on carbon monoxide derivatives have shown that close, nonbonded contacts between the bound CO and amino acid residues in the vicinity of the distal site (His E7 and Val E11) seem to result in a bent and/or tilted geometry for this ligand [17]. The structural difference between the bondings of CO and O_2 has been proposed as a natural mechanism for lowering the toxicity of CO in natural systems.

From these structural and chemical features considered necessary to mimic oxyhemoglobin or oxymyoglobin, there are at least two minimum requirements that any realistic models must satisfy: (1) formation of a five-coordinate heme precursor having a proximal base (imidazole, pyridine and so on) and (2) limitation of pathways that lead to irreversible oxidation.

If we use iron(II) porphyrins without facial protection as models of the active site of hemoproteins, the five-coordinate state does not form. Addition of aromatic, nitrogen-based ligands in a noncoordinating solvent preferentially gives symmetrical six-coordinate complexes. The formation of such complexes, called hemochromes, is favored over pentacoordination because the equilibrium constant is greater for the addition of the second ligand (K_B^B) than for the first (K_B)



where P represents the porphyrin.

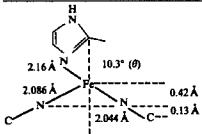
For example, in benzene at 25 °C, the binding constants of pyridine to iron(II) mesotetraphenylporphyrin [$\text{Fe}^{\text{II}}(\text{TPP})$] have been estimated as $K_{\text{B}} = 1500 \text{ M}^{-1}$ and $K_{\text{B}}^{\text{B}} = 1.9 \times 10^4 \text{ M}^{-1}$ [18]. This atypical occurrence arises from ligand field stabilization energy. The d^6 , six-coordinate hemochromes are low spin and gain electronic stabilization relative to the high-spin state of pentacoordination [19]. With $K_{\text{B}}^{\text{B}} > K_{\text{B}}$, the five-coordinate species cannot be present in any significant amount in solution. It can only be obtained if $K_{\text{B}}^{\text{B}} \ll K_{\text{B}}$.

That is the case when appropriately sterically hindered axial ligands are used. Collman and Reed [20] have discovered that 2-methylimidazole (2-MeIm) as an axial ligand gave five-coordinate iron(II) hemes (Table 1). They reasoned that the steric interaction between the methyl group and the heme would not hinder pentacoordination but would prevent the iron atom from moving into the porphyrin ring. The out-of-plane iron displacement is $\sim 0.5 \text{ \AA}$, as predicted by Hoard [21]. Furthermore, like deoxymyoglobin ($\mu = 5.1 \mu_{\text{B}}$), the magnetic moment of $5.2 \mu_{\text{B}}$ at 25 °C is close to the spin-only value for a high-spin ($S = 2$) ion(II) ion ($\mu = 4.9 \mu_{\text{B}}$). The high-spin state was confirmed by Mössbauer measurements [22].

The second major problem in studying flat, open iron(II) porphyrins as models of active sites of hemoproteins is their rapid and irreversible oxidation in the presence of dioxygen, even in protic solvents. At least two general mechanisms have been identified depending on the conditions: the well-accepted μ -peroxo mechanism, and the less understood proton-catalyzed superoxide mechanism.

The first mechanism results from the observations by Caughey and coworkers [23, 24], showing that the autoxidation of deuterohemochrome in nonaqueous solvents with pyridine as an axial ligand is second order in iron(II) and first order in dioxygen. These results suggested the formation of

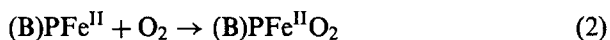
Table 1 Structural parameters for five-coordinate iron(II) models and deoxymyoglobin

$\text{Fe}^{\text{II}}(\text{TPP})(2\text{-MeIm})$	Parameter	(5)(2-MeIm) ^a	(26d)(1-MeIm) ^b	Deoxymyoglobin
	$\text{Fe}-\text{P}_{\text{N}}(\text{\AA})$	0.40	0.3	0.42
	$\text{Fe}-\text{P}_{\text{C}}(\text{\AA})$	0.53	0.34	0.55
	$\text{Fe}-\text{N}_{\text{pyrolo}}(\text{\AA})$	2.072	2.075	2.03
	$\text{Fe}-\text{N}_{\text{im}}(\text{\AA})$	2.095	2.134	2.1
	$\theta(^{\circ})$	11	4.85	10.7

^aFor the structure of (5) see Scheme 1.

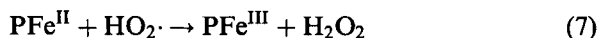
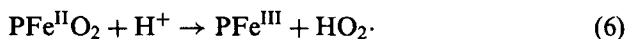
^bFor the structure of (26d) see Scheme 8.

a μ -peroxo iron(III) dimer intermediate. Characterization of the μ -peroxodiiron(III) complex has been achieved by Balch and coworkers [25, 26]. This species rapidly breaks down, presumably via a ferryl intermediate, to give a stable μ -oxodiiron(III) complex [27]. The oxidation mechanism is summarized by



This irreversible autooxidation of iron(II) porphyrins upon exposure to dioxygen considerably limits the use of the simplest iron(II) porphyrins as models of active sites of hemoproteins. In hemoproteins it is clear that the globin environment plays a vital role in their function by preventing the close approach of two hemes and their subsequent oxidation.

Another autooxidation mechanism has been proposed. It involves electron transfer from iron(II) to O_2 to give a superoxide species. The generation of the superoxide demonstrated by Caughey and coworkers [28] and Shikama [29] involves a transfer mechanism catalyzed by nucleophilic agents. For example, the capture of a superoxide ion by a proton of water to form $HO_2\cdot$ is a general autooxidation feature for a large number of mutant hemoglobins [10] and myoglobins [30]. These observations show that the hydrophobic cavity which surrounds the heme is essential for a good stabilization of the oxygenated species.



2.2 Single-Face-Hindered Porphyrins

In 1973, Baldwin and Huff [31] reported the synthesis of the iron(II) octaazamacrocyclic (2) (Figure 2), the first nonporphyrin model which acts as a reversible dioxygen carrier at relatively low temperature. The sterically hindered substituents form a cavity in which the dioxygen is fixed and retard μ -oxo dimer formation.

The first successful approach was the elegant steric modification of the porphyrin developed by Collman *et al.* [32–34]. The “picket-fence” porphyrin tetra($\alpha\alpha\alpha$ -*o*-pivalamidophenyl)porphyrin (5) (TpivPP) has steric bulkiness constructed with pivalamido groups on one side of the porphyrin, leaving the

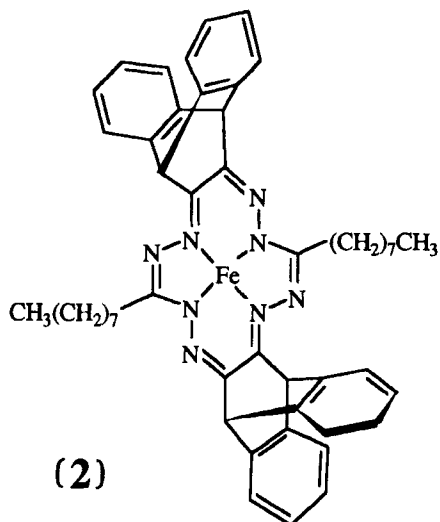
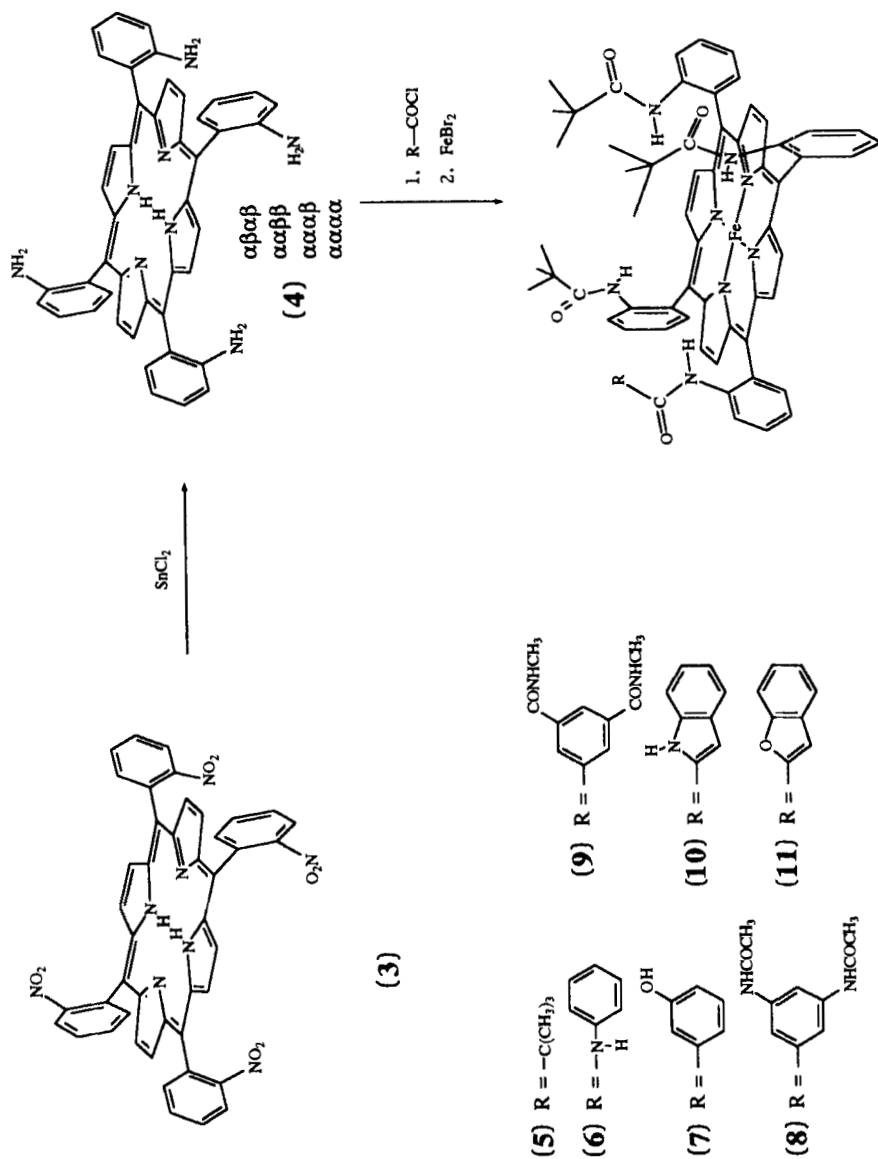


Figure 2 Structure of the iron complex of the octaazamacrocycle [31]

other side unencumbered. The general synthetic scheme for the picket-fence porphyrins is outlined in Scheme 1. Condensation reaction of *o*-nitrobenzaldehyde and pyrrole in the Rothmund reaction [35] gave the mesotetra(*o*-nitrophenyl)porphyrin (**3**), which was reduced with tin(II) chloride to the mesotetra(*o*-aminophenyl)porphyrin (**4**). Four atropisomers ($\alpha\beta\alpha\beta$, $\alpha\alpha\beta\beta$, $\alpha\alpha\alpha\beta$ and $\alpha\alpha\alpha\alpha$) were obtained and were separated by chromatography. The least polar isomer was the desired $\alpha\alpha\alpha\alpha$ -isomer, which was obtained in very low yield. However, interconversion of the atropisomers in the presence of silica gel in toluene under reflux predominantly gave the $\alpha\alpha\alpha\alpha$ -isomer. Reaction of the amino groups with pivaloyl chloride afforded the picket-fence porphyrin (TpivPP). Metalation can be effected by one of several methods. Usually, iron is incorporated as iron(II), but purification treatment gave the iron(III) derivative. Reduction steps under an inert atmosphere gave Fe^{II}($\alpha\alpha\alpha\alpha$ -TpivPP). The iron(II) derivative reversibly binds dioxygen in the presence of any of a number of axial ligands [36]. In dry benzene solution at 25 °C under an atmosphere of dioxygen and with three equivalents of 1-MeIm, the half-life of the resulting oxygenated derivative is approximately two months. Crystal structures of oxygenated and carbonylated complexes show that the gaseous ligand is bound onto the iron atom in the cavity formed by the picket-fence substituents, providing effective protection against irreversible μ -oxo dimer formation [33, 37–39]. The imidazole ligand is coordinated to the unhindered side of the porphyrin. However, this compound has too much and highly constrained steric hindrance to inhibit hemochrome formation in the presence of an unhindered ligand.



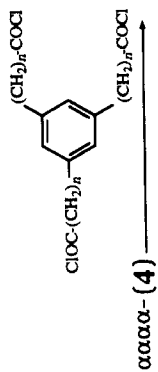
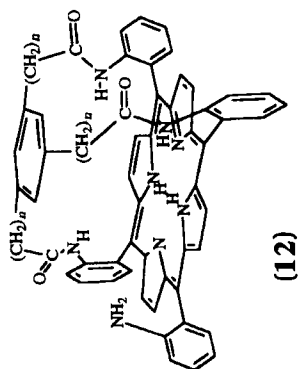
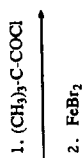
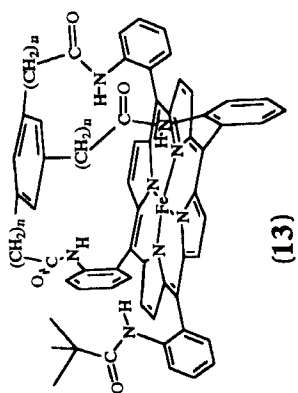
Scheme 1

As the formation of five-coordinate complexes with nitrogenous bases largely depends on the size of the host cavity, single-face-hindered porphyrins have been developed: pocket [40], cyclophane [41–44], bridged [45], crowned [46], capped [47–53], strapped [54–60] and hybrid [61]. In these compounds, the size and the chemical nature of the superstructure can be conveniently varied by changing the number of methylene groups and the aromatic substituent incorporated.

Two fundamentally different approaches have been adopted for the synthesis of single-face-hindered porphyrins. The first consists of the coupling of the constrained superstructure with a functionalized tetraphenylporphyrin (TPP) or a β -substituted porphyrin. This strategy has been applied to the synthesis of pocket porphyrins by Collman *et al.* [40] and strapped porphyrins by Ogoshi *et al.* [54, 55], Battersby *et al.* [45] and Traylor and coworkers [41, 42]. In the case of the pocket porphyrins (**13**) (Scheme 2), the protecting structure is linked to three free amino groups of the $\alpha\alpha\alpha\alpha$ -atropisomer of tri(*o*-amino)mono(*o*-pivalamido)phenylporphyrin. This general synthetic scheme is also used in the synthesis of strapped porphyrins (**15**) (Scheme 3). It consists of condensing simple polymethylene chains or bridges containing more bulky groups (e.g. biphenyl, anthracene or naphthalene) with the porphyrin ring at opposite β -positions under high-dilution conditions.

The second strategy was adopted by Dolphin and coworkers [59] and Baldwin *et al.* [56, 57]. Here the porphyrin cyclization was achieved during the final step. The synthesis of capped porphyrins (**16**) was an adaptation of the Rothmund synthesis. All four aldehyde groups destined to form the meso positions are provided from the pyromellitoyl derivative obtained in two steps from salicylaldehyde (Scheme 4). Dolphin adopted another strategy based on the cyclization of a bis(dipyrrylmethane) in which the dipyrrylmethane units are linked at the pyrrolic β -positions by a pure hydrocarbon strap. In numerous examples of these compounds the straps contain a great variety of bulky blocking groups (Scheme 5).

In a noncoordinating solvent such as toluene or methylene chloride, binding of unhindered imidazole to four-coordinate iron(II) single-face-hindered porphyrins does not give hemochrome formation because the sixth-ligand affinity is drastically lowered. However, large differences in the affinity constants for the formation of five-coordinate compounds are observed. They seem to depend on the nature of the porphyrin. This is reflected by the values measured during the titration of capped porphyrins [62] with 1-MeIm, which are low in comparison with the values in other systems. The X-ray crystallographic data of the free base and the chloroiron(III) complex of this superstructured porphyrin show a significant doming of the porphyrin ring toward the cap, which was suggested to cause the unusual ligand behavior. However, *cis*-effect cannot be excluded [61]. Such an argument has been used to explain the difference in affinity constants between compounds

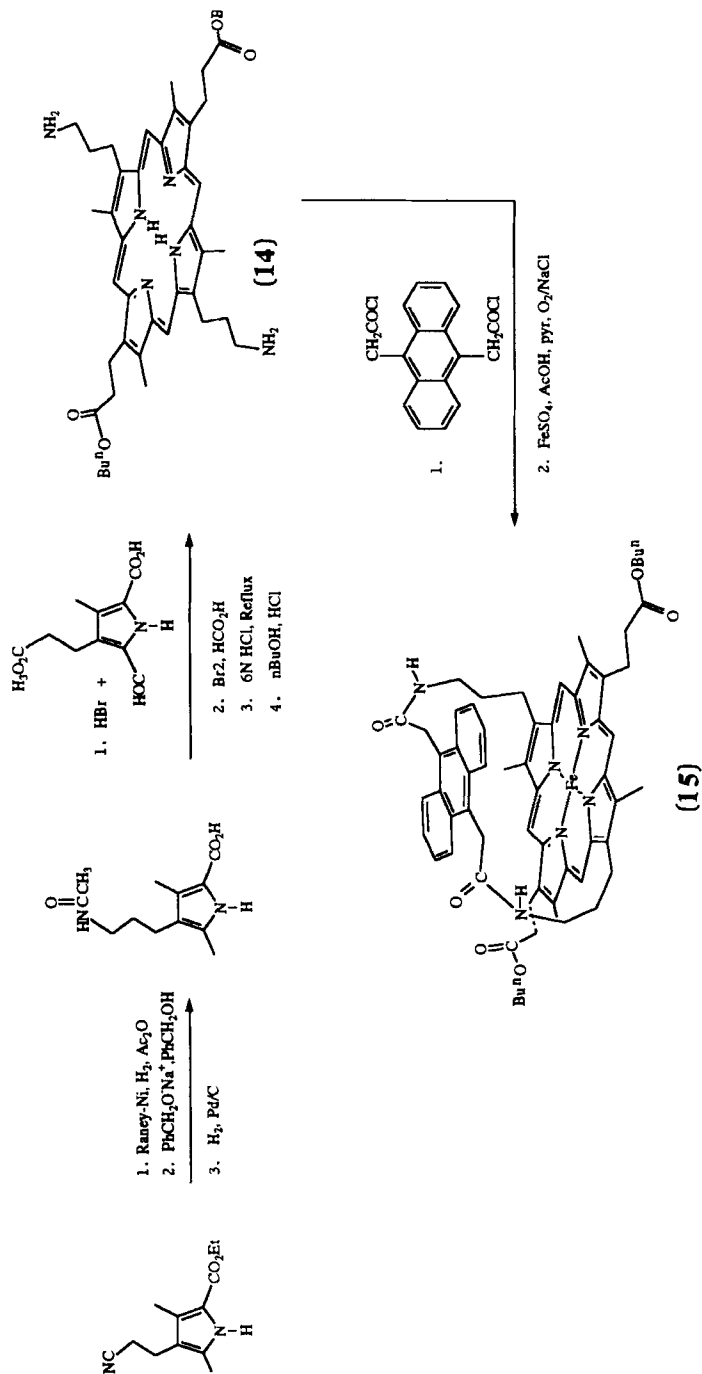


(a) $n = 1$, Fe-Poc Piv

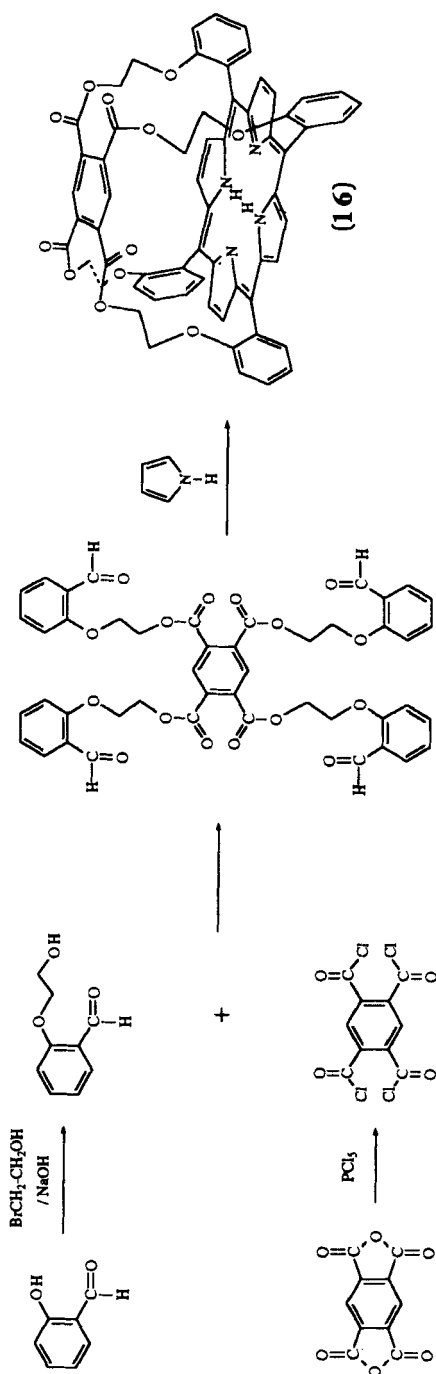
(b) $n = 2$, Fe-Med Piv

(c) $n = 3$, Fe-Tal Piv

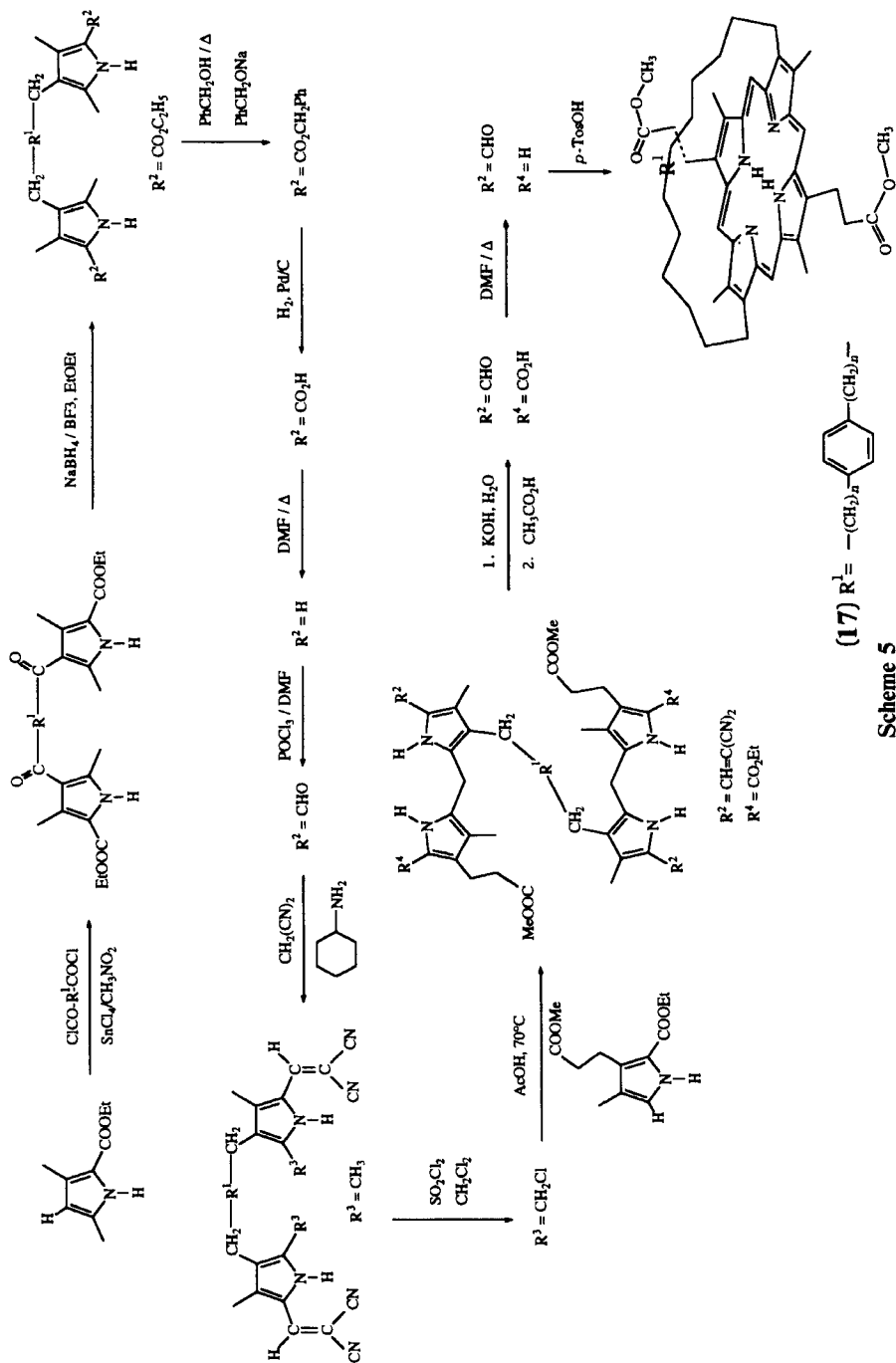
Scheme 2



Scheme 3 Reproduced from *J. Am. Chem. Soc.*, **101**, 4748 (1979) by permission of the American Chemical Society



Scheme 4



Scheme 5

which differ in the chemical nature of the group linking the superstructure to the macrocycle. Single-face-hindered five-coordinate iron(II) complexes have been characterized by a number of methods including UV-visible spectroscopy [40], resonance Raman [63, 64] and NMR [50]. Only one has been crystalized and characterized with 1-MeIm as the proximal axial ligand [65]. Despite the slightly distorted porphyrin core of this hybrid iron(II) complex with a short methylene chain (C_8), the pyramidal geometry at the iron is typical of high-spin ($S=2$) complexes. This spin state was confirmed by Mössbauer spectroscopy, which gave data in agreement with the magnetic susceptibility measurements ($\mu = 5.4 \mu_m$). It is important to note that the crystal structure reveals a smaller out-of-plane distance (0.31 \AA) for the iron atom than such distances observed in other iron(II) five-coordinate complexes having a 2-methylimidazole as the axial ligand ($\sim 0.40 \text{ \AA}$) [37, 66]. Detailed comparison of X-ray structures of these two complexes allows us to consider them as good analogues of the active site of deoxyhemoglobin in the R-state and T-state, respectively (Table 1). In fact, the steric constraint resulting from the presence of the 2-methyl group induces a tension between the iron and the proximal ligand. This tension is relaxed in the iron(II) complex with 1-MeIm, which induces a low out-of-plane iron displacement and lower imidazole tilt. These changes are in the direction of those that must occur upon dioxygen binding. As is revealed by the dioxygen binding, if the imidazole is prevented from moving along this direction, the dioxygen affinity is lowered.

Most of the dioxygen-binding studies have been carried out in an organic solvent in the presence of various axial ligands including 1-alkylimidazoles, 1,2-dimethylimidazole, 2,5-dicyclohexylimidazole and pyridine, always in excess. In such conditions, all these compounds show reversible O_2 binding at room temperature. However, in nonpolar solvents, the lifetimes of dioxygen adducts largely depend on the nature and the concentration of the exogenous base. For example, at a low concentration of imidazole, undesired μ -oxo dimer formation still takes place on the unprotected side of the heme.

2.3 Both-Faces-Hindered Porphyrins

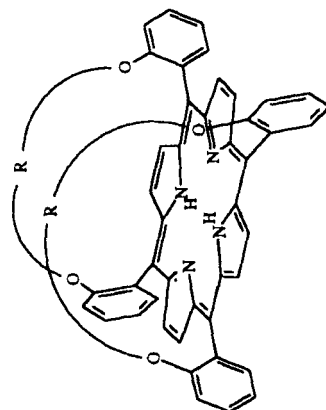
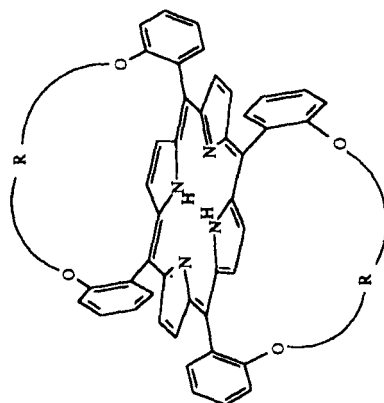
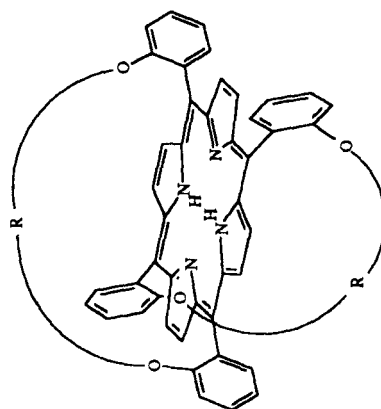
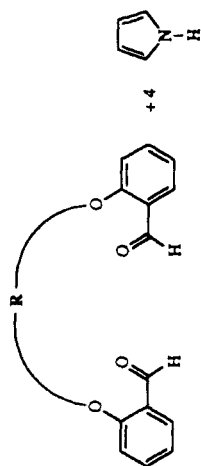
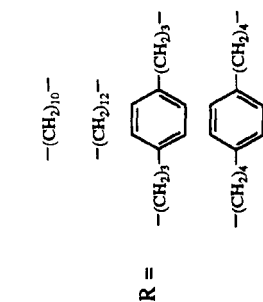
Sterically, single-face-hindered porphyrins may still be susceptible to μ -oxo bridge formation on the unprotected side of the heme. Dioxygen-binding studies have been carried out in nonpolar organic solvents, in which these compounds are soluble in the presence of a great variety of axial ligands, always in excess. Under such conditions, they show varying degrees of reversible O_2 binding at room temperature. The lifetimes of the dioxygen adducts depend on the nature and the concentration of the exogenous base.

Steric encumbrance on both faces of the porphyrin ring must prevent the bimolecular oxidation pathway but often still allows ligand binding. This approach has been proposed by several groups: there are the two-pocket porphyrins of Amundsen and Vaska [67], Cense and Le Quan [68] and Suslick and Fox [69]; the double-sided porphyrins of Tsuchida and coworkers [70, 71]; the basket-handle porphyrins of Momenteau *et al.* [72–75], Rose and coworkers [76], Walker and coworkers [77], Mansuy *et al.* [78] and Reddy and Chandrashekar [79]; and the jellyfish porphyrins of Uemori and coworkers [80, 81].

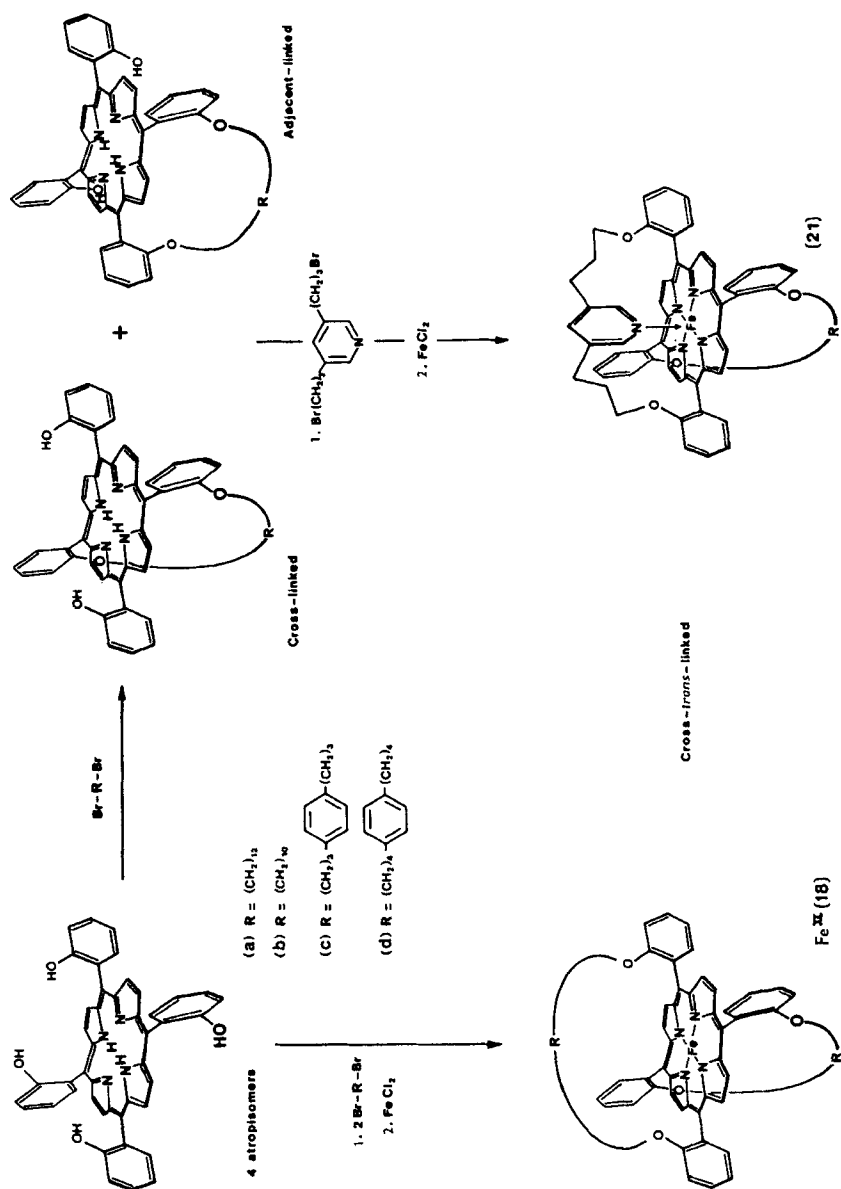
Among these new classes of compounds, the so-called “basket-handle” porphyrin (BHP) appears to be the most promising. In a strategy reminiscent of the capped porphyrin syntheses [56, 57], the sodium salt of salicylaldehyde was reacted with a variety of convenient dibromoalkyl or *p*-(dibromoalkyl)benzene chains to give dialdehyde derivatives [72]. The TPP ring was then formed by condensing the dialdehydes with pyrrole in refluxing propionic acid. After removal of polymeric materials, three isomers [cross-*trans*-linked (**18**), adjacent-*trans*-linked (**19**) and adjacent-*cis*-linked (**20**)] (Scheme 6) were obtained in low overall yield. To increase the yield of the most interesting cross-*trans*-linked isomers, the basket handle was linked to the tetra(*o*-hydroxyphenyl)porphyrin previously prepared (Scheme 7). Alkylation with the dibromo derivatives was performed under high dilution in dimethylformamide (DMF) at 100 °C [73]. The desired cross-*trans*-linked isomer was the major product isolated after chromatography.

A similar basket-handle porphyrin in which the bridges are linked to the macrocycle by means of amide groups has also been reported by Momenteau *et al.* (Scheme 8) [75]. The possibility of isolating the $\alpha\beta\alpha\beta$ -atropisomer of mesotetra(*o*-aminophenyl)porphyrin in pure form and acylating it with a diacid chloride at room temperature (conditions that do not cause significant isomerization of the atropisomers) allows us to obtain the desired cross-*trans*-linked porphyrin (**22**) in 32% yield after chromatography.

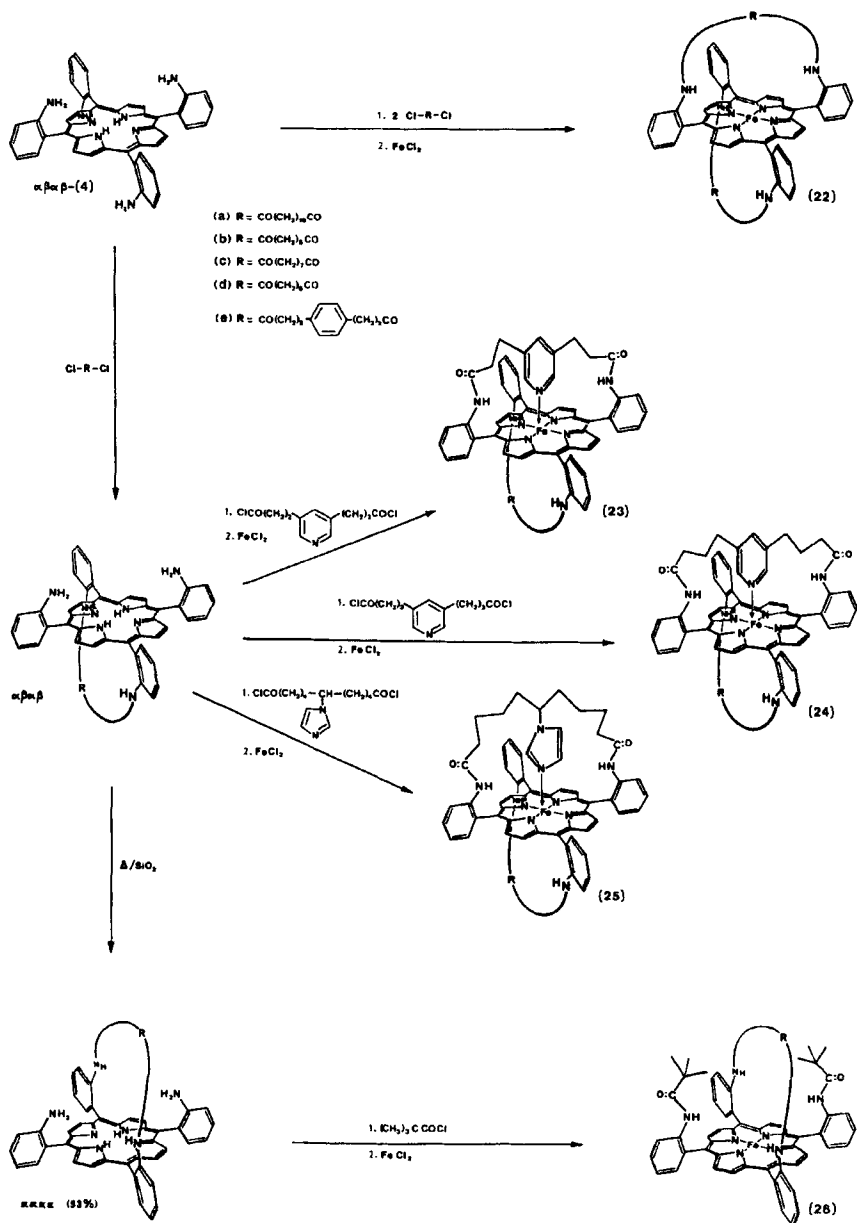
The degree of steric hindrance is indicated by the rates of autoxidation of iron(II) species. Thus, in the presence or absence of a nitrogenous base, giving six- or four-coordinate complexes, respectively, iron(II) complexes exhibit very good redox stability toward oxidation when exposed to 1 atm of dioxygen at room temperature [72]. For example, Momenteau and coworkers reported that in the absence of 1-MeIm, Fe^{II}(**18**) in the cross-*trans*-linked configuration has a half-life ($t_{1/2}$) for oxidation to hematin (Fe^{III}OH) derivatives of 1.5–10.5 min. On the other hand, the less hindered isomers in the adjacent-*cis*-linked configuration are oxidized to μ -oxo complexes in 7.5 s under the same conditions. Similarly, in toluene at 25 °C under O₂ (1 atm), the half-lives for oxidation of six-coordinate iron(II) are 11–25 min for the cross-*trans*-linked



Scheme 6



Scheme 7 Reproduced from *Pure Appl. Chem.*, **58**, 1493 (1986) by permission of IUPAC



Scheme 8 Reproduced from *Pure Appl. Chem.*, **58**, 1493 (1986) by permission of IUPAC

isomers compared to 1.5–12 min for the other two isomers. The steric encumbrance of both faces in these compounds inhibits the oxidation mechanism via μ -peroxo dimer formation. The ultimate oxidation products in toluene or methylene chloride solutions exhibit optical and ESR spectra characteristic of monomeric $\text{Fe}^{\text{III}}\text{OH}$ derivatives [82] whose main structural parameters have been determined by extended X-ray absorption fine-structure spectroscopy (EXAFS) [83]. A mechanism was proposed using ^{17}O NMR spectroscopy [84].

2.4 Integrated Compounds

In an effort to obtain realistic deoxymyoglobin models, several groups designed both-faces-hindered porphyrins in which the nitrogenous base (pyridine or imidazole) was inserted into one of the straps. In these types of compounds, double attachment of the nitrogenous base ensures a high degree of iron pentacoordination and eliminates the need for excess free ligand in solution. Thus, the preparation of such compounds marks an important advance and a further refinement in the design of synthetic dioxygen carriers because the incorporation of a nitrogen donor ligand simulates the “proximal” base of natural systems, whereas the steric hindrance provided by the second strap creates a protected “distal” cavity for dioxygen ligation.

Baldwin *et al.* [85] built the capped strapped porphyrin (**27**) in which a pyridine is covalently bound to two opposing meso phenyl rings forming a strap over the porphyrin face opposite to the cap (Figure 3). In dry toluene, this compound undergoes reversible dioxygen binding, with good stability toward autoxidation reactions.

Momenteau *et al.* [74, 75, 86] synthesized “hanging base” porphyrins (in ether and amide series) with pyridine or imidazole as the axial ligand (Schemes 7 and 8). The synthetic strategies were derived from those developed for the preparation of symmetric both-faces-hindered porphyrins in ether and amide series by two-step procedures. The first step involved the formation of singly bridged porphyrins containing the distal protecting chain. The doubly bridged porphyrins were obtained in a second step by coupling the pyridine or imidazole chain with a singly bridged intermediate. Condensation of the four atropisomers of tetra(*o*-hydroxyphenyl)porphyrin with one equivalent of a dibromoalkane gave a mixture of two singly handled intermediates depending on whether adjacent or opposite meso phenyl groups were linked. This mixture was then treated with a dibromopyridine derivative to afford the desired cross-*trans*-linked isomer (**21**) isolated by preparative chromatography. Analogous amide compounds (**23**), (**24**) and (**25**) were prepared from $\alpha\beta\alpha\beta$ -tetra(*o*-aminophenyl) porphyrin.

This strategy has also been independently proposed by Battersby and coworkers [87–89] to produce doubly strapped porphyrins. They used the diacid chloride of coproporphyrin I (**28**) as the starting compound. Coupling reactions with anthracenediol gave the single-faced-hindered porphyrin (**29**).

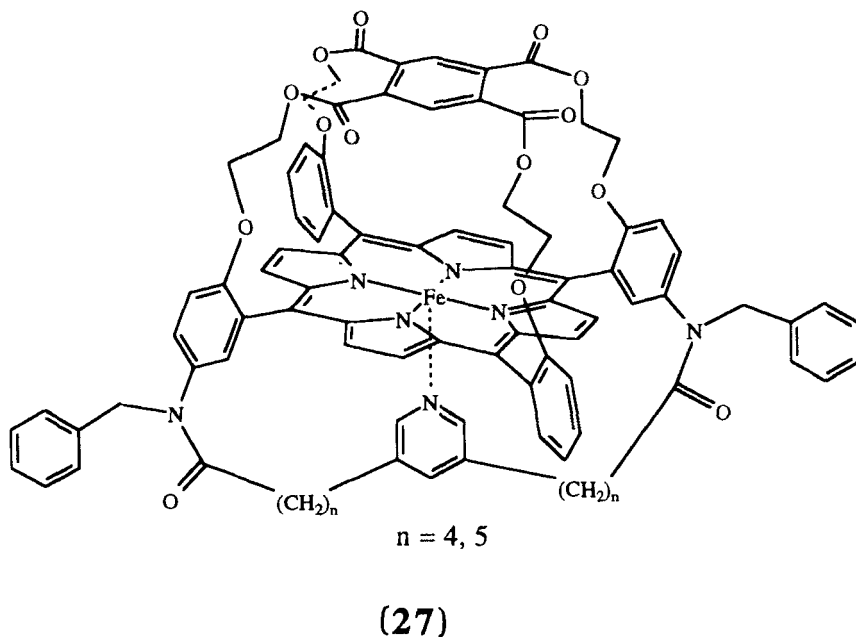


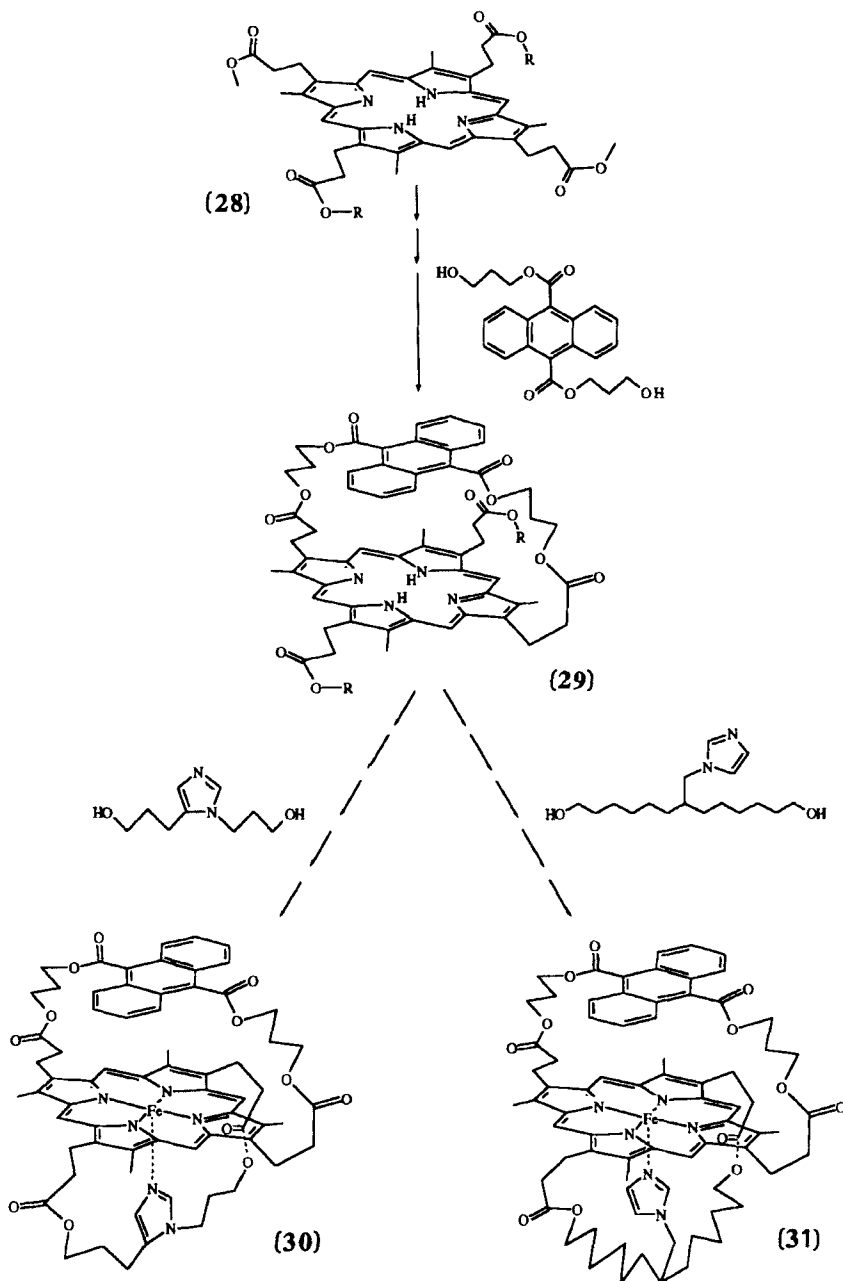
Figure 3 Structure of the hanging base capped porphyrin. Reproduced from *J. Chem. Soc., Dalton Trans.*, 1739 (1984) by permission of the Royal Society of Chemistry

Subsequent condensation with 7-(imidazole-1-yl-methyl)-tridecane-1,13-diol 1,5-di(3-hydroxypropyl)imidazole or gave the nitrogenous-base-strapped porphyrins (30) or (31) (Scheme 9).

After iron insertion and reduction, both visible absorption [74, 75] and ^1H NMR [90] spectra were consistent with five-coordinate high-spin ($S = 2$) iron(II) complexes. The NMR spectrum of such a complex in which an axial pyridine is inserted in the handle shows that the isotropic shifts are mainly contact in nature. From this observation, it was concluded that the complexes remain predominantly pentacoordinated in the absence of a gaseous ligand.

2.5 Studies of Dioxxygen and Carbon Monoxide Binding

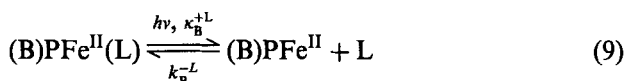
What are the consequences of the mode of attachment of the superstructure, the chemical nature of the superstructure and the nature of the axial base on O_2 and CO binding? In order to answer this question, thermodynamic and kinetic studies have been performed. The numerous chemical and stereochemical factors which can be individually controlled should permit the evaluation of



Scheme 9

the influence of the proximal base restraint, the distal steric hindrance and distal site polarity on gas binding.

The experimental approach to the reactivity of heme models and hemoproteins is essentially based on simple chemical relaxation principles. Fortunately, many six-coordinate complexes undergo a reversible photodissociation which provides a convenient means for measuring ligand recombination rates [91, 92]. The recombination reaction is exponential when conditions of pseudoorder are satisfied, namely when the concentration of L (O₂, CO, base, water and so on) is much higher than that of the heme or the axial base (B). For the reaction



the observed recombination rate k_{r}^{L} is given by the relation

$$k_{\text{r}}^{\text{L}} = k_{\text{B}}^{+\text{L}}[\text{L}] + k_{\text{B}}^{-\text{L}} \quad (10)$$

from which the association (k^{+}) and the dissociation (k^{-}) rate constants can be obtained from the slope and the intercept of the linear plot of k_{r}^{L} against [L].

In the case of oxyhemochromes (L = O₂), a direct study is impracticable owing to their irreversible autoxidation. Furthermore, base elimination can take place with dioxygen dissociation and the quantum yields are low [93]. This is not the case for carboxyhemochrome (L = CO).

A convenient method for the determination of the kinetic constants for O₂ binding is offered by the technique of phototriggered ligand replacement, an indirect but elegant solution to solve the problem of autoxidation [94]. This flash photolysis method was originally proposed by Gibson and coworkers [95] for the investigation of hemoproteins. Because carbon monoxide protects most model systems against oxidation and the carboxyhemochrome is the dominant species, in the presence of CO and O₂, the Gibson equation can be used to estimate both association and dissociation rates for dioxygen binding. However, the Gibson equation cannot be applied to the study of oxyhemochromes which bind dioxygen weakly ($K_{\text{O}_2} \leq 1000 \text{ M}^{-1}$). A modified equation was proposed by Momenteau and coworkers [96–98] to generalize it

$$\frac{1}{R} = \frac{1}{k^{-\text{O}_2}} \frac{k^{\text{O}_2}}{k_{\text{r}}^{\text{CO}}} \quad (11)$$

In a typical experiment, the photodissociation of the carboxyhemochrome leads to the formation of carbon monoxide and the five-coordinate iron(II), then O₂ and CO compete for rebinding. If we choose adequate ligand

concentrations, it is generally possible to adjust the reaction rates such that O_2 recombination is faster than CO recombination. Consequently, the oxyhemochrome is formed in an initial step (from $\sim 100 \mu s$ to a few microseconds depending on the conditions) as a transient species which later undergoes a ligand replacement reaction, restoring the initial carboxyhemochrome in several milliseconds. As a consequence, many experiments can be successively performed without any significant porphyrin degradation.

(a) *Distal polar effect*

In 1981, Phillips and Schoenborn [16], using neutron diffraction analysis, demonstrated that the bound dioxygen forms a hydrogen bond with the imidazole of distal histidine E7 in oxymyoglobin, as initially proposed by Pauling [99]. These studies yielded an $NH \cdots O$ distance of 2.97 \AA . Similarly, a hydrogen bond appears to exist in the α -subunits of oxyhemoglobin and a weaker one in the β -subunits. This electrostatic intermolecular interaction was revealed by Shaanan [15] using X-ray diffraction, giving $NH \cdots O$ distances of 2.7 \AA and $3.2\text{--}3.4 \text{ \AA}$ for the α -subunits and β -subunits, respectively. The relative strength of these hydrogen bonds could contribute to the control of the affinity for dioxygen of natural dioxygen carriers and the stabilization of the dioxygen adduct. Synthetic models have been used to study this interaction and to demonstrate its consequences on the kinetic data for O_2 binding.

Momenteau and coworkers, in a systematic study with hanging base basket-handle porphyrins [86, 100, 101], revealed that polar amide groups in close proximity to the binding site of the O_2 dramatically affect the equilibrium constants. They compared the O_2 binding affinities for compounds having ether or amide groups as the attachment mode of both the proximal and distal handles, using compounds which had the same aliphatic C_{12} chains and pyridine as the proximal ligand [compounds (21a) and (23a)]. While the CO affinities are nearly identical, the equilibrium constant for O_2 is 10 times larger in the amide compound than in the ether one. In fact, such a difference is due exclusively to a 10-fold reduction of the O_2 dissociation rate, whereas the association rate is not significantly modified (Table 2). This increase of stability in the oxygenated amide species is attributed to the presence of the amide linkages and the possibility of hydrogen bonding with the terminal oxygen atom of the bound dioxygen molecule. The 1H NMR spectra of oxygenated complexes have provided evidence for such a hydrogen bond [102]: the observed inequivalence of the pyrrole protons and the shifts of the amide protons suggest a preferred orientation of the dioxygen molecule toward the NH groups. The $NH \cdots O$ distance is close to 3 \AA , consistent with intramolecular interaction. IR, ^{17}O NMR and Raman spectra of dioxygen complexes of these porphyrins corroborate the structure assignment [61, 64, 84]. The greater stability of the amide BHP relative to the ether BHP

Table 2 Rate and equilibrium constants for O₂ and CO binding to model hemes and hemoproteins at 20 °C in toluene

Compound	O ₂			CO ₂			<i>M</i> ^b
	<i>k</i> ⁺ /10 ⁷ (M ⁻¹ s ⁻¹)	<i>k</i> ⁻ /10 ³ (s ⁻¹)	<i>K</i> /10 ³ (M ⁻¹)	<i>k</i> ⁺ /10 ⁷ (M ⁻¹ s ⁻¹)	<i>k</i> ⁻ /10 ⁻³ (s ⁻¹)	<i>K</i> /10 ⁸ (M ⁻¹)	
(21a)	30	40	7.5	6.8	69	10	130 000
(23a)	36	5	70	3.5	30	11.6	16 500
(25a)	31.4	0.620	500	4	6.7	60	12 000
(24a)	30	47	6.4	1.9	160	1.2	18 800
(21c)	10	400	0.25	3	0.018	1.7	680 000
(23e)	12	11	11.4	0.9	0.82	11	96 500
(5)(1-MeIm)	43	0.29	140	3.6	8	45	32 000
Myoglobin ^a	2	0.01	2000	0.05	17	0.29	15
Hemoglobin ^a	5.9	0.012	4900	0.65	10	6.5	130
Myoglobin aplysia ^a	1.5	0.07	220	0.05	0.2	0.25	114

^aIn 0.1 M phosphate buffer at pH 7.^bThe partition coefficient, defined as K_{CO}/K_{O_2} .

corresponds to gain in free energy of 5.4 kJ mol⁻¹, which is certainly due, in part, to the interaction with the amide protons.

In contrast, examination of the structural data for the oxygenated picket-fence porphyrin developed by Collman indicates only weak hydrogen bonding in spite of there being four amide groups. According to the crystal structures of (O₂)(5)(1-MeIm) and (O₂)(5)(2-MeIm), the Fe–O–O plane is fourfold statistically disordered, bisecting the N–Fe–N right angles of the equatorial porphyrin (Figure 4) [33, 37]. In these orientations, the NH···O distances are 3.88 Å and 4.19 Å, corresponding respectively to two of the four positions that the terminal oxygen atom can occupy [28]. Although the NH···O distances are ~1 Å longer than conventional hydrogen bonds and the NH···O groups of atoms do not adopt a linear arrangement, Jameson and Drago [103] considered that there is a substantial net attraction between the dioxygen moiety and the amide groups. While dipole–dipole interactions exist at distances longer than conventional hydrogen bonds, they are sufficiently important in the stabilization of the oxygenated adduct to lower the off-rate relative to the on-rate.

In an attempt to model hydrogen bonding more precisely, Reed and coworkers [104] developed new compounds (6)–(11) derived from a picket-fence porphyrin (Scheme 1). Here, substitution of one of the *t*-butyl groups in a picket by an OH or NH group may modulate the strength of the hydrogen-bonding interaction. Only the compound bearing a *m*-hydroxyphenyl substituent shows a substantial decrease in the dissociation rate constant as compared to the picket-fence porphyrin [98]. This effect may be attributed to hydrogen bond stabilization of dioxygen with the proton of the phenol-substituted picket.

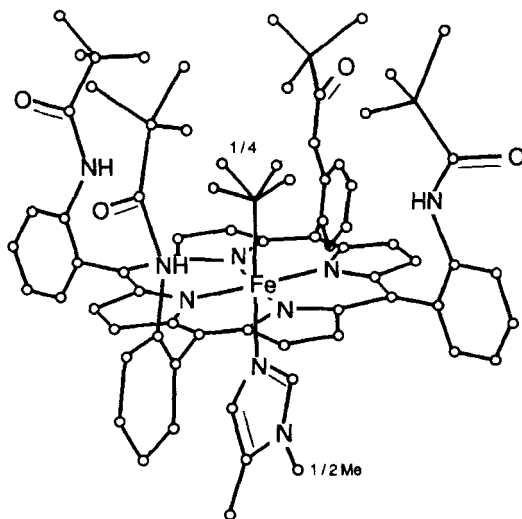


Figure 4 Perspective view of the O_2 adduct of the iron(II) picket-fence porphyrin. Reproduced from *Proc. Natl. Acad. Sci. USA*, **71**, 1326 (1974) by permission of the National Academy of Sciences of the USA

In this context, the control of O_2 affinity by the distal environment of the heme group in hemoproteins can be probed by comparison of wild-type compounds with mutants which do not contain distal histidine [105]. Replacement of distal histidine by glycine results in a 10-fold decrease in O_2 affinity. Within the hemoproteins themselves, the lack of distal histidine in aplysia myoglobin compared to horse myoglobin increases the dissociation rate constant by a factor of six, whereas the association rate constants are identical for both systems. The data are again consistent with the stabilization of bound O_2 via hydrogen-bonding in horse myoglobin.

Thus, there is a clear indication that this stabilization of oxygenated derivatives is consistent with the dipolar nature of the iron–dioxygen bond ($Fe^{\delta+}-O_2^{\delta-}$). This was confirmed by Chang and Traylor [91], who demonstrated increased dioxygen affinities with increasing solvent polarity using various systems. These authors have shown that tail-base heme complexes bind O_2 with a lower dissociation rate constant in water than in nonpolar solvents. Similar conclusions were drawn earlier by Basolo and coworkers [106] with capped porphyrins and by Suslick and Fox [69] with both-faces hindered, nonpolar two-pocket porphyrins. These investigations confirmed the possibility that the polarity at the binding site might have a significant effect on O_2 affinity. It should be noted that the dipolar distal effects mentioned here do not contribute to carbon monoxide binding [91, 107–110].

(b) Proximal base effect

Two factors appear predominant in O₂ and CO binding: the nature of the nitrogenous base and the steric hindrance of the nitrogenous base.

The first factor is an electronic one. Studies of O₂ binding with a single iron(II) porphyrin at low temperature show that the basicity of the proximal ligand is expected to be a determinant parameter. The equilibrium data in Table 2 show that increased basicity increases dioxygen affinity. A change in basicity seems to affect both the association and dissociation rate constants of dioxygen binding, whereas the rates of carbon monoxide binding are little affected. Momenteau and coworkers [100] confirmed this by comparing basket-handle porphyrins which had an imidazole or pyridine base attached through relatively unstrained linkages to the distal handle [compounds (25a) and (23a)]. The replacement of pyridine by an imidazole group enhances the affinity of the five-coordinate complex for O₂ by a factor of seven. This increase is manifested almost entirely in lower dissociation rates. The electronic stabilization of the dioxygen adduct suggests a strong dipolar or ionic iron–dioxygen bond. The imidazole then acts in a synergistic way with the electronegative oxygen through both σ -backbonding and π -backbonding into the π^* -orbital of O₂. According to this point of view, modification of the basicity of the proximal ligand that interacts with the strong Fe⁺–O₂[–] dipole would affect the dioxygen affinity.

This electronic factor can be counterbalanced by a steric pull on the proximal base. This is the second factor which contributes to the modulation of O₂ and CO affinity. Collman *et al.* [111] have analyzed the effects on O₂ and CO binding of replacing 1-methylimidazole with 1,2-dimethylimidazole (1,2-Me₂Im). The introduction of a methyl group in the 2-position of the axial ligand increases the O₂ affinity by a factor of 10–100 and the CO affinity by a factor of ~ 50 (Table 3). The effect is predominantly in increased off-rates. More recently, Momenteau and coworkers [75, 100] have introduced proximal base strain in amide BHPs by modification of the proximal handle length with pyridine. The increase in the number of methylene carbon atoms in the chain connecting the pyridine ring to the macrocycle [from C₃ to C₄ for compounds (23) and (24), respectively] decreases the equilibrium constant by a factor of 10, principally because of a larger dissociation rate. ¹H NMR spectroscopy provided useful information on this surprising result. The spectrum of the pyridine C₃ derivative shows that the pyridine ring executes a continuous libration around its average position in the plane directed along the meso carbon atoms. In contrast, the pyridine ring in the C₄ compound is confined in two equivalent planes passing through the pyrrole nitrogen, and it undergoes a flip–flop movement. This constraint imposed on the proximal base in the latter compound may oppose the necessary reorganization of the proximal base accompanying the movement of the iron atom toward the porphyrin plane on ligation with O₂ or CO.

Table 3 Comparison of rate and equilibrium constants for O₂ and CO binding to model hemes in the R-state and T-state at 20 °C in toluene

Compound	O ₂			CO			<i>M</i>
	$k^+/10^7$ (M ⁻¹ s ⁻¹)	k^- (s ⁻¹)	$K/10^5$ (M ⁻¹)	$k^+/10^7$ (M ⁻¹ s ⁻¹)	$k^-/10^{-3}$ (s ⁻¹)	$K/10^8$ (M ⁻¹)	
(13a)(1-MeIm)	0.22	9	2.4	0.058	8.6	0.67	270
(13a)(1,2-Me ₂ Im)	0.19	280	0.068	0.01	55	0.018	216
(26b)(1-MeIm)	3	27	11	0.18	2	9	814
(26b)(1,2-Me ₂ Im)	1.5	540	0.28	0.017	50	0.034	120
(23a)	36	5000	0.7	3.5	30	11.6	16 500
(24a)	30	47 000	0.064	1.9	160	1.2	18 800
Hb-R ^a	3.3	13.1	25.2	0.46	9	5.1	200
Hb-T ^a	0.3	180	0.17	0.022	90	0.024	140

^aIn 0.1 M phosphate buffer at pH 7.*(c) Influence of the central steric hindrance*

A particularly intriguing problem is whether the heme cavity within a hemoprotein sterically discriminates between O₂ and CO. Within oxygenated hemoproteins, the O₂ unit is coordinated in a bent geometry with an Fe–O–O angle of ~120°, while within carbonylated heme proteins the CO unit is bent and/or tilted from the perpendicular of the porphyrin plane [112, 113]. Crystallographic data of models indicate that O₂ has a similar geometry but that the Fe–CO unit, as in all simple metal carbonyls, is linear and normal to the mean porphyrin plane [114–117]. The structural difference between carbonylated natural compounds and heme models would be related to close, nonbonded contacts between the bound ligand and distal residues (His E7 and Val E11) in hemoproteins. It has been proposed that distortion of the Fe–CO unit can reduce CO affinities without affecting the O₂ affinity of the inherently bent Fe–O₂ group.

To study this discrimination, generally expressed as an *M* value, the ratio of the O₂ and CO equilibrium constant values, researchers have used sterically hindered porphyrins (capped, pocket and hybrid porphyrins) with a view to providing an environment which would permit normal binding of dioxygen whilst hindering the binding of carbon monoxide. Kinetically, the major effect is a decrease in CO association rates, consistent with steric blocking in productlike transition states.

Collman *et al.* [40] have reported the preparation and characterization of a series of sterically hindered pocket porphyrins (FePocPiv, FeMedPiv and FeTalPiv) (Scheme 2). These porphyrins have a benzene ring attached to three of the phenyl rings of the tetraphenylporphyrin through chains consisting of an amide group and one or more methylene groups. The fourth phenyl ring carries a pivaloyl group. The length of the bridges that connect the top benzene ring

and the phenyls can be varied and hence the size of the pocket. Measurements of O₂ and CO affinities for these compounds have been compared to those for open-cavity picket-fence porphyrins (Table 4). Whereas the dioxygen affinities are comparable, there is a considerable decrease in CO affinity. This difference is interpreted as being due to steric encumbrance close to the binding site preventing the binding of CO in a linear fashion, thus lowering CO association rates. Concerning O₂ binding, the association and dissociation rates are both reduced, leaving the O₂ affinity essentially unaffected. The relative CO/O₂ affinities for the three different models in this pocket porphyrin series show that the partition coefficient *M* is reduced from 3500 in the largest structure to 215 in the tightest. Crystallographic study of the CO-containing FePocPiv complex with 1,2-Me₂Im as the proximal ligand has shown that the CO ligand exhibits a slight but detectable distortion from linearity, being both bent and tilted off the axis normal to the porphyrin plane [118]. The Fe–C–O bond angle is 172.5(6)° and the off-axis displacements for the carbon and oxygen atoms of the carbonyl are 0.18 Å and 0.38 Å. This modest distortion of the carbonyl subunit is accompanied by considerable ruffling of the porphyrin.

The capped porphyrins prepared by Baldwin *et al.* [56, 57] are other model systems designed to test the consequences of steric hindrance on CO binding (Scheme 4). These compounds were reported to discriminate against dioxygen in favor of carbon monoxide [62, 119–121]. The CO affinity of the capped porphyrins differs by less than a factor of three from that of unprotected iron(II) tetraphenylporphyrin, while the dioxygen affinity is more than a factor of 100 lower. Kinetic studies of CO binding show that the CO dissociation rate constants are very similar to those of unprotected hemes. Recently, the X-ray crystal structure of a carbonylated complex of the smallest capped porphyrin was obtained [122]. The CO ligand is reported to deviate 7° and 4° from the heme normal, respectively, for each independent molecule present in the unit cell.

Table 4 Rate and equilibrium constants for O₂ and CO binding to sterically hindered model hemes at 20 °C in toluene

Compound	O ₂			CO			<i>M</i>
	$k^+/10^7$ (M ⁻¹ s ⁻¹)	k^- (s ⁻¹)	$K/10^5$ (M ⁻¹)	$k^+/10^7$ (M ⁻¹ s ⁻¹)	$k^-/10^{-3}$ (s ⁻¹)	$K/10^8$ (M ⁻¹)	
(13a)(1-MeIm)	0.22	9	2.4	0.058	8.6	0.67	270
(13b)(1-MeIm)	1.7	71	2.4	0.15	9.4	1.6	550
(5)(1-MeIm)	43	2900	1.4	3.6	8	45	32000
(26a)(1-MeIm)	62.3	130	48	6.3	2.65	238	5000
(26b)(1-MeIm)	3	27	11	0.18	2	9	814
(26c)(1-MeIm)	2.1	5	42.9	0.1	2.63	3.83	89
(26d)(1-MeIm)	0.22	3	13.7	0.008	8.16	0.1	7
(25a)(1-MeIm)	31.4	620	5.1	4	6.7	60	12000

The influences of steric effects have also been studied by Momenteau and coworkers [100] using basket-handle porphyrins in the ether-linked and in the amide-linked series which include a semiaromatic or a purely aliphatic chain as the distal handle. The difference between affinity and kinetic constants for O₂ and CO binding was interpreted as being the result of a distinction between central and peripheral steric effects due to the linkage mode of the handle to the macrocycle. The greater rigidity of the amide linkage compared to the ether linkage should reduce the amplitude of the lateral displacement of the handle. In the ether series a peripheral steric effect could decrease the dioxygen affinity more than the CO affinity since the terminal oxygen atom is more peripheral than central in the bent Fe–O₂ moiety. An opposite situation prevails in the amide series. However, the *M* values are not markedly different from those of unhindered hemes.

Such an observation may be explained by the fact that the distal handle could be displaced sideways from its average position in the Fe–C_{meso} plane, preventing a central steric affect from controlling the CO affinity. To solve this problem, Momenteau *et al.* [61] have used “hybrid” compounds (**26**) (Scheme 8). These single-face-hindered porphyrins have been designed to hold the distal handle in a central position with two flanking pivalamido pickets. They differ by the length of the handle, offering an increase in central steric hindrance to ligands when the handle length decreases. The systematic decrease of the available space for iron-bound CO in (**26a**) to (**26d**) produces a decrease in the affinity constants for this ligand by a factor of 10–100 as compared with amide basket-handle porphyrins (**25**). These reductions in affinity appear entirely in the association rates and are therefore attributed to central steric effects. No major change in the CO dissociation rates is observed. In contrast, their O₂ affinities are slightly higher than those of amide BHP analogues because of a greater stabilization of the dioxygen adducts. The values of the partition coefficients (*M*) decrease from 5000 to 7 for the least encumbered compound to the most hindered one, revealing a direct correlation with increased steric hindrance. These values are in reasonable agreement with those of hemoproteins (*M* ≈ 50–200).

Crystal structures of the carbonylated derivatives with 12, 10 and eight carbon atoms in the aliphatic chain have been obtained [117]. Even with the porphyrin which has the shortest handle, the coordinated CO ligand remains essentially linear. However, all the porphyrin cores are slightly domed and substantially ruffled.

(d) Water binding to iron(II)superstructured porphyrins

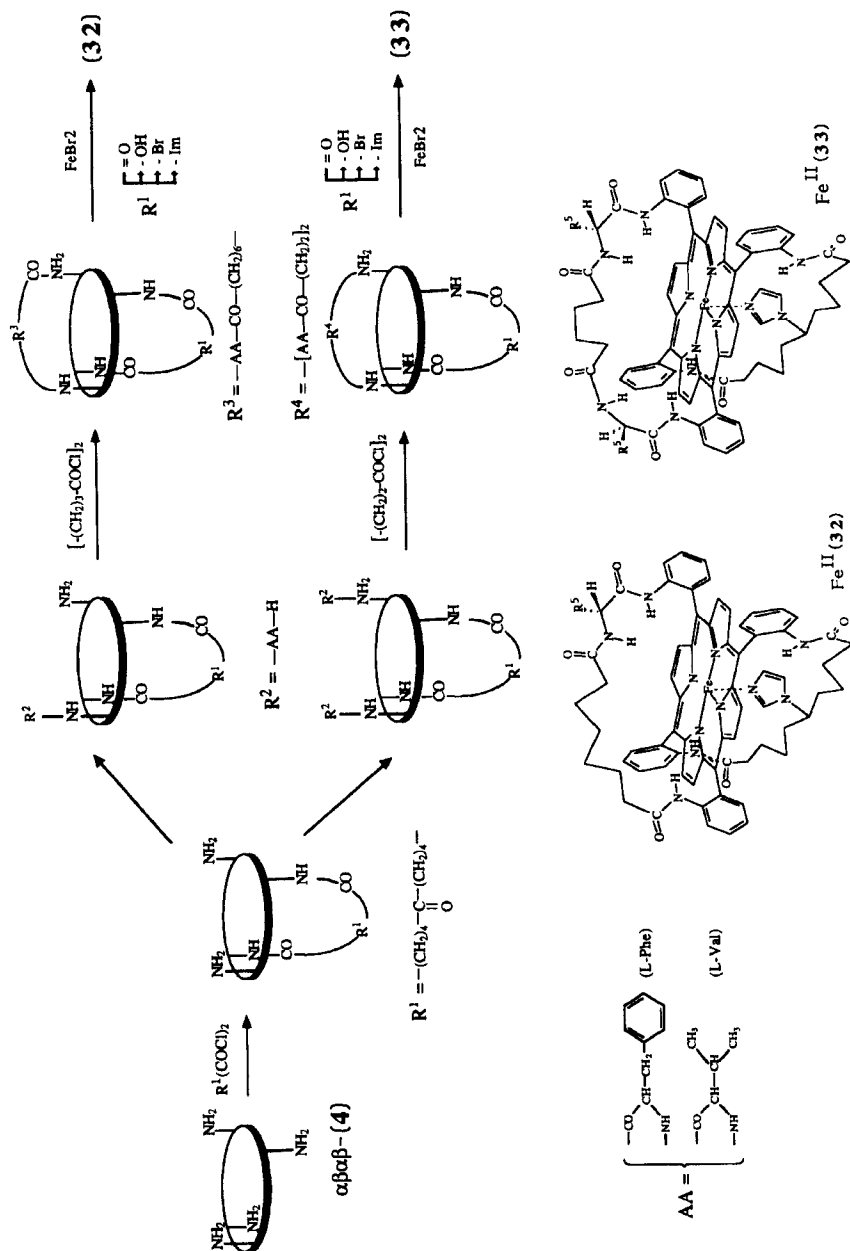
The above-mentioned studies of superstructured iron(II) porphyrins are of great significance because they have demonstrated steric and environmental effects on the O₂-binding and CO-binding reactions. Of particular relevance in

this context is the contribution of amide groups to strong stabilization of the oxygenated complexes by polar interactions (hydrogen bonds or dipole–dipole interactions).

In further studies, the number of secondary amide groups in the bridging chains should be increased in order to reinforce the affinity of the iron for O₂. Furthermore, an increase in the number of amide groups should be able to reinforce the rigidity of the handle and provide a stronger central, distal steric hindrance, a structural factor controlling both affinities and the discrimination between dioxygen and carbon monoxide. Good results have been achieved by the insertion of amino acids into the distal handle [123]. The original amide hanging base basket-handle porphyrin approach developed by Momenteau *et al.* has been extended to modified compounds in which there is an asymmetric environment on the two sides of the porphyrin plane: a “proximal” imidazole hangs on one of the two handles, whilst one or two amino acid residues (L-phenylalanine or L-valine) are inserted into the second and directly linked to the mesophenyl group via amide functions. Their synthesis first required the preparation of a single-face-hindered porphyrin in which the functional group was a ketone at the central carbon of the handle (Scheme 10). Free aminophenyl groups on the opposite face were coupled with an *N*-*t*-butoxycarbonyl amino acid. Coupling reactions were accomplished after activation of the carboxylated group of the amino acid with isobutylchloroformate in dry tetrahydrofuran at -15°C . This method allowed the chiral integrity of the amino acids to be maintained. Deprotection with trifluoroacetic acid, a treatment proceeding essentially without racemization, gave mono-amino and diamino acid derivatives. They were converted to basket-handle porphyrins by subsequent cyclization with suberoyl chloride and adipoyl chloride, respectively. The ketone function was easily converted into hydroxy then bromide prior to coupling with a large excess of imidazole to furnish the desired compounds (32) and (33).

Iron(II) complexes of compounds (32) and (33) were obtained by reduction of their hematin (Fe^{III}OH) forms in a heterogeneous two-phase system consisting of an organic solvent (toluene or methylene chloride) and aqueous sodium dithionite solution under argon [124]. Spectroscopic and magnetic (NMR) studies revealed an unusual behavior in their spin state depending on the presence of water in the organic solution. In wet toluene solution, they are found to be a mixture of high-spin five-coordinate ($S=2$) and low-spin six-coordinate ($S=0$) states at 295 K. At a lower temperature, the latter spin state is preferentially obtained. On the other hand, in dry solvent solution they exhibit a high-spin state, which characterizes five-coordinate deoxy forms of hemoproteins and models under these conditions. However, the spectra observed in wet conditions can be restored by addition of heavy water.

This magnetic difference is attributed to the uncommon coordination of water to the sixth coordination site of iron(II) in these complexes. Such



Scheme 10

coordination may be a result of the polarity of the distal cavity associated with the presence of amino acid residues. The water molecule should be even more strongly stabilized in compounds with two amino acids than in compounds with one amino acid because of the possibility of hydrogen-bonding interactions with the carbonyl groups of the "peptide" linkages (Figure 5). The presence of water in the cavity would favor the rapid autoxidation by formation of the superoxide species (HO_2^\cdot).

The affinities of compounds bearing one amino acid for carbon monoxide have been determined in dry solvents. They are reduced by a factor of ~ 50 in comparison to those of amide BHPs, while the affinities for dioxygen (K_{O_2}) remain almost unaffected. The reduction in K_{CO} results mainly from a decrease in the association rate constant together with a smaller increase in the dissociation rate constant indicative of the increase in steric hindrance. This structural parameter leads also to a decrease in both the association and dissociation rates for O_2 binding by a similar factor. In the case of compounds having two amino acids inserted into the distal chain, the determination of affinity and kinetic constants failed. This behavior is clearly a result of the steric hindrance which results from a shorter chain length and from a greater rigidity, giving a more packed conformation of the handle at a smaller distance from the iron owing to specific interaction with the chain.

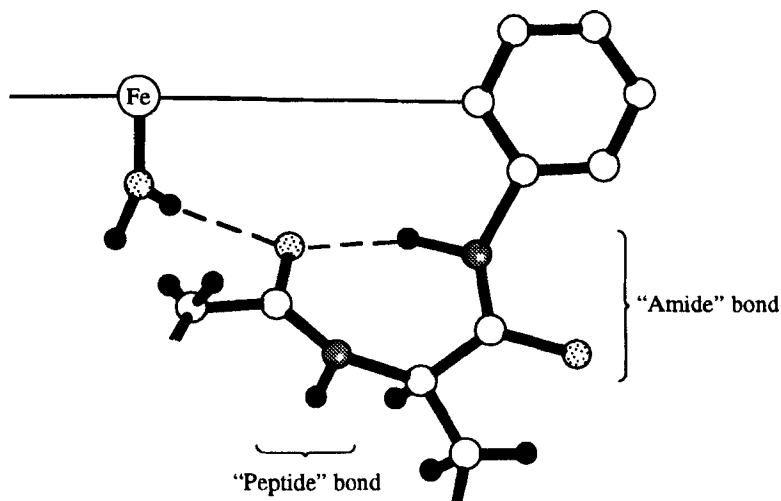


Figure 5 Suggested conformation of the handles bearing amino acids in compounds showing intramolecular hydrogen bonding between the H "amide" proton and the CO "peptide" oxygen, and the intermolecular hydrogen bonding between a coordinated water molecule and the CO "peptide" oxygen [124]. Reproduced from *J. Chem. Soc., Perkin Trans. 1*, 3285 (1988) by permission of the Royal Society of Chemistry

Water has already been considered as a potential ligand for iron(II) porphyrins. Numerous investigations by a variety of physical methods of anionic or cationic iron(II) porphyrins in water or in mixtures of polar organic solvents and water suggest water as an axial ligand [125–127]. Furthermore, Rougée and Brault have shown that water can play the role of a weak-field ligand during the titration of deuteroheme by carbon monoxide in wet toluene, and have measured the value of the affinity constant of water in these conditions to be $\sim 0.1 \text{ M}^{-1}$ at 295 K [128]. More recently, resonance Raman spectroscopy has shown that water can play the role of a fifth ligand in iron(II) tetra(*N*-*t*-butylcarbamoylphenyl)porphyrin [129]. This picket-fence-type porphyrin has the structural originality of reversed secondary amide groups (PhCONHR) connecting the pickets to the macrocycle [130]. The stabilization of this aquo complex is ascribed to the formation of (one or two) internal hydrogen bonds between the coordinated water molecule and one or two of the four carbamoyl carbonyl groups pointing toward the interior of the cavity generated by the porphyrin superstructure.

The use of the basket-handle porphyrins (32) and (33) containing iron(II) allowed us to determine, for the first time, the effect of an increasing number of secondary amide groups in the vicinity of the metal on the affinity and kinetic constants for water ligation (Table 5) [131]. The constants were obtained by the technique of phototriggered competitive rebinding in the presence of CO in wet toluene (see equation 9 where $L = \text{H}_2\text{O}$). Water binding was shown to be controlled by diffusion and was enhanced significantly in comparison to the binding with amide BHPs. With amide BHPs, the failure to detect any transient H_2O complex may be attributed entirely to the greater dissociation rate constant, which is estimated to be $> 3 \times 10^7 \text{ s}^{-1}$. The decrease in $k_{\text{H}_2\text{O}}$ by at least two orders of magnitude with compounds Fe(32) and Fe(33) reflects the stabilization of the water complex by hydrogen bonding associated with the carbonyl group or groups of one or two “peptide” bonds. This stabilization is greater with compounds where two amino acids are inserted, as apparent from the smaller values of the dissociation rate constants. The gain in free energy associated with hydrogen bond formation in the water complexes is estimated at 6–10 kJ mol^{-1} .

Binding of water has also been suspected in iron(II) deoxyhemoproteins. Using time-resolved resonance Raman spectra of the acidic form (pH 2–4) of deoxymyoglobin, Han *et al.* [132] found that the iron(II) protoheme remains in the five-coordinate high-spin state. They proposed the binding of a water molecule as a ligand in place of the normal Fe–His linkage broken by histidylimidazole protonation.

(e) Regulation of ligand binding

At physiological temperature, an innermost barrier in the binding of CO to myoglobin is reported to be the highest of a sequence of barriers, whereas the

Table 5 Rate and equilibrium constants for H₂O, CO and O₂ binding to iron(II) porphyrins in toluene at 20 °C

Compound	H ₂ O		CO		O ₂		<i>M</i>			
	$k^+ / 10^9$ (M ⁻¹ s ⁻¹)	$k^- / 10^5$ (s ⁻¹)	$K / 10^3$ (M ⁻¹)	$k^+ / 10^6$ (M ⁻¹ s ⁻¹)	$k^- / 10^{-3}$ (s ⁻¹)	$K / 10^8$ (M ⁻¹)		$k^+ / 10^7$ (M ⁻¹ s ⁻¹)	k^- (s ⁻¹)	$K / 10^5$ (M ⁻¹)
Fe ^{II} (32)(Phe)	5.9	25.0	2.4	3	27.3	1.1	2.2	60	3.6	305
Fe ^{II} (32)(Val)	9	12.0	7.5	2.5	22.5	1.1	1.8	25	7.2	152
Fe ^{II} (33)(Phe)	6.3	3.0	21.1	0.3						
Fe ^{II} (33)(Val)	7.0	5.4	12.9	0.5						
(25a)		>300	<0.2	40	6.7	60	31.4	620	5	12000

barriers for O₂ binding are of equal height [133–135]. With the most realistic models of hemoprotein active sites, the association of the gaseous ligand becomes a two-step reaction [136]. First, the ligand diffuses into the pocket under the superstructure; second, the actual bond formation occurs. The steric hindrance can thus affect the ligand binding in two different ways: (1) through a matrix effect by obstruction of diffusion into and out of the binding pocket, and (2) through a central steric effect by direct interaction with the ligand in its bound position.

Studies of these two reaction steps are difficult. In fact, kinetic measurements of the association and dissociation of the gaseous ligand reflect the overall reaction and say nothing about the individual steps. However, kinetic studies of ligand binding for some superstructured complexes over a large temperature range allow us to show the role of the macroenvironment which reproduces some of the dynamic characteristics found in hemoproteins. Using basket-handle porphyrins, Tétreau *et al.* [136] determined the relative heights of the reaction barriers for O₂ and CO binding as a function of the temperature. For most superstructured complexes, two steps are found which can be rate limiting. At low temperature the diffusion step is rate limiting, whereas the bond formation step is rate limiting at high temperatures. Thus, for the carbonyl complexes of hybrid basket-handle porphyrins, the barrier for bond formation is the highest of the two barriers in the entire measurable temperature range (180–300 K in toluene) [137]. This means that despite very low diffusion, the formation of the bond is rate limiting. For the corresponding dioxygen complex, the diffusion step becomes rate limiting at low temperatures. In this series of compounds, the rate constants for both association and dissociation of O₂ decrease when the handle becomes shorter. A decrease in the association rate constant for CO is also observed, while the rate constant for dissociation remains virtually constant. This could be explained by the fact that a weaker bond between the iron atom and the carbonyl ligand may compensate for the increase in diffusion obstruction caused by increasing steric hindrance. Since the CO ligand binds in its preferred straight manner along the heme normal, the reason for the Fe–C bond weakening appears to be reduced backbonding ability due to porphyrin core distortion in the more encumbered structures. This is in agreement with the decrease in the CO stretching frequency [61].

In conclusion, the superstructures which seem to be equivalent to a matrix induce barriers to the migration of the ligand inside the cavity surrounding the site of the iron atom. They can also induce a steric interaction, like some distal amino acids in hemoproteins, discriminating against carbon monoxide binding in favor of dioxygen. However, other factors, such as a hydrogen bond between a distal chemical group and the bound dioxygen, the intrinsic electronic properties of iron–ligand bonds or distortion of the porphyrin plane, could

occur in the regulation mechanism for gas binding not only in model systems, but also in hemoproteins.

3. CATALASES

3.1 Structure and Function

Catalases are hemoproteins able to catalyze the dismutation of hydrogen peroxide to water and dioxygen at a very high rate (10^5 s^{-1}) [138]. Most catalases are tetrameric compounds each of whose subunits contain iron protoporphyrin IX as a prosthetic group and axial tyrosinate ligation [139]. The prosthetic group is located $\sim 20 \text{ \AA}$ from the protein surface [140]. On the distal side an entrance channel allows access of small molecules (H_2O_2 , methanol) to the active site. The reaction cycle of the catalases (Figure 6) begins with the high-spin iron(III) state which reacts with a molecule of hydrogen peroxide to form the intermediate compound I which can be described as an oxoiron(IV) porphyrin radical cation [141, 142]. Next, a second hydrogen peroxide molecule reacts with compound I to yield dioxygen while

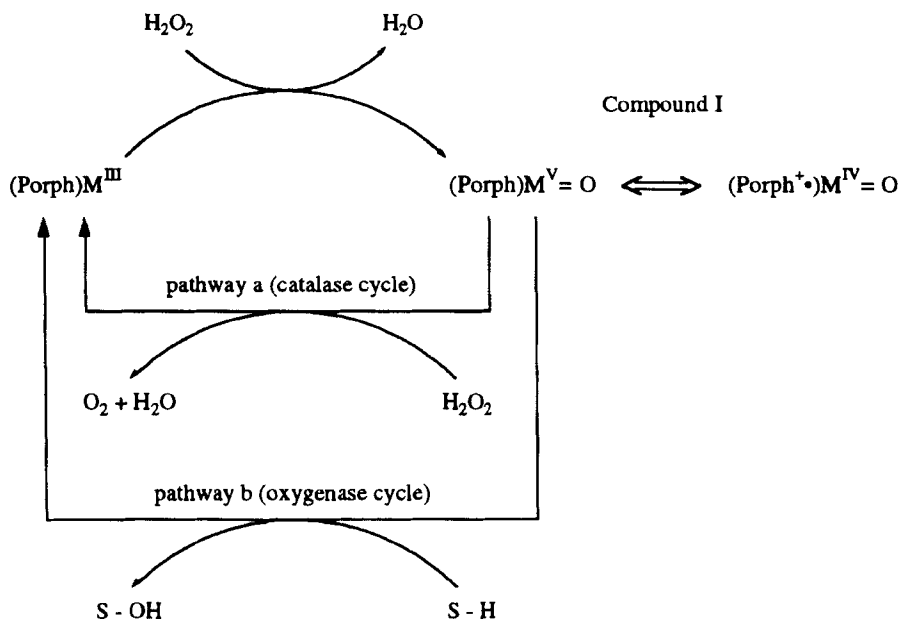


Figure 6 The catalase cycle versus the oxygenase cycle for oxometal porphyrin (P) complexes generated by hydrogen peroxide. Reproduced from *Inorg. Chem.*, **30**, 706 (1991) by permission of the American Chemical Society

restoring the native resting state. The heterolytic cleavage of the O—O bond of H_2O_2 appears possible because of the basic amino acid residues (His 74 and Asn 147) in the distal part of the heme pocket giving rise to a push-pull mechanism [143].

Such a dismutation of hydrogen peroxide is closely related to reactions mediated by peroxidases and chloroperoxidases for which a second oxidation state has been characterized in the catalytic cycle, namely compound II, formally an oxoiron(IV) porphyrin [144]. The oxoiron(IV) porphyrin radical cation is also generated in the peroxide shunt pathway of cytochrome P450 for the catalytic hydroxylation of hydrocarbon substrates by H_2O_2 as a single-oxygen donor [145]. These hemoproteins differ by the nature of the proximal ligand and its donor atom: an oxygen atom from tyrosine in catalase [140], a nitrogen atom from histidine in peroxidase [146, 147], a sulfur atom from a cysteine residue in cytochrome P450 [148] and a cysteine thiolate in chloroperoxidase [149].

At the molecular level it is interesting to understand all the factors which are involved in the control of the versatile reactivities of the different oxoiron species: the proximal axial ligand, the nature of the distal amino acids and the degree of access to the substrates. Catalase is not able to show oxygenase activity. Modeling studies might help in understanding the tuning of the catalytic activities in heme enzymes.

3.2 Biomimetic Models

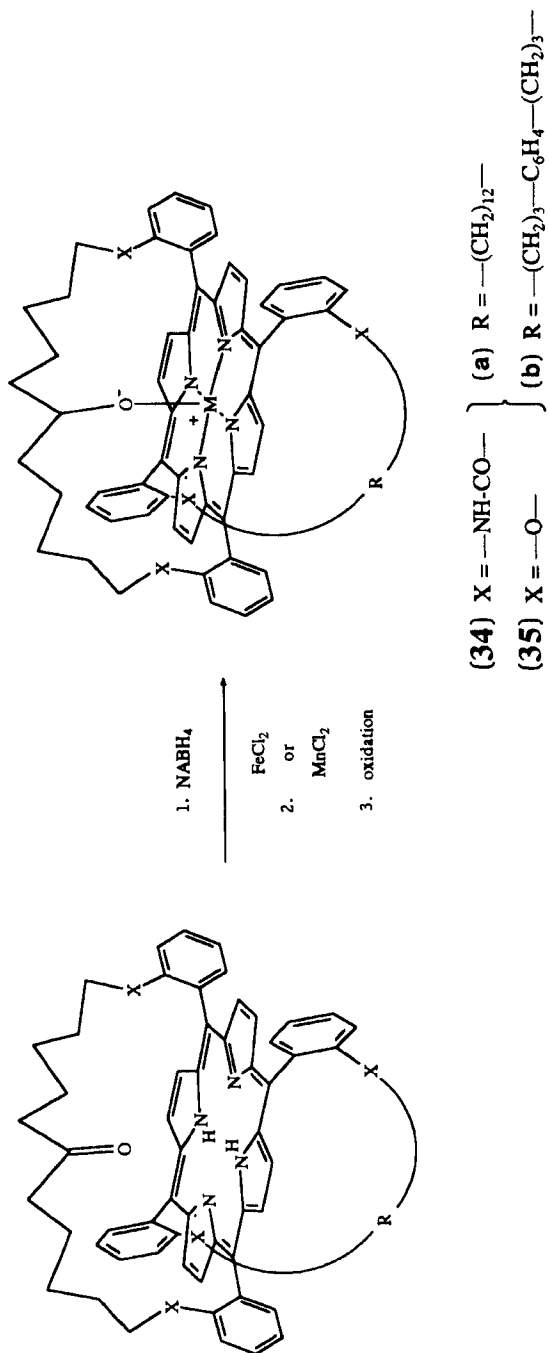
Synthetic metalloporphyrins have been used to model catalase. The catalase activity of iron porphyrins based on natural porphyrin ligands was recognized by Von Euler and Josephson [150] and Jones and coworkers [151, 152]. The activities of heme complexes are pH dependent, in contrast to the pH-independent dismutation activities of hemoproteins in the pH range 5–10. At pH 13 the activity of iron protoporphyrin is close to the activity of catalase, but an autoxidation of these flat metalloporphyrins takes place. Modified porphyrins with substituents at the *ortho*-positions of the meso phenyl groups have been successfully used as catalysts. This approach was developed by Bruce and coworkers using water-soluble iron derivatives of compounds with methyl groups creating sterically hindered cavities around the highly reactive oxometal species [153, 154]. They provide catalysts for the cleavage of hydrogen peroxide at basic pH. Traylor and Xu [155] reported that high-valence oxoiron complexes are able to abstract hydrogen radicals from alkyl hydroperoxides, but it remains to be shown that such a reaction occurs with hydrogen peroxide itself in catalase-type reactions. These studies did not describe the role of the proximal ligand in the reaction. In fact, the main difficulty in the preparation of structural catalase models is the formation of an alcoholate or phenolate as the axial ligand.

Momenteau *et al.* [156] designed the systems (34) and (35) to mimic the coordination of the central metal ion by oxygen ligands covalently linked to the metalloporphyrin. Functionalized basket-handle porphyrins incorporating oxygen donor groups attached to the central position of one of the two handles were prepared by the general strategy described previously for the preparation of hanging base derivatives in the ether series and amide series (Scheme 11). The key intermediate was a ketoporphyrin which was converted into a secondary alcohol derivative. In order to mimic in a more precise way the active site of catalase, Momenteau and coworkers prepared another model in which a phenol group was attached to two meso phenyl rings of the tetraphenylporphyrin via amide linkages [157]. Reaction of the diacid chloride of 4,4'-(1-methoxy-3,5-phenylene)dibutyric acid with a single-face-hindered diaminoporphyrin yielded the phenomethoxy-strapped porphyrin (70.5%). Demethylation with the boron tribromide–dimethyl sulfide complex gave the phenol basket-handle porphyrin (36) (Scheme 12).

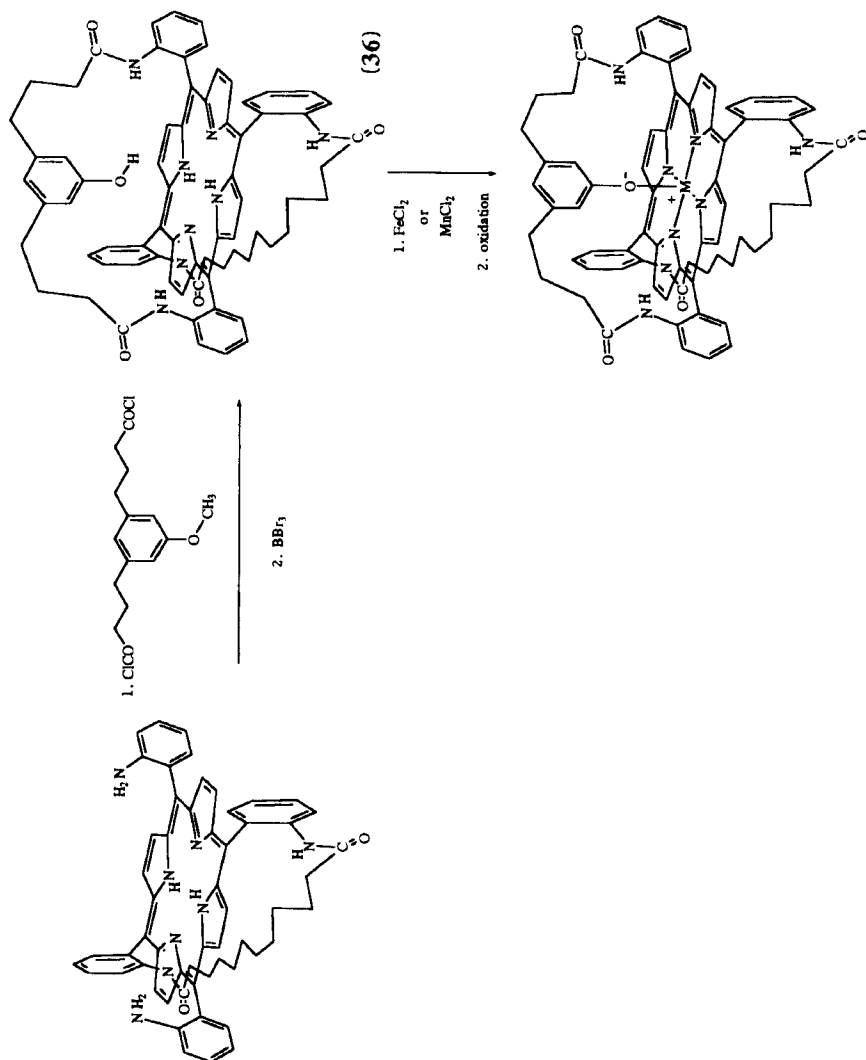
More recently, Bruce and coworkers [158, 159] have prepared the model catalase compound (37) based on a capped porphyrin (Scheme 13). The structure is designed such that a desired pendent phenol can be hung from the ceiling of a vaulted-dome capping structure with four legs that are anchored to the 2-positions of the four phenyl rings at C5, C10, C15 and C20 (all meso carbons) of the TPP (Scheme 13). Structural analysis by ^1H and ^{13}C NMR indicates that the proximal phenol is positioned within an adequate bonding distance of the metal and completely isolated from outside reagents. ^1H NMR, UV–visible and laser desorption mass spectroscopy have been carried out on the iron(III) complex and have revealed the coordination of the phenolate residue to the metal ion.

Such a coordination has also been revealed in the iron(III) and manganese (III) complexes of hanging alcohol (or phenol) basket-handle porphyrins using electron paramagnetic resonance (EPR) and UV–visible spectroscopy. However, the coordination of the oxygen atom to the metal ion depends on two main factors: (1) the central atom itself and (2) the basicity of the metalloporphyrin solution [160]. In toluene or methylene chloride solution, an equilibrium was observed between two forms: one with a free alcohol or phenol function and one with the oxygen atom linked to the metal. Whereas the equilibrium is completely shifted to the O-linked form in the case of manganese, addition of a noncoordinating base is necessary to force the iron complex to be in the O-linked form [161]. This process can be summarized as shown in Scheme 14.

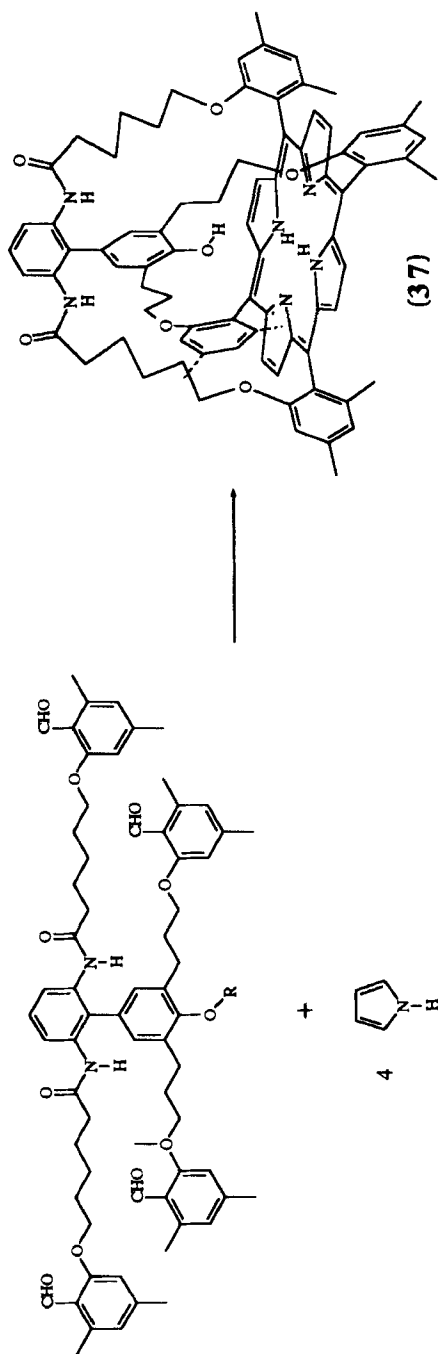
However, for the compounds in the amide series, the O-linked form is almost totally formed in the absence of base. In fact, in such systems, the secondary amide groups present in close vicinity to the porphyrin ring induce greater stabilization by dipole–dipole interactions between the NH dipoles and the central negative charges in comparison to compounds having ether-linked



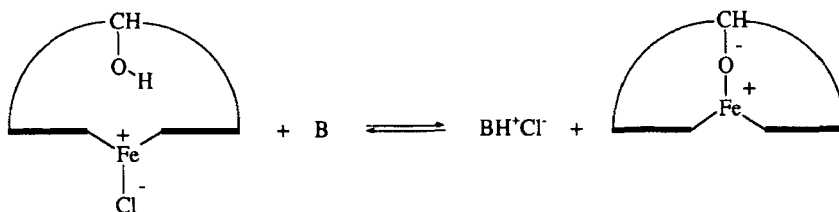
Scheme 11



Scheme 12



Scheme 13 Reproduced from *J. Am. Chem. Soc.*, **112**, 6434 (1990) by permission of the American Chemical Society



Scheme 14 Reproduced from *Inorg. Chem.*, **25**, 4577 (1986) by permission of the American Chemical Society

chains. It can be noticed that this "local solvation" by secondary amide groups located in the superstructure also exerts a strong influence on the redox behavior of the central metal for reactions that involve an increase of the negative charge as well as on the ligand-binding thermodynamics [162–164].

These systems were able to reproduce the dismutation of hydrogen peroxide displayed by catalases, at least from a qualitative point of view [165]. In a biphasic system of CH_2Cl_2 and buffered water at pH 7.0, a striking observation is that this reaction is made easier by the presence of manganese complexes and more difficult by the corresponding iron catalysts. In addition, these results are comparable to those obtained for basket-handle porphyrin analogues which have an imidazole as the hanging base. Work with such porphyrins shows further oxygenase activity in the presence of H_2O_2 and a key role of the proximal imidazole ligand in the oxygen-transfer reaction from the high-valence oxometal porphyrin complex. In contrast, complexes with an oxygen atom as the proximal ligand are not able to catalyze the epoxidation of cyclohexene significantly. This fact suggests that a possible role of the axial oxygen ligand in catalase is to inhibit any oxygenase activity of the oxoiron species generated from hydrogen peroxide.

Taking into account the results of catalase activity for different superstructured metalloporphyrins, one can speculate that the distal chain acts as a screen and enhances the steric discrimination between possible substrates for the high-valence oxometal intermediate complex [157]. The approach of hydrogen peroxide, a smaller molecule than cyclohexene (or other organic substrates), to the active site is less restricted with basket-handle porphyrin complexes with large steric hindrance compared to complexes with a more open cavity. Thus, the control of oxidant and substrate uptakes by the protein channel appears to be an additional and important factor to be taken into consideration for the catalytic activities of catalases. Furthermore, the influence of the medium on hydrogen peroxide dismutation was studied in a single-phase system of acetonitrile and buffered water at pH 7.0, where the ratio of acetonitrile to water could be varied in order to model a hydrophilic active site such as that in catalase [160]. A maximum for the dismutation reaction was observed at 40% water, a percentage close to the water content of

a folded protein. Above this value, substantial solvation of the oxometal species by surrounding water molecules would create a protective screen, shielding the approach of the second H_2O_2 molecule implicated in the dismutation reaction. This is in agreement with the observed decrease in catalase activity [165].

4. CYTOCHROME-P450-DEPENDENT MONOOXYGENASES

4.1 Structure and Function

Cytochrome P450 is a generic name for heme proteins which occur widely in microsomal and mitochondrial fractions of animal tissues as well as in plants and microorganisms. Their catalytic activity corresponds to the monooxygenation of a variety of organic compounds [5, 166]. In their catalytic reactions, one oxygen atom of the heme-bound dioxygen is incorporated into a substrate, while the other oxygen is converted into water, following the overall reaction

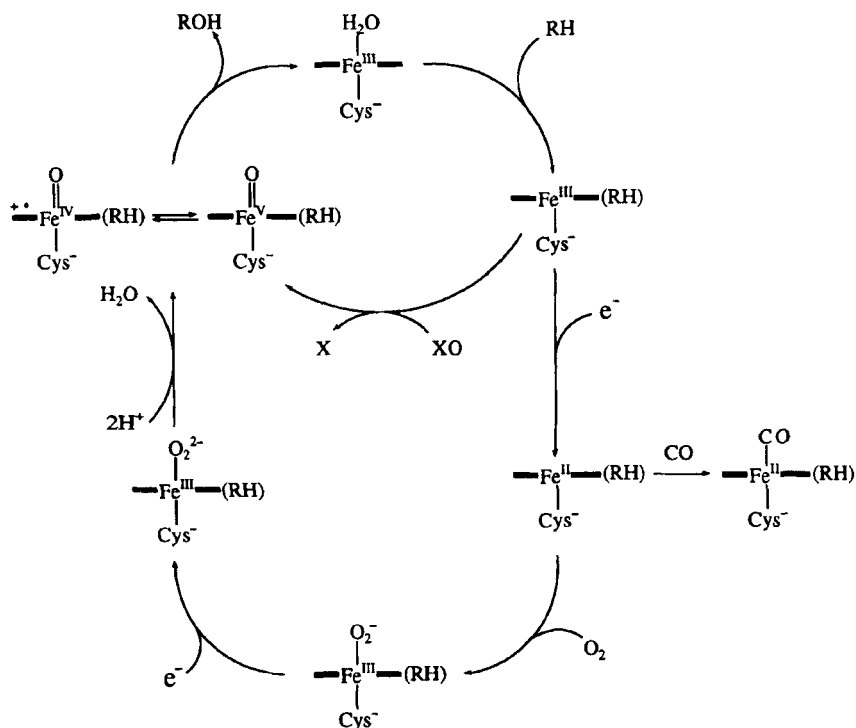


In addition to the conversion of unactivated alkanes to alcohols, cytochrome P450 hemes transform alkenes to epoxides, arenes to phenols, and sulfides to sulfoxides to sulfones. Furthermore, they are involved in the biosynthesis and biodegradation of endogenous compounds such as steroids, fatty acids, prostaglandins and leukotrienes. Under anaerobic conditions, P450 will reductively dehalogenate haloalkanes to the corresponding alkanes.

All P450 enzymes share a common reaction cycle with four well-characterized, stable intermediates: a low-spin iron(III) resting state, a high-spin iron(III) complex resulting from binding of the substrate, a high-spin iron(II) state from a one-electron transfer and a low-spin dioxygen complex. The reactive oxoferryl complex and water are then formed after addition of the second electron and two protons to oxycytochrome P450. It is generally thought that the oxoferryl complex may be formulated as an iron(V) complex or an iron(IV) porphyrin radical formed upon heterolytic cleavage of the O—O bond of the peroxide intermediate (Scheme 15).

An alternative reaction pathway, called the peroxide shunt, is obtained by the association of various oxygen atom donors (PhIO , ClO^- , ROOH , H_2O_2 , KHSO_5 , and so on) with the high-spin iron(III) substrate-bound enzyme. Such additions lead directly to the oxo species.

Since the discovery of cytochrome P450 hemes, many questions have been resolved using iron porphyrin model systems. The first question concerns the nature of the iron complexes involved as intermediates in the catalytic cycle of dioxygen activation and substrate hydroxylation or epoxidation. The understanding of the mechanisms by which cytochrome P450 hemes act during the



Scheme 15

oxidation reactions is the second question. A third question concerns the possibility of building up catalytically active chemical systems able to reproduce the main reactions catalyzed by cytochrome P450 hemes. This is an important challenge because the catalytic activities of cytochrome P450 hemes are highly regioselective and stereoselective.

4.2 Structural Modeling of the Active Site

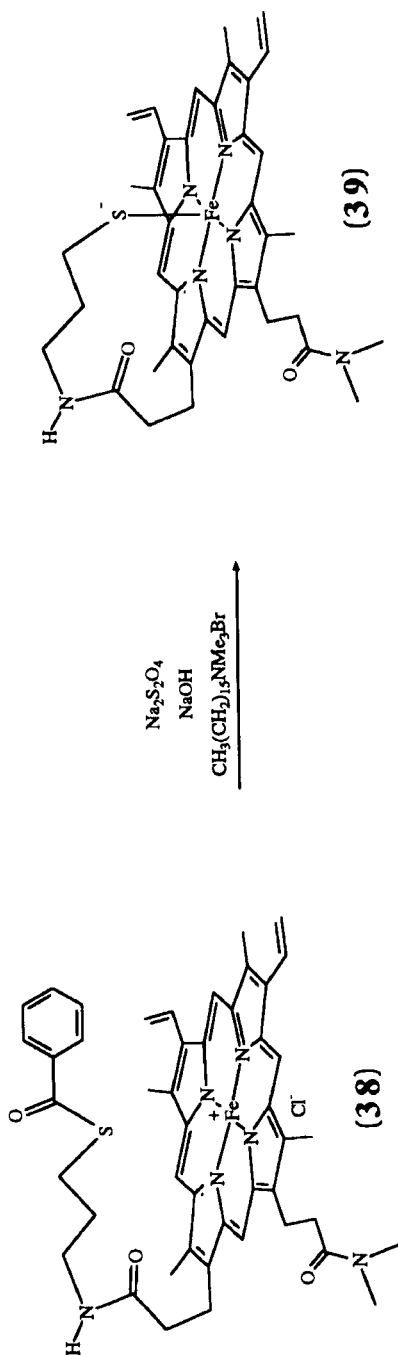
Cytochrome P450 monooxygenases, which are protoheme proteins, present an unusually red-shifted Soret band for the reduced CO complex at 450 nm [167]. Upon denaturation by various treatments, the cytochromes are always able to bind CO reversibly by losing their unique spectral properties as well as their catalytic activities. The spectral properties of the reduced carbonylated complexes of the denaturated form called P420 are identical to those of the dioxygen-carrying hemoproteins ($\lambda_{\text{max}}=420\text{ nm}$). These facts indicate that the unusual spectral properties of cytochrome P450 closely relate to its function.

Many efforts have been made to elucidate the structural bases of these unique spectral properties. In 1975, Chang and Dolphin [168] synthesized iron(II) protoporphyrin IX dimethyl ester coordinated with some alkylthiolate-crown ether complexes. The Soret bands of these complexes appeared at 408 nm and were shifted to 451 nm upon addition of CO, suggesting that the proximal axial ligand was a thiolate sulfur from a cysteine residue. A large body of chemical and spectroscopic data from techniques including EPR, resonance Raman, magnetic circular dichroism and EXAFS spectroscopy provided strong evidence for thiolate ligation at the fifth coordination position [169]. More recently the X-ray crystal structure of P450cam has given a clear picture of the active site, with the iron axially bound to the sulfur atom of cysteine 357 [148, 170]. In this P450 complex, the camphor molecule is maintained in a distal hydrophobic cavity close to the heme mainly by a hydrogen bond between the camphor oxo group and a tyrosine residue of the protein.

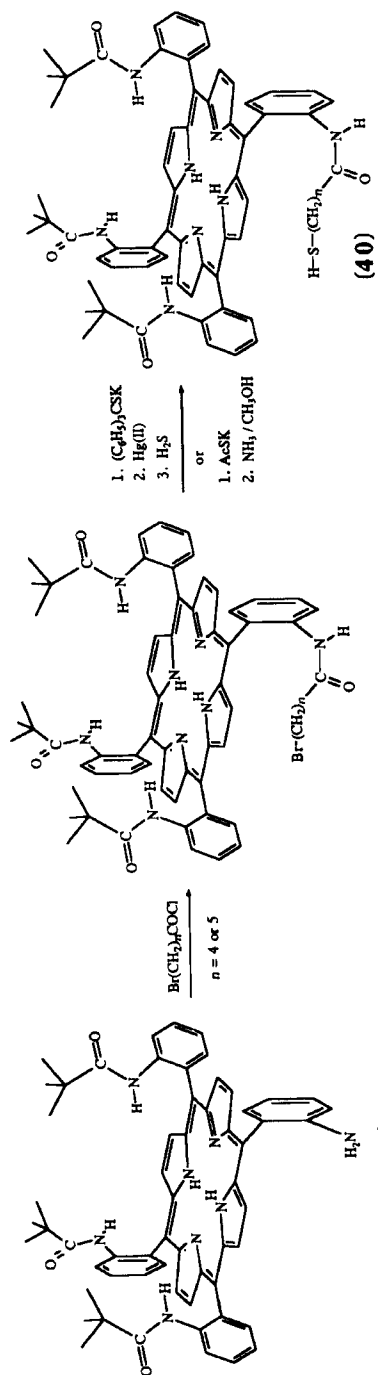
Chang and Dolphin [171] reported also that their protoheme-sulfide complexes bind O₂ at -45°C in dimethylacetamide without deterioration of the dioxygen adduct after 1 h. However, Ruf and Wende [172] showed that the visible spectrum of the presumed dioxygen adduct was the same as that of the iron(III)dithiolate complex.

In an effort to prepare model compounds of cytochrome P450, a chelated heme strategy was developed by several groups. Thus, Traylor *et al.* [173] prepared simple thiol "tailed" protohemes in which a covalently attached sulfide at the porphyrin periphery was realized in order to avoid the addition of an external ligand always in excess (Scheme 16). They found that iron(III)sulfide systems are stabilized and that iron(II) derivatives form five-coordinate thiolate adducts. In the presence of carbon monoxide, these compounds exhibited P450-like CO spectra. The carbonyl carbon in the ¹³CO adduct presents a very similar chemical shift (197 ppm) [173] to that of the ¹³CO-P450 complex (200 ppm) [174]. In contrast, O₂ complexation gives rise to irreversible oxidation. Other chelated hemes have been synthesized and show similar properties. For example, Collman and Groh [175] have prepared models based on TpiVPP and TPP derivatives bearing thiols attached by a "tail" (Scheme 17). To avoid competing thioester formation, they introduced the thiols as their *S*-trityl or *S*-acetyl derivatives (for the alkyl thiols) and as the disulfide derivatives (for the aryl thiols). After removal of protecting groups and iron insertion, all these compounds were found to be extremely sensitive to a combination of light and air. UV-visible and magnetic circular dichroism spectra of the sulfide-carbonyl complexes generated by treatment with a strong base (KNPhCOMe) in the presence of CO displayed the characteristic hyperporphyrin features of CO-P450.

Functionalized bridge and basket-handle porphyrins were designed to hold the thiolate firmly in a suitable position for coordination to the iron atom by

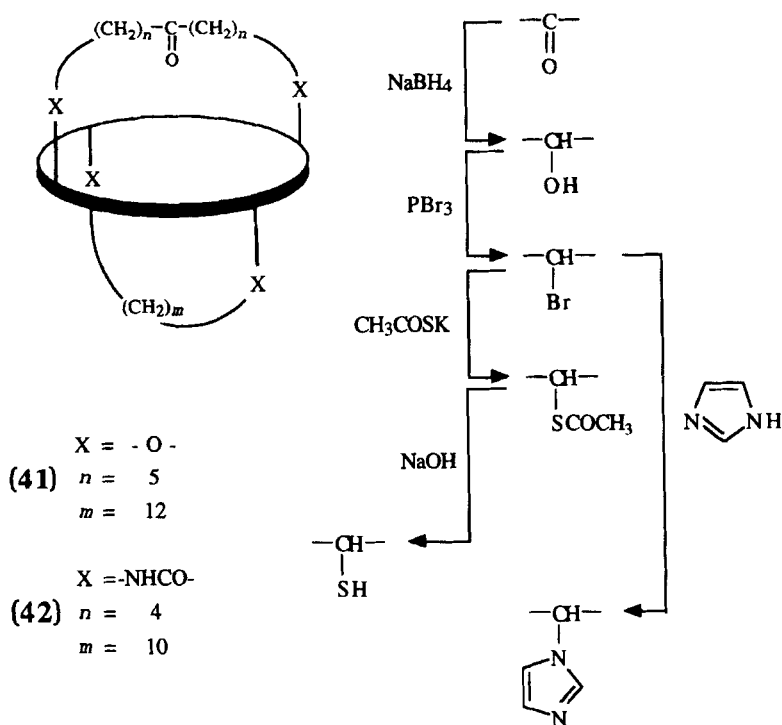


Scheme 16



Scheme 17

bridging it across one face of the porphyrin ring. The strategies of synthesis parallel those used for the "integrated" models of dioxygen carriers (see above). In the case of the bridged porphyrins reported by Battersby *et al.* [176], the building of the bridge was performed with a 5-acetyl derivative. After insertion of an iron(III) ion, the thiolate group was generated by exposure to dimethyl sodium, giving directly the five-coordinate iron(II) derivative. Exposure to CO yielded a six-coordinate complex which displayed the characteristic hyperporphyrin spectrum of P450. The ^{13}CO complex showed a single resonance at 196.8 ppm. Momenteau *et al.* [177] have also prepared cytochrome P450 models based on the both-faces-hindered porphyrins. The synthesis involved preparation of hanging alcohol basket-handle porphyrins, followed by bromination with triphenylphosphine-carbon tetrabromide (Scheme 18). Upon treatment with potassium thioacetate in dimethylformamide at 100 °C followed by saponification with 5% aqueous potassium hydroxide under argon and acidification, such porphyrins give the thiol derivatives. In agreement with other reports on superstructured iron(II) models, these compounds were found to exhibit identical electronic spectra for



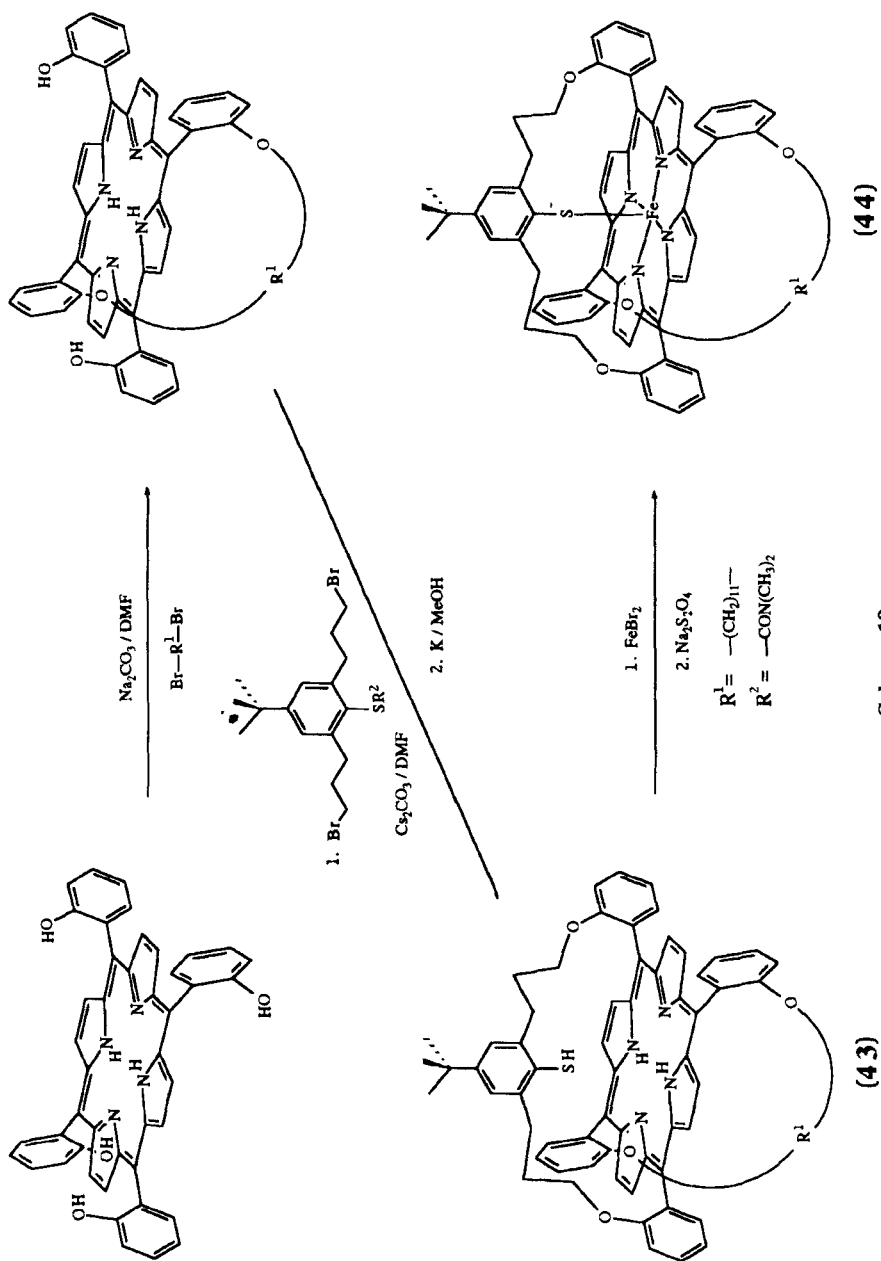
Scheme 18

the carbonylated derivatives with thiol (423 nm) and thiolate anion (453 nm) as the proximal axial ligands in polar solvents (e.g. DMF).

Kinetic studies of CO and O₂ binding require good solubility and stability of the compounds in aprotic media like toluene. This is not the case for thiolate derivatives which are very reactive species, giving rise to numerous redox reactions. Most of them rapidly oxidize at room temperature and dioxygen can react with the thiolate to give a disulfide. For such reasons, Woggon and coworkers [178–180] designed a functionalized basket-handle porphyrin to hold the thiolate firmly in a suitable position for coordination to the iron atom and to inhibit, even in the presence of O₂, dimerization via disulfide linkages between two molecules (Scheme 19). This basket-handle porphyrin has a *p-t*-butyl thiophenolate inserted into a bridge stretching diagonally over one face of the porphyrin; the second handle across the second face forms a cavity, allowing controlled metal oxidation in the presence of O₂. This compound allows production of a P450-like CO complex of iron(II) and binding of dioxygen at 10 °C in toluene.

Studies of models for cytochrome P450 have always shown that an aryl thiolate is more stable than an alkyl thiolate. Furthermore, the introduction of electron-withdrawing substituents onto the arene ring significantly stabilizes the aryl thiolate toward oxidation. Weiss and coworkers [181–185] have exploited this along with the steric protection offered by picket-fence porphyrins to make crystalline models of each of the reaction states of P450. They observed in the crystal structures of three thiolate derivatives of the type [Na(222)]⁺[Fe(TpivPP)(SR)][−] (R = Et, Ph and 2,4,5-C₆H₂Cl₃) that the sulfur donor ligand was coordinated to the iron(II) ion within the cavity formed by the pivalamido pickets. However, using the bulkier, less reducing thiolate 2,3,5,6-tetrafluorothiophenolate, they were able to get reversible dioxygen binding within the picket cavity. The remarkable stability of these compounds, even at room temperature, has allowed their characterization by IR [181], resonance Raman [182], magnetic dichroism [186] and Mössbauer spectroscopic techniques [183, 184].

The crystal structures of two oxycytochrome P450 models have also been reported by Weiss and coworkers [185] and Dawson and Cramer [186]. They are [K(C222)]⁺[Fe(TpivPP)(SC₆HF₄(O₂))][−] and [Na(16C6)]⁺[Fe(TpivPP)(SC₆HF₄(O₂))][−] (where 16C6 is 16-crown-6). The main structural data are almost identical, but the two structures differ by the rotational disorder of the O₂ molecule in a bent, end-on geometry. Two nonequivalent positions are clearly found for the former complex, while the O₂ molecule occupies three sites in the latter. This disorder, which may be static or dynamic in the former complex, seems to be the result of factors arising from the particular orientation of the *trans*-thiolate ligand rather than specific interactions with the pickets.



Scheme 19

4.3 Metalloporphyrins Mimicking Cytochrome-P450-Dependent Monooxygenases

Previous attempts to mimic either the long catalytic cycle or the shortened catalytic cycle of cytochrome P450 using synthetic iron(III) porphyrins and alkyl thiolate ligands were unsuccessful because of the susceptibility to reduction of iron(III) to iron(II) under such reduction conditions [168] or the formation of a disulfide bridge in the presence of O₂ and other oxygen donors. This problem has been partially circumvented by Patzelt and Woggon [180] by employing doubly bridged iron(III) porphyrins with an aryl thiolate inserted into one bridge. They found that this superstructured compound performs catalytic hydroxylation of the distal bridge in the presence of O₂. An oxidation of the axial thiolate ligand into the corresponding sulfonate was also detected.

(a) Structured porphyrins

Groves and coworkers first reported an application of the peroxide shunt pathway in model systems. They described [187, 188] the use of a simple 5,10,15,20-tetraphenylporphyrinatoiron(III) chloride [Fe(TPP)Cl] to catalyze oxygen transfer from iodosylbenzene (PhIO) to alkanes and alkenes. Such a system was found to be able to generate the high-valence oxometal intermediate PFe=O. Since that time, numerous efficient model systems based on metalloporphyrin catalysts and single-oxygen donors have been developed [6]. A wide range of catalytic activities have been achieved through variation in the nature of the metal, the proximal ligand and distal environments, and in the degree of accessibility of the metal center. Manganese porphyrins which are able to form PMn^V=O have been shown to be more effective than iron systems in reproducing most reactions of cytochrome-P450-dependent monooxygenases with a variety of single-oxygen donors [189].

The efficiency of these systems is further increased by the addition of a basic axial ligand such as pyridine or imidazole as a cocatalyst. Their presence provides increased reaction rates and higher degrees of regio- and stereoselectivity [190, 191]. This was firmly confirmed using superstructured models in which the axial ligand was covalently linked to the porphyrin ring through only one flexible chain [192, 193] or hung in the middle of a flexible bridge connecting two opposite mesophenyl rings of a porphyrin [194]. Such a coordination “*trans*” to the metal–oxygen active species by electron-donating molecules results in increased electron density at the metal center, leading to easy generation of a high-valence oxometal moiety [195].

Furthermore, the regioselectivity of hydroxylation of alkanes or epoxidation of alkenes appears to be dependent on the nature of the distal environment of the metal center [196, 197]. It has been postulated that the access to the iron is controlled either by the superstructures in model compounds or by the protein chains present in the vicinity of the iron in the hemoprotein active site. Thus,

the investigation of linear alkane oxidation using iron(III) complexes of basket-handle porphyrins (**18**) as catalysts has revealed a hydroxylation of the more accessible 1-position (ω) and 2-position ($\omega-1$) of the alkane [198]. On the other hand, with simple Fe(TPP)Cl or Mn(TPP)Cl this regioselectivity does not occur and an almost statistical hydroxylation is observed.

In a similar way, Collmann *et al.* [199] have described the synthesis of the “picnic-basket” porphyrins (**45**) and (**46**) (Figure 7) by condensation of tetra(*o*-aminophenyl)porphyrin ($\alpha\alpha\alpha\alpha$ -atropisomer) with various diisophthaloyl acid chlorides. These systems possess a rigid cavity on one face of the macrocycle. The unhindered face of the manganese complex is blocked by 3,5-di-*t*-butyl phenoxide. Comparison of the oxidation activities of the superstructured metalloporphyrins shows that the selectivity is largely dependent on the steric hindrance of the catalytic site: too small a cavity does not accommodate alkene recognition, whereas too large a cavity does not provide high selectivity [200,201].

Another interesting approach toward regioselective systems was reported by Groves and Neumann [202]. They used the steroid-linked porphyrin (**48**) in which hydrophobic steroid pickets are linked on both sides of the porphyrin ring. Iron(III) or manganese(III) complexes included in a bilayer membrane of a phospholipid gave regioselective hydroxylation of cholesterol at C25, while the more reactive but less accessible Δ^5 -double bond was unreacted (Figure 8) [203].

Substituents in the porphyrin ring systems may confer stability and selectivity toward oxidation; these attributes are fundamental to the development of efficient model systems mimicking hemoprotein activities. Metalloporphyrins are very vulnerable to destructive oxidation of the porphyrin ligand under strongly oxidizing conditions. Thus, Groves *et al.* [204] demonstrated that a high-valence oxoiron porphyrin system could be observed with the tetramesitylporphyrinatoiron(III) chloride system, or Fe^{III} (**49**)Cl (see Figure 9). The presence of bulky *ortho*-substituents on the phenyl groups could be important in preventing self-oxidation of the catalyst by keeping the metal centers apart.

(b) Polyhalogenated porphyrins

The introduction of electron-withdrawing substituents onto the four mesoaryl rings induces a stabilization of metalloporphyrins toward oxidative degradation during catalysis. This fact was first reported by Chang and Ebina [205], who described the robustness of tetrakis(pentafluorophenyl)porphyrin (**50**) toward oxidation during the conversion of cyclohexane to cyclohexene oxide in 95% yield. They concluded that the electron deficiency of the active site at the metal, caused by the electron-withdrawing nature of substituted meso phenyl groups, enhanced the stability of the catalyst and also increased the reactivity toward the substrate by generating a more electrophilic oxoiron intermediate.

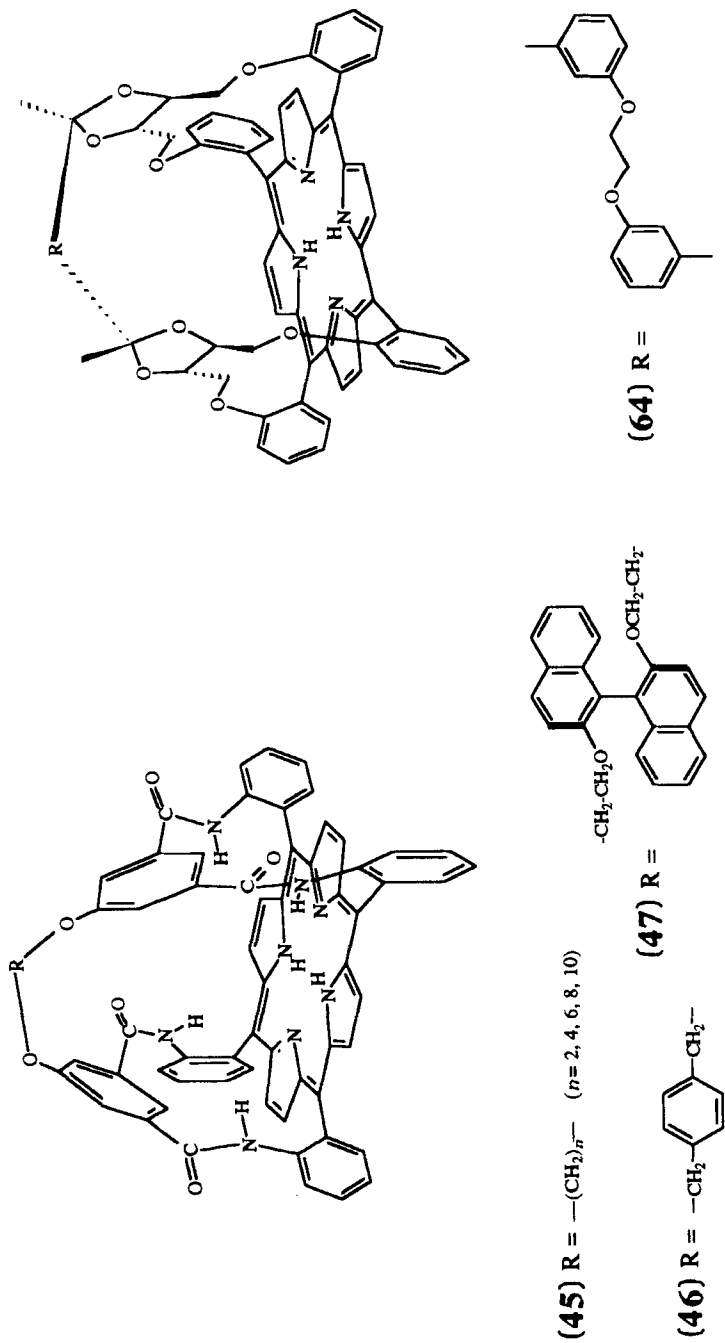


Figure 7 Structures of picnic-basket porphyrins [199, 200]

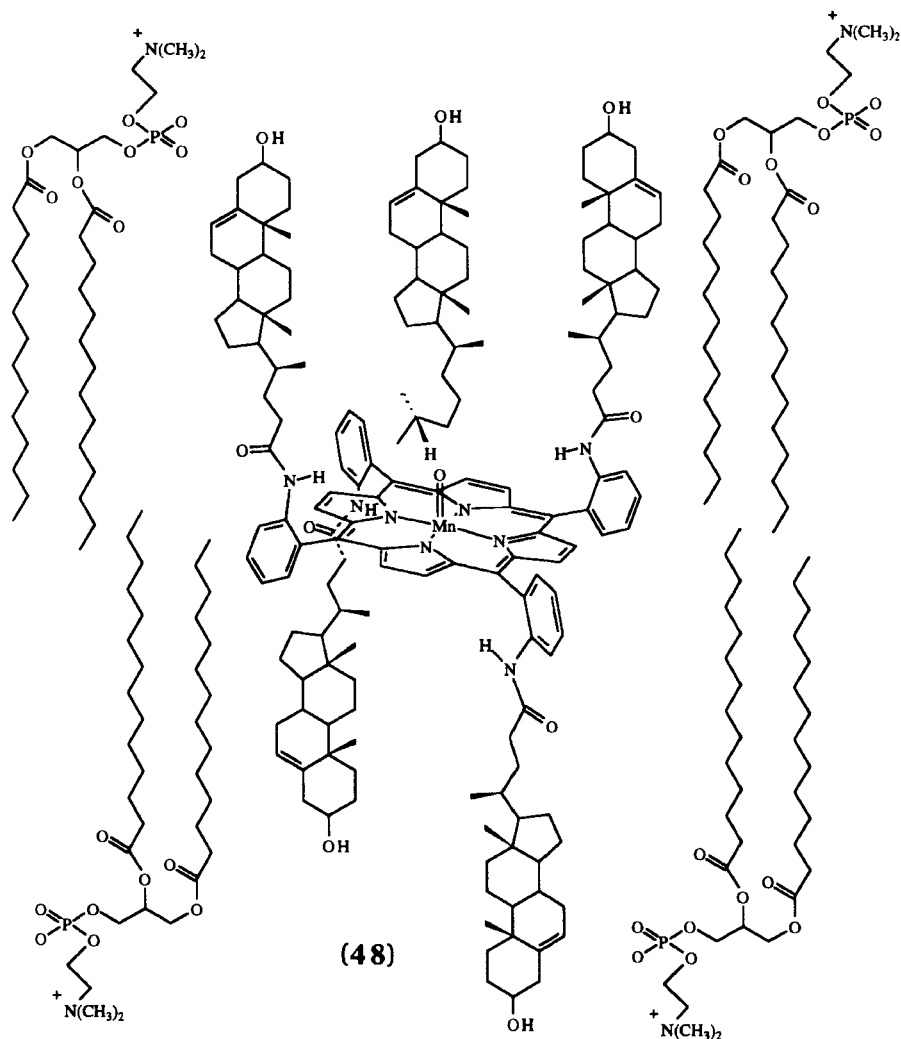


Figure 8 Structure of a lipid bilayer vesicle including a steroid-linked picket-fence porphyrin [202]. Reproduced from *J. Org. Chem.*, **53**, 3891 (1988) by permission of the American Chemical Society

Other groups, one of which being Traylor *et al.* [206], subsequently applied this new concept in the synthesis of so-called second-generation metalloporphyrins. The presence of a great number of chloro substituents on the meso aryl rings renders the oxometal active species much more reactive and provides steric protection of the vulnerable meso positions. Remarkable stability of these new catalysts was observed even in the presence of very strong oxidative

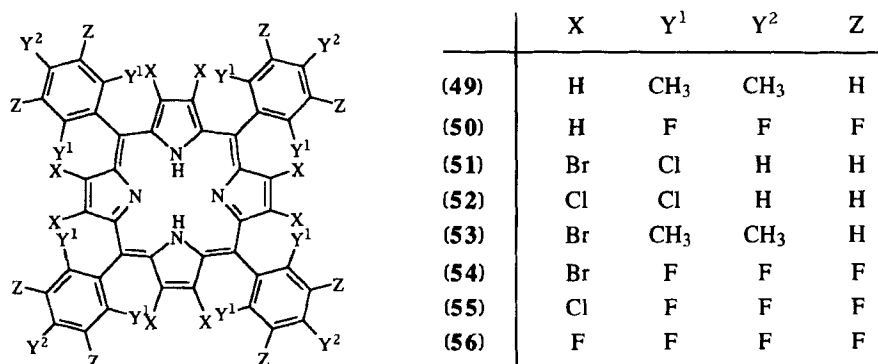


Figure 9 Formulas of polyhalogenated porphyrins used in model systems for cytochrome P450

donors. Furthermore, such catalysts can be adapted for use in aqueous media. Dolphin *et al.* [207] prepared a water-soluble compound by introducing sulfonic acid groups onto the phenyl moieties.

However, these ligands still contain oxidation-vulnerable C–H bonds in the pyrrole rings. In order to obtain more robust catalysts, polyhalogenated metalloporphyrins bearing electron-withdrawing substituents not only on the mesoaryl rings but also at the β -pyrrole positions have been prepared (Figure 9). The first compound to be used in the third-generation metalloporphyrins, namely mesotetrakis(2,5-dichlorophenyl)- β -octabromoporphyrin (51), was reported by Traylor and Tsuchiya [208]. It was obtained by the bromination of tetrakis(2,6-dichlorophenyl)porphyrinatozinc using *N*-bromosuccinimide. Numerous other compounds have been described recently in which β -pyrrole carbons bear fluoro [209], bromo [210, 211], chloro [212], sulfonato [213, 214] and nitro [215] substituents.

These metalloperhaloporphyrin complexes are more robust and more active than the partially halogenated catalysts corresponding to the second generation. Of importance here are the lipophilic environment used to attract the alkane to the active site and the saddle-shaped structure for the tetrapyrrole ring [216]. However, their catalytic activity depends on the nature of the halide substituents and the degree of halogenation. Mansuy and coworkers [217] examined a series of electronegative porphyrins and compared the yields of alkane oxidation by PhIO versus the degree of halogenation. The yields increase as the number of electron-withdrawing groups on the periphery of the macrocycle increases. These authors propose that there is a greater tendency for the active species to behave more like $\text{PFe}^{\text{IV}}\text{O}\cdot$ than $\text{PFe}^{\text{IV}}=\text{O}$ with increased electron withdrawal from the porphyrin ring. This appears to be directly related to the iron(III)–iron(II) reduction potential [212].

(c) *Hydroxylation of aromatic substrates*

The hydroxylation of arenes represents a predominant mechanism for the enzymatic detoxification of these compounds by cytochrome P450: the substrate-binding site is lined with hydrophobic residues which provide a driving force for the complexation of lipophilic substrates. For instance, cyclohexane is one of the more rapidly hydroxylated substances, whereas polar substrates such as alcohols have a much lower affinity for the active site.

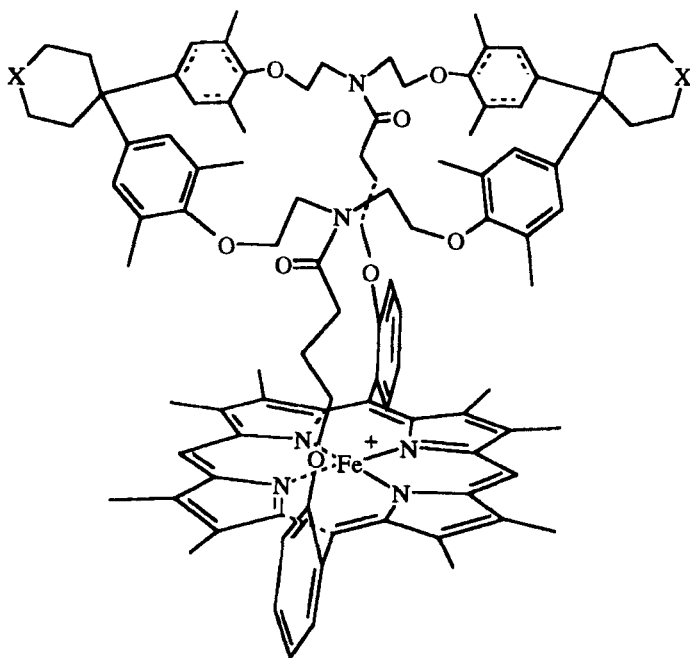
Whereas important progress has been made regarding the use of metalloporphyrins as catalysts for alkene epoxidations and alkane hydroxylations, work concerning the mechanism of hydroxylation of aromatic hydrocarbons has received only limited attention. In fact, the main problem encountered with the design of systems capable of performing such oxidative reactions is in the preparation of superstructured porphyrins for the selective complexation of aromatic compounds.

The first iron(III) porphyrin designed to have an efficient apolar binding site for arene complexation in close proximity to the porphyrin ring was synthesized by Diederich and coworkers [218]. The porphyrin cyclophane (**57**) (Figure 10) was obtained by following the protocol previously developed by Baldwin for the construction of strapped porphyrins. In the presence of a variety of polycyclic aromatic hydrocarbons (anthracene, naphthalene, acenaphthylene, phenanthrene and so on), complexation occurs [219]. The ^1H NMR spectra showed remarkably large upfield shifts, indicating that the substrates are incorporated deep in the cyclophane cavity. It has also been reported that the iron(III) complex in the presence of iodosylbenzene catalyzes the direct oxidation of acenaphthylene to acenaphthen-1-one in 65% yield. Under similar conditions, isotetralin is converted with high catalytic turnover to 1,4-dihydronaphthalene and naphthalene. This interesting catalytic activity mimics that of cytochrome P450 aromatase.

Iron and manganese complexes of the water-soluble sulfonatoporphyrins were found to be suitable catalysts in the oxidation of lignin dimer models [220, 221]. They catalyze the oxidation of methoxyarenes to *p*- or *o*-quinones [213]. Recently, Tsuchiya and Seno [222] prepared the perfluoro porphyrinatoiron complex $\text{Fe}(\text{TPPF}_{28})\text{Cl}$ by treating $\text{Fe}(\text{TPP})$ with CoF_3 in pyridine [TPPF_{28} is (**56**) in Figure 9]. This catalyst was able to oxidize benzene to phenol with H_2O_2 , but surprisingly was unable to oxidize cyclohexane with the same oxygen donor.

(d) *Catalysts for asymmetric epoxidation*

The most attractive aspect of cytochrome P450 monooxygenases is that they are able to perform chiral recognitions and enantioselective oxygenations which are induced by the protein around the active site. This aspect can be mimicked using synthetic chiral catalysts.



(57) $X = \text{EtHN}^+\text{Br}^-$

Figure 10 Structure of the iron(III) porphyrin cyclophane. Reproduced from *Angew. Chem., Int. Ed. Engl.*, **29**, 191 (1990) by permission of VCH Verlagsgesellschaft

Groves and Myers [223] reported the first example of asymmetric induction using vaulted iron or manganese binaphthylporphyrins (Figure 11). Compounds (58) and (59) were synthesized by the condensation of the optically active diacid chloride of 1,1'-binaphthyl-2,2'-dicarboxylic acid with the alternating ($\alpha\beta\alpha\beta$) atropisomer of tetra(*o*-aminophenyl)porphyrin. The binaphthyl group creates a relatively large and rigid chiral cavity around the iron porphyrin core of the catalyst. Epoxidation of styrene with PhIO gave (*R*)-styrene oxide in 48% enantiomeric excess (ee) [the ee is the percentage excess of the (*R*)-enantiomer over the (*S*)-enantiomer], but enantiomeric excesses varied considerably with other substrates probably owing to the conformational mobility of the chiral substituents and the degradation of the catalyst.

Mansuy *et al.* [78] have prepared the basket-handle porphyrin (60) bearing two amino acids (phenylalanine) in each handle (Figure 11). The iron(III) complex was found to be active as a catalyst for *p*-chlorostyrene epoxidation by iodosylbenzene in 50% ee.

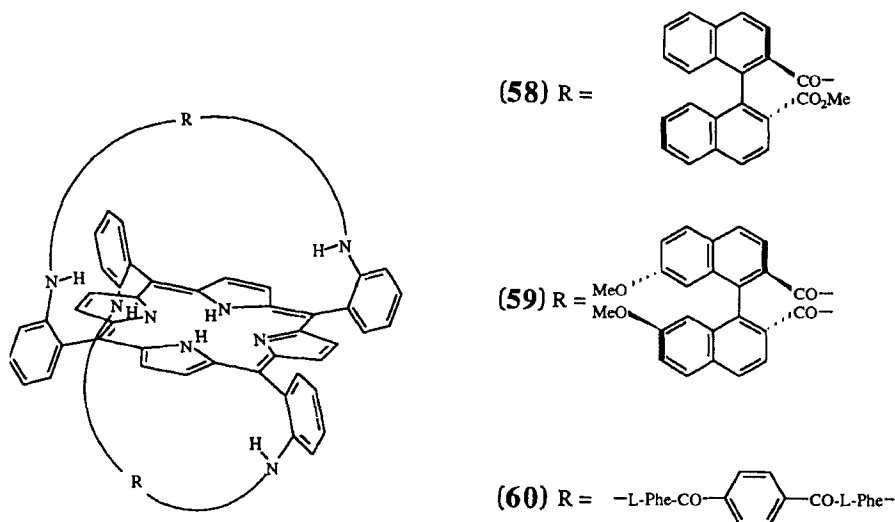


Figure 11 Structures of chiral basket-handle porphyrins [78, 223]

This approach has been used by many research groups to produce a wide variety of chiral catalysts. These compounds were designed to enforce the rigidity of the chiral environment for the central metal ion and were based on mesotetra(*o*-aminophenyl)porphyrin. However, since porphyrins bearing carboxamido groups are somewhat fragile under oxidation conditions, porphyrins containing chiral substituents linked by a C–C bond or an ether bond were synthesized. These compounds appear to be more robust than those with the carboxamido groups and give better results for the asymmetric epoxidation of alkenes.

Thus, O'Malley and Kodadek [224] prepared the “chiral wall” porphyrin ligand (**61**) by condensation of (*R*)-binaphthaldehyde with pyrrole (Figure 12). The corresponding manganese complex associated with NaOCl produced epoxidation of various styrene derivatives in 20–40% ee with extremely high catalytic efficiency. Furthermore, this complex is quite robust under oxidation conditions.

Naruta *et al.* [225, 226] designed the “twin-coronet” porphyrin ligands (**62**) and (**63**) with binaphthyl derivatives as chiral substituents (Figure 13). Each face of the macrocycle is occupied by two binaphthyl units and the ligand has C_2 symmetry. Iron complexes of these compounds can be very effective catalysts in the epoxidation of electron-deficient alkenes. Thus, nitro-substituted styrenes are readily epoxidized in 76–96% ee [226]. The degree of enantioselectivity can be explained on the basis of electronic interactions between the substrate aromatic ring and the chiral substituents rather than on the basis of steric interactions.

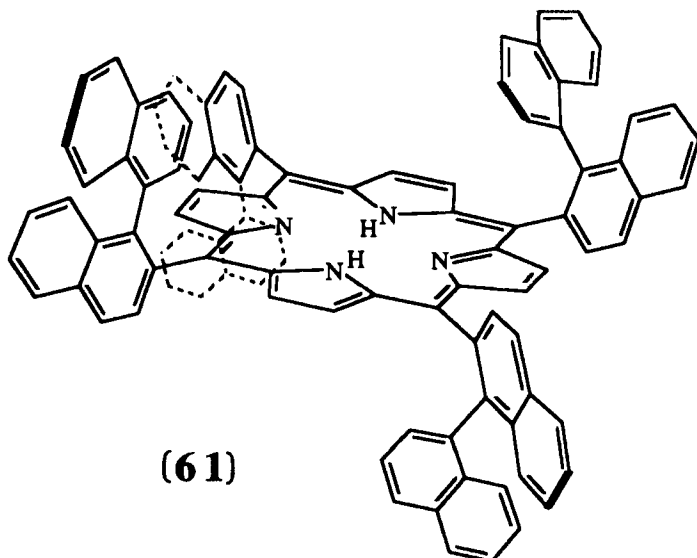


Figure 12 Structure of the chiral wall porphyrin. Reproduced from *J. Am. Chem. Soc.*, **111**, 9116 (1989) by permission of the American Chemical Society

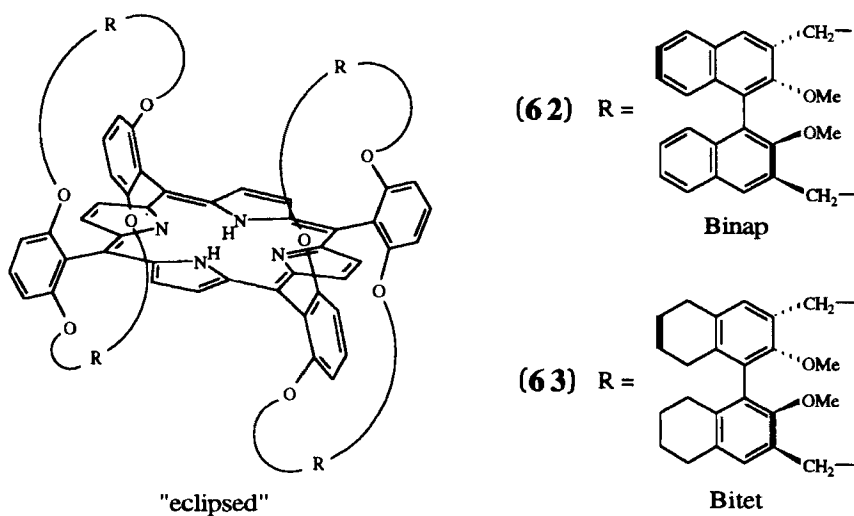


Figure 13 Structures of twin-coronet porphyrins. Reproduced from *J. Am. Chem. Soc.*, **113**, 6865 (1991) by permission of the American Chemical Society

Additional chiral binaphthyls in the central part of the superstructure of the picnic-basket porphyrins (Figure 7) developed by Collman *et al.* [227, 228] do not enhance catalytic effectiveness or low enantioselectivity in comparison to the systems of Naruta *et al.* Manganese complexes of compound (47) give only 13% ee in the epoxidation of styrene when phenoxide is used to block the unhindered face of the catalyst [199]. This low optical yield suggests a weak interaction of the substrate with the chiral binaphthyl unit, which is not very close to the active site ($> 6 \text{ \AA}$ distant). This handicap has been overcome more recently by Collman *et al.* by using "threitol-strapped" porphyrins (Figure 14) (64) [200]. Introduction of such chiral superstructures enforces a more effective asymmetric epoxidation by optimization of the chiral environment of the catalyst. Up to 88% ee can be obtained in the epoxidation of 1,2-dihydronaphthalene with manganese derivatives when a bulky imidazole ligand is used to block the unhindered face of the macrocycle.

Attachment of acetylated glucose units to an *ortho*-substituted tetraphenylporphyrin by ether linkage forms chiral substrate-binding sites on both faces of the porphyrin ring (Figure 14). These compounds, reported by Momenteau and coworkers [229–232], contain multistereogenic centers. Manganese(III) and iron(III) complexes of tetrakis[(2,3,4,5-tetraacetyl-*O*- β -glucosyl)phenyl]porphyrin (64) catalyze the epoxidation of styrene derivatives in 23–33% ee depending on the atropisomer [233]. These low stereospecificities of oxidation when PhIO or other oxidants such as NaOCl and KHSO₅ [234] are used could be attributed to the great steric hindrance of the glycosylated groups very close to the active site.

These porphyrins with chiral superstructures are expected to be insufficiently robust against oxidative catalyst destruction when H₂O₂ is used as the source

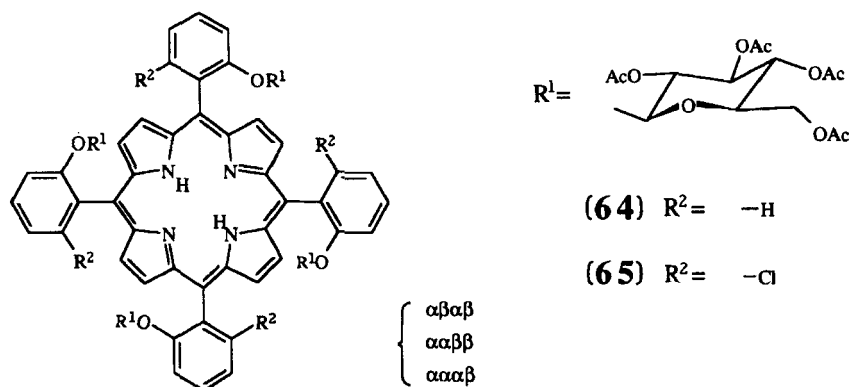


Figure 14 Structures of glycosylated porphyrins [229, 230]

of dioxygen. In response to this limitation, Momenteau and coworkers [231] have developed new glycosylated compounds of type (65) whereby electron-withdrawing substituents are introduced at each meso aryl position. In these compounds, regarded as second-generation catalysts, the tetraacetylglucosyl substituents linked at the *ortho*-positions of the meso phenyl groups give a chiral environment to the catalytic site, whereas the presence of chloro substituents at the other *ortho*-positions reinforces the stability of the catalysts. Low enantiomeric excesses (22%) are obtained with manganese complexes in the presence of 4-*t*-butylpyridine for the epoxidation of 4-chlorostyrene by H_2O_2 , but only a very low destruction of the catalyst ($\sim 5\%$) results after 4 h of epoxidation.

The possibility that chiral substituents close to the reactive oxometal group may promote better enantioselectivity of alkene epoxidation has encouraged several groups to seek new porphyrin types. This can be achieved by the synthesis of "chiorporphyrins" with chiral moieties borne directly on the meso carbon atoms (Figure 15). Such compounds can be synthesized in a single step by reacting chiral aldehydes with pyrrole under Lindsey conditions. This possibility overcomes the handicap of the multistep synthesis of superstructured chiral porphyrins derived from the mesotetraphenylporphyrin generally accompanied by rather poor yields in some steps. The first attempt to introduce chiral fragments into the meso positions was reported by Proess and Hevesi [235]. They have prepared the mesotetra(fenchylidenylmethyl)porphyrin (66) using the regioselective reaction of an α , β -unsaturated selenoacetal with pyrrole in 20% yield. With the manganese derivative, NaOCl as oxidant and pyridine as coligand, a 50% yield and 12% ee were reported for the epoxidation of *o*-chlorostyrene, without destruction of the catalyst at the end of the reaction (60 h). The enantiomeric excess is rather low, perhaps a result of the presence of various atropisomers which may differ greatly in their catalytic efficiencies.

Synthesis of the chiorporphyrins (67) and (68) was achieved by reacting the chiral aldehydes (1*R*)-(-)-*cis*-caronaldehyde acid methyl ester and (1*R*)-(-)-myrhenal with pyrrole [236]. Chloromanganese(III) derivatives of the D_2 -symmetric $\alpha\beta\alpha\beta$ -atropisomers, which appear to be the most abundant, were applied to the epoxidation of some unfunctionalized aromatic alkenes with PhIO. A high ee value (70%) was obtained in the epoxidation of dihydronaphthalene with this type of catalyst whereas it was significantly lower when functionalized substrates were used (17% for *p*-chlorostyrene).

Momenteau and coworkers [237] developed a series of glycosylated porphyrins where four protected sugar substituents are directly attached to the meso positions. Contrary to the observations mentioned above, the manganese complex of the xylofuranosylporphyrin (69) catalyzes the epoxidation of *p*-chlorostyrene to the (*S*)-epoxide in 20% ee [238]. Further investigations are being carried out to try to explain that result.

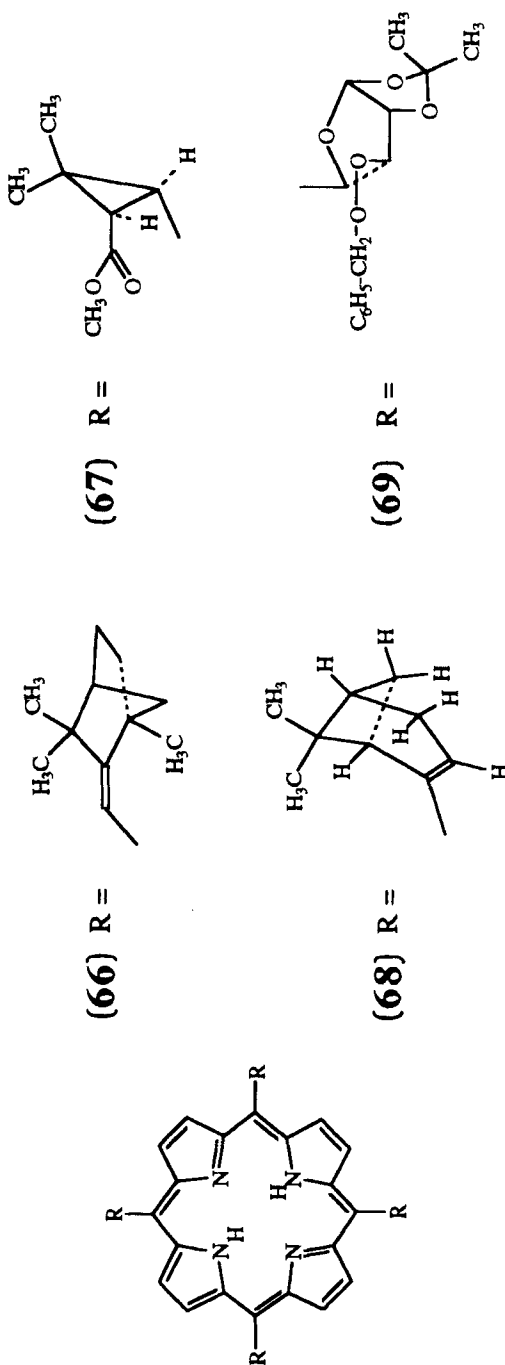


Figure 15 Structures of chirophyrins (arrows indicate attachment points of R groups) [234–236]

5. CONCLUSION

During the last two decades, a general trend in biomimetic chemical approaches has been developed to give a better understanding of the various chemical and stereochemical parameters which govern the electronic, magnetic and coordination properties, and the chemical reactivities of hemoprotein active sites. Superstructured metalloporphyrins have provided much information about structure and function that cannot be obtained from investigations of the natural systems themselves. Thus, we have seen a demonstration of the relative importance of proximal, distal and other effects in intramolecular interactions, host-guest recognition processes and specific reactions. The supramolecular structures obtained by a great variety of chemical strategies are capable of strongly influencing the reactivity of reaction centers in a manner that is reminiscent of the modulation of the reactivity of the prosthetic group by the surrounding protein chains in hemoproteins.

The development of new well-defined and robust compounds suitable for efficient applications in dioxygen transport or carbon monoxide detoxification and in catalytic regioselective and stereoselective oxidations of various compounds will be the major challenge in the near future.

6. ACKNOWLEDGMENTS

Much of the work described herein was carried out in my laboratory at the Institut Curie and was supported by the Centre National de la Recherche Scientifique. It is a great pleasure to acknowledge the collaborators and coworkers whose names can be found in the literature citations, in particular B. Looock and N. Marie for their assistance in the preparation of this manuscript.

7. REFERENCES

1. J.-P. Collman, T. R. Halbert and K. S. Suslick, in *Metal Ion Activation of Dioxygen* (ed. T. G. Spiro), Wiley, New York, 1980, p. 1.
2. B. Morgan and D. Dolphin, *Struct. Bonding*, **64**, 115 (1987).
3. M. Momenteau, *Pure Appl. Chem.*, **58**, 1493 (1986).
4. M. Momenteau and C. A. Reed, *Chem. Rev.*, **94**, 659 (1994).
5. D. Mansuy, P. Battioni and J.-P. Battioni, *Eur. J. Biochem.*, **184**, 267 (1989).
6. B. Meunier, *Chem. Rev.*, **92**, 1411 (1992).
7. J. P. Collman, X. Zhang, V. J. Lee, E. S. Uffelman and J. I. Brauman, *Science*, **261**, 1404 (1993).
8. S. B. Ungashe and J. T. Groves, in *Advances in Inorganic Biochemistry* (eds G. L. Eickhorn and L. Marzelli), Elsevier, New York, 1993, p. 1.
9. D. Mansuy, *Pure Appl. Chem.*, **66**, 737 (1994).
10. R. A. Sheldon, *Metalloporphyrins in Catalytic Oxidations*, Dekker, New York, 1994.

11. R. E. Dickerson and I. Geis (eds), *Hemoglobin: Structure, Function, Evolution and Pathology*, Benjamin/Cummings, Menlo Park, CA, 1983, p. 1.
12. G. Fermi, *J. Mol. Biol.*, **97**, 237 (1975).
13. S. E. V. Phillips, *Nature*, **273**, 247 (1978).
14. S. E. V. Phillips, *J. Mol. Biol.*, **142**, 531 (1980).
15. B. Shaanan, *Nature*, **296**, 683 (1982).
16. S. E. V. Phillips and B. P. Schoenborn, *Nature*, **292**, 81 (1981).
17. E. J. Heidner, R. C. Ledner and M. F. Perutz, *J. Mol. Biol.*, **104**, 707 (1976).
18. D. Brault and M. Rougée, *Biochemistry*, **13**, 4591 (1974).
19. W. R. Scheidt and C. A. Reed, *Chem. Rev.*, **81**, 543 (1981).
20. J. P. Collman and C. A. Reed, *J. Am. Chem. Soc.*, **95**, 2048 (1973).
21. J. L. Hoard, *Science*, **174**, 1295 (1971).
22. K. Spartalian, G. Lang, J. P. Collman, R. R. Gagne and C. A. Reed, *J. Chem Phys.*, **63**, 5375 (1975).
23. L. A. Cohen and W. S. Caughey, *Biochemistry*, **7**, 636 (1968).
24. N. Sadasivan, H. I. Eberspaecher, W. H. Fuchsman and W. S. Caughey, *Biochemistry*, **8**, 534 (1969).
25. L. Latos-Grazynski, R. J. Cheng, G. N. La Mar and A. L. Balch, *J. Am. Chem. Soc.*, **104**, 5992 (1982).
26. D. H. Chin, J. Del Gaudio, G. N. La Mar and A. L. Balch, *J. Am. Chem. Soc.*, **99**, 5486 (1977).
27. A. L. Balch, Y. W. Chan, R. J. Cheng, G. N. La Mar, L. Latos-Grazynski and M. W. Renner, *J. Am. Chem. Soc.*, **106**, 7779 (1984).
28. W. J. Wallace, R. A. Houtchens, J. C. Maxwell and W. S. Caughey, *J. Biol. Chem.*, **257**, 4966 (1982).
29. K. Shikama, *Coord. Chem. Rev.*, **83**, 73 (1988).
30. R. E. Brantley, S. J. Smerdon, A. J. Wilkinson, E. W. Singleton and J. S. Olson, *J. Biol. Chem.*, **268**, 6995 (1993).
31. J. E. Baldwin and J. J. Huff, *J. Am. Chem. Soc.*, **95**, 5757 (1973).
32. J. P. Collman, R. R. Gagne, T. R. Halbert, J. C. Marchon and C. A. Reed, *J. Am. Chem. Soc.*, **95**, 7868 (1973).
33. J. P. Collman, R. R. Gagne, C. A. Reed, W. T. Robinson and C. A. Rodley, *Proc. Natl. Acad. Sci. USA*, **71**, 1326 (1974).
34. J. P. Collman, R. R. Gagne, C. A. Reed, T. R. Halbert, G. Lang and W. T. Robinson, *J. Am. Chem. Soc.*, **97**, 1427 (1975).
35. P. Rothmund, *J. Am. Chem. Soc.*, **57**, 2010 (1935).
36. J. P. Collman, *Acc. Chem. Res.*, **10**, 265 (1977).
37. G. B. Jameson, F. Molinaro, J. A. Ibers, J. P. Collman, J. J. Brauman, E. Rose and K. S. Suslick, *J. Am. Chem. Soc.*, **102**, 3224 (1980).
38. G. B. Jameson, G. A. Rodley, W. T. Robinson, R. R. Gagne, C. A. Reed and J. P. Collman, *Inorg. Chem.*, **17**, 850 (1978).
39. G. B. Jameson, F. Molinaro, J. A. Ibers, J. P. Collman, J. J. Brauman, E. Rose and K. S. Suslick, *J. Am. Chem. Soc.*, **100**, 6769 (1978).
40. J. P. Collman, J. J. Brauman, T. J. Collins, B. L. Iverson, G. Lang, R. B. Pettman, J.-L. Sessler and M. A. Walters, *J. Am. Chem. Soc.*, **105**, 3038 (1983).
41. H. Diekmann, C. K. Chang and T. G. Traylor, *J. Am. Chem. Soc.*, **93**, 4068 (1971).
42. T. G. Traylor, D. Campbell and S. Tsuchiya, *J. Am. Chem. Soc.*, **101**, 4748 (1979).
43. H. Ogoshi, H. Sugimoto and Z. Yoshida, *Tetrahedron Lett.*, **49**, 4477 (1976).
44. T. G. Traylor, N. Koga, L. A. Deardurff, P. N. Swepston and J. A. Ibers, *J. Am. Chem. Soc.*, **106**, 5132 (1984).

113. J. C. Hanson and B. P. Schoenborn, *J. Mol. Biol.*, **153**, 117 (1981).
114. S. M. Peng and J. A. Ibers, *J. Am. Chem. Soc.*, **98**, 8032 (1976).
115. L. Ricard, R. Weiss and M. Momenteau, *J. Chem. Soc., Chem. Commun.*, 818 (1986).
116. I. Ascone, A. Bianconi, E. Dartyge, S. Della Longa, A. Fontaine and M. Momenteau, *Biochem. Biophys. Acta*, **915**, 168 (1987).
117. C. Tétreau, D. Lavalette, M. Momenteau, J. Fischer and R. Weiss, *J. Am. Chem. Soc.*, **116**, 11 840 (1994).
118. K. Kim, J. Fetting, J. L. Sessler, M. Cyr, J. Hugdahl, J. P. Collman and J. A. Ibers, *J. Am. Chem. Soc.*, **111** 403 (1989).
119. J. R. Budge, P. E. Ellis, R. D. Jones, J. E. Linard and F. Basolo, *J. Am. Chem. Soc.*, **101**, 4760 (1979).
120. J. R. Budge, P. E. Ellis, R. D. Jones, J. E. Linard, T. Szymanski and F. Basolo, *J. Am. Chem. Soc.*, **101**, 4762 (1979).
121. J. E. Linard, P. E. Ellis, J. R. Budge, R. D. Jones and F. Basolo, *J. Am. Chem. Soc.*, **102**, 1896 (1980).
122. K. Kim and J. A. Ibers, *J. Am. Chem. Soc.*, **113**, 6077 (1991).
123. P. Maillard, C. Schaeffer, C. Huel, J.-M. Lhoste and M. Momenteau, *J. Chem. Soc., Perkin Trans. 1*, 3285 (1988).
124. P. Maillard, C. Schaeffer, C. Tétreau, D. Lavalette, J.-M. Lhoste and M. Momenteau, *J. Chem. Soc., Perkin Trans. 2*, 1437 (1989).
125. D. Mansuy, M. Lange, J. C. Chottard, J. F. Bartoli, B. Chevrier and R. Weiss, *Agnew. Chem., Int. Ed. Engl.*, **17**, 781 (1978).
126. P. A. Forshey and T. Kuwana, *Inorg. Chem.*, **20**, 693 (1981).
127. J. Silver, B. Lukas and G. Al-Jaff, *Inorg. Chim. Acta*, **91**, 125 (1984).
128. M. Rougée and D. Brault, *Biochemistry*, **14**, 4100 (1975).
129. L. Leondiadis, M. Momenteau and A. Desbois, *Inorg. Chem.*, **31**, 4691 (1992).
130. L. Leondiadis and M. Momenteau, *J. Org. Chem.*, **54**, 6135 (1989).
131. C. Tétreau, L. Leondiadis, D. Lavalette and M. Momenteau, *J. Chem. Soc., Perkin Trans. 2*, 73 (1992).
132. S. Han, D. L. Rousseau, G. Giacometti and M. Brunori, *Proc. Natl. Acad. Sci. USA*, **87**, 205 (1990).
133. R. H. Austin, K. W. Beeson, L. Eisenstein, M. Frauenfelder and I. C. Gunsalus, *Biochemistry*, **14**, 5355 (1975).
134. R. J. Morris and Q. H. Gibson, *J. Biol. Chem.*, **17**, 8050 (1980).
135. W. Doster, D. Beece, S. F. Boisne, E. E. Di Iorio, L. Eisenstein, H. Frauenfelder, L. Reinish, E. Shyamsunder, K. H. Winterhalter and K. T. Yue, *Biochemistry*, **21**, 4831 (1982).
136. C. Tétreau, D. Lavalette, M. Momenteau and J. M. Lhoste, *Proc. Natl. Acad. Sci. USA*, **84**, 2267 (1987).
137. C. Tétreau, M. Momenteau and D. Lavalette, *Inorg. Chem.*, **29**, 1727 (1990).
138. J. M. McCord and I. Fridovich, *J. Biol. Chem.*, **244**, 6049 (1969).
139. J. E. Frio and P. Jones, *Adv. Inorg. Bioinorg. Mech.*, **3**, 175 (1984).
140. I. Fita and M. G. Rossmann, *J. Mol. Biol.*, **185**, 21 (1985).
141. D. Dolphin and R. H. Falton, *Acc. Chem. Res.*, **7**, 26 (1974).
142. D. Dolphin, A. Forman, D. C. Borg, J. Fajer and R. H. Felton, *Proc. Natl. Acad. Sci. USA*, **68**, 614 (1971).
143. J. H. Dawson, *Science*, **240**, 433 (1988).
144. B. M. Kincaid and R. G. Shulman, *Adv. Inorg. Biochem.*, **2**, 303 (1980).
145. J. T. Groves, *Adv. Inorg. Biochem.*, **1**, 119 (1979).
146. B. C. Finzel, T. L. Poulos and J. Kraut, *J. Biol. Chem.*, **259**, 13027 (1984).

80. Y. Uemori and E. Kyuno, *Inorg. Chim. Acta*, **125**, L45 (1986).
81. Y. Uemori, H. Miyakawa and E. Kyuno, *Inorg. Chem.*, **27**, 377 (1988).
82. D. Lexa, M. Momenteau, J.-M. Savéant and F. Xu, *Inorg. Chem.*, **24**, 122 (1985).
83. C. Cartier, M. Momenteau, E. Dartyge, A. Fontaine, G. Tourillon, A. Michalowicz and M. Verdaguer, *J. Chem. Soc., Dalton Trans.*, 609 (1992).
84. I. P. Gerotheranassis, M. Momenteau and B. Looock, *J. Am. Chem. Soc.*, **111**, 7006 (1989).
85. J. E. Baldwin, J. H. Cameron, M. J. Crossley and E. J. Dagley, *J. Chem. Soc., Dalton Trans.*, 1739 (1984).
86. M. Momenteau, B. Looock, D. Lavalette, C. Tétreau and J. Mispelter, *J. Chem. Soc., Chem. Commun.*, 962 (1983).
87. A. R. Battersby, S. G. Hartley and M. D. Turnbull, *Tetrahedron Lett.*, 3169 (1978).
88. A. R. Battersby and A. D. Hamilton, *J. Chem. Soc., Chem. Commun.*, 117 (1980).
89. A. R. Battersby, S. A. J. Bartholomew and J. Nitta, *J. Chem. Soc., Chem. Commun.*, 1291 (1983).
90. J. Mispelter, M. Momenteau and J.-M. Lhoste, *Biochimie*, **63**, 911 (1981).
91. C. K. Chang and T. G. Traylor, *Proc. Natl. Acad. Sci. USA*, **72**, 1166 (1975).
92. D. K. White, J. B. Cannon and T. G. Traylor, *J. Am. Chem. Soc.*, **101**, 2443 (1979).
93. D. Lavalette, C. Tétreau and M. Momenteau, *J. Am. Chem. Soc.*, **101**, 5395 (1979).
94. M. Brunori, R. W. Noble, E. Antonini and J. Wyman, *J. Biol. Chem.*, **241**, 5238 (1966).
95. R. W. Noble, Q. H. Gibson, M. Brunori, E. Antonini and J. Wyman, *J. Biol. Chem.*, **244**, 3905 (1969).
96. M. Momenteau and D. Lavalette, *J. Am. Chem. Soc.*, **100**, 4322 (1978).
97. D. Lavalette and M. Momenteau, *J. Chem. Soc., Perkin Trans. 2*, 385 (1982).
98. D. Lavalette, C. Tétreau, M. Momenteau, J. Mispelter, J.-M. Lhoste, G. E. Wuenschell and C. A. Reed, *Laser Chem.*, **10**, 297 (1990).
99. L. Pauling, *Nature*, **203**, 182 (1964).
100. D. Lavalette, C. Tétreau, J. Mispelter, M. Momenteau and J.-M. Lhoste, *Eur. J. Biochem.*, **145**, 555 (1984).
101. M. Momenteau and D. Lavalette, *J. Chem. Soc., Chem. Commun.*, 341 (1982).
102. J. Mispelter, M. Momenteau, D. Lavalette and J.-M. Lhoste, *J. Am. Chem. Soc.*, **105**, 5165 (1983).
103. G. B. Jameson, and R. S. Drago, *J. Am. Chem. Soc.*, **107**, 3017 (1985).
104. G. E. Wuenschell, C. Tétreau, D. Lavalette and C. A. Reed, *J. Am. Chem. Soc.*, **114**, 3346 (1992).
105. J. S. Olson, A. J. Mathews, R. J. Rohlfs, B. A. Springer, K. D. Egeberg, S. G. Sligar, J. Tame, J.-P. Renaud and K. Nagai, *Nature*, **336**, 265 (1988).
106. T. Hashimoto, R. L. Dyer, M. L. Crossley, J. E. Baldwin and F. Basolo, *J. Am. Chem. Soc.*, **104**, 2101 (1982).
107. T. G. Traylor, N. Koga and L. A. Deardurff, *J. Am. Chem. Soc.*, **107**, 6504 (1985).
108. T. G. Traylor and A. Berzinis, *Proc. Natl. Acad. Sci. USA*, **77**, 3171 (1980).
109. V. S. Sharma, H. M. Ranney, J. F. Geibel and T. G. Traylor, *Biochem. Biophys. Res. Commun.*, **66**, 1301 (1975).
110. T. G. Traylor, S. Tsuchiya, D. H. Campbell, M. Mitchell, D. V. Stynes and N. Koga, *J. Am. Chem. Soc.*, **107**, 604 (1985).
111. J. P. Collman, J. I. Brauman, B. L. Iverson, J.-L. Sessler, R. M. Morris and Q. M. Gibson, *J. Am. Chem. Soc.*, **105**, 3052 (1983).
112. J. M. Baldwin, *J. Mol. Biol.*, **136**, 103 (1980).

45. A. R. Battersby, D. G. Buckley, S. G. Hartley and M. D. Turnbull, *J. Chem. Soc., Chem. Commun.*, 879 (1976).
46. C. K. Chang, *J. Am. Chem. Soc.*, **99**, 2819 (1977).
47. J. Almog, J. E. Baldwin, R. L. Dyer and M. Peters, *J. Am. Chem. Soc.*, **97**, 226 (1975).
48. J. Almog, J. E. Baldwin and J. R. Huff, *J. Am. Chem. Soc.*, **97**, 227 (1975).
49. J. Almog, J. E. Baldwin, M. J. Crossley, J. F. Debernardis, R. L. Dyer, J. R. Huff and M. K. Peters, *Tetrahedron*, **37**, 3589 (1981).
50. M. R. Johnson, W. K. Seok and J. A. Ibers, *J. Am. Chem. Soc.*, **113**, 3998 (1991).
51. W. Ma, C. Slebodnick and J. A. Ibers, *J. Org. Chem.*, **58**, 6349 (1993).
52. W. F. K. Schnatter, O. Almarsson and T. C. Bruice, *Tetrahedron*, **47**, 8687 (1991).
53. H. Y. Zhang, A. Blasko, J. Q. Yu and T. C. Bruice, *J. Am. Chem. Soc.*, **114**, 6621 (1992).
54. H. Ogoshi, M. Sugimoto and Z. Yoshida, *Tetrahedron Lett.*, **49**, 4481 (1976).
55. H. Ogoshi, M. Sugimoto, M. Miyake and Z. Yoshida, *Tetrahedron*, **40**, 579 (1984).
56. J. E. Baldwin, T. Klose and M. Peters, *J. Chem. Soc., Chem. Commun.*, 881 (1976).
57. J. E. Baldwin, M. J. Crossley, T. Klose, E. A. O'Rear and K. M. Peters, *Tetrahedron*, **38**, 27 (1982).
58. J. E. Baldwin, M. J. Crossley and J. Debernardis, *Tetrahedron*, **38**, 685 (1982).
59. T. P. Wijesekera, J. B. Paine, III and D. Dolphin, *J. Org. Chem.*, **53**, 1345 (1988).
60. D. El-Kasmi, C. Tétreau, D. Lavalette and M. Momenteau, *J. Chem. Soc., Perkin Trans. 2*, 1799 (1993).
61. M. Momenteau, B. Looock, C. Tétreau, D. Lavalette, A. Croisy, C. Schaeffer, C. Huel and J.-M. Lhoste, *J. Chem. Soc., Perkin Trans. 2*, 249 (1987).
62. P. E. Ellis, J. E. Linard, T. Szymanski, R. D. Jones, J. R. Budge and F. Basolo, *J. Am. Chem. Soc.*, **110**, 1889 (1980).
63. T. G. Spiro and J. M. Burke, *J. Am. Chem. Soc.*, **98**, 5482 (1976).
64. A. Desbois, M. Momenteau and M. Lutz, *Inorg. Chem.*, **28**, 825 (1989).
65. M. Momenteau, W. R. Scheidt, C. W. Eigenbrot and C. A. Reed, *J. Am. Chem. Soc.*, **110**, 1207 (1988).
66. J.-L. Hoard, in *Porphyrins and Metalloporphyrins* (ed. K. M. Smith), Elsevier, Amsterdam, 1985, p. 317.
67. A. R. Amundsen and L. Vaska, *Inorg. Chim. Acta*, **14**, 249 (1975).
68. J. M. Cense and R. M. Le Quan, *Tetrahedron Lett.*, 3725 (1979).
69. K. S. Suslick and M. M. Fox, *J. Am. Chem. Soc.*, **105**, 3507 (1983).
70. T. Komatsu, E. Hasegawa, S. Kumamoto, H. Nishide and E. J. Tsuchida *J. Chem. Soc., Dalton Trans.*, 3281 (1991).
71. T. Komatsu, K. Arai, H. Nishide and E. Tsuchida, *Chem. Lett.*, 799 (1992).
72. M. Momenteau, B. Looock, J. Mispelter and E. Bisagni, *Nouv. J. Chim.*, **3**, 77 (1979).
73. M. Momenteau, B. Looock, J. Mispelter and E. Bisagni, *J. Chem. Soc., Perkin Trans.*, **1**, 189 (1983).
74. M. Momenteau, J. Mispelter, B. Looock and J.-M. Lhoste, *J. Chem. Soc., Perkin Trans.*, **1**, 61 (1985).
75. M. Momenteau, J. Mispelter, B. Looock and J.-M. Lhoste, *J. Chem. Soc., Perkin Trans.*, **1**, 221 (1985).
76. A. Lecas, B. Boitrel and E. Rose, *Bull. Soc. Chim. Fr.*, **128**, 407 (1991).
77. U. Simonis, F. A. Walker, P. L. Lee, B. J. Hanquet, D. J. Meyerhoff and W. R. Scheidt, *J. Am. Chem. Soc.*, **109**, 2659 (1987).
78. D. Mansuy, P. Battioni, J.-P. Renaud and P. Guerin, *J. Chem. Soc., Chem. Commun.*, 155 (1985).
79. D. Reddy and T. K. Chandrashekar, *J. Chem. Soc., Dalton Trans.*, 619 (1992).

147. V. Thanabal, J. S. de Ropp and G. N. La Mar, *J. Am. Chem. Soc.*, **109**, 7516 (1987).
148. T. L. Poulos, B. C. Finzel and A. J. Howard, *Biochemistry*, **25**, 5314 (1986).
149. J. H. Dawson and M. Sono, *Chem. Rev.*, **87**, 1255 (1987).
150. H. Von Euler and K. Josephson, *Justus Liebigs Ann. Chem.*, **456**, 111 (1927).
151. P. Jones, T. Robson and S. B. Brown, *Biochem. J.*, **135**, 353 (1973).
152. H. C. Kelly, D. M. Davies, M. J. King and P. Jones, *Biochemistry*, **16**, 3543 (1977).
153. M. F. Zippies, W. A. Lee and T. C. Bruice, *J. Am. Chem. Soc.*, **108**, 4433 (1986).
154. P. N. Balasubramanian, E. S. Schmidt and T. C. Bruice, *J. Am. Chem. Soc.*, **109**, 7865 (1987).
155. T. G. Taylor and F. Xu, *J. Am. Chem. Soc.*, **109**, 6201 (1987).
156. M. Momenteau, B. Looock, C. Huel and J.-M. Lhoste, *J. Chem. Soc., Perkin Trans.*, **1**, 283, (1988).
157. A. Robert, B. Looock, M. Momenteau and B. Meunier, *Inorg. Chem.*, **30**, 706 (1991).
158. C. H. Lee, B. Garcia and T. C. Bruice, *J. Am. Chem. Soc.*, **112**, 6434 (1990).
159. A. Blasko, B. Garcia and T. C. Bruice, *J. Org. Chem.*, **58**, 5738 (1993).
160. R. Belal, M. Momenteau and B. Meunier, *New J. Chem.*, **13**, 853 (1989).
161. C. Schaeffer, M. Momenteau, J. Mispelter, B. Looock, C. Huel and J.-M. Lhoste, *Inorg. Chem.*, **25**, 4577 (1986).
162. D. Lexa, M. Momenteau, J.-M. Savéant and F. Xu, *J. Am. Chem. Soc.*, **108**, 6937 (1986).
163. C. Gueutin, D. Lexa, M. Momenteau, J.-M. Savéant and F. Xu, *Inorg. Chem.*, **25**, 4294 (1986).
164. D. Lexa and J.-M. Savéant, in *Redox Chemistry and Interfacial Behavior of Biological Molecules* (eds G. Fryhurst and K. Miki), Plenum Press, New York, 1987, p. 1.
165. B. Meunier, in *Catalytic Oxidation with Hydrogen Peroxide as Oxidant* (ed. G. Strukul), 1992, p. 153.
166. T. J. McMurphy and J. T. Groves, in *Cytochrome P450: Structure, Mechanism and Biochemistry*, (ed. P. R. Ortiz de Montellano), Plenum Press, New York, 1986, p. 1.
167. R. W. Estabrook, D. Y. Cooper and O. Rosenthal, *Biochem. Z.*, **338**, 741 (1963).
168. C. K. Chang and D. Dolphin, *J. Am. Chem. Soc.*, **97**, 5948 (1975).
169. J. H. Dawson and K. S. Eble, *Advances in Organic and Bioinorganic Mechanisms*, Academic Press, New York, 1986, p. 1.
170. T. L. Poulos, B. C. Finzel, I. C. Gunsalus, G. C. Wagner and J. Kraut, *J. Biol. Chem.*, **260**, 16122 (1985).
171. C. K. Chang and D. Dolphin, *J. Am. Chem. Soc.*, **98**, 1607 (1976).
172. H. H. Ruf and P. J. Wende, *J. Am. Chem. Soc.*, **99**, 5499 (1977).
173. T. G. Traylor, T. C. Mincey and A. P. Berzini, *J. Am. Chem. Soc.*, **103**, 7084 (1981).
174. A. P. Berzini and T. G. Traylor, *Biochem. Biophys. Res. Commun.*, **87**, 229 (1979).
175. J. P. Collman and S. E. Groh, *J. Am. Chem. Soc.*, **104**, 1391 (1982).
176. A. R. Battersby, W. Howson and A. D. Hamilton, *J. Chem. Soc., Chem. Commun.*, 1266 (1982).
177. M. Momenteau, B. Looock, C. Huel and J. M. Lhoste, *J. Chem. Soc., Perkin Trans. 1*, 283 (1988).
178. B. Staubli, H. Fretz, U. Piantini and W. D. Woggon, *Helv. Chim. Acta*, **70**, 1173 (1987).
179. W. D. Woggon, *Nachr. Chem. Tech. Lab.*, **36**, 890 (1988).
180. H. Patzelt and W. D. Woggon, *Helv. Chim. Acta*, **75**, 523 (1992).

181. M. Schappacher, L. Ricard, R. Weiss, R. Montiel-Montoya, E. Bill, U. Gonser and A. X. Trautwein, *J. Am. Chem. Soc.*, **103**, 7646 (1981).
182. G. Chottard, M. Schappacher, L. Ricard and R. Weiss, *Inorg. Chem.*, **23**, 4557 (1984).
183. R. Montiel-Montoya, E. Bill, A. X. Trautwein, H. Winkler, L. Ricard, M. Schappacher and R. Weiss, *Hyperfine Interact.*, **29**, 1411 (1986).
184. L. Ricard, M. Schappacher, R. Weiss, R. Montiel-Montoya, E. Bill, U. Gonser and A. X. Trautwein, *Nouv. J. Chim.*, **7**, 405 (1983).
185. M. Schappacher, L. Ricard, J. Fischer, R. Weiss, E. Bill, R. Montiel-Montoya, H. Winkler and A. X. Trautwein, *Eur. J. Biochem.*, **168**, 419 (1987).
186. J. H. Dawson and S. P. Cramer, *FEBS Lett.*, **88**, 127 (1978).
187. J. T. Groves, T. E. Nemo and R. S. Myers, *J. Am. Chem. Soc.*, **101**, 1032 (1979).
188. J. T. Groves and T. E. Nemo, *J. Am. Chem. Soc.*, **105**, 5786 (1983).
189. T. J. Groves, Y. Watanabe and T. J. De Murry, *J. Am. Chem. Soc.*, **105**, 4489 (1983).
190. P. Battioni, J. P. Renaud, J.-F. Bartoli and D. Mansuy, *J. Chem. Soc., Chem. Commun.*, 341 (1986).
191. P. Battioni, J. P. Renaud, J. F. Bartoli, M. Reina-Artiles, M. Fort and D. Mansuy, *J. Am. Chem. Soc.*, **110**, 8462 (1988).
192. S. Banfi, F. Legramandi, F. Montanari, G. Pozzi and S. Quici, *J. Chem. Soc., Chem. Commun.*, 1285 (1991).
193. P. L. Anelli, S. Banfi, F. Legramandi, F. Montanari, G. Pozzi and S. Quici, *J. Chem. Soc., Perkin Trans. 1*, 1345 (1993).
194. O. Bortolini, M. Momenteau and B. Meunier, *Tetrahedron Lett.*, **25**, 5773 (1984).
195. R. D. Arasasingham, G. X. He and T. C. Bruice, *J. Am. Chem. Soc.*, **115**, 7985 (1993).
196. D. Mansuy, J. Leclaire, M. Fontecave and M. Momenteau, *Biochem. Biophys. Res. Commun.*, **119**, 319 (1984).
197. K. S. Suslick and B. R. Cook, *J. Chem. Soc., Chem. Commun.*, 200 (1987).
198. D. Mansuy, J. F. Bartoli and M. Momenteau, *Tetrahedron Lett.*, **23**, 2781 (1982).
199. J. P. Collman, X. Zhang, R. H. Hembre and J. I. Brauman, *J. Am. Chem. Soc.*, **112**, 5356 (1990).
200. J. P. Collman, V. J. Lee, X. Zhang, J. A. Ibers and J. I. Brauman, *J. Am. Chem. Soc.*, **115**, 3834 (1993).
201. J. P. Collman, J. I. Brauman, J. P. Fitzgerald, P. D. Hampton, Y. Naruta and T. Michida, *Bull. Chem. Soc. Jpn.*, **61**, 47 (1988).
202. J. T. Groves and R. Neumann, *J. Am. Chem. Soc.*, **111**, 2900 (1989).
203. J. T. Groves and R. Neumann, *J. Org. Chem.*, **53**, 3891 (1988).
204. J. T. Groves, R. C. Haushalter, M. Nakamura, T. E. Nemo and B. J. Evans, *J. Am. Chem. Soc.*, **103**, 2884 (1981).
205. C. K. Chang and F. Ebian, *J. Chem. Soc., Chem. Commun.*, 778 (1981).
206. P. S. Traylor, D. Dolphin and T. G. Traylor, *J. Chem. Soc., Chem. Commun.*, 279 (1984).
207. D. Dolphin, T. Nakano, T. E. Maione, T. K. Kirk and R. K. Farrell, in *Lignin Enzymic and Microbial Degradation* (ed. E. Odier), INRA, Paris, 1987, p. 157.
208. T. G. Traylor and S. Tsuchiya, *Inorg. Chem.*, **26**, 1338 (1987).
209. P. Bhyrappa and U. Krishnan, *Inorg. Chem.*, **30**, 241 (1991).
210. P. Hoffman, A. Robert and B. Meunier, *Bull. Soc. Chim. Fr.*, **129**, 85 (1992).
211. P. Hoffman, G. Labat, A. Robert and B. Meunier, *Tetrahedron Lett.*, **31**, 1991 (1990).

212. T. Wijesekera, A. Matsumoto, D. Dolphin and D. Lexa, *Angew. Chem., Int. Ed. Engl.*, **29**, 1028 (1990).
213. I. Artaud, H. Grennberg and D. Mansuy, *J. Chem. Soc., Chem. Commun.*, 1036 (1992).
214. I. Artaud, K. Ben Aziza, C. Chopard and D. Mansuy, *J. Chem. Soc., Chem. Commun.*, 31 (1991).
215. J. F. Bartoli, P. Battioni, W. R. De Foor and D. Mansuy, *J. Chem. Soc., Chem. Commun.*, 23 (1994).
216. D. Mandon, P. Ochsenbein, J. Fischer, R. Weiss, K. Jayaraj, R. N. Austin, A. Gold, P. S. White, O. Brigaud, P. Battioni and D. Mansuy, *Inorg. Chem.*, **31**, 2044 (1992).
217. J. F. Bartoli, O. Brigard, P. Battioni and D. Mansuy, *J. Chem. Soc., Chem. Commun.*, 440 (1991).
218. D. R. Benson, R. Valentekovich and F. Diederich, *Angew. Chem., Int. Ed. Engl.*, **29**, 191 (1990).
219. D. R. Benson, R. Valentekovich, S. W. Tam and F. Diederich, *Helv. Chim. Acta*, **76**, 2034 (1993).
220. I. Artaud, K. Ben Aziza and D. Mansuy, *J. Org. Chem.*, **58**, 3373 (1993).
221. G. Labat and B. Meunier, *New. J. Chem.*, **13**, 801 (1989).
222. S. Tsuchiya and M. Seno, *Chem. Lett.*, 263 (1989).
223. J. T. Groves and R. S. Myers, *J. Am. Chem. Soc.*, **105**, 5791 (1983).
224. S. O'Malley and T. Kodadek, *J. Am. Chem. Soc.*, **111**, 9116 (1989).
225. Y. Naruta, F. Tani and K. Maruyama, *Chem. Lett.*, 1269 (1989).
226. Y. Naruta, F. Tani, N. Ishihara and K. Maruyama, *J. Am. Chem. Soc.*, **113**, 6865 (1991).
227. J. P. Collman, J. I. Brauman, J. F. Fitzgerald, P. D. Hampton, Y. Naruta, J. W. Sparapany and J. A. Ibers, *J. Am. Chem. Soc.*, **110**, 3477 (1988).
228. J. P. Collman, X. Zhang, V. J. Lee and J. I. Brauman, *J. Chem. Soc., Chem. Commun.*, 1647 (1992).
229. Ph. Maillard, J.-L. Guerquin-Kern, C. Huel and M. Momenteau, *J. Org. Chem.*, **58**, 2774 (1993).
230. S. Vilain, Ph. Maillard and M. Momenteau, *J. Chem. Soc., Chem. Commun.*, 1697 (1994).
231. S. Vilain, Ph. Maillard and M. Momenteau, *J. Mol. Catal.* in press (1996).
232. Ph. Maillard, J.-L. Guerquin-Kern, M. Momenteau and S. Gaspard, *J. Am. Chem. Soc.*, **111**, 9125 (1989).
233. Ph. Maillard, J.-L. Guerquin-Kern and M. Momenteau, *Tetrahedron Lett.*, **32**, 4901 (1991).
234. S. Vilain, A. Robert, Ph. Maillard, B. Meunier and M. Momenteau, *J. Mol. Catal.* in press (1996).
235. G. Proess and L. Hevesi, *J. Mol. Catal.*, **80**, 395 (1993).
236. M. Veyrat, O. Mauray, F. Faverjoin, D. E. Over, R. Ramasseul, J. C. Marchon, I. Turowaka-Tyrk and W. R. Scheidt, *Angew. Chem., Int. Ed. Engl.*, **33**, 220 (1994).
237. Ph. Maillard, C. Huel and M. Momenteau, *Tetrahedron Lett.*, **33**, 8081 (1992).
238. S. Vilain, Ph. Maillard and M. Momenteau, unpublished results.

Chapter 5

Recent Developments in the Design of Self-Replicating Systems

EDWARD A. WINTNER AND JULIUS REBEK JR

Massachusetts Institute of Technology, Cambridge, MA, USA

1. ABIOTIC REPLICATORS

The synthetic design of self-replicating systems is a relatively new field in chemistry; work on molecules which produce copies of themselves began in the 1980s and has since become a significant facet of the broader field of molecular recognition. This chapter details the work of our laboratory group in the design of replicating systems, from our entrance into the field in 1989 to our current generation of replicators. The excellent work of our many colleagues in the field, mentioned only briefly here, can best be read in their own words [1–10].

Life, by definition, is self-replicating, and perhaps the ultimate goal in the study of self-replicating systems is to gain insight into the precepts and definitions of life. While the replication of life as we know it is now understood in a general molecular sense, it is clear that the DNA-based cell is well evolved from what must have been the first living systems. One may speculate on the existence of very simple molecules or groups of molecules able to reproduce themselves – simple chemical cycles which could scarcely be termed “life.” Modern research into self-replication seeks to emulate such phenomena, if only in a synthetic, abiotic environment, with the goal of understanding the principles which must have governed the molecular transition from chaotic solution to the pockets of decreasing entropy known as ordered life.

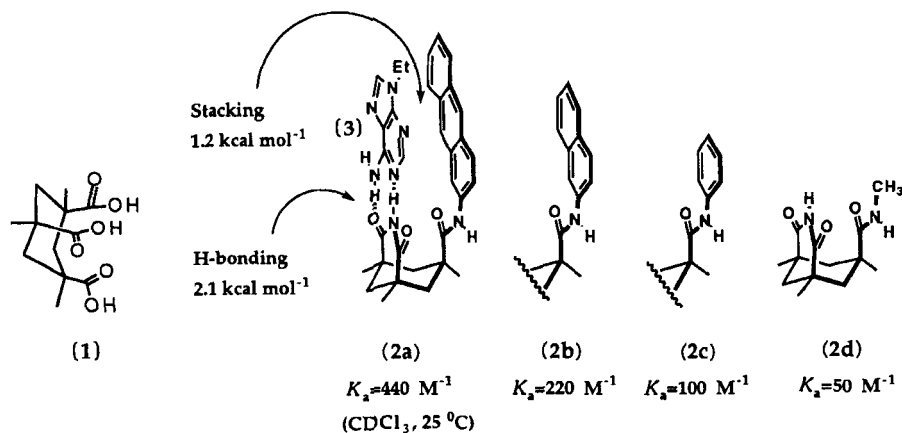


Figure 1 Energetics of aryl stacking and hydrogen bonding in the complexation of 9-ethyladenine (3)

While the most obvious (and glamorous) reason for exploring the world of self-replicating molecules is to search for insight into the origins of life, our work did not begin as an investigation into the so-called primordial soup of prebiotic earth. Instead, our replicators grew out of a more general interest in molecular recognition of nucleic acids. Early on, we had discovered the utility of derivatives of Kemp's triacid (1) [11] (Figure 1) to create molecules with the ability to recognize certain substrates; the U-turn inherent in the Kemp's triacid moiety allowed us to effect the convergence of multiple functionalities at a single location [12]. In 1987, we used this U-turn to bring both hydrogen-bonding and aryl-stacking interactions to bear on the nucleic acid adenosine [13]. Series of molecules such as (2a)–(2d) in Figure 1 allowed us to evaluate the energetics of aryl stacking versus hydrogen bonding in the complexation of 9-ethyladenine (3). From here, replicating molecules were just an idea away.

The key idea was that of self-complementarity: designing the size, shape and chemical surface of a structure such that the molecule has an affinity for itself. Given a self-complementary molecule, one has in theory only to break the structure into two parts to produce a self-replicating system; alternatively stated, linking two complementary molecules in an appropriate way can give rise to a self-complementary, replicating structure. In the schematic replicating system depicted in Figure 2, the two complementary components A and B react in an intermolecular fashion to form template T. Owing to the self-complementary nature of the template, two additional units of A and B form a complex with the template T–A–B. Weak intermolecular forces (e.g. hydrogen bonding and aryl stacking) anchor A and B on the template surface, while an intracomplex reaction takes place to produce the dimer 2T. The dimer

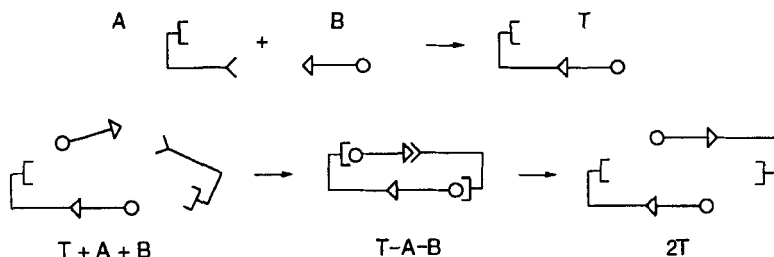


Figure 2 Schematic representation of self-complementary, template-based autocatalysis

dissociates and repeats the process, completing replication of the template, and the molecules are called replicators.

Autocatalysis in self-complementary systems is generally due to an efficient reaction within the complex $T-A-B$. If the reaction has no intermediate, or formation of an intermediate is rate limiting, rate enhancement is derived from the reduction in entropy caused by bringing together the reagents on a template. If breakdown of an intermediate is rate limiting (as in the case with our amide-forming replicators), rate enhancement is derived from template stabilization of an intermediate $A-B$ such that product formation is favored over reversion to substrates.

The enhancement of reactions by complementary surfaces lies at the heart of many processes in the laboratory and in nature. Template effects, leading to reduced activation entropies or stabilized intermediates, are responsible for the autocatalysis observed in our replicators, in nucleic acid replicators [1–5, 9], in bisubstrate reaction systems [8] and in a number of other processes [10], as well as countless biological reactions. The most relevant biological template effect was revealed in Watson and Crick's structure of double-stranded DNA. It was clear to them that during replication, one strand of DNA acted as a template for the other. This feature led to the inspired experiments of Orgel and coworkers at the Salk Institute [4], and there, in 1986, von Kiedrowski showed that a short, self-complementary segment of DNA could act as a template for its own formation, even without the aid of enzymes [1]. The complementary trideoxynucleotides CCG and CGG (C =cytosine, G =guanine) were coupled in the presence of a water-soluble condensation agent to form the self-complementary hexadeoxynucleotide by an autocatalytic process, thus creating the first abiotic self-replicating system. Subsequent improvements were made in the efficiency of autocatalysis; greater efficiency led to parabolic growth in the hexadeoxynucleotide concentration, reflecting the exponential nature of an autocatalytic process [2].

As shown above, molecular replication is simply an autocatalytic reaction where the product of a chemical transformation acts to catalyze that

transformation through the directed production of copies of the molecule. We distinguish here between self-replication and other forms of autocatalysis; while there are many examples of the latter – the bromination of acetone and the formose reaction (involving the polymerization of formaldehyde) [14] being among the oldest examples – self-replication is a special subset of autocatalytic reactions in which molecular recognition plays a role. It must be noted, however, that self-complementarity is not necessary for self-replication; other types of autocatalytic systems exist in which more general physical entities are created.

The replication of physical structures has been extensively explored by Luisi and coworkers [6a, 7], who have observed autocatalytic generation of micelles or reverse micelles in both aqueous and organic media. The recognition event in these types of systems is the preferential binding of a substrate to the micelle, whereby the exposure of the starting material to reagents, which are typically biphasic, is enhanced. The autocatalytic product in these systems, the micelle, is an aggregate of the reaction products with a loosely defined size and structure. These systems differ from template-based replication in that the latter is more strictly defined in its requirements of a complementary fit and stoichiometry in the recognition event. The difference is sufficiently great that “self-reproduction” has been proposed as the terms for the behavior of the micellelike systems [6b].

As already stated, our first self-replicating system evolved from work on the molecular recognition of adenine. By attaching an adenosine moiety to the aryl end of molecule (2b) in Figure 1, self-complementary molecules such as (6) were created. In the system, the Kemp's imidenaphthoylpentafluorophenyl ester (5) reacts with 5'-amino-5'-deoxy-2',3'-isopropylideneadenosine (4) to form the self-complementary autocatalytic template (6) (Figure 3) [15]. The system was tested in chloroform with 1% triethylamine base at $21 \pm 1^\circ\text{C}$, following the generation of template (6) by HPLC. The autocatalytic nature of the reaction was evident from the rate acceleration caused by seeding the reaction with its product (Figure 4) [16]. At 8.2 mM initial concentrations of reactants, adding 20% of compound (6) produced an average 43% increase in initial rate of product formation, and adding 50% of compound (6) produced a 73% increase in initial rate.

In general, the rate-limiting step for ester aminolysis in aprotic solvents is the breakdown of the zwitterionic tetrahedral intermediate [17–20]. We propose that the autocatalysis observed in our system is the result of the ability of the product to gather on its framework the two components of which it is formed and stabilize the tetrahedral intermediate thus created – complex (7) in the case of Figure 3. Noncovalent binding of the two ends of the substrate favors the elimination of pentafluorophenol from the tetrahedral intermediate, and leads to product. Depending on the mode of base pairing (Watson–Crick, Hoogsteen, reverse Watson–Crick, etc.), several geometric possibilities for a

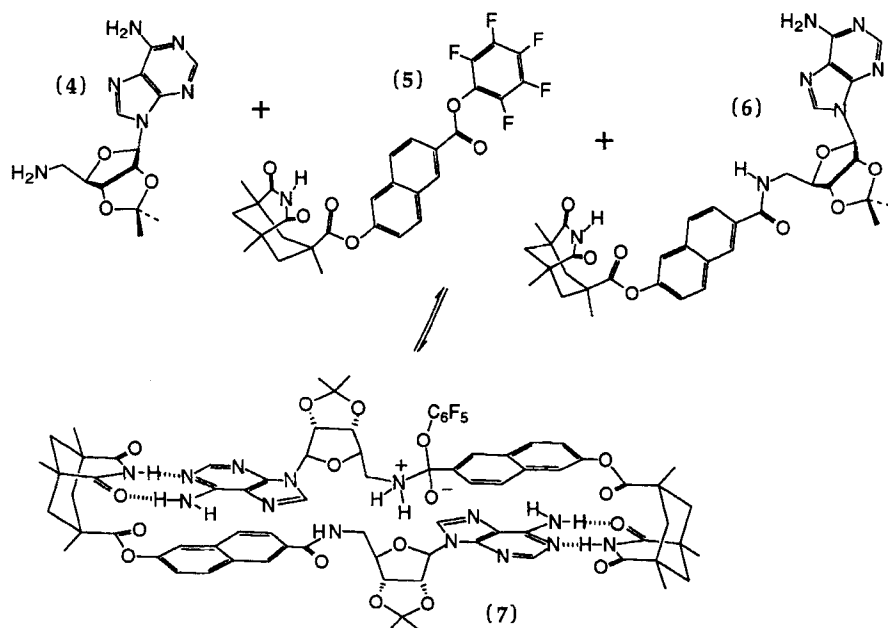


Figure 3 An abiotic self-replicating system

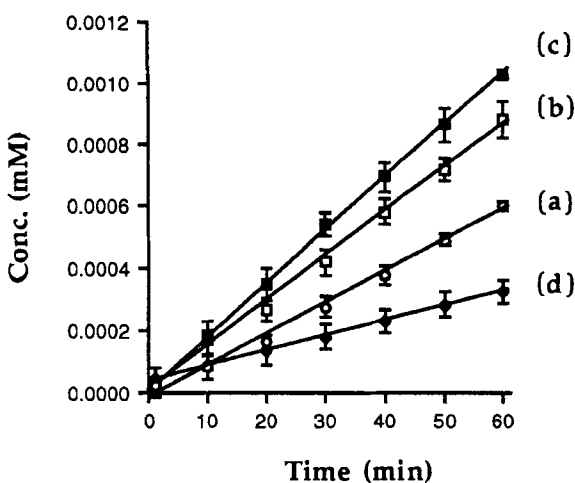


Figure 4 Formation of (6) in CHCl₃ (as followed by HPLC) at 21 ± 1 °C for 8.2 mM initial concentrations of (4) and (5) and with 1% triethylamine (TEA) base added: (a) baseline reaction of (4) with (5); (b) baseline reaction plus a fifth of an equivalent of product (6); (c) baseline reaction plus half an equivalent of product (6); and (d) baseline reaction plus one equivalent of adenine binder (21) (see Figure 15)

productive complex (7) are possible, but all result in the covalent coupling of substrates to give a replica of the template catalyst in dimeric form.

In order to affirm that template effects were the true cause of catalysis in these reactions, we gathered evidence from a wide range of experiments, and these are detailed in Section 2. After many years of testing the system in Figure 3, we are now convinced that it is a real if modest example of self-replication. As already stated, the key to the system lies in the catalytic efficiency of the template, and ever since, it has been our goal to enhance the template process relative to the more random background reactions of amine and ester. Chemical catalysis, positioning acids and bases on the template surface, is one means to this goal; such hydrogen-donating and -accepting functions could be trained on the tetrahedral intermediate to assist breakdown of the zwitterion to an amide. To begin, however, we used an alternative tactic: reduce the rate of background reactions.

One of the complications of the naphthoyl-derived system was that in both Hoogsteen and Watson–Crick binding modes, coupling between the amine and ester could occur within a complex of the two precursors (Figure 5). The initial product of this bimolecular preassociative mechanism was postulated to be a *cis*-amide which isomerized to the *trans*-amide, the active form of the template. In fact, this appears to be the major background pathway for product formation [16]. By lengthening the spacer element in this molecule from a 2,6-naphthoyl to a 4,4'-biphenyl, the ester and amine were moved away from each other [21]. Intracomplex reaction could now occur only if the adenosine were bound in the more extended Watson–Crick mode as shown in Figure 6. By reducing the amount of preassociative catalysis, the effect of the autocatalytic pathway became apparent in the initial rate of growth of the product. At 50 mM, 20% of added biphenyl template increased the rate of coupling of (4) and (8) by 60%. Upon following the time course of the reaction, we discovered the gentle sigmoidal product growth curve expected of an efficient self-replicating system [21], a feature which had already been observed for nucleic acid replicators [2]. This result was further exploited for a study of molecular competition and “mutation” using derivatives of adenosine substituted at N6 with the benzyloxycarbonyl group (see Section 3) [22].

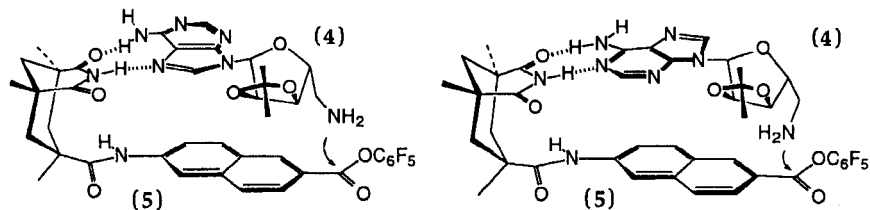


Figure 5 Hoogsteen-type and Watson–Crick-type intracomplex reactions in the naphthoyl self-replicating system

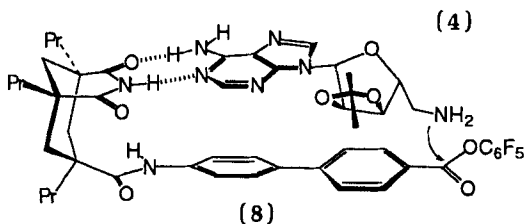


Figure 6 Intracomplex reaction in the biphenyl self-replicating system

The next logical step was to remove the remaining preassociative bimolecular pathway with a still longer spacer, and thus the terphenyl derivative (9) (Figure 7) was synthesized. Computer modeling showed that this spacer left only two reaction pathways to formation of the template: random bimolecular collision and template-directed catalysis of the tetrahedral intermediate. As shown in Figure 7, no preassociative bimolecular pathway is available to the terphenyl molecule. Unfortunately, addition of the terphenyl spacer took away not only the preassociative bimolecular pathway, but also the termolecular pathway. The molecule did not replicate, and the only reaction seen was the slow, bimolecular background reaction of ester and amine. NMR titration of the terphenyl molecule (9) with 9-ethyladenine (3) revealed that the structure no longer provided adequate binding of adenosine; practical concerns had been overlooked in the design of the molecule.

What was needed was a new adenosine-binding structure which could hold its substrate fixed even in an elongated molecule. The spacer element in the receptor had to be of sufficient length to keep the amine and ester groups from reacting in a bimolecular complex, yet the affinity of the components for each other had to be high. These criteria were fulfilled by using a diaminocarbazole-based diimide module developed in our efforts at molecular recognition of polynucleotides [23]; structure (10) (Figure 8) had proven to be a nearly ideal complement to the purine nucleus of adenine [24,25]. The imides in molecule (10) chelate the purine through simultaneous Watson-Crick and Hoogsteen base pairing, and the extended heterocyclic surface of the carbazole stacks

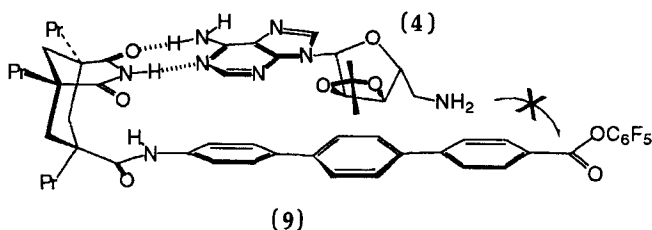


Figure 7 Intracomplex reaction is prohibited in the terphenyl system

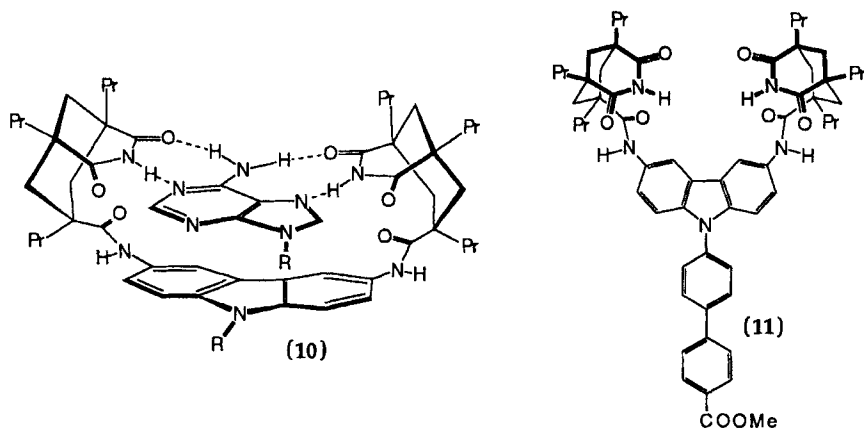


Figure 8 The carbazolediimide backbone in two molecules

against the purine. Not only is the binding affinity for adenosine derivatives extremely high ($K_a \approx 10^5 \text{ M}^{-1}$ in CDCl_3), but with triplexlike chelation of the adenine moiety [25], conformational ambiguities from the switching of bound adenine between Watson–Crick and Hoogsteen binding modes were eliminated.

Attaching a biphenyl substituent on N9 of the carbazolediimide created a new backbone for self-replication [26, 27], shown as the methyl ester in structure (11). Figure 9 shows the computer-predicted geometry of a bimolecular complex between (11) and aminoadenosine (4) [28], and from the figure it is clear that the amine and ester are separated by a significant distance, $>5.5 \text{ \AA}$ in the model. This distance is well defined, as the diimide-bound adenine has only limited motion within the complex, and since the two reactive centers cannot approach each other within the complex, a bimolecular preassociative pathway is ruled out. By addressing distance considerations, separation of ester and bound amine was achieved just as in the case of the terphenyl molecule (Figure 7), yet the diimide function of the new carbazole structure retained the ability to bind adenosine tightly.

The new self-replicating system, pictured in Figure 10, thus achieved precise positioning of aminoadenosine and a pentafluorophenyl ester, and reaction of (4) and (12) to form the self-complementary template molecule (13) had to occur either in an unassisted intermolecular fashion or through the template-catalyzed complex (13)–(12)–(4). Kinetic studies of the coupling reaction (Figure 11) were performed in 13% THF-CHCl_3 using the pentafluorophenyl active ester (12) and the amine (4). Appearance of the amide product (13) was followed by HPLC. The reaction was found to be autocatalytic; at 6.2 mM in 13% THF-CHCl_3 , 50% added (13) increased the coupling of (4) and (12) by an average of 54%. While this rate of autocatalysis was not greater than that

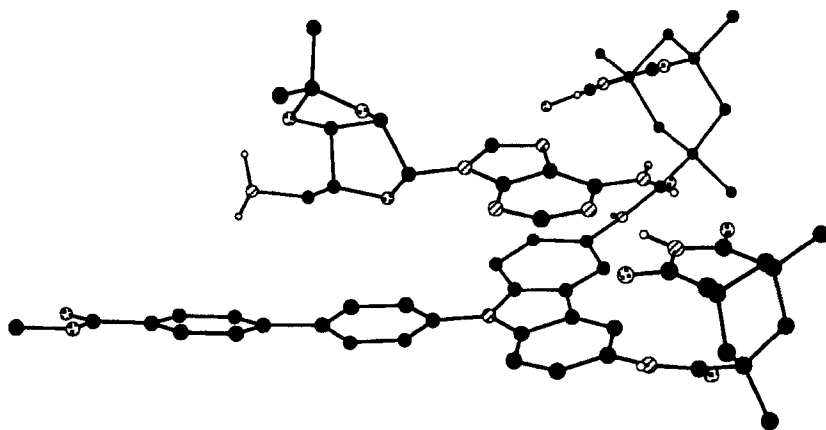


Figure 9 Computer-generated complex [28] between the biphenylcarbazole (11) and aminoadenosine (4)

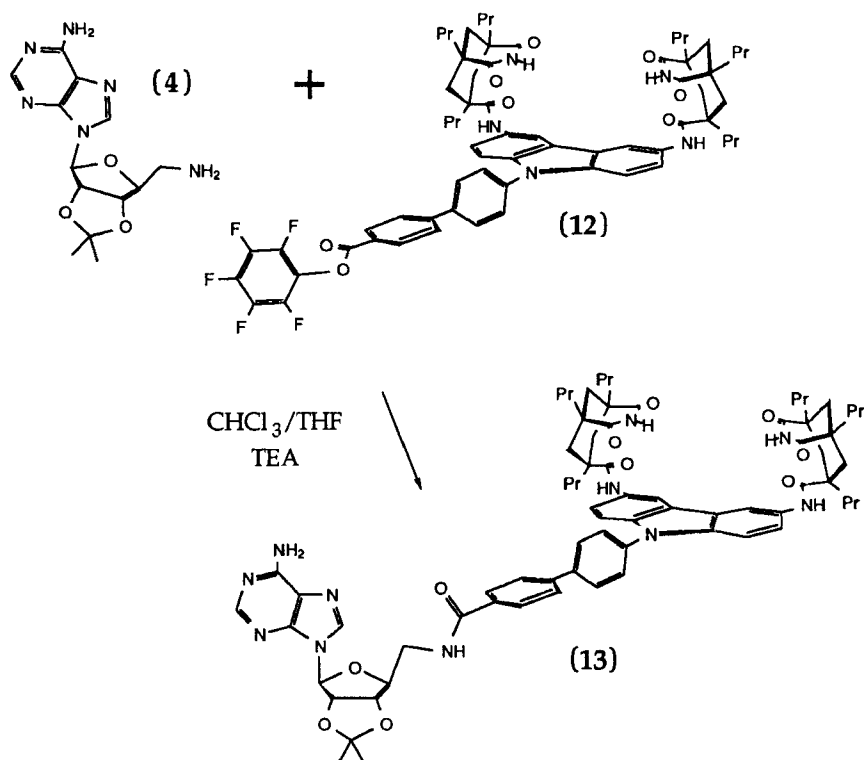


Figure 10 A diimide-based replicator

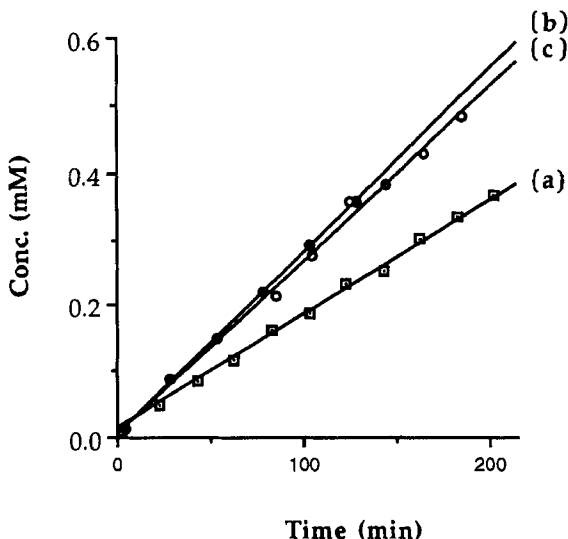


Figure 11 Representative kinetic plots of the formation of template (13) in 13% THF-CHCl₃ (as followed by HPLC) at $21 \pm 1^\circ\text{C}$ for 6.2 mM initial concentrations of (4) and (12) and with 1% TEA base added: (a) baseline reaction of (4) with (12); (b) baseline reaction plus half an equivalent of product (13); and (c) baseline reaction plus half an equivalent of monopyridyl template (14)

which we had previously achieved, it was at least evidence of termolecular autocatalysis in a system where all other likely pathways had been excluded. The tetrahedral intermediate for the complex (13)-(12)-(4) is modeled [28] in Figure 12.

After much experimentation [27], it was concluded that the diimide replicator was not more efficient because it suffered from severe product inhibition. From several NMR studies (see Section 2), the dimerization constant of diimide template (13) was calculated to be $\sim 10^9$ in 13% THF-CHCl₃, and thus very little template (on the order of $1\ \mu\text{M}$) is present as a monomer in solution. The concentration of template monomer at 3.1 mM total template concentration (Figure 11b; half an equivalent of template added) was calculated by estimating a single binding event at $8.6 \times 10^4\ \text{M}^{-1}$ in 13% THF-CHCl₃ (between $10^5\ \text{M}^{-1}$ and $576\ \text{M}^{-1}$) and taking the dimerization constant of the template to be the square of that value. Values were inserted into a model of autocatalysis developed by Nowick (see [11]). The concentration of template monomer may also be approximated using $K_{\text{dim}} = [\text{template dimer}] / [\text{template monomer}]^2$. As NMR titrations showed that the association constant between the two starting materials is reduced from $\sim 10^5\ \text{M}^{-1}$ in CHCl₃ to $576\ \text{M}^{-1}$ in pure THF, an attempt was made to decrease dimerization by increasing solvent polarity. Because the reaction was relatively fast in THF,

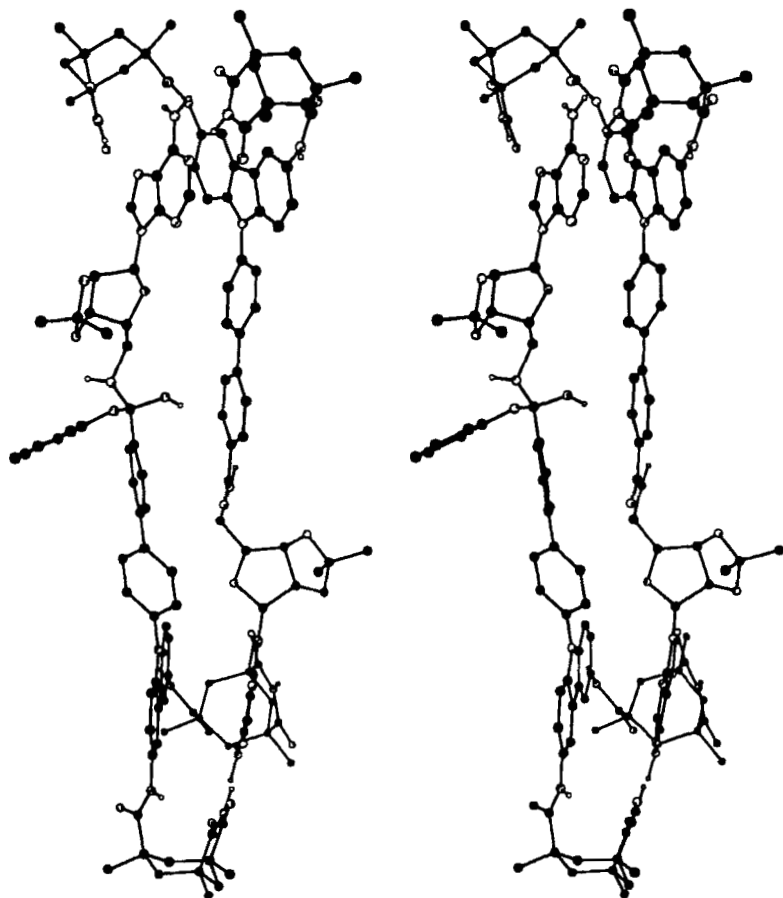


Figure 12 Computer-generated structure [28] of the tetrahedral intermediate for the complex (13)–(12)–(4), modeled as the neutral tautomer (stereoview). Hydrogens attached to carbon have been omitted for clarity

experiments were conducted at 0.07 mM. Formation of (13) was followed by coupling (4) with the 2,4-dinitrophenyl ester of (12) and monitoring the release of 2,4-dinitrophenol by UV–visible spectroscopy. Variation of the makeup of the THF–CHCl₃ solvent led to a catalytic peak at ~15% THF, with a quick drop in catalysis thereafter (Figure 13). While NMR studies show that a more polar solvent does decrease dimerization of the template, higher polarity also enhances the rate of the background bimolecular reaction such that any gain in catalysis is “swamped out”.

We were thus left with a system which showed promise, but was not sufficiently catalytic owing to the small amount of free template in solution. That so little free template gave rise to a 54% increase in rate indicates the

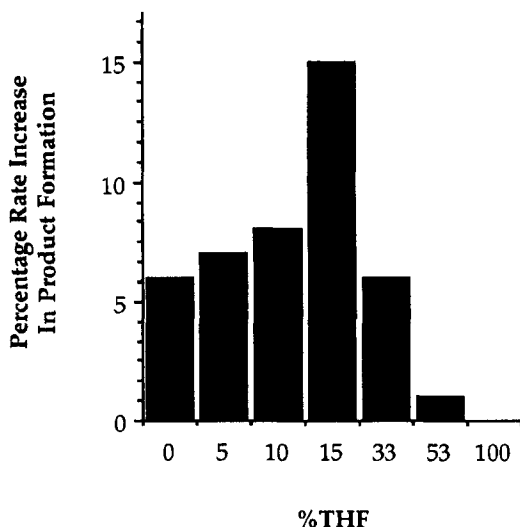


Figure 13 Catalytic enhancement of reaction rate in THF-CHCl₃ mixtures. Each bar shows the rate enhancement of the reaction between (4) and the 2,4-dinitrophenyl ester of (12) in the presence of 50% product (13). The system was examined under dilute conditions (0.07 mM ester 0.04 mM amine, 0.035 mM template, 8 mM TEA) by monitoring the release of 2,4-dinitrophenol using UV-visible spectroscopy

success of (13) in positioning its substrates for reaction. If such molecular recognition could be trained specifically on the transition state of the reaction at the expense of the ground-state dimer, a new level of efficiency in self-replication might be achieved. We are presently designing molecules of similar structure in which functional groups are incorporated into the template for chemical catalysis of the replication step at the point of amide formation. These include functionalities which can enhance proton transfers within the tetrahedral intermediate formed and destroyed along the coupling pathway.

To date, only the two pyridyl templates (14) and (15) (Figure 14) have been tested as catalysts for the reaction of (4) and (12). It was hoped that the pyridine nitrogens might act as a general base to catalyze the breakdown of the tetrahedral intermediate, but so far these molecules have not shown enhanced catalytic activity. The bipyridyl molecule (14) was ill behaved in solution, showing aggregation (beyond dimerization) according to NMR analysis, and affording no catalysis to the system according to HPLC. The monopyridyl template (15) acted much as its biphenyl predecessor (13), 50% of added template catalyzing the reaction by an average of 54% at 6.2 mM concentration (Figure 11). However, the pyridine nitrogen did not appear to increase catalysis of the system.

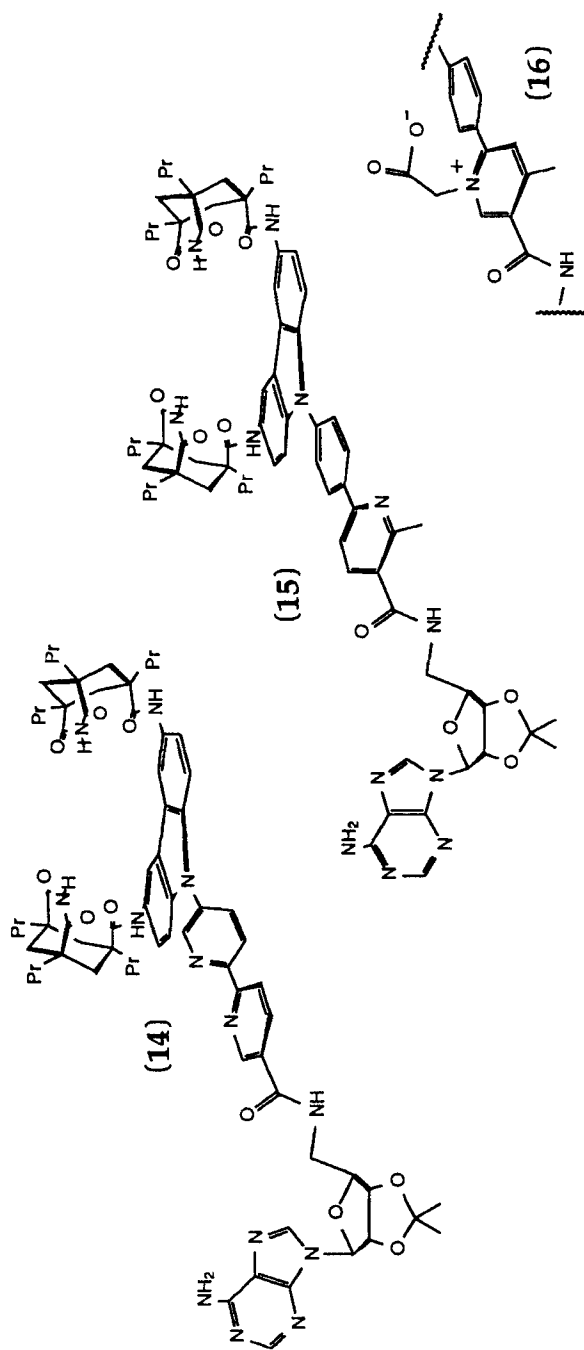


Figure 14 Proposed pyridyl templates for chemical catalysis at the point of amide formation

In summary, we have shown the viability of creating abiotic self-replicating systems, and we have successfully modified our molecules to focus on the autocatalytic pathways of the systems. Detailed evidence of self-replication is given in Section 2. Truly outstanding autocatalysis (e.g. a 10-fold rate enhancement) has so far eluded us, but the search for greater efficiency in replicative systems is our constant goal. Further functionality of the pyridine of (15) may be possible in the future, such as in the pyridinium carboxylate molecule (16). A second option is to attempt to create a similar system with slightly reduced hydrogen-bonding affinity, thus lowering product inhibition and increasing turnover. Using a recognition element such as guanine, cytosine or a modified base might lessen binding to the carbazolidiimide. In the meantime, we have used our existing systems to delve into some of the interesting questions which one may pose of replicating systems, and these explorations are detailed in Section 3.

2. EVIDENCE FOR REPLICATION

The naphthoyl-based self-replicating system shown in Figure 3 was our first success in the field of replication and has been examined more thoroughly than any other system which we created [15, 16, 29, 30]. When seeded with its product, the system shows autocatalysis at 16.0 mM, 8.2 mM and 2.2 mM concentrations of starting materials (4) and (5) in CHCl_3 at ambient temperature. As noted in Section 1, under conditions of 8.2 mM, addition of a fifth of an equivalent of product (6) produced an average 43% increase in the reaction rate (Figure 4). With varied amounts of added product, the rate enhancements are not directly proportional to product concentration, but rather to its square root [16]. Thus, under the same conditions, addition of half an equivalent produced a 73% increase in the reaction rate. This “square root law” was described by von Kiedrowski and coworkers [1, 2] to characterize nucleic acid replicators in which the autocatalytic entity exists largely in dimeric form.

But what is it about this system that makes us call it self-replicating? How could we show that the system progresses through directed template catalysis rather than through simple chemical autocatalysis? After all, (6) bristles with functional groups. The imide, amide, ribose and purine functionalities must all be considered as possible explanations for the autocatalysis observed. For example, imidazole is a well-known catalyst for acylation reactions, and the purine contains such a subunit. Could not this functionality be the cause? The potentially catalytic functions of the product molecule had to be individually tested in the structural context of (6) and under the conditions where (6) acts as an autocatalyst.

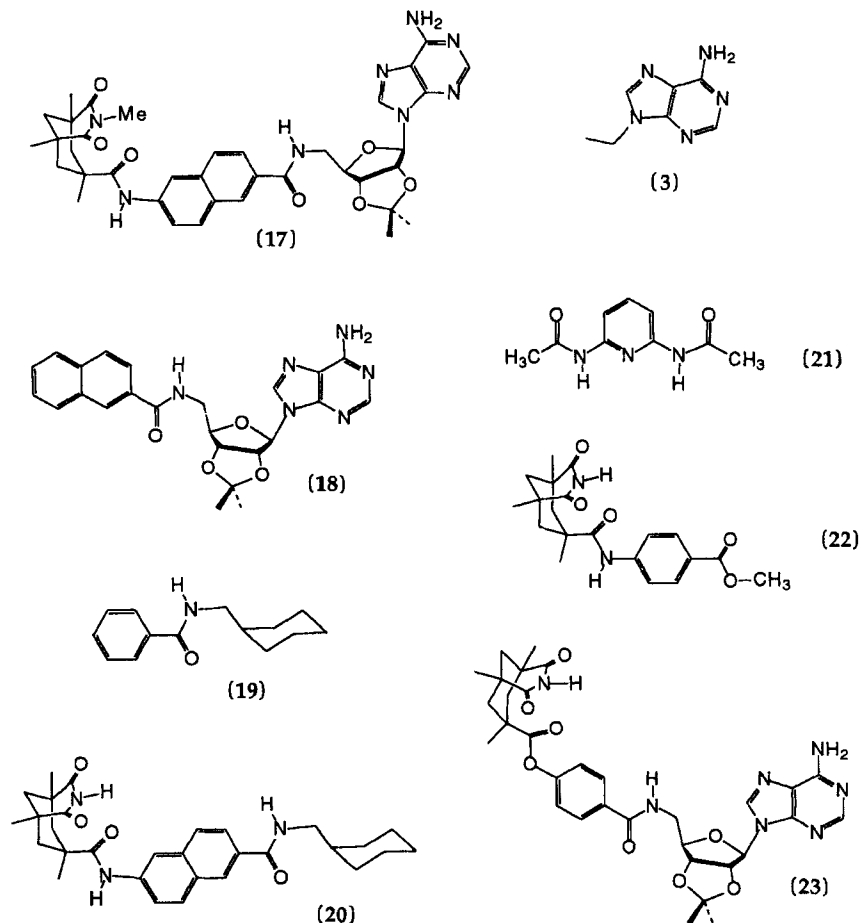


Figure 15 Control additives for the reaction of (4) and (5)

We proceeded, through overlapping control experiments [29, 30a, 30b], to exclude each individual function of the product molecule as a source of simple chemical catalysis. The control additives are shown in Figure 15 and the results are summarized in Table 1. In CHCl_3 at 2.2 mM concentrations of (4) and (5), a 50% increase in initial rate was observed when the reaction was seeded with half an equivalent of product (6) (Table 1, entry 2). Our control experiments, detailed below, show that this 50% increase is the result of replication, i.e. a template effect as shown in Figure 3, complex (7).

(1) The question of purine catalysis was answered by the addition of 9-ethyladenine (3) and the naphthoylated ribosyl derivative (18) (Table 1, entries

Table 1 Effect of various additives on the formation of (6) in CHCl_3 (as followed by HPLC) for 2.2 mM initial concentrations of (4) and (5), at $22 \pm 1^\circ\text{C}$ and with 1% added triethylamine (TEA) [9]

Entry	Additive (half an equivalent)	Average initial rate of product formation ($\pm 5\%$) ($\mu\text{M min}^{-1}$)	Fraction of baseline rate (%)
1		0.54	
2	(6)	0.81	150
3	(3)	0.55	102
4	(17)	0.55	102
5	(18)	0.50	93
6	(19)	0.52	96
7	(20)	0.56	104
8	(22)	0.56	104
9	(23)	0.57	106
10	(28) ^a	0.63	117

^aSee Figure 18.

3 and 5). The absence of catalysis in these experiments excluded the purine nucleus and the ribose of (6) as the sources of catalysis in Table 1, entry 2.

(2) Control experiments with added secondary *trans*-amides such as (19) showed that an external, secondary amide function [presented in the steric environment of (6)] was unable to catalyze the reaction (Table 1, entry 6). This excluded the amide of (6) as the sole culprit of catalysis.

(3) The inability of control molecule (22) to catalyze the reaction allowed us to exclude the Kemp's imide moiety of (6) as a source of direct chemical catalysis (Table 1, entry 8).

(4) A most telling control experiment involved the *N*-methylated imide (17). In the presence of (17), no rate enhancement in product formation was seen (within the 5% experimental error) at either high (16 mM) or low (2.2 mM) concentrations of reactants (Table 1, entry 4). Merely *N*-methylating the imide shut down autocatalysis. Since the imide had already been excluded as a chemical catalyst [control molecule (22)], this study pointed to base pairing between the imide and adenine as necessary for catalysis by molecule (6). Support for such base pairing was obtained with the use of (21). Diacylaminopyridines such as (21) are much admired as hydrogen-bonding complements to imides [31], and addition of (21) inhibited the replication reaction (Figure 4) [16].

(5) Using control molecules (18) and (20), we excluded catalytic intermediates (24) and (25) (Figure 16) involving the amide and one of the two base-pairing sites of (6). Both complexes (24) and (25) imply that the amide chemically assists the breakdown of the tetrahedral intermediate, but as neither (18) nor (20) was a catalyst under these conditions, it was concluded that the full template (6) is necessary for autocatalysis (Table 1, entries 5 and 7). Merely

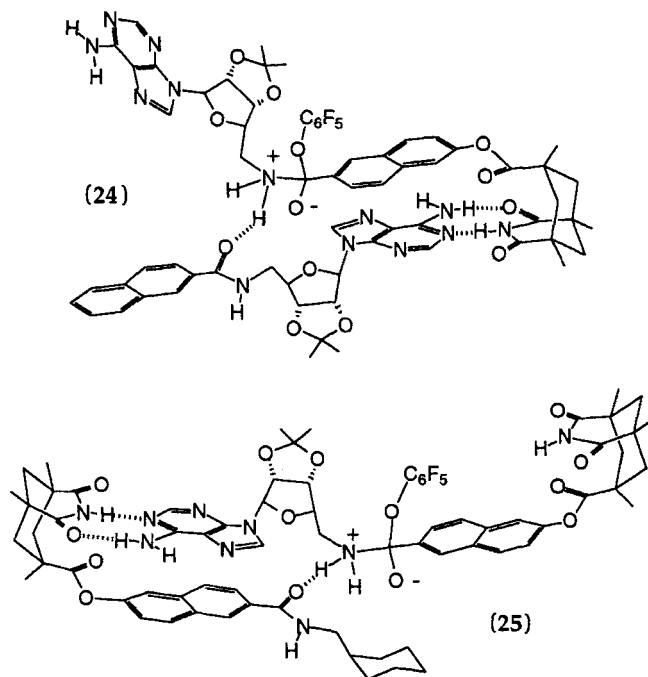


Figure 16 Two possible intermediates of catalysis excluded by experiments with molecules (18) and (20)

positioning one of the two substrates (or one end of the tetrahedral intermediate) on the template backbone is not sufficient.

The isolated, individual features and functionalities of (6) are, therefore, unable to account for the autocatalysis observed. Rather, the whole product molecule is more effective than the sum of its parts. The most economical explanation for these results involves complex (7) in Figure 3. Template-catalyzed replication, in which (6) binds (4) and (5), stabilizes the tetrahedral intermediate that forms and favors its breakdown to an amide, is the source of autocatalysis.

Even in the light of these experiments, another laboratory contended that the system did not replicate through directed template catalysis [32], instead asserting a mechanism of simple amide catalysis by the product (6). Control experiments with molecules (17), (19) and (22) – all amides – had already excluded this pathway, and controls with (18) and (20) had further excluded a more subtle pathway of internal amide catalysis (Figure 16). Nevertheless, additional evidence against amide catalysis by product (6) was desired, and thus experiments were conducted that involved coupling (4) with molecule (26)

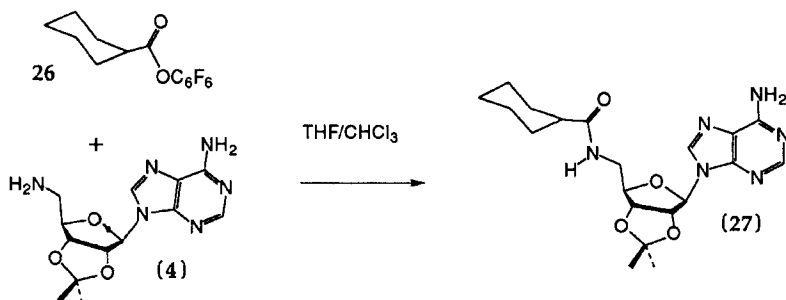


Figure 17 Control molecules used to test the proposed mechanism of formation of complex (25)

(Figure 17). Molecule (26) has neither stacking nor hydrogen-bonding capability, and any catalysis by template (6) would support a mechanism of amide catalysis. However, it was shown that (6) did not act as a catalyst to form (27) (Table 2). Accordingly, the full template mechanism of complex (7) was upheld: catalysis is dependent not on the amide functionality of (6), but rather on the ability of the template to bind both substrates through stacking and hydrogen bonding. Recently, the self replicative mechanism which we assert for this system was confirmed by a third party [30c].

Having established the ability of our molecule to replicate, we became interested in the generality of this shape for autocatalysis. To probe the spacing requirements for an effective template, we examined the effects of exchanging the naphthoyl spacer in ester (5) for a longer biphenyl and a shorter phenyl spacer [33]. While lengthening the spacer had beneficial effects (discussed in Section 1), almost no catalysis was observed with the shorter (23) (Table 1, entry 9); there are clearly certain steric requirements which have to be met for effective replication to occur.

Catalysts other than the template (6) *can* be found for this system. The action of bifunctional catalysts in acylation reactions and glucose mutarotation

Table 2 Generation of product (27) as a function of time, as followed by HPLC. All reactions were performed at 2.0 mM initial concentrations of reactants (4) and (26) in CHCl₃ with 1% TEA base added and at 22 ± 1 °C

Concentration of ester (26) and amine (4) (mM)	Number of equivalents of template (6)	Average initial rate of formation of (27) (μM min ⁻¹)	Relative rate
2.0	0	15.0	1
2.0	0.5	15.0	1.00
2.0	0.7	15.2	1.01

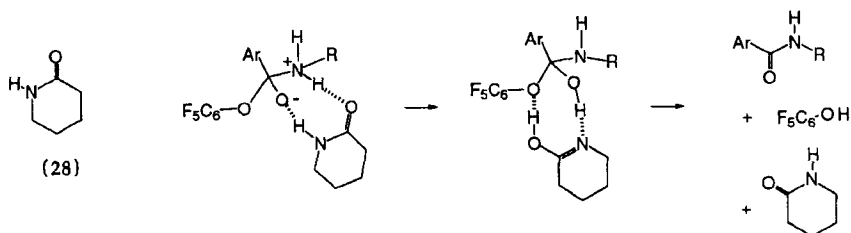


Figure 18 A possible role for valerolactam in the catalysis of ester aminolysis [17]

is well known [17], and it was indeed found that the *cis*-amide valerolactam (28) increases the initial rate of formation of (6) by 17% when added to the reaction of (4) and (5) (Table 1, entry 10). Figure 18 depicts a possible catalytic role for valerolactam in the breakdown of the tetrahedral intermediate [17]. The acidic and basic sites on valerolactam can stabilize the zwitterionic tetrahedral intermediate and facilitate the required proton transfers for product release, ultimately regenerating the catalyst. Probably by the same mechanism, primary amides such as acetamide catalyzed the reaction of (4) and (5) [32]. At 2.2 mM concentrations of starting materials, we found that 50% added acetamide increased the initial rate of formation of (6) by 35%.

Valerolactam and primary amides have a common capability: their acidic and basic sites, being on the same edge of the molecule, can act in concert. A *trans*-amide, however, such as that in molecule (6), has no such feature. While Su and Watson [19] showed that under certain conditions small *trans*-amides (even tertiary amides such as dimethylacetamide) can hydrogen bond to the tetrahedral intermediates in related reactions and catalyze their breakdown to products, in the light of the failure of the many secondary amides in Table 1 to catalyze the reaction of (4) and (5), the *trans*-amide of (6) cannot be a significant contributor to the autocatalysis observed under these conditions. This was confirmed in control experiments forming simple amides in CDCl_3 . As shown in Figure 19 and Table 3, even at 20 mM concentrations of pentafluorophenyl ester (29) and benzylamine (30), amide (32) was not a significant catalyst of amide formation.

The most plausible explanation, then, for the autocatalytic nature of (6) remains its ability to act as a template for its parts. The forces of hydrogen bonding and aryl stacking position the amine and active ester on the surface of the template, stabilizing the tetrahedral intermediate formed [complex (7), Figure 3]. Subsequent collapse to the amide bond is favored over reversion to a termolecular complex, and this results in an exact replica of the catalyst in the form of a template dimer. The weak intermolecular forces which stabilize the dimer also permit its dissociation [a dimerization constant of 630 M^{-1} was measured for the product (3) in CDCl_3], and monomeric template is generated.

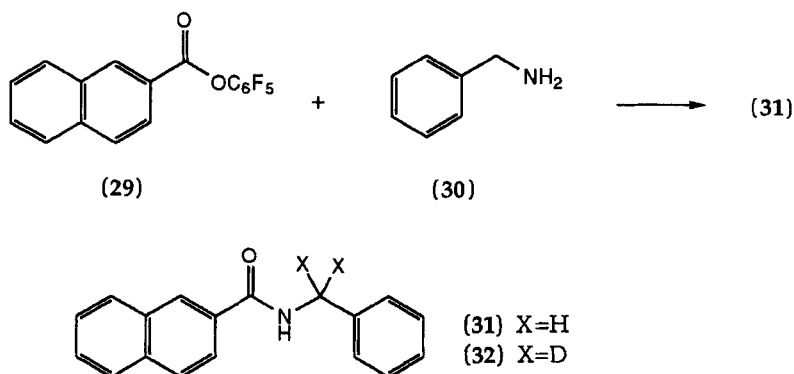


Figure 19 Molecules for amide formation control experiments

Thus, the template, through specific noncovalent contacts, has produced a copy of itself – the molecule replicates.

In our studies of replicator (6) [16] we presented a minimalist kinetic model for the formation of product, taking into account all possible bimolecular and termolecular complexes of (4), (5) and (6). This model was effective at low concentrations (8 mM or less), but did not predict the rate of product formation quantitatively at higher concentrations, predicting a rate which was higher than that observed. We have not pursued such simulations further owing to a lack of the necessary equilibria; with dimerization constants in the hundreds, it is likely that trimers, tetramers and so on appear at higher

Table 3 Amide formation control experiments at 25 °C, as followed by NMR. The reactions involved coupling of (29) and (30) in CDCl_3 with or without the addition of amide (32). Initial velocities of reaction were determined through integration of the methylene peak of the product amide (31) at 4.72 ppm relative to the methylene peak of (30) at 3.88 ppm

Concentration of ester (29) and amine (30) (mM)	Number of equivalents of amide (32)	Average initial rate of formation of (31) ($\mu\text{M min}^{-1}$)	Relative rate
4	0	42	1
	0.5	42	1.00
8	0	84	1
	0.5	84	1.00
16	0	168	1
	0.5	174	1.04
20	0	258	1
	0.5	282	1.09

concentrations. These species (and even one form of the dimer) all feature "frayed ends", namely unpaired imides and adenines which provide sites for binding their respective complements. Such species would isolate the reaction components from each other and would inhibit the reaction; a concrete example of this isolation effect is given in Section 3 (Figure 31). Accordingly, our recent modeling efforts have been limited to computer minimizations [28] in which we measure distances between functionalities in hydrogen-bonded complexes (e.g. Figure 9).

The second class of replicators which we studied in depth was the carbazolediimide series (Figure 10) [26,27]. These molecules are marked by a high affinity of the biphenylcarbazolediimide structure for 2',3'-isopropylideneadenosine, and their binding properties were studied at length by NMR. The binding constant between the diimide methyl ester (**11**) (Figure 8) and 2',3'-isopropylideneadenosine in CDCl_3 could only be estimated as 10^5 M^{-1} ; slow exchange of the adenosine complex led to highly broadened ^1H NMR spectra during titration. The components are readily soluble in THF, and the association constant between (**11**) and 2',3'-isopropylideneadenosine was measured by ^1H NMR titration in $\text{THF-}d_8$ to be 576 M^{-1} at 298 K based on the downfield shift of the imide proton from 9.65 ppm to 12.87 ppm.

Variable-temperature ^1H NMR spectra for a 5 mM solution (CDCl_3) of the self-complementary template (**13**) (Figure 10) showed two sharp imide peaks centered at 13 ppm at -55°C (Figure 20). The inherent asymmetry of the chelated adenine causes the chemical environments of the Watson-Crick and Hoogsteen binding modes to differ, giving rise to two different imide chemical shifts when exchange is slowed [25]. Two-dimensional nuclear Overhauser effect spectroscopic (NOESY) studies of a related carbazolediimide at low temperature suggested that the downfield imide proton forms the Hoogsteen bond [34]. The shape of the adenine-diimide complex mandates that the hydrogen bonds on either side of the purine be of unequal length, and this was reflected in the different responses of the two imide shifts to temperature change. The imide resonances began to broaden at -25°C , with more broadening of the downfield imide, and coalesced to a single broad resonance between 35°C and 45°C . With a maximum $\delta\nu$ of 311 Hz (-55°C), standard dynamic NMR theory [35] gives a barrier to conversion between the two imides at the coalescence temperature (taken to be 40°C) of $\sim 14.3 \text{ kcal mol}^{-1}$.

With an association constant on the order of 10^5 M^{-1} in chloroform and 576 M^{-1} in THF, a single binding event in 13% THF-CHCl_3 was estimated at $8.6 \times 10^4 \text{ M}^{-1}$. The dimerization constant of template (**13**) in 13% THF-CHCl_3 was thus crudely estimated to be on the order of 10^9 M^{-1} (K_a^2); in the absence of either negative or positive cooperativity, the dimerization interaction energy will be at least the sum of two individual association energies [36]. The dimerization of (**13**) appears so strong, in fact, that dimerization occurs even in DMSO despite the highly competitive nature of this solvent for hydrogen-

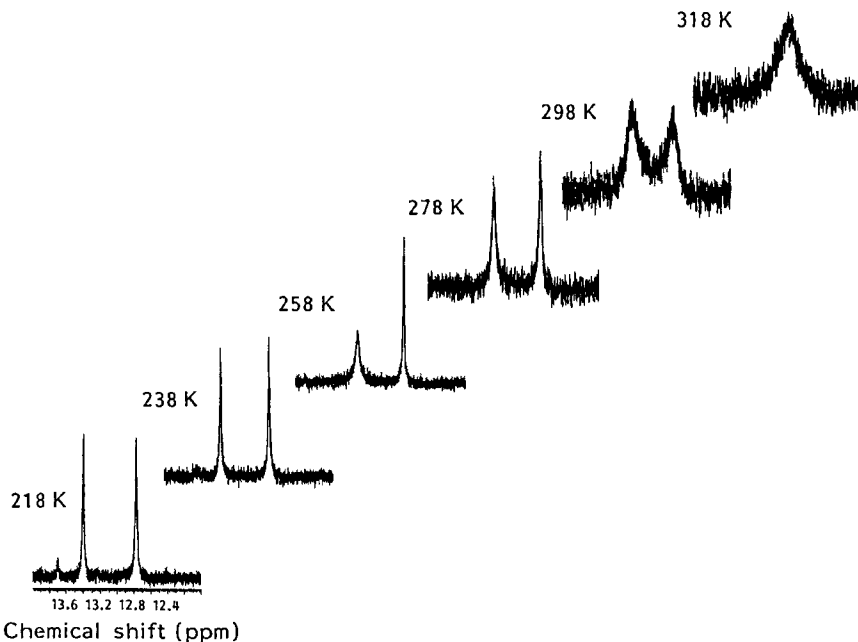


Figure 20 Variation of the imide region of the ^1H NMR spectrum of (13) with temperature (CDCl_3 solvent)

bonding sites. A dimerization constant of 169 M^{-1} was calculated based on ^1H NMR dilution studies in $\text{DMSO}-d_6$ (0.068 mM to 6.13 mM).

As already noted in Section 1, autocatalysis occurs in the carbazolediimide system. Addition of the product increased the rate of the coupling reaction of the ester (12) with amine (4) in 13% $\text{THF}-\text{CHCl}_3$. Experiments at 6.2 mM showed a 54% increase in initial rate with half an equivalent of added (13). Just as with the naphthoyl-based replicator, the carbazolediimide system was extensively tested using various control molecules to assure that autocatalysis was due to molecular recognition and not to trivial chemical catalysis by some functionality of the template. The results are summarized in Figure 21 and Table 4.

The experiments revealed firstly that the diimide function alone is not the source of the autocatalysis. This was established by control experiments with the diimide methyl ester (11) (Figure 8). This molecule did not catalyze the reaction of (12) with (4); rather, inhibition resulted, probably as a consequence of its sequestering the aminoadenosine in an unproductive complex. Additional experiments with (22) (Figure 15), which competes only poorly for adenosines, further supported the conclusion that an imide is an ineffective catalyst.

Our controls further showed that the phenylamide does not catalyze the reaction. The coupling rate of (12) with (4) was not increased by the addition of

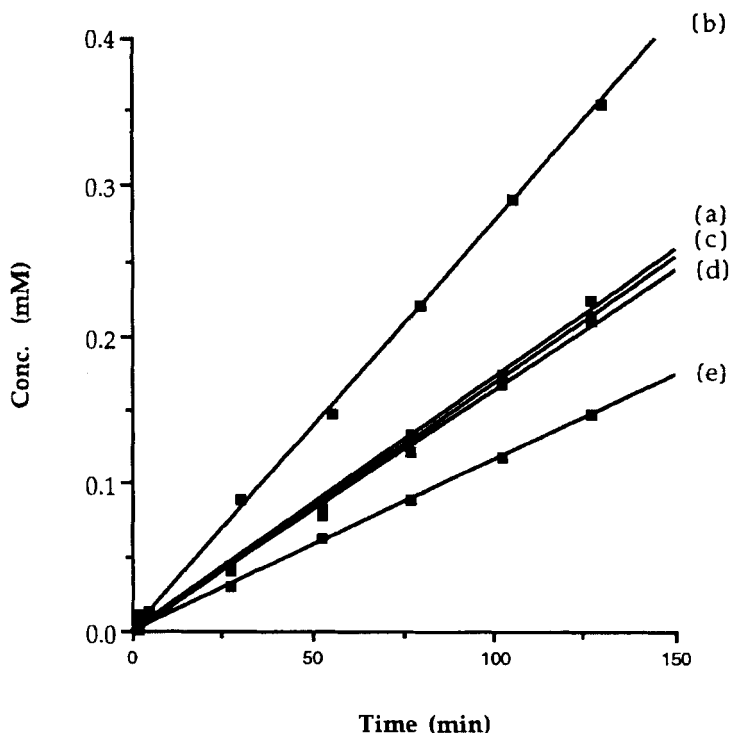


Figure 21 Representative kinetic plots of the generation of product (**13**) as a function of time (initial 5% of reaction). All reactions were performed at 6.2 mM initial concentrations of reactants (**4**) and (**12**) in 13% THF-CHCl₃ with 1% TEA base added and at 22 ± 1 °C. All the individual slopes (reaction rates) are given in Table 1: (a) baseline reaction of (**4**) with (**12**); (b) baseline reaction plus half an equivalent of product (**13**); (c) baseline reaction plus half an equivalent of imide methyl ester (**22**); (d) baseline reaction plus one equivalent of amide (**19**); and (e) baseline reaction plus half an equivalent of diimide methyl ester (**11**)

the benzoyl derivative (**19**) (Figure 15), which presents a secondary amide function in a steric environment similar to the one in (**13**), but lacks recognition elements. Finally, previous control experiments with adenosines [9-ethyladenine (**3**) and naphthoyl derivatives (**18**)] had shown that neither the purine nor the ribose was effective as a catalyst for an acylation reaction [29], and these results were upheld in 13% THF-CHCl₃ by the data in Table 5 (see later).

The above experiments all pointed toward self-replication. Separated, the individual features and functionalities of (**13**) are unable to account for the autocatalysis observed; like the naphthoyl replicator, the effect of the whole molecule is greater than the sum effect of its parts. The autocatalytic nature of (**13**) is most easily explained by postulating that the molecule serves as a

Table 4 Generation of product (**13**) as a function of time. All reactions were performed at 6.2 mM initial concentrations of reactants (**4**) and (**12**) in 13% THF-CHCl₃ with 1% TEA base added and at 22 ± 1 °C

Part of Figure 21	Additive	Individual initial rates of product formation ($\mu\text{M min}^{-1}$)	Average initial rate of product formation ($\mu\text{M min}^{-1}$)	Relative rate
(a)	Nothing	1.72, 1.77, 1.63, 1.69, 1.74, 1.63, 1.80, 1.72	1.71 ± 0.06	1.00
(b)	Product (13) (half an equivalent)	2.75, 2.60, 2.49, 2.68	2.63 ± 0.11	1.54 ± 0.08
(c)	Imide (22) (half an equivalent)	1.73, 1.71, 1.70, 1.75	1.72 ± 0.02	1.01 ± 0.04
(d)	Amide (19) (one equivalent)	1.44, 1.58, 1.60, 1.63	1.56 ± 0.08	0.91 ± 0.06
(e)	Diimide (11) (half an equivalent)	1.26, 1.05, 1.15, 1.27	1.18 ± 0.10	0.69 ± 0.06

template for its own replication: the initial reaction to form (**13**) is relatively slow, but once present, it can form the productive complex (**13**)–(**12**)–(**4**) stabilized by complementary recognition surfaces. Within the complex, hydrogen bonding and aryl stacking hold the tetrahedral intermediate in place (as modeled in Figure 12) and favor breakdown to amide (**13**) over reversion to (**12**) and (**4**).

In further control experiments, we found that under these conditions, autocatalysis is not a general feature of ester aminolysis. Parallel experiments with the naphthoyl ester (**29**) and amine (**4**) (Figure 22) showed that within experimental error, the amide product (**33**) did not significantly catalyze its own formation (Table 5). Interestingly, complexation of (**4**) with the diimide methyl ester (**11**) inhibited the reaction of (**4**) with (**29**) just as it did the reaction of (**4**) with (**12**). In both cases, the inhibition is presumably due to the ability of the diimide (**11**) to sequester (**4**) in an unproductive complex.

What are the consequences of complexation for replicators? The rate of formation of (**13**) compared with that of (**33**) under identical conditions revealed that recognition slows the rate of coupling by a factor of two; in the presence of (**4**), pentafluorophenyl ester species which are unable to complex (**4**) [such as (**29**)] are twice as reactive toward amines than is ester (**12**). For the same reason, however, noncomplexed esters are also more exposed to side reactions. Structures which recognize each other and form complexes become stabilized; the surfaces in contact are protected from external, often harmful reagents, and the protected structures react primarily with molecules which are specifically complexed with them [37]. Accordingly, molecular recognition

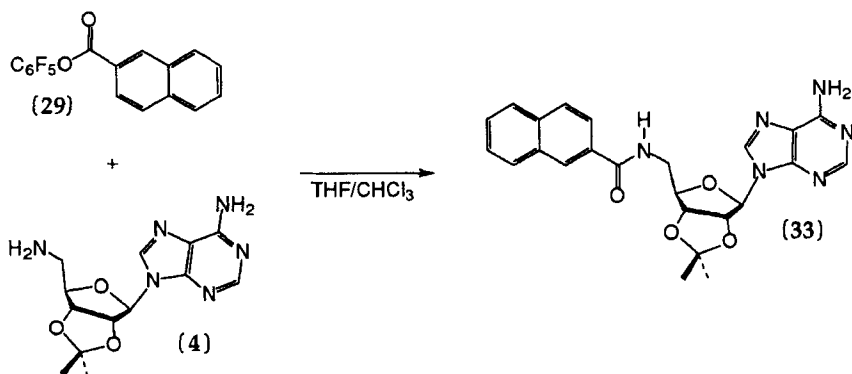


Figure 22 A nonreplicating system

Table 5 Generation of product (33) as a function of time. All reactions were performed at 6.2 mM initial concentrations of reactants (4) and (29) in 13% THF-CHCl₃ with 1% TEA base added and at 22 ± 1 °C

Additive	Individual initial rates of product formation (μM min ⁻¹)	Average initial rate of product formation (μM min ⁻¹)	Relative rate
Nothing	3.76, 3.84, 3.73	3.78 ± 0.06	1.00
Amide (33) (half an equivalent)	4.11, 4.05, 4.07	4.08 ± 0.03	1.08 ± 0.02
Diimide (11) (one equivalent)	2.32, 2.64, 2.85	2.60 ± 0.27	0.69 ± 0.07

offers advantages for evolution at the molecular level; survival, as well as replication, is enhanced.

3. EXPLORATIONS

The above insight into possible evolutionary advantages, gained through an examination of complexation in the carbazodiiimide system, is the type of windfall which we had hoped to reap in our studies of self-replication. Once we had functioning replicators, it was a small step to modify the systems to simulate artificially various aspects of evolution. While one may debate the relevance of these model systems to prebiotic chemistry or biology – we are, after all, dealing only with small rate enhancements and are contemplating only small structural changes in synthetic structures – our molecules allowed us to explore several engaging aspects of self-replication.

We began with our biphenyl replicating system of (4) and (8), and modified the adenine component (Figure 23) [22]. The exocyclic amine of the purine was outfitted with urethane-type blocking groups: a benzyloxycarbonyl was attached in (34), and an *o*-nitrobenzyloxycarbonyl was attached in (35). These changes were known to reduce base-pairing possibilities, as the blocking groups protrude on the Watson–Crick hydrogen-bonding edge of the purine and force molecules which bear them to base pair on the Hoogsteen edge [38]. Both (34) and (35) coupled to the biphenyl (8) in the familiar manner, giving the respective self-complementary products (37) and (38). They were each replicators; hobbled as they were in their base-pairing capacities, they could not be terribly efficient, but they did catalyze their own formation. They also made mistakes; as shown in the generic complex (39), there is no means by which either template can distinguish between those molecules bearing the benzyloxycarbonyl group and those bearing the *o*-nitrobenzyloxycarbonyl group. The behavior of these molecules was reciprocal: one catalyzed the formation of the other and vice versa.

These molecules were, of course, contrived to make a point. We intended to show that a change in environment could alter the system such that a third

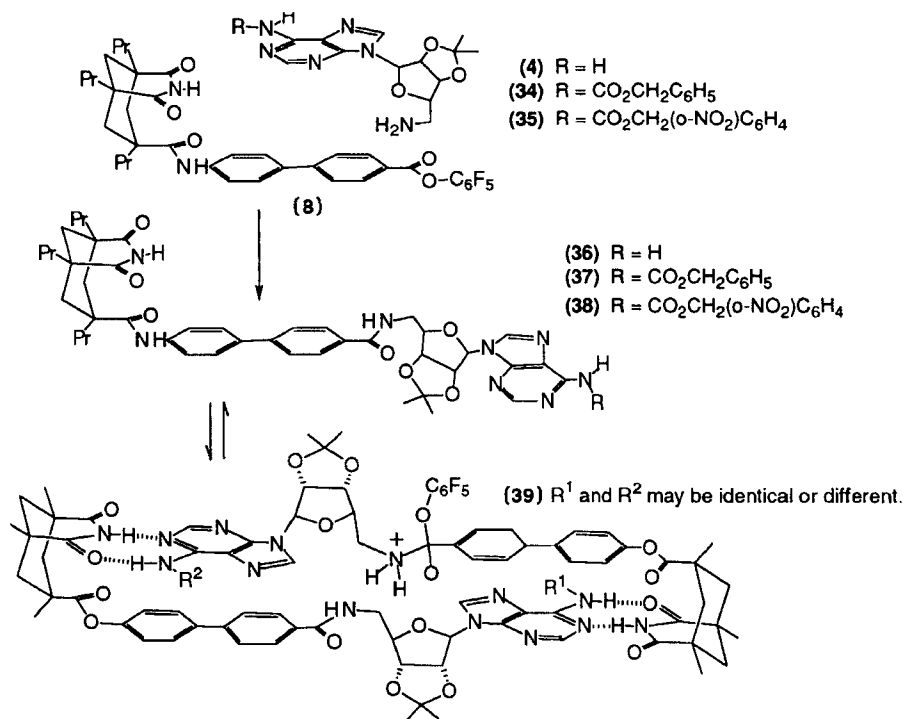


Figure 23 Molecules for a mutation experiment

replicator was produced which was more efficient than either (37) or (38). Our change in environment was the introduction of light to the system; when the molecules bearing the *o*-nitrobenzyloxycarbonyl group were irradiated, the photolabile blocking group was cleaved [39].

In the experiment [22], amines (34) and (35) were allowed to compete for a limited amount of active ester (8). The result (Figure 24) was that the nitro derivative was a slightly more effective replicator; more (38) was formed than (37). The solution was then irradiated, causing the photolabile nitro groups to be removed [the photocleavage product of (35) is (4) and that of (38) is (36)]. The new replicator (36) generated in this manner had a profile which permitted Watson-Crick as well as Hoogsteen base pairing; it had a statistical advantage over either (37) or (38). Now, when more active ester was added to the medium, the new molecule was more effective at replication, and it took over the resources of the system. The permanent change in structure caused by light created a self-replicating molecule more fit to the environment of the experiment.

Inspired by the rapidly emerging model systems of artificial life [40], we were confronted with the question of whether synthetic replicators shuffle their components to generate new hybrid replicators. To answer this, we made use of a self-replicating system developed at the same time as the adenine biphenyl replicator, but which had never been fully explored. The replicator, pictured at the top of Figure 25, was based on molecular recognition of thymine derivative (41) and xanthene derivative (40) by template (42). Coupling of the

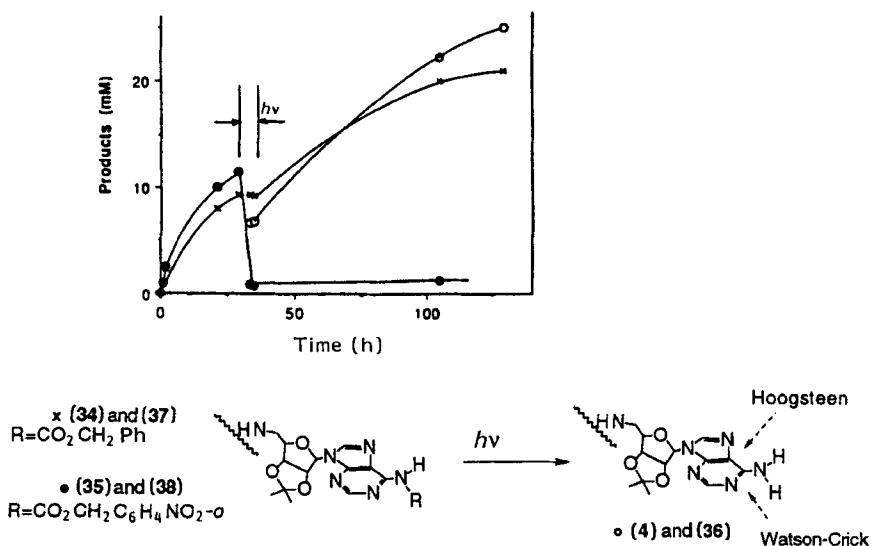


Figure 24 Kinetics of a mutation experiment

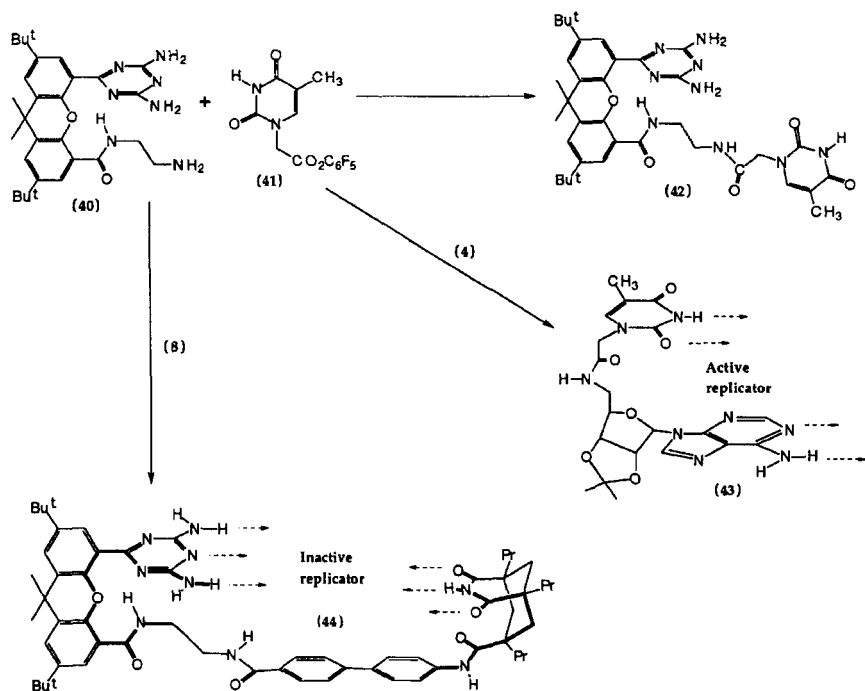


Figure 25 A recombinate experiment with two different replicators

components in an amide bond gave self-complementary structure (42), which showed autocatalytic behavior when added to its starting materials [41] just as in the adenine-based systems described above.

In the experiment, the components of the new replicator were mixed with the components of our biphenyl replicator [42], and we expected to generate four self-complementary, replicating systems. We assumed that self-complementarity of structure was sufficient for replication; after all, had not all our replicators (and those of others [43]) shared this feature? All possible combinations of (4), (8), (41) and (40) were duly synthesized (Figure 25), and their behavior taught us a lesson concerning molecular shape. One of the shuffled replicators, the adenine–thymine product (43), resembles DNA, but with an amide backbone. It turned out to be the most effective synthetic replicator we have encountered to date (perhaps this is not mere coincidence). The other shuffled replicator (44) was unable to catalyze its own formation.

The reasons for the differing behaviors of (43) and (44) are implicit in their molecular shapes. The adenine–thymine product can present its recognition surfaces [arrows on structure (43)] in such a way that a productive complex can be assembled with its precursors. No such conformation is available to the hapless (44). Because it is made up of two U-shaped components (xanthene and

Kemp's triacid skeletons), the overall conformation of (**44**) is either a C shape (shown) or an S shape (not shown). In the C-shaped conformation, recognition surfaces converge [arrows on structure (**44**)], and the component parts cannot fit within the cleft. In the S-shaped conformation, a complex can form, but it is not productive; the recognition surfaces diverge and reactive centers are too far apart from each other to form a covalent bond. Accordingly, self-complementarity is insufficient for replication; it is necessary for the replication product to be able to achieve a cyclic conformation.

To this point we had created replicators which were self-complementary and thus reproduced through a single templating event; however, many replicating systems are based on cycles. Nucleic acid replication is the paradigm in biology: one strand acts as a template for the other, and the new strand in turn acts as a reciprocal template. This pattern of template-directed catalysis has been used before in abiotic systems [44–49], and we saw that by modifying our carbazolediimide replicator, we could synthesize a similar two-cycle system as shown schematically in Figure 26.

We began with our existing aminoadenosine and carbazolediimide structures, as both the carbazole portion of the receptor and the ribose portion of adenosine are well suited for synthetic elaboration. For the reciprocal system, each was outfitted with amine nucleophiles and active ester electrophiles for covalent coupling reactions [50]. Two amines and two *p*-nitrophenyl esters were prepared [(**4**), (**45**), (**46**) and (**47**), Figure 27], as well as the two templates (**48**) and (**49**) (Figure 28). Two reference templates (**50**) and

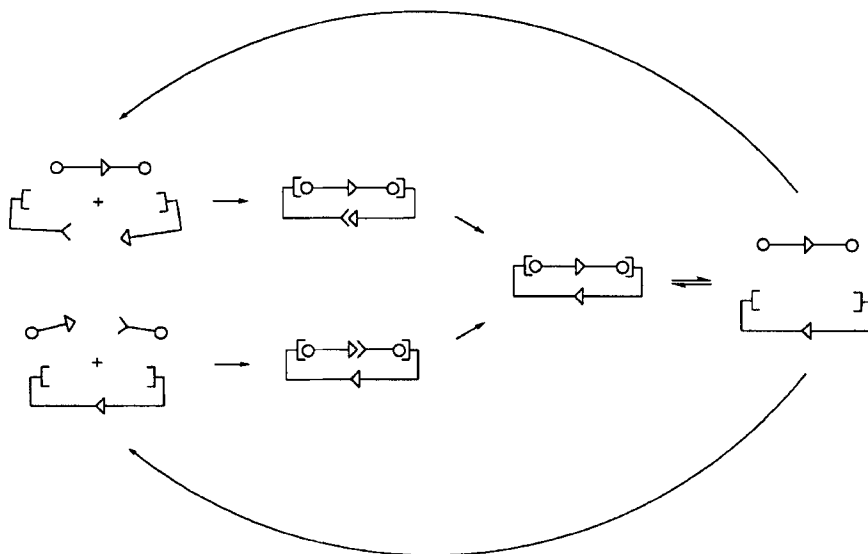


Figure 26 Schematic representation of a replication cycle of reciprocal templates

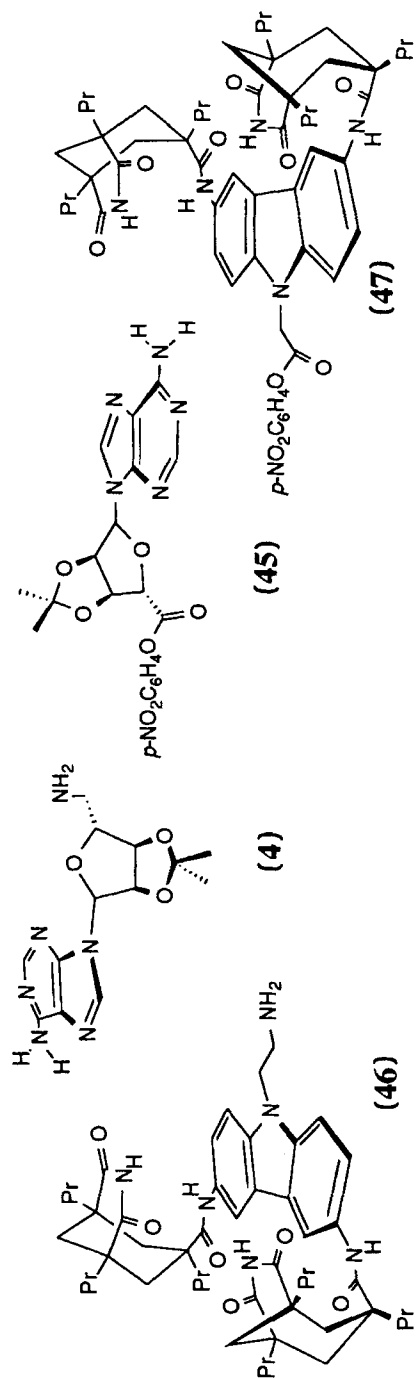


Figure 27 Pieces of a two-cycle replication system

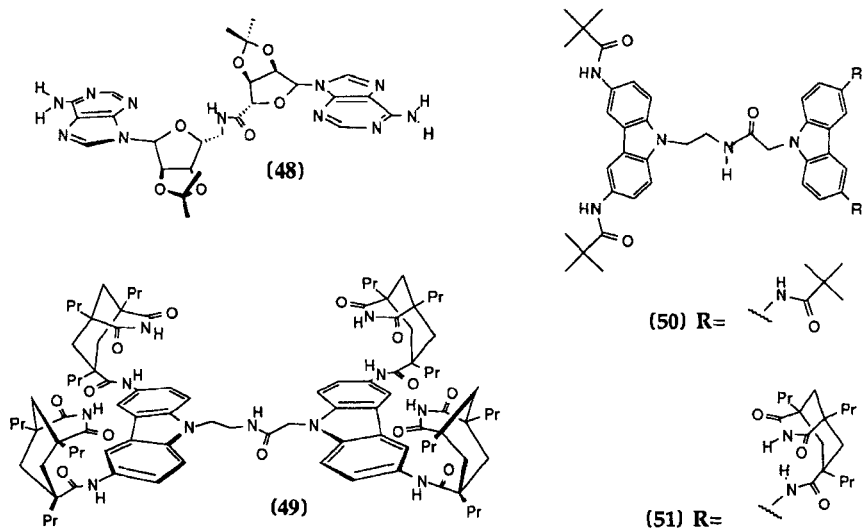


Figure 28 Templates for the evaluation of coupling reactions between (4), (45), (46) and (47)

(51) were also prepared; they contained many of the structural features of template (49) but lacked both recognition sites and one recognition site, respectively.

Template effects on the coupling of (4) with (45) and (46) with (47) were systematically evaluated [50]. Coupling reactions in CHCl_3 were carried out at 25°C and monitored spectrophotometrically, following the release of *p*-nitrophenol. The results are summarized in Table 6. The first reaction studied was the coupling between (4) and (45); at a concentration of 0.05 mM each in CHCl_3 in the presence of triethylamine, the coupling proceeded with an initial rate of $1.5 \times 10^{-8} \text{ M min}^{-1}$ (Figure 29) to give the product amide (48). The reaction was then run in the presence of one equivalent of (49) [the product of (46) and (47)]. Compound (49) accelerated the coupling reaction between (4) and (45) by a factor of 10. This acceleration was reduced when competitive binders were added: the product (48) (one equivalent) reduced the acceleration to roughly threefold, whereas a large amount of 9-ethyladenine (10 equivalents) lowered the acceleration to twofold. The rate of the uncatalyzed reaction is unaffected by these compounds. Compound (51), having one receptor site, slightly reduced the initial coupling rate (by $\sim 25\%$). This is presumably due to the fact that molecules bound by (51) are less accessible for reaction with other molecules in solution. The reference compound (50), which lacks both receptor sites and contains only amide functionalities, had no effect on the rate of the reaction. This is in keeping with earlier studies of amide

Table 6 Initial rates of amides formation [50c]

Reaction ^a	Concentrations (mM)					Initial rate ^b (10 ⁻⁹ M min ⁻¹)	Relative rate
	(48)	(49)	(3)	(50)	(51)		
(4) + (45)						15	1
(4) + (45)	0.05					16	1.1
(4) + (45)		0.05				150	10
(4) + (45)	0.05	0.05				42	2.8
(4) + (45)		0.05	0.5			30	2
(4) + (45)			0.5			15	1
(4) + (45)				0.05		15	1
(4) + (45)					0.05	11	0.7
(46) + (47)						4.3	1
(46) + (47)	0.05					23	5.3
(46) + (47)		0.05				4.3	1
(46) + (47)	0.05	0.05				13	3
(46) + (47)	0.05		0.5			15	3.5
(46) + (47)			0.5			4.8	1.1
(45) + (46)						5.3 × 10 ⁴	1
(45) + (46)			0.5			1.4 × 10 ⁴	0.3
(4) + (47)						2200	1
(4) + (47)			0.5			600	0.3

^aBoth components were present at 0.05 mM in CHCl₃ at 25 °C with 4 mM TEA.

^bValues are averaged from multiple independent runs. Standard deviations are ± 15%.

catalysis of nitrophenyl ester aminolysis [19], in which amide catalysis appeared only at concentrations over 100-fold greater than in our studies.

Reciprocally, (48) catalyzed the formation of (49). An initial rate of $4.3 \times 10^{-9} \text{ M min}^{-1}$ was measured for the coupling of (46) and (47) (Table 6), and addition of one equivalent of (48) increased the initial coupling rate roughly fivefold. Both product (49) and 9-ethyladenine acted as competitive inhibitors; both reduced the acceleration while having no significant effect on the background reaction rate.

All of the observed rate enhancements are consistent with a mechanism in which the template binds two reactive components and stabilizes the tetrahedral intermediate. An energy-minimized structure [28] of the proposed coupling of (4) and (45) is shown in Figure 30. The model suggests that both adenosine derivatives can be accommodated simultaneously by template (49), and that the binding permits close proximity of the two reactive groups. In the reaction of (46) with (47), acceleration is likely due to a similar termolecular complex, but this time the “outside” amide is formed instead of the “inside” one. The reactions of (4) with (45) and (46) with (47) are related in a special

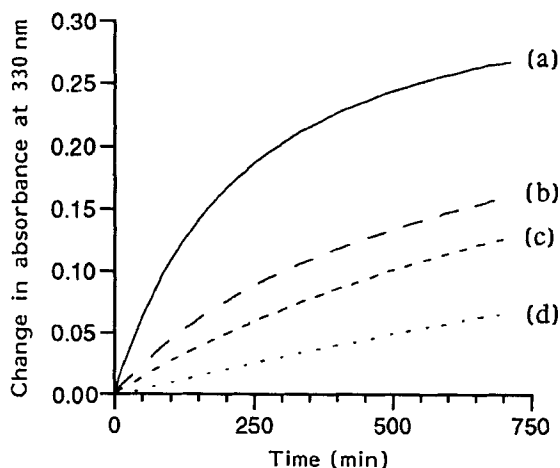


Figure 29 Plots for the reaction between (4) and (45) (both at 0.05 mM) in CHCl_3 at 25 °C with 4 mM TEA and with (a) one equivalent of (49), (b) one equivalent of (49) and one equivalent of (48), (c) one equivalent of (49) and 10 equivalents of 9-ethyladenine (3), and (d) no additives (background)

way, since the product of one reaction is a template for the other: these reciprocally templated reactions constitute a formal replication cycle [44].

More support for this mechanism came from experiments in which the concentration of added template was varied. Increasing the amount of (49) increased the initial coupling rate of (4) with (45) to a maximum at two equivalents of template (Figure 31). Further addition resulted in lower coupling rates, because the two reactive components became increasingly separated as bimolecular complexes on different template molecules. As shown by the solid line in Figure 31, these data fit a theoretical curve [50b, 50c] for such a system in which the template binds each substrate with a K_a of $1.4 \times 10^4 \text{ M}^{-1}$, and this K_a is in good agreement with the experimentally observed association constants for similar carbazolediimide receptors [25].

The remaining coupling combinations of the starting materials (Figure 27) are the reactions between (4) and (47) and between (45) and (46). These reactions involve complementary bimolecular components and are both about three orders of magnitude faster than those previously discussed (Table 6). The high rates are due to the association of the two reaction partners, resulting in complexes in which the reactive groups are almost always in close proximity [Figure 32 depicts complex (45)–(46)] [51]. Thus, as was the case in our earlier self-complementary replicators, these combinations suffer from a preassociative bimolecular effect. In experiments in which the four reactants (4), (45), (46) and (47) are all present, preassociative bimolecular pathways dominate, and template effects of (48) and (49) become negligible. Nevertheless, reciprocal

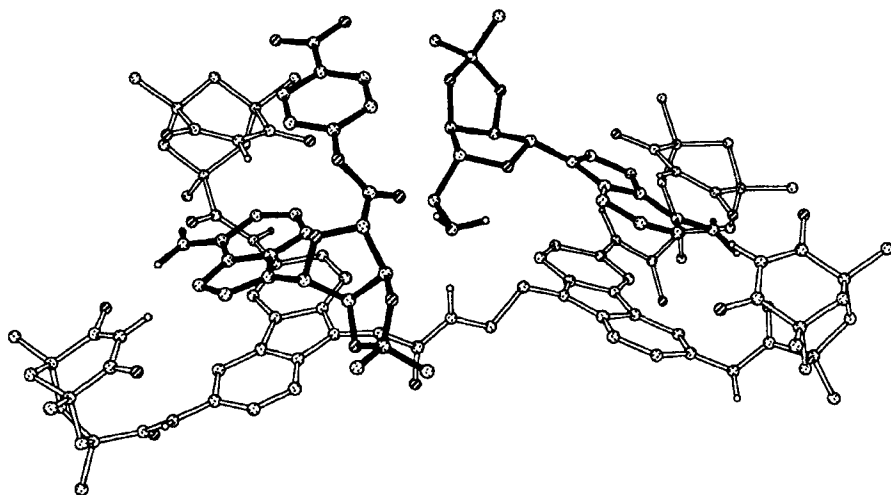


Figure 30 Computer-generated structure [28] of the termolecular complex (4)-(45)-(49)

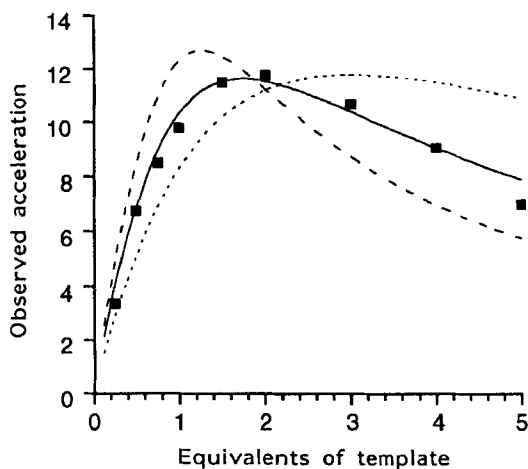


Figure 31 Plots for the reaction between (4) and (45): (■) observed acceleration of the reaction between (4) and (45) versus the amount of template (49) (0.05 μM of each reagent, 4 μM TEA in CHCl_3 at 25 $^\circ\text{C}$); (—) calculated concentration (under the same conditions) of productive complex (4)-(45)-(49) for a diimide-adenine affinity of $1.4 \times 10^4 \text{ M}^{-1}$; (- - -) calculated concentration of productive complex (4)-(45)-(49) for $K = 5000 \text{ M}^{-1}$; (- · - ·) calculated concentration of productive complex (4)-(45)-(49) for $K = 4.5 \times 10^4 \text{ M}^{-1}$. Note that no vertical scale is intended for the calculated data, as the scale is different for each line. Calculations were based on the assumption that the template binds each substrate independently and with the same intrinsic affinity K [50b, 50c]

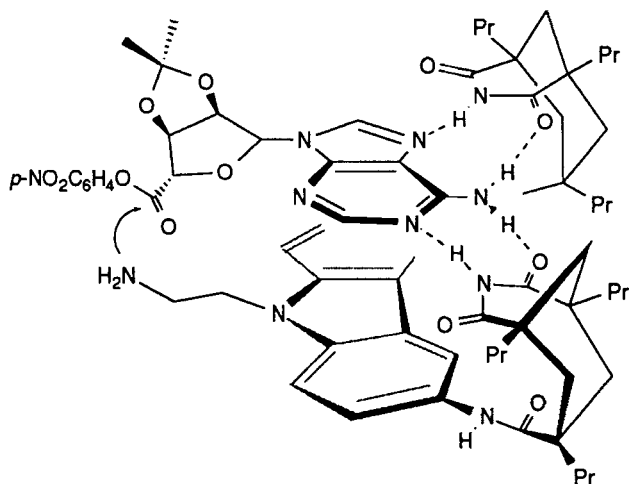


Figure 32 Bimolecular complex proposed for the fast reaction between (45) and (46)

templates (48) and (49) undergo a formal replication cycle in which covalent coupling reactions are individually accelerated by up to 13-fold. The rate enhancements here are comparable to those observed by Kelly *et al.* in reaction templates for bimolecular S_N2 reactions [8], and are considerably larger than those observed in template effects involving our self-complementary structures (see above). Whether these cycles are generally more efficient than the minimalist self-complementary replicators is the subject of ongoing research; it is perhaps no accident that the strands of DNA are complementary, and not self-complementary.

In the above experiments, we explored replication, mutation and recombination through simplistic molecular analogues. By continuing to enhance various qualities of our replicating systems, we hope to continue to probe questions of how evolution might function at the molecular level. Our replicators are abiotic, existing in chloroform and ranging far from the structure of DNA, and yet these simple chemicals exhibit traits which one generally associates with biology. Perhaps this is in itself an insight into the origins of life; perhaps our results are trying to tell us that if structures capable of selective molecular recognition are at hand, life is no coincidence but rather a phenomenon of chemistry just waiting to occur.

4. ACKNOWLEDGMENTS

We thank the many present and former coworkers whose work is described herein: Morgan Conn, Roland Pieters, Ivan Huc, Belinda Tsao, Jong-In Hong, Vince Rotello, James Nowick, Tae Kyo Park, Quing Feng, Tjama Tjivikua,

Pablo Ballester, Michael Famulok, Amalia Galan, Ghislain Deslongchamps, Ben Askew, Sharon Jones, Chris Buhr, Kyu-Sung Jeong, Kevin Parris, Kevin Williams and Mary Killoran. We also thank Professor Javier de Mendoza for his collaborative efforts. We are grateful to the National Science Foundation for financial support.

5. REFERENCES

1. G. von Kiedrowski, *Angew. Chem., Int. Ed. Engl.*, **25**, 932 (1986).
2. G. von Kiedrowski, B. Wlotzka, J. Helbing, M. Matzen and S. Jordan, *Angew. Chem., Int. Ed. Engl.*, **30**, 423 (1991).
3. A. Terfort and G. von Kiedrowski, *Angew. Chem., Int. Ed. Engl.*, **31**, 654 (1992).
4. L. E. Orgel, *Cold Spring Harbor Symp. Quant. Biol.*, **52**, 9 (1987); G. F. Joyce, *Cold Spring Harbor Symp. Quant. Biol.*, **52**, 41 (1987).
5. L. E. Orgel, *Nature*, **358**, 203 (1992).
6. (a) P. A. Bachmann, P. Walde, P. L. Luisi and J. Lang, *J. Am. Chem. Soc.*, **113**, 8204 (1991); (b) P. L. Luisi, personal communication.
7. P. A. Bachmann, P. L. Luisi and J. Lang, *Nature*, **357**, 57 (1992).
8. (a) T. R. Kelly, G. J. Bridger and C. Zhao, *J. Am. Chem. Soc.*, **112**, 8024 (1990); (b) T. R. Kelly, C. Zhao and G. J. Bridger, *J. Am. Chem. Soc.*, **111**, 3744 (1989).
9. J. T. Goodwin and D. G. Lynn, *J. Am. Chem. Soc.*, **114**, 9197 (1992).
10. For reviews of template effects see (a) S. Anderson, H. L. Anderson and J. K. M. Sanders, *Acc. Chem. Res.*, **26**, 469 (1993); (b) R. Hoss and F. Vögtle, *Angew. Chem., Int. Ed. Engl.*, **33**, 375 (1994).
11. D. S. Kemp and K. S. Petrakis, *J. Org. Chem.*, **46**, 5140 (1981); an improved synthesis is given by J. Rebek Jr, B. Askew, M. Killoran, D. Nemeth and F.-T. Lin, *J. Am. Chem. Soc.*, **109**, 2426 (1987).
12. For a review see J. Rebek Jr., *Angew. Chem., Int. Ed. Engl.*, **29**, 245 (1990).
13. (a) J. Rebek Jr, B. Askew, P. Ballester, C. Buhr, A. Costero, S. Jones and K. Williams, *J. Am. Chem. Soc.*, **109**, 6866 (1987); (b) B. Askew, P. Ballester, C. Buhr, K. S. Jeong, S. Jones, K. Parris, K. Williams and J. Rebek Jr, *J. Am. Chem. Soc.*, **111**, 1082 (1989); (c) K. Williams, B. Askew, P. Ballester, C. Buhr, K. S. Jeong, S. Jones and J. Rebek Jr., *J. Am. Chem. Soc.*, **111**, 1090 (1989).
14. (a) S. F. Mason, *Chemical Evolution: Origins of the Elements, Molecules and Living Systems*, Clarendon Press, Oxford (1991); (b) A. H. Weiss, R. F. Socha, V. A. Likholobov and M. M. Sakharov, *CHEMTECH*, **10**, 643 (1980).
15. T. Tjivikua, P. Ballester and J. Rebek Jr., *J. Am. Chem. Soc.*, **112**, 1249 (1990).
16. J. S. Norwick, Q. Feng, T. Tjivikua, P. Ballester and J. Rebek Jr, *J. Am. Chem. Soc.*, **113**, 8831 (1991).
17. P. R. Rony, *J. Am. Chem. Soc.*, **91**, 6090 (1969); C. G. Swain and J. F. Brown Jr, *J. Am. Chem. Soc.*, **74**, 2538 (1952).
18. F. M. Menger and A. C. Vitale, *J. Am. Chem. Soc.*, **95**, 4931 (1973); F. M. Menger and J. H. Smith, *J. Am. Chem. Soc.*, **94**, 3824 (1972).
19. C. Su and J. W. Watson, *J. Am. Chem. Soc.*, **96**, 1854 (1974).
20. J. C. Hogan and R. D. Gandour, *J. Org. Chem.*, **57**, 55 (1992).
21. V. Rotello, J. I. Hong and J. Rebek Jr, *J. Am. Chem. Soc.*, **113**, 9422 (1991).
22. J.-I. Hong, Q. Feng, V. Rotello and J. Rebek Jr, *Science*, **255**, 848 (1992).
23. A. Galán, J. de Mendoza, C. Toiron, M. Bruix, G. Deslongchamps and J. Rebek Jr, *J. Am. Chem. Soc.*, **113**, 9424 (1991).

24. G. Deslongchamps, A. Galán, J. de Mendoza and J. Rebek Jr, *Angew. Chem., Int. Ed. Engl.*, **31**, 61 (1992).
25. M. M. Conn, G. Deslongchamps, J. de Mendoza and J. Rebek Jr, *J. Am. Chem. Soc.*, **115**, 3548 (1993).
26. M. M. Conn, E. A. Wintner and J. Rebek Jr, *Angew. Chem., Int. Ed. Engl.*, **33**, 1577 (1994).
27. E. A. Wintner, M. M. Conn and J. Rebek Jr, *J. Am. Chem. Soc.*, **116**, 8877 (1994).
28. For details on MacroModel 3.5X see F. Mohamadi, N. G. Richards, W. C. Guida, R. Liskamp, M. Lipton, C. Caufield, G. Chang, T. Hendrickson and W. C. Still, *J. Comput. Chem.*, **11**, 440 (1990).
29. E. A. Wintner, M. M. Conn and J. Rebek Jr, *Acc. Chem. Res.*, **27**, 198 (1994).
30. (a) M. M. Conn, E. A. Wintner and J. Rebek Jr, *J. Am. Chem. Soc.*, **116**, 8823 (1994); (b) E. A. Wintner, B. Tsao and J. Rebek Jr, *J. Org. Chem.*, **60**, 7997 (1995); (c) D. N. Reinhoudt, D. M. Rudkevich and F. de Jong, *J. Am. Chem. Soc.*, **118**, in press (1996).
31. A. D. Hamilton and D. Van Engen, *J. Am. Chem. Soc.*, **109**, 5035 (1987).
32. F. M. Menger, A. V. Eliseev and N. A. Khanjin, *J. Am. Chem. Soc.*, **116**, 3613 (1994).
33. T. Tjivikua, PhD Thesis, University of Pittsburgh, 1990, p. 73.
34. M. M. Conn, PhD Thesis, Massachusetts Institute of Technology, 1994, p. 29.
35. J. Sandström, *Dynamic NMR Spectroscopy*, Academic Press, London, 1982.
36. R. Breslow and S. Halfon, *Proc. Natl. Acad. Sci. USA*, **89**, 6916 (1992).
37. There are earlier examples of a template slowing down a reaction but improving the yield of the desired molecule; for example, see Ch. Dietrich-Buchecker and J. P. Sauvage, *New J. Chem.*, **16**, 277 (1992).
38. G. Dodin, M. Dreyfus and J.-E. Dubois, *J. Chem. Soc., Perkin Trans. 2*, 438 (1979).
39. A. Patchornik, B. Amit and R. B. Woodward, *J. Am. Chem. Soc.*, **92**, 6333 (1970).
40. S. Levy, *Artificial Life: The Quest for a New Creation*, 1st edn, Pantheon, New York, 1992, p. 390.
41. T. K. Park, Q. Feng and J. Rebek Jr, *J. Am. Chem. Soc.*, **114**, 4529 (1992).
42. Q. Feng, T. K. Park and J. Rebek Jr, *Science*, **256**, 1179 (1992).
43. However, see F. Persico and J. D. Wuest, *J. Org. Chem.*, **58**, 95 (1993).
44. For a recent experimental study of reciprocal effects in nucleic acid chemistry see D. Sievers and G. von Kiedrowski, *Nature*, **369**, 221 (1994).
45. C. J. Walter, H. L. Anderson and J. K. M. Sanders, *Chem. Soc. Chem. Commun.*, 458 (1993).
46. B. Odell, M. V. Reddington, A. M. Z. Slawin, N. Spencer, J. F. Stoddart and D. J. Williams, *Angew. Chem., Int. Ed. Engl.*, **27**, 1547 (1988).
47. C. O. Dietrich-Buchecker, J. P. Sauvage and J. M. Kern, *J. Am. Chem. Soc.*, **106**, 3043 (1984).
48. W. L. Mock, T. A. Irra, J. P. Wepsiec and M. Adhya, *J. Org. Chem.*, **54**, 5302 (1989).
49. J. T. Goodwin and D. G. Lynn, *J. Am. Chem. Soc.*, **114**, 9197 (1992).
50. (a) R. J. Pieters, I. Huc and J. Rebek Jr, *Angew. Chem., Int. Ed. Engl.*, **33**, 1579 (1994); (b) I. Huc, R. J. Pieters and J. Rebek Jr, *J. Am. Chem. Soc.*, **116**, 10296 (1994); (c) R. J. Pieters, I. Huc and J. Rebek Jr, *Tetrahedron*, **51**, 485 (1994).
51. For related systems see (a) P. Tecilla and A. D. Hamilton, *J. Chem. Soc., Chem. Commun.*, 1232 (1990); (b) M. W. Göbel, J. W. Bats and G. Dürner, *Angew. Chem., Int. Ed. Engl.*, **31**, 207 (1992); (c) J. M. Lehn and C. Sirlin, *Chem. Soc., Chem. Commun.*, 949 (1978); (d) D. J. Cram and H. E. Katz, *J. Am. Chem. Soc.*, **105**, 135 (1983); (e) G. L. Trainor and R. Breslow, *J. Am. Chem. Soc.*, **103**, 154 (1981).

Chapter 6

Synthetic Control of DNA Triplex Structure Through Chemical Modifications

**KRISHNA N. GANESH, VAIJAYANTI A. KUMAR
AND DINESH A. BARAWKAR**

National Chemical Laboratory, Pune, India

1. INTRODUCTION

Nucleic acids (DNA, RNA) are the most important of all biopolymers. DNA is primarily responsible for the storage of genetic information, while its expression occurs through the participation of RNA. Nucleic acids perform their vital functions in cell replication and the regulation of biological activity through interaction with a variety of small and large molecules with specific molecular recognition. Indeed, nature has reached evolutionary perfection in endowing nucleic acids with chemical structures highly optimized for the self-recognition and interaction with other molecules so essential for information storage and transfer within the cell. Accurate DNA replication is most necessary for survival of the cell, and at a molecular level this is achieved through Watson–Crick (WC) specific hydrogen bonding between the complementary base pairs TA (T = thymine, A = adenine) and CG (C = cytosine, G = guanine) [1]. The mutual specific recognition of bases by use of two hydrogen bonds in TA and three hydrogen bonds in CG (Figure 1) primarily ensures the fidelity of DNA transcription and translation. The four base pair combinations AT, TA, CG and GC are geometrically isomorphous, and when linked through the sugar phosphate backbone lead to the classical antiparallel double-helical structure for DNA in which two strands held together by

hydrogen bonds are twisted around each other (Figure 2). The bases in each pair generally reside in a plane which is perpendicular to the double-helical axis. *N*-Glycosyl linkages between sugars and bases are on opposite sides of the lower edge of the base pair plane. This arrangement places the backbones of the two strands closest to each other at this edge of the base pairs, giving rise to major and minor grooves in a double-stranded helix. From a functional point of view the grooves are key, as the most specific interactions of the DNA duplex with other species such as proteins, drugs, water and metal ions take place in these grooves [2]. Three modes of interaction (Figure 3) are possible

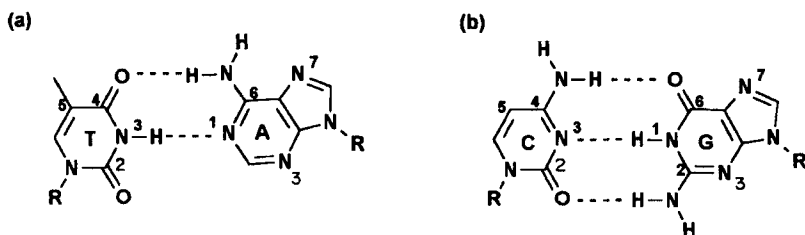


Figure 1 Watson-Crick hydrogen-bonding schemes for (a) TA and (b) CG base pairs

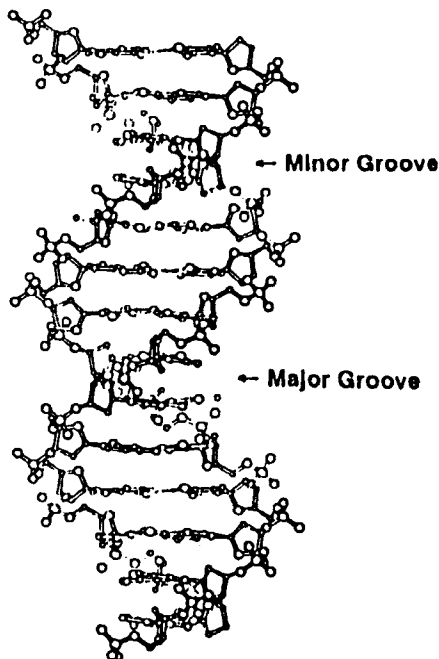


Figure 2 Structure of B-DNA depicting the major and minor grooves

for DNA recognition: (1) surface binding by interionic interactions with positively charged ligands; (2) specific recognition in major and minor grooves via hydrophobic and hydrogen-bonding interactions; and (3) intercalation of polycyclic aromatic rings in between the base stacks. Among the three basic components of DNA – sugar, phosphate and heterocyclic bases – the sugar and phosphate provide centres for nonspecific hydrophobic and electrostatic interactions, respectively, while the heterocyclic bases are responsible for specific hydrogen-bonding interactions in the major and minor grooves. Many molecules use combinations of the above modes to generate high sequence specificity in DNA recognition.

Among other patterns of hydrogen bonding, the Hoogsteen (HG) [3] and wobble [4, 5] base pairs are the most significant (Figure 4). Hoogsteen base pairing is not isomorphous with Watson–Crick base pairing and has importance in triple-helix formation. In wobble base pairing, a single purine (Pu) is able to recognize a noncomplementary pyrimidine (Py) (e.g. GU, where U = uracil). Wobble base pairs have importance in the interaction of messenger RNA (m-RNA) with transfer RNA (t-RNA) on the ribosome during protein synthesis (codon–anticodon interactions). Several mismatched base pairs and anomalous hydrogen-bonding patterns have been seen in X-ray studies of synthetic oligodeoxynucleotides [6, 7].

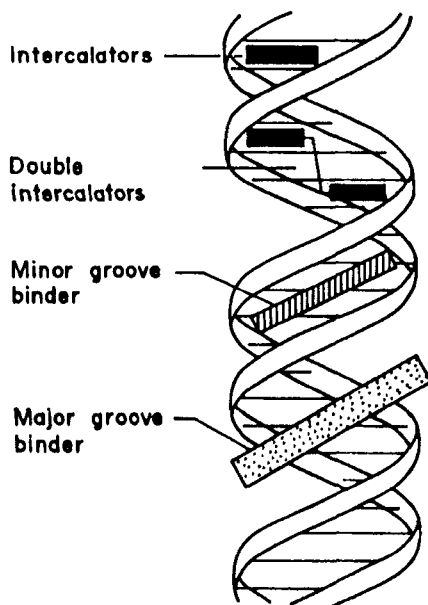


Figure 3 DNA–ligand interactions: intercalation and groove binding

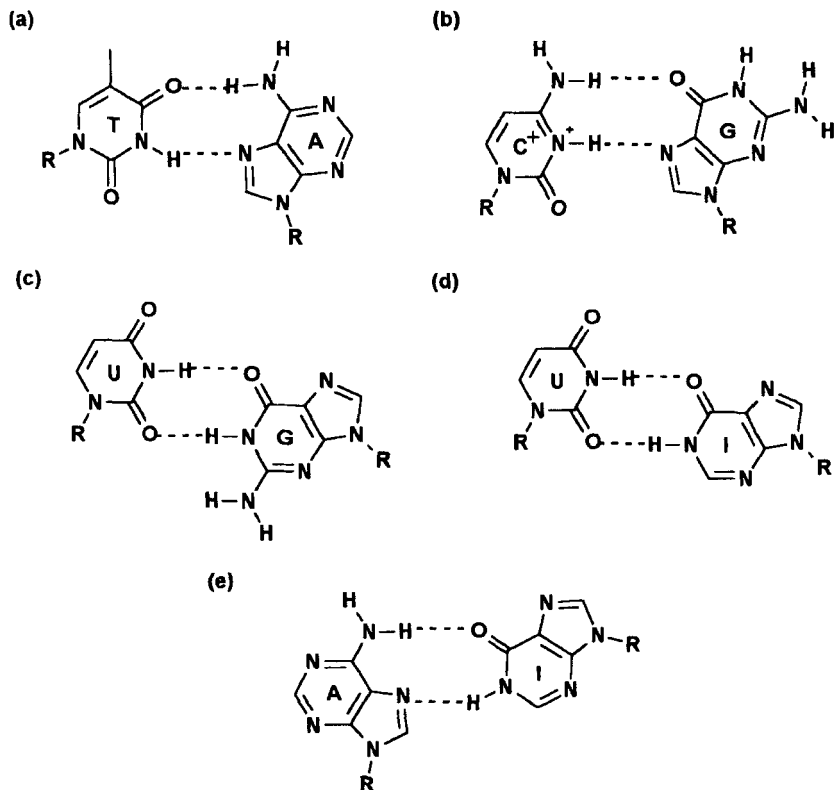


Figure 4 (a, b) Hoogsteen and (c-e) wobble base-pairing schemes. I = inosine

1.1 A-DNA, B-DNA and Z-DNA: Double-Helical Polymorphs

Depending on the base sequence and environment, the DNA duplex can exist in three major conformations: A-DNA, B-DNA and Z-DNA (Figure 5) [2]. A-DNA and B-DNA are regular major secondary structures with right-handed double helices. B-DNA has a wide major groove and a narrow minor groove and the structure is maintained by an *anti*-glycosidic conformation with a C2'-*endo*-sugar pucker (Figure 6). The detailed X-ray analysis of the dodecamer d(CGCGAATTCGCG) (where d signifies the 2'-deoxysugar) and its analogues has given much insight into our present understanding of the structural versatility of B-DNA [8, 9]. The minor groove in the AT regions is narrower than that in the GC regions and is characterized by a spine of hydration. The steric clashes between adjacent purine rings on complementary strands are compensated by local changes in DNA helical structural elements such as base stacking, propeller and helical twist, curvature and so on. Base stacking [10] plays an important role in the sequence control of DNA structure with

5'PuPy3' structures differing from 5'PyPu3' sequences for the same base combinations, and the energetic requirements are accommodated by changes in the sugar phosphate backbone conformation. Mismatched base pairs cause local structural irregularities. A particular hallmark of the B-DNA conformation is its flexibility and capacity to modulate local helix structure in response to base sequence changes [11]. In contrast, A-DNA has a more rigid structure with a deep, narrow major groove and a broad, shallow minor groove, showing little sequence-dependent variation in structure. The structure comprises *anti*-glycosidic torsion with a C2'-*endo*-sugar geometry. Z-DNA [12] is a left-handed double helix with a characteristic zig zag phosphate backbone in which purines adopt a *syn*-conformation with a C3'-*endo*-sugar pucker. It is favoured for alternating GC sequences and stabilized by high concentrations of salt and ethanol. Structural transitions from one form of DNA [2] to another are possible as a response to a change in environment such as salt, solvent and pH, and easily monitored by optical spectroscopic techniques, in particular circular dichroism.

1.2 Molecular Recognition in the Major and Minor Grooves of Duplex DNA

The major and minor grooves of DNA differ significantly in their electrostatic potential, hydrogen-bonding character [13], steric effects, hydration [14] and dielectric strength [15]. Hydrogen bonds can be accepted by AT and TA base pairs from ligands bound in the major groove via the C4 carbonyl of T and N7 of A, while in the minor groove hydrogen bonding occurs through the C2 carbonyl of T and N3 of A (Figure 7). The only hydrogen bond donor in the

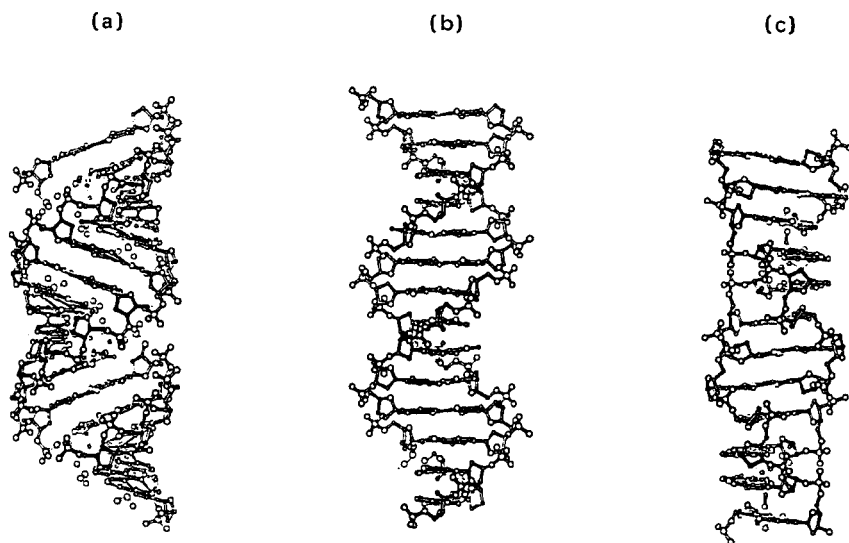


Figure 5 DNA structural polymorphs: (a) A-DNA, B-DNA and (c) Z-DNA

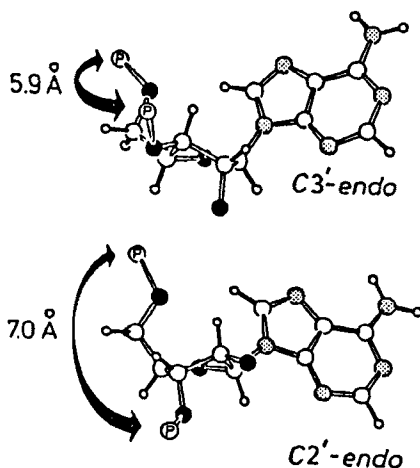


Figure 6 Sugar puckers and glycosidic torsions in DNA structure

major groove for the AT base pair is the N6 amino of A, while none exists in the minor groove. The picture is different for CG and GC duplets, the hydrogen bond acceptors in the major groove being N7 and O6 of G, and in the minor groove C2 of C and N3 of G. The hydrogen bond donor in the major groove for CG is the N4 amino of C, and in the minor groove it is the N2 amino of G.

The salient outcome of this distribution of hydrogen bond donors and acceptors in the naturally occurring base pairs is that the binding molecules can discriminate the AT base pair from CG efficiently from the major groove side but not so well in the minor groove [13]. Two further features of molecular discrimination are noteworthy. In AT and TA base pairs, the C5 methyl of T offers substantial hydrophobic recognition in the major groove which is absent for CG and GC base pairs. However, in the CG and GC duplets, the N2 amino of G presents a steric block to hydrogen bond formation at N3 of G and the C2 carbonyl of C in the minor groove. It is possible to distinguish AT from TA and CG from GC in the major groove since the horizontally ordered arrays of hydrogen-bonding sites and hydrophobic centres differ among the four pairs (Figure 7). The negative electrostatic potential due to phosphate charges is greater in the AT minor groove than in GC-rich regions, and this provides an additional important source for AT-specific minor groove recognition [14].

1.3 Scope and Aims

An understanding of the macrostructural organization of nucleic acids at a molecular level becomes important in discerning the three-dimensional

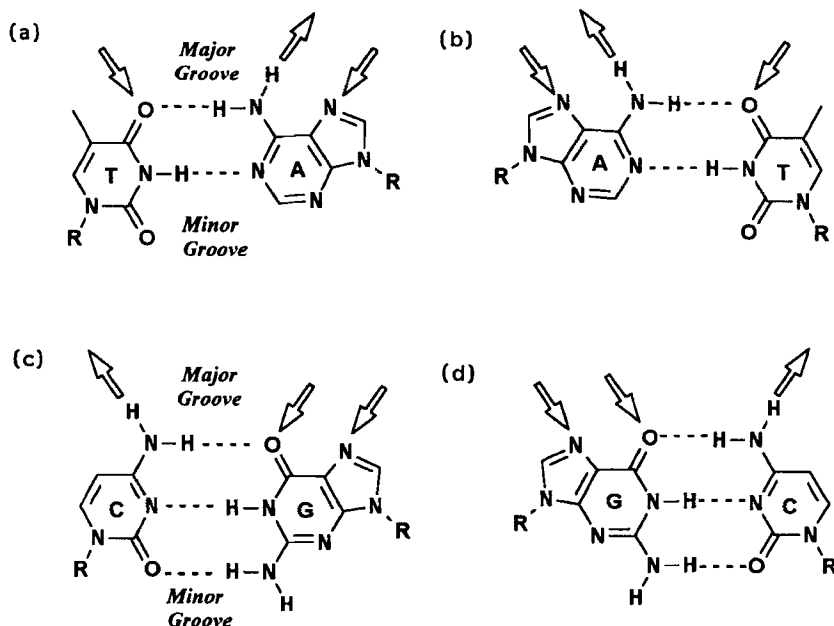


Figure 7 Hydrogen bond donor and acceptor sites in the major groove of duplex DNA at (a) TA, (b) AT, (c) CG and (d) GC base pairs. Arrows pointing to the atoms indicate acceptor sites; arrows pointing away from the atoms indicate donor sites

recognition codes and allows the design of new supramolecular systems of practical importance. In DNA, a vertical combination of the horizontally ordered hydrogen bond donor and acceptor sites characteristic of each base pair in a helix generates a three-dimensional grid which is unique to each DNA sequence. This pattern is recognized in the major or minor groove by ligands possessing complementary sites. When the ligand is another strand of DNA having Hoogsteen or reverse Hoogsteen complementarity to the duplex in the major groove, the binding leads to formation of a DNA triplex. The synthetic control of the structure and stability of such a triplex can be exercised either by varying the sequence of bases, giving rise to different motifs, or by a chemical modification of the nucleobase or phosphate backbone within a particular motif. In this article, a brief description of the general features of triplex structure is followed by examples of specific chemical modifications and emerging biological applications. No attempt is made to review exhaustively all the literature on triplexes, and the scope of the article is limited to presentation of the chemical logic of each structural modification by considering specific examples and their consequences on triplex stability.

2. DNA TRIPLE HELIX: GENERAL FEATURES AND NATURAL MOTIFS

One of the most exciting developments in DNA molecular recognition with a high potential for practical utility is the discovery of triple-stranded DNA complexes. Moser and Dervan [16] were the earliest to demonstrate site-specific binding of an oligonucleotide to the major groove of a DNA duplex (Figure 8). Le Doan and coworkers [17] simultaneously reported the formation of a triplex between an unnatural α -oligonucleotide and its cognate DNA duplex sequence. This new strategy for the recognition of double-stranded DNA sequences has fuelled studies unabated, with far-reaching implications in the fields of genetics, biochemistry and medicine [18].

2.1 Triple-Helical Motifs

Pyrimidine oligonucleotides bind in the major groove of Watson–Crick double-stranded DNA with polypurine stretches resulting in triple-stranded structures [16]. The specificity in triple-helix formation is derived from Hoogsteen hydrogen bonding in which thymine recognizes the AT base pair (T·AT triplet) and protonated cytosine the GC base pair (C^+ ·GC triplet) (Figure 9). The notable features of this motif, called the “pyrimidine motif” (Y·RY), are that (1) while AT base pairs are recognized by neutral T, the base pair GC requires protonated C (C^+) for triad formation, and (2) the third strand (HG) is parallel

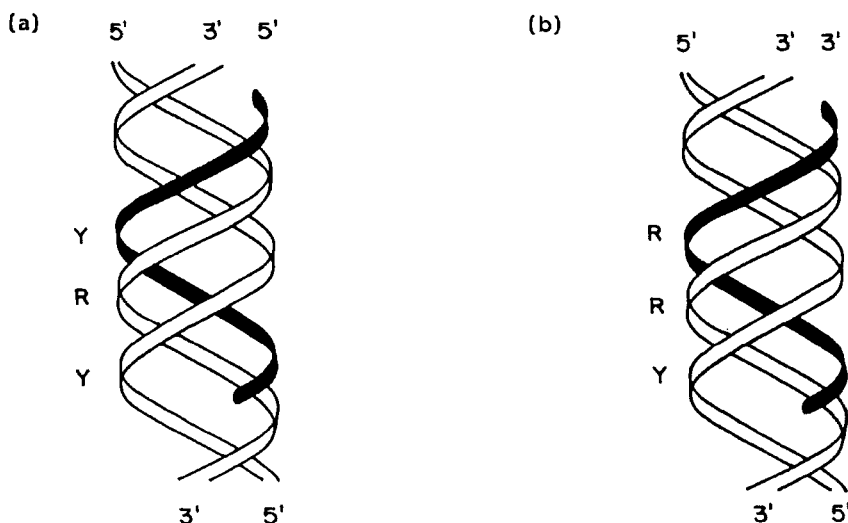


Figure 8 DNA triple helices with the third-strand ODN in the major groove (a) parallel (Y·RY motif) and (b) antiparallel (R·RY motif)

to the central purine strand. In the “purine motif” (R·RY) [19, 20], oligodeoxyribopurines are capable of forming triplexes, but again through interaction with a homopurine tract of double-stranded DNA. These triplexes are characterized by A·AT and G·GC triplets, and, unlike in the pyrimidine motif, no protonation of pyrimidines is required for GC recognition; in addition, the third strand is antiparallel to the central purine strand. A common feature of both motifs is the necessity of a purine in the central position of the triad. Thus, among the four possible duplets AT, GC, CG and TA, only the first two are “allowed” to recognize the incoming purine or pyrimidine third strand. In addition to the formation of specific base triplets, triple-helix formation is also sensitive to several structural and environmental factors such as the length of the third strand, single mismatches, cation concentration and valency, temperature, and backbone composition of the three strands [16]. In order to realize the full potential of triplex formation, there is widespread interest in expanding the scope of triplex recognition to all four duplex base pairs within a single triple-helical motif. These approaches have mainly involved invention and use of several synthetic heterocycles which are either mimics of protonated C or provide complementary neutral hydrogen-bonding sites to the duplex base pair. Synthetic control of DNA structures via chemical modifications of backbones and heterocyclic base components provides an innovative strategy for triplex stabilization [18].

2.2 Triplex Structure

Triplex formation with natural bases is limited by several important structural requirements. Recognition of any sequence in one of the WC strands is achieved by the formation of specific sets of hydrogen bonds (Hoogsteen or reverse Hoogsteen) with complementary base pairs in the other strand (Figure 7).

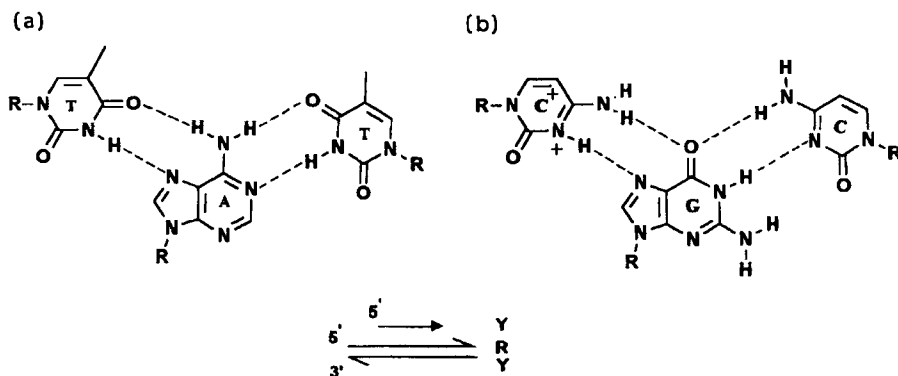


Figure 9 Base-pairing schemes in Y·RY motif (a) T·AT and (b) C⁺·GC triads. The arrows indicate the relative 5'→3' directionalities of the three strands

Because of steric and electrostatic considerations, interaction of a third-strand nucleic acid with a double-stranded target site occurs almost exclusively within the major groove with sequence restrictions. Pyrimidine bases provide only one hydrogen-bonding site at C4 in the major groove of a WC-type duplex, whereas purine bases afford two sites at C6 and N7. The 5-methyl group on T in DNA can sterically block hydrogen-bonding interactions within the major groove. The donor and acceptor patterns in the major groove for A and G are distinct from each other, and therefore sequence-specific recognition through the formation of pairs of hydrogen bonds occurs only at purine bases. A regular placement of a third strand in the major grooves requires that all purine complements of WC base pairs are on the same strand. Hence, triplex formation is limited to polypyrimidine–polypurine duplex sites.

Considerable progress in understanding the structure of triple-stranded oligonucleotides has been achieved in recent years. The complexity of the problem has demanded a wide variety of approaches to the solution, ranging from biochemical (gel electrophoresis [20], footprinting and affinity cleavage [16] and biophysical (spectroscopy, mainly NMR [21] and optical spectroscopy, and calorimetry for energetics [18]) to molecular biological (gene inhibition) techniques [19b, 22]. A parallel orientation of the third strand relative to the purine strand in Y·RY triplexes was established by affinity cleavage and chemical modification experiments [16] in intermolecular and intramolecular complexes. Direct evidence for the Hoogsteen hydrogen bond pairing in T·AT and C⁺·GC triplets was provided by high-resolution NMR studies of intermolecular triplexes [23, 24], which also showed that WC interactions were unaffected upon triplex complexation. The *anti*-glycosidic torsion angles and S-type sugar conformations (C2'-*endo*) are like those found in B-form helices. However, the inter- and intrastrand overlaps of heterocyclic bases are more like those in the A-form. Thus, Y·RY triplexes adopt an overall conformation that is distinct from both A-form and B-form helices [21].

The relative orientation of purine strands in R·RY triplexes was shown to be antiparallel by protection and affinity cleavage experiments [19b, 25]. The three permissible triplets in the R·RY motif are G·GC, T·AT and A·AT (Figure 10) [19b]. These are stabilized by two reverse-Hoogsteen-type hydrogen bonds between bases in the third strand and the purine strand of the WC duplex, and possess *anti*-glycosidic torsion angles. The G·GC, T·AT and A·AT triplets in the R·RY motif are nonisomorphous, and hence noticeable structural perturbations are found at junctions between G·GC and T·AT triplets. These involve underwinding of the helix and other compensating effects including a high-energy (*gauche*, *trans*) state for phosphodiester torsion angles [26]. A poor overlap between neighbouring base moieties in the third strand, deviations from S-type sugar pucker for thymines and a high *anti*-glycosidic conformation for G all characterize the third strand of the R·RY motif. In the WC duplex

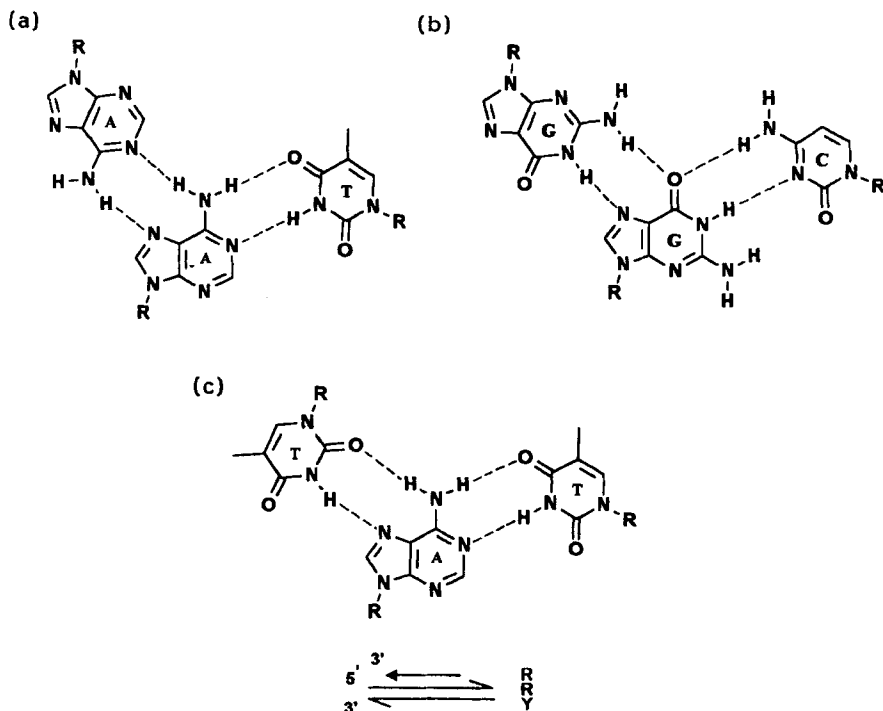


Figure 10 Base-pairing schemes in R·RY motif (a) A·AT, (b) G·GC and (c) T·AT triads. Note the reverse HG mode for the third-strand T in (c) as compared to T·AT in Figure 9

region, the base pairs are displaced towards the minor groove by 1 \AA , with base stacking reminiscent of A-form DNA with S-type sugar pucker and *anti*-glycosidic torsion.

2.3 Triplex Grooves

The binding of the third strand in the Y·RY motif induces global conformational changes in the WC-paired duplex region of the triplex. As a result, WC base pairs move towards the minor groove by 1 \AA to overcome the nonbonded interactions with the incoming third strand in the major groove, accompanied by a slight unwinding of the helix. The third strand partitions the major groove of DNA, leading to three distinct grooves in triple helices (Figure 11) [21]. Among these, in the Y·RY motif, the Crick–Hoogsteen (CH) groove is quite narrow ($2\text{--}3 \text{ \AA}$) with an ordered, interconnected network of water molecules. These water molecules not only solvate the macromolecule but also screen the repulsive interactions between negatively charged phosphate groups in the narrow groove. The Watson–Hoogsteen (WH) groove is wide ($>7 \text{ \AA}$)

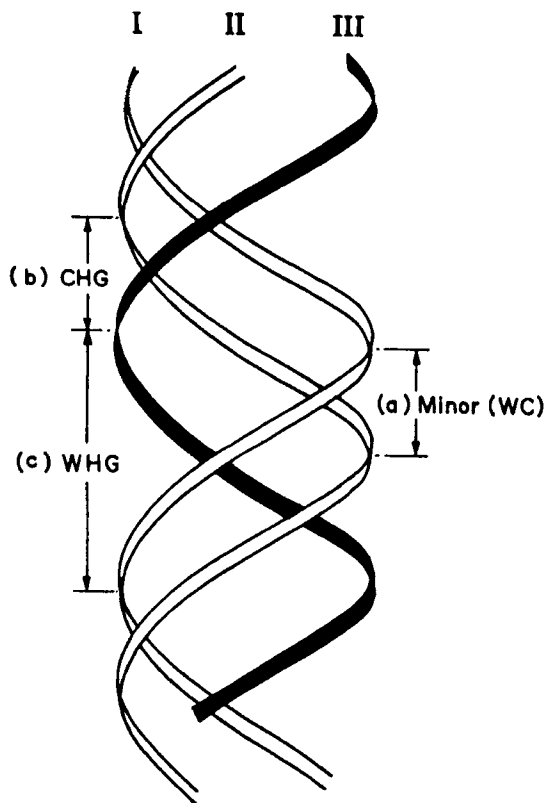


Figure 11 Triple-helix grooves: (a) the Watson–Crick (strands I and II) minor groove of the duplex; (b) the Crick–Hoogsteen (strands II and III) groove; and (c) the Watson–Hoogsteen (strands I and III) groove. The grooves in (b) and (c) are formed by partition of the major groove of the DNA duplex by a Hoogsteen strand

and somewhat hydrophobic owing to the presence of the 5-methyl groups of T moieties. The Watson–Crick (WC) groove ($6\text{--}7\text{ \AA}$) is similar to the minor groove of B-DNA with hydration sites located near H2 of A. The CH groove in the R·RY motif is narrow (3 \AA) and somewhat shallow with extensive hydration. The WH groove, despite its width (8 \AA), has water molecules positioned along the inner edges close to the phosphate oxygens. Thus, hydration is an important determinant in the stability of R·RY duplexes.

2.4 Sequence Control of Triplex Stability

There are four different ways (Figure 12) to assemble Y·RY triple helices from oligonucleotides (ODNs) (1) mixing of appropriate homopurine and

homopyrimidine ODNs in a stoichiometry of 1:2; (2) addition of a complementary homopyrimidine guest strand to a host hairpin duplex with a polypurine–polypyrimidine stem; (3) adding a complementary homopurine strand to a palindromic pyrimidine sequence; and (4) successive folding of a single contiguous ODN to yield an intramolecular triplex. Depending on the nature of the ODNs chosen, the relative contributions of various thermodynamic parameters for triplex stabilization differ. For the Y·RY triplex model in Figure 12(a), assembled from a 15-mer all-pyrimidine single strand (Y_{15}) and a WC 21-mer duplex composed of a polypurine-rich (R_{21}) and a pyrimidine-rich (Y_{21}) DNA, spectroscopic and calorimetric studies indicated two distinct, well-resolved transitions [27]. The first low-temperature UV transition ($t_m \approx 30^\circ\text{C}$, where t_m is the midpoint of the melting curve) was pH dependent and was attributed to dissociation of Y_{15} from the $R_{21}Y_{21}$ duplex. The second, pH-independent, transition (pH 6–7) corresponds to melting of duplex $R_{21}Y_{21}$. Calorimetric measurements at pH 6.5 show the triplex to be enthalpically stabilized by $2.0 \pm 0.1 \text{ kcal mol}^{-1}$ of base triplets, in contrast to $6.3 \pm 0.3 \text{ kcal mol}^{-1}$ of base pair stabilization for the duplex. These correspond to free energies of stabilization of $1.3 \pm 0.1 \text{ kcal mol}^{-1}$ for the triplex and $17.2 \pm 1.2 \text{ kcal mol}^{-1}$ for the duplex. The stabilization of $dA_{10} \cdot 2dT_{10}$ and $d(C_3^+T_4C_3^+) \cdot d(G_3A_4G_3)d(C_3T_4C_3)$ triple helices was observed with NaCl and $MgCl_2$ at pH 5.5 [28]. The binding affinity of the third strand is two to five

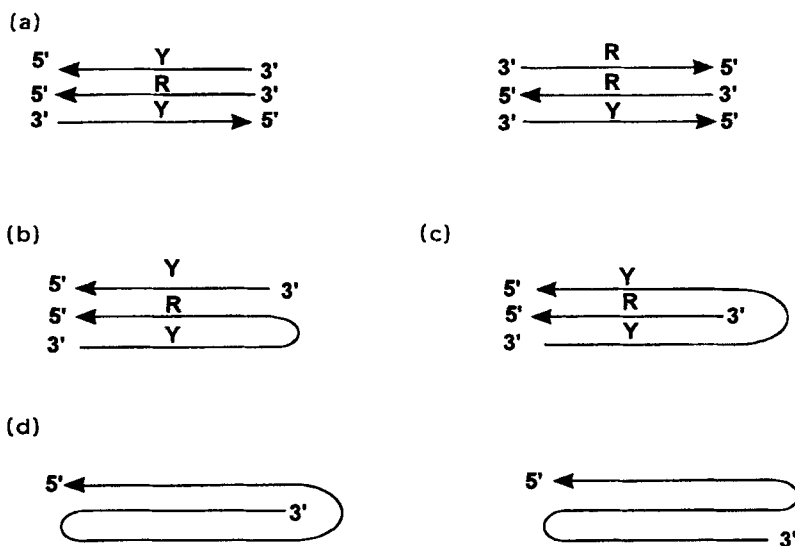


Figure 12 Schematic illustration of modes of inter- and intramolecular triple-helix formation: (a) termolecular Y·RY and R·RY motifs; (b) bimolecular from a hairpin duplex (RY) and a single strand (Y); (c) bimolecular from a hairpin loop (YY) and a single strand (R); and (d) single-strand intramolecular

orders of magnitude lower than that of the two strands forming the underlying duplex. While the two HG base pairs TA and C⁺G have similar stability in the presence of Mg²⁺ at low pH, HG base pairs are 0.22–0.64 kcal mol⁻¹ less stable than WC base duplets.

Another study [29] of the model Y·RY triplex in Figure 12(a) involved a 34-mer duplex pairing with a variable-length third strand of dT_n with *n* = 10, 12 and 15. The results indicated that (1) even at low pH, T·AT triplets are more stable than C⁺·GC triplets; (2) triplex DNA is stabilized by the addition of salts (NaCl) and polyamines (spermine); (3) the stability of the triplex is dependent on the length of the third strand, with *n* = 15 showing *t*_m 5 °C and 10 °C higher than *n* = 12 and 10, respectively; and (4) mismatches in the HG strand destabilize the triplex. In the R·RY motif as in d(G₃A₄G₃)·d(G₃A₄G₃)d(C₃T₄C₃), studies [30] by polyacrylamide gel electrophoresis (PAGE) have shown an antiparallel orientation of the third purine strand with respect to the central purine strand of the duplex, while ¹H NMR provided evidence for the existence of purine–purine HG hydrogen bonds. The triplex was stabilized by Mg²⁺ ions even at neutral pH, and the triplex dissociated upon heating. The free energy of triplex formation (−26 ± 0.5 kcal mol⁻¹) was approximately twice that of duplex formation (−12.6 ± 0.7 kcal mol⁻¹); interestingly, under identical conditions, the stability of the third strand was greater than in the analogous Y·RY motif sequence d(C₃⁺T₄C₃⁺)·d(G₃A₄G₃)d(C₃T₄C₃). This enhanced stability, coupled with a lack of acidic pH requirement, is appealing for potential *in vivo* applications of R·RY triplexes.

Singleton and Dervan [31a] employed quantitative affinity cleavage titration (QACT) to compute thermodynamic parameters for triplexes of type Y·RY (Figure 12a) using long duplex stretches (33 base pairs) and 15-base third strands equipped with an iron complex of ethylenediaminetetraacetic acid (EDTA). The equilibrium binding constants measured at 24 °C were in the region of 10⁶ M⁻¹, corresponding to a free energy of −9.0 ± 0.2 kcal mol⁻¹, which was also dependent on the length of the third strand. Removal of one T and one C from the 3'-end reduced the free energy of stabilization by 0.5 kcal mol⁻¹, while removal of two T and two C reduced Δ*G* by 1.1 kcal mol⁻¹. Single internal-base triplet mismatches resulted in more destabilization of the local structure by 2.5–3.0 kcal mol⁻¹. A van't Hoff analysis of temperature-dependent *K* data revealed that the triplex is enthalpically stabilized by 2 kcal mol⁻¹ of base triplets, in agreement with the literature [31b]. The buffer species, pH and sequence have significant effects on the experimentally measured values for thermodynamic parameters, as shown by a systematic study on the triplex formation of d(T₄C)₃T₄·d(A₄G)₃A₄d(T₄C)₃T₄ in the Y·RY motif under different environments [32].

The association constants for the formation of 16 Y·RY triple helices having variation at a single common position [Z·XY, where Z = A, G,

5-methylcystosine (m^5C) or T and $XY = AT, GC, CG$ or TA] were determined by QACT of a 242-base-pair DNA duplex with a 15-mer DNA third strand [33]. The K_a ranged from $10^4 M^{-1}$ ($Z \cdot XY = A \cdot CG$) to $10^7 M^{-1}$ ($Z \cdot XY = T \cdot AT$) under identical conditions with the stability orders $T \cdot AT > T \cdot GC$, $T \cdot CG$ and $T \cdot TA$ by $\geq 2-3 \text{ kcal mol}^{-1}$, $m^5C^+ \cdot GC > m^5C \cdot AT$, $m^5C \cdot CG$ and $m^5C \cdot TA$ by $\geq 1.4 \text{ kcal mol}^{-1}$, and $G \cdot TA > G \cdot CG$ and $G \cdot GC$ by $\geq 0.8 \text{ kcal mol}^{-1}$. Among the favoured triplets, the order of stability is $T \cdot AT > G \cdot TA > m^5C^+ \cdot GC$, and the results are only for one sequence composition context. The dependence of triple-helix energetics on sequence composition is yet to be determined.

Significant stability effects have been seen for intermolecular R·RY motifs where GT oligonucleotides, dodecamers in length, on the third strand were most capable of triplex formation [34]. Shorter ODNs significantly impaired the triplex-forming ability, while longer ODNs exhibited no correlation between length and binding affinity. The 3'-extension sequences on the third strand seem to play a more important role in determining triplex stability than the 5'-ends, and the mismatches at the 3'-ends are far more destabilizing than those at the 5'-ends. These results indicate that in the R·RY motif, important interactions occur between the ODN 3'-end and duplex DNA, leading to an asymmetry in purine motif triplex formation. These effects may arise owing to the propensity of GT-rich oligonucleotides to self-associate either intramolecularly or intermolecularly into DNA structures which are resistant to triplex formation, and understanding the molecular basis of such effects would have practical benefits in designing GT-rich, triplex-forming ODNs (TFOs).

An example of a triplex corresponding to the type shown in Figure 12(b) was provided by the specific recognition of a 26-mer hairpin duplex (h26) by an undecamer pyrimidine ODN (s1) [35]. The triplexes were characterized by retardation in gel electrophoresis, the band at 212 nm in the CD spectrum, which is characteristic of the Y·RY triplex, and their biphasic melting behaviour. Analysis of the melting curves with a three-state model gave an enthalpy change of $-6.6 \pm 0.4 \text{ kcal mol}^{-1}$ for pyrimidine binding. One-dimensional and two-dimensional NMR investigations of a 15-mer polypurine-polypyrimidine hairpin at low pH showed the formation of Y·RY triplexes by asymmetric self-association, and the enthalpy of triplex formation as estimated by NMR was 16 kcal mol^{-1} [35].

The type of triple helix shown in Figure 12(c) can be formed by binding at pH 5 of an undecamer purine (dR_{11}) with a 24-mer pyrimidine (dY_{24}) containing a "mirrored" repeated sequence [36]. The 3'-half of dY_{24} forms a conventional antiparallel duplex, while the 5'-half binds to the major groove of this duplex by folding back, leading to a mimic of H-DNA occurring *in vivo*. The triplex formed at pH 5 shows all the characteristic features such as gel retardation, a band at 212 nm in the CD spectrum and resistance to deoxyribonuclease (DNAase) I. The $dR_{11}dY_{24}$ mixture exhibits a monophasic, thermally induced cooperative transition directly into single strands. The ΔH

values calculated from UV transitions ($137 \pm 13 \text{ kcal mol}^{-1}$) and differential scanning calorimetry (DSC) ($129 \pm 6 \text{ kcal mol}^{-1}$) were mutually consistent and corresponded to an average ΔH of $5-8 \pm 0.6 \text{ kcal mol}^{-1}$ per triad, in agreement with the literature.

Two types of single-stranded, intramolecular triple helices of the type shown in Figure 12(d) are possible by double-hairpin formation [37]. This was demonstrated for the R·RY motif by the design of suitable 18-mer sequences containing two G tracts to fold in an antiparallel fashion. The salient features of this intramolecular triplex motif are that (1) Mg^{2+} is not essential, (2) compared to the intermolecular version, a shorter triplex stem can be formed in a much lower DNA concentration, and (3) acidic conditions are not required as it is the R·RY motif. The evidence for triplex existence came from the observation that duplex-hairpin intercalator binders such as actinomycin D, chromomycin A₃ and ethidium bromide bind poorly.

A 38-mer ODN composed of $d(\text{R}_{10}\text{C}_4\text{Y}_{10}\text{T}_4\text{Y}_{10})$ undergoes a pH-induced sequential folding (Figure 13) from a random coil structure via a hairpin to an intramolecular triplex (Y·RY motif), and the secondary structures on the folding path were characterized by spectroscopic and enzymatic means [38]. The ODN is in a random coil state at pH 12, which at pH 8 forms a hairpin helix between the 5'-purine decamer and the consecutive pyrimidine decamer, leaving the second pyrimidine decamer as a dangling, disordered 3'-extension. Reduction of the pH to 5.5 causes the folding of the second pyrimidine stretch back into the major groove to yield an intramolecular triplex. The thermal dissociation was biphasic with the spectroscopic (van't Hoff, $69.9 \pm 3.5 \text{ kcal mol}^{-1}$) and calorimetric ($71.7 \pm 3 \text{ kcal mol}^{-1}$) ΔH values in complete agreement with each other, but showing a slightly higher average ΔH of $7.0 \text{ kcal mol}^{-1}$ per base triplet.

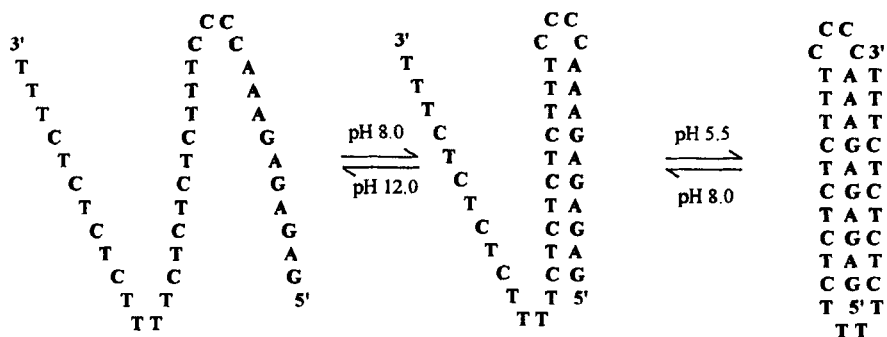


Figure 13 An example of pH-dependent intramolecular triplex formation. Reproduced by permission from *J. Mol. Biol.*, **230**, 1278 (1993)

2.5 Kinetics of Triple-Helix Formation

A knowledge of the kinetics of triple-helix formation is important since triple-helix-forming ODNs have to compete with other duplex-DNA-binding agents *in vivo* such as proteins, transcription activators and so on. Studies on the thermal denaturation–renaturation kinetics of a 22-base third strand with a 22-mer duplex have indicated a hysteresis effect with nonsuperimposable heating and cooling curves [39]. The association constant K_{on} is independent of the nature of the base and the presence of mismatches, but decreases linearly with salt concentration. The dissociation constant K_{off} shows an opposite trend, being independent of salt concentration but dependent on the nature of the base in the third strand and increasing with the presence of base mismatches. These features are characteristic of the presence of a quasistable intermediate, supporting a nucleation zipper model for the formation of a triplex from a duplex and a third strand. This is a slower process compared to duplex formation from two single strands. The energies of activation for association (E_{on}) and dissociation (E_{off}) also show opposing behaviours, with the overall activation energy being negative and corresponding to the formation of three to five base triplets in nucleation. The replacement of a single base pair in the Y·RY motif is highly detrimental to triple-strand binding, with a mismatch at the end less destabilizing [39]. Nucleation requires about five base triplets, the remaining complexation being formed in a highly cooperative way. A mismatch in the centre disrupts the cooperativity between neighbouring base triplets.

In another approach, a filter-binding assay was found to be of value to study the kinetics of triplex formation by 19-mers in the R·RY motif [40]. It was found that the K_{off} is pH dependent owing to a rapid acid–base equilibrium of Y single strands, and is temperature independent at low pH while strongly temperature dependent at higher pH. K_{on} decreases with increasing pH and temperature, and the associated negative activation energy suggests that the process goes through a quasistable intermediate as in the nucleation zipper model.

2.6 Polymorphism in Triplex Structures

If third strands could be constructed to recognize any given double-stranded DNA, the triple-helix strategy would be of utmost practical utility. However, there are numerous theoretical possibilities, and attempts have been made to discard systematically the lame ones [41]. In principle, when based on natural nucleosides, the third strand may recognize the canonical WC duplex in eight different conformations: sugars can be α or β , base torsion can be *anti* or *syn*, and the third strand can be parallel or antiparallel to the duplex. From these considerations, a complete structural database of 32 triplets was analysed using simple building rules encompassing helical symmetry, base pairing, allowable

glycosidic torsions and isomorphism. The analysis indicated that among all possibilities, the triplets T-TG, T-GC, A-TA and G-GC exhibit a high probability for stable triplets. Investigations by molecular dynamics and computer modelling of triplex (T-AT)_n in both A-form and B-form duplex structures indicated that in the A-form, the sugar phosphate backbone of the third strand clashes with poly(dA) in the major groove, enforcing an alteration in duplex geometry [42]. A WC duplex in the triplex indicates a unique geometry differing from both the A-form and B-form. Theoretical calculations taking into consideration the counterion and the hydration pointed to a major role for solvation in determining the third-strand orientation of R-RY triplexes with either HG or reverse HG base pairing possible between the two purine strands [43]. An experimental attempt to find a general solution to triple-helix-mediated recognition of natural DNA sequences including secondary structural and context effects has involved the use of combinatorial techniques [44]. Some 10¹⁰–10¹² randomized RNA molecules were screened against a number of homopurine–homopyrimidine targets. Five successive rounds of selection with increased stringency gave RNA transcripts which were transcribed into complementary DNAs for amplification by a polymerase chain reaction (PCR). The results indicated that a number of secondary structural elements such as interior and hairpin loops can be accommodated in triple-helical motifs, and a higher conformational flexibility in the third strand may facilitate recognition of mixed and nonstandard sequences such as C⁺·AT, U(T)·GC and so on without impairing triplex formation.

3. NUCLEOBASE MODIFICATIONS

3.1 Pyrimidine Modifications to Alter the N3 pK_a

In general, the stability of Y-RY triplexes containing cytosine residues in the third strand decreases as the pH of the solution is raised from acidic to alkaline values [27, 45, 46]. This is due to a decreased protonation at the N3 of C with increased pH. The triplex stability reaches a maximum around pH 5.8, close to the pK_a of the N3 of C. Various approaches have been described to overcome this pH limitation (Figure 14), since any triplex-dependent *in vivo* applications demand stable triplexes at physiological pH. Since the R-RY motif does not involve any charged triad bases, its stability is independent of pH.

(a) C5-substituted pyrimidines

The first category of modifications involved substitutions at C5 of the pyrimidine nucleobase (Figures 14 and 15) [47]. It is well known that C5 substitutions control the pK_a of the N3 of C in nucleosides and drastically alter the hydrophobic driving force, base stacking and electronic complementarity

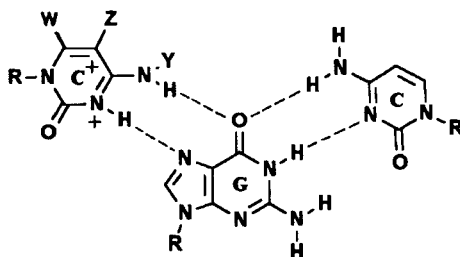


Figure 14 The $C^+ \cdot GC$ triad with various base modifications in the third strand. Possibilities include $W = Y = H$, $Z = \text{Me}$ or H ($C^+ / m^5 C^+ \cdot GC$); $W = Y = H$, $Z = C \equiv \text{CMe}$ ($p^5 C^+ \cdot GC$); $W = Z = H$, $Y = \text{Bu}^n$, $(\text{CH}_2)_2$, CO_2H or $(\text{CH}_2)_4\text{NH}_2$ (N^4 -alkyl- $C^+ \cdot GC$); $W = H$, $Z = \text{Me}$, $Y = (\text{CH}_2)_3\text{NH}(\text{CH}_2)_4\text{NH}(\text{CH}_2)_3\text{NH}_2$ (N^4 -spermine- $C^+ \cdot GC$); and $W = \text{NH}_2$, $Z = Y = H$ (6-amino- $C^+ \cdot GC$)

of hydrogen bonding in duplex formation [2]. There are two opposing electronic effects from C5 substituent X which influence the hydrogen-bonding ability of X^5U and A. An electron-withdrawing substituent (e.g. bromine) increases the acidity of the N3 amino (making it a better hydrogen bond donor) but decreases the electron-donating properties of the carbonyl lone pair, making it a poorer hydrogen bond acceptor. An electron-donating substituent such as a methyl would have the opposite effect of stabilizing protonation at N3, which is thus favourable for triplex formation.

The effect of methylcytosine was first observed in the triplex of poly(dGdA)·poly[d(Tm⁵C)], which formed even at pH 8 in contrast to its unmethylated analogue [45]. It is well known that m⁵C also enhances the stability of the double helix [2]. The pH-dependent affinity cleavage experiments with ODNs incorporating Br⁵dU and m⁵C in the third strand have indicated that (1) substitution of Br⁵U for T increases the binding affinity without changing the pH profile greatly, (2) incorporation of m⁵C for C increases the triplex binding only marginally but extends the pH range to 7 and (3) substitution of both m⁵C and Br⁵U results in a large increase in binding

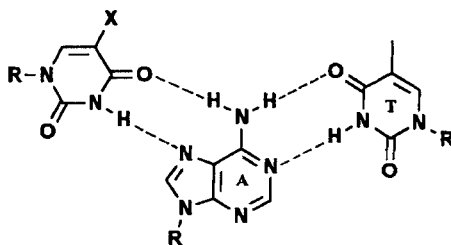


Figure 15 The $Y \cdot AT$ triad with various substitutions in the third-strand pyrimidine. Possibilities include $X = \text{Br}$ ($\text{Br}^5U \cdot AT$), $C \equiv \text{CMe}$ ($p^5U \cdot AT$) and Me ($m^5U \cdot AT$)

over an extended pH range [47]. The relative stabilities of base triplets are in the order $\text{Br}^5\text{U}\cdot\text{AT} > \text{T}\cdot\text{AT} > \text{U}\cdot\text{AT}$ and $\text{m}^5\text{C}^+\cdot\text{GC} > \text{C}^+\cdot\text{GC}$, suggesting that 5-methylation in general increases the binding affinity irrespective of the methylated pyrimidine. Thus, the substitution of methyl for hydrogen at C5 promotes binding by a hydrophobic effect, while bromine substitution strengthens binding by increasing acidity at N3 or enhancing hydrophobicity or both.

5-Methylcytosine The “5-methyl hydrophobic effect” was used to inhibit the recognition of double-helical DNA by prokaryotic modifying enzymes and a eukaryotic transcription factor via oligonucleotide-directed triple-helix formation in which ODNs containing m^5C conferred substantially more efficient inhibition than those with C [22]. Triple-helix formation also selectively protects the DNA duplex from restriction methylation, and the specificity of 15 base pairs is useful for chromosome mapping.

Thermodynamic analysis has indicated that the additional stability imparted to the triplex by 5-methylcytosine is entropic in origin [27, 48]. The methyl group should fill a space in the major groove, causing a release of hydrating water molecules from the double helix to bulk solvent, a source of positive entropy change. The protonated state of cytosine is stabilized by $1.5 \text{ kcal mol}^{-1}$, while N3-protonated m^5C is stabilized by $1.8 \text{ kcal mol}^{-1}$ in the triplex. This stabilization comes from (1) interactions such as hydrogen bonding between the C^+ heterocycle and the proximal base and (2) coulombic interaction between the positively charged N3 of C^+ and the anionic phosphate ($0.5 \text{ kcal mol}^{-1}$). In addition to hydrogen bonding and solvation, another likely source of stabilization is the increased base-stacking interactions. Methyl substitution increases the molecular polarizability and thereby the free energy of stacking, and may stabilize the complex through increased stacking energy without directly influencing the protonation event.

The kinetic analysis of ODN-directed triplex formation with a 21-mer ODN containing 10 m^5C substitutions indicated a pseudo-first-order association rate constant (k_2) (at concentrations > 10 -fold excess over DNA) of $\sim 1000 \text{ M}^{-1}$ [49]. It was found that divalent and multivalent cations (e.g. Mg^{2+} , spermine) were superior to monovalent cations (e.g. Na^+) in triplex stabilization [48]. The monovalent cations not only decreased the association rate but also enhanced the dissociation rate, indicating a significant role for the counterions in triple-helix formation. A similar effect was observed upon increasing the pH from 6.8 to 7.2. The observed dissociation constant of 10 nM is similar to that seen for sequence-specific DNA-binding proteins, and a half-life of 12 h for triplexes suggests an efficient *in vivo* binding to target DNA by competition with DNA-binding proteins. ODNs containing m^5C (undecamers with six m^5C groups) also recognized the purine tract of a double-helical stem of a 26-mer and at pH 6.8 where only the 5-methylated ODN was effectively binding, whereas a

standard ODN did not. Thus, cytosine methylation expands the pH range compatible with triplex formation by one unit, and the t_m of triplex transition was enhanced by 10 °C. Thus, m^5C has become an important structural element for inducing stabilization of $C^+ \cdot GC$ -containing triple helices under physiological conditions.

C⁵-(1-propynyl)-2'-dC The logic of entropic and stacking stabilization provided by m^5C has been extended to investigate the effect of a 1-propynyl substituent at C5 [50]. The propyne modification (Figure 14) is planar with respect to the heterocycles and allows for increased stacking of bases. It is also more hydrophobic than the methyl group, allowing a further increase in the entropy of binding. It was found that the C5 propyne analogue of 2'-deoxyuridine stabilizes the triple-helical complex relative to thymidine; conversely, the C5 propyne analogue of 2'-dC destabilizes the triple helix, perhaps owing to a decrease in the pK_a of the heterocycle. Both, however, cause an increase in the t_m of the double helix formed with RNA. These results are valuable since the increased hydrophobicity of propyne analogues relative to dT and m^5C may also facilitate permeation of ODNs into cells, with potential therapeutic applications.

5-Methyl-2'-O-methylcytidine It was recently demonstrated that the triplex of a 2'-O-methylpyrimidine RNA oligomer with a duplex DNA is thermally more stable than the corresponding DNA triplex [51]. The 2'-O-methyl oligoribonucleotides are chemically more stable and relatively nuclease resistant compared to unmodified RNAs. These facts led to the study of triplex stability for ODNs containing 5-methyl-2'-O-methyluridine and 5-methyl-2'-O-methylcytidine bound to duplex DNA. It was observed that while 5-methyl-2'-O-methyluridine formed a more stable triple helix with double-stranded DNA than the 5-unmodified parent probe, 5-methyl-2'-O-methylcytidine destabilized the triplex. This effect is similar to that observed with the 5-propynylpyrimidines, where the dU derivatives enhanced triplex stability while the dC analogues exhibited the opposite effect. The cause of the destabilization was thought to be the lower N3 pK_a of the cytosine derivatives.

(b) Carbocyclic m^5C

The carbocyclic analogue (Figure 16) of m^5C (cm^5C), having a higher pK_a of 4.8 than the parent nucleoside with a pK_a of 4.5, may facilitate protonation at N3. It was found that incorporation of cm^5C into the third strand resulted in an increase in t_m of 3.9 °C per substitution over strands containing m^5C at pH 7.2 [52]. Interestingly, carbocyclic T (ct) showed an opposite trend, with a decrease in t_m of 1.7 °C per substitution at pH 6.6 relative to the ODN containing T. Thus, the hydrophobic interaction of the carbocyclic ring is

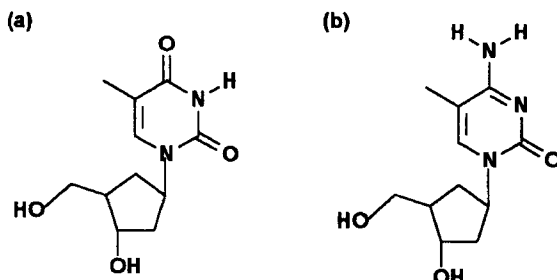


Figure 16 The carbocyclic pyrimidines (a) cT and (b) cm⁵C

probably not responsible for the increased t_m of cm⁵C. The C1'-*exo*-conformation of the cyclopentane ring is unfavourable for triplex formation, and the observed enhanced stability is due to pK_a effects. Since the carbocyclic analogues of nucleosides exhibit greater enzymatic stability to cleavage of the glycosidic linkages, they may prove useful in therapeutic applications.

(c) *N*⁴-Alkyl-C

Another site for easy modification of cytosine is N4, which can be derivatized by means of a sulfite-catalysed transamination reaction [53, 54]. This selectively introduces aminoalkyl or carboxyalkyl linker arms into a single deoxycytidine residing in an ODN which also contains m⁵C. This is possible since m⁵C do not react in the transamination reaction. Oligonucleotides which carry side chains at N4 form duplexes and triplexes (Figure 14) with complementary single-stranded or double-stranded ODN target molecules. The transaminated oligomers were found to be capable of forming triplexes with a double-stranded DNA target, but the triplexes were considerably more destabilized than those formed with an unmodified third-strand oligomer. The decrease in triplex stability was attributed to either steric interactions between the side chain and the components of the major groove or a higher pK_a of the modified cytosine, which decreases the N3-protonating ability.

(d) *N*⁴-Spermine-m⁵C

Interestingly, however, when N4 of m⁵C carried a polycationic side chain such as spermine (Figure 14) in the third-strand oligodeoxynucleotides, stable triplex formation with a complementary duplex occurred even at neutral pH [55]. Under identical conditions, control ODNs carrying m⁵C without any spermine conjugation did not form triple helices. Remarkably, the triplexes from spermine conjugates had foremost stability at neutral pH, unlike the behaviour of normal ODNs whose optimal stability is at acidic pH. The molecular origin of this stability could be the polycationic side chain which decreases the net negative charge on the triplex by intramolecular

neutralization, hydrophobic desolvation and internal molecular recognition of the duplex by the spermine chain through hydrogen bonding. These derivatives are likely to have significant implications for antigene therapeutics, since in addition to triplex stabilization, the spermine-ODN conjugates may have better membrane permeability owing to a decreased net charge. It may be pointed out here that 21-mer homopyrimidines conjugated with polyamines at the 5'-end formed a triple helix of a higher stability with appropriate complementary duplexes in the Y·RY motif but without showing the pH effect as in ODNs containing spermine at N4 [56].

(e) *N*⁴-ethano-C

Substitution of *N*⁴-ethano-m⁵dC in the third strand in place of a C⁺ residue would allow the placement of an electrophilic methylene near nucleophilic N7 or O6 of G in the triplex (Figure 17) [57]. The acidic environment in the major groove of DNA enhances the reactivity, leading to a very efficient, irreversibly crosslinked stable DNA triple helix. The reaction does not require light or addition of any external reagent and occurs under physiological conditions, making it promising for *in vivo* application of triple-helix-mediated, sequence-specific regulation of genes.

(f) 6-Amino-C

It was realized that N3 in 6-aminodeoxycytidine has a higher p*K*_a (6.8) compared to the unsubstituted analogue, and hence 6-amino-2'-*O*-methyl-C was incorporated as a protonated cytidine analogue for triple-helix binding (Figure 14) [58]. These ODNs showed significantly lowered binding to duplex DNA relative to control 2'-*O*-methyl-C. The 6-amino modification might perturb the glycosidic conformation to the *syn*-form, and thus disfavour binding to the duplex DNA.

3.2 Neutral Mimics of C⁺

Charge repulsion disfavors protonation at N3 of all cytosines and m⁵C in contiguous C⁺·GC and m⁵C⁺·GC triplets. The p*K*_a values of N3 of G and m⁵G

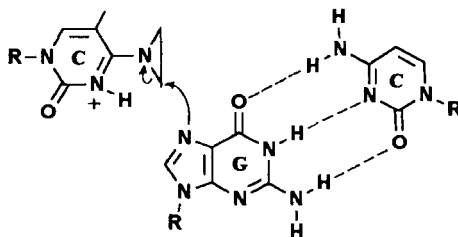


Figure 17 The *N*⁴-ethano-C⁺·GC triad

in $C^+ \cdot GC$ and $m^5C^+ \cdot GC$ are sequence dependent, limiting the utility of m^5C for ODN-directed triplex formation for G-rich sequences. Also, as seen from the above discussion, N3 protonation of C seems to be a critical factor in determining the triplex stability, and this has led to a search for neutral, nonprotonated C^+ mimics. These may not only reduce the pH-dependent effects but also eliminate the destabilization of the triplex due to charge repulsions (which are operative even in neutral conditions) between cations on neighbouring protonated C or m^5C bases.

(a) *Pseudoisocytidine*

The first example in this approach is the use of the pseudoisocytidine derivative (ΨiC , where i denotes the isonucleoside), which has the ability to form both Hoogsteen-type (Figure 18a) and Watson–Crick-type (Figure 18b) base pairings to hydrogen bond with guanine under neutral conditions [59]. This is possible since it has a hydrogen at N3 for hydrogen bonding with N7 of G, leading to the $\Psi iC \cdot GC$ triad in neutral conditions (Figure 18). The uncharged-base-containing ODN would be helpful in forming a triplex with double-stranded DNA containing a 2'-deoxyguanine cluster. A 16-mer ODN containing six contiguous ΨiC s formed a stable triplex with a 22-mer duplex containing a tract of six guanines under conditions where the analogous 16-mer ODN containing m^5C instead of ΨiC did not form a triplex. The ΨiC used here contained 2'-*O*-methylsugars as these are stable to nucleases.

(b) *8-Oxo-dA*

Oligonucleotides with 8-oxoadenine (Figure 19) were found to be capable of forming stable triplexes with GC of double-stranded DNA under neutral and basic pH, eliminating the necessity for protonation of the base in the third strand [60–62]. Thus, 8-oxoadenosine in the *syn*-conformation could be a logical mimic of C^+ in which the hydrogen of the N7 of 8-oxo-dA and the 6-amino would act like the protonated N3 and 4-amino of C^+ , respectively. N^6 -Methyl-8-oxo-2'-dA (Figure 19) when present with thymidines in the ODN

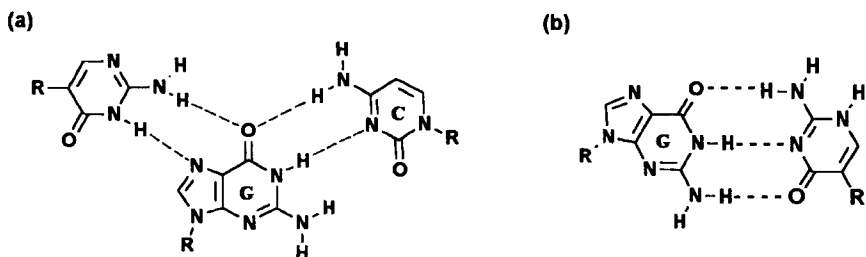


Figure 18 (a) The $\Psi iC \cdot GC$ triad in the Y·RY motif. (b) The G ΨiC WC base pairing

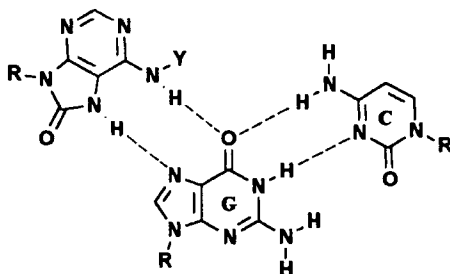


Figure 19 The 8-oxo-dA·GC triad, where Y = H or Me (see text)

formed a triple helix in the Y-RY motif which is not only pH independent but also superior to m^5C in conferring increased affinity under physiological salt conditions [63]. Formation of the triplex was supported by CD spectral studies, DNA footprinting and so on, and the oligopyrimidine containing this substitution prevented *in vitro* transcription, making 8-oxo-dA a useful alternative for C and m^5C . A third strand containing up to eight 8-oxo-A bases exhibited stable triplex formation insensitive to pH changes in the region 6.0–7.4 [60]. Surprisingly, triplex formation took place with a negligible change in UV absorption (hypochromicity), and could not be detected by conventional thermal denaturation experiments. In the absence of any satisfactory reason to explain the lack of hypochromicity, triplex formation was supported by gel retardation assay and triplex-directed photocrosslinking of a psoralen-conjugated third strand.

(c) 8-Oxo-dG

Although affinity cleavage methods have been extensively used for sequence-specific cleavage of a single target site on the duplex, little is known about the relationship between the thermal stability of the triple helix and the cleavage efficiencies of targeted strands, having the mismatched HG hydrogen bonds. To gain insight into this relationship, comparative studies on the thermal stability and duplex cleavage efficiency by a DNA third strand linked to 1,10-phenanthroline were performed [64]. In addition to the four natural bases A, G, C and T, the base analogues I (hypoxanthine), X (xanthine), m^5C and Br^5C were incorporated systematically into the third strand to generate ($8 \times 4 = 32$) combinations of triplets. The results indicated that increased cleavage yields reflect higher thermal stability in most cases except for G·AT, which is the least stable triplex and showed the highest cleavage yield. In principle, it is possible that Cu^{2+} can mediate and strengthen the G·AT recognition at the O6 of dG and the N7 of dA. This could partially be true as in the presence of Cu^{2+} , the t_m of the G·AT-containing triplex increased by $\sim 14^\circ C$ without an alteration in the thermal stability of the WC duplex during melting. Alternatively, the

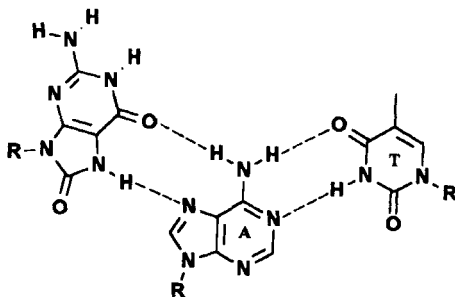


Figure 20 The 8-oxo-dG·AT triad in the Y·RY motif

hydroxy radicals produced during the DNA cleavage reaction can oxidize G at the 8-position to yield 8-oxo-dG. This indeed was the case, as demonstrated by the actual incorporation of 8-oxo-dG into the third strand, which exhibited both high thermal stability ($\Delta t_m = 19^\circ\text{C}$) and cleavage yields like those of the triplex containing the G·AT triplet. This stability could come from two hydrogen bonds: one between O6 of 8-oxo-dG and the 6-amino of dA, the other between the N7 hydrogen of 8-oxo-dG and N7 of dA (Figure 20). The introduction of the 8-keto group forces the dG residue to adopt a *syn*-conformation such that the N7 proton and O6 mimic the base-pairing face of thymidine.

(d) 6-Oxo- $m^5\text{C}$

Another pyrimidine modification in the Y·RY motif consists of employing 4-amino-5-methyl-2,6-[1*H*,3*H*]pyrimidione (6-oxo- $m^5\text{C}$), a 6-keto derivative of $m^5\text{C}$ which effectively is a bidentate hydrogen bond donor to O6 and N7 of target G through its imido and amino groups (Figure 21) [65]. The structural advantages of this moiety are that its pyrimidine like system minimizes anomalous conformational changes in the triplex backbone and the presence of a 5-methyl group contributes to the formation of a potentially important and stabilizing hydrophobic spine. Compared to C and $m^5\text{C}$ analogues, 6-oxo- $m^5\text{C}$ ODNs show triplex t_m values which are largely pH independent in the range 6.4–8.5. In contrast to a t_m difference of 20–25 $^\circ\text{C}$ between C and $m^5\text{C}$ ODNs, the modified 6-oxo- $m^5\text{C}$ exhibits only a 2 $^\circ\text{C}$ difference. Interestingly, in the pH range 6.4–7.0, 6-oxo- $m^5\text{C}$ -containing ODNs show a lower triplex t_m than C and $m^5\text{C}$ analogues, while at pH 7.5 the situation is reversed. This is perhaps a result of the fact that C and $m^5\text{C}$ at pH 6.5–7.0 form charged hydrogen bonds which result in enhanced complex stability, while beyond pH 7.5 a decrease in the extent of protonation leads to weaker triplexes. In 6-oxo- $m^5\text{C}$ -containing triplexes, neutral hydrogen bonds persist and dominate the stability throughout the pH range.

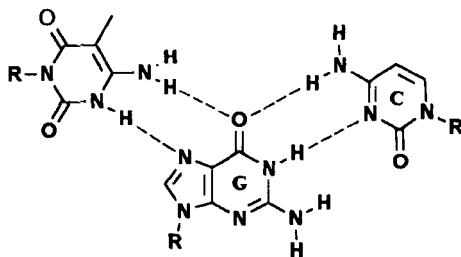


Figure 21 The 6-oxo- m^5C ·GC triad

(e) *N7-dG*

7-(2-Deoxy- β -D-*erythro*-pentofuranosyl)guanine is N7-glycosylated guanine which, upon incorporation into a pyrimidine oligonucleotide, binds to WC GC duplets (Figure 22) with remarkable specificity [66]. The third-strand orientation in such N7-G·GC triplexes is reversed compared to the conventional $R \cdot RY$ motif and becomes parallel to the purine WC strand. N7-dG is specific for GC base pairs, and the stability order of triplets containing this modified base as determined from QACT against a 314-base pair duplex DNA is $N7-G \cdot GC > N7-G \cdot CG > N7-G \cdot AT \approx N7-G \cdot TA$. New parallel-stranded purine motifs can thus be constructed with all N7 purines, thus eliminating protonated C in the third strand.

(f) N^4 -(6-Aminopyridinyl)-2'-dC

Oligopyrimidines containing N^4 -(6-aminopyridinyl)-2'-dC formed stable triplexes with duplexes containing opposing AT, TA, GC and CG base pairs [67]. Triplexes of different stabilities were observed with each base pair combination in the duplex opposing the modified nucleoside (X). The base pairs AT and CG in the complementary duplex showed t_m values 12–14°C higher than TA and GC. Hydrophobic interactions between the pyridinyl ring and neighbouring bases may contribute to the stability in all cases. X·AT and X·CG triplexes may

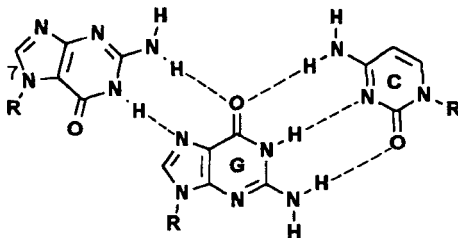


Figure 22 The N7-dG·GC triad in the Y·RY motif

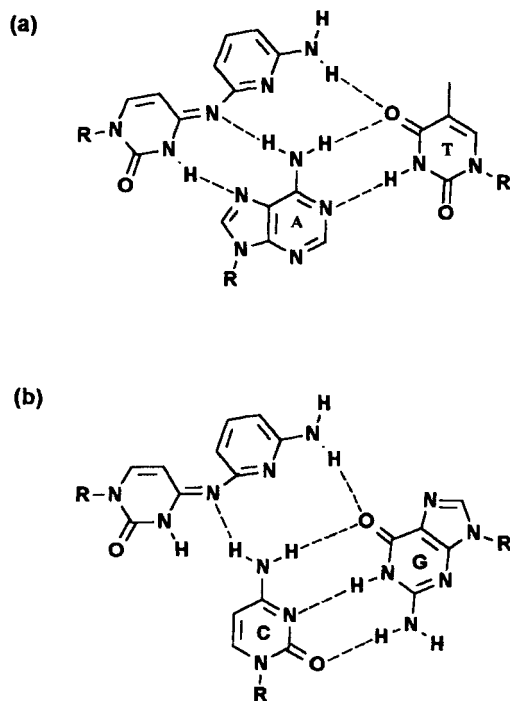


Figure 23 The (a) N^4 -(6-aminopyridinyl)-dC·AT and (b) N^4 -(6-aminopyridinyl)-dC·CG triads in the Y·RY motif

involve hydrogen-bonding interactions as shown in Figure 23, invoking an unusual imino tautomer. Support for the presence of this rare species came from ^1H NMR and UV spectra of the nucleoside monomer.

(g) *Nonnatural heterocyclic analogues*

The use of nonnatural heterocyclic systems circumvents the molecular problems in triplex formation. The rationale is to use a molecular frame that places hydrogen bond donors and acceptors in appropriate positions to form two specific hydrogen bonds to GC pairs while maintaining a deoxyribose phosphate backbone geometry compatible with the Y·RY motif. The nucleosides P1 and P2 are pyrazole analogues which possess a donor–acceptor hydrogen-bonding pattern on one edge, mimicking the N3-protonated cytosine, and can form two hydrogen bonds to G in GC of the duplex without protonation of the base in the third strand (Figure 24) [68a].

From affinity cleavage analysis, the stabilities of the base triplets were found to decrease in the order $\text{P1} \cdot \text{GC} > \text{P1} \cdot \text{CG} > \text{P1} \cdot \text{AT}$, $\text{P1} \cdot \text{TA}$ at pH 7.4, thus demonstrating a sequence-selective binding of P1 to GC. ODNs containing P1

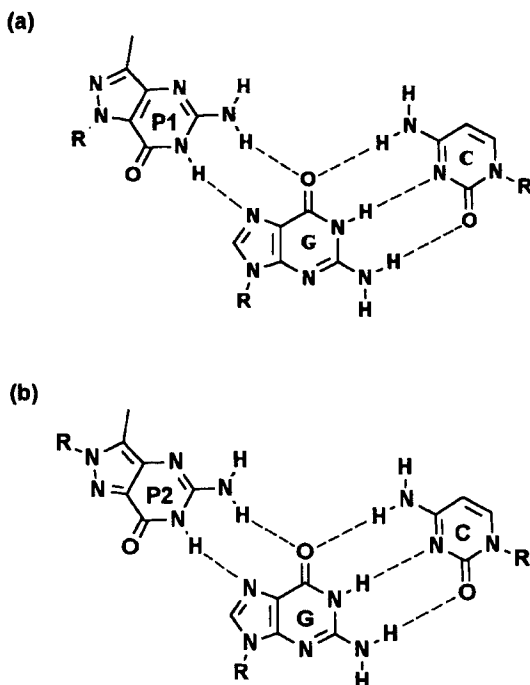


Figure 24 The (a) P1-GC and (b) P2-GC triads in the Y-RY motif

bind to plasmid DNA in a single 15-base-pair site containing five GC base pairs and a single 16-base-pair site containing six contiguous GC base pairs at pH 7.4–7.6. The triplex affinity was even higher than that achievable with six contiguous m⁵C moieties [68b]. There was a marked difference in the behaviour of the isomeric nucleoside P2 in the recognition of the GC base pair, suggesting the importance of the deoxyribose phosphate backbone and the glycosidic conformation in matching the hydrogen bond donors and acceptors of heterocycles for base-specific triple-helix formation. Efficient cleavage was seen when P1 was opposite a GC base pair, and a moderate cleavage for P2 at the same position. The weaker cleavage for the P2-GC triplet indicates an energetically unfavourable distortion of the third-strand backbone, or the methyl group disfavouring the *anti*-conformation of P2 in the triple helix.

The detailed nuclear Overhauser effect (NOE) analysis of contacts between P1 and its flanking thymidine residues involving imino and methyl protons attested to a stacked-in conformation for this base, with a regular right-handed helical conformation [69]. Cross-strand NOE patterns between protons on adjacent triplexes suggested no structural distortions with an altered width for the groove formed by purines and pyrimidines in the third strand. The P1 base was found to be readily accommodated in an otherwise all-pyrimidine third

strand while participating in the hydrogen-bonding interactions consistent with the proposed pairing alignment.

3.3 Recognition of the Pyrimidine Base in the Central Strand

Although ODN-directed triplex formation offers a powerful chemical approach for sequence-specific recognition of double-helical DNA, both Y·RY and R·RY motifs provide only a limited recognition code since they specify for only the purine tracts of double-helical DNA. A general solution to the methods of recognition of mixed sequences containing all four base pairs of duplex DNA has led to the engineering of base components that (1) sterically match the edges of the pyrimidine–purine WC base pairs in the major groove, (2) position the hydrogen bond donors and acceptors to form hydrogen bonds with CG or TA base pairs in the major groove, (3) maintain a backbone geometry compatible with the Y·RY motif and (4) allow the energetically favourable stacking of bases in the third strand.

(a) 4-Phenylimidazole and 4-(3-benzamidophenyl)imidazole

The above logic resulted in the design of the nonnatural base analogues 4-phenylimidazole (D2) and 4-(3-benzamidophenyl)imidazole (D3) [70]. A single bond connecting the two aromatic rings allows rotational degrees of freedom for the nonnatural base to adopt a favourable geometry for interaction with Py–Pu base pairs. While D2 may recognize CG with a single hydrogen bond (Figure 25a), D3 spans both strands of the WC CG base pair (Figure 25b). D2 exhibits a weak binding affinity for all four base pairs, as expected for the natural base triplet mismatches. D3 was found to have a novel binding affinity and sequence specificity different from that anticipated by the above rationale. It recognized both YR base pairs (TA and CG) in preference to RY pairs (AT and GC) in the Y·RY motif, giving rise to an expanded recognition code for D3·TA and D3·CG ($D3\cdot TA \approx D3\cdot CG > > D3\cdot AT > D3\cdot GC$). The results were analysed from binding of an 18-base-pair sequence in SV 40 plasmid DNA, and the differences between D2 and D3 suggested that the benzamido group is responsible for the site-specific interaction; when this is replaced by acetamido, cyclohexanecarboxamide or -naphthamide, diminished affinity and lower specificity are observed, suggesting a probable shape selectivity. Neighbouring base triplets influenced the stabilities of D3·TA and D3·CG triplets, which were most stable when flanked by T·AT and less stable when C⁺·GC was on the 3'-side. The limitations are that D3 does not distinguish TA and CG base pairs and nearest-neighbour interactions matter. It was found that D3 selectively recognizes both TA and CG in WC base pairs in the Y·RY motif. In a triplex containing D3·TA, only the 3'-neighbouring triplet affected stability with the best results obtained from TA and CA followed by AA and GA. The triple-helix complementation was tested in an intramolecular triplex where the

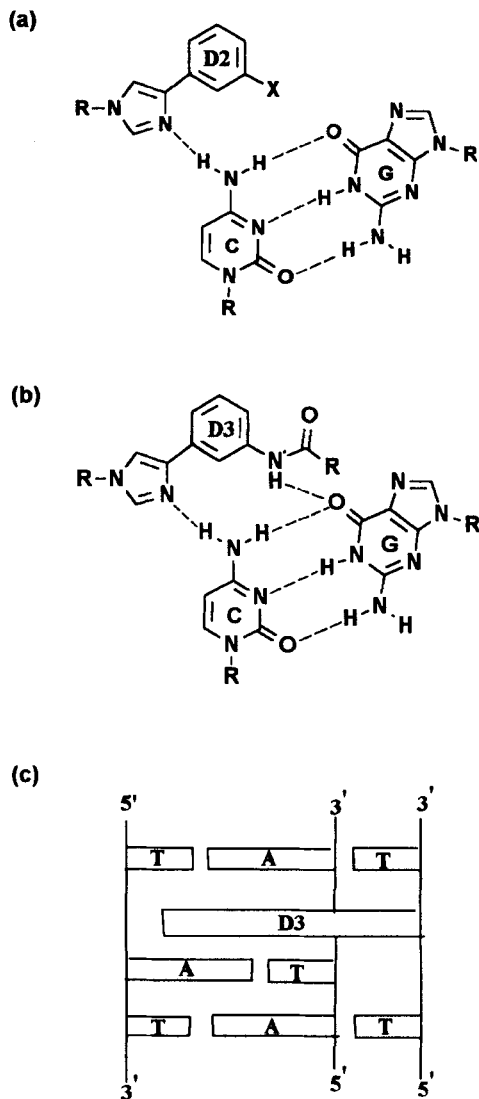


Figure 25 The (a) D2-CG and (b) D3-CG proposed triads forming one and two hydrogen bonds, respectively. (c) Intercalative binding by D3

modified base assumed an HG position. NMR studies indicated that D3 on the third strand binds the duplex in an intercalative mode (Figure 25c) [71]. The binding mode of D3 is unique in that it not only binds by intercalation but also skips a potential base pair to do so. This certainly opens the way to new designs for achieving sequence specificity and stability in mixed DNA sequences.

(b) G·TA triad

Griffin and Dervan [72] examined the relative affinities of common bases for all four pairs within a Y·RY motif by the affinity cleavage method. All the 20 possible base triplet combinations were examined (including those of I), and it was found that in addition to the expected T·AT and C⁺·GC triplexes, the next-highest affinity was that of G·TA (Figure 26). This, apart from extending the triple-helix specificity to three of the four base pairs, indicated that the specificity may differ for each structural motif because of a different alignment of the deoxyribosyl phosphodiester backbone and consequently the heterocyclic bases along the major groove. Thus, within a pyrimidine motif, G prefers to bind to the TA base pair, whereas in the purine motif G binds the GC base pair. The base-pairing structure of a single G·TA triplet present in a 32-base DNA oligonucleotide capable of forming an intramolecular triple-helical structure was investigated by NMR [73, 74]. It was shown that this triplet involves a single hydrogen bond from the G amino group to O4 of T, leaving the guanine imino proton free. The G in the third strand adopts a C3'-*endo*-sugar pucker, which effectively orients the guanine such that its sugar is near the thymine methyl group. A purine base in an otherwise all-pyrimidine third strand causes distortion in the helical structure, which is possibly relieved by adopting an N-type (C3'-*endo*) sugar pucker within a Y·RY motif [73, 74]. The G·TA triplet is significantly more stable than other noncanonical triplets, but less stable than either T·AT or C⁺·GC. The nature of the neighbouring triplet affects the stability of triplexes containing the G·TA triplet. While T·AT neighbours tolerate G·TA, two neighbouring C⁺·GC triplets decrease the stability of the triplexes. The stacking interactions play an important role in the stability of noncanonical triplets in DNA triplexes.

(c) T·CG triad

An addition to the recognition of the WC base pairs AT, GC and TA by T, C⁺ and G bases in the third strand (T·AT, C⁺·GC and G·TA) is the identification

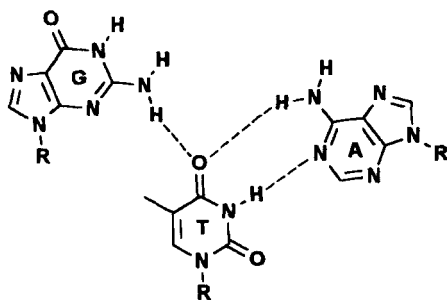


Figure 26 The G·TA triad in the Y·RY motif

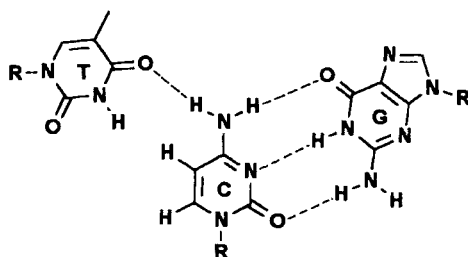


Figure 27 The T·CG triad in the Y·RY motif

of the triad T·CG (Figure 27) [33, 39a]. This extends the recognition scheme to all four combinations of WC base pairs. The preference for a pyrimidine in the third strand was attributed to a lower steric hindrance [39a]. T·CG was preferentially stabilized over C·CG under physiological conditions. The occurrence of such triplets involving HG interaction of two pyrimidines (U·CG) *in vivo* was found in sequences of phylogenetically conserved group I introns [75]. Thus, T shows degenerate recognition of both AT and CG WC base pairs (T·AT and T·CG), with the former more stable than the latter. The solution structure of a Y·RY triplex containing the T·CG triplet was determined by two-dimensional NMR [76]. Evidence for a single hydrogen bond between O2 of T and the N4 amino of C in the WC CG base pair was found. This produces large variations in the helical twist at dinucleotide steps involving T and localized perturbations around C in the central purine-rich strand, similar to those changes seen in triplexes containing the G·TA triplet.

(d) Y/R·UA triad

Triplex formation by oligodeoxyribonucleotides involving formation of X·UA triads in the Y·RY motif has been systematically investigated by Miller and Cushman [77]. Triplexes are observed in X·CG when X is T or U, in which the C4 carbonyl of T or U serves as a hydrogen bond acceptor for the N4 amino of C. In the case of X·TA the triplex was observed only when X was G, whereas in the X·UA system stable triplexes were seen when X was C, m⁵C, T or U, and thus the UA duplex pair is a much more versatile participant in triad formation than TA. A possible hydrogen-bonding scheme is shown in Figure 28. In the case of C or m⁵C, N3 protonation provides a hydrogen bond to the C4 carbonyl of U of the duplex. Interestingly, as compared to G·TA stable triads, G·UA triads were not formed, indicating that factors in addition to the availability of a C4 carbonyl hydrogen bond acceptor group influence the formation of G·TA versus G·UA triads.

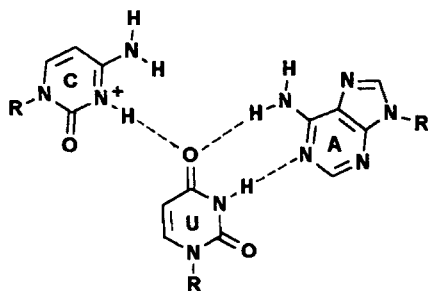


Figure 28 The $C^+ \cdot UA$ triad in the $Y \cdot RY$ motif

(e) ψ -Pyrimidines

On the basis of isomorphous base-pairing geometries and novel hydrogen-bonding recognition schemes, various triple-stranded helices may be generated at single-strand target sites of unrestricted sequence by addition of two ODN probes. In a remarkable theoretical paper, Trapane and Ts'O [78] have proposed the recognition of any single target DNA strand ODN by two probe strands (Figure 29), one of which is a complementary strand to the target DNA generated by use of standard purine nucleosides G and A and the modified pyrimidine nucleosides ψC , ψiC and ψU . The major groove of the initial duplex will have a unique configuration of hydrogen-bonding sites for recognizing the second probe strand. In these patterns, either a homopyrimidine or a homopurine third strand binds in the major groove of the duplex formed by target and probe strands. The design was achieved by identifying 10 distinct geometries, each one consisting of four isomorphous base triads which recognize C, G, A or T(U) in the target strand. To maintain specific hydrogen bonding and to construct isomorphous triads, Trapane and Ts'O used several nonstandard bases (ψC , ψiC , iC , ψU and iG). The hydrogen-bonding interactions involved in base triads for base pairing are those well recognized within the common bases in nucleic acids. The proposed model involving binding of synthetic probe strands (with nonstandard bases) to recognize a single strand with a sequence of any arrangement of natural bases has wide potential application. It will unravel several novel duplex hydrogen-bonding patterns hitherto unknown in standard WC duplexes. The formation of a target strand–second strand (first probe) duplex will also generate a site for the third strand (second probe), which is unique in cellular duplex DNA, thus increasing the recognition fidelity. Hence, triple-strand formation at single-stranded target sites of any sequence will be possible. Experimental and theoretical results demonstrated that triple-helix formation is highly sequence specific, at least as high as for double-helix formation.

(a)	Target	Probes	
		P ₁	P ₂
		↑	↑
	A	ψU	C
	C	G	ψiC
	G	ψiC	iC
	U	A	T
	↓		
	WC	HG	

(b)	Target	Probes	
		P ₁	P ₂
		↑	
	A	ψU	G
	C	G	iG
	G	ψiC	I*
	U	A	A
	↓		↓

Figure 29 Recognition of a single target strand with two probe strands. The target strand has only natural bases, while the probe (P₁ and P₂) strands have natural and pseudobases. (a) Parallel triplexes form P₂·P₁X triads, each containing two pyrimidines and one purine in any combination. (b) Antiparallel triplexes form P₂·P₁X triads, each with two purines and one pyrimidine in any combination. I* = 5-aza-7-deazainosine

Use of pyrimidine ψ-isonucleoside residues on the second strand is structurally essential to the proposed model. These provide an extra hydrogen-bonding site in the major groove of a WC-type duplex for third-strand recognition, which can alleviate the restriction on triplex formation to pyrimidine–purine target sites. All standard bases pair with ψU through the formation of two hydrogen bonds. The donor–acceptor patterns of ψU and ψiC in the major groove of a duplex in which they are WC base paired to A are different from those of UA and CG, respectively (Figure 30). Such patterns can

be used in specific recognition sites in biological systems. The species ψC has two distinct tautomeric forms, allowing it to base pair either via WC ($\text{G}\psi\text{C}$) (Figure 18b) or HG ($\psi\text{C}\cdot\text{GC}$) (Figure 18a) hydrogen bonds.

The possible success of the strategy envisaged in the model of Trapane and Ts'O has been demonstrated by the recognition of a mixed TA target sequence by two probe strands containing pseudodeoxyuridines in polypurine stretches and a polypyrimidine methyl phosphonate backbone, respectively [79]. This has also demonstrated base-pairing interactions in the $\text{C}\cdot\psi\text{UA}$ triad (Figure 31), and that a homopyrimidine strand can bind a WC duplex of mixed purine and pyrimidine content. More examples using these principles will certainly emerge to exploit the full versatility of molecular recognition in natural and nonnatural nucleobases.

(f) *Inverted motif*

An inverted motif for the oligonucleotide triplex ($\text{R}\cdot\text{YR}$) is possible when the central position of a triad is occupied by pseudouridine, as in $\text{A}\cdot\psi\text{UA}$ (Figure 32) [80]. As shown by a UV melting experiment, successful triplex formation can be achieved when this inverted triad is accommodated in $\text{T}\cdot\text{AT}$ triplexes. The two A moieties in the inverted repeat are not likely to be identical, and the issue is yet to be resolved as to whether the two have different glycosidic torsions and so on. These examples involving pseudopyrimidines in the central position have really extended the triplex recognition motifs and allow the construction of additional patterns with pyrimidines involved in nonstandard WC pairs.

3.4 Base Modifications in the Purine Motif ($\text{R}\cdot\text{RY}$)

The base modifications discussed so far are mostly concerned with those permissible in the pyrimidine motif ($\text{Y}\cdot\text{RY}$). In the purine motif ($\text{R}\cdot\text{RY}$), the permitted triads are $\text{A}\cdot\text{AT}$, $\text{T}\cdot\text{AT}$ and $\text{G}\cdot\text{GC}$, and the following examples illustrate the permissible base modifications in this motif.

(a) *2'-Deoxynebularine*

Nebularine (N) is a naturally occurring nucleoside found in certain mushrooms. In its *anti*-glycosidic conformation it would allow favourable stacking interactions in the third strand, but it provides a single hydrogen bond acceptor (N1) site to the exocyclic amino group of either cytosine or adenine. 2'-Deoxynebularine (dN) was shown to recognize cytosine (Figure 33) or adenine of WC CG or AT base pairs through one specific hydrogen bond [81]. The stability order of $\text{N}\cdot\text{CG}$, $\text{N}\cdot\text{AT}$, $\text{N}\cdot\text{GC}$ and $\text{N}\cdot\text{TA}$ was studied in the purine motif at pH 7.4. The high specificity under physiological conditions was demonstrated by its binding to a 15-base-pair purine tract within plasmid

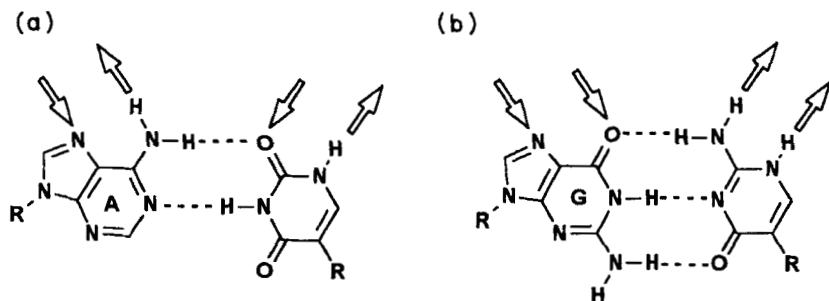


Figure 30 Altered arrays of hydrogen-bonding sites available in the major groove of duplex DNA with WC pairing of ψ -bases. Compare (a) A ψ U and (b) G ψ iC with AT and GC in Figures 7 (b) and 7(d), respectively

DNA. T is the only natural base that binds to some extent to CG base pairs in the R-RY motif; however, it also interacts equally well with the AT base pair. In contrast, 2'-deoxynebularine can bind with CG as strongly as T, but shows a weak binding with AT unlike T, making dN more specific for CG than T. The formation of a T-CG triplet in an intramolecular R-RY motif is supported by NMR studies which indicated slight perturbation around the T-CG site extending to two adjacent base triplets but with no overall change [82]. T-CG inversion triads have also been studied in a wide number of sequences with identical results [83].

(b) 2'-Deoxyformycin A

Formycin A is a naturally occurring nucleoside antibiotic with structural similarity to adenine. It has a C-glycosidic bond and consequently it is capable of donating two hydrogen bonds to a biacceptor (Figure 34) (such as G or A), and hence is homologous to G. Analysis by the band-shift method indicated that a 2'-deoxyformycin-A-containing ODN displayed a 10-fold increase in affinity as compared to its unmodified control [84]. This indicates an alternative

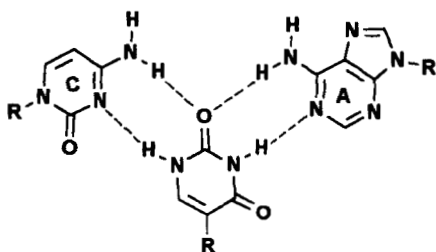


Figure 31 The C- ψ UA triad in the Y-RY motif

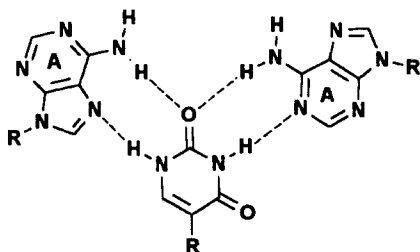


Figure 32 The A-ψUA triad in the Y·RY motif

way to accommodate CG inversion sites within target sites for the antiparallel R·RY motif.

(c) 7/9-Deaza-2'-dG

In contrast to the Y·RY triple-helix motif, the recognition of a duplex target by the R·RY motif faces another serious drawback. There is evidence to show that the G-rich ODNs (third strands in the R·RY motif) in such triplex-forming oligonucleotides (TFOs) have the potential to self-associate and form stable G tetrads (Figure 35a) in the presence of alkali cations through strong stacking interactions and coordination of the four O6 atoms of the G moieties with the alkali cations [85]. As both Na^+ and K^+ are present in significant amounts in physiological environments, G-rich ODNs may self-associate to some degree *in vivo*. The formation of such structures may reduce the ability of TFOs to bind to the intended target duplex, depending on the triplex–tetraplex equilibrium, thus reducing their therapeutic efficacy. In the recent literature, there have been reports of some efforts to circumvent this shortcoming in the R·RY motif through base modifications.

One approach is to replace the hydrogen bond acceptor site N7 with carbon, as in 7-deaza-2'-dG [85a], or convert it into a donor site, as in 9-deaza-2'-dG (Figure 35b) [86]. Both modifications result in a decrease in the capacity of the

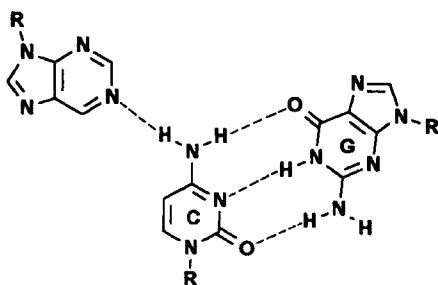


Figure 33 The dN·CG triad in the R·RY motif

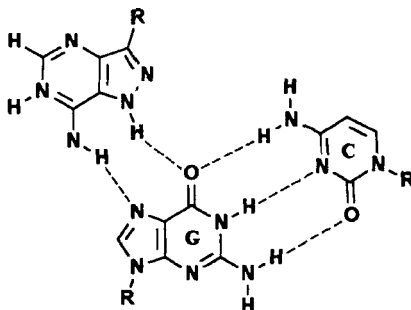


Figure 34 The formycin-CG triad in the R·RY motif

ODNs to form tetraplexes under physiological conditions. However, both of these ODNs were also found to form triplexes with decreased stability.

(d) 2'-Deoxy-6-thioguanosine

Another way of preventing G tetrad formation involves the incorporation of 2'-deoxy-6-thioguanosine in place of dG, since the thio group can interfere with the coordination of alkali cations by reducing the strength of the hydrogen bond. Additionally, the larger van der Waals radius of sulfur relative to oxygen might lead to significant steric repulsion in the tetrad. It was recently demonstrated [86] that partial incorporation of S6-dG in TFOs is effective in inhibiting the formation of dG tetrads in dG-rich ODNs, thus facilitating triplex formation in potassium-containing buffers. The incorporation of 7-deaza-6-thioxanthosine into G-rich ODNs did not lead to any enhancement in triplex formation [85a]. This strategy was further combined with the imidazole nucleosides to recognize TA inversion sites in the *neu* gene by triple-helix formation [87].

(e) 7-Deaza-2'-deoxyxanthosine

A second limitation of antiparallel triplexes in the R·RY motif is that their high-affinity binding requires that the target contain at least 60–65% of G in one strand. The TFOs containing mixed G and T in the presence of K^+ and Mg^{2+} do not bind to the target duplex. However, if T is replaced by the purine analogue 7-deaza-2'-deoxyxanthosine (Figure 35c), stable triplexes are formed with a 100-fold greater affinity for the target duplex than shown by the unmodified T [87]. This purine analogue of T might be disrupting the formation of G tetrad structures of the modified ODNs, consequently favouring triplex formation. 7-Deaza-2'-deoxyxanthosine was found to be unique in its ability to enhance triplex stability in the antiparallel motif. A different replacement of T is by its benzo derivative, namely quinazoline-2,4-dione, which may provide additional stacking interactions. This choice,

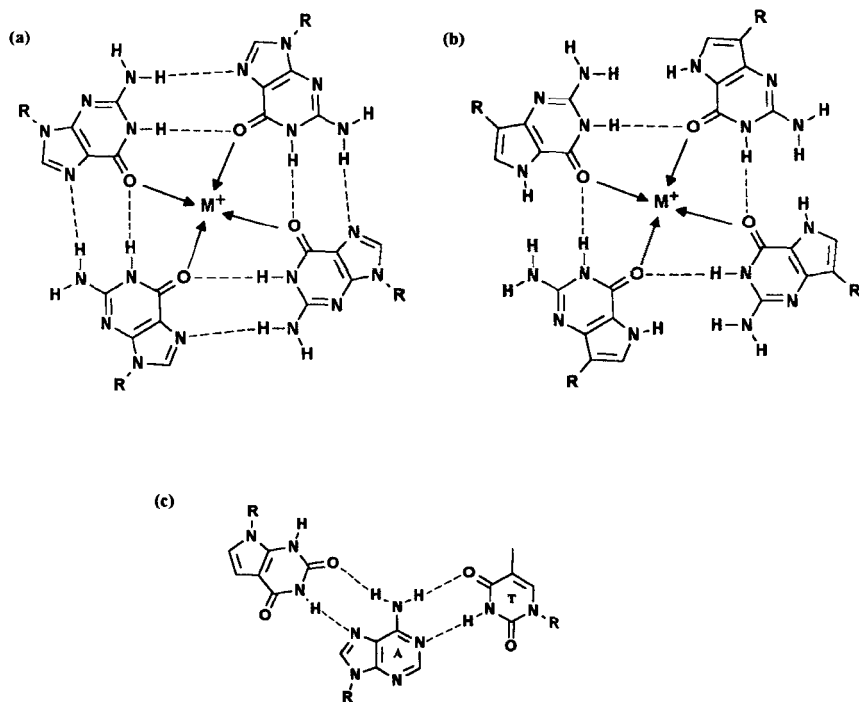


Figure 35 Some G tetrads formed by (a) dG and (b) 9-deaza-2'-dG. (c) The 7-deaza-2'-deoxyxanthosine-AT triad in the R·RY motif

however, caused decreased stability of triple helices in both parallel and antiparallel motifs [88a]. The nonnatural heterocycle pyrido[2,3-*d*]pyrimidone nucleoside [88b] was found to recognize the AT base pair with high specificity. The various nucleobase modifications and their effects on triplex stabilities are summarized in Table 1.

3.5 Triplex Formation by α -Oligonucleotides

Natural nucleic acids are constructed from β -anomers of nucleotide units. Oligonucleotides containing α -anomeric nucleobases have been synthesized and their binding to double-stranded DNA investigated by a number of techniques. α -Oligopyrimidines form triplexes with duplex DNA with the orientation of the third strand depending on the sequence. In the Y·RY motif, an α -T_n ODN binds parallel to poly(dA), while an α -ODN containing both T and C binds antiparallel to the target duplex and engages in reverse HG interactions [17]. This avoids the distortion of the backbone, resulting in a parallel orientation since T·AT and C⁺·GC are not isomorphous in the reverse

HG configuration. Triple helices from α -ODNs are less stable than those from the β -analogues, but can be stabilized by attaching intercalating agents at the 3'-end. The nuclease resistance of α -ODNs makes them attractive for development as *in vivo* therapeutic agents.

4. TRIPLEX STABILIZATION BY BACKBONE MODIFICATIONS

Delineation of all factors contributing to triple-helix stability is pivotal to the application of ODN-directed, sequence-specific recognition of duplexes for *in vivo* applications. Structural modifications of the sugar phosphate backbones in ODNs provide an excellent opportunity to alter the conformations of triplex components to enhance stability, introduce nuclease resistance and increase the cellular permeability of ODNs. While the use of RNA strands instead of DNA is the simplest variation in backbone structure, chemical modifications of the natural system include introduction of methyl phosphonates and phosphorothioates. Phosphorothioates are successfully emerging as first-generation antisense lead compounds. Currently, several dephosphono analogues which are nonionic and neutral are being designed, synthesized and studied as potential antigene and antisense agents.

4.1 RNA–DNA Hybrid Triplexes

In principle, functional triplexes can be formed from some combination of RNA (R) and DNA (D) strands, and eight such permutations, wherein each strand is either DNA or RNA, are possible for each motif. These are D·DD, R·DD, R·DR, D·DR, R·RD, R·RR, D·RR and D·RD. DNA can adopt either A-form or B-form geometry (corresponding to C3'-*endo*-sugar and C2'-*endo*-sugar puckers), whereas RNA overwhelmingly prefers the A-form. Non-covalent RNA–DNA hybrid duplexes adopt an overall A-form as revealed by X-ray crystallography, whereas in solution only the RNA strand in the hybrid appears as the A-form [89]. In comparison, solution NMR studies of DNA triple helices have shown that the pyrimidine strands adopt both C3'-*endo*-sugar and C2'-*endo*-sugar puckers, while the purines are completely in the C2'-*endo*-sugar form [90].

Systematic analyses of the stability of various RNA–DNA hybrid triplexes by electrophoretic gel mobility, affinity cleavage, UV melting and molecular modelling techniques [91, 92] have been reported. Among the eight possible combinations for the Y·RY motif, the most stable is the R·DR hybrid, and the order of stabilization is shown in Figure 36. Comparison of triplex stabilities with the stabilities of underlying complementary WC duplexes has led to the discovery of an important anticorrelation between the two: relatively stable duplexes give rise to unstable triplexes, the only exceptions being in the RD and

Table 1 Third-strand base modifications and duplex recognition specificity^a

R or Y	AT	TA	CG	GC	UA	Reference
T	+		+		+	16, 33, 39a, 77
U			+			77
A	+				ψUA	80
C				+	+	77
G		+		+	+	16, 72
m ⁵ C				+	+	77
p ⁵ C				+		50
cm ⁵ C				+		52
2'-Methoxy-m ⁵ C				—		51
cT	—					52
N ⁴ -Alkyl-C				—		53, 54
N ⁴ -Spermine-C				+		55
N ⁴ -Ethano-C				+		57
6-Amino-C				—		58
ψiC				+		59
8-Oxo-dA				+		59
8-Oxo-dG	+					64
6-Oxo-m ⁵ C				+		65
N7-dG			+	+		66
N ⁴ -(6-Aminopyridimyl)- dC	+		+			67
P1, P2			+	+		68
D2			+			70
N	+		+			81
F			+			84
7/9-Deaza-2'-dG				+		85, 86
7-Deaza-dX	+					85a
6-Thio-G				+		86
Pyridopyrimidone	+					88b

^aThe entries + and — indicate stabilization and destabilization of triplexes consisting of specific triads relative to control triads having no chemical modifications.

RR duplexes and the derived triplexes. This could be a consequence of stable duplex structures which need more energy to become distorted to accommodate the third strand. The stability order of various RNA–DNA hybrid triplexes indicates that duplexes with DNA in the purine strand readily bind to either RNA or DNA to form triplexes. In contrast, a purine RNA duplex binds only RNA on a third strand. It was recently shown that RNA cannot be a part of a triplex with the R·RY motif [92c]. These studies point to the fundamental role of sugars in controlling nucleic acid recognition through conformational switches. Since RNA–DNA hybrids are cellular targets for a number of

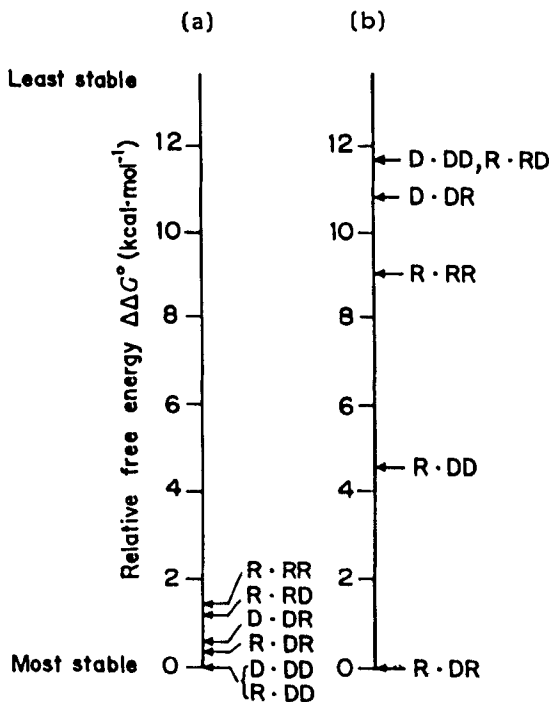


Figure 36 Relative stabilities of RNA–DNA hybrid triplexes in the Y·RY motif. (a) Data from Ham and Dervan [92a], Escude *et al.* [92b] and Semerad and Maher [92c]. (b) Data from Roberts and Crothers [91]

important enzymes including RNAase H, reverse transcriptase and so on, studies on RNA–DNA hybrid triplexes have an important bearing for their physiological applications.

4.2 Methyl Phosphonates and Phosphorothioates

Short oligodeoxynucleotides containing methyl phosphonates were shown to form stable triplexes [93]. However, it was subsequently demonstrated that methyl phosphonate ODNs require a >10-fold higher concentration for binding to duplexes relative to the natural phosphodiester. Methyl phosphonates of d(CT)₈ formed triplexes with the unmodified duplex d(AG)₈d(CT)₈ at pH 4.8, which is lower than that of the control d(CT)₈ at pH 5.6. It is possible that a lower stability and pH requirement for triplex formation from nonionic methyl phosphonates may arise owing to the absence of favourable interactions between the negatively charged phosphodiester backbone and positively charged C⁺. In a contrasting report

[94], it was shown that in the Y·RY motif comprising the T·AT triplex, replacement of any of the chains with the corresponding methyl phosphonates failed to result in triplex formation as detected by UV, t_m or gel analysis. Further studies are needed to assess the real potential of methyl phosphonate backbones in triplex stability.

The ability of homopyrimidine phosphorothioate (Y_{11}) oligonucleotides to recognize and bind a DNA hairpin duplex was investigated using PAGE, CD and UV melting techniques [95]. The all-thioate ODN exhibited a 17°C destabilization compared to the all-phosphate ODN ($\sim 2^\circ\text{C}$ t_m depression per thioate linkage). A van't Hoff analysis indicated a free energy depression of 2.7–5.4 kcal mol⁻¹ depending on the number of thioate linkages in the third strand. Some 20-mer ODNs with a 45% C content and 10–20% of thioate groups strongly repressed transcription of bacteriophage T7 RNA polymerase using this strategy.

4.3 Dephosphono Congeners

The formacetal and thioformacetal linkages (Figure 37) have been shown to be competent for sequence-specific triple helix binding when placed in a m⁵CT context [96]. Between these two, 3'-thioformacetal is better than formacetal, but shows a lower binding compared to the unmodified analogue. The binding of 3'-thioformacetal to single-stranded RNA, single-stranded DNA and double-stranded DNA was enhanced when used in conjunction with the modified nucleobase C5-propyne-dU [97]. Thus, heterocyclic and backbone modifications can be mutually compatible, and such a combinational approach may provide a useful solution since these ODNs possess both nuclease resistance and better cellular permeability properties. More such examples are sure to follow rapidly.

4.4 Peptide Nucleic Acids

The most promising backbone modification involves the newly emerged peptide nucleic acids (PNAs) which have nucleobases on an achiral peptide backbone (Figure 38) [98]. PNAs containing mixed purine and pyrimidine bases bind to complementary DNA or RNA strands by WC base pairing to yield duplexes of higher thermal stability than the corresponding DNA–DNA or DNA–RNA duplexes [99]. An all-thymine PNA (PNA-T₁₀) was shown to form stable, sequence-specific complexes of unprecedented thermal stability with DNA dA₁₀ [100]. The cause for this turned out to be the formation of a (PNA)₂–DNA triplex in which a single DNA strand was bound to two PNA strands, one via WC and the other by HG base pairing. When added to the preformed DNA duplex dA₁₀dT₁₀, PNA-T₁₀ again formed the triplex (PNA)₂–DNA by strand displacement binding [101]. PNA-T₁₀ first displaces dT₁₀ from the duplex to result in the triplex. With PNAs containing mixed C and T,

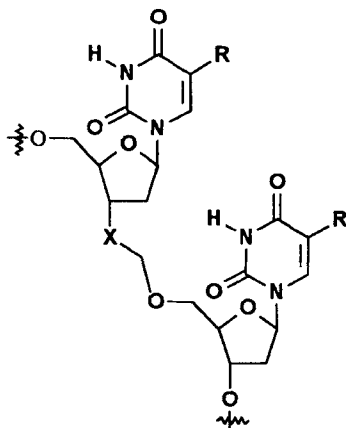


Figure 37 Dephosphono analogues used in triplex formation. Substituents include X=O, R=Me; X=O, R=C≡CMe; X=S, R=Me; and X=S, R=C≡CMe

strand displacement triplex binding was pH dependent in the pH 5–7 range. Triplex formation by strand displacement is restricted to all-pyrimidine PNAs and is not observed with mixed purine–pyrimidine PNAs, which give only duplexes [102]. Among the various PNA backbones that have been synthesized by using glycine–ethylenediamine (eda), β -alanine–eda and glycine–propylenediamine combinations with bases conjugated through an acetyl or propionyl moiety (Figure 38), the best turned out to be the one with the glycine–eda–acetyl combination [102].

4.5 Triplexes with Interchain Linkers

Covalent connection of the ODNs involved in triplexes by nonnucleotide linkers reduces the molecularity of complexation from biomolecular to monomolecular. Owing to a consequently more favourable entropic factor, thermodynamic stabilization of triplexes may be achieved. Such a strategy was employed [103] for the recognition of a single-stranded DNA target by interconnected bis(DNA) strands which form both WC and HG hydrogen bonds. The target single-stranded DNA was 29 nucleosides long with a stretch of 16 purines, and the recognition DNA was derived by linking two pyrimidine tracts (Y_{18} and Y_{16}) by a hexaethylene glycol bridge (Figure 39). Y_{18} formed WC base pairing, while Y_{16} gave HG bonding. Acridine linked at the 5'-end of the Y_{16} stretch further locked the triple-helical system by intercalation.

In a conceptual variation, linkers containing a rigid spacer such as terephthalamide were used to cap a pair of complementary ODNs and thereby enhance the stability of the derived duplexes [104]. When a pair of thymidylate oligomers were joined with this linker, the compound exhibited an unusually

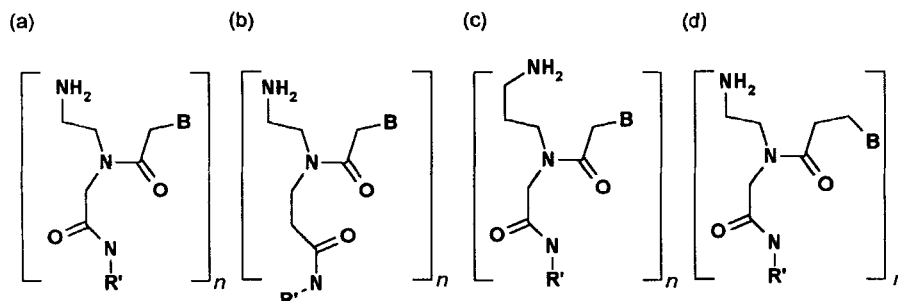


Figure 38 Peptide nucleic acid backbones: (a) glycine–ethylenediamine, (b) β -alanine–ethylenediamine and (c) glycine–propylene diamine. All have bases (B) linked by acetyl groups, except for (d) which has a propionyl linker

high affinity for an oligo(dA) strand, leading to a stable bimolecular triplex in the Y·RY motif. This linker was also used to join two complementary strands and a third strand sequentially to form an intramolecular triplex with high stability.

Another example of the entropic stabilization of triplexes through conformational rigidity is offered by the use of biocyclo-DNA (bc-DNA) (Figure 40), which contains an additional ethylene bridge between C3' and C5' of the ribose sugar [105]. This restricts the freedom of rotation around the C3'–C4' and C4'–C5' bonds. In duplex studies, it was noticed that while bcdT₁₀ paired less strongly to complementary DNA and RNA than its natural analogue, bcdA₁₀ formed stronger triplexes with dT₁₀ in the Y·RY motif compared to dA₁₀. Other examples of triplex stabilization by conformational restriction involve the use of riboacetal DNA analogues [106a] and a propanediol linker [106b] which skips destabilizing interruptions in a target duplex.

4.6 Circular DNA Triplexes

The interstrand connections described above provide entropic stabilization by a preorganization of the components. An ingenious way to achieve this more efficiently was demonstrated by D'Souza and Kool [107] using circular DNA. In this strategy, the two binding domains are interconnected by two pentanucleotide DNA loops (CACAC) to form a single-stranded circular DNA. Two polypyrimidine stretches (2Y₁₂) in the circular DNA can bind a polypurine sequence (R₁₂) (Figure 41a) using the Y·RY motif. This recognition of single-stranded targets by circular DNA was thermodynamically favoured by a higher enthalpy of complexation, greater loss of entropy and larger association constants ($>10^3$ – 10^4 M^{–1}) compared to appropriate controls. Other interesting features included destabilization of the triplex by added

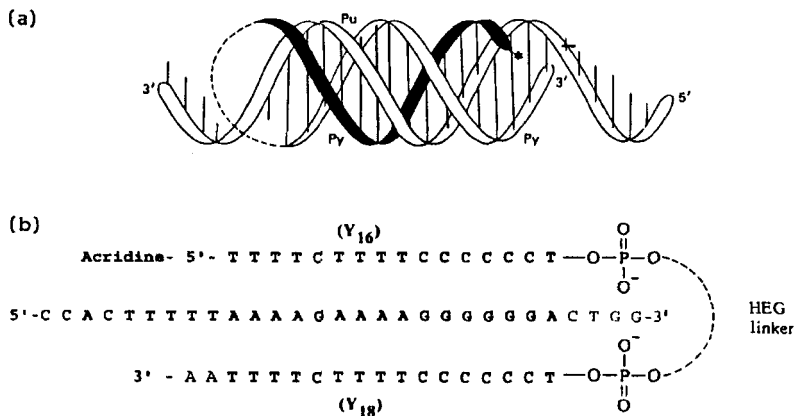


Figure 39 (a) Schematic representation of a triple helix constituted from a single-stranded ODN with a homopurine stretch and a dimeric ODN linked by a hexaethylene glycol (HEG) linker. (b) The sequences of ODNs involved in triplex formation, indicating WC and HG complements

ethanol, in contrast to linear duplexes, and a large difference in the pK_a values of C in the loop and helix regions ($\Delta pK_a \approx 2-3$). These findings suggest that the binding event is not compatible with an ethanol-inducible B-form \rightarrow A-form conformational change, and that the local environment has an effect on the basicity of C. Spermine was 100 times more effective than Mg^{2+} , which was 300 times more stabilizing than Na^+ on a molar basis.

The recognition of polypyrimidine-rich sequences by interconnected polypurines (Figure 41b) in the R·RY motif encounters problems owing to competition from stable secondary structures of polypurines. However, the use of appropriate circular DNA circumvents such limitations in the recognition of pyrimidine sequences [108]. The circular oligomer with polypurine domains binds the target pyrimidine strand with a high thermal stability compared to the hairpin control ($t_m = 68.4^\circ C$, $\Delta t_m \approx 5-6^\circ C$). An added advantage is that the same circular DNA also binds a single-stranded pyrimidine RNA with the same high affinity ($t_m = 65.3^\circ C$). Thus, both DNA and RNA strands can be bound with the same ligand in the R·RY motif, in contrast to the RNA-dependent and DNA-dependent stabilities of the Y·RY motif. As expected for the R·RY motif, no pH dependence of binding is observed.

An extension of this concept is in the design of a 35-mer circular DNA which can bind to different polypurine sequences, leading to a total recognition of 48 nucleotides [109]. The 35-mer circular DNA contained sequences related by a pseudomirror plane of symmetry containing domains for binding in the forward (5'–3') or reverse (3'–5') direction by simply switching the roles of WC and HG domains. In addition to a high binding strength and specificity, circular DNA triplexes offer the practical benefits of being stable to biological

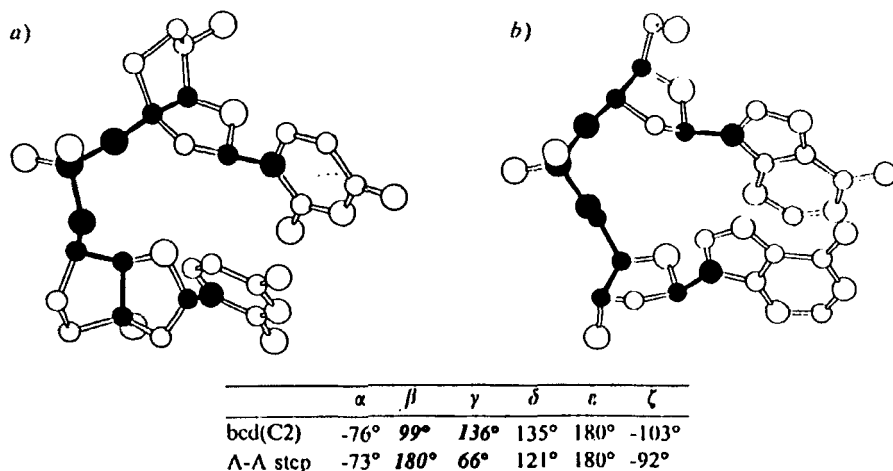


Figure 40 Comparison of the partial backbone structures of (a) bicyclo-DNA (bcd) and (b) unmodified DNA (A-A step). Reproduced by permission from *Helv. Chim. Acta*, 77, 716 (1994)

media and accelerating duplex unwinding. The multisite binding of circular DNA may be useful in devising ways for the inhibition of gene expression by targeting more than one site in a gene or more than one gene in an organism.

The origin of the large differences in stability of RNA and DNA double and triple helices has been addressed to delineate the effects of C5 methyl groups and 2'-hydroxy groups using bimolecular triplexes formed from circular pyrimidine ODNs with purine target strands [110]. It was found that the two types of effects are independent of one another, with C5 methyl groups stabilizing in all cases and 2'-hydroxy groups stabilizing or destabilizing depending on the type of complex. The two effects vary with secondary structure and reinforce or oppose each other in their influence on the triplex stability of hybrids.

4.7 Alternate-Strand Recognition

A strategy for triplex recognition in duplexes containing alternate stretches of homopurine and homopyrimidine sequences consists of engineering third-strand ODNs with polarity inversion. These ODNs, termed "switch back ODNs", contain linker elements replacing the normal 3'-5' phosphodiester bond; they enable the inversion of strand direction required for the recognition of alternate stretches (Figure 42). Triplex formation at adjacent, alternating sites by 5'-5'-linked oligomers can be stabilized in the presence of ethidium bromide [111]. ODNs containing a 3'-3' internucleotide junction made from a xylose nucleoside linker (Figure 42b) bind on opposite strands of duplex DNA

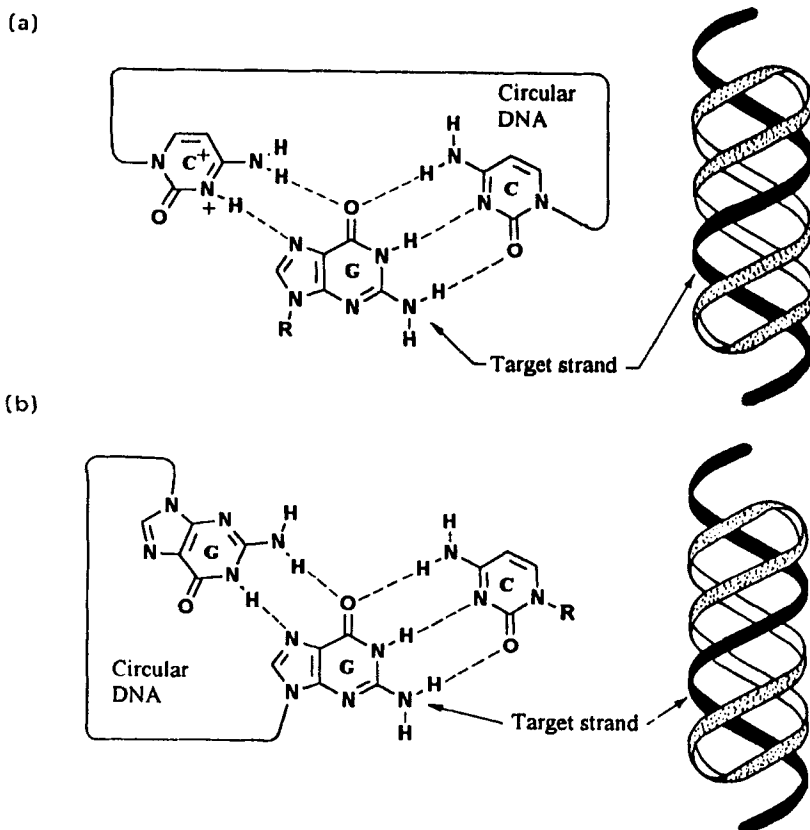


Figure 41 Strategies for binding a single-stranded ODN by circular DNA for (a) purine recognition and (b) pyrimidine recognition

with a high degree of cooperativity [112]. ODNs have also been linked through their 3'-terminal nucleobases via N4 of C with short alkyl chains to achieve triplexes with alternate-strand recognition (Figure 43) [113a]. Such nucleobase tethering via 5'-terminal bases has been reported recently, but without any details of triplexing ability [113b]. Alternate-strand DNA triplex formation has also been achieved using short, acridine-linked ODNs in which the intercalation of acridine at GT or AC steps stabilizes the triplex [114].

4.8 Cooperativity in Triplex Formation and Triplex-Directed Chemical Reactions

ODN-directed triplex formation at adjacent sites on a duplex is subject to significant cooperative effects. As detected by QACT, a 20-fold enhancement in

K_a was observed for an undecamer pyrimidine binding in the presence of a neighbouring bound third strand (Figure 44) [115]. A further increase in cooperativity was achieved by the use of ODNs containing the modified bases m^5C and 5-(1-propynyl)-dU (p^5dU), which are known to enhance the triplex stabilities by increasing stacking effects (Figure 44b) [116]. The equilibrium binding constant of an octamer in the presence of a neighbouring bound octamer, both modified ODNs, was enhanced by a factor of 40 compared to the control, as detected by QACT. This enhancement is due to a favourable stacking overlap at 5'-3' junctions, in which a 5'T p^5dU 3' stacks better than a 5' p^5dUT 3'. Cooperativity was not seen when the two sites were separated by one base pair. The sources for such cooperative [115] interaction may include the propagation of conformational transitions between adjacent sites and base stacking of 5'-terminal and 3'-terminal bases. This effect has been usefully employed to achieve chemical ligation (Figure 45) of two 15-mer ODNs bound to a 37-base-pair duplex at neighbouring sites in a head-to-tail fashion in the Y·RY motif [117]. The ligation was carried out using imidazole-cyanogen bromide. This provides a duplex template for macromolecular information transfer of a nonself-replicating type.

The third strand of a triplex when equipped with an electrophile (Figure 46) such as an aromatic chloroethylamine [118a], *N*-bromoacetyl [118b] or ethano- m^5dC [57] reacts with the proximal N7 of a G on the duplex, leading to a covalent linking of the ODN to the target sequence. Site-specific incorporation

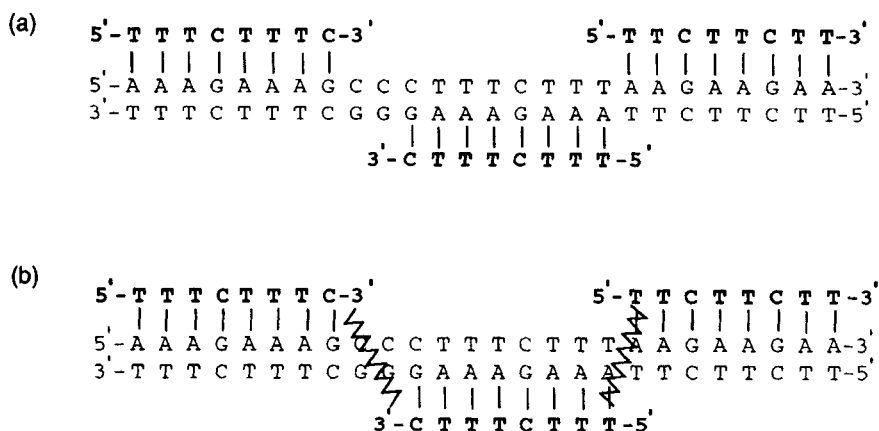


Figure 42 Schematics of binding of third strands by alternate-strand recognition of duplex DNA, sharing (a) unlinked third strands and (b) 3'-3'-linked and 5'-5'-linked third strands

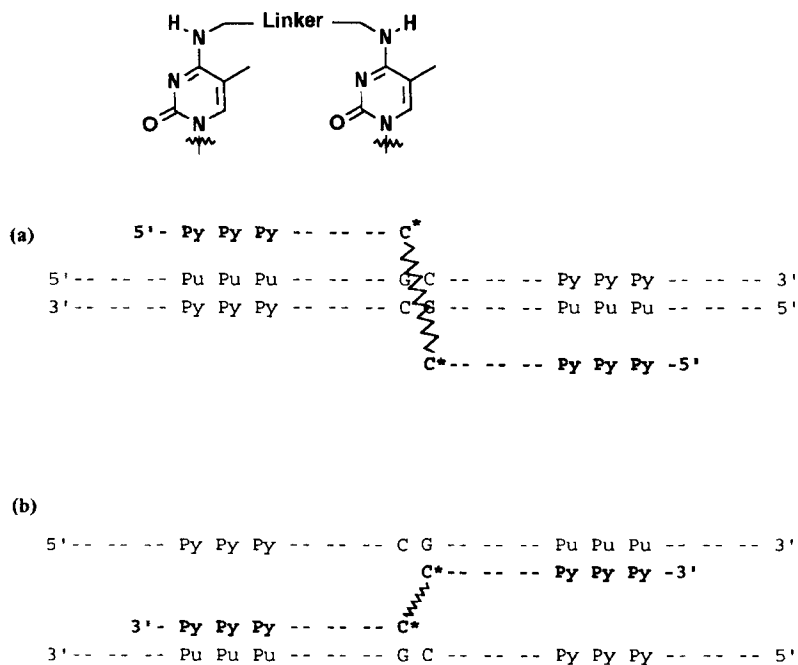


Figure 43 Alternate-strand triple-helix formation via oligomers bridged through N4 of C with (a) 3'-3' linkers and (b) 5'-5' linkers

of disulfide crosslinks into nucleic acids can stabilize DNA and RNA secondary-structural perturbations as shown by bridging the N3 positions of a terminal TT mismatch with thioethyl linkers [119]. Extension of this strategy for the stabilization of an unfavoured T·TA triplet within the intramolecular Y·RY motif involves crosslinking of C5 of the central T with N3 of T in the HG strand (Figure 47) [120]. Such positioning of thiols for crosslinking was achieved by synthesis of ODNs containing 3-thioethyl-T (N-3S) at the 3'-end of the HG strand and C5-thioethyl-dU (C5-S) at the opposing site on the complementary WC duplex. Oxidative S-S crosslinking yielded a triplex stabilized by 40 °C over a noncrosslinked control triplex.

ODNs equipped with a cleaving agent have been designed to recognize and cleave single-stranded hairpin structures by simultaneous formation of a WC duplex and HG pairing [121]. These ODNs contain two different domains for recognition by each mode (Figure 48), which was experimentally proved by gel retardation and spectroscopic experiments. Conjugation of the ODN with a

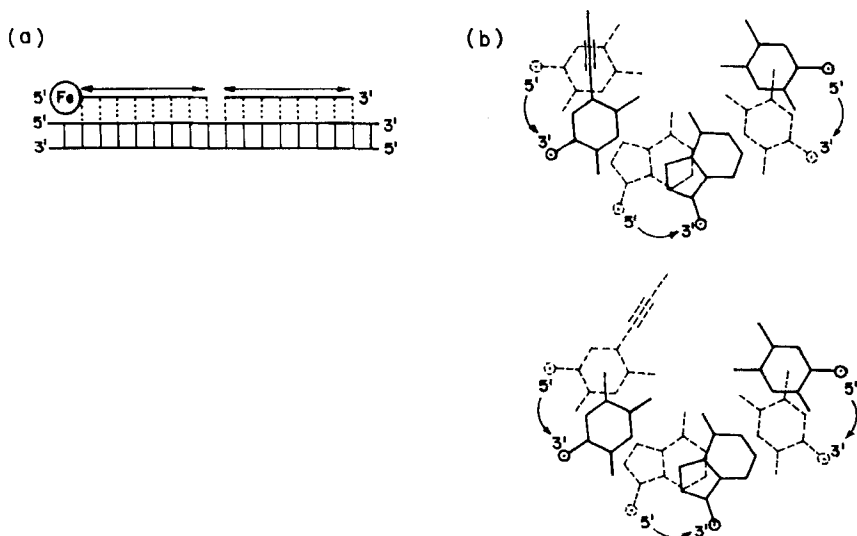


Figure 44 (a) Schematic representation of a triple helix composed of two TFOs binding at adjacent sites on double-helical DNA. (b) The base-stacking configuration of the p⁵ dU·AT triad. Reproduced by permission from *J. Am. Chem. Soc.*, **116**, 785 (1994)

phenanthroline complex of copper induced specific cleavage in the double-stranded hairpin stem. The WC and HG ODNs might be very useful in an antisense strategy for preventing the translation of stabilized hairpin forms, particularly in RNA which has a preference for such secondary structures.

Duplex and triplex stability can also be modulated via cooperative hydrophobic interactions, as demonstrated by the use of cholesteryl-conjugated oligonucleotides [122]. Cholesteryl moieties on complementary strands can be arranged such that hybridization of the two strands brings them into proximity, and the resulting intercholesteryl hydrophobic interaction would enhance the stability of the duplex or triplex. This occurs in a 5',3'-bis(cholesterol) oligomer capable of forming a clamp-shaped, triple-stranded complex in which the cholesterol linked to the termini of duplex-forming and triplex-forming domains effect a 30 °C stabilization of the triplex compared to a suitable control.

4.9 Triple-Helix-Binding Ligands

There are three grooves in triple-helical DNA which can be targeted for binding by ligands either covalently or noncovalently. The third strand of a triplex is positioned asymmetrically in the major groove and the vacant minor

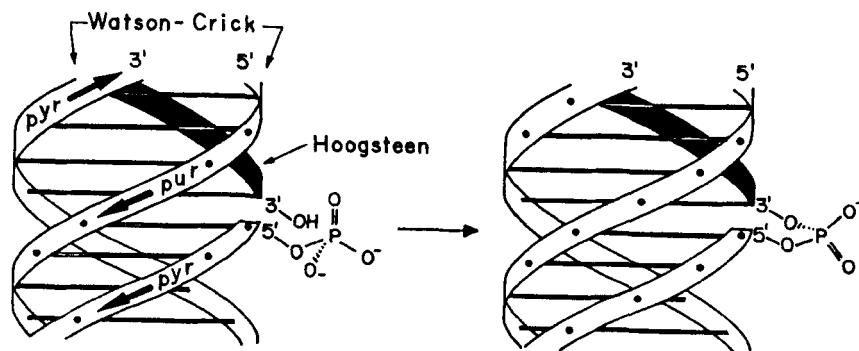


Figure 45 Chemical ligation of a third-strand ODN induced by triple-helix formation. Reproduced by permission from *J. Am. Chem. Soc.*, **111**, 8733 (1989)

groove can be a target for DNA-binding ligands. This and the possibility of intercalation can provide additional mechanisms for triplex stabilization.

(a) Intercalation

Intercalating ligands are well known to stabilize duplex DNA [2], and there have been recent efforts to study this phenomenon in triple helices. The classical cationic, planar chromophore ethidium bromide was shown to intercalate into an intermolecular 22-mer triplex in the Y·RY motif corresponding to mixed T·AT and C⁺·GC sequences [123]. The binding to the triple helix occurred at a lower affinity relative to the corresponding duplex (AT)_n, with the intercalator occupying only four sites on the triplex. Relative to the favoured CpG or TpA steps for intercalation in the duplex, intercalation of ethidium bromide in the triplex is preferred only at TpA steps, away from CpG steps. This is the result of a repulsion of positive charges on DNA and the intercalator, with a negative cooperativity and moderate destabilization. This binding preference could be reversed by a benzo[*e*]pyridoindole (Figure 49a) derivative, which strongly intercalated with the triplex rather than the duplex [124]. This triple-helix-specific intercalator showed a sequence-specific inhibition of the transcription initiation of a specific gene by *E. coli* RNA polymerase in the presence of an appropriate third-strand ODN. Furthermore, upon photoirradiation, it effected covalent modification within the triplex structure. An intercalator similar to acridine was linked to the 5'-end of an ODN (Figure 49b) which bound the complementary duplex and inhibited restriction enzyme cleavage at a site within the duplex [125]. The length, flexibility and chemical composition of the linkers substantially influence the binding affinity [126]. Taking into consideration the aromatic surface area required for stacking into a triplex, the torsional freedom required to match the

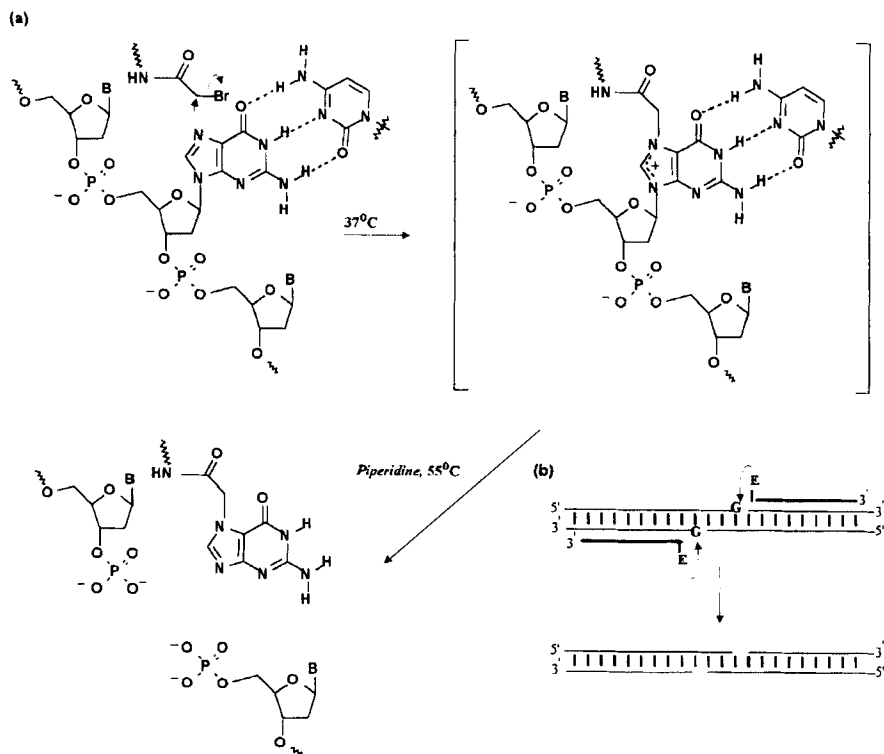
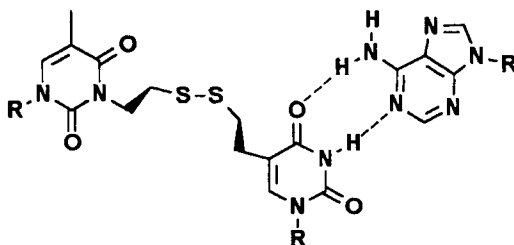


Figure 46 (a) An *N*-bromoacetyl electrophile localized in the major groove by triplex formation proximal to the GC base pair on the duplex target site leads to N7 alkylation of G followed by depurination and strand cleavage. (b) Schematic diagram of target duplex cleavage by covalent electrophiles in the third strand. Reproduced by permission from *J. Am. Chem. Soc.*, **114**, 5934 (1992)

propeller twist of triple-base interactions and charge effects, Wilson *et al.* prepared a series of quinolone derivatives carrying various aryl substituents at the 2-position (Figure 49c) [127]. Among these, the naphthylquinolone gave good stacking and stability of the triplex with a 30 °C enhancement in the triplex t_m compared to the duplex t_m . This intercalator was also more effective in the stabilization of triplexes with 5'-acridine linker ODNs and exhibited a better stabilization of a parallel triplex than an antiparallel triplex [128]. The compound was suggested to bind at T·AT triplets and prevent transmission of structural changes into the flanking duplex.

Another chromophore, namely oxazolopyridocarbazole (OPC) (Figure 49d), related to the ellipticine series, is a strong, reversible intercalator with no major preference for any DNA sequence [129]. This, upon conjugation at the 5'-ends of TFOs, showed a higher stabilization of both Y·RY and R·RY motifs, with the target being the HIV-1 U3 (human immunodeficiency virus type 1, gene



U3) end sequence. The Y_n -OPC conjugate binds in a pH-dependent manner, while R_n -OPC has no pH dependence. Molecular modelling indicated that intercalation of OPC is favoured at the triplex–duplex junction, accompanied by a small unwinding at the neighbouring exclusion site.

Netropsin, a minor-groove-specific ligand for duplex DNA [130], was studied for its ability to bind to triplexes in the Y-RY motif. It was established by spectroscopic and calorimetric means that the binding of netropsin does not displace the third strand from the major groove of the triplex, and, in contrast to duplex stabilization, this binding destabilizes the triplex [131]. The intramolecular triplex $T_{12} \cdot A_{12} T_{12}$ constructed using hexaethylene glycol as the interchain linker, bound netropsin as evidenced by CD, and induced destabilization by affecting the equilibrium in which the third strand was expelled from the major groove [132]. In contrast to this, distamycin 2, a netropsin analogue, was reported to destabilize the short triplex $T_6 \cdot A_6 T_6$, while

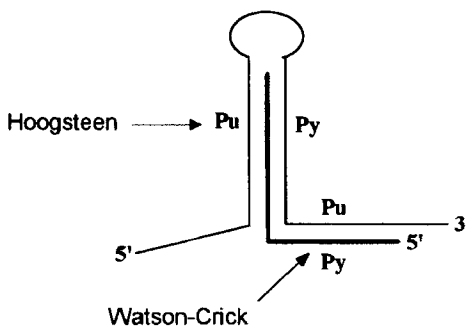


Figure 48 Schematic diagram of triplex stabilization by simultaneous formation of a WC duplex and HG pairing in separate domains. Reproduced by permission from *Biochemistry*, **34**, 65 (1995)

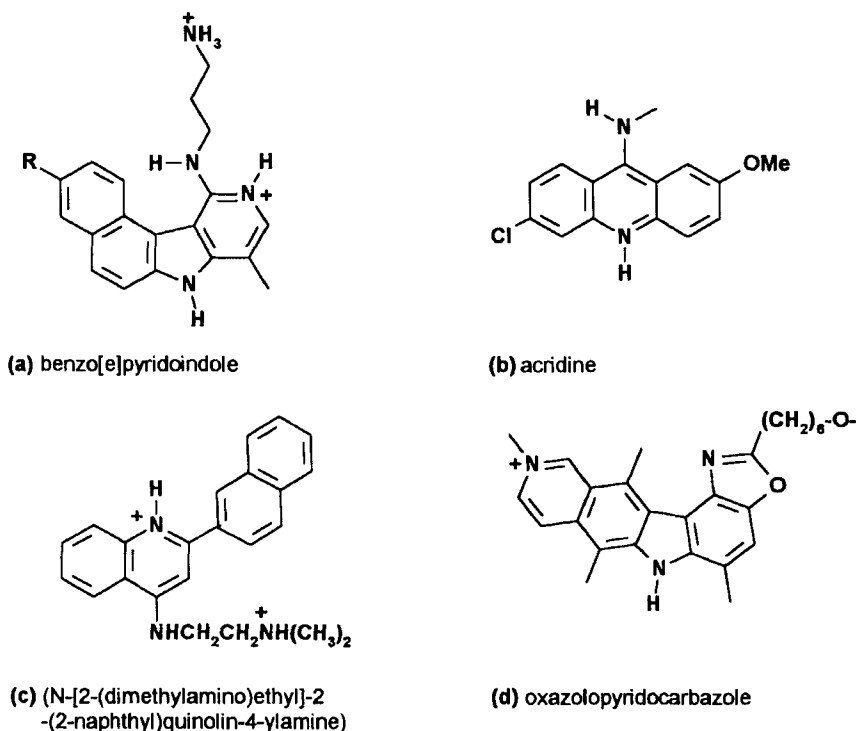


Figure 49 Triple-helix intercalators

it stabilized the duplex A_6T_6 [133]. The DNA-binding drug duocarmycin, when targeted to the minor groove in an intramolecular Y-RY triplex, reacted with N3 of A to form a covalent complex [134]. Similarly, the anthracycline SN-07, when bound to an intramolecular triplex, specifically at a T-CG site, formed a covalent adduct by reaction with the exocyclic N2 amino of G in the minor groove [135]. This last complex interacts with triplex DNA by both groove recognition and intercalation. These studies not only establish that triplex grooves are potential targets for binding ligands, but also suggest significant intergroove “crosstalk” modulating the interactions. From the above observations, a rational design of sequence-specific DNA ligands seems to be a practical reality, with bright prospects for artificial control of gene expression [136].

5. BIOLOGICAL APPLICATIONS OF TRIPLEX-FORMING OLIGONUCLEOTIDES

The triplex-forming ODNs can be perceived to affect biological processes which involve the use of duplex DNA as a matrix [137, 138]. These are

transcription, replication, DNA repair, recombination, action of topoisomerases and alterations in chromatin superstructure. In addition, several proteins and factors bind to DNA to regulate gene expression, and these are all potential targets for sequence-specific interference by triplex ODNs. When the triplex-forming site overlaps with the recognition binding site of one of the components such as the transcription activator, basal factor, RNA polymerase or replication machinery, competition for this site by the ODN exerts a direct effect on the biological process [18, 137, 138]. The DNA conformational change accompanying triplex formation, such as bending, stiffening and so on, may perturb the binding of protein factors and enzymes. These changes may extend to distant regions outside the triplex-forming site and modulate the biological effects. Initiation of transcription and replication may be inhibited by a triplex-forming ODN bound close to a promoter site or origin of replication, thus interfering in the function of RNA or DNA polymerase. A duplex-bound ODN may also present a steric block for transcription or replication enzymes. In addition to the inhibition of an enzymatic process, local triple-helix formation may also lead to activation by negative regulation through relieving inhibition effects. When third-strand ODNs are not strong enough ligands to stop the enzymatic machinery, irreversible reactions induced by conjugated ligands at the ODN-binding site may deactivate the biological complexes.

5.1 Inhibition of Restriction Enzyme Cleavage

A triplex-forming ODN can protect a restriction site from enzyme cleavage and from methylation by methylase when the recognition sites for both overlap. Such effects have been demonstrated for Y·RY triplexes containing Ava I [22], EcoRI [139], KSP 6321 [140] and Dra I [141] cleavage sites partially overlapping the triplex-binding site in recombinant plasmids. A physical overlap of sites may not be a prerequisite since long-range conformational effects induced by triplexation on the DNA duplex, as detected by chemical probes [142], may also be effective in suppressing the biological effects.

5.2 Inhibition of Transcription *in vitro* and *in vivo*

Oligonucleotides containing CT, GT and GC sequences have been used to inhibit the binding of transcription factors at specific sites in promoter regions, both *in vitro* and in cell cultures. Poly(dG)·poly(dC) sequences at the 5'-end of thymidine kinase promoter form intramolecular triplexes (H-DNA) to inhibit transcription factor binding [143]. Poly(dG)·poly(dC) also strongly augments gene expression when placed at the 5'-end of a promoter, and the activity shows a dependence on the length. The blocking effect of triplex ODNs in the binding of transactivating factor Sp1 in eukaryotic promoters has been examined [137, 138]. An oligonucleotide bound immediately downstream of *E.*

coli RNA pol was shown to inhibit transcription of the β -lactamase gene. The inhibition was made irreversible by psoralen crosslinking with the target sequence [144]. In the presence of specific triplex intercalators such as benzo[e]pyridoindole, transcription initiation at the β -lactamase promoter was inhibited at low ODN concentration [124]. A transient arrest of transcription at a eukaryotic pol II promoter site was demonstrated upon ODN binding [145]. Transcription initiation by T7 RNA pol was inhibited by ODN-directed triplex formation at a site overlapping with a polymerase-specific promoter [146].

It is always difficult to show that oligonucleotide-induced effects on biological processes inside cells are a direct consequence of triplex formation. The binding of a triplex-forming ODN to the *myc* gene was demonstrated by showing that a DNAase-I-hypersensitive site was masked by the ODN in cell nuclei [147]. A 28-mer GT ODN targeted to the α -subunit of the IL2R α -receptor promoter region effected a 32% decrease in the IL2R α m-RNA level without any effect on the control gene [148]. A 15-mer TFO ODN containing m⁵C and a 5'-linked acridine with a four-base-pair overlap between the binding site for NF-K β transcription factor and the triplex site inhibited protein binding [149]. A human protein containing a cold shock domain (BP-8) has been shown to bind specifically to H-DNA in a region upstream from human γ -globin genes [150].

In an approach to overcome inefficient cellular uptake, intracellular sequestration and rapid cellular degradation, the *in vivo* generation of highly abundant, sequence-specific ODNs for triplex gene regulation has been attempted [151]. The ODNs could be generated from a vector containing promoter, capping and terminator sequences from the human small-nuclear U6 gene surrounding a synthetic sequence of interest. *In vivo*, these ODNs were produced constitutively in levels up to 5×10^6 copies per cell, and no cell type specificity was observed. The HER-2/*neu* oncogene is overexpressed in breast cancer and human malignancies and contains a purine-rich sequence in the promoter region, favourable for R-RY triplex formation. An ODN targeted to this region was shown to prevent protein binding to the target *in vitro* [152]. A purified DNA helicase unwinds a triple-helical substrate in a similar manner to the situation with the duplex [153]. Thus, the formation of triple helices may not seriously inhibit DNA replication or recombination *in vivo* since DNA polymerases are preceded by helicases in the fully assembled holoenzyme.

The effects of ligand structure and properties, DNA backbone modifications and DNA sequence on the interactions of various well-known groove-binding agents have been studied [154]. ODNs designed to bind the promoter elements (m-RNA-capping and Sp1-binding sites) of HIV-1 by DNA triple-helix formation and modified with a 3'-amino to enhance intracellular stability have been shown to suppress HIV-1 m-RNA production in intact mammalian cell lines [155]. The HIV-integrase-binding site located in U3 LTR contains the

purine motif 5'-GGAAGGG-3', which can be selectively targeted by ODN intercalator conjugates, resulting in the prevention of integrase function *in vitro* [156]. A short purine ODN was shown to form a highly stable triple helix with the promoter of murine c-pim-1-proto oncogene [157].

5.3 Inhibition of DNA Replication

An ODN–intercalator conjugate targeted to the origin of replication of SV 40 inhibited the cytopathic effect of SV 40 virus on CV1 cells in culture and blocked viral DNA replication without any toxic effects on host cells [158]. When single-stranded DNA was used as a template for either *E. coli* (Klenow) or Taq. DNA polymerase, replication stopped in the middle owing to the presence of a polypurine tract which may form triplexes (H-DNA) by complementation with the replicated strand [159]. A monoclonal antibody raised against a triplex DNA cross-reacted with metaphase chromosomes and interphase nuclei, as observed by fluorescence microscopy of mouse myeloma cells [160]. Immunopositive regions corresponding to condensed chromatin rings have also been seen in polytene chromosomes of *C. tentans* and *D. melanogaster* [161]. The abundance of polypurine–polypyrimidine sequences in the DNA of eukaryotes makes it likely that H-DNA can form under topological constraints [18a, 162].

Genetic information exchange in living organisms proceeds through either homologous or site-specific recombination. Homologous recombination is thought to occur via a triple-stranded intermediate which is facilitated by recombinases such as Rec A [163]. These enzymes act by lowering the activation energy for the duplex–triplex transition, and since the third strand is homologous, this may involve a parallel orientation to the same strand in the duplex, defining a novel structural motif [164, 165]. Characterization of these intermediates may indicate newer biological targets for triplex activity.

6. FUTURE PROSPECTS

Although nucleic acid triplexes were first described more than 30 years ago [166], it is only during the last eight years that their practical importance has been realized. The demonstration of recognition and binding of ODNs in the major groove of duplex DNA to generate triplexes has far-reaching implications for molecular genetics and medicinal chemistry, and this has opened new vistas for the development of DNA-based therapeutic agents. In particular, the increasing incidence of their biological occurrence has provided the much-needed driving force to pursue this strategy. The present article summarizes the current activity in this area, particularly in the synthetic control of triplex structure and stability via chemical modifications of nucleobases, the sugar phosphate backbone and ligand conjugation. There

has been tremendous growth during the past three or four years in the understanding of the thermodynamics and kinetics of triplex formation, the structural basis for extending triplex recognition to code random sequences of double-stranded DNA, the design of alternative modes of duplex recognition and the modulation of triplex activity by covalent conjugation of reactive ligands and intercalators. The synthesis of ODN analogues and study of their physicochemical and biological properties will continue to occupy a central position, providing new principles and concepts for the development of newer strategies. Several biological applications are fast emerging towards addressing important disease targets, both *in vitro* and *in vivo*. The future challenge lies in unequivocally demonstrating direct triplex involvement in the observed biological effects and overcoming the hurdles facing *in vivo* applications, such as the stability of ODNs in biological media, cell uptake, intracellular distribution and pharmacokinetics.

7. REFERENCES

1. J. D. Watson and F. H. C. Crick, *Nature*, **171**, 737 (1953).
2. W. Saenger, *Principles of Nucleic Acids Structure*, Springer, New York, 1984.
3. K. Hoogsteen, *Acta Crystallogr.*, **16**, 907 (1963).
4. F. H. C. Crick, *J. Mol. Biol.*, **19**, 548 (1966).
5. D. Soll, J. D. Cherayil and R. M. Bock, *J. Mol. Biol.*, **19**, 97 (1966).
6. R. E. Dickerson, in *Unusual DNA Structures* (eds R. D. Wells and S. C. Harvey Sr), Springer, New York, 1988.
7. O. Kennard and W. N. Hunter, *Q. Rev. Biophys.*, **22**, 337 (1989).
8. R. M. Wing, H. R. Drew, T. Takano, C. Broka, S. Tanaka, K. Itakura and R. E. Dickerson, *Nature*, **287**, 755 (1980).
9. H. R. Drew, R. M. Wing, T. Takano, C. Broka, S. Tanaka, K. Itakura and R. E. Dickerson, *Proc. Natl. Acad. Sci. USA*, **78**, 2179 (1981).
10. C. A. Hunter, *J. Mol. Biol.*, **230**, 1025 (1993).
11. R. E. Dickerson and H. R. Drew, *J. Mol. Biol.*, **149**, 781 (1981).
12. A. H.-J. Wang, G. J. Quigley, F. J. Kolpak, G. van der Marel, J. H. van Boom and A. Rich, *Science*, **211**, 171 (1980).
13. N. C. Seeman, J. M. Rosenberg and A. Rich, *Proc. Natl. Acad. Sci. USA*, **73**, 804 (1976).
14. (a) W. Saenger, W. N. Hunter and O. Kennard, *Nature*, **324**, 385 (1986); (b) E. Westhof, *Int. J. Biol. Macromol.*, **9**, 185 (1987).
15. (a) R. Jin and K. G. Breslauer, *Proc. Natl. Acad. Sci. USA*, **85**, 8939 (1988); (b) D. A. Barawkar and K. N. Ganesh, *Nucleic Acids Res.*, **23**, 159 (1995).
16. H. E. Moser and P. B. Dervan, *Science*, **238**, 645 (1987).
17. (a) T. Le Doan, L. Perrouault, D. Praseuth, N. Habboub, J. L. Decout, N. T. Thuong, J. Lhomme and C. Helene, *Nucleic Acids Res.*, **15**, 7749 (1987); (b) D. Praseuth, L. Perrouault, T. Le Doan, M. Chasseigne, N. Thuong and C. Helene, *Proc. Natl. Acad. Sci. USA*, **85**, 1349 (1988).
18. (a) R. D. Wells, D. A. Collier, J. C. Harvey, M. Schimizu and F. Wohlrat, *FASEB J.*, **2**, 2931 (1988); (b) N. T. Thuong and C. Helene, *Angew. Chem., Int. Ed. Engl.*, **32**, 666 (1993).

19. (a) M. Cooney, G. Czernyszowsky, E. H. Postel, S. J. Flink and M. E. Hogan, *Science*, **241**, 456 (1988); (b) P. A. Beal and P. B. Dervan, *Science*, **251**, 1360 (1991).
20. K. Yoon, C. A. Hobbs, J. Koch, M. Sandaro, R. Kuntz and A. Weis, *Proc. Natl. Acad. Sci. USA*, **89**, 3840 (1992).
21. I. R. Radhakrishnan and D. J. Patel, *Biochemistry*, **33**, 11 405 (1994).
22. L. J. Maher, B. Wold and P. B. Dervan, *Science*, **245**, 725 (1989).
23. C. de los Santos, M. Rosen and D. J. Patel, *Biochemistry*, **28**, 7282 (1989).
24. P. Rajagopal and J. Feigon, *Biochemistry*, **28**, 7859 (1989).
25. Y. Kohwi and T. Kohwi-Shigematsu, *J. Mol. Biol.*, **231**, 1090 (1993).
26. (a) I. Radhakrishnan, D. J. Patel, E. S. Priestley, H. M. Nash and P. B. Dervan, *Biochemistry*, **32**, 11 228 (1993); (b) I. Radhakrishnan, C. de los Santos and D. J. Patel, *J. Mol. Biol.*, **234**, 188 (1993).
27. G. E. Plum, Y. W. Park, S. F. Singleton, P. B. Dervan and K. J. Breslauer, *Proc. Natl. Acad. Sci. USA*, **87**, 9436 (1990).
28. D. S. Pilch, R. Brousseau and R. H. Shafer, *Nucleic Acids Res.*, **18**, 5743 (1990).
29. R. G. Shea, P. Ng and N. Bischofberger, *Nucleic Acids Res.*, **18**, 4859 (1990).
30. D. S. Pilch, C. Levenson and R. H. Shafer, *Biochemistry*, **30**, 6051 (1991).
31. (a) S. F. Singleton and P. B. Dervan, *J. Am. Chem. Soc.*, **114**, 6957 (1992); (b) S. F. Singleton and P. B. Dervan, *J. Am. Chem. Soc.*, **116**, 10 376 (1994).
32. W. D. Wilson, H. P. Hopkins, S. Mizan, D. D. Hamilton and G. Zon, *J. Am. Chem. Soc.*, **116**, 3607 (1994).
33. G. C. Best and P. B. Dervan, *J. Am. Chem. Soc.*, **117**, 1187 (1995).
34. (a) A.-J. Cheng and M. W. Van Dyke, *Nucleic Acids Res.*, **22**, 4742 (1994); (b) L. E. Xodo, G. Manzini, F. Quadrioglio, G. A. van der Marel and J. H. van Boom, *Nucleic Acids Res.*, **19**, 5625 (1991).
35. M. M. W. Mooren, D. E. Pulleybank, S. S. Wijmenga, M. J. J. Blommers and C. W. Hilbers, *Nucleic Acids Res.*, **18**, 6523 (1990).
36. L. E. Xodo, G. Manzini and F. Quadrioglio, *Nucleic Acids Res.*, **18**, 3557 (1990).
37. F. M. Chen, *Biochemistry*, **30**, 4472 (1991).
38. (a) J. Volker, D. P. Botes, G. G. Lindsey and H. H. Klump, *J. Mol. Biol.*, **230**, 1278 (1993); (b) G. E. Plum and K. J. Breslauer, *J. Mol. Biol.*, **248**, 679 (1995).
39. (a) J.-L. Mergny, J.-S. Sun, M. Rougee, T.-M. Garestier, F. Barcelo, J. Comilier and C. Helene, *Biochemistry*, **30**, 9791 (1991); (b) M. Rougee, B. Faucon, J.-L. Mergny, F. Barcelo, C. Giovannangeli, T. Garestier and C. Helene, *Biochemistry*, **31**, 9269 (1992).
40. H. Shindo, H. Torigoe and A. Sarai, *Biochemistry*, **32**, 8963 (1993).
41. J. M. Piriou, Ch. Ketterle, J. Gabarro-Arpha, J. A. H. Cognet and M. Le Bret, *Biophys. Chem.*, **50**, 323 (1994).
42. C. Y. Sekharudu, N. Yatindra and M. Sundaralingam, *J. Biomol. Struct. Stereodynam.*, **11**, 225 (1993).
43. Y.-K. Cheng and B. M. Pettit, *J. Am. Chem. Soc.*, **114**, 4465 (1992).
44. D. Pei, H. D. Ulrich and P. G. Schultz, *Science*, **253**, 1408 (1991).
45. J. S. Lee, M. L. Woodsworth, L. J. P. Latimer and A. R. Morgan, *Nucleic Acids Res.*, **12**, 6603 (1984).
46. J. S. Lee, M. L. Woodsworth and L. J. P. Latimer, *Biochemistry*, **23**, 3277 (1984).
47. T. J. Povsic and P. B. Dervan, *J. Am. Chem. Soc.*, **111**, 3059 (1989).
48. L. J. Maher III, P. B. Dervan and B. J. Wold, *Biochemistry*, **29**, 8820 (1990).
49. S. F. Singleton and P. B. Dervan, *Biochemistry*, **31**, 10 995 (1991).
50. B. C. Froehler, S. Wadwani, T. J. Terhorst and S. R. Gerrard, *Tetrahedron Lett.*, **33**, 5307 (1992).

51. M. Shimizu, T. Koizumi, H. Inoue and E. Ohtsuka, *Bioorg. Med. Chem. Lett.*, **4**, 1029 (1994).
52. B. C. Froehler and D. J. Ricca, *J. Am. Chem. Soc.*, **114**, 8320 (1992).
53. P. S. Miller and C. D. Cushman, *Bioconj. Chem.*, **3**, 74 (1992).
54. C.-Y. Huang, C. D. Cushman and P. S. Miller, *J. Org. Chem.*, **58**, 5048 (1993).
55. (a) D. A. Barawkar, V. A. Kumar and K. N. Ganesh, *Biochem. Biophys. Res. Commun.*, **205**, 1665 (1994); (b) D. A. Barawkar, K. G. Rajeev, V. A. Kumar and K. N. Ganesh, *Nucleic Acids Res.*, **24**, 1229 (1996).
56. C.-H. Tung, K. J. Breslauer and S. Stein, *Nucleic Acids Res.*, **21**, 5489 (1993).
57. J.-P. Shaw, J. F. Milligan, S. H. Krawczyk and M. Matteucci, *J. Am. Chem. Soc.*, **113**, 7765 (1991).
58. J. S. Pudlo, S. Wadwani, J. F. Milligan and M. D. Matteucci, *Bioorg. Med. Chem. Lett.*, **4**, 1025 (1994).
59. A. Ono, P. O. P. Ts'O and L.-S. Kan, *J. Org. Chem.*, **57**, 3265 (1992).
60. M. C. Jetter and F. W. Hobbs, *Biochemistry*, **32**, 3249 (1992).
61. P. S. Miller, P. Bhan, C. D. Cushman and T. L. Trapane, *Biochemistry*, **31**, 6788 (1992).
62. E. C. Davison and K. Johnsson, *Nucleosides Nucleotides*, **12**, 237 (1993).
63. S. H. Krawczyk, J. F. Milligan, S. Wadwani, C. Moulds, B. C. Froehler and M. D. Matteucci, *Proc. Natl. Acad. Sci. USA*, **89**, 3761 (1992).
64. M. Shimizu, H. Inoue and E. Ohtsuka, *Biochemistry*, **33**, 606 (1994).
65. G. Xiang, W. Soussou and L. W. McLaughlin, *J. Am. Chem. Soc.*, **116**, 11 155 (1994).
66. J. Hunziker, E. S. Presley, H. Brunav and P. B. Dervan, *J. Am. Chem. Soc.*, **117**, 2421 (1995).
67. C.-Y. Huang and P. S. Miller, *J. Am. Chem. Soc.*, **115**, 10456 (1993).
68. (a) J. S. Koh and P. B. Dervan, *J. Am. Chem. Soc.*, **114**, 1470 (1992); (b) E. S. Priestley and P. B. Dervan, *J. Am. Chem. Soc.*, **117**, 4761 (1995).
69. I. Radhakrishnan, D. J. Patel, E. S. Priestley, H. M. Nash and P. B. Dervan, *Biochemistry*, **32**, 11 228 (1993).
70. L. C. Griffin, L. L. Kiessling, P. A. Beal, P. Gillespie and P. B. Dervan, *J. Am. Chem. Soc.*, **114**, 7976 (1992).
71. K. M. Koshlap, P. Gillespie, P. B. Dervan and J. Feigon, *J. Am. Chem. Soc.*, **115**, 7908 (1993).
72. L. C. Griffin and P. B. Dervan, *Science*, **245**, 967 (1989).
73. E. Wang, S. Malek and J. Feigon, *Biochemistry*, **31**, 4838 (1992).
74. I. Radhakrishnan and D. J. Patel, *Structure*, **2**, 17 (1994).
75. F. Michel, A. D. Ellington, S. Coutre and J. W. Szostak, *Nature*, **347**, 578 (1990).
76. I. Radhakrishnan and D. J. Patel, *J. Mol. Biol.*, **241**, 600 (1994).
77. P. S. Miller and C. D. Cushman, *Biochemistry*, **32**, 2999 (1993).
78. T. L. Trapane and P. O. P. Ts'O, *J. Am. Chem. Soc.*, **116**, 10 437 (1994).
79. T. L. Trapane, M. S. Christopherson, C. D. Roby, P. O. P. Ts'O and D. Wang, *J. Am. Chem. Soc.*, **116**, 8412 (1994).
80. R. Bandaru, H. Hashimoto and C. Switzer, *J. Org. Chem.*, **60**, 786 (1995).
81. H. U. Stilz and P. B. Dervan, *Biochemistry*, **32**, 2177 (1993).
82. K. Dittrich, J. Gu, R. Tinder, M. Hogan and X. Gao, *Biochemistry*, **33**, 4111 (1994).
83. R. H. Durland, T. S. Rao, G. R. Revankar, J. H. Tinsley, M. A. Myrick, D. M. Seth, J. Rayford, P. Singh and K. Jayaraman, *Nucleic Acids Res.*, **22**, 3233 (1994).
84. T. S. Rao, M. E. Hogan and G. R. Revankar, *Nucleosides Nucleotides*, **13**, 95 (1994).
85. (a) J. F. Milligan, S. H. Krawczyk, S. Wadwani and M. D. Matteucci, *Nucleic Acids Res.*, **21**, 327 (1993); (b) A.-J. Cheng and M. W. van Dyke, *Nucleic Acids*

- Res.*, **21**, 5630 (1993); (c) W. M. Olivas and L. J. Maher, *Biochemistry*, **34**, 278 (1993); (d)
T. S. Rao, A. F. Lewis, R. H. Durland and G. R. Revankar, *Tetrahedron Lett.*, **34**, 6709 (1993).
86. (a) T. S. Rao, R. H. Durland, D. M. Seth, M. A. Myrick, V. Bodepudi and G. R. Revankar, *Biochemistry*, **34**, 765 (1995); (b) T. S. Rao, A. F. Lewis, T. S. Hill and G. R. Revankar, *Nucleosides Nucleotides*, **14**, 1 (1995).
87. J. E. Gee, G. R. Revankar, T. S. Rao and M. E. Hogan, *Biochemistry*, **34**, 2042 (1995).
88. (a) B. K. Bhattacharya, M. V. Chari, R. H. Durland and G. R. Revankar, *Nucleosides Nucleotides*, **14**, 45 (1995); (b) A. B. Staubli and P. B. Dervan, *Nucleic Acids Res.*, **22**, 2637 (1994).
89. S.-H. Chou, P. Flynn and B. Reid, *Biochemistry*, **28**, 2435 (1989).
90. (a) R. Macaya, E. Wang, P. Schultze, V. Sklenar and J. Feigon, *J. Mol. Biol.*, **225**, 755 (1990); (b) R. F. Macaya, P. Schultz and J. Feigon, *J. Am. Chem. Soc.*, **114**, 781 (1992).
91. R. W. Roberts and D. M. Crothers, *Science*, **258**, 1463 (1992).
92. (a) H. Han and P. B. Dervan, *Proc. Natl. Acad. Sci. USA*, **90**, 3806 (1993); (b) C. Escude, J. C. Francois, J. S. Sun, G. Ott, M. Sprinze, T. Gareshier and C. Helene, *Nucleic Acids Res.*, **21**, 5547 (1993); (c) C. L. Semerad and L. J. Maher, *Nucleic Acids Res.*, **22**, 5321 (1994).
93. D. E. Callahan, T. L. Trapane, P. S. Miller, P. O. P. Ts'O and L.-S. Kan, *Biochemistry*, **30**, 1650 (1991).
94. L.-K. Herzog, B. Keil, G. Zon, K. Shinozuka, S. Mizan and W. D. Wilson, *Nucleic Acids Res.*, **18**, 3545 (1990).
95. L. Xodo, M. Alunnifabroni, G. Manzini and F. Quadrifoglio, *Nucleic Acids Res.*, **22**, 3322 (1994).
96. (a) M. Matteucci, K.-Y. Lin, S. Butcher and C. Moulds, *J. Am. Chem. Soc.*, **113**, 7767 (1991); (b) R. J. Jones, K.-Y. Lin, J. F. Milligan, S. Wadwani and M. D. Matteucci, *J. Org. Chem.*, **58**, 2983 (1993).
97. K.-Y. Lin, J. S. Pudlo, R. J. Jones, N. Bischofberger, M. D. Matteucci and B. C. Froehler, *Biomed. Chem. Lett.*, **4**, 1061 (1994).
98. M. Egholm, O. Buchardt, P. E. Nielsen and R. H. Berg, *J. Am. Chem. Soc.*, **114**, 1895 (1992).
99. M. Egholm, O. Buchardt, L. Christensen, C. Behrens, S. M. Frier, D. A. Driver, R. Berg, B. Norden and P. E. Nielsen, *Nature*, **365**, 566 (1993).
100. S. Kim, P. E. Nielsen, M. Egholm, O. Buchardt and B. Norden, *J. Am. Chem. Soc.*, **116**, 785 (1994).
101. P. E. Nielsen, M. Egholm, R. H. Berg and O. Buchardt, *Science*, **254**, 1497 (1991).
102. P. E. Nielsen, M. Egholm and O. Buchardt, *Bioconj. Chem.*, **5**, 3 (1994).
103. C. Giovannangeli, T.-M. Garestier, M. Rougee, M. Chassignol, N. T. Thuong and C. Helene, *J. Am. Chem. Soc.*, **113**, 7775 (1991).
104. M. Salunkhe, T. Wu and R. L. Letsinger, *J. Am. Chem. Soc.*, **114**, 8768 (1992).
105. M. Tarkoy, M. Bolli and C. Leumann, *Helv. Chim. Acta*, **77**, 716 (1994).
106. (a) R. J. Jones, S. Swaminathan, J. F. Milligan, S. Wadwani, B. C. Froehler and M. D. Matteucci, *J. Am. Chem. Soc.*, **115**, 9816 (1993); (b) C. Mayfield and D. Miller, *Nucleic Acids Res.*, **22**, 1909 (1994).
107. D. J. D'Souza and E. T. Kool, *Biomed. Chem. Lett.*, **4**, 965 (1994).
108. S. Wang and E. T. Kool, *J. Am. Chem. Soc.*, **116**, 8857 (1994).
109. E. Rubit and E. T. Kool, *Angew. Chem., Int. Ed. Engl.*, **33**, 1004 (1994).
110. S. Wang and E. T. Kool, *Biochemistry*, **34**, 4125 (1995).

111. A. Ono, C.-N. Chen and L.-S. Kan, *Biochemistry*, **30**, 9914 (1991).
112. B. C. Froehler, T. Terhorst, J.-P. Shaw and S. N. McCurdy, *Biochemistry*, **31**, 1603 (1992).
113. (a) U. Asseline and N. T. Thuong, *Tetrahedron Lett.*, **34**, 4173 (1993); (b) U. Asseline and N. T. Thuong, *Tetrahedron Lett.*, **35**, 5221 (1994).
114. E. Washbrook and K. R. Fox, *Biochem. J.*, **301**, 569 (1994).
115. N. Colocci, M. D. Distefano and P. B. Dervan, *J. Am. Chem. Soc.*, **115**, 4468 (1993).
116. (a) N. Colocci and P. B. Dervan, *J. Am. Chem. Soc.*, **116**, 785 (1994); (b) N. Colocci and P. B. Dervan, *J. Am. Chem. Soc.*, **117**, 4781 (1995).
117. K. J. Leubke and P. B. Dervan, *J. Am. Chem. Soc.*, **111**, 8733 (1989).
118. (a) O. S. Fedorova, D. G. Knorre, L. M. Podust and V. F. Zarytova, *FEBS Lett.*, **228**, 273 (1988); (b) T. J. Povsic, S. A. Strobel and P. B. Dervan, *J. Am. Chem. Soc.*, **114**, 5934 (1992).
119. J. T. Goodwin and G. D. Glick, *Tetrahedron Lett.*, **35**, 1647 (1994).
120. J. T. Goodwin, S. E. Osborne, P. C. Swanson and G. D. Glick, *Tetrahedron Lett.*, **36**, 4527 (1995).
121. J.-C. Francois and C. Helene, *Biochemistry*, **34**, 65 (1995).
122. S. M. Gryaznov and D. H. Lyod, *Nucleic Acids Res.*, **21**, 5909 (1993).
123. J.-L. Mergny, D. Collier, M. Rougee, T. M. Garestier and C. Helene, *Nucleic Acids Res.*, **19**, 1521 (1991).
124. J.-L. Mergny, G. D. Valentin, Ch. Nguyen, L. Perrouault, B. Faucon, M. Rougee, T. M. Garestier, E. Bishani and C. Helene, *Science*, **256**, 1681 (1992).
125. D. A. Collier, N. T. Thuong and C. Helene, *J. Am. Chem. Soc.*, **113**, 1457 (1991).
126. F. M. Orson, B. M. Kinsdy and W. M. McShan, *Nucleic Acids Res.*, **22**, 479 (1994).
127. W. D. Wilson, F. A. Tarrions, S. Mizan, S. Yao, A. Y. Kiselyov, G. Zon and L. Strekowski, *Biochemistry*, **32**, 10614 (1993).
128. S. A. Cassidy, L. Strekowski, W. D. Wilson and K. R. Fox, *Biochemistry*, **33**, 15338 (1994).
129. J. F. Mouscadet, C. Ketterle, H. Goulaonic, S. Couteau, F. Subra, M. L. Bret and C. Auclair, *Biochemistry*, **33**, 4187 (1994).
130. C. Zimmer and U. Wahnert, *Prog. Biophys. Mol. Biol.*, **47**, 31 (1986).
131. Y. W. Park and K. J. Breslauer, *Proc. Natl. Acad. Sci. USA*, **89**, 6653 (1992).
132. M. Durand, N. T. Thuong and J. C. Maurizot, *J. Biol. Chem.*, **267**, 24394 (1992).
133. K. Umemato, M. H. Sarma, G. Gupta, J. Luo and R. H. Sarma, *J. Am. Chem. Soc.*, **112**, 4539 (1990).
134. C. H. Lin and D. J. Patel, *J. Am. Chem. Soc.*, **114**, 10658 (1992).
135. X. Ye, K. Kimura and D. J. Patel, *J. Am. Chem. Soc.*, **115**, 9325 (1993).
136. C. Helene, *Pure Appl. Chem.*, **66**, 663 (1994).
137. C. Helene, *Anti-Cancer Drug Des.*, **6**, 569 (1991).
138. L. J. Maher, *Bioessays*, **14**, 807 (1992).
139. J. C. Hancey, M. Shimizu and R. D. Wells, *Nucleic Acids Res.*, **18**, 157 (1990).
140. J. C. Francois, S. Behmoaras, T. Thuong and C. Helene, *Biochemistry*, **28**, 9617 (1989).
141. J. S. Sun, C. Giovannangeli and J. C. Francois, *Proc. Natl. Acad. Sci. USA*, **88**, 6023 (1991).
142. D. A. Collier, J. L. Mergny, N. T. Thuong and C. Helene, *Nucleic Acids Res.*, **19**, 4219 (1991).
143. L. B. Maher III, P. B. Dervan and B. J. Wold, *Biochemistry*, **31**, 70 (1992).

144. G.-D. Valentin, N. T. Thuong and C. Helene, *Proc. Natl. Acad. Sci. USA*, **89**, 504 (1992).
145. S. L. Young, S. H. Krawczyk, M. D. Matteucci and J. J. Toole, *Proc. Natl. Acad. Sci. USA*, **88**, 10023 (1991).
146. L. J. Maher, *Biochemistry*, **31**, 5787 (1992).
147. E. H. Postel, S. J. Flint, D. J. Kessler and M. E. Hogan, *Proc. Natl. Acad. Sci. USA*, **88**, 8228 (1991).
148. E. M. Orson, D. W. Thomas, W. M. Meshan, D. J. Kessler and M. E. Hogan, *Nucleic Acids Res.*, **19**, 3435 (1991).
149. M. Grigoviev, D. Praseuth, P. Robin, A. Heman, T. Behmoras, A.-D. Varsat, N. T. Thuong, C. Helene and A.-H. Bellan, *J. Biol. Chem.*, **267**, 3389 (1992).
150. E. M. Horowitz, A. K. Maloney and T. J. Lee, *J. Biol. Chem.*, **269**, 14130 (1994).
151. S. B. Noonberg, G. K. Scott, M. R. Garovoy, C. C. Benz and C. A. Hunt, *Nucleic Acids Res.*, **22**, 2830 (1994).
152. S. W. Ebbinghaus, J. E. Gee, B. Rodu, A. C. Mayfield, G. Sanders and D. M. Miller, *J. Clin. Invest.*, **92**, 2433 (1993).
153. I. P. Maine and T. Kodadek, *Biochem. Biophys. Res. Commun.*, **204**, 1119 (1994).
154. W. D. Wilson, S. Mizan, F. A. Torrious and S. Yao, *J. Mol. Recogn.*, **7**, 89 (1994).
155. W. M. McShan, R. D. Rossem, A. H. Laughter, J. Trial, D. J. Kessler, J. G. Zendegeu, M. E. Hogan and F. M. Orson, *J. Biol. Chem.*, **267**, 5712 (1992).
156. J. F. Mouscadet, S. Carteau, H. Goulaouic, F. Subra and C. Auclair, *J. Biol. Chem.*, **269**, 21635 (1994).
157. F. Svinarchuk, J. R. Bertund and C. Malvy, *Nucleic Acids Res.*, **22**, 3742 (1994).
158. F. Birg, D. Praseuth, A. Zerial, N. T. Thuong, U. Asseline, T. Le Doan and C. Helene, *Nucleic Acids Res.*, **18**, 2901 (1990).
159. N. Baran, A. Lapidot and H. Manor, *Proc. Natl. Acad. Sci. USA*, **88**, 507 (1991).
160. J. S. Lee, G. D. Burkholder, L. J. P. Latimer, B. L. Hang and R. P. Braun, *Nucleic Acids Res.*, **15**, 1047 (1987).
161. G. D. Burkholder, L. J. P. Latimer and J. S. Lee, *Chromosoma*, **101**, 11 (1991).
162. H. Htun and J. E. Dahlberg, *Science*, **243**, 1571 (1989).
163. B. J. Rao, B. Jwang and C. M. Radding, *J. Mol. Biol.*, **213**, 789 (1990).
164. B. J. Rao and C. M. Radding, *Proc. Natl. Acad. Sci. USA*, **91**, 6161 (1994).
165. V. B. Zhurkhin, G. Raghunathan, N. B. Ulyanov, R. D. Camerini-Otero and J. L. Jernigan, *J. Mol. Biol.*, **239**, 181 (1994).
166. G. Felsenfeld, D. R. Davies and A. Rich, *J. Am. Chem. Soc.*, **79**, 2023 (1957).

Cumulative Author Index

This index comprises the names of contributors to Volumes 1 and 2 of **Perspectives in Supramolecular Chemistry**

Bell, Ian M., *see* Hilvert, Donald, **1**, 73.

Benkovic, S. J., *Macrocycles and Antibodies as Catalysts*, **1**, 149.

Chang, Ning-Leh, *see* Davis, Raymond E., **2**, 63.

Cramer, Friedrich, *Emil Fischer's Lock-and-Key Hypothesis after 100 Years – Towards a Supracellular Chemistry*, **1**, 1.

Dance, Ian, *Supramolecular Inorganic Chemistry*, **2**, 137.

Davis, Raymond E., *Molecular Shape as a Design Criterion in Crystal Engineering*, **2**, 63.

Desiraju, Gautam R., *Crystal Engineering and Molecular Recognition – Twin Facets of Supramolecular Chemistry*, **2**, 31.

Dunitz, Jack D., *Thoughts on Crystals as Supermolecules*, **2**, 1.

Fagan, Paul J., *Molecular Engineering of Crystals by Electrostatic Templating*, **2**, 107.

Glusker, Jenny P., *The Protein as a Supermolecule: The Architecture of a ($\beta\alpha$)₈ Barrel*, **2**, 235.

Hilvert, Donald, *New Biocatalysts via Chemical Modifications*, **1**, 73.

Horovitz, Ammon, *see* Katchalski-Katzir, Ephraim, **1**, 25.

Katchalski-Katzir, Ephraim, *Molecular Recognition in Biology: Models for Analysis of Protein–Ligand Interactions*, **1**, 25.

Krishnamohan Sharma, C. V., *see* Desiraju, Gautam R., **2**, 31.

Kuhn, Hans, *A Model of the Origin of Life and Perspectives in Supramolecular Engineering*, **1**, 247.

Lahav, Meir, *Lock-and-Key Processes at Crystalline Interfaces: Relevance to the Spontaneous Generation of Chirality*, **1**, 173.

Lancet, Doron, *see* Katchalski-Katzir, Ephraim, **1**, 25.

Lehn, Jean-Marie, *Perspectives in Supramolecular Chemistry – From the Lock-and-Key Image to the Information Paradigm*, **1**, 307

Leiserowitz, Leslie, *see* Lahav, Meir, **1**, 173.

Popovitz-Biro, Ronit, *see* Lahav, Meir, **1**, 173.

Smithrud, D. B., *see* Benkovic, S. J., **1**, 149.

Vlassov, V. V., *Oligonucleotides: Superspecific Ligands for Targeting Nucleic Acids and Proteins and Development of Molecular Devices*, **1**, 89.

Ward, Michael D., *see* Fagan, Paul J., **2**, 107.

Waser, Jürg, *see* Kuhn, Hans, **1**, 247.

Weissbuch, Isabelle, *see* Lahav, Meir, **1**, 173.

Whitesell, James K., *see* Davis, Raymond E., **2**, 63.

Wong, Man-Shing, *see* Davis, Raymond E., **2**, 63.

Cumulative Title Index

	Vol.	Page
A Model of the Origin of Life and Perspectives in Supramolecular Engineering (<i>Kuhn and Waser</i>)	1	247
Crystal Engineering and Molecular Recognition – Twin Facets of Supramolecular Chemistry (<i>Desiraju and Krishnamoran Sharma</i>)	2	31
Emil Fischer's Lock-and-Key Hypothesis after 100 Years – Towards a Supracellular Chemistry (<i>Cramer</i>)	1	1
Lock-and-Key Processes at Crystalline Interfaces: Relevance to the Spontaneous Generation of Chirality (<i>Weissbuch, Popovitz-Biro, Leiserowitz and Lahav</i>)	1	173
Macrocycles and Antibodies as Catalysts (<i>Smithrud and Benkovic</i>)	1	149
Molecular Engineering of Crystals by Electrostatic Templating (<i>Fagan and Ward</i>)	2	107
Molecular Recognition in Biology: Models for Analysis of Protein–Ligand Interactions (<i>Lancet, Horovitz and Katchalski-Katzir</i>)	1	25
Molecular Shape as a Design Criterion in Crystal Engineering (<i>Davis, Whitesell, Wong and Chang</i>)	2	63
New Biocatalysts via Chemical Modifications (<i>Bell and Hilvert</i>)	1	73
Oligonucleotides: Superspecific Ligands for Targeting Nucleic Acids and Proteins and Development of Molecular Devices (<i>Vlassov</i>)	1	89
Perspectives in Supramolecular Chemistry – From the Lock-and-Key Image to the Information Paradigm (<i>Lehn</i>)	1	307
Thoughts on Crystals as Supermolecules (<i>Dunitz</i>)	2	1
The Protein as a Supermolecule: The Architecture of a ($\beta\alpha$) ₈ Barrel (<i>Glusker</i>)	2	235

Index

- A-DNA, 266
 α -amino acids *p*-nitrophenyl esters, 120
 α -helicity, 35, 36
 α -oligopyrimidines, 302
acetylcholine, 70, 145
acetylcholinesterase, 145
acridine, 307, 311
actinomycin D, 278
acylaminopyridine, 25, 30
adenine-thymine, 252
adenosine 5'-triphosphate binding, 44
affinity cleavage, 272
Ag₂O crystallites, 134
alkali metal ion extraction, 45
alkali metal transport, 35
alkaline hydrolysis, 113
alkane hydroxylation, 204, 209
alkene epoxidation, 204, 209, 214
allosteric properties, 156
alternate-strand recognition, 310
Amber force field, 29
trans-amides, 240, 243
6-amino-cytosine, 285
amino- β -cyclodextrins, 44
AMP receptor, 70, 75
amphiphilic molecules, 101
8-anilinonaphthalene-1-sulfonate, 43
anion complexation, 69
anion recognition, 66
anthracene-based fluorescent sensor, 86
anthranilamides, 56
antibiotics, 103
arene hydroxylation, 209
aromatic templating, 16
Arrhenius profile, 121
artificial life, 251
asymmetric epoxidation of alkenes, 211
autocatalysis, 227, 238, 242
autopoiesis, 108
autoxidation, 168
 β -cyclodextrin, 42
B-DNA, 266
 β -lactamase gene, 320
 σ -backbonding, 179
bacteriophage T7 RNA polymerase, 305
barrel-shaped aggregate, 22
base stacking, 266
base-pairing, 250
benzimidazole, 10
4-(3-benzamidophenyl)imidazole, 292
benzo[e]pyridoindole, 315
bilayer membrane, 205
bilayer, 104
bile acid–drug conjugates, 61
bile-acid-based receptors, 60
bile-acid-derived macrocycles, 62
bilirubin, 80
bimolecular triplexes, 310
biocyclo-DNA, 308
biomineralization, 134
biphasic kinetic behavior, 127
bis(2,9-diphenyl-1,10-phenanthroline)
copper(I), 29
bis(2-pyridyl)pyrazine, 25
5,10-bis(4-pyridyl)-15,20-diphenyl-
porphine, 17
bis(amino acid) derivatives, 34
bis(β -cyclodextrin), 83

- bis(benzimidazole), 35
- bis(bipyridine), 6
- bis(crown ether), 45
- bis(cyclodextrin), 43, 44
- bis(guanidinium) receptors, 54
- bis(phenanthroline), 6, 18, 20
- bis(phosphonate) receptor, 58
- bis(terpyridine), 24, 32, 36
- bis(terpyridine), complexes iron(II), 32
- bis(terpyridine), complexes ruthenium(II), 32
- bis(urea) receptor, 94
- bis-(benzimidazole), 10
- bis-(benzimidazole), complexes cobalt(II), 12
- bis-(benzimidazole), complexes copper(I), 11
- bis-(benzimidazole), complexes zinc(II), 13
- bite angle α , 11
- bola surfactants, 106
- boronic-acid-based receptors, 62
- box structures, 15
- breakdown of the tetrahedral intermediate, 240
- C2'-endo-sugar* pucker, 266, 303
- C3'-endo-sugar* pucker, 267
- C3'-endo-sugar*, 303
- C⁵-(1-propynyl)-2'-dC*, 283
- C5*-substituted pyrimidines, 280
- cage complex, 16
- calixarenes, 49
- calixfuran, 49
- calixspherands, 51
- calix[4]arene UO_2 -salen complex, 66
- calix[4]arene, 49, 68, 71, 85
- calix[4]arenediquinone crown, 90
- calix[6]arenes, 51, 53, 71
- calix[8]arenes, 89
- carbazolediiimide, 232, 238, 253
- carbocyclic m^2C , 283
- carbon monoxide binding, 173
- carboxyhemochrome, 175
- carcaplex, 93
- carcerands, 74
- catalyses, 189
- catenanes, 17, 29
- [2]catenane, 18
- [3]catenane, 18
- cation complexation, 68
- cation- π interaction, 92
- cationic amphiphile, 121, 145
- cationic surfactants, 126
- cationic vesicles, 114
- cellular triplex uptake, 320
- CH- π interactions, 49
- charge-charge interactions, 132
- charge-polarizability, 93
- charge-quadrupole, 93
- chemosensor, 85, 86
- chiral helix, 7
- chiral metalloaggregates, 120
- chiral podands, 74
- chiral recognition, 74
- chiral, 209
- chiroporphyrins, 214
- chloroperoxidases, 190
- cholacrown, 46
- cholaphanes, 61
- cholesteric liquid crystal, 63
- cholesterol hydroxylation, 205
- cholesterol, 63
- cholesteryl-conjugated oligonucleotides, 314
- cholic acid, 46, 60
- choline, 70
- chromogenic effect, 29
- chromogenic reagent, 89
- chromomycin A_3 , 278
- circular DNA, 308
- cis*-amide, 243
- codon-anticodon interactions, 265
- combinatorial methods, 77, 280
- compartmentalization, 137
- competitive inhibitors, 256
- cooperative transition into single strands, 277
- cooperativity in triplex formation, 311
- cooperativity, 6, 9, 108
- Cotton effect, 8
- Crick-Hoogsteen groove, 273
- critical micelle concentration, 103, 109, 118
- crown ether, 45, 198
- cryptand, 89
- cryptophane, 70, 75
- CTAB, 103, 110, 123
- cycloinulohexose, 46
- cyclophane receptor, 77
- cyclophane, 34, 71

- cytochrome P450 models, 202
cytochrome-P450, 136, 196, 209
- D-glucose-derived crown ethers, 46
D-hexopyranosides, 46
deamination, 119
7-deaza-2'-deoxyxanthosine, 301
7/9-deaza-2'-dGuanosine, 300
decapsulation, 145
2'-deoxyformycin A, 299
deoxyhemoglobin R-state T-state, 167
deoxymyoglobin, 158
2'-deoxynebularine, 298
2'-deoxy-6-thioguanosine, 301
dephosphono congeners, 305
desmosterol, 138
diacylaminopyridines, 240
dicarboxylic acid binding, 27
Diels-Alder reaction, 85
differential scanning calorimetry, 278
dihexadecyl phosphate, 135
dimyristoylphosphatidylcholine, 138
2,4-dinitrophenyl ester, 235
dioxygen binding, 160
distal histidine, 176
distal polar effect, 176
DNA bending, 319
DNA duplex, 264
DNA helicase, 320
DNA polymerase, 319
DNA stiffening, 319
DNA-based therapeutic agents, 321
dopamine transport, 65
double-hairpin, 278
double-helical structures, 2, 11, 19
drug discovery, 143
duocarmycin, 318
duplex-triplex transition, 321
- edge-to-face interaction, 95
electrochemical sensors, 89
electrochemical studies, 68
electron paramagnetic resonance, 191
electron transport in membranes, 136
electrostatic interactions, 265
enantioselective oxygenations, 209
enantioselectivity, 118, 123
environment effects on self-replication, 250
- enzymes in hydrocarbon solution, 133
epoxidation of alkenes, 136
error checking, 9
ester aminolysis, 228
ethidium bromide, 278, 310, 315
ethyl caprylate, 109
ethylenediaminetetraacetate, 276
- ferricytochrome c, 142
ferrocene-crown ether conjugate, 90
ferryl intermediate, 159
flash photolysis, 175
flavin, 140
flip-flop in membranes, 105, 124, 125
fluorescence sensor, 63, 92
footprinting, 272
formacetal, 305
four-helix bundle, 36
frayed ends, 245
- gel electrophoresis, 272, 276
gel state, 112
glucose mutarotation, 242
glutaric acid complexation, 27
glycopeptide antibiotics, 103
glycosides, 58, 61
gridlike arrangement, 22
groove binder-triplex complexes, 317
G•TA triad, 294
- hairpin duplex, 275
helicate, 6
hemicaracerands, 74
hemochromes, 157
hemoglobin, 156
hemoglobin, hydrogen bonding, 157
hemoproteins, 156
heterohelicene, 15
hexaethylene glycol bridge, 307
hexakis(metal) complex, 22
hexosammonium, 53
high-spin five-coordinate Fe(II), 183
high-spin iron(II), 196
high-spin iron(III), 189
high-valence oxometal, 204
holand, 51
homologous recombination, 321

- homopurine tract of double-stranded DNA, 271
homopurine-homopyrimidine, 280
Hoogsteen, 228, 232, 265, 271, 286
Hückel molecular orbital, 11
hydrogen bonds, 54, 60, 177, 238, 265
hydrogen peroxide dismutation, 195
hydrophobic interactions, 34, 70, 94, 106, 132, 289, 265
hydrophobic polyelectrolytes, 146
hypoxanthine, 287
- imidazole cocatalyst, 204
imidazole cyanogen bromide, 312
imidazole, 114
imprinted polymer, 73
inhibition of DNA replication, 321
inhibition of gene expression, 310
inhibition of restriction enzyme cleavage by triplexes, 319
intercalation, 315
intergroove crosstalk, 318
intramolecular triplex, 292
inverted motif, 298
iodonium ions, 17
iodosylbenzene, 204, 209
ionic surfactants, 108
ionochromic response, 89
isomorphism, 280
2',3'-isopropylidene-adenosine, 245
- Job plot, 33
- Kemp's imide, 240
Kemp's triacid, 45, 73, 226, 253
kinetic data in aggregates, quantitative treatment, 151
kinetic model of replication, 244
kinetics of triple-helix formation, 279
knot, 19
- L-phenylamine transport, 65
Langmuir-Blodgett films, 135
lateral diffusion of lipids, 124
libraries, 77
ligand field stabilization, 13
linear free energy relationship, 92
lipase in benzene, 133
liposomes, 104, 112, 143
low-spin five-coordinate Fe(II), 183
low-spin iron(III), 196
- μ -oxo dimer, 167
 μ -oxodiiron(III) complex, 159
macrocyclic surfactants, 106
MacroModel, 29
magic rings, 18
melamine, 60
membrane transport, 66
metal permeation, 128
metal-templated receptors, 25, 34
metal-templated self-assembly, 27
metallomicelle copper(II) complexes, 116
metallomicelles, 115
metalloperhaloporphyrin complexes, 208
metallovesicles, 128
5-methylcytosine, 277, 282
5-methyl-2'-O-methylcytidine, 283
5-methylterpyridine, 32
2-methylimidazole, 158
methyl phosphonates, 305
methylcytosine, 281
methylviologen, 135
micellar catalysis, 109, 112
micelles, 72, 103
micelles, autocatalytic generation, 228
micelles, kinetics of formation, 104
Michael addition, 84
Michaelis-Menten, 151
macrocyclic lipids, 126
microemulsions, 106
minimalist replicators, 259
minor groove, 266, 267
molecular boxes, 46
molecular cleft, 57, 81
molecular clumps, 132
molecular knots, 19
molecular polarizability, 282
molecular torsion balance, 95
molecular trench, 77
molecular tweezer, 62, 77, 82
molecular zipper, 59
monooxygenases, 136
morphological changes, 123
mutation, 259
myoglobin, 156

- N-alkyl-cytosine, 284
N⁴-(aminopyridinyl)-2''-dcytosine, 289
N⁴-ethano-cytosine, 285
N⁴-spermine-m⁵ cytosine, 284
N⁷-glycosylated guanine, 289
naphthylquinolone, 316
negative cooperativity, 315
neighboring exclusion, 317
netropsin, 317
nickel(II), 5
nitrophenyl ester aminolysis, 256
nonnatural heterocyclic analogues of
 DNA bases, 290
nuclear Overhauser effect, 291
nucleation zipper model for the formation
 of a triplex, 279
nucleic acid replicators, 227
nucleoside antibiotic, 299
- octaazamacrocyclic, 160
oligosaccharide mimics, 36
oxazopyridocarbazole, 316
oxidative S-S crosslinking triplex, 313
8-oxo-dAdenine, 286
8-oxo-dGuanosine, 287
oxoiron(IV) porphyrin radical cation, 189
6-oxo-m⁵Cytosine, 288
p-(dimethylamino)benzamide, 42
 π -backbonding, 179
p-nitrophenol-functionalized surfactants,
 124
p-nitrophenyl hexanoate, 114
 π -stacking, 10, 22, 94
p-*t*-butyl thiophenolate, 202
P450cam, 198
peptide library, 76
peptide nucleic acids, 306
peptide receptor, 76
peroxidases, 190
peroxide shunt pathway of cytochrome
 P450, 190, 196
phase transition temperature, 105, 112,
 122
phenanthroline, 5, 6, 18, 19, 25, 58, 314
1,10-phenanthroline, 287
phenazine, 82
phenothiazine-linked terpyridine, 25
phenylboronic acid, 62, 65
4-phenylimidazole, 292
phosphatidylcholine vesicles, 114, 134
phosphine oxide macrocycle, 69
phosphodiesterase, 84
phospholipid, 205
phosphorothioates, 303, 305
photo-dissociation of CO, 175
photocleavage self-replicator, 251
photoinduced electron-transfer, 23
phototriggered competitive rebinding, 186
pimelate binding, 33
poly(ethylene glycol)-functionalized
 lipids, 143
polyanion sensor, 85
polymerase chain reaction, 280
polypeptides bound micelles, 104
polypurine-rich DNA, 275
porphyrin, 17, 74, 136, 138, 142, 158
porphyrin, basket-handle, 168, 179, 186,
 191, 201
porphyrin, binaphthyl, 210
porphyrin, both-faces-hindered, 167
porphyrin, capped, 162, 178, 181
porphyrin, capped strapped, 172
porphyrin, chiral wall, 211
porphyrin, cyclophane, 209
porphyrin, doubly strapped, 172
porphyrin, hanging base, 172
porphyrin, picket-fence, 159, 177, 202
porphyrin, picnic-basket, 205
porphyrin, polyhalogenated, 205
porphyrin, single-face-hindered, 159
porphyrin, steroid-linked, 205
porphyrin, strapped, 162
porphyrin, superstructured iron(II), 182
porphyrin, threitol-strapped, 213
porphyrin, twin-coronet, 211
porphyrin, vaulted-dome, 191
porphyrin, xylofuranosyl, 214
preaggregates, 131
preassociative bimolecular pathway, 231
prebiotic chemistry, 249
product inhibition, 234
protoheme-sulfide complexes, 198
protohemes thiol "tailed", 198
protoporphyrin IX, 157, 189
proximal base effect, 179
pseudo-first-order rate constant, 152
pseudoisocytidine, 286
pseudophase characteristics, 104
pseudophase exchange model, 110
pseudophases, 111
pseudopyrimidines, 298

- purine, 238
- pyridine, 16
- pyridine-2,6-dicarboxamide, 56
- pyrido[2,3-d]pyrimidone, 302
- pyrido[3,2-g]indole, 56
- 1,2-(4-pyridyl)ethane, 16
- pyrimidine motif, 270
- pyrimidine oligonucleotides, 270
- pyrimidine, 265
- pyrimidine-rich DNA, 275
- ϕ -pyrimidines, 296

- quantitative affinity cleavage, 276
- quinazoline-2,4-dione, 301
- quinquepyridine, 4

- racemization, 118
- rack-type arrangement, 21
- random coil- α -helix transition, 43
- rate enhancement from template stabilization, 227
- reactivity in organized assemblies, 107
- reciprocal templates, 253
- recombination, 259
- replication, 259
- reverse Hoogsteen, 269, 271
- riboacetal DNA, 308
- ribose, 238
- RNA-DNA hybrid triplexes, 303
- rotaxanes, 20
- Rothemund reaction, 160

- S-type sugar pucker, 272
- salen, 35
- sapphyrin, 66
- Scatchard analysis, 9
- second-order rate constants, 111, 117, 152
- self-assembled ionophores, 35
- self-assembled porphyrin receptor, 59
- self-assembled receptor, 82
- self-complementarity, 226
- self-recognition, 9
- self-replicating systems, 225, 238
- self-replication, 238, 249
- self-reproduction, 108

- sexipyridine, 2
- sexipyridine, complexes cadmium(II), 3
- sexipyridine, complexes copper(I), 4
- sexipyridine, complexes manganese(II), 3
- sexipyridine, complexes silver(I), 4
- sodium dodecyl sulfate, 72
- spectroscopic reporter group, 28
- spermine, 284, 309
- spine of hydration, 266
- starburstlike coordination oligomers, 24
- Stealth liposomes, 143
- steric hindrance in O₂ and CO binding, 180
- Stern layer, 107, 110
- steroid-functionalized porphyrin, 139
- steroidal cyclopeptide, 61
- strand displacement binding, 306
- styrene epoxidation, 213
- superoxide, 185
- surfactants, 101
- switch back oligonucleotides, 310

- teicoplanin, 103
- template catalysis, 241
- template dimerization, 235
- template synthesis, 5
- terpyridine, 2, 5, 21, 32
- tetrahedral intermediate, 228
- tetrakis(metal) complex, 22
- tetraphenylporphyrin, 162
- tetrathioalix[4]arene, 50
- thermodynamic control, 22
- thioformacetal, 305
- thioindigocrown, 45
- thiourea, 32
- transactivating factor Spl, 319
- tripeptides, 122
- triple-helix, 10, 13, 14, 35
- triple-helical structures, 2
- triple-stranded DNA, 270
- triplex-helix-binding ligands, 314
- triplex-tetraplex equilibrium, 300
- triplexes, 269
- tris terpyridinyl benzene, 24
- tris(phenanthroline), 20
- tris-(bipyridine), complexes copper(I), 8
- tris-(bipyridine), complexes nickel(II), 14
- tris-(bipyridines), 8
- T \bullet CG triad, 294

- valerolactam, 243
- vesicle bilayer, 105
- vesicles multilayer, 105
- vesicles, 104, 123, 130
- viologen-linked terpyridine, 25

- water ligation to Fe(II), 186
- water-soluble cyclophane, 74, 80, 102
- water-soluble macrocycle, 70
- Watson–Crick, 227, 232, 265, 286
- Watson–Hoogsteen groove, 273

- Williamson ether synthesis, 18
- wobble base pairing, 265

- xanthene, 56
- xanthine, 287

- Y/R•UA triad, 295

- Z-DNA, 266